Late Quaternary radiolarians as proxies for past environmental conditions in the eastern and southern sectors of the Indian Ocean

by

John Rogers

July, 2009

Research School of Earth Sciences
The Australian National University

A thesis submitted for the degree
of
Doctor of Philosophy
of
The Australian National University

Except where otherwise acknowledged in the text, this thesis represents original research by the author

John Rogers

Acknowledgements

Ensuring that everyone who brought me through the long gestation of this thesis is included in the acknowledgement and is properly thanked is, perhaps, the most difficult part of the whole project. Deciding the order in which they should be listed is even worse.

Equal first place must, of course, go to my ever-supportive supervisor, Patrick De Deckker, and to my long-suffering wife, Leonie. Patrick kindly left me alone when he thought I was managing but was always there to answer a question, point to a reference, suggest a new approach, and to push me when I was lagging. Leonie protected me from all the day-to-day time-consumers, prepared the food, watched the paint peel off the walls for want of maintenance, and generally suffered the lack of excursions, holidays, etc.

Next come my three advisors, Drs. Michael Ellwood, Stephen Eggins, and George Charpronière – always ready to answer even the most stupid questions. Thank you all. Two people who were not official advisors: Drs. Andrew Hogg and Brad Opdyke. Brad frequently filled in the gaps in my palaeoclimatology and Andy enthusiastically approached the obtuse oceanography questions I put to him – and, almost accidentally, provided an invaluable tip on how turn this thesis into an actual printed document. Thanks to you both.

I should also like to thank all the staff and students of the erstwhile Department of Earth and Marine Sciences, especially Judith Shelley for always being able to find the bits and pieces I needed in the laboratory, Brian Harrold for unstinted help with IT problems, Maree Coldrick for advice on the administrative aspects, and Nigel Crady for logistic aid. Thanks are also due to Susanne Hutchinson who, since the DEMS/RSES merger, has found herself shouldering some of the administrative load. To all those whose ears I bent in the DEMS common room and elsewhere, thanks for putting up with me and for the moral support and advice you gave me. Thanks too for succeeding in not looking bored!

Much of the material on which I worked was product of *RV. Marion Dufresne I and II* research cruises, including some which were part of the PAGES (Past Global Changes) IMAGES Programme (http://www.images-pages.org/home.html). My research would not have been possible without the cooperation of members of the Laboratoire des Sciences du Climat et de l'Environnement (LSCE), CNRS-CEA, Gif-sur-Yvette, France. Especial thanks for the welcome I received from Drs Elisabeth Michel, Claire Waelbroeck, Marie-Alexandrine Sicre, Jean-Claude Duplessy, and numerous others on my visit to LSCE in 2008 and to Professor Jean-Louis Turon, Drs Thierry Corrège, Xavier Crosta, Bruno Malaize, and their colleagues at EPOC, Université de Bordeaux I. Dr Monique Labracherie, who requested the radiolarian slides from cores MD88-769 and MD88-770, and Marie-Hélène Castera, who prepared them, contributed more than they can know to this thesis by giving me hundreds of beautifully prepared samples which were kindly loaned by J-L Turon. The visits to EPOC and LSCE were made possible by a scholarship from the Australian-French Association for Science and Technology in Canberra.

My research would have been impossible without access to several online databases for which thanks go to Professors Kjell Bjørklund, Demetrio Boltovskoy, and Jean-Pierre Caulet, and Drs Jane Dolven, and Annika Sanfilippo. Thanks also to the members of the International Association of Radiolarian Paleontologists – too many to mention all by name but including Drs Giuseppe Cortese, Chris Hollis, Stanley Kling, Kozo Takahashi, and William Riedel.

On the statistical front, this thesis would never have been completed without the advice of Dr Steve Juggins of the University of Newcastle (UK) during and after his course in

Adelaide in 2007. Thanks go also to Dr Øyvind Hammer of the University of Oslo, to Dr Jeff Wood of the ANU's Statistical Consulting Unit. and to Dr Joël Guiot.

My two sons also made valuable contributions. James built the device to connect my camera to the microscope: without it none of the thousands of photographs would have been possible. Luke scoured the libraries of Yale to give me overnight access to the journal articles which the ANU did not hold. My daughters provided morale support throughout.

Critical also to my ability to study was an Australian Postgraduate Award scholarship and the AINSE grant (no. 0736) provided to Patrick De Deckker for the dating of a number of the core-tops from which radiolaria were extracted. The opportunity (arranged by Professor De Deckker) to obtain sea experience on the University of the Sea 2005 on the *RV. Marion Dufresne II* and on two cruises of the *RV Southern Surveyor* was also invaluable.

Last but not least, thanks to staff and students from all round the ANU – the library and its very helpful librarians, especially Chris Harney, the Academic Skills and Learning Centre, PARSA, the SIGN mentoring programme, MEP, SCUNA, and all those other people and university institutions which kept me on the right track, happy, and busy.

Abstract

This study falls into two parts. The first comprises a detailed study of the radiolarian sub-fossils from surface sediment samples from two sectors of the Indian Ocean – an eastern sector lying between 12°S and 31°S and between 107°E and 128°E, and a southern sector between 31°S and 63°S and between 48°E and 111°E. The second part of the thesis consists of the reconstruction of palaeoenvironmental conditions from four cores extracted from the southern Indian Ocean between the Kerguelen Plateau and the Southeast Indian Ridge.

The study's first part establishes the existence of eleven radiolarian assemblages, six in the eastern Indian Ocean (EIO) and five in the southern Indian Ocean (SIO). The EIO assemblages can be associated with the sector's currents, at least one of them being subsurface. The SIO assemblages correspond to the inter-frontal zones of the Southern Ocean. The first part of the study also establishes relationship between radiolarian taxa distributions and a number of oceanic variables (temperature, salinity, *in situ* density, dissolved oxygen, nitrate, phosphate, silicate, and alkalinity) at depths from the ocean's surface down to 500 metres below sea level. These relationship do not always hold for all depths in the water column or for all parts of the study area, thus demonstrating the need for care when attempting palaeoenvironmental reconstructions over a wide geographical area. The validity of the relationship between the radiolarian census data and sea-surface temperature (SST) is confirmed by reconstructing Last Glacial Maximum SSTs and comparing them with Barrows and Juggins' (2005) SST study which is based on foraminifera and is generally accepted as the source of the best SST estimates for the Indian Ocean thus far.

In the second part of this thesis, the palaeoenvironmental conditions over approximately the last 40 ka at the sites of four sediment cores (MD88-769, MD88-770, MD94-102, and MD94-103: all located in the southern Indian Ocean between the Kerguelen Plateau and the

Southeast Indian Ridge) are reconstructed. From this data, the displacements of the Subantarctic and the Polar Fronts over time are adduced. The two fronts were closer together during the last glacial period (19-35 ka) than at present, indicating a steeper subduction gradient for the surface waters. The fronts also moved further north in the region of the Kerguelen Plateau than adjacent to the Southeast Indian Ridge. The variation on the fronts' movements from place to place may have been due to permanent glaciation on the Kerguelen Plateau. The study also attempts to find, in its radiolarian-based palaeoenvironmental reconstructions, reflections of interactions between the Southern Ocean and the North Atlantic. Sicre *et al.* (2005) report peaks in foraminiferally-derived Southern Ocean SSTs coincident with Heinrich Events, and the present study specifically includes provision of the corresponding radiolarian-based SSTs. This thesis strongly suggests a connection between SIO warming and Heinrich Events H1 and H2a but associations with other Heinrich Events are insufficiently robust to be conclusive. The intention exists to investigate these putative relationships more deeply using higher resolution reconstructions.

This thesis also includes considerable investigation of the available statistical techniques for the analysis and reconstruction of plankton census data. It concludes that a number of the traditional techniques, whilst useful when computer power was severely limited, are unsuitable for employment in regions as complex as the Indian Ocean. The number of surface samples available for this study is insufficient to attempt reconstructions using the theoretically very advantageous "modern analog technique" (Hutson, 1980), and the most successful technique available proved to be weighted-averaging – partial least squares (ter Braak and Juggins, 1993; ter Braak *et al.*, 1993).

In summary, my research for this thesis confirms and expands the knowledge of Indian Ocean radiolarian assemblages. It allows the reconstruction (under certain conditions) of palaeo temperature, salinity, *in situ* density, dissolved oxygen, nitrate, phosphate, silicate, and

alkalinity in the eastern and southern sectors of the Indian Ocean. It provides palaeo-reconstructions of these oceanic variables for four SIO cores over approximately the last 40 ka and deduces from these reconstructions the movements of the Subantarctic and Polar Fronts by a new and robust method. The research also suggests associations between the Southern Ocean and Heinrich Events in the North Atlantic. Finally, it demonstrates the efficacy of modern statistical techniques when compared with traditional methods.

Table of Contents

List of Figures

List of Tables

"ES" indicates the table is contained in the Electronic Supplement

Chapter 1: Introduction

A detailed knowledge of the oceans and how they change over time is imperative because of the impact they have on humans and their activities, especially in a world deeply concerned by the possibility of adverse climate change within the next century. The oceans, which cover over 70% of the planet, are the world's main surface heat-store with a capacity far larger than that of the atmosphere. They transfer heat from the tropics to higher latitudes, making large areas of the Earth far more habitable than otherwise would be the case. As a heat-store, they are slow to warm and slow to cool, generally ameliorating the extremes of atmospheric temperatures but also, on occasion, providing the energy for violent storms (Charnock, 1996). Evaporation from the oceans is the ultimate source of all the water vapour which, by precipitation, transports water onto the land, maintaining conditions suitable for life over wide areas (Linacre and Geerts, 1997; Tomczak and Godfrey, 2003). Water vapour is also the most important greenhouse gas: without it, the Earth would have surface temperatures close to those of Mars (Oke, 1987).

Palaeoceanography is a primary source of information on the drivers of climate change. Although, in some places, detailed direct observations go back up to 350 years or so (Walker and King, 2008), such a period is far too short to draw sound conclusions on the causes of change. To establish the climate change drivers and to confirm the prognostications of climate modellers, it is necessary to reconstruct palaeoenvironmental conditions over many millennia, and one of the principal sources of this information lies as calcareous and siliceous oozes at the bottom of the sea. The other major source is glacial ice, particularly in the Greenland and Antarctic (see, for example, Greenland Project (GRIP) Members, 1993; Petit *et al.*, 1999).

Despite research since the 1950s (e.g. Emiliani, 1955), understanding of the past oceanic environment is far from complete. Some potentially important oceanic variables lack proxies and, where proxies exist, the resolution of palaeo-reconstructions, in terms of both time and global coverage, is poor (Meissener, 2007). The present study seeks to make a small contribution to filling the gaps.

The objectives of this study are:

- to provide a database for the reconstruction of palaeoenvironmental conditions from a detailed record of the radiolarian sub-fossil assemblages in the surface sediments of the eastern and southern sectors of the Indian Ocean;
- to establish which palaeoceanic variables might be reconstructed using the distribution of radiolarian taxa as proxy, and what limitations would have to be placed on the reconstructions;
- to reconstruct oceanic variables from some individual samples from the eastern Indian Ocean and to reconstruct, with a high degree of resolution, the last 40 ka from core samples from four southern Indian Ocean sites situated between the Kerguelen Plateau and the Southeast Indian Ridge on either side of the Subantarctic Front;
- where possible, to seek confirmation of the oceanic variable reconstructions by comparing them with the work of other researchers using different proxies (e.g. foraminifera or diatoms); and
- to estimate the movement of southern Indian Ocean water masses and fronts over the last forty millennia.

Chapter 2: Radiolaria

2.1. Description and classification

In 1860 Haeckel used the term "radiolarian" to describe a group of unicellular marine organisms which are now considered to constitute three distinct classes of Protozoa: Polycystinea, Phaeodarea, and Acantharea (for a definition of Protozoa see Cavalier-Smith, 1993). The tests of both Polycystinea and Phaeodarea (of those species that have them, that is; some species lack hard body parts) are siliceous with those of Phaeodarea being hollow and of Polycystinea solid. Phaeodarean tests dissolve easily and are rarely fossilised; acantharean tests, consisting of strontium sulphate, dissolve immediately the organism dies. In micropalaeontology today, the term Radiolaria is frequently used to refer to Polycystina alone (because the other members of the superclass Actinopodea leave few or no fossils) and this is the way it is used throughout this study.

The classification of Radiolaria below the level of class has traditionally been based on morphology with three long-accepted orders: Spumellaria, Nassellaria, and Collodaria (sometimes subsumed in Spumellaria). Recently radiolarians' specialist group, the International Association of Radiolarian Paleontologists (InterRad), has proposed three new orders, Albaillellaria, Archaeospicularia, and Latentifistularia, to cover certain Palaeozoic radiolaria. In addition, the InterRad confirms the Spumellaria/Collodaria split and distinguishes a third modern order, Entactinaria. The distinction between Collodaria and Entactinaria on the one hand and Spumellaria on the other is the fact that the formers' tests grow from spicules like the other orders, whereas Spumellaria grow from micro- or macrospheres. For the most part, test morphology is sufficient for the researcher to separate Spumellaria from Collodaria at sight but this is not true of Entactinaria where the presence or absence of an initial spicule must be determined (De Wever *et al.*, 2001).

Recent phylogenic studies support the introduction of Entactinaria. Spumellaria (as now defined) and Acantharia have been found to share a clade and Nassellaria, Collodaria, and Entactinaria to share a separate clade (Zettler *et al.*, 1997; Zettler *et al.*, 1999; Takahashi, O. *et al.*, 2004; Yuasa *et al.*, 2005; Kunitomo *et al.*, 2006). Allocation of radiolarian species to the four modern orders is still at a fairly early stage (De Wever *et al.*, 2001).

2.2. Physiology and ecology

Radiolaria are, for the most part, holoplanktonic, i.e. floating organisms dwelling only in the open ocean (Casey, 1967a), living in waters of salinity greater than 30 . Just one species has been found living in brackish waters (Boltovskoy *et al.*, 2003). The absence of Radiolaria from shallow, coastal, waters may result from an excess of predators or from the high particulate load overwhelming their food capture system (Swanberg, 1983). They do, however, thrive in deep coastal waters like the Norwegian fiords (Swanberg and Bjørklund, 1986, 1992), even in "polls", i.e. fiords with a very shallow entrance sill (Cortese and Bjørklund, 1998).

Most Radiolaria are solitary but some form colonies with a common gelatinous mass which, if spherical, may be up to 1 cm in diameter and, if filiform, several metres long (Anderson, O. R., 1981, 1983; Anderson, A. and Gupta, 1998). They have some control of their position in the water column. Firstly, probably as a result of CO_2 production during nocturnal respiration and use during diurnal photosynthesis, there is a daily shift of 200-350 metres through the water column. Secondly, they can eject their vacuolar content to decrease density and dive. Finally, the loss of ectoplasm and axopodia during reproduction tends to cause sinking (De Wever *et al.*, 2001).

Anderson, Swanberg, Sugiyama, and others (Swanberg, 1983; Swanberg and Anderson, 1985; Anderson, O. R. *et al.*, 1988; 1989; Anderson, O. R., Bennett and Bryan, 1989; Anderson, O. R. *et al.*, 1990; Sugiyama and Anderson, 1997) have shown that Radiolaria comprise a number of trophic types. Casey (1993) suggests six or seven types in all with different types living at different ocean depths and in different geographical regions. Casey is supported by, for instance, Dworetsky and Morley (1987) who demonstrate that Nassellaria prefer greater depths than Spumellaria and by Swanberg (1983) who comments on the dominance of symbiotrophic colonial radiolaria in the top centimetre of warm oligotrophic waters. To a degree, Anderson contradicts the differentiation by pointing out that *Euchitonia elegans* (bacterial and phytoplankton feeders) and *Spongaster tetras tetras* (picoplankton), and some Nassellarida (nanoplankton) can inhabit the same water mass, despite being of similar size, probably because they do not compete for food (Anderson, O. R., Bennett, Angel *et al.*, 1989) and by discovering the wide temperature tolerance of *Didymocyrtis tetrathalamus* (Anderson, O. R. *et al.*, 1990).

2.3. Taphonomy

The true picture of radiolarian distribution seems to be of different communities at different levels in the water column at any particular geographical area. When viewed as a fossil or sub-fossil collection, all the communities in the water column will be mixed but the mixture should change from place to place, depending on variables such as temperature, salinity, and nutrient concentrations, which may allow the categorisation of water masses by their radiolarian assemblages (Casey, 1967a, b). For instance, *Cycladophora davisiana* live no deeper than 500 metres in the Okhotsk Sea and *Actinomma boreale* at the same depth in Norwegian fiords but both are found at 1000-2000 metres in the Sea of Japan, probably because that sea's deep-water mass is well oxygenated, at the right temperature, and independent of the over-lying water-mass (Itaki, 2003).

It not known what may prey upon radiolaria (De Wever *et al.*, 2001). It has even been suggested that the small size of open ocean populations is a strategy which prevents them being the target species for any particular predator (Swanberg, 1983). However, they present a good source of organic compounds and minerals and, in most of this study's samples, there was little evidence of test dissolution, suggesting that predation is rife and that most tests reach the seafloor in faecal pellets.

Once a radiolarian dies, its cytokalymma decomposes, leaving the test open to dissolution in a sea which is typically under-saturated in dissolved silicon (Casey, 1967a). Rates of dissolution vary, principally according to the dissolved silicon concentrations over the various water masses through which the test falls. Rates of dissolution are high close to the surface but decease with increasing depth so that below 1000 metres very little further dissolution takes place until the test reaches the ocean floor (Berger, 1968; Renz, 1976). Some species are so susceptible to dissolution that they are essentially only known from plankton traps, almost never appearing in sediments (De Wever *et al.*, 2001).

Once tests have reached the ocean floor, their dissolution is thought to be determined by the rate of sediment deposition (Sanfilippo *et al.*, 1985), although the potentially different solubilities of different species will continue to have an effect. Until tests are buried below the depth subject to bioturbation, they will continue to dissolve. Thus, the higher the sedimentation rate the better the preservation: 10-25 metres/ma is adequate in calcareous-siliceous oozes and 4-5 metres/ma below the Calcite-Compensation Depth in siliceous oozes (Sanfilippo *et al.*, 1985).

The fact that shallow-dwelling radiolarian tests have to fall through as much as 1000 metres more of the water column than the tests of the deeper-dwelling species (and that the portion of the column where most silica dissolution takes place) must tend to bias the proportion of the tests found in sediments to deep-dwelling rather than shallow-dwelling species. As a result, sediment samples may be more reflective of deeper-dwelling species, and, therefore, of the ocean variables below the mixed layer. A bias in favour of deeper-dwelling species would strengthen this study's attempts to establish relationships between subsurface water masses and census counts of species found in sediments.

Chapter 3: Previous work

3.1. Introduction

As Berggren (1978) relates, the first detailed studies of marine plankton date from the early 19th century. In the case of radiolarian species, both living and fossilised, Meyen published the first description in 1834 (in Kling, 1978), Ehrenberg provided the first classification and introduced the name *Polycystina* in 1838, and Müller coined the name *Radiolaria* (Ehrenberg and Müller are cited by De Wever *et al.*, 2001). Haeckel (1887) greatly extended the knowledge of radiolaria, as well as that of many other oceanic biota, in his report of the *HMS Challenger* voyage of 1873-6 and his other researches. In the 1950s, Riedel reinvigorated radiolarian studies by applying them to Tertiary tropical biostratigraphy (Kling, 1978) and, with the advent of the Deep Sea Drilling Program (DSDP) in the 1960s, this work bore fruit and has kept its importance in biostratigraphy ever since (Casey, 1993). De Wever (2001) comprehensively summarises the use of radiolaria in biostratigraphy.

Murray (1897, cited by Berger and Garner, 1975) first proposed the use of fossil plankton (*Foraminifera*) to reconstruct palaeo-SSTs but, until the late-1960s, neither the technology to recover suitable oceanic samples nor the computing power to analyse the data were available. The use of fossil radiolaria in palaeoceanography is another product of the 1960s. The most common applications have been in the reconstruction of SSTs (just a few examples of many studies are Hays *et al.*, 1976; Pisias *et al.*, 1997; Abelmann *et al.*, 1999; Dolven *et al.*, 2002; Wang *et al.*, 2003; Cortese *et al.*, 2007; Lüer *et al.*, 2009), in the reconstruction of palaeo-salinity (Gupta, 2002), the occurrence of upwelling (Haslett, 1995), the study of water masses (Casey, 1967b; Dow, 1978), and oceanic productivity (Ragueneau *et al.*, 2000; Wang *et al.*, 2003).

Researchers into radiolarian sub-fossils from surface sediments have either tended to concern themselves with whole oceans – for instance, the South Atlantic (Boltovskoy, 1998) and the central Pacific (Renz, 1976) – or on semi-isolated regions like the East China Sea (Chang, F. *et al.*, 2003) or the Sea of Okhotsk (Nimmergut and Abelmann, 2001; Hays and Morley, 2004). Earlier census data investigations tended to select a small number of species (20 to 40) to count (for example Lozano and Hays, 1976; Johnson and Nigrini, 1980, 1982), presumably because the computing power of the period limited the amount of data which it was practical to analyse. Some researchers restricted themselves to a single species like *Cycladophora davisiana* (Hays *et al.*, 1976; Brathauer *et al.*, 2001) which they used to construct a biostratigraphy for the last 200 ka approximately. The surveys which attempt to identify every specimen usually find around 100 to 200 species per site in the tropics and subtropics (Welling, 2003; Kamikuri *et al.*, 2008), falling to 50 to 60 in the high latitudes (Boltovskoy, 1998).

3.2. Radiolaria in the Indian Ocean

The previous investigations of radiolaria in surface sediments from the eastern and southern Indian Oceans were mainly conducted in the period 1965-1990. Investigations of the eastern Indian Ocean are few. Nigrini (1967) examined strewn slides (processed through a 64 micron sieve) from 87 sites from 10°N to 45°S in the Indian Ocean. She described 45 species chosen for their abundance, ease of recognition, and the understanding of the groups to which they belong, but indicates many more are present. Nigrini provided census counts for these species based on counts of 500 specimens per slide. She found high radiolarian abundance between 10°N and 20°S and between 35°S and 45°S, with the subtropical gyral region in between virtually devoid of radiolaria. From her abundance counts, Nigrini (1967) identifies two assemblages, one low-latitude, the other mid-latitude. Nigrini's 87 sites omit any from the present study's eastern Indian Ocean sector (the area from 10°S to 32°S and

from 105°E to 125°E), apparently because her smear slide examinations indicated a lack of specimens. Fifteen of her sites fall into this study's southern sector (from 31.5°S to 62.5°S and from 50°E to 111°E).

Petrushevskaya (1967) examined an area between approximately 10°N and 70°S and 20°E and 180°E, and found Antarctic, bipolar (Arctic and Antarctic dwelling), warm water, cool water, and cosmopolitan species. She identified some associations between species, but did not describe larger assemblages. Johnson and Nigrini (1982) analysed radiolaria in the eastern Indian Ocean between 10°N and 52°S and 81°E and 115°E as a complement to their earlier (1980) study of the western Indian Ocean. They identified six recurrent groups of radiolaria and nine radiolarian assemblages. They related these assemblages to various oceanographic conditions including currents and physico-chemical parameters. Six of the 74 core tops they studied came from within this study's eastern sector and eighteen from the southern sector.

Many of the eastern Indian Ocean samples used in the present study have previously been analysed for clays (Gingele *et al.*, 2001), pollen (van der Kaars and De Deckker, 2003), calcareous nannofossils (Takahashi, K. and Okada, 2000), planktonic foraminifera (Martínez *et al.*, 1998), benthic foraminifera (Murgese and De Deckker, 2005), and dinoflagellates (Young, 2006).

The CLIMAP Project (CLIMAP Project Members, 1981, 1984, 1997) was devoted to understanding palaeoenvironmental conditions in the southern Indian Ocean, and its members made considerable use of radiolarian census counts (CLIMAP Project Members, 1976, 1981; Molfino *et al.*, 1982; Howard and Prell, 1984; Morley, 1989). Morley (1989) studied the southern Indian Ocean between 31.7°S and 59.0°S and between 27.3°E and

130.0°E, an area which includes the whole of this study's southern sector but only one of his sites lies in its eastern sector. He identified four geographically distinct radiolarian assemblages and generated a transfer function for summer and winter sea-surface temperatures (SSTs). Dow (1978) reconstructed palaeotemperatures in cores taken from an area between approximately 40°S and 65°S and 80°E and 120°E using Q-mode factor analysis (QMFA). She estimated from her reconstructions of SSTs that, during the LGM, the Antarctic Convergence lay approximately 5° north of its present position. Granlund (1986) investigated the morphology of *Antarctissa* in the southern sector and concluded that the genus' shape is influenced by sea temperature and salinity.

The southern Indian Ocean cores investigated during this study have been extensively researched from other viewpoints. Pichon *et al.* (1992) and Bareille *et al.* (1998) considered biogenic silica distribution and accumulation, Bareille *et al.* (1994) examined the origin of detrital flux, Waelbroeck *et al.*, (1995) compared SST reconstructions with the Vostok core findings, Labeyrie *et al.* (1996) researched hydrographic changes. There are studies of the sediment redistribution by bottom currents (Dezileau *et al.*, 2000), the barium distribution in surface sediments (Fagel *et al.*, 2002), and authigenic uranium enrichment in glacial sediments (Dezileau *et al.*, 2002). Salvignac (1998) used census counts of planktonic foraminifera to reconstruct summer and winter SSTs for three of the cores used in this study (MD88-769, MD88-770, and MD94-102) but her work remains unpublished. Sicre *et al.* (2005) have proposed a connection between SST reconstructions from core MD94-103 located near the Southeast Ocean Ridge and Heinrich Events in the North Atlantic. Considerable use has been made of these researches in the present study, especially those involving SST reconstruction (particularly Barrows and Juggins, 2005) and relationship with North Atlantic phenomena (Sicre *et al.*, 2005).

Chapter 4: The Oceanographic Setting

4.1. The southern Indian Ocean

4.1.1. The Frontal System

The southern Indian Ocean (SIO) is part of that which Tomczak and Godfrey (2003) term, for brevity, 'the Southern Ocean', i.e. that part of the world ocean bordering on Antarctica and south of the Subtropical Convergence (STC). The Southern Ocean is split into a number of circumpolar bands bounded by fronts. These fronts are zones of sharp change in the values and vertical profiles of such oceanic variables as temperature, salinity, and nutrients. In their 1996 paper, Belkin and Gordon mainly use temperature and salinity as the defining variables but, as can be seen from figures (Figures 4.1a-n), the STC and the Antarctic Convergence are also marked by acute changes in dissolved oxygen and silicate, nitrate and phosphate concentrations. Further, Gille (1994) has been able to establish the locations of the SAF and PF by measuring mean sea surface height using the Geosat altimeter.

The STC is a subduction zone for Southern Ocean waters. It is where the permanent thermocline reaches the surface and lies between 38° and 42°S, its position depending on both the topography of the sea floor and the season (Tchernia, 1980). The southern limit of the STC is the Subtropical Front (STF) (Figure 4.2) or, where both exist, the Southern Subtropical Front (SSTF – between 38° and 42°S) rather than the Northern STF (NSTF – between 31° and 38°S) (Belkin and Gordon, 1996). A second convergence, the Antarctic Convergence (AC) (Figure 4.2), lies south of the STC and comprises the two-step transition formed by the Subantarctic Front (SAF) at around 45°S and the Polar Front (PF – around 50°S) (Tomczak and Godfrey, 2003). The PF marks the location where northward-moving Antarctic surface water dives sharply and the temperature minimum descends to the 400

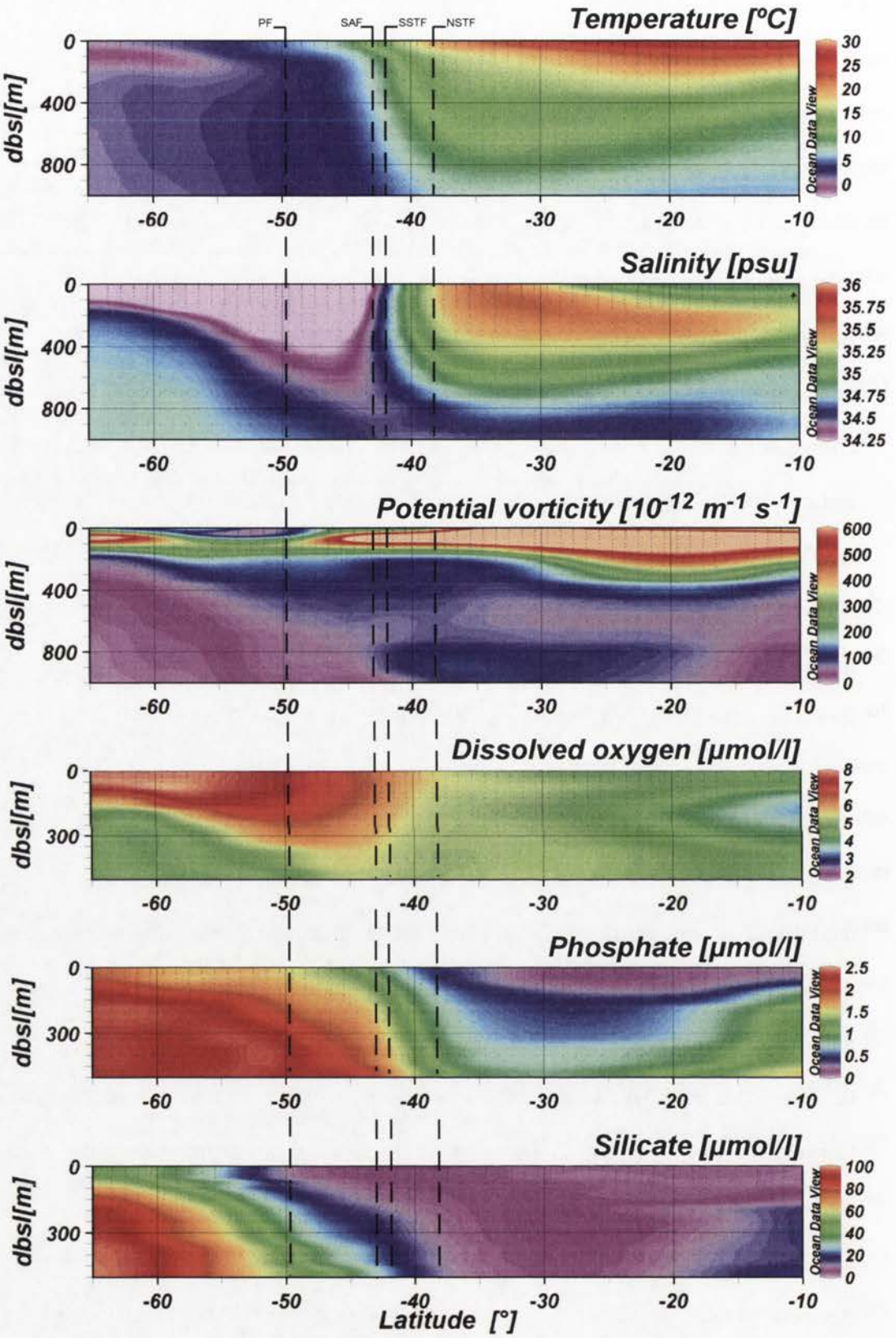

Figure 4.1a: A vertical section of the Indian Ocean at longitude 50.5°E based on WOA-05 austral summer (JFM) data showing the PF, SAF, SSTF and NSTF. At this longitude, which is in Belkin and Gordon's (1999) Crozet Front Area, the AF (not shown), SAF and SSTF are virtually confluent, and go to form the "Crozet Front".

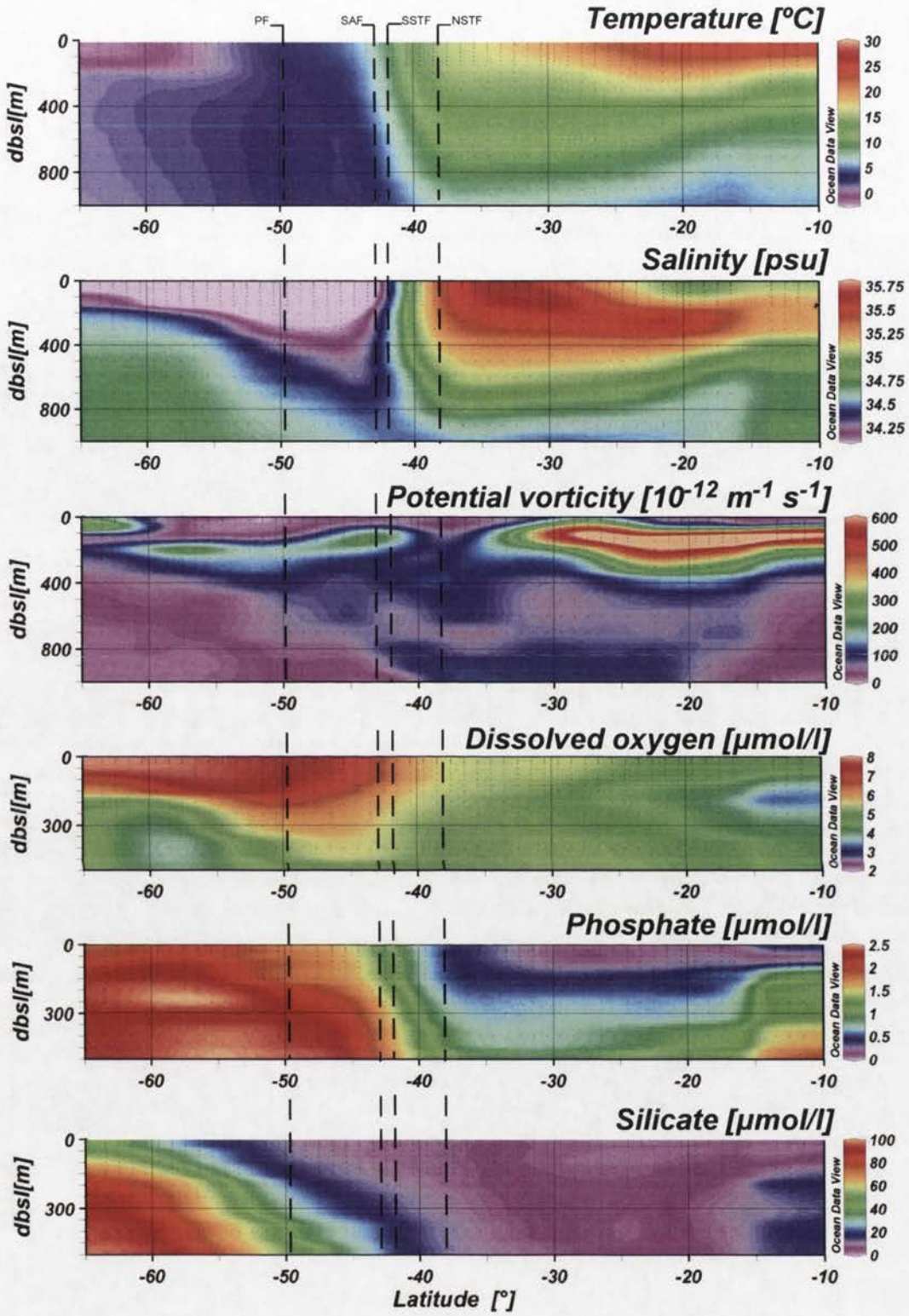

Figure 4.1b: A vertical section of the Indian Ocean at longitude 50.5°E based on WOA-05 austral winter (JAS) data showing the PF, SAF, SSTF and NSTF. At this longitude, which is in Belkin and Gordon's (1999) Crozet Front Area, the AF (not shown), SAF and SSTF are virtually confluent, forming the "Crozet Front".

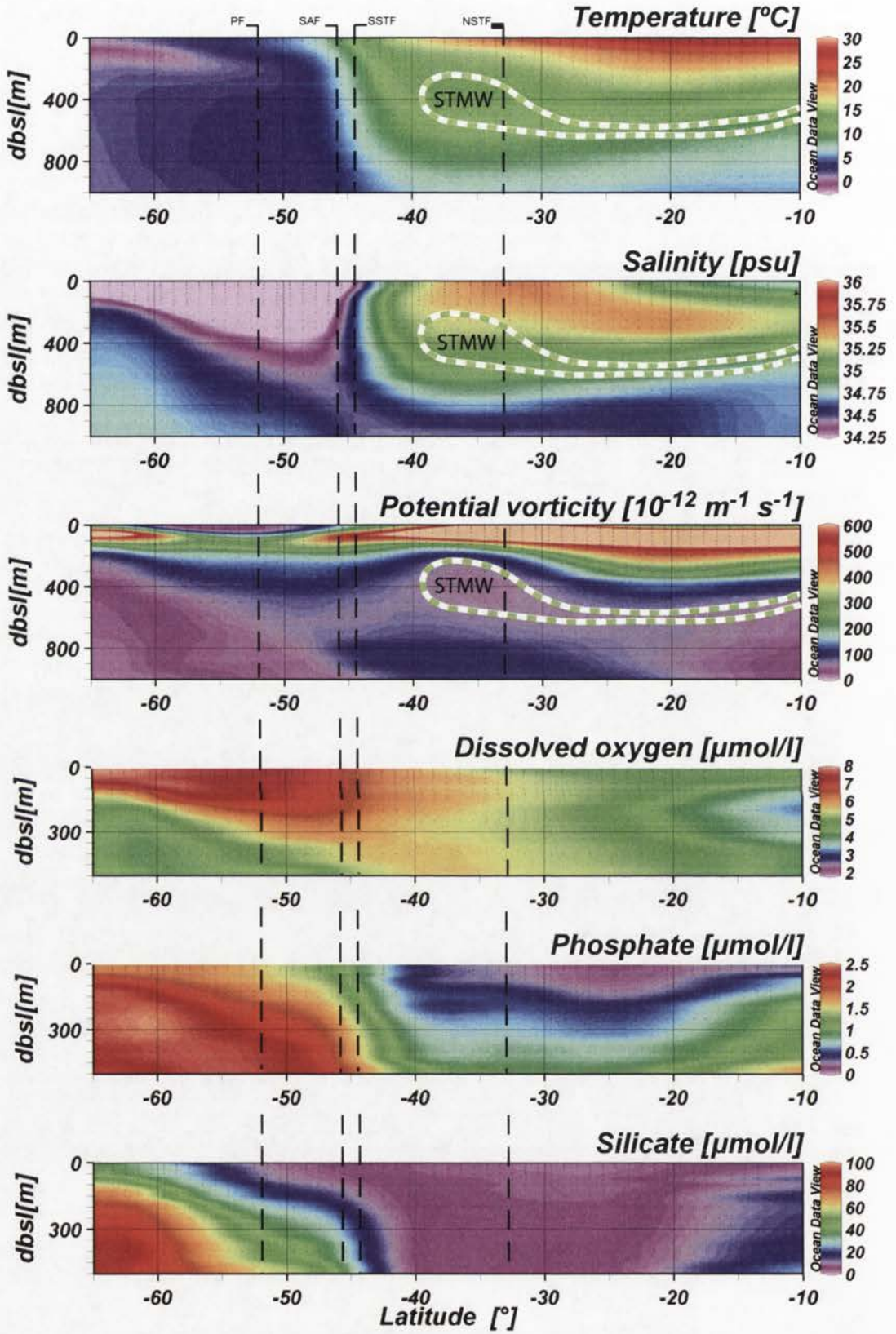

Figure 4.1c: A vertical section of the Indian Ocean at longitude 65.5°E based on WOA-05 austral summer (JFM) data showing the PF, SAF, SSTF and NSTF. The Subtropical Mode Water (STMW) is identified by its low potential vorticity.

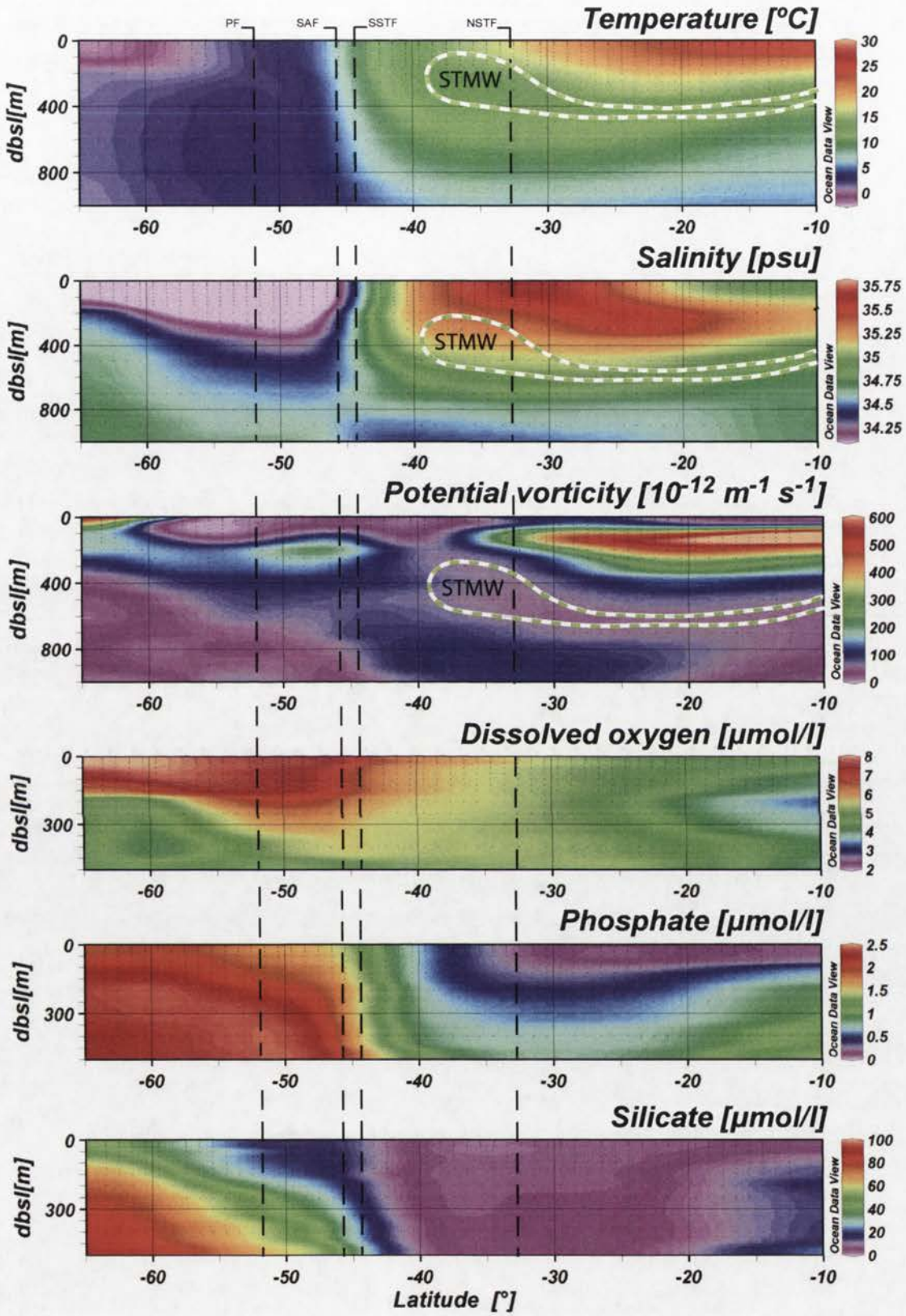

Figure 4.1d: A vertical section of the Indian Ocean at longitude 65.5°E based on WOA-05 austral winter (JAS) data showing the PF, SAF, SSTF and NSTF. The Subtropical Mode Water (STMW) is identified by its low potential vorticity.

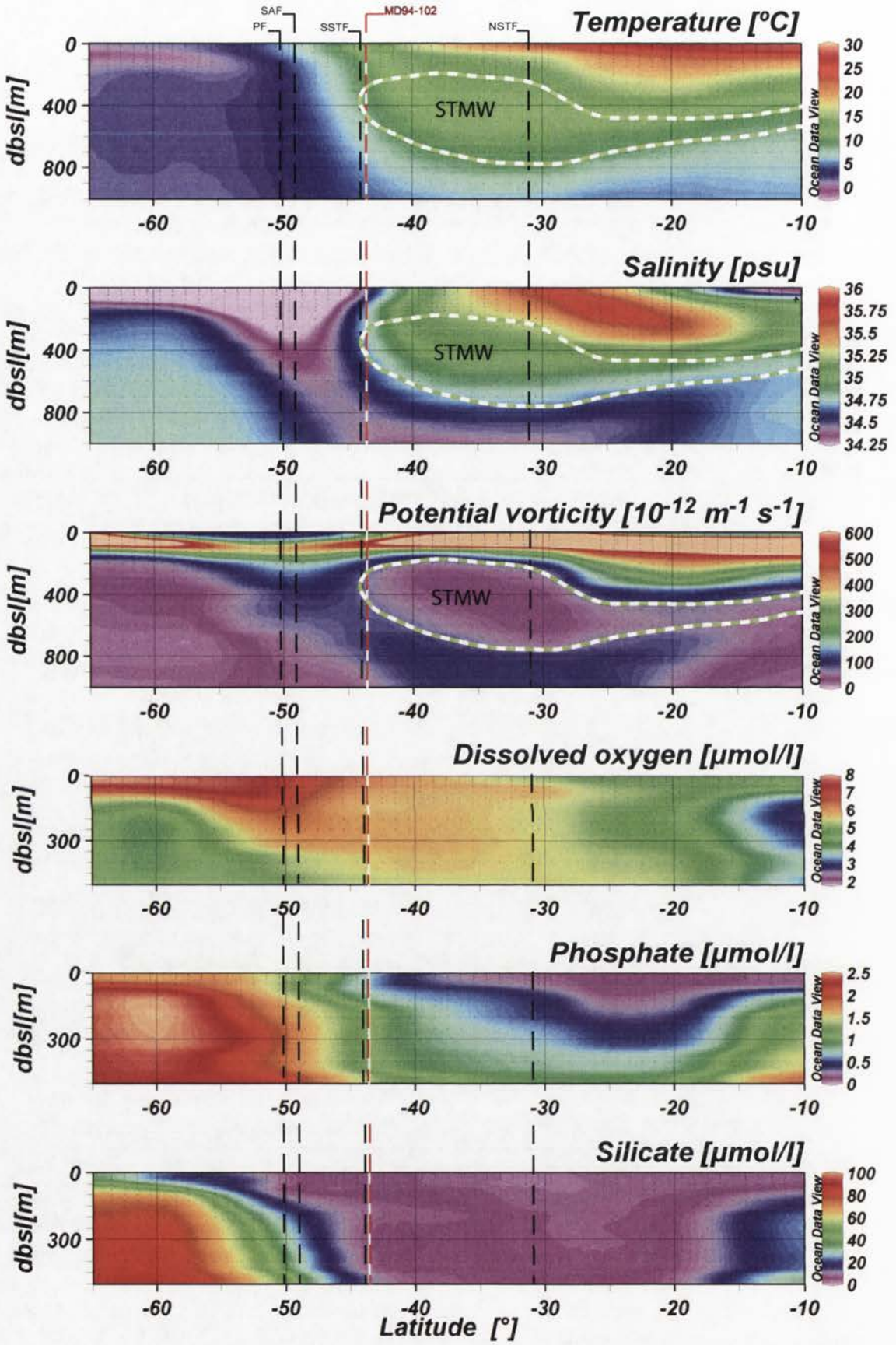

Figure 4.1e: A vertical section of the Indian Ocean at longitude 79.5°E based on WOA-05 austral summer (JFM) data. The locations of PF, SAF, and STF, and MD94-102 are also shown. The Subtropical Mode Water (STMW) is identified by its low potential vorticity.

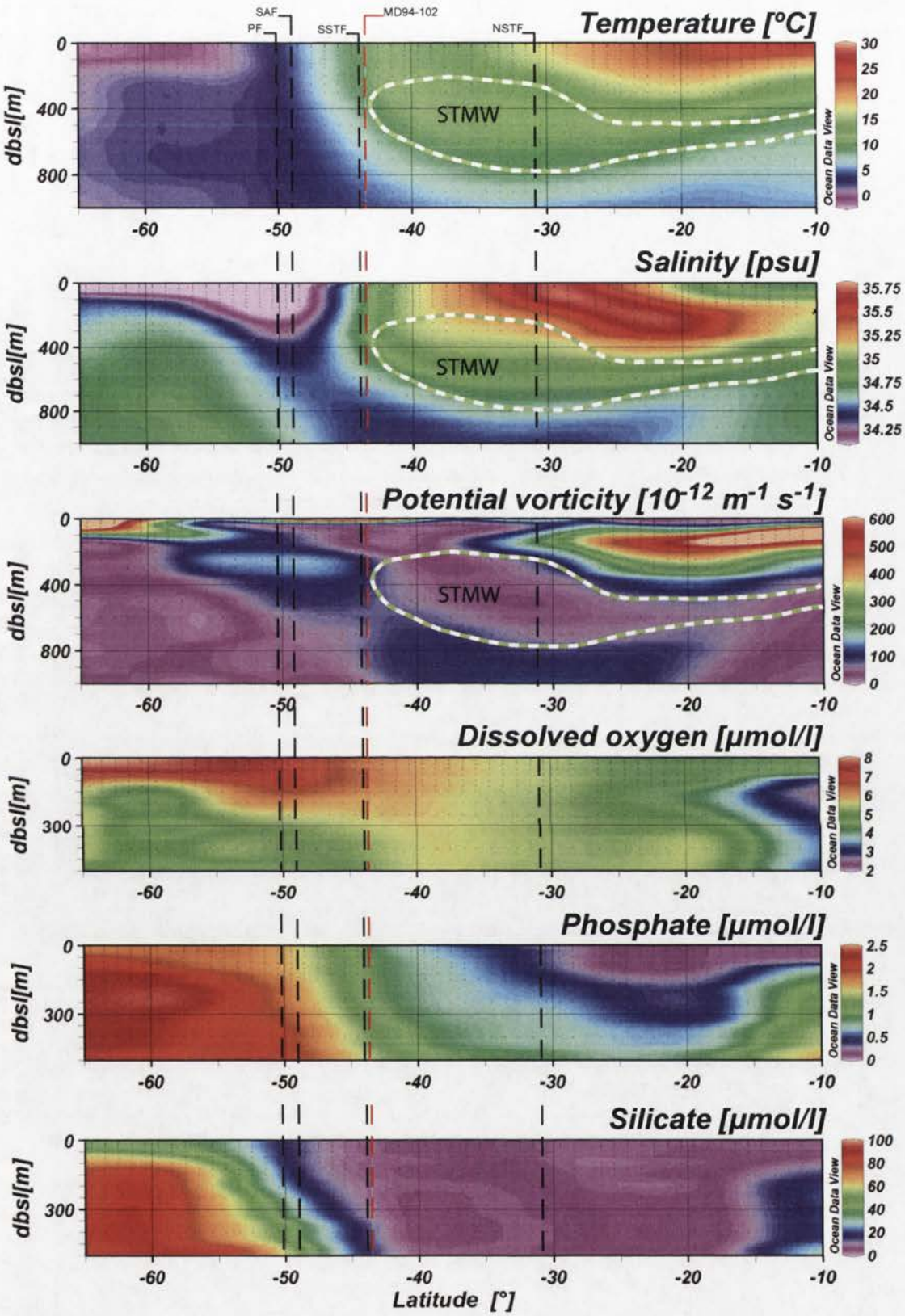

Figure 4.1f: A vertical section of the Indian Ocean at longitude 79.5°E based on WOA-05 austral winter (JAS) data. The PF, SAF, and STF are also shown as is the location of station MD94-102. The Subtropical Mode Water (STMW) is identified by its low potential vorticity.

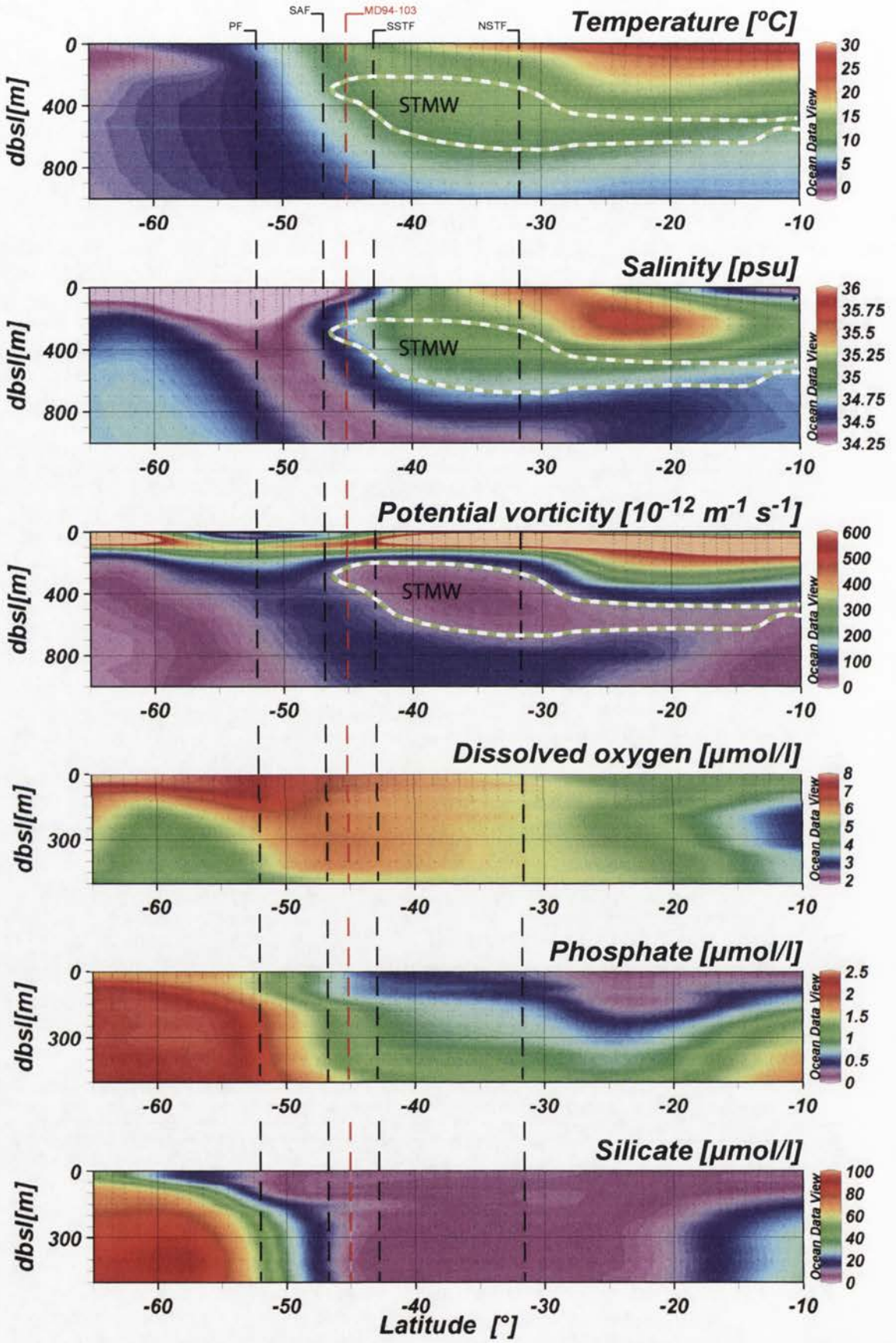

Figure 4.1g: A vertical section of the Indian Ocean at longitude 86.5°E based on WOA-05 austral summer (JFM) data showing the locations of the PF, SAF, STF, and MD94-103. The Subtropical Mode Water (STMW) is identified by its low potential vorticity.

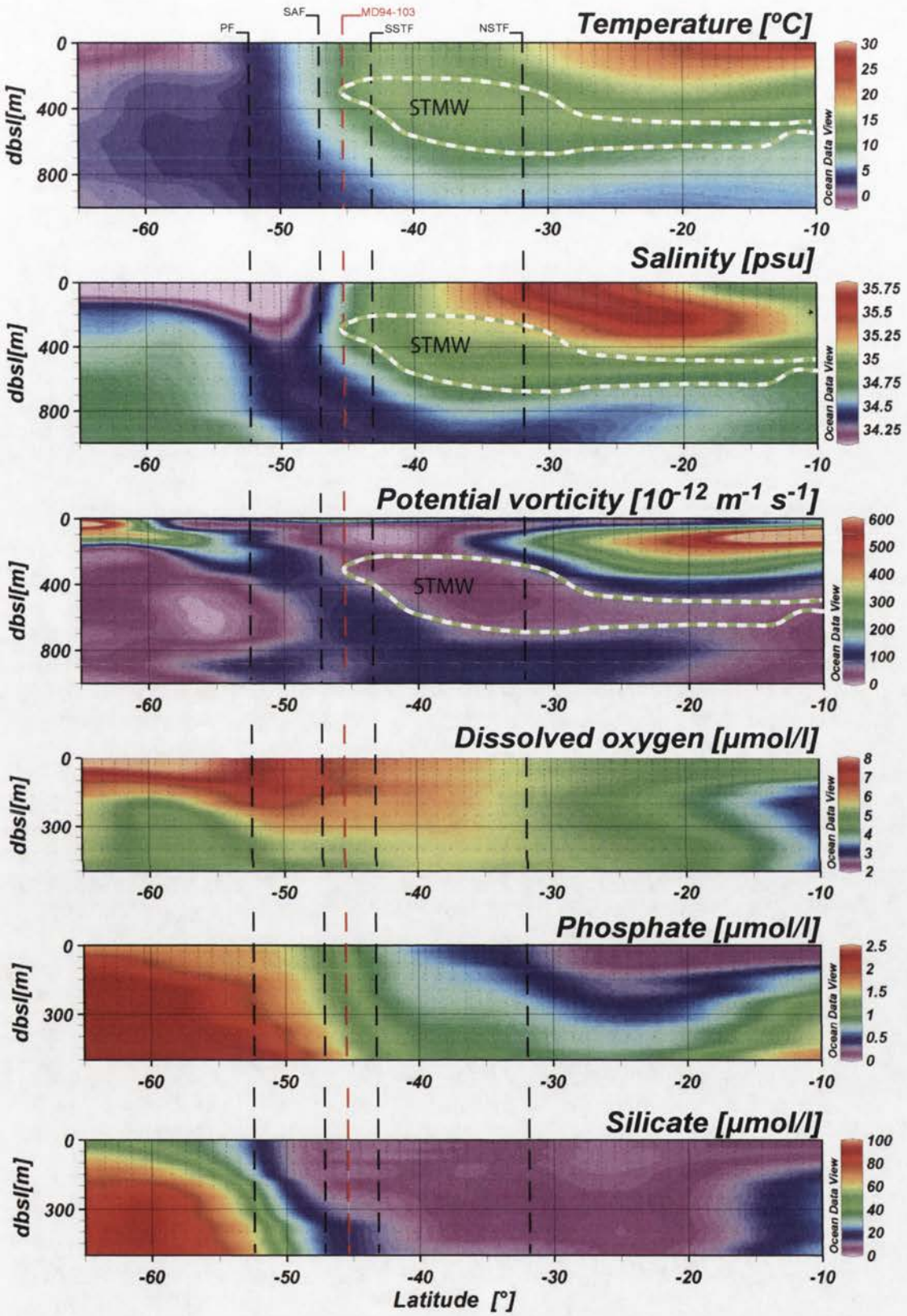

Figure 4.1h: A vertical section of the Indian Ocean at longitude 86.5°E based on WOA-05 austral winter (JAS) data showing the PF, SAF, and STF. The Subtropical Mode Water (STMW) is identified by its low potential vorticity. The location of site MD94-103 is indicated.

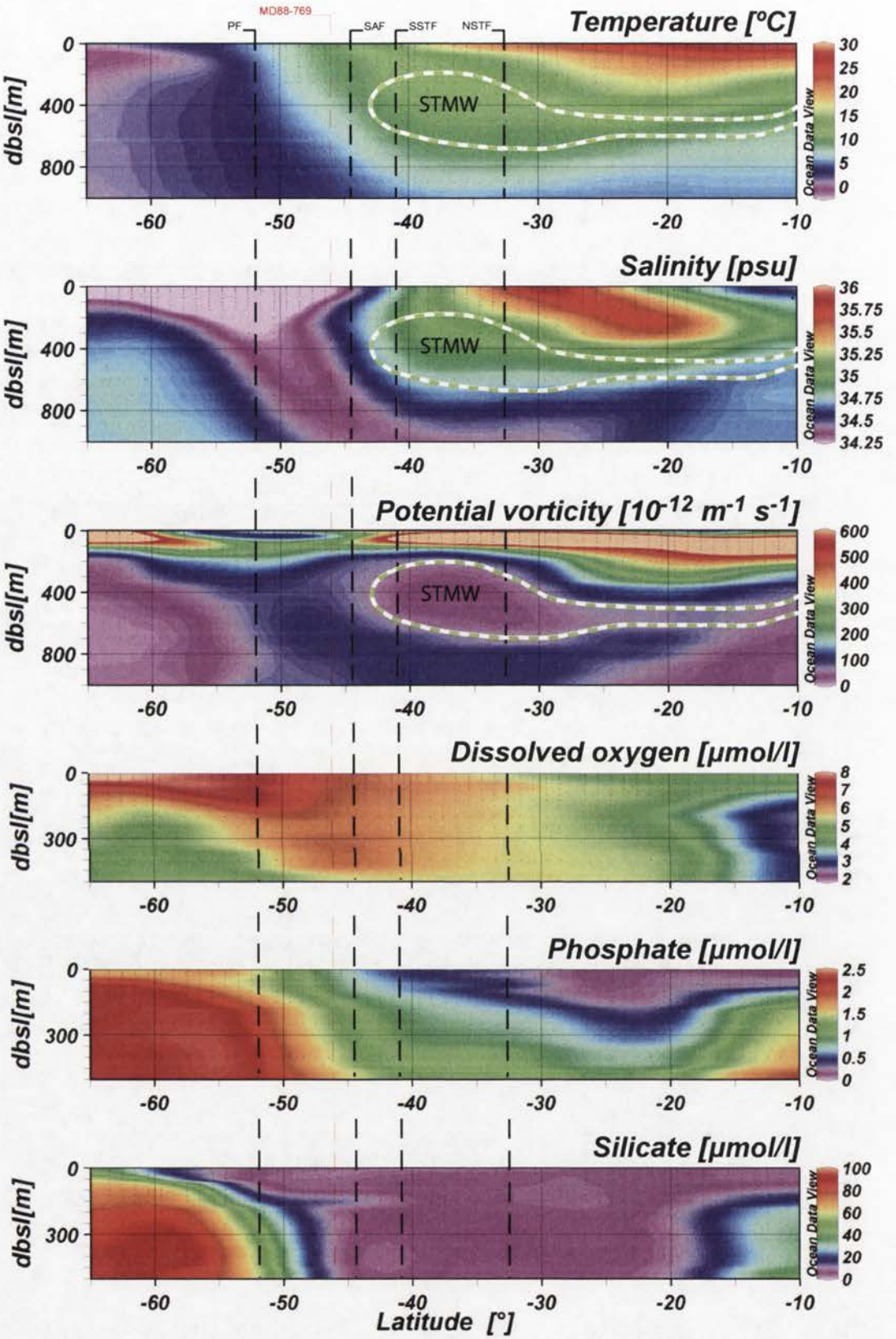

Figure 4.1i: A vertical section of the Indian Ocean at longitude 90.5°E based on WOA-05 austral summer (JFM) data showing the locations of the PF, SAF, STF, and MD88-769. The Subtropical Mode Water (STMW) is identified by its low potential vorticity.

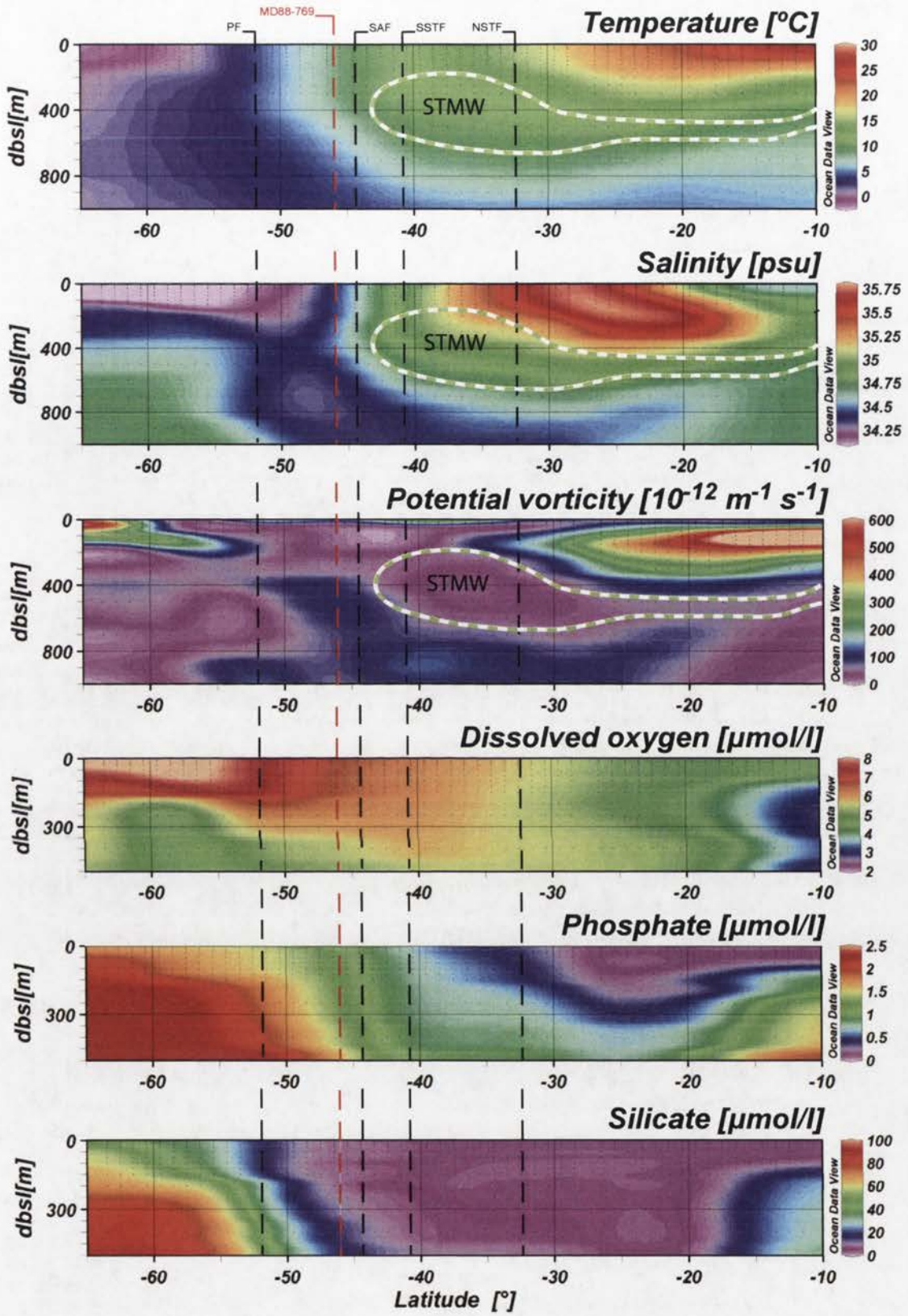

Figure 4.1j: A vertical section of the Indian Ocean at longitude 90.5°E based on WOA-05 austral winter (JAS) data showing the locations of the PF, SAF, STF and MD88-769. The Subtropical Mode Water (STMW) is identified by its low potential vorticity.

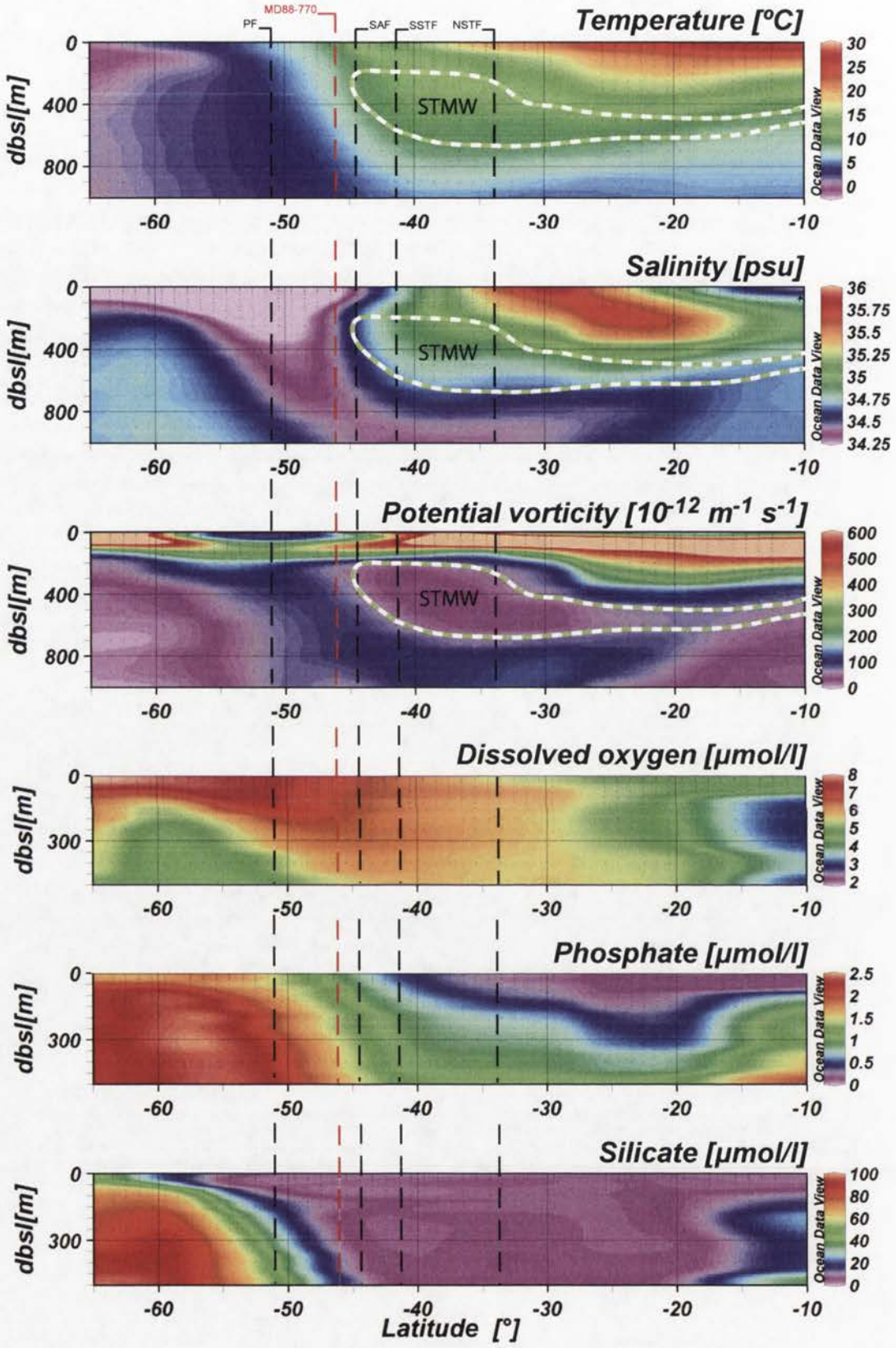

Figure 4.1k: A vertical section of the Indian Ocean at longitude 96.5°E based on WOA-05 austral summer (JFM) data showing the locations of the PF, SAF, STF and MD88-770. The Subtropical Mode Water (STMW) is identified by its low potential vorticity.

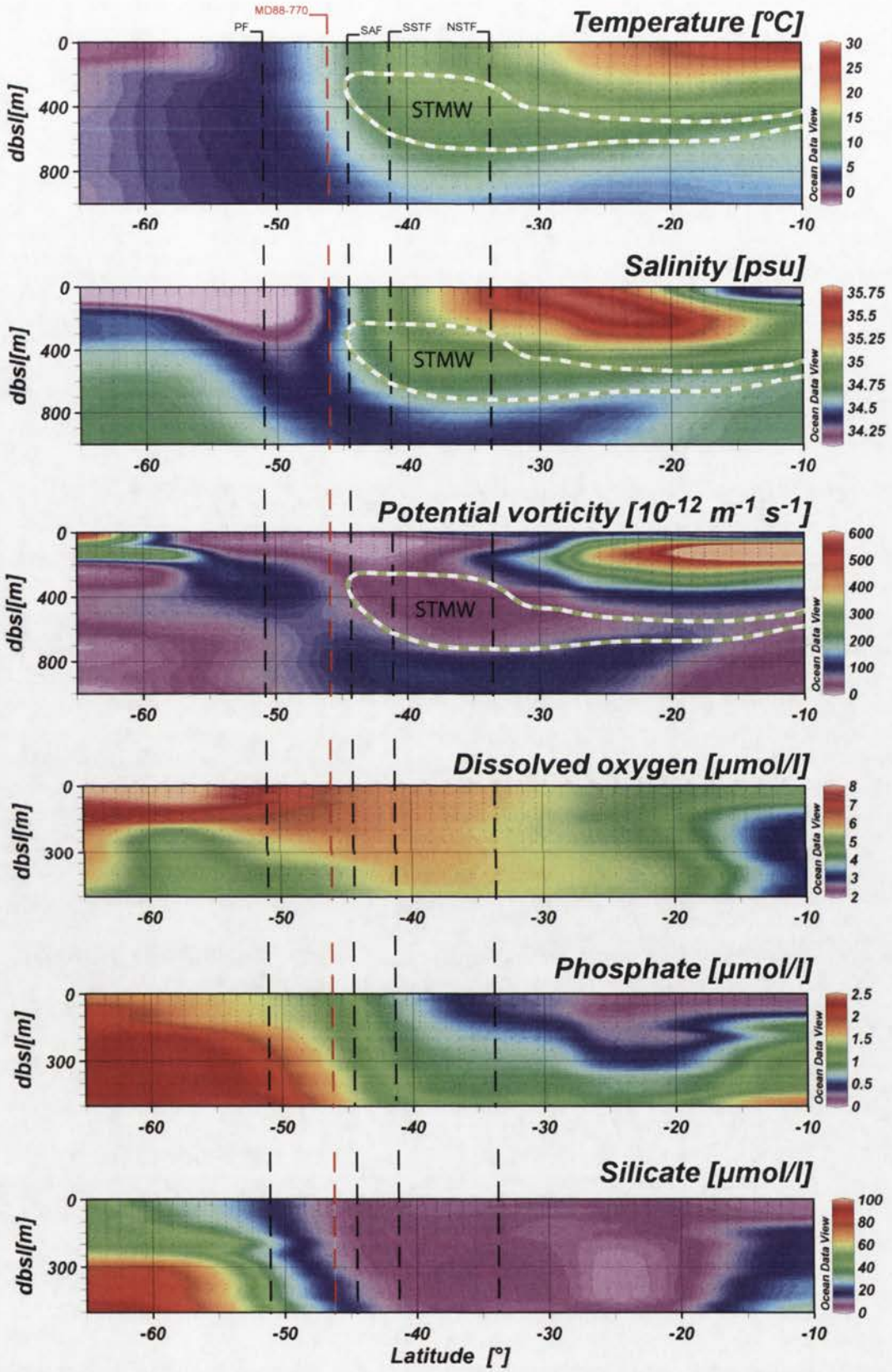

Figure 4.1l: A vertical section of the Indian Ocean at longitude 96.5°E based on WOA-05 austral winter (JAS) data showing the locations of the PF, SAF, STF and MD88-770. The Subtropical Mode Water (STMW) is identified by its low potential vorticity.

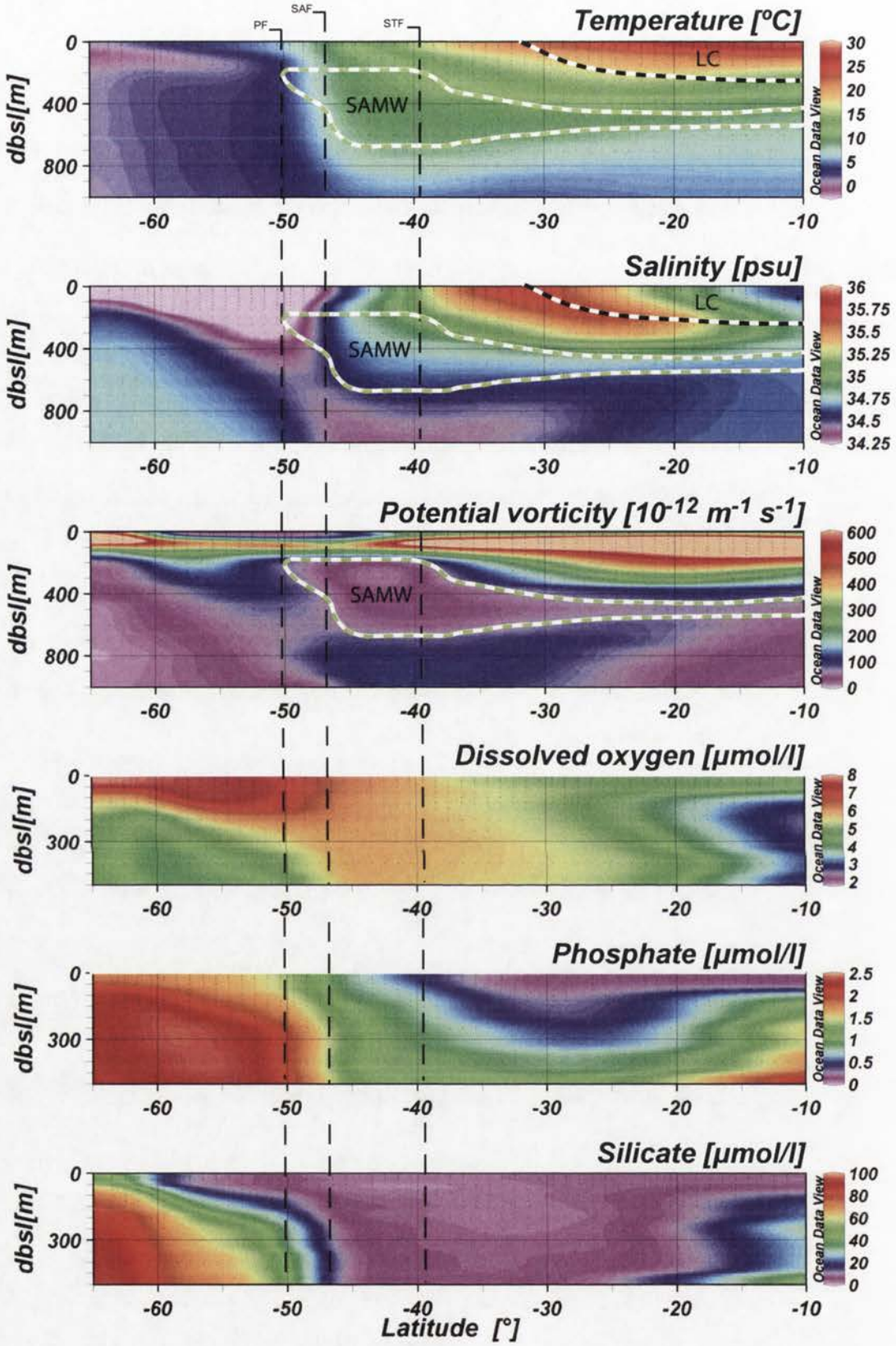

Figure 4.1m: A vertical section of the Indian Ocean at longitude 110.5°E based on WOA-05 austral summer (JFM) data showing the PF, SAF, and STF. The Subantarctic Mode Water (SAMW) is identified by its low potential vorticity and the Leeuwin Current (LC) by its high temperature and low salinity.

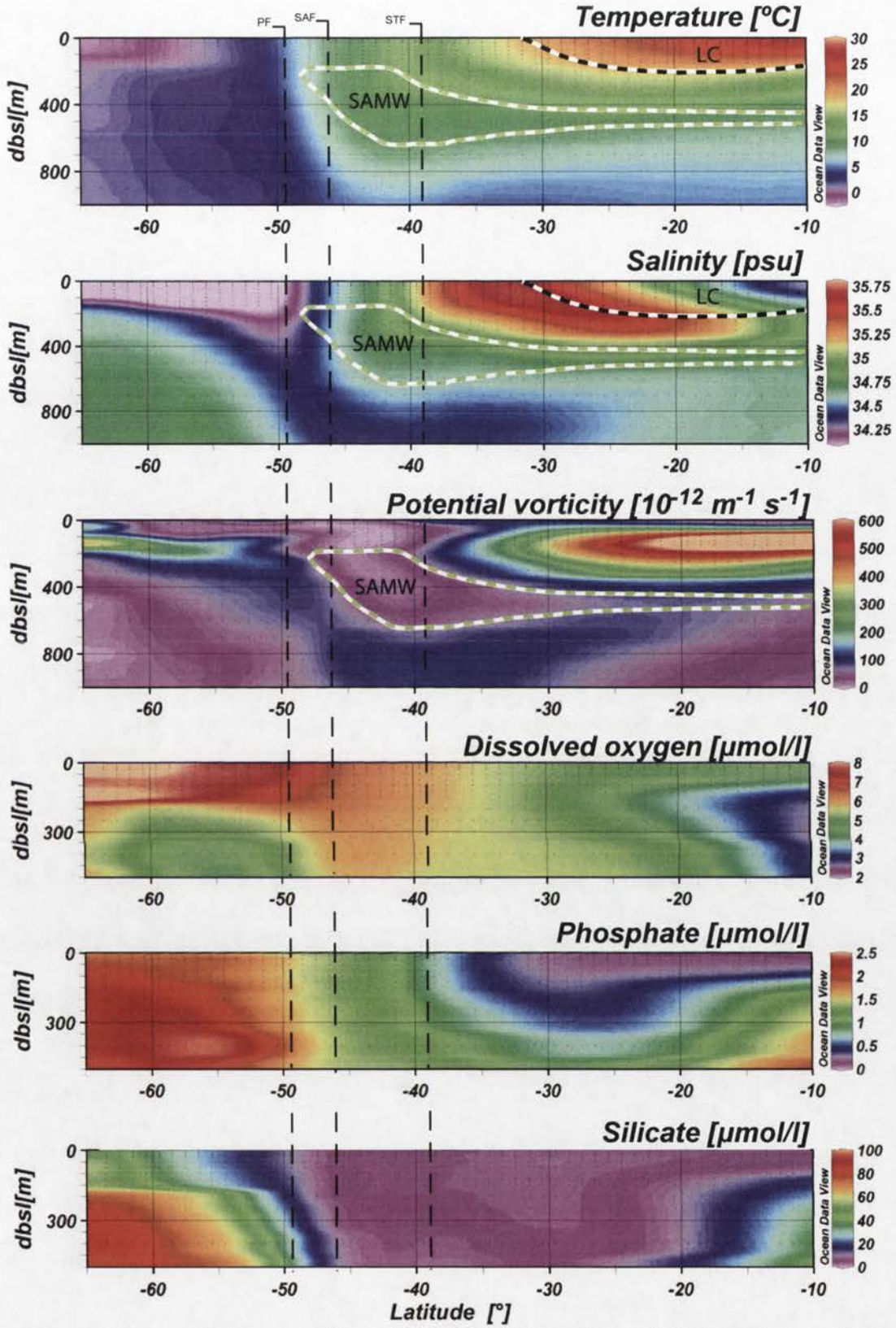

Figure 4.1n: A vertical section of the Indian Ocean at longitude 110.5°E based on WOA-05 austral winter (JAS) data showing the PF, SAF, and STF. The Subantarctic Mode Water (SAMW) is identified by its low potential vorticity and the Leeuwin Current (LC) by its high temperature and low salinity.

metre layer (Belkin and Gordon, 1996). The circumpolar band of ocean between the (S)STF and the SAF is known as the Subantarctic Zone, that between the SAF and the PF as the Polar Frontal Zone, and that south of the PF as the Antarctic Zone (Tomczak and Godfrey, 2003).

Belkin and Gordon (1996) divide the SIO meridionally into five regions: the South African Sector (10°-35°E), the Crozet Plateau Area (35°-60°E), the Kerguelen-Amsterdam Region (60°-80°E), the Southeast Indian Ocean (80°-115°E), and the Australian Sector (115°-150°E), on the basis of their frontal configurations (Figure 4.2 – the South African Sector is not shown). East of 20°E the Agulhas Front (AF) and the NSTF are essentially confluent, the SSTF is also close, whereas the SAF and the PF are distinct from these three and each other, lying some way to the south. In the eastern part of this region, the SAF and the PF both loop, first south, then north/northeast round the mid-ocean ridge.

In the Crozet Plateau Area, the SAF moves northward [Belkin and Gordon (1996) assume this is the result of the topography of the ocean floor] to join the SSTF; the AF lies further north. At about 50°E, the AF turns south to join the SAF and the SSTF as the "Crozet Front". East of the Crozet Islands, the Crozet front turns south, possibly because of a loss of topographic control in the deeper waters of the Crozet Basin. Belkin and Gordon (1996) consider the PF normally loops north round the Kerguelen Plateau, approaching, possibly joining, the Crozet Front but Olbers *et al.* (2004) and Park *et al.* (1993) suggest it may pass south of Kerguelen. It is also in the Kerguelen-Amsterdam Region that the NSTF is at its furthest from the SSTF, the two fronts surrounding the source of the Subtropical Mode Water (STMW) (McCartney, 1982).

The southern Indian Ocean surface currents

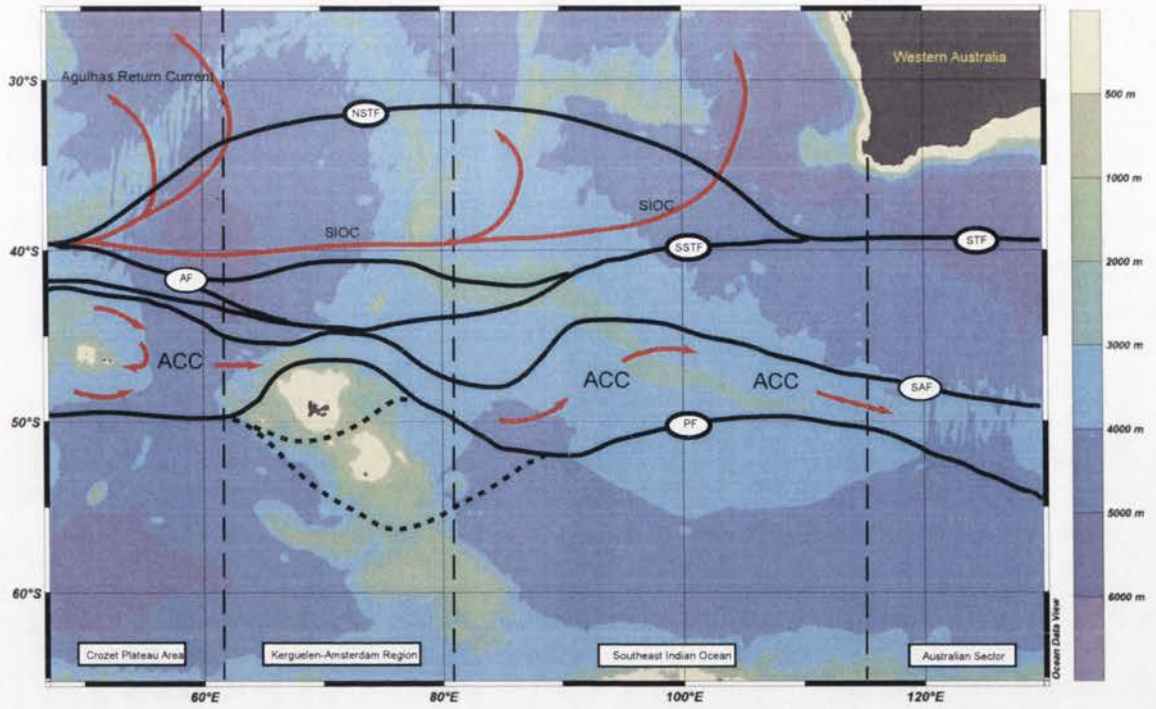

Figure 4.2: The southern Indian Ocean showing the fronts, the surface currents, and Belkin and Gordon's (1996) meridional divisions [Crozet Plateau Area, etc]. Fronts plotted using Belkin and Gordon (1996) data: NSTF - Northern Subtropical; SSTF - Southern Subtropical; STF - Subtropical; AF - Agulhas; SAF - Subantarctic; PF - Polar (Park et al., 1993; Gille, 1994; Belkin and Gordon, 1996, Tomczak and Godfrey, 2003; Pollard et al., 2007). Currents (drawn): Agulhas Return Current; SIOC - South Indian Ocean Current; ACC - Antarctic Circumpolar Current (Stramma, 1991; Rintoul et al., 2001).

The southern Indian Ocean sub-surface currents

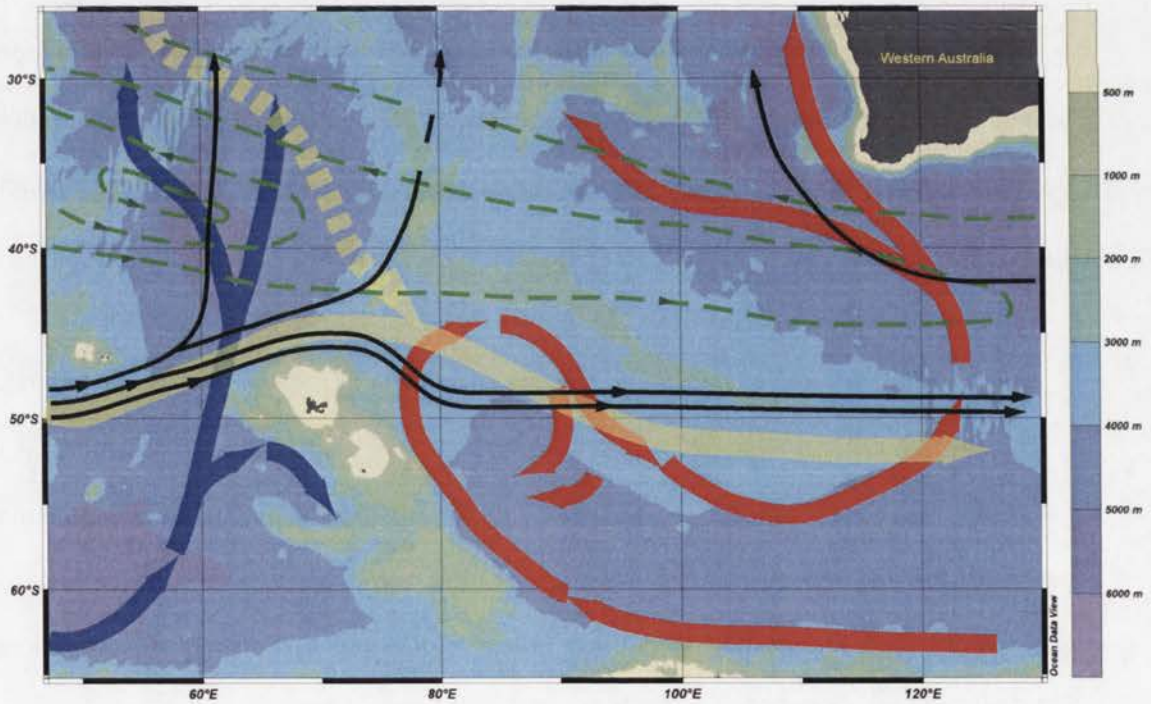

Figure 4.3: The southern Indian Ocean showing the Subantarctic Mode Water (SAMW - black line) (McCartney, 1979), the Southern Hemisphere Supergyre (green dashes), the Circumpolar Deep Water (CDW - yellow), the North Indian Deep Water (NIDW - yellow dashes), and the Antarctic Bottom Water (AABW) with the Weddell Sea-sourced AABW in blue and that from the Ross Sea and Adélie Coast in red (Kolla *et al.*, 1976, Corliss, 1979; Fine, 1992; Park *et al.*, 1993, Toole and Warren, 1993; Rintoul *et al.*, 2001; Ridgeway and Dunn, 2007; Aoki *et al.*, 2008).

At around 115°, the boundary between the Southeast Indian Ocean and Australian Sectors, the NSTF and the SSTF merge, reducing the system to one of three fronts, the STF, the SAF, and the PF, all trending southwards and with a conspicuous layer of Subantarctic Mode Water between the STF and the SAF (Belkin and Gordon, 1996).

4.1.2. Surface currents

The SIO (Figure 4.2) has, in essence, only one surface current, the Antarctic Circumpolar Current (ACC), and, because the permanent thermocline reaches the surface at the Subtropical Convergence, the ACC is not restricted to the first few hundred metres of water depth but extends deeply enough to be affected significantly by the topography of the ocean floor (Tomczak and Godfrey, 2003; Barker and Thomas, 2004).

The ACC is a mainly wind-driven current generated by the belt of westerlies at 45-55°S (Barker and Thomas, 2004) and it is estimated that 40-70% or more of its transport is carried by the SAF and the PF as two narrow Gaussian jets (Gille, 1994; Craneguy and Park, 1999; Barker and Thomas, 2004). The STF is not continuous due to intervening continents, so does not contribute to the ACC's transport. However, Orsi *et al.* (1995) identify the "southern ACC front", south of the PF , as a third element in ACC transport.

In the SIO, the ACC has no geographically constraints like the Drake Passage to hinder its eastward flow, so topographical effects are the major cause of eddies and of deviations in the fronts' east-west alignment. Bathymetric features less than 2000-2500 metres deep may cause two or more fronts to merge or a single front to split, with the process being reversed west of the obstruction (Craneguy and Park, 1999; Pollard and Read, 2001; Durgadoo *et al.*, 2008). Over the obstruction the waters may be relatively stagnant, or eddying may even reverse the current direction (Pollard and Read, 2001; Durgadoo *et al.*, 2008). In deeper

waters, where the ACC may not extend to the ocean floor, the fronts are relatively free to meander (Belkin and Gordon, 1996; Moore, J.K. *et al.*, 1999).

It is important to this study to recognise that the strength of the frontal jets and the fact that the currents usually extend to the ocean bed would tend either to prevent sedimentation and/or cause substantial reworking of bottom sediments along the lines of the fronts. It is also important that the westerly winds which drive the ACC may have migrated meridionally over geological time, perhaps moving north during glacials and south again during interglacials. This migration is likely to have caused a corresponding shift in the location of the fronts with the concomitant disruption in fossil deposition as the front passes (cf. Bareille *et al.*, 1994; Dezileau *et al.*, 2000).

Although outside the area of Tomczak and Godfrey's (2003) Southern Ocean, relevant to this study is another surface current, the South Indian Ocean Current (SIOC), found by Stramma (1991) to flow at around 40°S just north of the STF from 30°E to 90°E before turning northeast at 95°E, then north at 110°E to close the south Indian Ocean subtropical gyre (Stramma, 1991).

4.1.3. Mode and Intermediate Waters

"Mode water" is a term applied to a thick isopycnal layer which is vertically as well as horizontally homogeneous in a range of water properties such as temperature, salinity, and oxygen. Mode water is formed by convective mixing down to 500 metres in winter followed by the isolation of the thermostad by the spring warming of surface waters. Formation is on the less dense (and, thus, warmer) side of a front; thereafter the layer extends by advection much beyond its source (McCartney, 1977; Hanawa and Talley, 2001).

McCartney (1977) identifies the Subantarctic Mode Water (SAMW) north of the SAF, i.e. in the Subantarctic Zone (SAZ). Three western boundary currents, the East Cape Current (east of New Zealand), the East Australian Current, and the Agulhas Current, feed the SAZ with warm water. In the SAZ these waters are cooled, freshened, and vertically homogenised, and finally advect into the subtropical gyres, their original sources (McCartney, 1982). In the southeastern Indian Ocean the SAMW is at its deepest and most homogeneous, with a temperature of approximately 14.5°C and a salinity greater than 35 psu. (McCartney, 1977). (Figure 4.3). A further body of mode water, the Subtropical Mode Water (STMW), is formed in the area bounded by the NSTF and the SSTF (33°-45°S, 60°-90°E –Figure 4.3) (McCartney, 1982; Belkin and Gordon, 1996). The STMW is also advected into the SIOC.

The structure and location of the SAMW is significant in relation to the present study because many species of radiolaria live at depths below the immediate surface layers (Kling, 1975, 1979; Dworetzky and Morley, 1987; Kling and Boltovskoy, 1995; Abelmann and Gowing, 1996; Yamashita *et al.*, 2002; Itaki, 2003; Itaki *et al.*, 2003; Okazaki *et al.*, 2004; Takahashi, K. and Yamashita, 2004; Lazarus *et al.*, 2006). Radiolaria are, therefore, likely to act as proxies for water properties at these depths as well as the surface layers, the latter being the source of much of their food (Casey, 1993).

Less important to this study is the Antarctic Intermediate Water (AAIW) which is found below the SAMW. The AAIW starts at a depth of 500 metres at the SAF and sinks to 1000-1200 metres north of the STF. It is identified by its low salinity and high oxygenation, and its main flow is eastwards parallel to the SAF but with some northward transport west of 65°E (Fine, 1993; McCarthy and Talley, 1999; Rintoul *et al.*, 2001).

4.1.4. The Southern Hemisphere Supergyre

North of the ACC and at a depth of 400 to 2000 metres, the Southern Hemisphere Supergyre (SHSG – Figure 4.3) connects the South Pacific gyre and the Southern Indian Ocean gyre (Ridgway and Condie, 2004; Ridgway and Dunn, 2007; Roemmich, 2007). Above 400 metres the South Pacific gyre flows north of Australia, contributing to the Indonesian Throughflow. Below that level, part of the South Pacific gyre flows south of Australia. That part splits, some joining the Western Australian Current (also known as Leeuwin Undercurrent) which flows north under the Leeuwin Current and the rest continuing west under the WAC to join the westward leg of the Southern Indian Ocean Current (Ridgway and Condie, 2004; Ridgway and Dunn, 2007; Roemmich, 2007)

4.1.5. Deep and Bottom Waters

The largest water mass in the Southern Ocean is the Circumpolar Deep Water (CDW – Figure 4.3) which is approximately 2000 metres thick. The top of the Upper CDW is marked by an oxygen minimum and that of the Lower CDW by a salinity maximum reflecting the North Atlantic Deep Water's major contribution to the CDW. The water mass's flow is broadly eastward (Fine, 1993; McCarthy and Talley, 1999; Rintoul *et al.*, 2001). The North Indian Deep Water (NIDW – Figure 4.3), which flows from the western Mascarene Basin, spreads south of Amsterdam in the western Crozet Basin (Park *et al.*, 1993), appears to be the only southward-flowing current in the vicinity of SIO cores investigated during this study.

The Antarctic Bottom Water (AABW – Figure 4.3) lies below the CDW and, in contrast to the CDW, is mainly northward-flowing. AABW is formed in the Weddell Sea, moves eastwards into the Atlantic-Indian Basin, generates a gyre west of the Kerguelen Plateau, and then moves north in two parts. One part passes through the Agulhas Basin to enter the Mozambique Basin and the second enters the Crozet Basin and on to the Central Indian Basin

(Kolla *et al.*, 1976; Toole and Warren, 1993). AABW formed in the Ross Sea and along the Adélie Coast flows west at about 70°S before turning north parallel to the Kerguelen Plateau. It swings east along the southern edge of the eastern arm of the Mid Indian Ridge, where it generates a gyre east of the Kerguelen Plateau, before crossing the Ridge at about 120°E and entering the South Australian Basin, finally reaching the Wharton Basin (Kolla *et al.*, 1976; Corliss, 1979).

4.2. The eastern Indian Ocean

The oceanography of the eastern Indian Ocean is complex and still the subject of much investigation. However, it is broadly evident that (within this study's area of interest – 5°-35°S and 105°-135°E), north of about 20°S conditions in the top 500m of the ocean are dominated by the Indonesian Throughflow (ITF) and the South Java Current (SJC), whereas south of 20°S the major influences are the Eastern Gyral (EGC), the Leeuwin (LC), the Western Australian (WAC) , and the South Indian Ocean (SIOC) Currents (Figure 4.4).

In the equatorial Pacific, the southeasterly Trade Winds drive water westward towards the Indonesian Archipelago. The resultant large-scale pressure gradient between the Pacific and Indian Oceans causes the "Indonesian Throughflow" of waters from the Pacific into the Sulawesi, Flores, Banda, and Arafura Seas and onward into the Indian Ocean between northwest Australia and Indonesia (Wijffels *et al.*, 1996; Tomczak and Godfrey, 2003). The Throughflow then becomes a tributary to the South Equatorial Current (SEC) which flows west in a broad band between 7°S and 15°S (Quadfasel *et al.*, 1996), and to the LC which flows south along the coast of Western Australia (Fieux *et al.*, 1994).

The westward component of the ITF close to the surface (where the majority of radiolarian species dwell - Petrushevskaya, 1967; Kling and Boltovskoy, 1995; Boltovskoy, 1998) is seasonally constrained by the SJC. The SJC, as defined by Meyers et al. (1995), is an eastward-flowing water mass which passes south of Sumatra and Java, driven in part by the Equatorial Counter-current (ECC) and in part by windstress along the Sumatran and Javan coastlines. In February, the ECC is at its most southerly due to the Monsoon and the SJC-maximum that results partially counteracts the ITF, causing a minimum in the ITF. In August, the ECC migrates north, relieving the pressure and allowing the Throughflow to push west and south again (Meyers *et al.*, 1995; Tomczak and Godfrey, 2003). Thus, the SJC is only active from April-May until June-July and in October-November, some authors (Quadfasel and Cresswell, 1992; Tomczak and Godfrey, 2003) treating it as a semi-annually reversing current. At greater depths, the SJC does not exist and the ITF is constantly westward because it is the outfall of the net flow across the Pacific from Chile to Australia (Tomczak and Godfrey, 2003).

The ITF is, itself, strongly seasonal: the northeast Monsoon creates a minimum in the Throughflow in April and the southeast Monsoon a maximum in September. Further, the November transition between the monsoons coincides with the semi-annual cessation of the SJC (Wijffels *et al.*, 1996). In the austral summer (December to March), winds are mainly westerly and the currents weak as a result. The current may even reverse and some upwelling occur when the winds are at their strongest. In the austral winter (May to August), southeast winds contribute to the southwestward strength of the Throughflow (Pearce and Cresswell, 1985). On an inter-annual scale, the pressure gradient which drives the Throughflow is significantly affected by ENSO events, being distinctly stronger than average in La Niña, and weaker in El Niño, years (Pearce and Phillips, 1988; Feng *et al.*, 2003). The interannual effects are still being investigated (Vranes and Gordon, 2005).

The eastern Indian Ocean currents

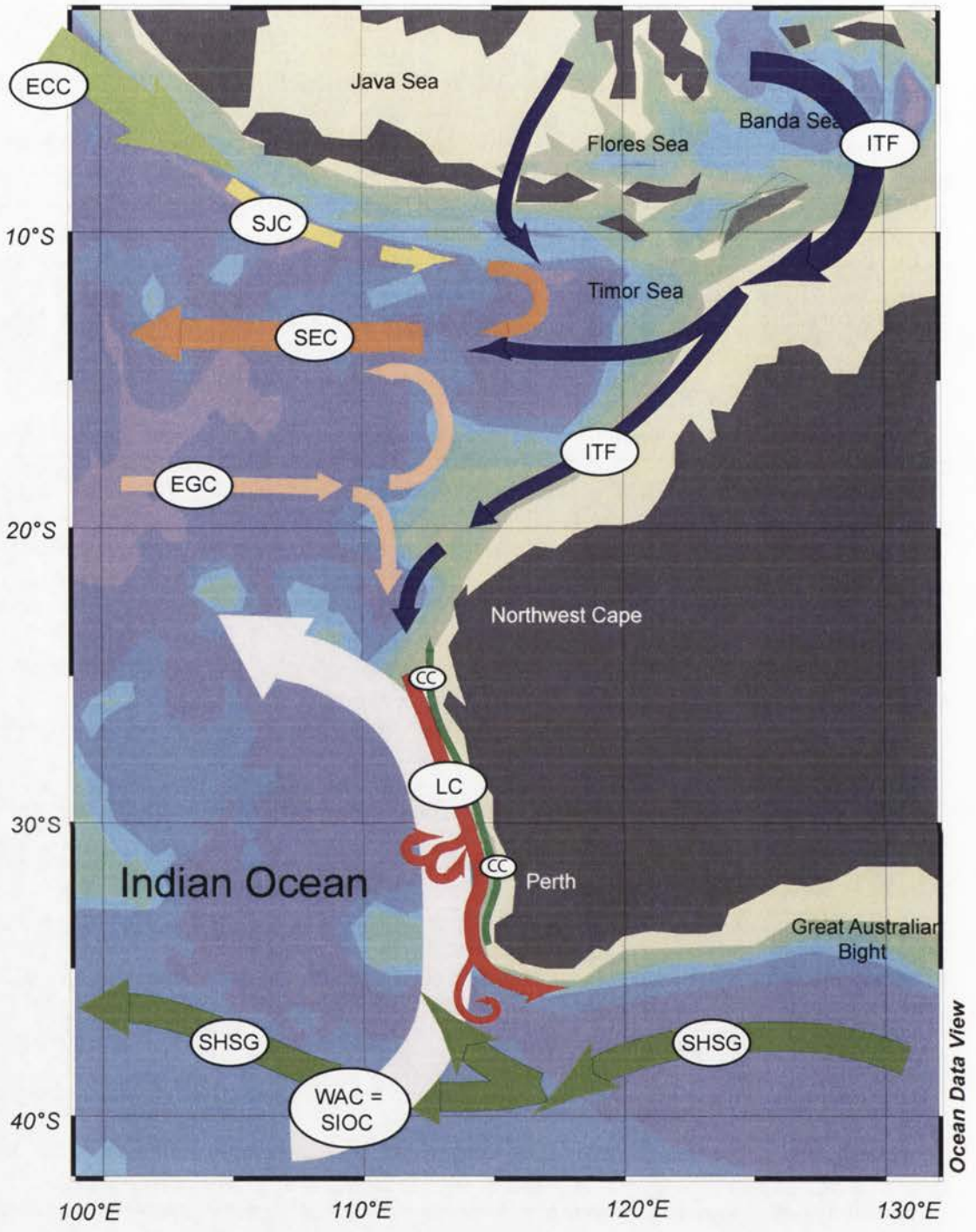

Figure 4.4: The currents of the eastern Indian Ocean.
ITF - Indonesian Throughflow; ECC - Equatorial Counter-current; SJC - South Javan (seasonal); SEC - South Equatorial Current; EGC - Equatorial Gyral Current; LC - Leeuwin Current; CC - the Cape and other coastal currents; WAC - Western Australian Current - also called the South Indian Ocean Current (SIOC) and the Leeuwin Undercurrent; SHSG -Southern Hemisphere Super Gyre.

Because of their origins in low-latitude waters with high precipitation, both the SJC and the ITF are warm and low in salinity and, hence, of low density. Fieux *et al.* (1994) report upwelling of high-salinity, low-oxygen water close to the coast of Bali – the Java Upwelling System – a phenomenon active at the northwest extremity of the study area.

Between 10° and 15°S, part of the ITF combines with the northward-flowing portion of the Eastern Gyral Current (EGC) and the SJC (when extant) to form the SEC (Quadfasel *et al.*, 1996). The remainder of the ITF passes southwest to meet the southwest-flowing component of the EGC to form the Leeuwin Current (LC). There is a sharp rise in the salinity of the waters (at least to 200m depth) as the EGC and the ITF merge (Quadfasel *et al.*, 1996; WOA05, 2005) but the LC is still a relatively warm, fresh, watermass (Cresswell and Golding, 1980; Thompson, 1983).

The Leeuwin Current (Figure 4.4) is a belt of water which flows close (30-100km) to the west Australian coast from North-West Cape to Cape Leeuwin before turning east and on towards the Great Australian Bight (Pearce and Cresswell, 1985). It is separated from the coast by seasonally-reversing coastal currents (Pearce and Pattiaratchi, 1999; Taylor and Pearce, 1999). The LC is shallow [never more than 250m deep, and usually much less (Pearce and Cresswell, 1985; Smith *et al.*, 1991)] and narrow [around 50km wide (Pearce and Cresswell, 1985)], its width and course variable, and there are eddies which are large relative to the current itself, particularly along its western (seaward) edge where it is bounded by the West Australian Current (WAC) (Pearce, 1991). Although it flows all year round (1995), the LC's strength varies with the seasons (Cresswell, 1991; Pearce, 1991; Smith *et al.*, 1991), and with the El Niño-Southern Oscillation (Pearce and Phillips, 1988; Feng *et al.*, 2003).

Temperature

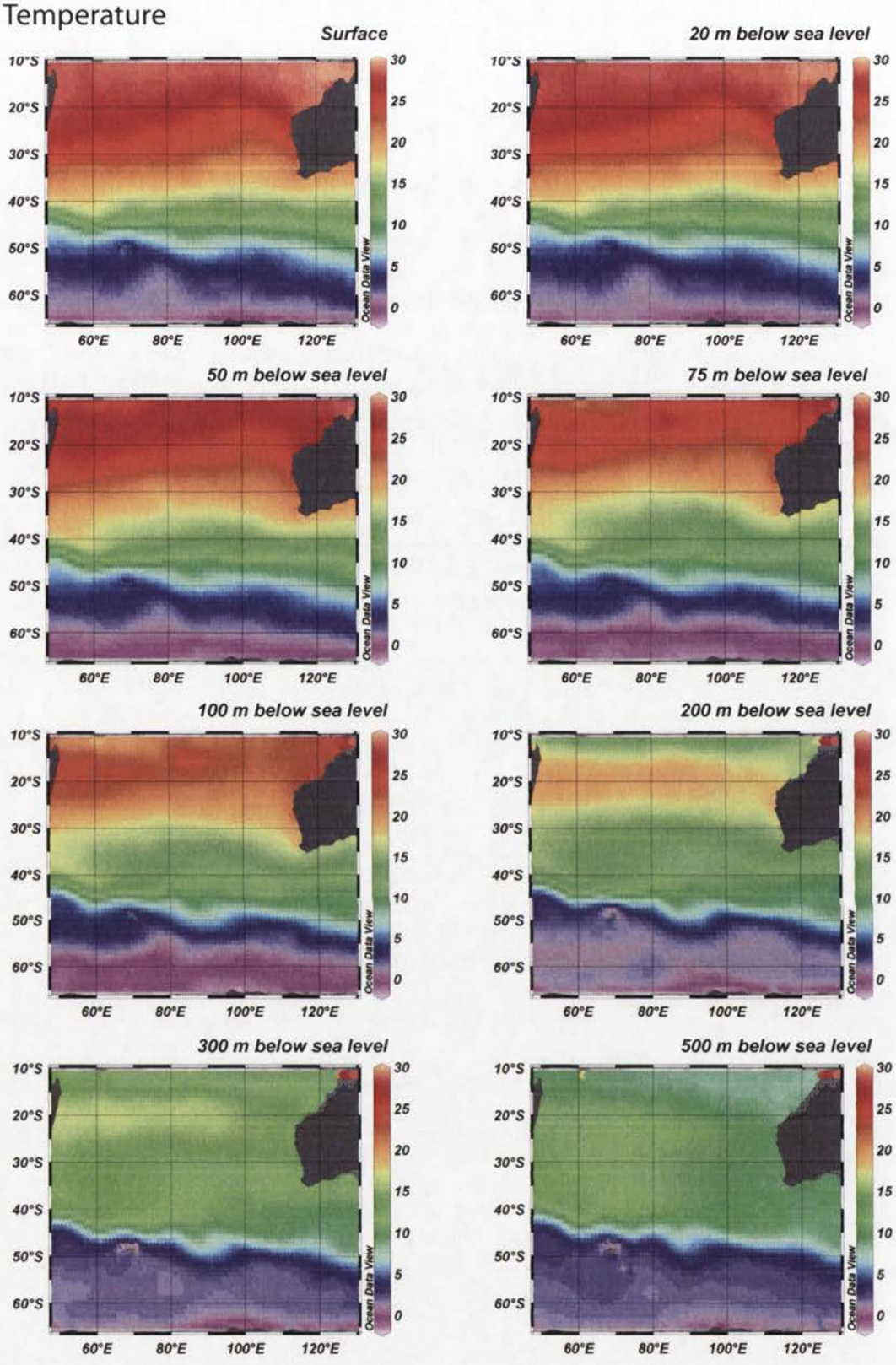

Figure 4.5a: Sea temperature at a succession of depths for the austral summer (JFM). The temperature increases from south to north at all depths except 200 metres below sea level where the maximum is at approximately 20°S. At all levels there is a particularly sharp change at the Antarctic Convergence (~50°S) and a less severe change at the Subtropical Convergence (~40°S at the surface but further north at greater depths, reflecting the advection of the Subantarctic Mode Water).

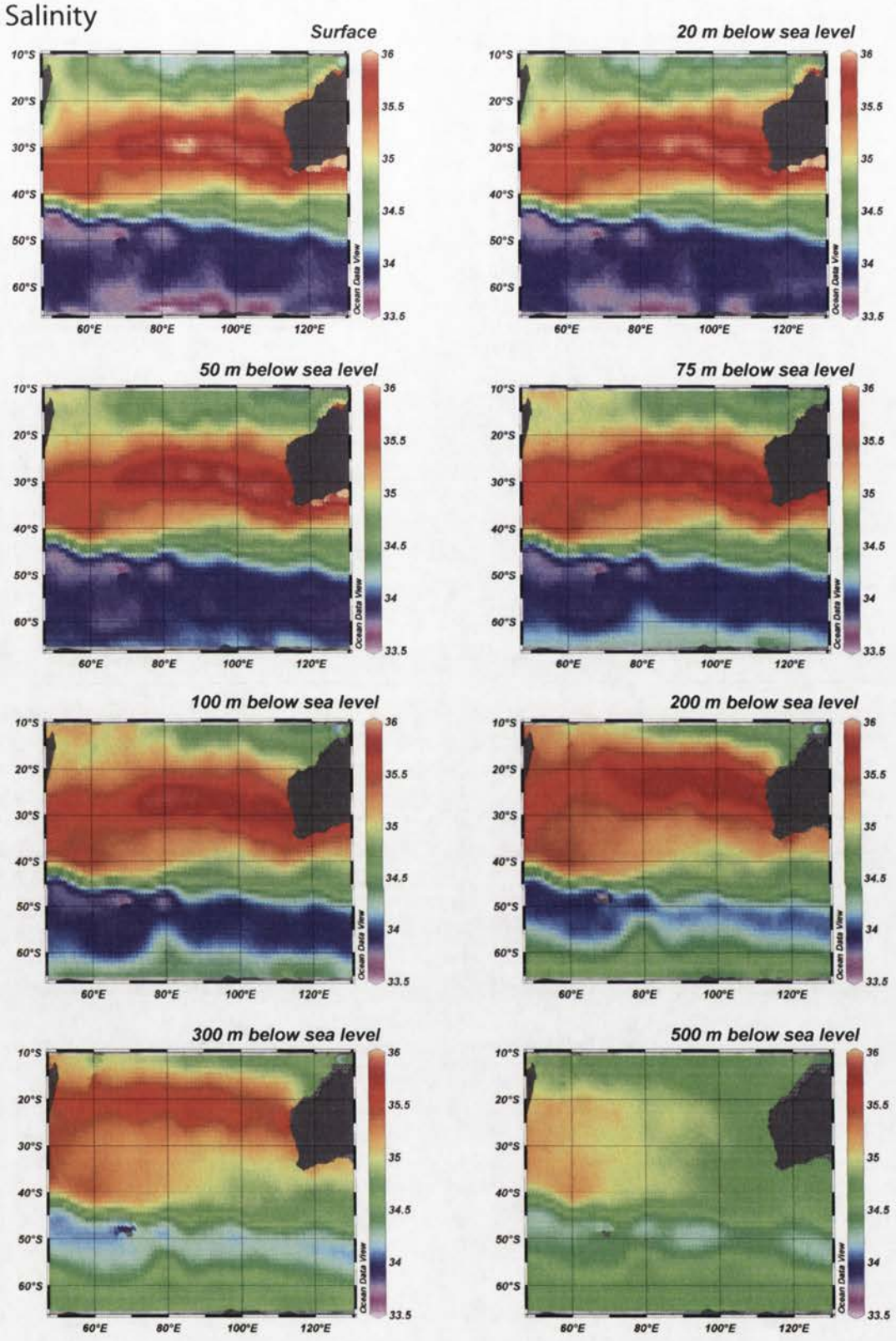

Figure 4.5b: Austral summer (JFM) ocean salinity [psu] at a succession of depths. From south to north the salinity increases to a maximum at approximately 30°S at all depths to 300 m. before decreasing again further north. The absence of this maximum at 500 m. in the eastern Indian Ocean reflects the transport of low-salinity Antarctic Intermediate Water into the Southern Indian Ocean gyre. There are sharp salinity increases at the surface at the Antarctic Convergence and at the Subtropical Convergence (~40°S). Both increases are less acute at greater depth.

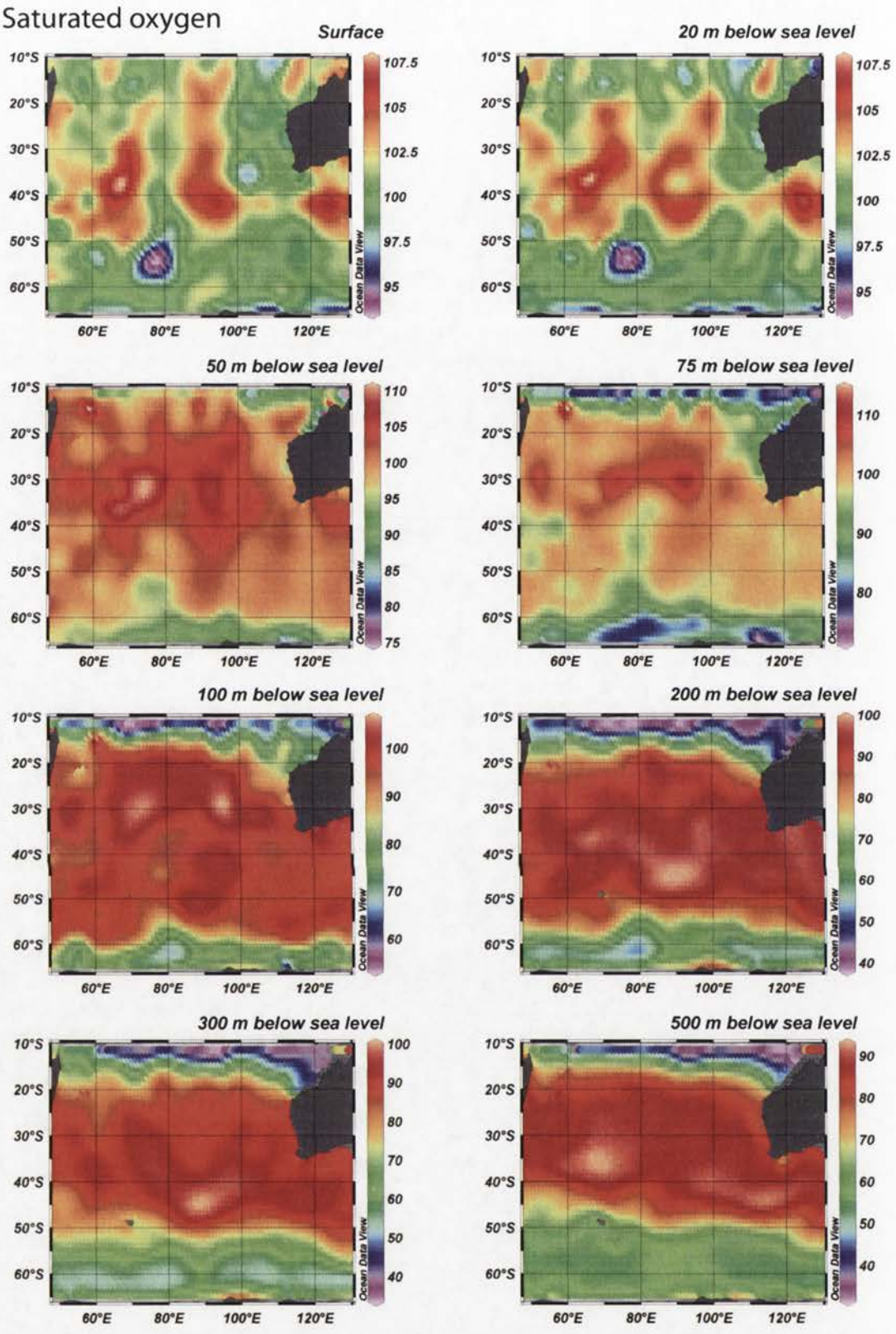

Figure 4.5c: Saturated oxygen [µmol/l] at a succession of depths for the austral summer (JFM). There are sharp increases associated with the Antarctic Convergence and at about 10-20°S at all levels.
Note: concentration scales vary with depth to accommodate the ranges.

Dissolved oxygen

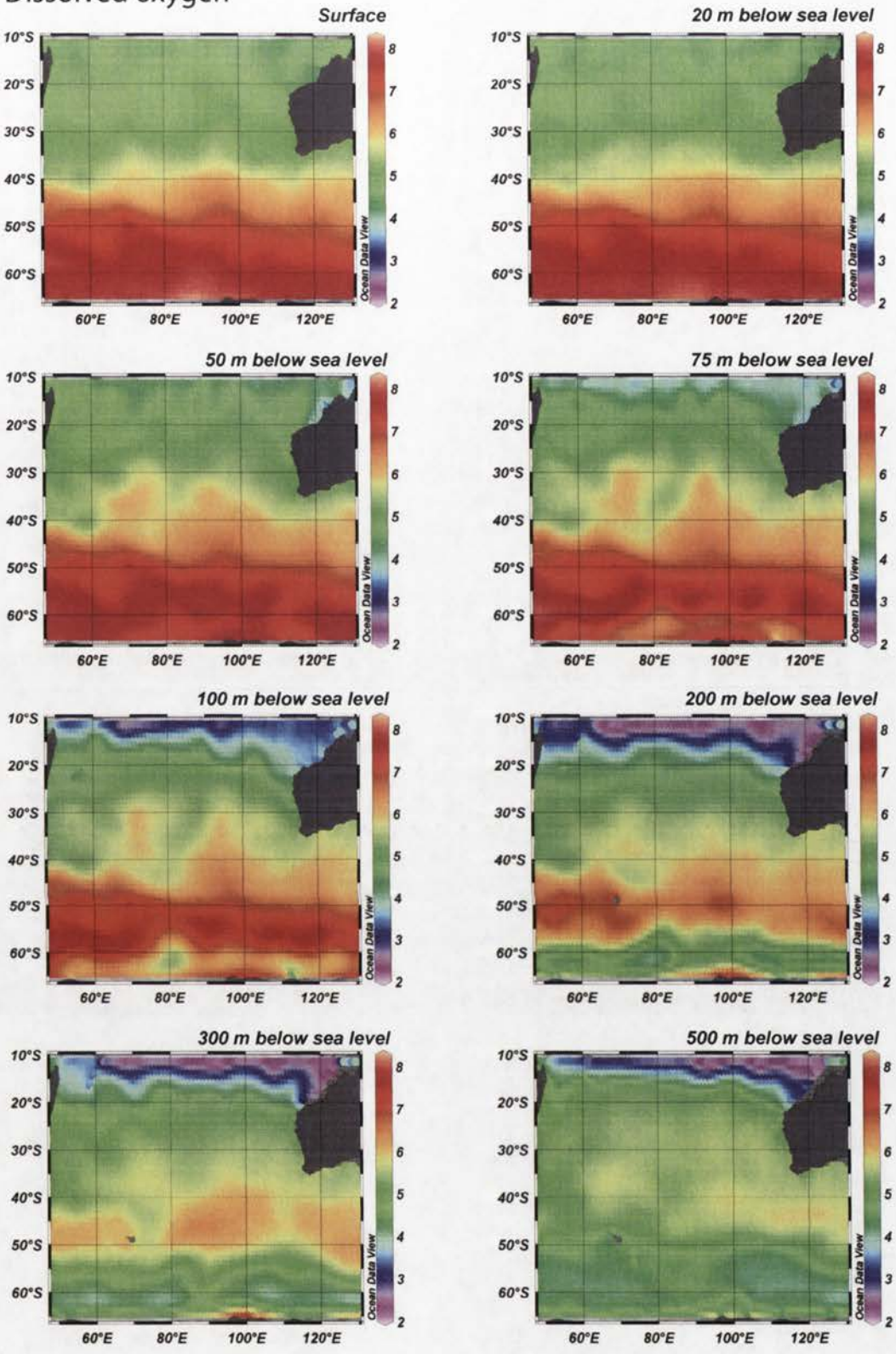

Figure 4.5d: Dissolved oxygen concentrations [µmol/l] at a succession of depths for the austral summer (JFM). The relatively high concentrations in the high latitudes decrease sharply in the Subantarctic Zone and at about 10-15°S at all levels.

Nitrate Concentrations

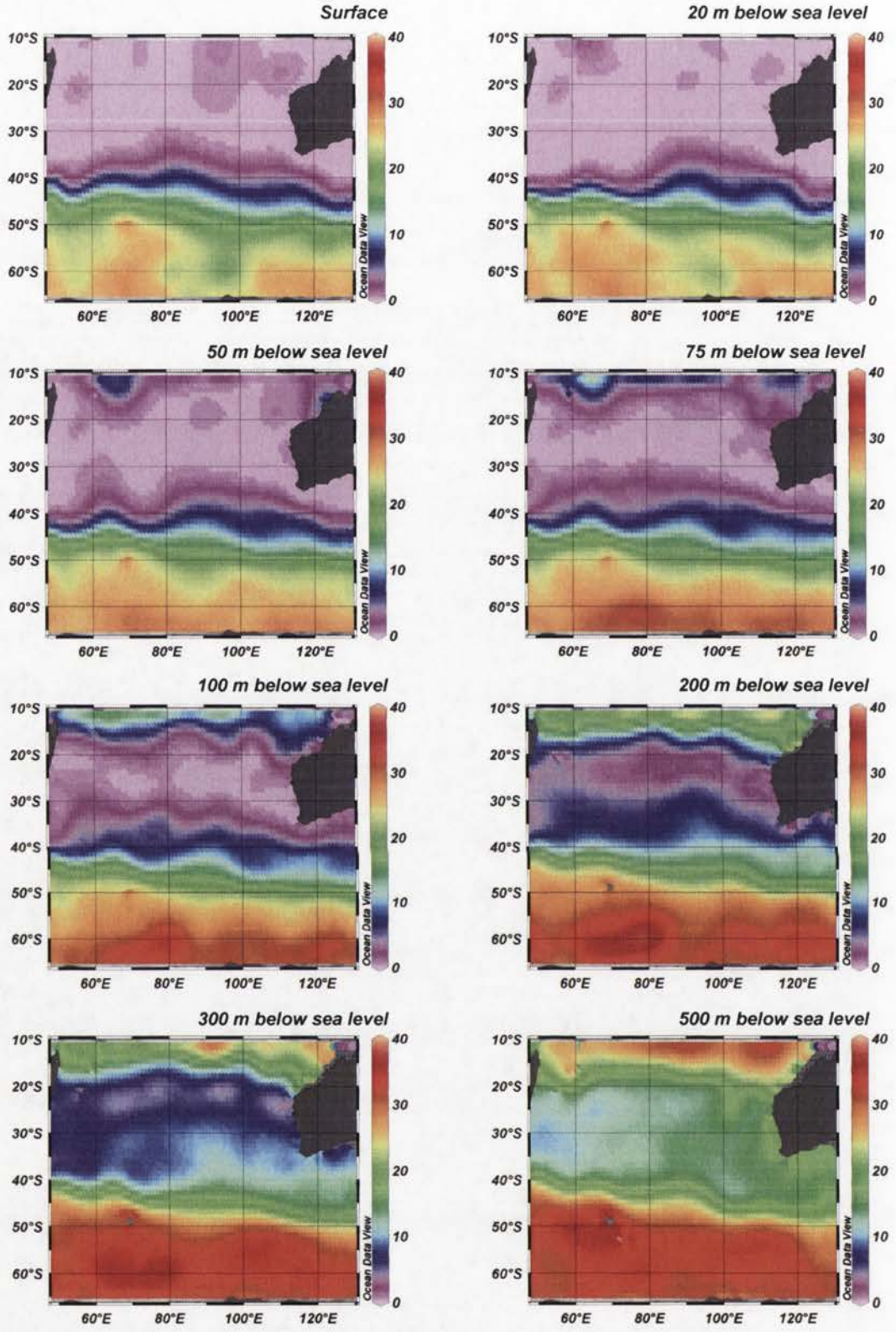

Figure 4.5e: Nitrate concentrations [µmol/l] at a succession of depths for the austral summer (JFM). The relatively high concentrations in the high latitudes decrease sharply in the Subantarctic Zone and at about 10-15°S at all levels to give a minimum centred on 25°S.

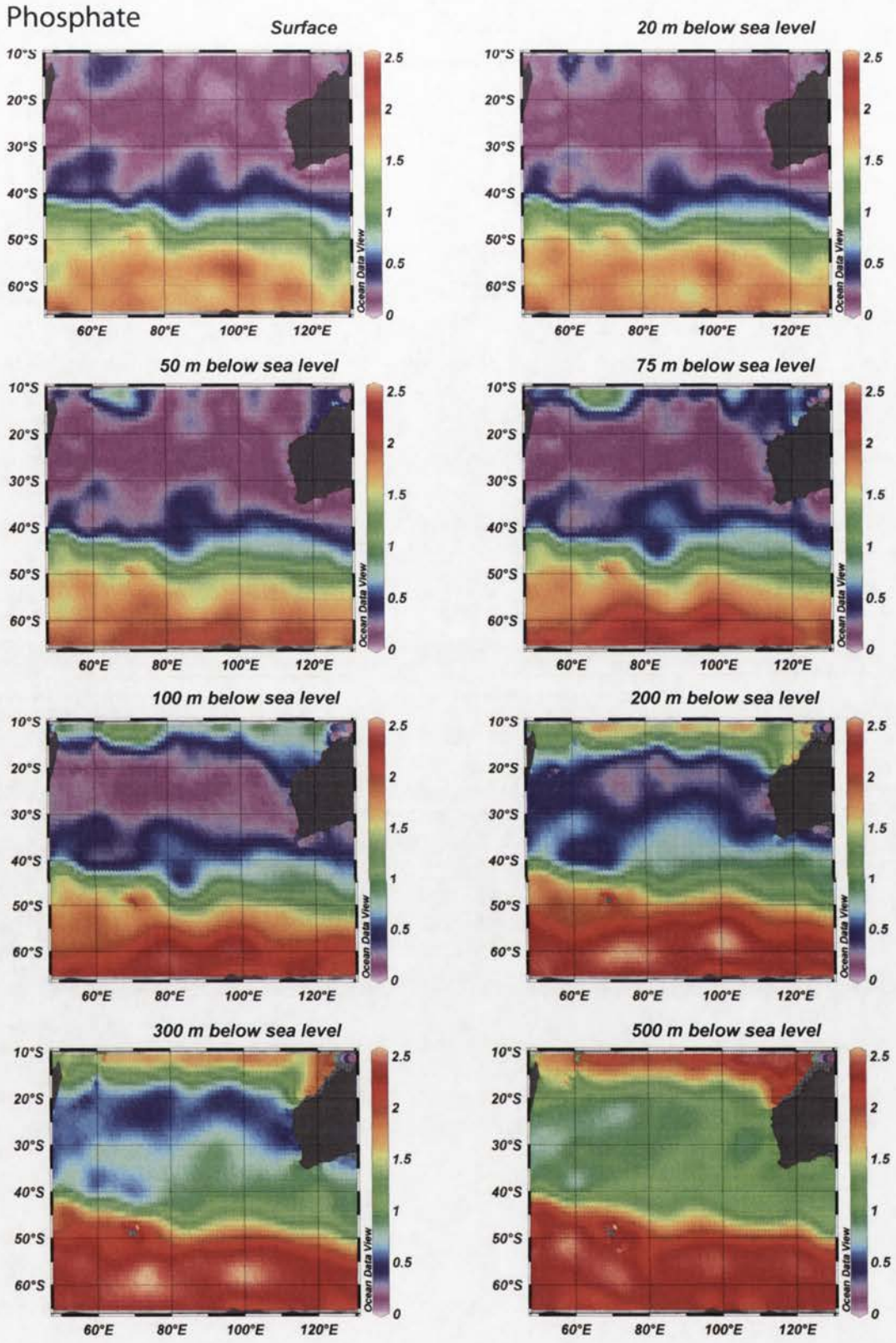

Figure 4.5f: Phosphate concentrations [µmol/l] for a succession of depths for the austral summer (JFM). The relatively high concentrations in the high latitudes decrease sharply in the Subantarctic Zone and at about 10-15°S at all levels to give a minimum centred on 25°S.

Silicate

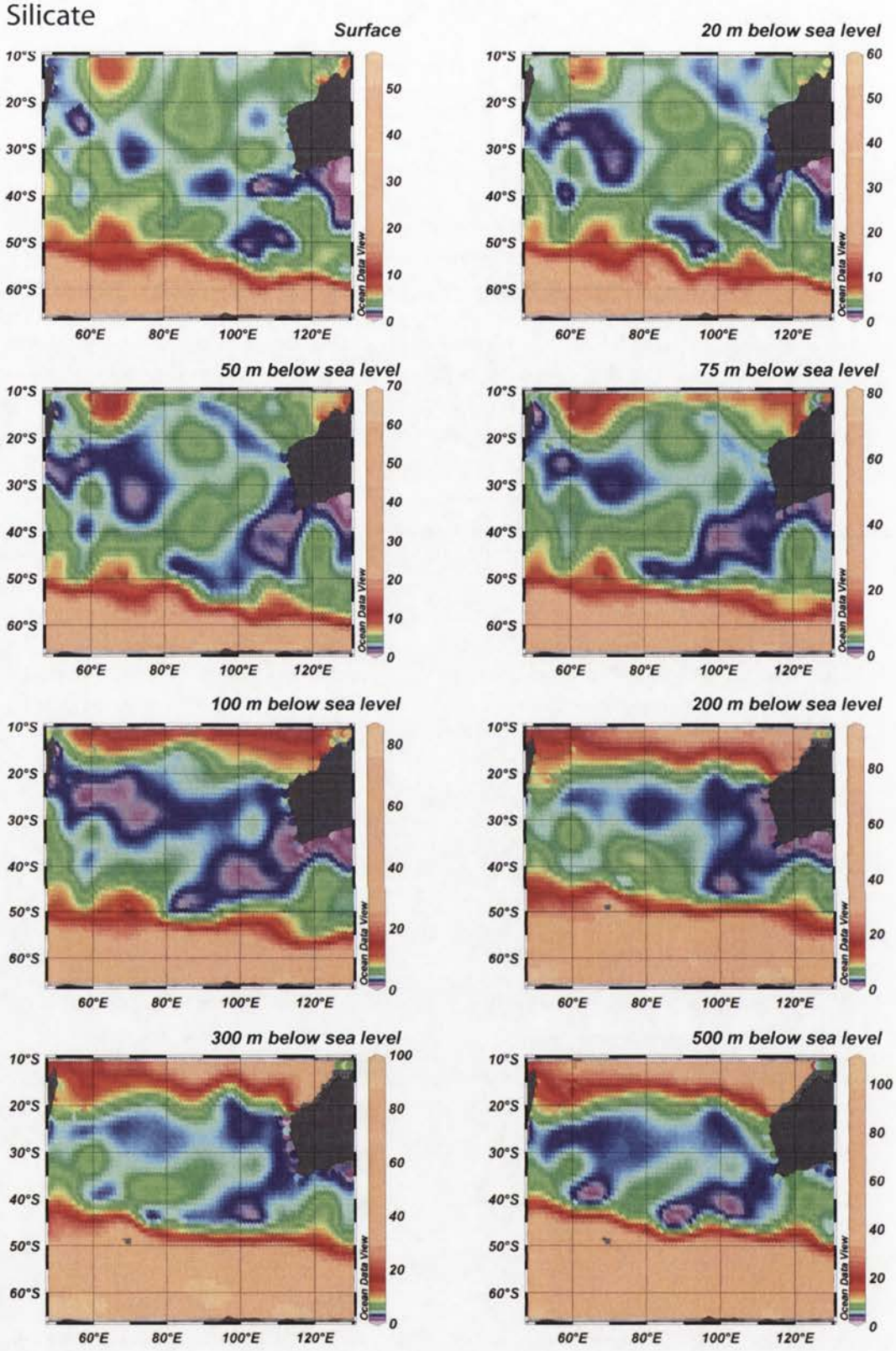

Figure 4.5g: Silicate concentration [µmol/l] at a succession of depths for the austral summer (JFM). Just south of the Polar Front (PF) there is a sudden change in the silicate concentration, values changing from greater than 6 µmol/l to less than 4.5 µmol/l. The change moves north with increasing depth, reflecting the gradient of the PF. A similar change is seen at 10-20°S.
Note: the silicate concentration scales vary with depth to accommodate the ranges.

The West Australian Current [as Pearce (1991), not Andrews' (1977), uses the name] constitutes the northward leg of the South Indian Ocean gyre in the eastern Indian Ocean and is part of the current Stramma (1991) calls the South Indian Ocean Current (SIOC – see Figure 4.2and 4.4). It has been recently discovered that the SIOC is part of a Southern Hemisphere Supergyre and that an element of the South Pacific gyre which flows just south of Australia contributes to the SIOC (Ridgway and Condie, 2004; Ridgway and Dunn, 2007). By analogy with the eastern boundary currents off the west coasts of South America and southern Africa, the WAC, as an equatorward-flowing surface current, should cause upwelling along the Western Australian coast. However, because the WAC is cold and saline, it flows under the fresh, warm, LC to form the Leeuwin Undercurrent (LUC), extending northward to beyond 20°S (Thompson, 1983; Smith *et al.*, 1991). As a surface current, the WAC is evident beyond the western limits of the LC (Pearce, 1991).

4.3. The SIO's physico-chemical properties

The (US) National Oceanographic and Atmospheric Agency (NOAA) publishes objectively analysed data for nine oceanographic variables at the International Association of Physical Oceanography standard set of depths below sea-level (dbsl). These variables are temperature, salinity, chlorophyll, dissolved oxygen, apparent oxygen utilisation (AOU), oxygen saturation, and nitrate, phosphate, and silicate concentrations. Seven of the data are interpolations of direct measurements: AOU and oxygen saturation are statistically derived. For some variables, the set of depths is limited to the upper 500 metres of the ocean or less.

Figure 4.5a shows temperatures derived from NOAA data (Locarnini *et al.*, 2006) down to 500 metres. From 65°S to 10°S temperature down to about 100 metres below sea level increases monotonically. Between 100 and 400 metres there is a temperature maximum centred at around 20°S which is associated with the Equatorial Gyral Current (EGC)

(Tomczak and Godfrey, 2003). The increase, which is no more than about 1°C, is at its least in the eastern Indian Ocean and, thus, is unlikely to have a significant effect on the present study.

In the study area, the NOAA data for salinity (Antonov *et al.*, 2006) increases from a minimum associated with the AC and from the Equator to a strong maximum between 25°S and 35°S which, in the eastern Indian Ocean, extends to a depth of approximately 300 metres, and deeper in the west. The AC minimum results from the influx of fresh waters from Antarctica and the tropical maximum is due to the high evaporation and lack of precipitation (Figure 4.5b).

Except close to the surface where levels are continually replenished even to the point of supersaturation (Sarmiento and Gruber, 2006) (Figure 4. 5c), the level of dissolved oxygen is principally determined by biological activity: south of 36°S oxygen is taken up by the ocean; north of that it is out-gassed (Sarmiento and Gruber, 2006) (Figure 4.5d). In addition, oxygen solubility decreases with increasing temperature and salinity (Tchernia, 1980), and the levels decrease with the length of time the water has been isolated from the surface (Pickard and Emery, 1982). From the AC northwards, dissolved oxygen levels decline monotonically (Figure 4.5d).

The concentrations of nutrients, nitrate, phosphate, and silicate, fall sharply to the north of the SAF at all depths down to 500 metres; a similar decline is seen from 75 metres down between 10°S and 20°S (Figure 4.5e-g). The concentrations (Figure 4.6) are well below the levels set for Martin *et al's* (1994) high-nitrate, low-chlorophyll (HNLC) areas (nitrate>10.8±0.4 μmol/l, phosphate>0.92±0.02 μmol/l, and silicate>3.9 ±0.1 μmol/l). This lack of nutrients might be expected to constrain plankton growth severely. Unfortunately,

data on some of the ocean environmental variables which might be related to radiolarian distribution are either limited or no existent. For instance, only some very sparse measurements of pH and alkalinity are available from NOAA (Figure 4.7a-b) . Alkalinity, however, is a second order function of temperature and can be estimated at the surface of the ocean (Millero *et al.*, 1998). Iron, for which there are no comprehensive data, may be an important determinant in radiolarian development (Blain *et al.*, 2007; Moore, C., Hickman *et al.*, 2007; Moore, C., Seeyave *et al.*, 2007; Sedwick *et al.*, 2008). Lack of iron in Southern Ocean may account for low phosphate utilisation even in the presence of high nitrate, phosphate, and silicate concentrations (Martin *et al.*, 1994; Sarmiento and Gruber, 2006). Upwelling in the southern Indian Ocean is limited to areas such as the western boundaries of the Kerguelen Plateau and the Southeast Indian Ridge. Thus, aeolian dust is probably the major iron source in the SIO. Adjacency to the Australian continent means that dust deposition is substantial in the eastern Indian Ocean; deposition in the Southern Ocean is, however, very low (Gingele *et al.*, 2001; Erickson III *et al.*, 2003; Sarmiento and Gruber, 2006).

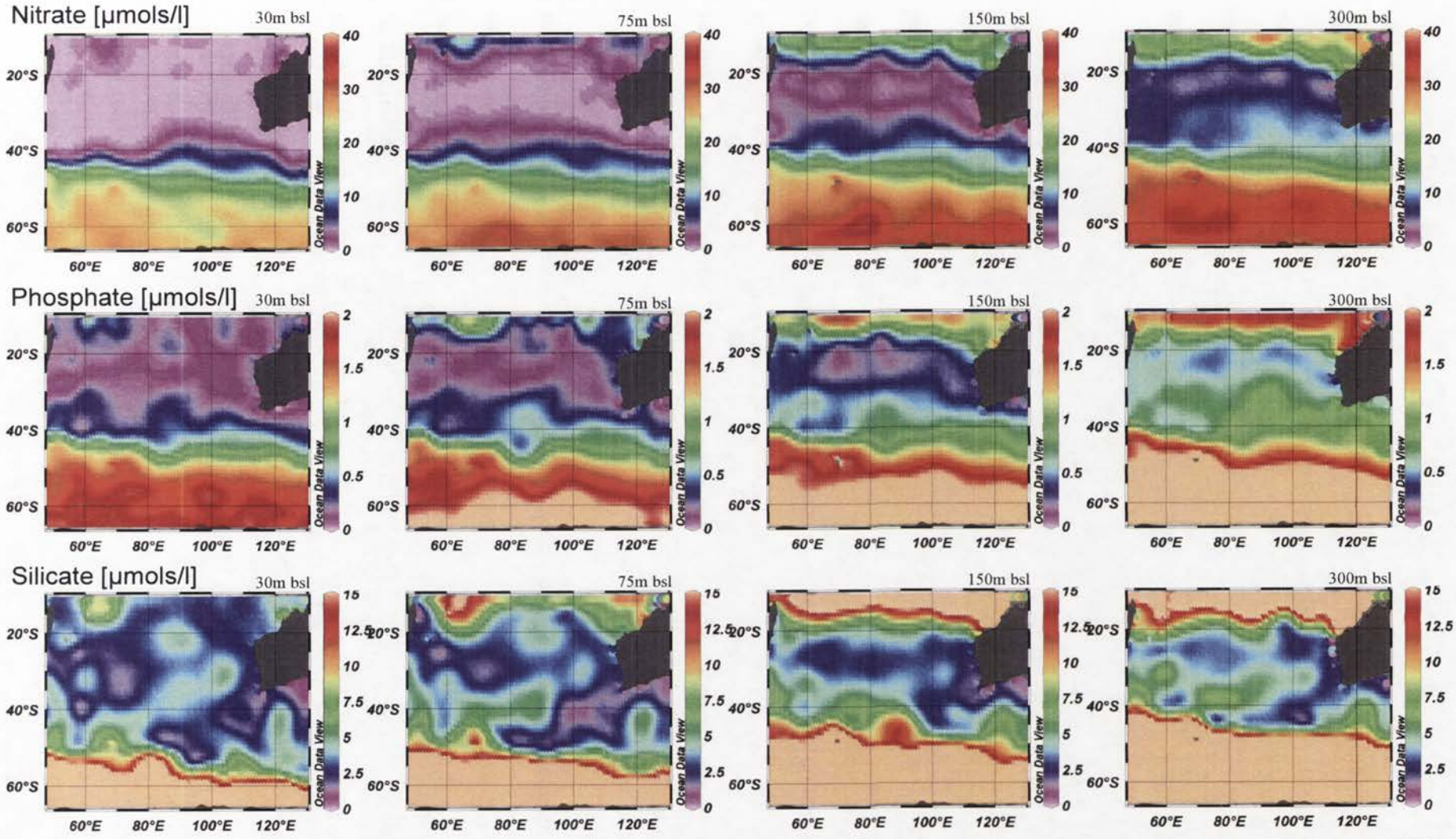

Figure 4.6: Nitrate, phosphate, and silicate concentrations at 30, 75, 150, and 300 metres below sea level (bsl) showing the Martin *et al's* (1994) areas deficient in nitrate (≤10.8±0.4 µmols/l), phosphate (≤0.92±0.02 µmols/l), and silicate (≤3.9±0.1 µmols/l) - mainly the dark blue and mauve areas - where phytoplankton growth might be nutrient constrained.

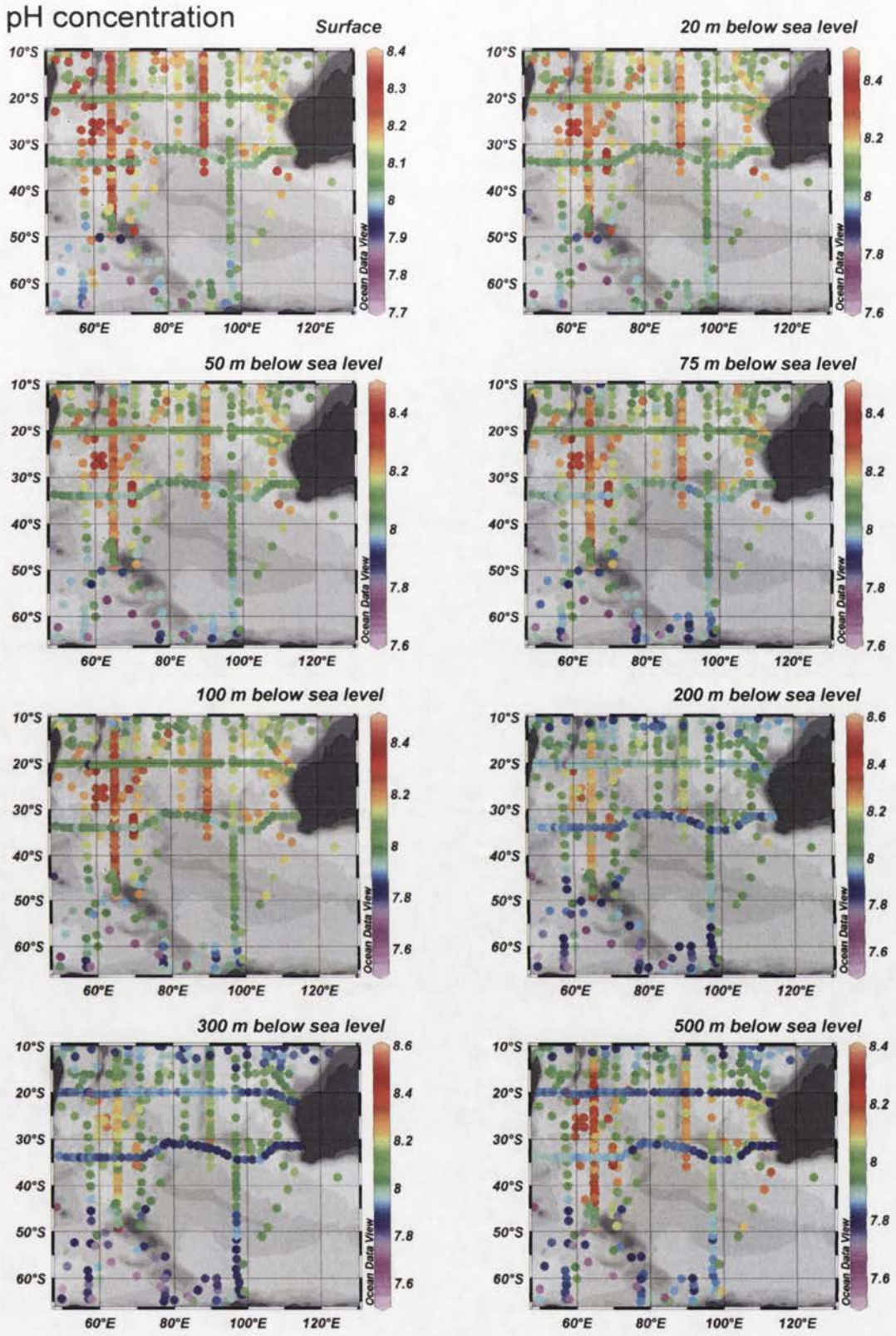

Figure 4.7a: pH for a succession of depths for the Austral Summer (JFM) showing the sparse nature of the records available in the World Ocean Database 2005.

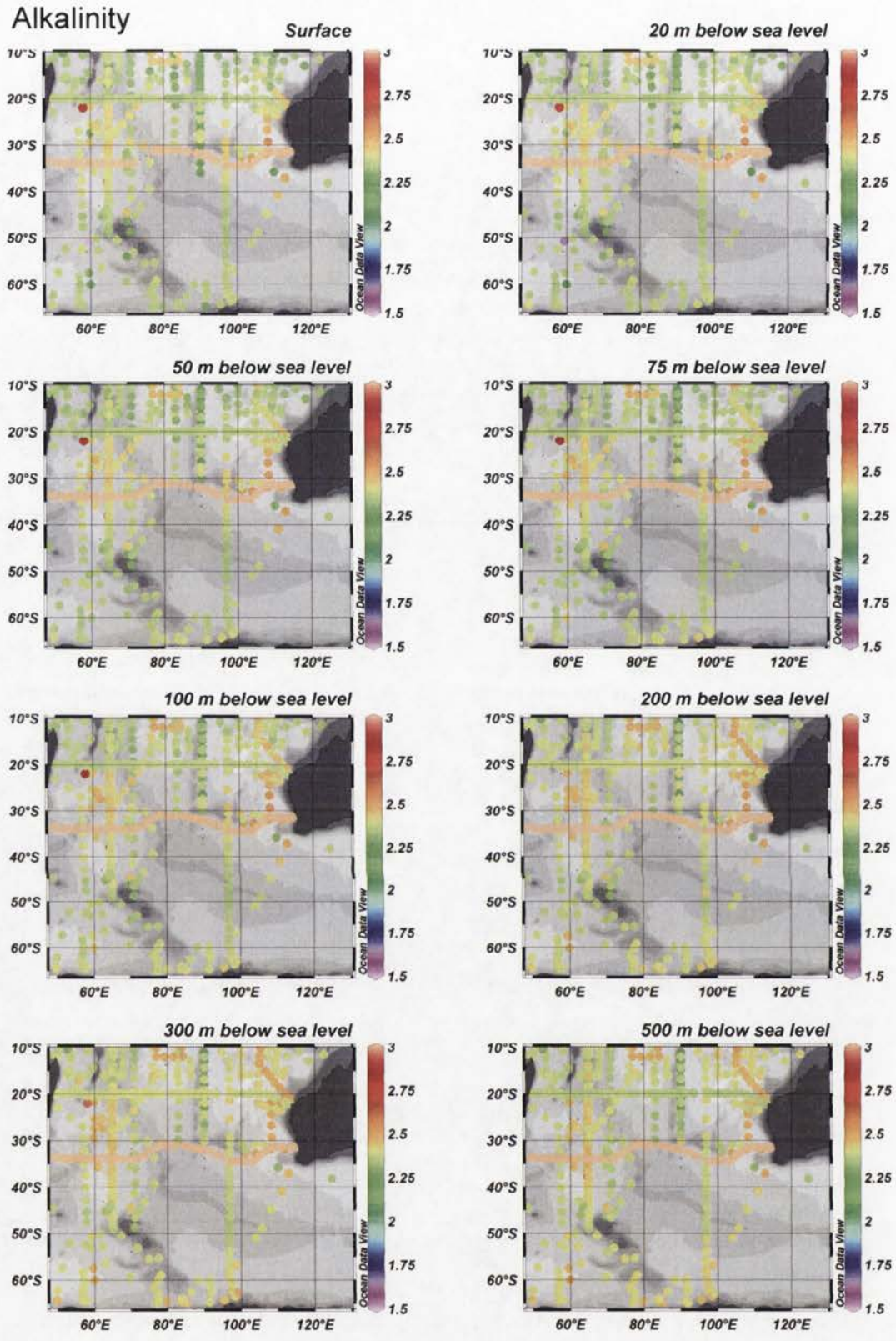

Figure 4.7b: Alkalinity [meq/l] for a succession of depths for the Austral Summer (JFM) showing the sparse nature of the records available in the World Ocean Database 2005.

Chapter 5: Materials and Methods

5.1. Radiolarian samples

The study has two parts. The first ("Part I") attempts to relate radiolarian census data in surface sediments to the modern environmental data for the sediment sources. In order to establish the utility of these results for palaeoenvironmental reconstruction, six Last Glacial Maximum (LGM) sea-surface temperatures (SSTs) from the eastern Indian Ocean (EIO) and three from the southern Indian Ocean (SIO) were reconstructed and compared with estimates made by Barrows and Juggins (2005), considered the most accurate to date. The second half of the study ("Part II") uses the results from the first to reconstruct aspects of the Quaternary palaeoenvironment from four southern Indian Ocean cores.

5.1.1. The surface sample database

The first half of the study is based on 100 core tops drawn from a succession of cruises that took place between 1988 and 2004 at the locations listed in Table 5.1 and shown in Figures 5.1 and 5.2. With the exception of one sample collected by the *RV. Marion Dufresne* II in 2000, the eastern Indian Ocean samples all come from two cruises of the Australian national research facility, *RV. Franklin.* The first cruise ["Fr10-95], which yielded 29 samples, took place in December, 1995; it began in Darwin and ended in Fremantle. Broadly following the 1500 metre isobath, all but a few samples from waters close to Darwin were taken at water depths ranging from 500 to 4090 metres with an average depth of 2500 metres. The second *RV. Franklin* cruise ["Fr02-96] in February and March, 1996, took a more seaward route than Fr10-95 so the 29 samples came from generally deeper seas – from 400 to 4100 metres with an average of 2600 metres.

The eastern Indian Ocean study area

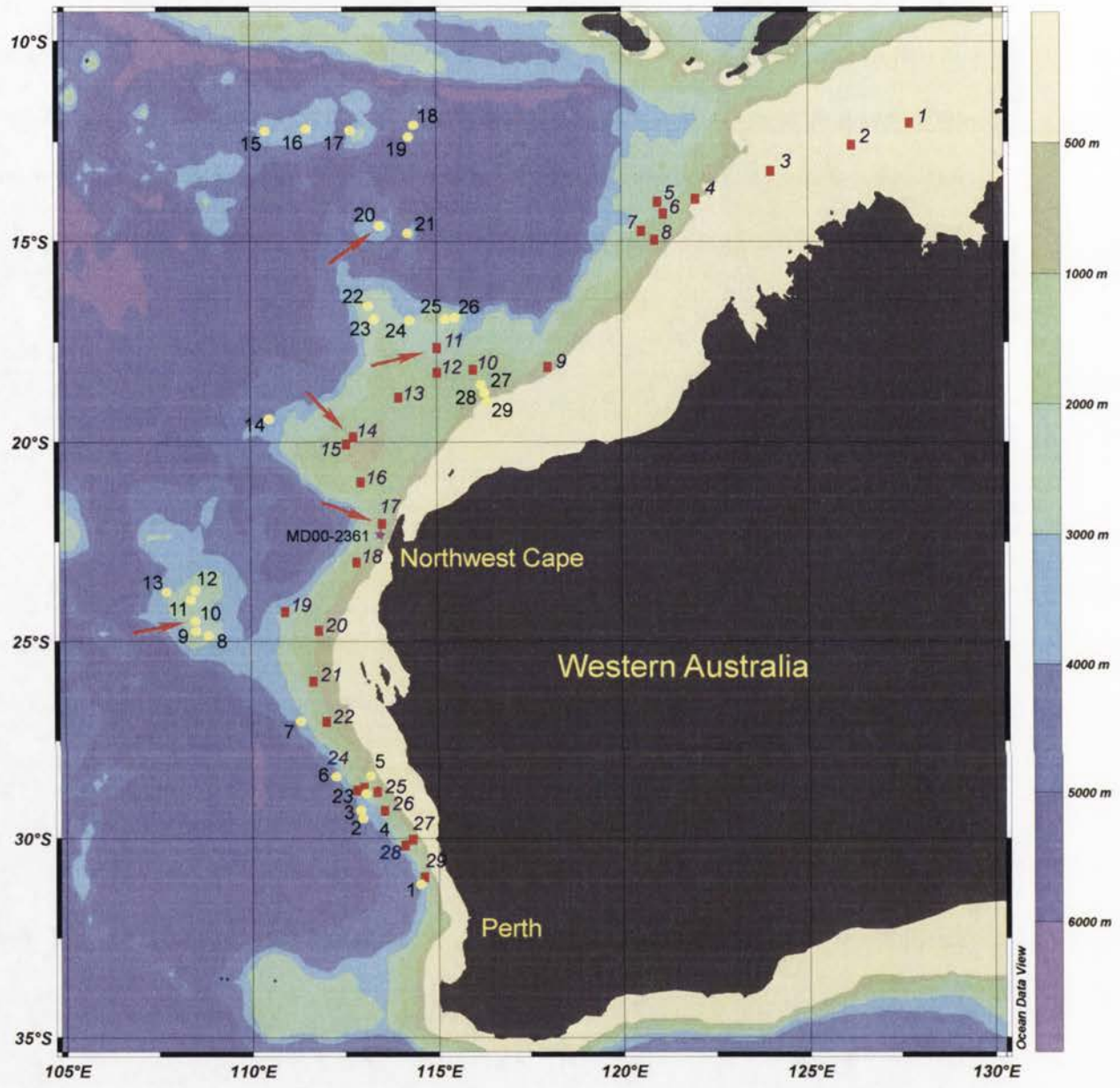

Figure 5.1: The eastern Indian Ocean sample sites.
RV Franklin 10-95 - red squares; 02-96 - yellow circles;
RV Marion Dufresne (one sample only) - star.
Except for the first four sample sites, which were taken in shallow water, the Fr10-95 cruise samples came from 800-2500 metres bsl (average 1500 m). The Fr02-96 samples came from much deeper waters (average 2500 m), and further out to sea, but, with one exception (Fr02-96 GC14), not from the deepest waters in the region.
The red arrows indicate the sites used for LGM reconstructions - see Chapter 10.

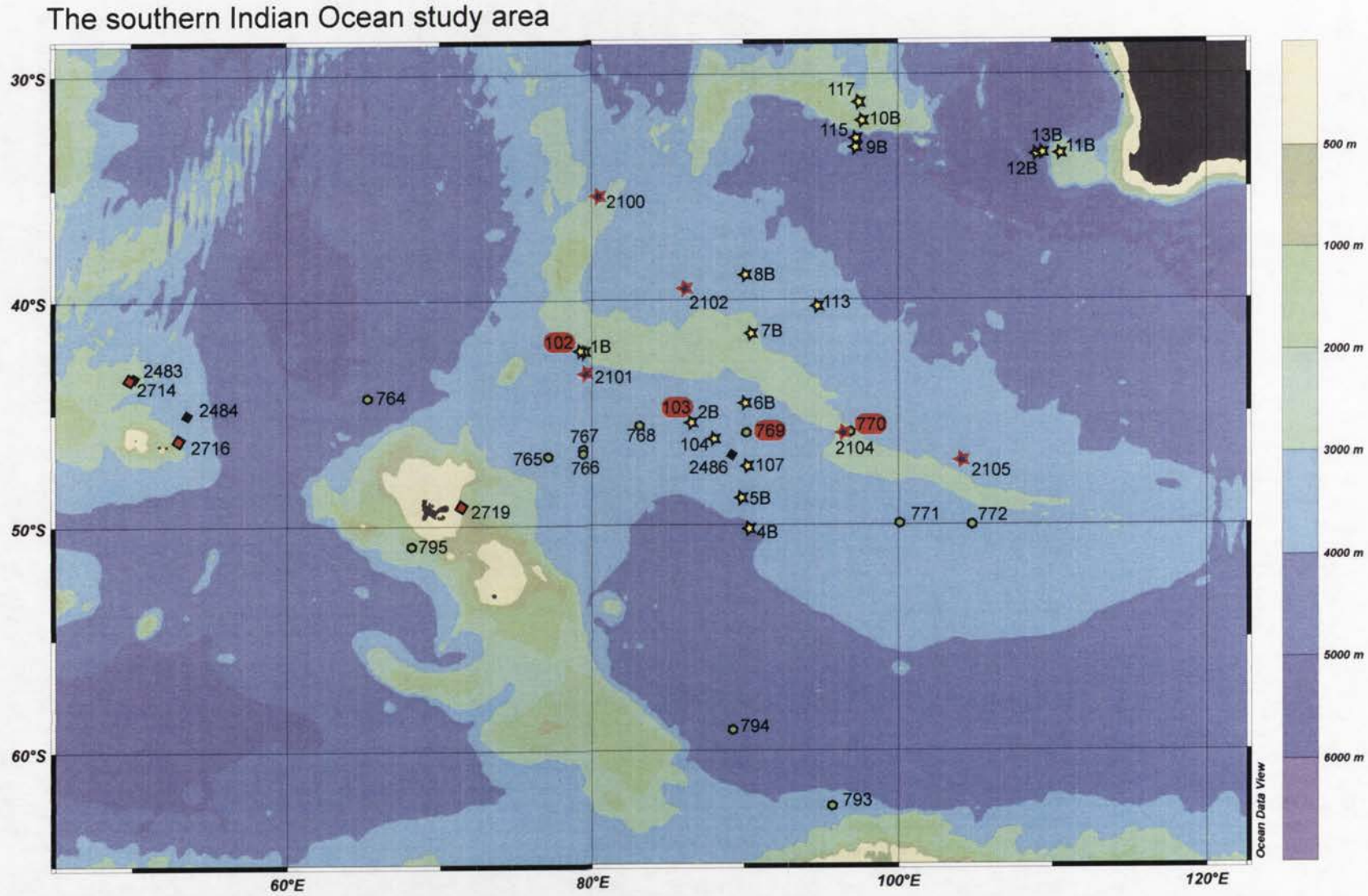

Figure 5.2: The southern Indian Ocean sites.
RV Marion Dufresne cruises: MD88 ○ MD94 ☆ MD97 ★ MD02 ◆ MD04 ◆
The names of the four SIO cores studied are highlighted with a red oval.

The RV *Franklin* samples were obtained from gravity cores which may fail to return the material from the sediment-water interface. However, this study's samples are the same as those used by Martínez et al. (1998) when studying planktonic foraminifera. Martínez took the top of each core onboard ship as it was recovered in order to minimise the risk of mixing and other forms of contamination. The Southern Ocean samples came from *RV. Marion Dufresne* I and II cruises in 1988, 1994, 1997, 2002, and 2004 and comprise a mixture of short-trigger, box, gravity, and piston cores. The 1988 cores and five of the 1994 cores were taken with Kullenburg (piston) corers. Twelve of the 1994 samples came from box cores; information on the coring method for the remaining *RV. Marion Dufresne* cores is not readily obtainable.

A number of the core tops were dated: twelve of the Fr10-95, fourteen of the Fr02-96, and nine of the *RV. Marion Dufresne* (see Table 5.1). Those more than 5000 ka (dates in red in Table 5.1) were considered too old to be considered likely to reflect modern ocean conditions and were excluded from Part I of the study. However, their census data was included, when applicable, in Part II. Three samples (Fr10-95/GC 1-3) also had to be omitted from almost all the analyses as they were taken in relatively shallow waters (less than 200 metres) and are virtually devoid of radiolaria. Eighty-five surface sediment samples remained for analysis.

5.1.2. LGM samples

Seven slides of fossil samples dated to the LGM (21,000±2000 cal. yr. BP) by Martínez *et al.* (1999) from the *Globigerinoides sacculifer* $\delta^{18}O$ record were prepared from six of the study's EIO cores. These cores were selected because they had been used by Barrows and Juggins (2005) for the estimation of LGM SSTs from the faunal analyses of planktonic foraminifera. The Fr10/95-GC29 sample yielded virtually no radiolaria and was rejected.

Table 5.1: Sample site locations (in latitude order)

Core	Latitude [°S]	Longitude [°E]	Depth [m]	Age [a]	Assemblage	WADE	URI
Fr10-95/GC01	12.0000	127.8333	124	[no rads]	-	na	na
Fr02--96/GC18	12.0862	114.4540	3189	4640±70	A01	7.90	0.80
Fr02--96/GC16	12.1882	111.5075	2714		A02	3.82	0
Fr02--96/GC15	12.2402	110.4283	3446	4910±70	A03	5.30	0
Fr02--96/GC17	12.2467	112.7378	2571		A04	8.14	0
Fr02--96/GC19	12.3793	114.2827	3355		A05	5.18	0
Fr10-95/GC02	12.5477	126.2473	80	[no rads]	-	na	na
Fr10-95/GC03	13.2422	124.0038	182	[no rads]	-	na	na
Fr10-95/GC04	13.9197	122.0252	470		B01	43.67	0
Fr10-95/GC05	14.0092	121.0263	2472	3442	B02	3.03	0
Fr10-95/GC06	14.3278	121.1635	2177	1390±45	B03	12.11	2.05
Fr02--96/GC20	14.5825	113.5082	2497	6070±80	-	8.05	0
Fr10-95/GC07	14.7097	120.5457	1440	14950±110	-	2.05	9.62
Fr02--96/GC21	14.8113	114.2728	2919		B04	6.86	0.48
Fr10-95/GC08	14.9162	120.9582	625		B05	12.09	1.12
Fr02--96/GC22	16.5785	113.1997	2501		B06	5.73	0
Fr02--96/GC26	16.9000	115.5167	1958		B07	9.90	1.38
Fr02--96/GC25	16.9108	115.2650	1666		B08	5.58	0
Fr02--96/GC23	16.9135	113.3357	1987	4780±60	C01	26.50	0
Fr02--96/GC24	16.9268	114.2577	1602.5		C02	12.33	0
Fr10-95/GC11	17.6428	114.9988	2458	3010±60	C03	7.82	0.53
Fr10-95/GC09	18.1272	118.0153	498		C04	114.00	0
Fr10-95/GC10	18.1488	116.0220	1462	1870±60	C05	17.62	1.38
Fr10-95/GC12	18.2450	114.9938	2034		C06	3.73	2.56
Fr02--96/GC27	18.5618	116.2668	1023.5		C07	6.25	0
Fr02--96/GC28	18.7988	116.3372	502	1740±50	C08	0	0
Fr10-95/GC13	18.8210	113.9740	1454	2310±50	C09	17.1	0
Fr02--96/GC29	18.9635	116.3920	344		C10	28.00	0
Fr02--96/GC14	19.4107	110.5067	4089.5	16870±130	-	6.36	1.49
Fr10-95/GC15	19.8958	112.7228	1393	10270±60	-	-	-
Fr10-95/GC14	20.0452	112.6622	997	2300	C11	53.5	0.74
Fr10-95/GC16	20.9972	112.9892	1221		C12	20.2	0
MD00/2361	22.0820	113.4772	1805		C13	4.97	0.77
Fr10-95/GC17	22.1290	113.5018	1093		C14	5.69	0
Fr10-95/GC18	22.9940	112.8310	1055		C15	4.62	3.12
Fr02--96/GC13	23.7292	107.7118	3189	45800±2000	-	1.5	0
Fr02--96/GC12	23.7372	108.5318	2100	10420±50	-	-	-
Fr02--96/GC11	23.9527	108.3690	2404		D01	9.80	0
Fr10-95/GC19	24.2352	111.0030	1974	5540±70	-	8.22	0.91
Fr02--96/GC10	24.4642	108.5102	2852		D02	13.07	0.41
Fr10-95/GC20	24.7445	111.8292	837	2800±60	D03	27.40	0
Fr02--96/GC09	24.7472	108.4877	2534	5980±70	-	18.33	3.49
Fr02--96/GC08	24.8460	108.8247	2670	1315±50	D04	1.90	0
Fr10-95/GC21	25.9963	111.6348	982		D05	0.25	0
Fr02--96/GC07	26.9793	111.3355	3090	3160±60	D06	8.82	1.77
Fr10-95/GC22	26.9920	112.0052	1049		D07	26.00	1.08
Fr02--96/GC05	28.3925	113.1595	735	1700±60	D08	11.88	0
Fr02--96/GC06	28.4202	112.2895	3575		D09	0	0
Fr02--96/GC04	28.7170	113.3887	935.5		D10	16.75	2.11

Core	Latitude [°S]	Longitude [°E]	Depth [m]	Age [a]	Assemblage	WADE	URI
Fr10-95/GC25	28.7322	113.3680	1010		D11	16.50	2.04
Fr10-95/GC23	28.7450	112.7823	2470	2975±50	D12	20.00	0
Fr10-95/GC24	28.7507	113.0645	1577		D13	5.64	0
Fr10-95/GC26	29.2403	113.5580	1734	2560±35	D14	4.17	1.18
Fr02-96/GC03	29.2963	112.9430	3343	3300±70	D15	4.50	0
Fr02-96/GC02	29.3492	112.9485	3377	5610±70	-	11.00	0
Fr10-95/GC27	30.0023	114.2773	853		D16	9.50	0
Fr10-95/GC28	30.0813	114.1418	1440		D17	2.50	0
Fr10-95/GC29	30.9932	114.5895	1200		D18	5.50	1.43
Fr02-96/GC01	31.1107	114.5482	2530		D19	5.53	0.64
MD94/117	31.6167	97.7138	2360		G01	1.75	7.55
MD94/10B box	32.1645	97.6957	1660		G02	0.89	0.93
MD94/115	33.1802	97.6125	4020		G03	1.00	0
MD94/12B box	33.5200	109.1500	4110		G04	2.62	1.14
MD94/13B box	33.5400	109.3000	3560		G05	2.41	5.60
MD94/11B box	33.5785	110.5848	2400		G06	5.08	0
MD94/09B box	33.5905	97.5978	4185		H01 [G]	1.13	1.60
MD97/2100	35.9642	80.9287	2510	7000±70	-	0.82	0
MD94/08B box	38.8637	90.1017	3491		H02	1.08	0.71
MD97/2102	39.9208	86.0068	3440		H03	1.73	0
MD94/113	40.6717	95.3550	3436		H04	0.80	0
MD94/07B box	41.7200	90.2785	2768		H05	1.14	0.53
MD94/01B box	42.5000	79.4167	2920	6260±60	-	4.25	0
MD02/2483	43.3933	49.7883	2300		K01	0.04	2.42
MD04/2714	43.3983	49.8200	2300		L01 [K]	0.32	0
MD97/2101	43.4957	79.8383	3145	3069±50	J01	1.00	0
MD94/102	43.5057	79.8363	3205	19300±180	J02	1.50	0
MD88/764	44.4000	65.1333	4530		J03	2.56	0
MD94/06B box	44.6650	90.0758	3315		H06	1.37	0
MD02/2484	45.0767	53.3300	3400		K02	0.09	0
MD94/02B box	45.5870	86.5167	3205		J04	0.69	1.49
MD88/768	45.7600	82.9333	3330		K03	0.41	0
MD88/770	46.0300	96.4667	3290	4080±70	J05	0.44	0.24
MD97/2104	46.0372	96.4833	3310		J06	0.39	1.57
MD88/769	46.0700	90.1167	3420	6193	-	1.32	0
MD04/2716	46.1650	52.9267	3320		K04	0.08	0
MD94/104	46.4828	88.0693	3460		J07	0.29	1.04
MD88/766	46.6700	79.4833	2930	4430±60	K05	0.24	0.90
MD88/767	46.6700	79.5000	2920		K06	0.26	0.46
MD02/2486	47.0033	89.1117	3380		J08	1.04	0.58
MD88/765	47.0300	76.9333	3420		L02 [K]	0.38	0
MD97/2105	47.1930	104.4762	3300		J09	0.41	0
MD94/107	47.7695	90.2368	3525		J10	0.24	1.83
MD94/05B box	48.8013	89.5413	3730		K07	0.16	0.39
MD04/2720	49.1267	71.3683	750		L03	0.02	0
MD88/771	49.9300	100.1167	3310	3560±60	K08	0.10	2.24
MD88/772	50.0300	104.9000	3240		K09	0.04	0
MD94/04B box	50.3808	90.2527	4036		K10	0.28	0
MD88/795	50.8500	68.0167	1870	980±50	L04	0.10	0
MD88/794	59.0000	89.4000	4595		L05	0.32	0
MD88/793	62.4833	95.9333	3790		L06	0.61	2.24

The SIO cores, MD88-769, MD88-770, and MD94-102, were also included in the Barrows and Juggins' (2005) study, so their LGM SSTs could be added to the EIO samples in the exercise to demonstrate the modern database's utility in palaeo-reconstruction. The LGM sample sites' locations are shown in Figures 5.1 and 5.2.

5.1.3. Core samples

Four southern Indian Ocean cores, MD88-769, MD88-770, MD94-102, and MD94-103, were investigated with the broad aim of reconstructing the last 40 ka at each site. All four cores come from locations close to southern Indian Ocean fronts (see Chapter 4). MD88-769 and -770 were selected because of the availability of over 600 slides of radiolaria (covering 200-300 ka in each core) prepared for Dr M. Labracherie of EPOC, University of Bordeaux I, but not subsequently examined. MD94-103 was selected on the recommendation of Dr J-L. Turon of EPOC and MD94-102 by agreement between Professor P. De Deckker and Dr E. Michel of CNRS-CEA. Dr Michel also provided samples of MD94-101 but time has not yet permitted their examination. MD94-101, -102, and -103 were provided as unprocessed core samples.

The MD88-769, MD88-770, and MD94-102 core samples examined during this study were from reasonably regular intervals down the cores to approximately 35-40 ka with some variation in interval and core-depth due to the availability of samples and time to conduct the counts. By contrast, the MD94-103 samples covered four specific areas where comparisons could be made with Sicre *et al's.* (2005) proposals concerning changes in the upper layer of the Southern Ocean induced by ENSO-like conditions during Heinrich events.

5.2. Laboratory methods

In order to make frequency counts of the radiolarian species, microscope slides were needed for each sample with as much extraneous material (clay, non-radiolarian tests, etc) removed as possible. Because the raw core tops were processed at different times and/or by different people, three different methods were used to prepare the slides. The core top and the EIO LGM sample slides were prepared by *Method I* (described below), the MD88 slides by *Method II*, and the MD94 slides by *Method III*. In a small number of cases, material was available to allow slides to be prepared by two different methods. Comparisons of census data from these slides were made and no statistically significant differences found. The one difference of importance lay in the interval between slide production and species identification. The gentle application of a toothpick to the cover slip of a new-produced slide whose mount medium is still soft allows tests to be rolled over and examined from various aspects. This facility, which is not available when examining older slides, often makes the difference between a firm identification or not. Whereas a test can usually be placed in to genus when viewed from any aspect, the ability to move specimens means a higher proportion will be identified to species.

5.2.1. Slide preparation: Method I

In order to dissolve any carbonates present, samples for the study (which came from the uppermost 1-2 cm of the cores) were digested with 10% hydrochloric acid until no further effervescence was evident. In the few cases, when this process did not also cause the clays to disaggregate completely, the samples were further treated with 3% hydrogen peroxide and placed in a gentle ultrasound bath for approximately 20 seconds. Sampling indicated that neither the hydrogen peroxide treatment nor the ultrasound had any adverse effects on the radiolarian tests but, as a precaution, these treatments were avoided as far as possible. Once all the unwanted material was fully digested or disaggregated, samples were washed through

a 63μm sieve with a gentle water jet and the coarse fraction transferred to vials. The samples were then allowed to settle at least overnight, after which time water was decanted from the vials by pipetting and replaced with ethanol. This process was repeated after further overnight settlings.

For each sample, a cover slip was gently warmed on a hot plate, a quantity of the sample residue sample micropipetted onto the cover slip with some ethanol to disperse the radiolarian specimens across the cover slip, and warming continued until all the liquid had evaporated. The cover slip was then mounted onto a slide, using Naphrax® as the mount-medium. The amount of residue transferred to a slide was determined by experience with the aim of ensuring there were at least 300 radiolarian tests to count for each core top, a number chosen to reduce to less than 1% the probability of failing to detect any taxon which comprised at least 1% of the population (see Fatela and Taborda, 2002). When necessary, a succession of slides was made from the same vial sample in an attempt to reach the 300 specimens. When the abundance of radiolaria was very low, additional samples were prepared from the core tops (if sufficient core material was still available), again with the aim of reaching the desired total of at least 300 specimens.

Using this method, it was not easy to ensure a even distribution of specimens over the slide: there was a strong tendency for the specimens to clump together. Clumping makes species counting difficult, part because one specimen will often obscure another and part because of the problem of keeping track of specimens to ensure each is counted once and once only.

5.2.2. Slide preparation: Method II

The MD88-769 and -770 slides were prepared at EPOC by M-H. Castera by the following method. Firstly, 10 gm of dry sediment was added to a litre of water, 870 ml of hydrogen peroxide and 42 gm of tetra-sodium diphosphate and, a few minutes later, heated in a bain-marie, stirring the while. Once effervescence ceased the mixture was left to cool (excess effervescence could be controlled by the addition of alcohol). The mixture was then sieved through a ***45*** μm filter, distilled water added to the residue, and the result dried in an oven at 60°C. Next, hydrochloric acid (first 10%, then 25%, and, finally, 50 %) was added to the residue in a beaker. After adding distilled water, the residue was allowed to stand for four hours, decanted with a filter pump, and re-sieved through the 45 μm filter. The residue from this procedure was made up to 50 cc with distilled water.

To mount a sample, a slide was placed in a Petri dish (a cover slip was used in place of a slide when mounting diatoms). The beaker containing the residue was shaken and as much liquid as seemed appropriate pipetted onto the slide. Enough water to cover the slide was then added to the Petri dish and knitting cotton (not wool or polyester) used as a siphon to drain the water. Draining could be expected to take one to two days. Once the slide was dry, it was placed on a hotplate at 250-300°C, a drop of Canada Balsam added and allowed to heat well. Finally, a cover slip was placed on the slide which was then allowed to cool at least five minutes.

This method produces slides with the specimens very well dispersed, a situation which aids fast and accurate counting. It has the disadvantage of requiring a relatively large amount of raw material (10 gm as compared with as little as 0.2 gm used in the other two methods). Comparisons demonstrated the use of a 45 μm filter instead of the 63 μm used at the ANU

had no significant effect on the census counts; relatively few sub-63 μm tests were seen on the Method II slides and the majority of them were not identifiable to species level.

5.2.3. Slide preparation: Method III

The author devised Method III to be the closest approximation to Method II possible when using a limited quantity of raw material. It, incidentally, proved a very speedy way to prepare slides, although not to the same very high quality as Method II.

The procedure followed was the same as Method I to the point where the coarse fraction from the 63 μm filter was transferred to a vial. Unlike in Method I, no attempt was made to minimise the water transferred to the vial and no ethanol was added (a side benefit of this is the fact that the samples in vials dry out far more slowly than those containing ethanol). A cover slip was placed in a small Petri dish and a quantity of the residue in the vial pipetted onto it. Water was added to Petri dish: this was done with care so as to encourage the radiolarian specimens to disperse evenly and to avoid causing the cover slip to float. Knitting cotton was then used as a siphon as in Method II and the Petri dish drained. When the cover slip was dry, two to three drops of Naphrax®, the mount-medium, were placed on a slide and the cover slip turned onto the slide. Prepared slides were then left in a fume cupboard overnight to allow any toxic solvent from the Naphrax® to evaporate safely.

5.3. Identification and counting of specimens

The slides were examined at a magnification of 100 or even higher when necessary, and the specimens identified mainly using the descriptions and photographs appearing in four online databases (Nigrini and Moore, 1979b; Boltovskoy, 1998; Dolven, 2004; Nigrini *et al.*, 2004). When the databases proved insufficient, identification was sometimes possible using a fairly extensive collection of journal and other publications featuring species descriptions

(for instance Haeckel, 1887; Campbell and Moore, 1954; Nigrini and Moore, 1979a; Takahashi, K., 1991). Unfortunately, the Catalogue of Polycystine Radiolaria (Foreman and Riedel, 1972), a comprehensive set of species descriptions on microfiche, was not available. Van de Paverd's (1995) PhD thesis with its large number of photographs was frequently used to obtain an initial identification but his taxa assignments were only accepted as a last resort because his classification proposals have yet to be peer-reviewed.

Because access to full species descriptions was limited, emphasis was placed on consistency in categorising specimens. In some instances, a taxon may have been misidentified but, provided the specimens grouped under its name come from a single species or genus, the statistical analysis of the census data is not compromised.

5.4. The database of modern radiolaria

During Part I of the study an average of 487 specimens per core top were counted: 281 taxa were observed, an average of 59 per core top. Not all of the taxa counted consisted of single species because it was not always possible to identify them to that level. To avoid the errors this might introduce, taxonomic groups of doubtful homogeneity were removed from the data for statistical analysis, as were the rarest species (<10 specimens observed or no site with five specimens) and the core tops with very few radiolarian specimens (<100). At the same time, the common requirement for a species to constitute 2% or more of at least one sample to be included was not implemented, the reasoning being that every exclusion results in information loss. In fact, some analyses of the data both with and without the rarer species were performed and the results found to differ only marginally.

5.5. Core samples

The tests in both the EIO LGM core samples and the SIO cores were counted in the same way as the core top samples. In most instances, there was more material available to count than for the core tops and the total number of tests counted per sample was often higher. Approximately 110 000 specimens were identified in the 185 core samples counted, about 610 per sample.

Specimens of 344 taxa were identified: 94 of these were represented by too few specimens to be included in statistical analyses. Fifty of these taxa (17 650 specimens) were unique to the SIO core samples (i.e. the taxa were not observed or were extremely rare in the surface samples). No identified taxa were unique to the surface samples. A few hundred specimens could not be identified to any taxon known to the author. Very few of the unidentified specimens seemed to belong to the same taxon and, therefore, perhaps to be representative of an undescribed species. The author believes that, at most, two or three undescribed species were observed. Species lists appear as Appendices 1 and 2. Plates containing light microscope photographs of the identified taxa are also appended. High-resolution photographs are included in the Electronic Supplement.

Three species, *Peromelissa* sp. cf. *P. scaphopodium* Haeckel 1862, *Lophophaena nadezdae* Petrushevskaya 1971, and *Lithomelissa setosa* Jørgensen 1900, all from the family Plagoniidae Haeckel 1881, emend. Riedel, 1967, constitute 55% of the core-unique taxa. Examination of their distribution against time shows that their number declined very sharply at the MIS-2 to MIS-1 transition, suggesting these three species are strong indicators of conditions south of the Polar Front.

5.6. The environmental database

In its World Ocean Atlas 2005 (WOA05, 2005), the US National Oceanographic and Atmospheric Agency publishes objectively analysed data for sea temperature, salinity, dissolved oxygen, apparent oxygen utilisation, percentage oxygen saturation, phosphate, nitrate, silicate, and chlorophyll concentrations at a selection of depths down to 5500 metres on annual, seasonal, and monthly time scales. An environmental database was created for this study from the World Ocean Atlas and consisted of austral summer (January to March), autumn (April to June), winter (July to September), and spring (October to December), where available, for each of the nine parameters at each site. Also included in the database were values for three derivative parameters: water density (Schlitzer, 2005) and Si*, where Si* = $[Si(OH)_4\text{-}]\text{-}[NO_3^-]$ (Sarmiento *et al.*, 2004), at the surface and depths of 10, 20, 30, 50, 75, 100, 150, 200, 250, 300, 500, and 1000 metres and salinity-normalised total alkalinity (NTA - Millero *et al.*, 1998) at the surface. The WOA-05 contains no values for chlorophyll below 100 metres; the Millero et al. (1998) formulae for NTA only provide surface values. The sites values were derived from the WOA-01 1° latitude by 1° longitude grid using linear interpolation.

5.7. Statistical analysis

For Part I of the study, the surface sample database was analysed to identify assemblages of radiolarian species and the assemblages found were associated with ocean currents and fronts. The surface sample database was also analysed in conjunction with the environmental database to establish which, if any, of the radiolarian census data could be used to reconstruct ocean variables and which ocean variables at which depths could be reconstructed. The reconstruction techniques were validated against the Barrows and Juggins' (2005) LGM SST estimates.

For Part II, the environmental conditions which Part I established as reconstructable, were reconstructed for the SIO cores MD88-769, MD88-770, MD94-102, and MD94-103.

The statistical methods used for the various analyses are described and discussed in Chapter 6.

Chapter 6: Analysis of the surface sediment database

6.1. Aims of the analysis

The aim of analysing the microfossil census data from the surface sediments was firstly to determine whether recent (<5ka) radiolarian deposits reflect present-day oceanic phenomena. The possible phenomena fall into two broad categories: the water masses associated with currents and fronts on the one hand, and physical conditions (such as temperature) and chemical composition (eg. salinity, nutrient concentrations) on the other. The second aim was to establish statistical associations which could be used to reconstruct palaeo-environmental conditions for any radiolarian-oceanic relationships which might exist.

6.2. Approach to analysis

The census data was, firstly, analysed as a single dataset (combined IO) and, then, as two datasets, one consisting of data from the eastern Indian Ocean (EIO) and the other from the southern Indian Ocean (SIO). The division between the EIO and the SIO made at 31°S, although one sample south of that line and a second just north of it were included in the EIO on the basis of cluster analysis (see below).

The analysis was chiefly achieved using software packages available through the R System (R Development Core Team, 2008). The scripting language, *Tinn-R* (Faria *et al.*, 2008), was used to develop R scripts. Italics are used to indicate R packages (and other software packages) when they are mentioned in the text – for example: *R:agnes, CANOCO.*

6.3. The clustering techniques used to establish relationships with currents and fronts

For a relationship with either ocean currents or fronts to exist, there must be geographically-based assemblages of radiolarian species corresponding to the various water

masses. The clustering of sample sites on the basis of their census data, if any, would point to the existence of such assemblages.

Choosing suitable clustering analysis techniques is very difficult (Jongman *et al.*, 1987). Techniques differ, firstly by the algorithm they use: there are agglomerative hierarchical methods (eg. *R:agnes*), divisive hierarchical methods (eg. *R:diana*), and optimal portioning methods (eg. *R:pam, R:fanny*), the last of these needing the expected number of clusters as input (Kaufman and Rousseeuw, 1990; Venables and Ripley, 2002). In addition, each method requires a similarity or dissimilarity measure – PAST (Hammer *et al.*, 2001) offers a choice of nineteen and theirs is not an exhaustive list, others being available in other software packages. These measures variously emphasise different features of the census data, for instance, the influence of the rarer or commoner species (Overpeck *et al.*, 1985). Some clustering methodologies also include a choice of metrics (single, average, etc) for deciding how the distances between clusters are to be measured (Venables and Ripley, 2002). Like the measures, the various metrics have their own peculiarities. For instance, some (eg. single linkage) tend to produce unbalanced dendrograms, whereas others produce clusters of very similar size (eg. complete linkage, Ward's method); some are sensitive to outliers (Ward's, complete linkage), others (centroid clustering) are more robust although less satisfactory in other ways (Hammer and Harper, 2006).

Clearly, it would have been impractical to explore every combination of clustering technique and, of course, there is a real danger of trying many and selecting the one that fits a prior hypothesis. The approach in this study was to use one typical configuration for each clustering algorithm and, in combination with the results from other multivariate analysis techniques, demonstrate a consistency of results and a geographical relationship for the

assemblages. The clustering techniques which were applied to the complete surface sample dataset, the EIO dataset, and the SIO, were:

- normal mixture modelling and model-based clustering (*R:Mclust, mclustBIC*) (Fraley and Raftery, 1998, 2006);
- agglomerative hierarchical clustering (*R:hclust*) using the Bray-Curtis measure and the *average* metric
- agglomerative nesting (*R:agnes*) using Ward's Method and the *manhattan* metric;
- partitioning around medoids (*R:pam*) with the *manhattan* metric;
- fuzzy analysis clustering (*R:fanny*) with principal components input and the *squared euclidean* measure;
- divisive analysis clustering (*R:diana*) using the *euclidean* metric.

The other multivariate analysis techniques applied were Linear Discriminant Analysis (LDA – *R:lda*) (Venables and Ripley, 2002), Non-metric Multidimensional Scaling (NMDS – *R:metaMDS*) (Faith *et al.*, 1987; Minchin, 1987), and (Artificial) Neural Networks (ANN – *R:nnet*) (Venables and Ripley, 2002) and the ordination techniques, Correspondence Analysis (CA – *R:cca*) (Legendre and Legendre, 1998) and Weighted Averaging-Partial Least Squares (WA-PLS – *R:mvr*) (ter Braak and Juggins, 1993; ter Braak *et al.*, 1993).

Clustering methodologies are potentially very subjective. Techniques (eg. *R:agnes, R:diana*) which do not require an initial estimate of the number of partitions for the data usually require a decision following examination of a dendrogram or similar graphical presentation of the output. (It is normally possible, but significantly harder, to make a decision based on numerical output from the clustering technique.) A typical dendrogram, in this case illustrating the results of applying *R:diana* to a dataset of taxa selected from the

combined EIO and SIO data by the Dufrêne and Legendre (1997) methodology (see below), appears as Figure 6.1. The dendrogram presents the distances between sample sites on the basis of the census counts. However, the number of clusters must be determined by inspection. In Figure 6.1, setting a threshold at a height of 70 would partition the sites into six assemblages, five in the SIO and one in the EIO. Three SIO (G01, G05, and G06) sites would be in the EIO assemblage. Although this arrangement could be justified because the three sites in question are close to the Western Australian coast, later analysis suggested that they should be include in SIO assemblage G. Setting the threshold much lower than 70 so as to separate the EIO sites would result in a plethora of SIO assemblages, many consisting of just one or two sites.

Some other techniques (eg. *R:fanny, R:pam*) require the number of partitions be supplied as input and, in this study, these values have been provided from the output of methods not requiring the number of partitions as input. One methodology, normal mixture modelling and model-based clustering (*R:Mclust, R:mclustBIC*) (Fraley and Raftery, 1998, 2006), attempts to decide the number of cluster without the researcher's intervention.

Statistical practice would suggest it would be desirable to use a Monte Carlo method to provide an estimate of the probability of each site belonging to a given cluster being correct. This would entail applying a clustering technique to a randomly selected number of sites and use the results to predict the cluster to which the remaining sites belong. This process would be repeated a large number of times and the results accumulated to provide a validity measure for the clusters. This approach does not appear common (I have found no prior

A typical cluster analysis dendrogram

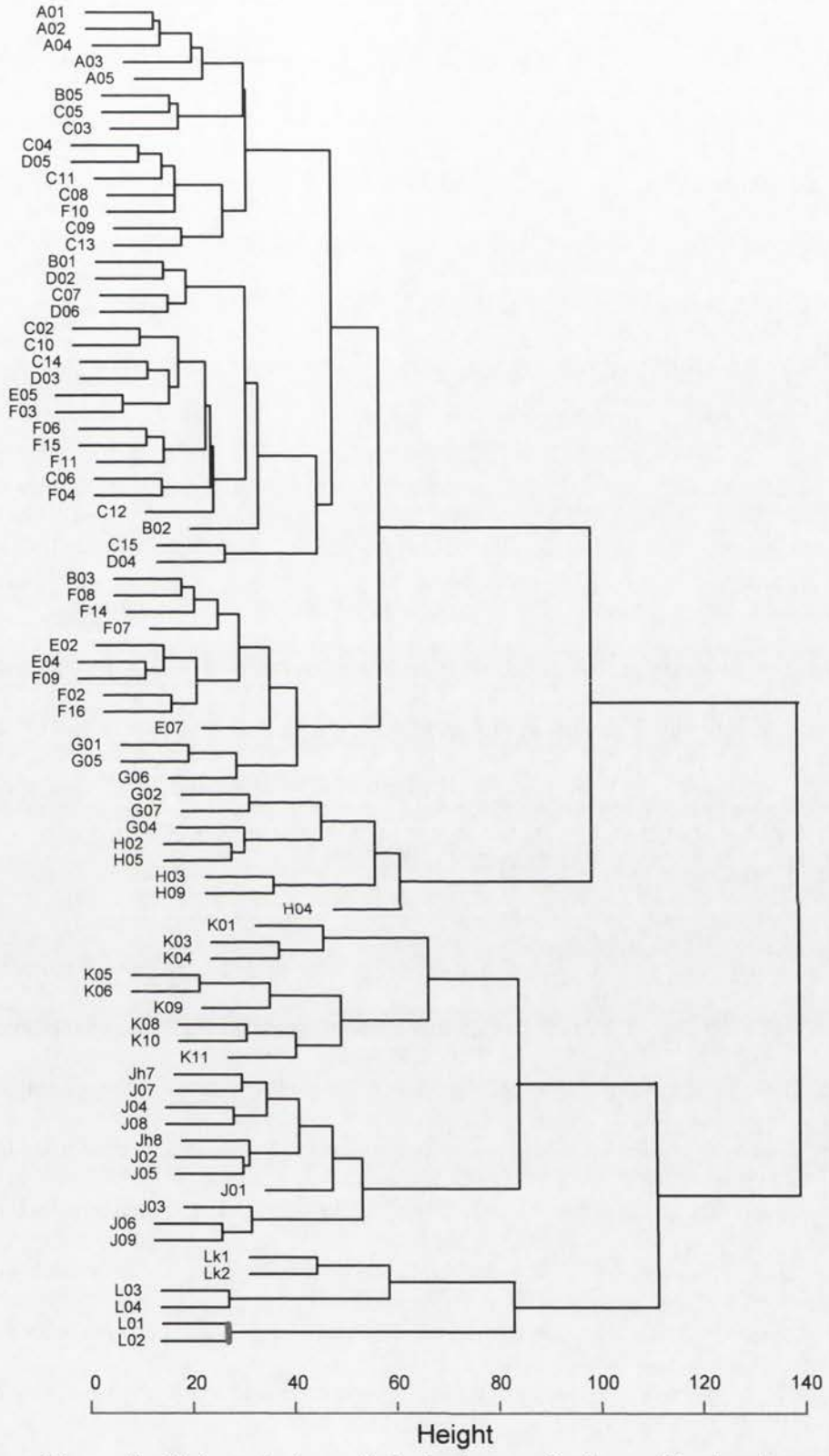

Figure 6.1: the *R:diana* cluster analysis dendrogram for the combined eastern and southern Indian Oceans (selected taxa only). Sites are designated A01, etc, the initial letter indicating their (provisional) assemblages. The *manhattan* metric was used and the divisive coefficient = 0.83.

reference to its use), probably because equating the clusters found at each iteration is relatively difficult to automate (or, even, to do by visual inspection). Clustering techniques depend critically on their starting points and do not give clusters the same designation, or even yield the same number of clusters, at each iteration. Thus, no iterative process of this sort can produce a definitive result but, *a priori,* would seem likely to give a more refined answer than a single application of the clustering technique to the whole data.

In preparation for a Monte Carlo cluster analysis, the eighty site samples of the census database with at least 100 specimens were listed in latitudinal order and allocated one of eleven cluster designators. Two possible initial allocations were provided. The "flat start" allocation was made by dividing first the EIO samples, then the SIO samples, into approximately equal groups, six for the EIO and five for the SIO, and giving each group a letter, A-L (omitting I for reasons of clarity). The other initial allocation was based on clustering revealed by Correspondence Analysis.

The five cluster analytic techniques, as well as WA-PLS, were each executed 200 times with 60 percent of site samples, randomly selected at each iteration, and the outcome used to predict the clustering of the whole dataset. After each execution, the resulting clusters were compared with the initial allocation to determine their most likely cluster designators, each new cluster receiving the designator that the majority of its members had in the initial allocation. A count of the cluster allocations was prepared and, for each site, the most frequently allocated determined. These allocations and their percentage occurrence were recorded. The percentages were intended to give an indication of the reliability of the cluster allocations.

A similar 200-iteration approach was also conducted using ANN and LDA although, in these cases, there was no necessity to find the most likely cluster designators because the two methods relate their predictions to the input cluster designators – which has the side effect that, unlike the situation with the other methods described above, no new clusters can be found.

In addition to the Monte Carlo approach, a "Single-Run" approach was investigated. The set of five cluster analysis techniques (*R:hclust, R:agnes, R:pam, R:fanny,* and *R:diana*) were run once with all the sites as input. The number of clusters for each run was decided by visual inspection. This process was applied to the combined IO, the EIO, and the SIO data and the results assembled in a table. By sorting the results and visual inspection, clusters could be identified by seeking the places where the majority of the techniques indicated a change from one cluster to the next.

It was felt possible that the information derivable from the census data could be enhanced by discriminating between those radiolarian taxa which are present in approximately the same proportion in every sample and those whose proportions varies widely between samples. Those taxa present in roughly the same proportions in every sample obviously provide little clustering information and, so, it could be beneficial to reject them and retain only those taxa whose proportions vary widely to maximise the difference between samples. Dufrêne and Legendre (1997) developed a method of "Indicator Species Analysis" (ISA) which, by application of a Monte Carlo method, gives an estimate of which taxa have indicator value. The method requires that the samples should be grouped before the process commences (because it was developed as a method of deciding when to stop subdividing the input into more clusters). The software is *R:duleg* and was run with the CA-based start only. A probability threshold (0.02 for the whole census data and the SIO, 0.1 for the EIO) was

employed to select the more indicative species – typically 30±5 were chosen. All the clustering methodologies were run with both the full census datasets and those containing the indicator species only.

The fact that the Dufrêne and Legendre (1997) methodology requires that the samples be grouped beforehand is clearly a disadvantage, potentially leading to a degree of subjectivity. Late in the study, it was realised that the disadvantage could, perhaps, be overcome by removing those taxa which were almost equally represented (on a percentage basis) at each site. It was also realised that such taxa could be recognised by applying the χ^2-test. For each taxon, in turn, a vector was formed consisting of the counts for the taxon (as a percentage of the site totals) taken over all the sites, the χ^2-test applied, and those taxa which deviated to a significant extent from the "flat distribution" (i.e. the situation where the taxon occurs the same number of times at each site) were selected as indicator species. The probability threshold used for the combined IO and the SIO datasets was 0.001; that for the EIO dataset was 0.7 – this, much higher, threshold for the EIO was necessary to ensure sufficient taxa were selected for the subsequent tests.

6.4. Ordination techniques used to establish associations with physico-chemical variables

Four ways of associating census data with environmental variables were investigated. Approach 1 consisted of employing, in turn, all nine World Ocean Atlas parameters and their derivatives, NTA, N* (Sarmiento and Gruber, 2006), Si* (Ribbe, 2004; Sarmiento *et al.*, 2004), and *in situ* density as the constraining variable in a Canonical Correspondence Analysis (CCA) of the radiolarian data. The proportion of the taxa variance explained by that environmental variable was then calculated by dividing the constrained inertia by the total inertia (*R:cca*) (Jongman *et al.*, 1987; ter Braak and Verdonschot, 1995; Legendre and Legendre, 1998). With the exception of chlorophyll and Normalised Total Alkalinity, where

data was only available for the sea surface, the eigenvalues for each environmental variable were plotted against depth below sea level (down to 500 metres). The plots provide a concise indication of which environmental variables might be reconstructed from core data. The investigations of N* and Si* were dropped early in the study due to poor correlation with the census data.

As a supplement to Approach 1, *CANOCO* (ter Braak and Šmilauer, 2004) was employed to perform CCA on the census data, the EIO and SIO regions being treated separately. Using *CANOCO* allowed convenient graphical display of the variables in relation to the site CCA scores and the inclusion of several variables at a time.

Approach 2 entailed calculating the R^2 values from the Root Mean Square Errors of Prediction (RMSEP) obtained by applying Weighted Average - Partial Least Squares (WA-PLS) (ter Braak and Juggins, 1993; ter Braak *et al.*, 1993) to the census data in conjunction with each environmental variable at every available depth bsl in turn. WA-PLS with cross-validation was applied to the sites' census data combined with the environmental data and the R^2 value calculated for the WA-PLS component which had the minimum bias-corrected cross-validation estimate. As with Approach 1, this approach was applied to the eastern and southern IO census data separately, and to the combined data, for all four seasons.

Approach 3 was to calculate the correlations between the census CA scores and the environmental data, using Spearman's method so that neither normality nor linearity of the input was assumed.

Approach 4 to relating the radiolarian data clusters to the environmental data was to employ multivariate regression trees (MVRT – *R:mvpart*) (Breiman *et al.*, 1984; De'ath,

2002), which are, in effect, constrained cluster analyses. Run iteratively (an option available in *R:mvpart*), MVRT will not only indicate which environmental variables relate well to the census data but the use of cross-validation error estimates limits data-partitioning to an appropriate number of splits (Maindonald and Braun, 2003). Because MVRT only guarantees each split will be optimal, not the tree as a whole (Maindonald and Braun, 2003), it was necessary to limit the number of environmental variables considered. This was achieved by choosing those variables which explained the highest proportion of taxa variance (Approach 1), the highest R^2 values under Approach 2, and the best correlations from Approach 3.

6.5. Other statistical investigations

The Upwelling Radiolarian Index (URI) (Nigrini and Caulet, 1992) and the Water Depth Ecology index (WADE) (Lazarus *et al.*, 2006) were calculated for each site (WADE and URI in Table 5.1). The definition of the taxa observed in our study as *warm, temperate, intermediate,* or *upwelling* was drawn from Lazarus et al. (2006). Fifty-two of the 62 taxa classified by these authors are represented amongst the 285 taxa presented here.

Chapter 7: Analytic results for the surface sediment database

7.1. Radiolarian assemblages

7.1.1. The identification of assemblages

7.1.1.1. Single-Run clustering

The procedures described in Chapter 6 for identifying clusters were run on the radiolarian census data. The Single-Run clustering was run on the combined Indian Ocean (IO), the eastern Indian Ocean (EIO), and the southern Indian Ocean (SIO) census counts using the whole data for each region (i.e. all radiolarian taxa that were observed at least five times and every site were more than 100 specimens were counted). The results for the three regions were combined and sorted by the classifications that the various clustering techniques returned. From this, the sites were allocated to groups considered to represent radiolarian assemblages. The results and the corresponding groups appear in the Electronic Supplement as Table 7.1a.

Next, Indicator Species Analysis (ISA) (Dufrêne and Legendre, 1997) was applied to reduce the taxa employed in clustering analysis to those likely to have the most predictive power. The Single-Run groups were used as (required) input. Single-Run procedure was rerun on combined IO, EIO, and SIO data but, this time, using the reduced taxa-set. Again, the results were combined and sorted to reveal the underlying assemblages: the outcome appears in the Electronic Supplement as Table 7.1b. Whereas using the Single-Run procedure with this reduced taxa-set appeared to yield an improved set of assemblages, using the improved set as input to further runs of the Single-Run procedure gave no further benefit. Repetition of the Single-Run procedure resulted in an oscillation between two sets of assemblages – and, so, the outcomes of such iterations are not reported here.

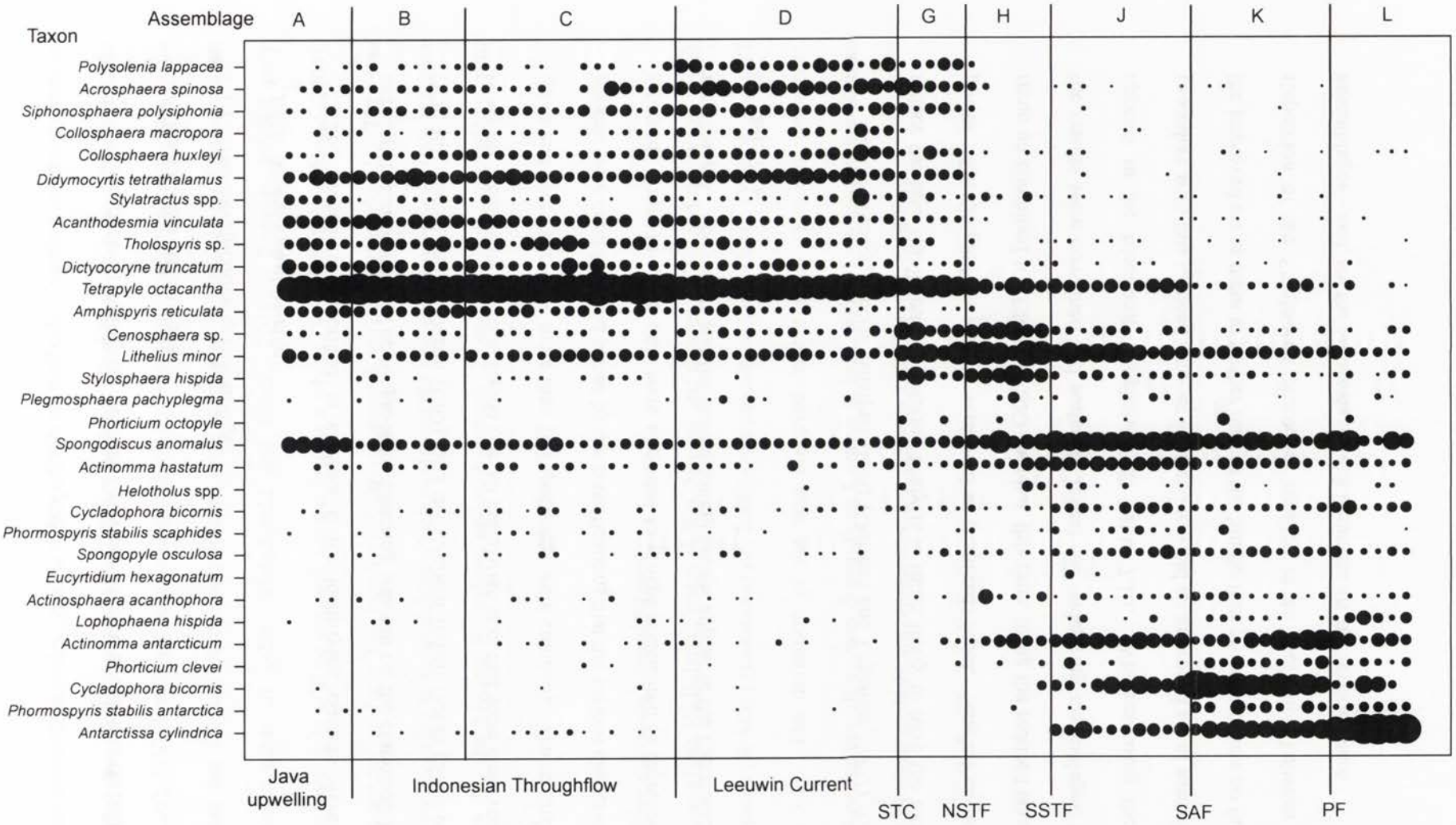

Figure 7.1: An abundance plot of predictive taxa selected using the chi-squared test. The size of the "inkspots" is proportional to the percentage of the corresponding taxa in the site sample. STC = Subtropical Convergence; N/S STF = Northern/Southern Subtropical Front; SAF = Subantarctic Front; PF = Polar Front. Note that the four eastern Indian Ocean assemblages (here labelled A-D) were subsequently increased to six following more detailed analysis.

The χ^2-test was also used to reduce the taxa dataset to one likely to be predictively powerful. The Single-Run clustering was rerun on all three census datasets reduced in this way. The results appear in the Electronic Supplement as Table 7.1c. An "inkspot" diagram illustrating the relative abundance of the selected taxa in the combined IO data appears as Figure 7.1. The corresponding diagram for ISA-selected taxa is very similar to that for the χ^2-selected taxa, so is not reproduced here. Neither are the diagrams for the EIO and SIO reproduced as they do not add much further information.

7.1.1.2. Monte Carlo clustering

The combined IO, the EIO, and the SIO census counts were subjected to the Monte Carlo procedure as described in Chapter 4. Six tables result from inputting the whole taxa-set: one for a "flat-start" and one for a "CA-based" start for each set (combined IO, EIO, and SIO) of census data. The tables appear in the Electronic Supplement as Tables 7.2a-f. A further six tables were generated from using the ISA-reduced taxa-set and appear as Tables 7.3a-f. As with the Single-Run clustering, the results were used in an attempt to improve the assemblage assignments.

7.1.1.3. Correspondence Analysis (CA) and Non-metric Multidimensional Scaling (NMDS) Clustering

CA and NMDS were applied after the other clustering techniques and were used as further confirmation of the assemblages. The CA results appear as Figures 7.2-7.4 and those for NMDS as Figures 7.5-7.6.

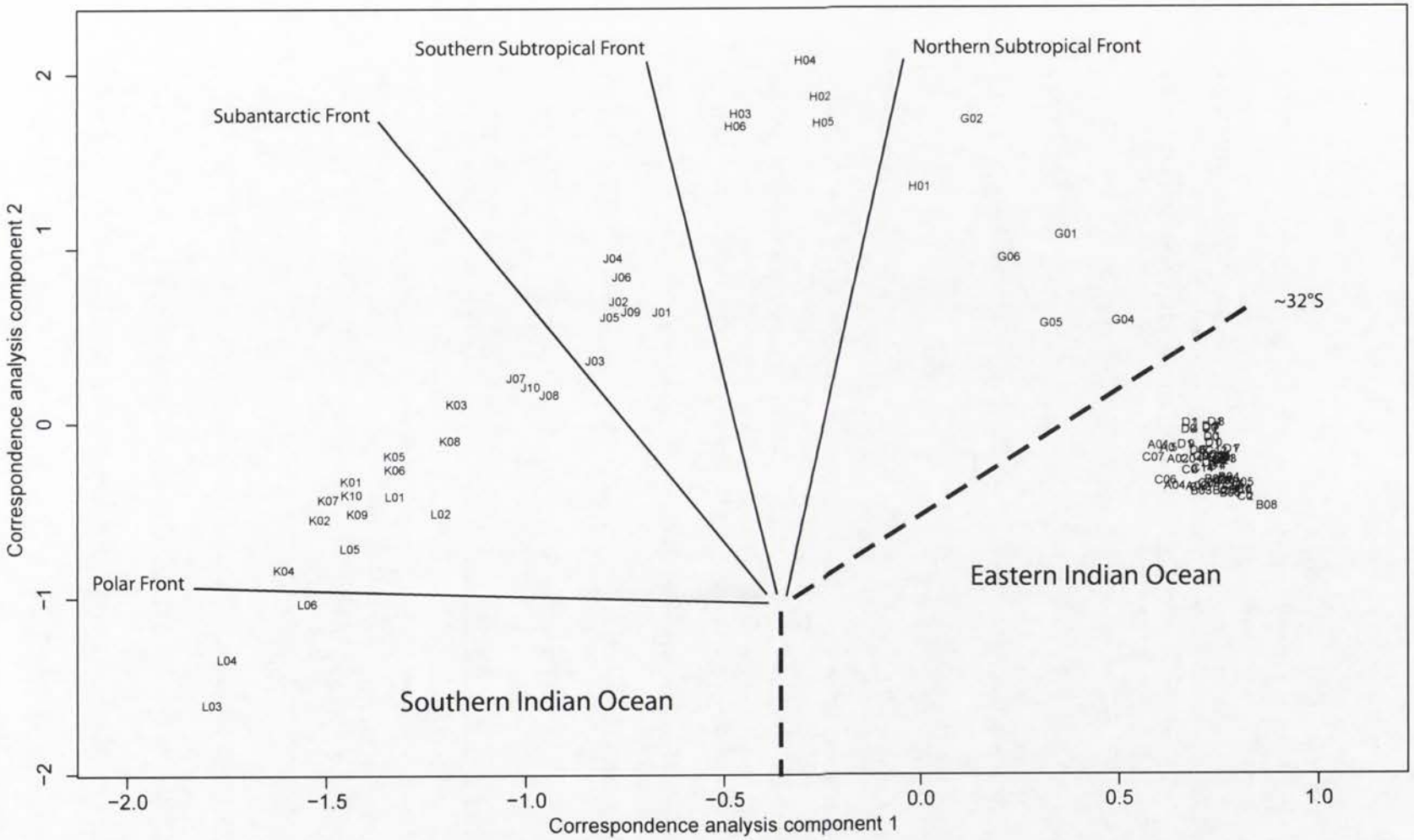

Figure 7.2: Plot of correspondence analysis component 1 against component 2 for the combined eastern and southern Indian Ocean sectors using those taxa selected as powerfully predictive on the basis of the chi-squared test. The labels indicate the assemblages determined by cluster analysis. The positions of the frontal demarcations are from Belkin and Gordon (1996). With the combined IO input data, radiolarian assemblages in the SIO can be discriminated but the EIO sites cannot be separated.

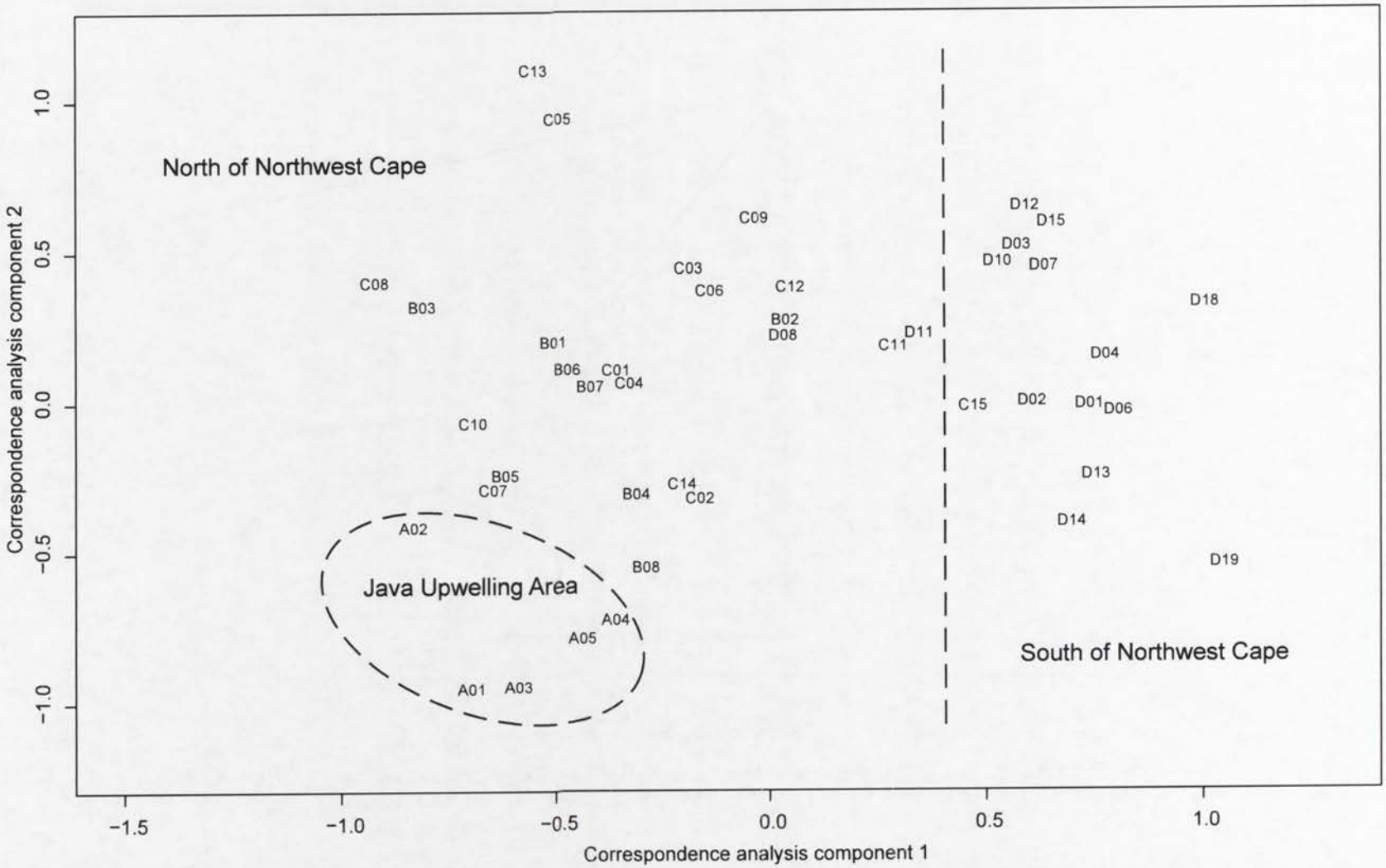

Figure 7.3: Plot of correspondence analysis components 1 and 2 for the eastern Indian Ocean. Input: chi-squared significant taxa only. Labels indicate the assemblages derived from cluster analysis.

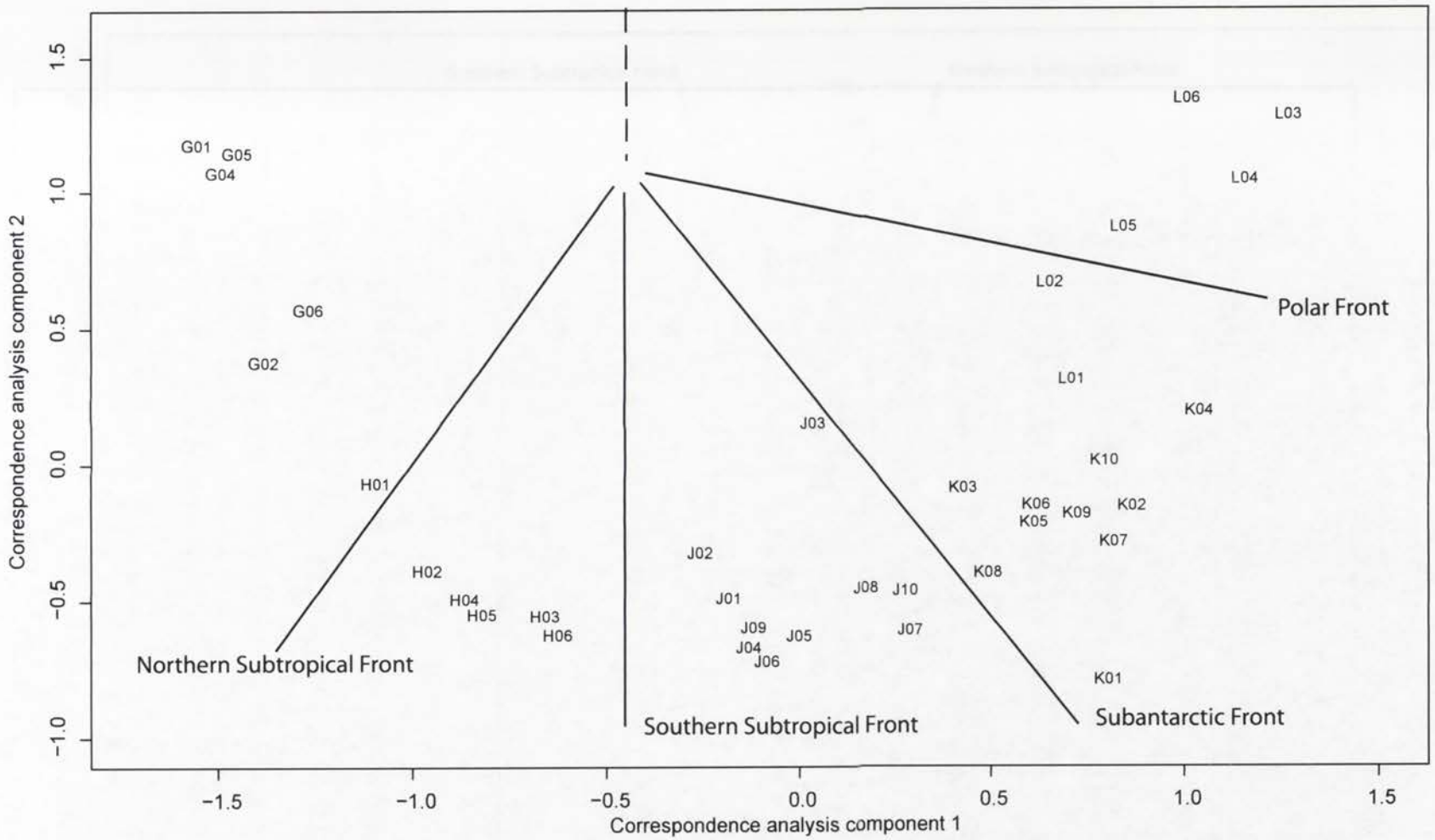

Figure 7.4: Plot of correspondence analysis components 1 and 2 for the southern Indian Ocean with only chi-squared significant taxa as input. The demarcation of the frontal zones is from Belkin and Gordon (196). Labels indicate the assemblages derived from cluster analysis.

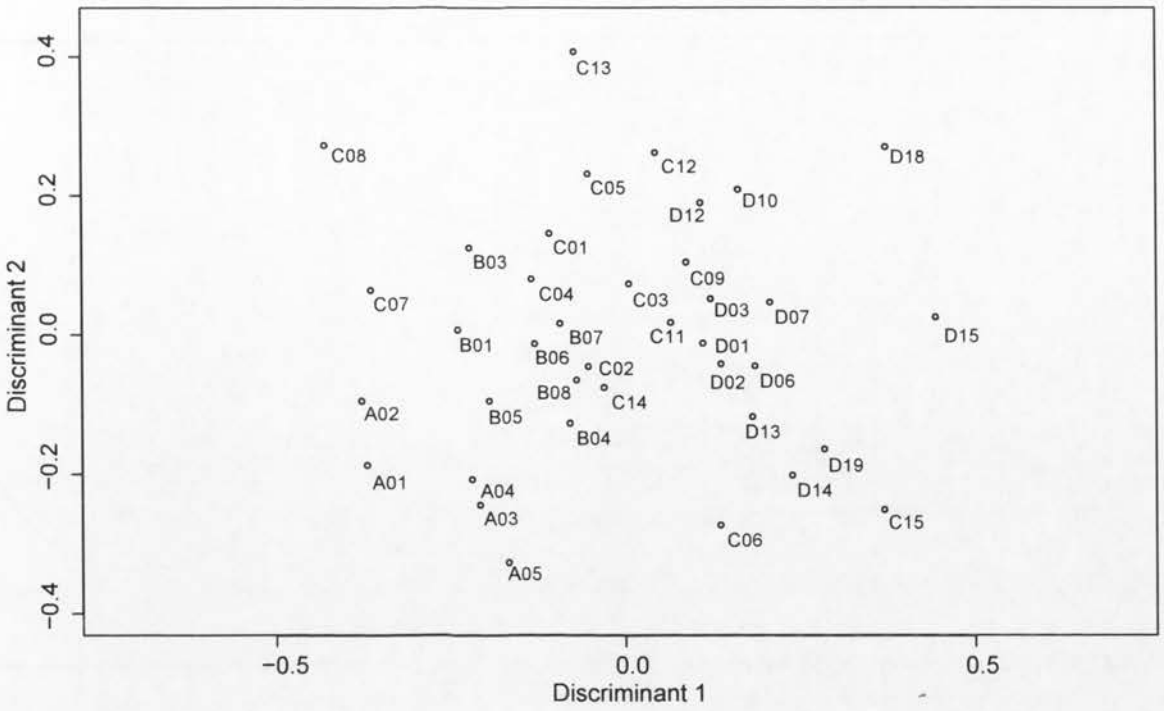

Figure 7.5: Nonmetric multidimensional scaling of Eastern Indian Ocean chi-squared selected taxa from the Eastern Indian Ocean census data. Assemblages A and D can be seen to plot separately, assemblages B and C are intermixed. However, in the absence of labels indicating the assemblages, the sites could not be partitioned.

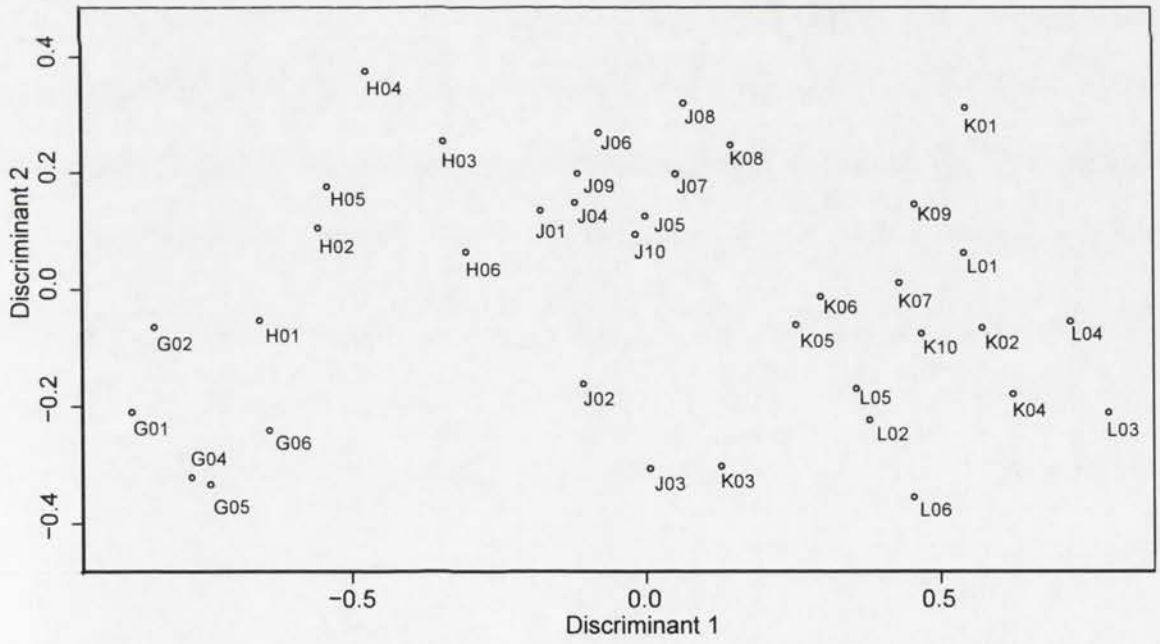

Figure 7.6: Nonmetric multidimensional scaling chi-squared selected taxa from the southern Indian Ocean census data. Whilst assemblages K and L are not separable, four groupings are discernable - assemblages G (assuming site H01 is a member), H, J, and a combined K/L.

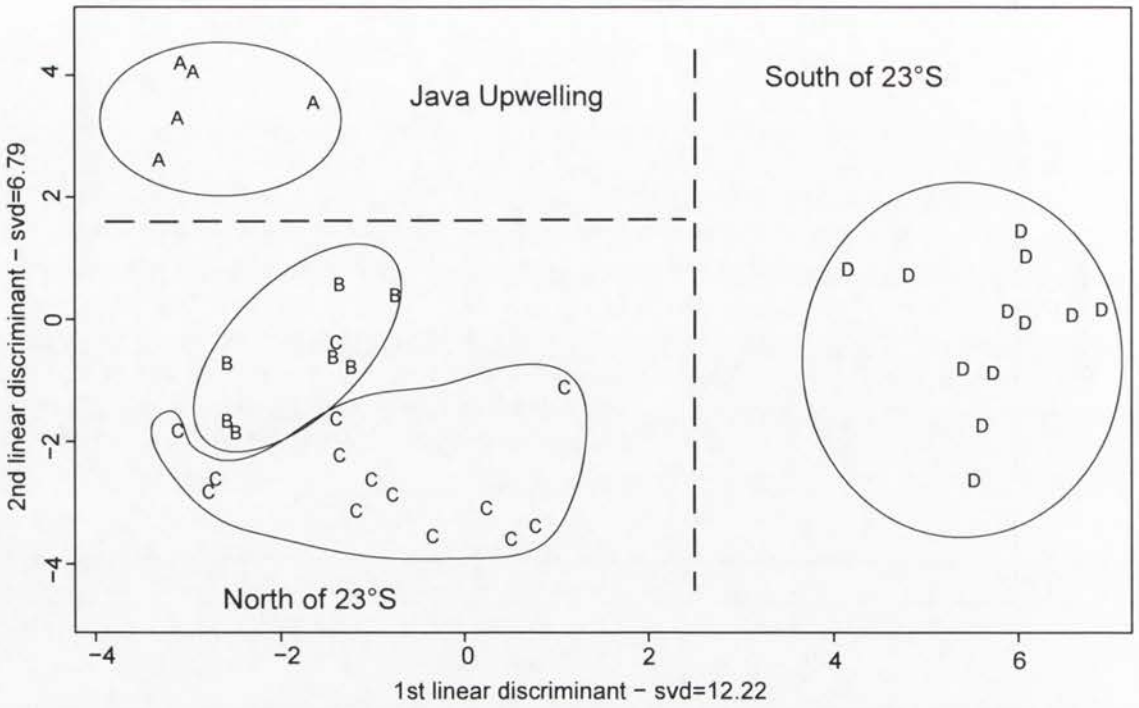

Figure 7.7: Eastern Indian Ocean - linear discriminant analysis plot with input assemblages determined from Single-Run clustering using chi-squared selected taxa. Note that, whereas assemblages A and D are widely separated, assemblages B and C could be a single assemblage.

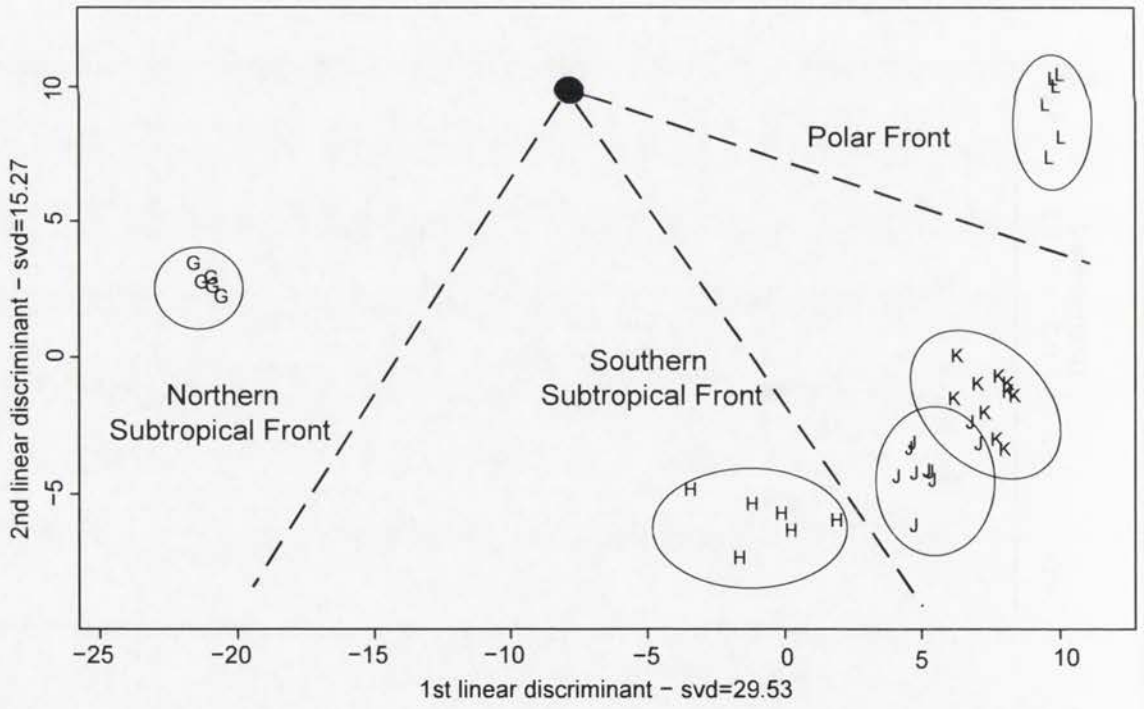

Figure 7.8: Southern Indian Ocean - linear discriminant analysis plot with input assemblages determined from Single-Run clustering using chi-squared selected taxa. Note that assemblages G and L are widely separated from the others. By contrast, assemblages J and K overlap or two sites are incorrectly identified as J members.

7.1.1.4. Summary of assemblage identification

Single-Run clustering allowed the partitioning of the EIO into four assemblages (hereafter referred to as assemblages A-D) although the evidence for the partition between assemblages B and C (an east-west line at 16.9°S) is tenuous. Applying the Single-Run technique to census data consisting of taxa selected by Indicator Species Analysis (Dufrêne and Legendre, 1997) or by employing the χ^2 test generally emphasised the differences between the assemblages, allowing assignment of sites to assemblage to be refined. [Note: the application of CCA caused assemblages B and D to be subdivided, giving six EIO assemblages in all – see §7.2.2 and Figure 9.1 below.]

Single-Run clustering suggested five assemblages in the SIO (labelled G-L). The distinctions between the assemblages was much more clear-cut than for the EIO and runs using selected taxa contributed little extra.

The conclusions from Single-Run clustering were largely confirmed by the Monte Carlo techniques. The EIO LDA plot (Figure 7.7) brings out the existence of at least three assemblages in the EIO whilst suggesting there is little to distinguish assemblage B from assemblage C. The CA (Figure 7.3), the NMDS (Figure 7.5), the LDA (Figure 7.7), and WA-PLS (Figure 7.10) results all support three, possibly four, assemblages in the EIO whilst showing little difference between assemblages B and C.

The SIO LDA plot (Figure 7.8) clearly partitions five assemblages. Similarly, the output of correspondence analysis (Figure 7.4), that of WA-PLS (Figures 7.9 and 7.11), and of NMDS (Figure 7.6), all lead to the same conclusion: there are five assemblages in the SIO.

The SIO LDA plot (Figure 7.8) suggests two sites assigned to the J assemblage might possibly be reassigned to K. Unfortunately, the software for linear discriminant analysis (*R:lda*) (Venables and Ripley, 2002) appears to have no provision for labelling individual sites and, thus, it is not possible to say which three sites should, perhaps, be reassigned. However, WA-PLS Monte Carlo output (Figure 7.11) points to the possibility that sites MD88-764 (J03), MD94-104 (J07), MD02-2486 (J08), and MD94-107 (J10) could constitute an additional cluster between J and K and, geographically, they lie between J and K. The strength of this evidence is diminished by the fact that both LDA and WA-PLS require the prior assignment of assemblages: those methods which do not require a prior assignment do not provide such strong evidence for the additional assemblage. Correspondence analysis (which assumes normality of taxon distribution over the explanatory variable gradient) places the sites between assemblages J and K (Figure 7.4), as does NMDS (Figure 7.6) which demands no prior assumptions and which Minchin (1987) describes as "the most robust unconstrained ordination method in community ecology".

Thus, the evidence for the addition of an assemblage or the reassignment of sites MD88-764 (J03), MD94-104 (J07), MD02-2486 (J08), and MD94-107 (J10) to assemblage K is insufficiently strong to settle for a change. Consequently they have been left in assemblage J. In contrast, the evidence for a reassignment for MD94-09B (H01) to assemblage G is very strong. Although the clustering techniques and LDA place it in assemblage H and WA-PLS produces no evidence, both NMDS and CA place it clearly in assemblage G and, geographically, this appears to be the correct grouping and it was reassigned, when appropriate, for reconstruction purposes. Similar arguments support the reassignment of MD04-2714 (L01) and MD88-765 (L02) to assemblage K and this also was done for reconstructions.

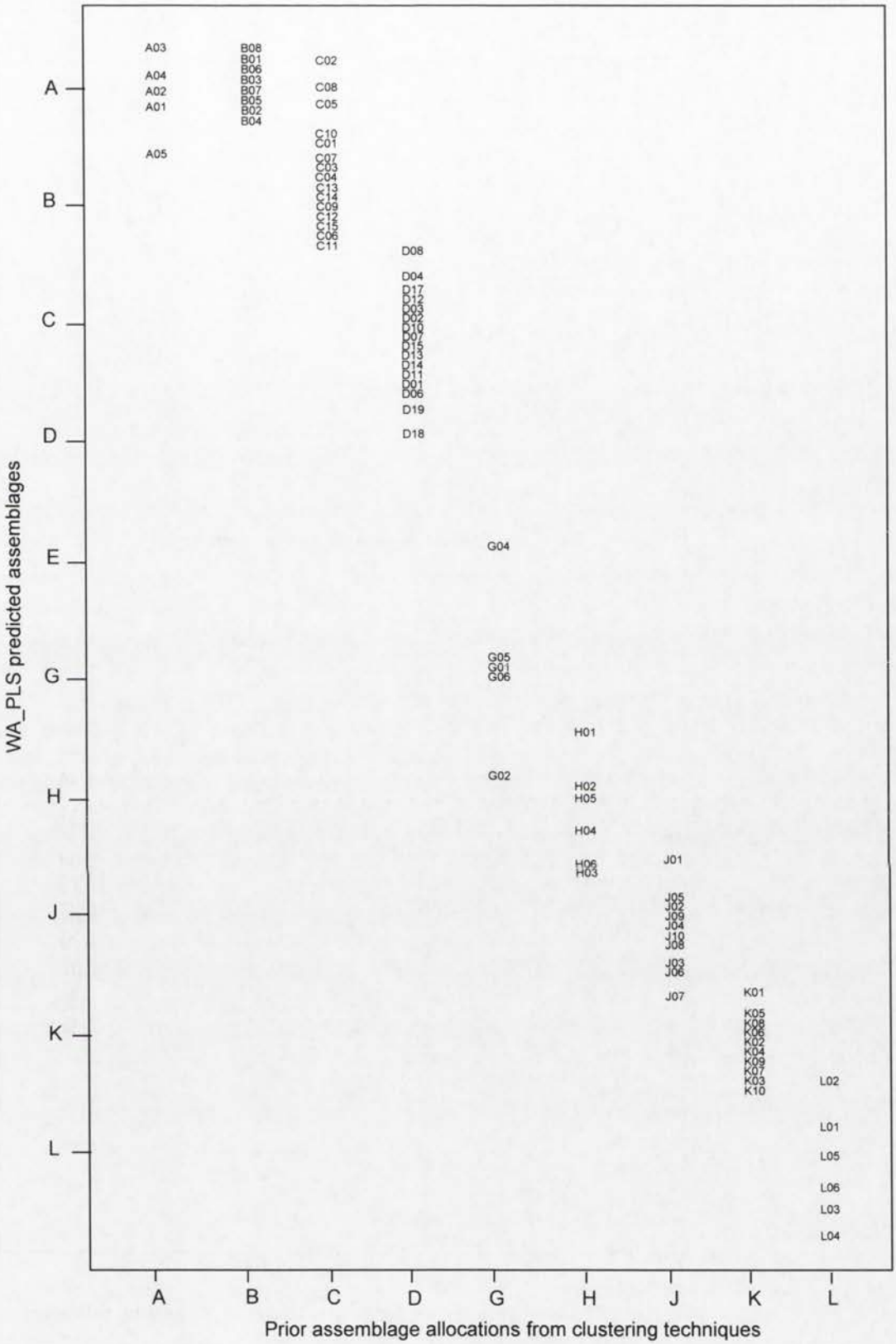

Figure 7.9: WA-PLS assemblage predictions plotted against the assemblage allocations from the Single-Run clustering technique applied to the combined eastern and southern Indian Ocean census counts. Rather than refining the cluster allocations, the predictions tend to indicate the quality of the clustering by the extent to which the predictions do or do not overlap. However, there is some suggestion that sites G02, H01, J01 K01, and L02 should be reassigned to assemblages H, G, H, J, and K respectively.

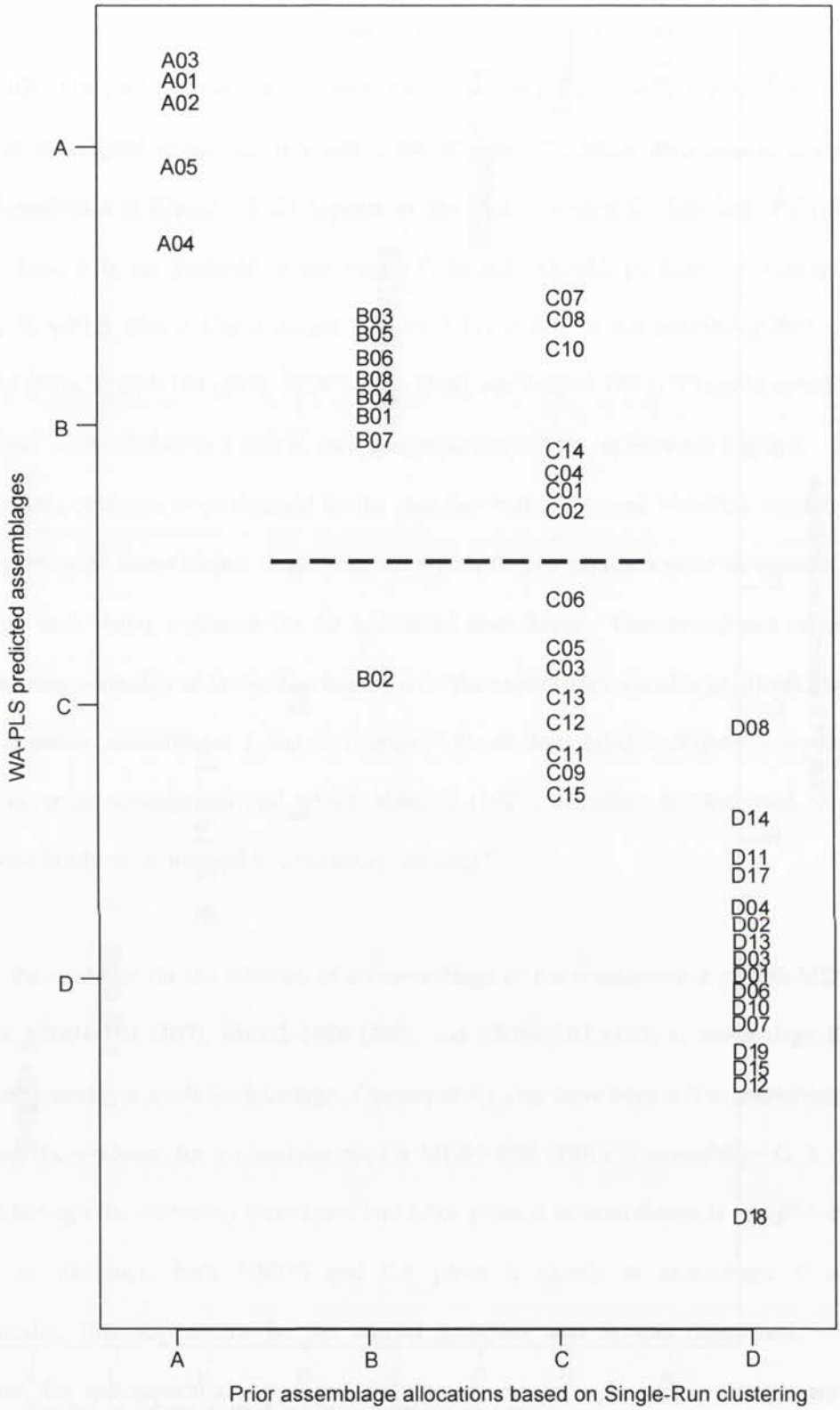

Figure 7.10: WA-PLS predictions of eastern Indian Ocean assemblages using Single-Run clusters derived from chi-squared selected taxa. The plot shows that A and D are distinct assemblages but that B and C may be a single entity. Alternatively, the "B" and "C" sites above the dotted line constitute one assemblage and those below another. Some site labels have been moved slightly for legibility but the vertical spread of the predicted assemblages have been maintained.

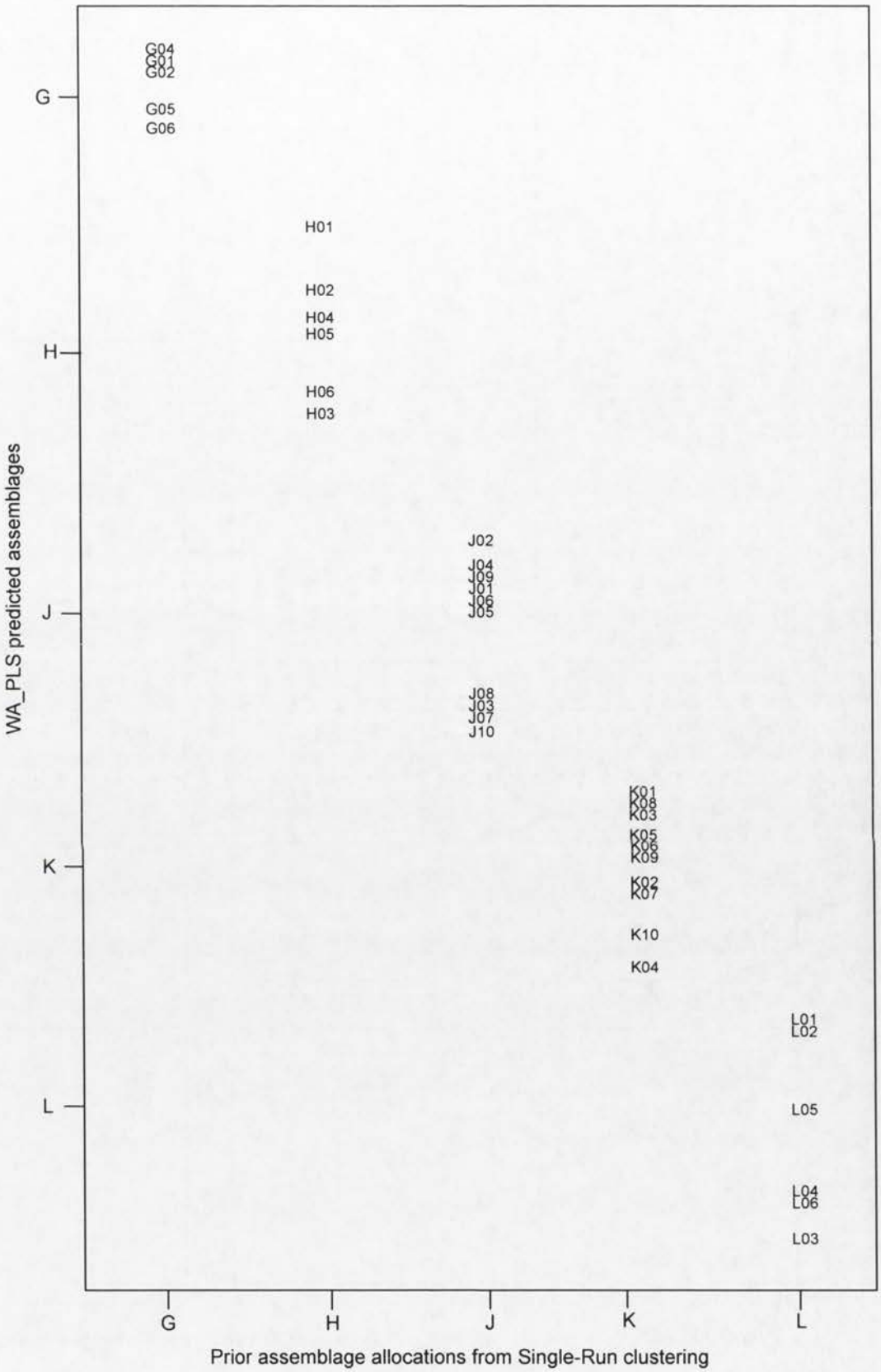

Figure 7.11: WA-PLS predictions of assemblages from Single-Run clustering applied to the southern Indian Ocean census counts. The lack of overlaps between the WA-PLS predicted assemblages indicates the strength of the assemblage assignments.

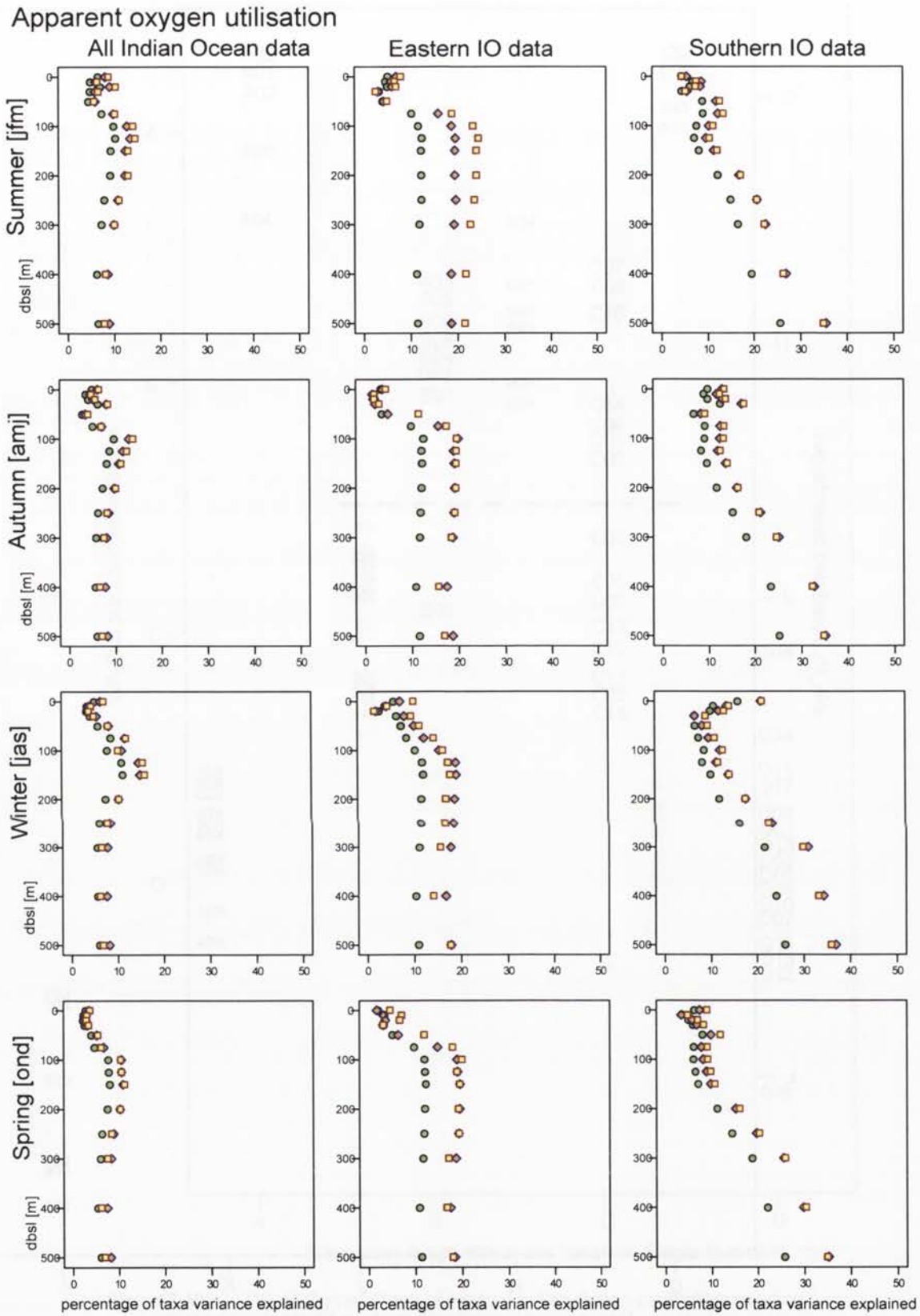

Figure 7.12a: The percentage of taxa variance explained by apparent oxygen utilisation for the four (austral) seasons. Plots are provided for all the radiolarian census data and for the eastern and southern sectors of the Indian Ocean. Circles indicate all the taxa were included, diamonds the Dufrêne and Legendre significant taxa alone, and squares the chi-squared significant taxa alone.

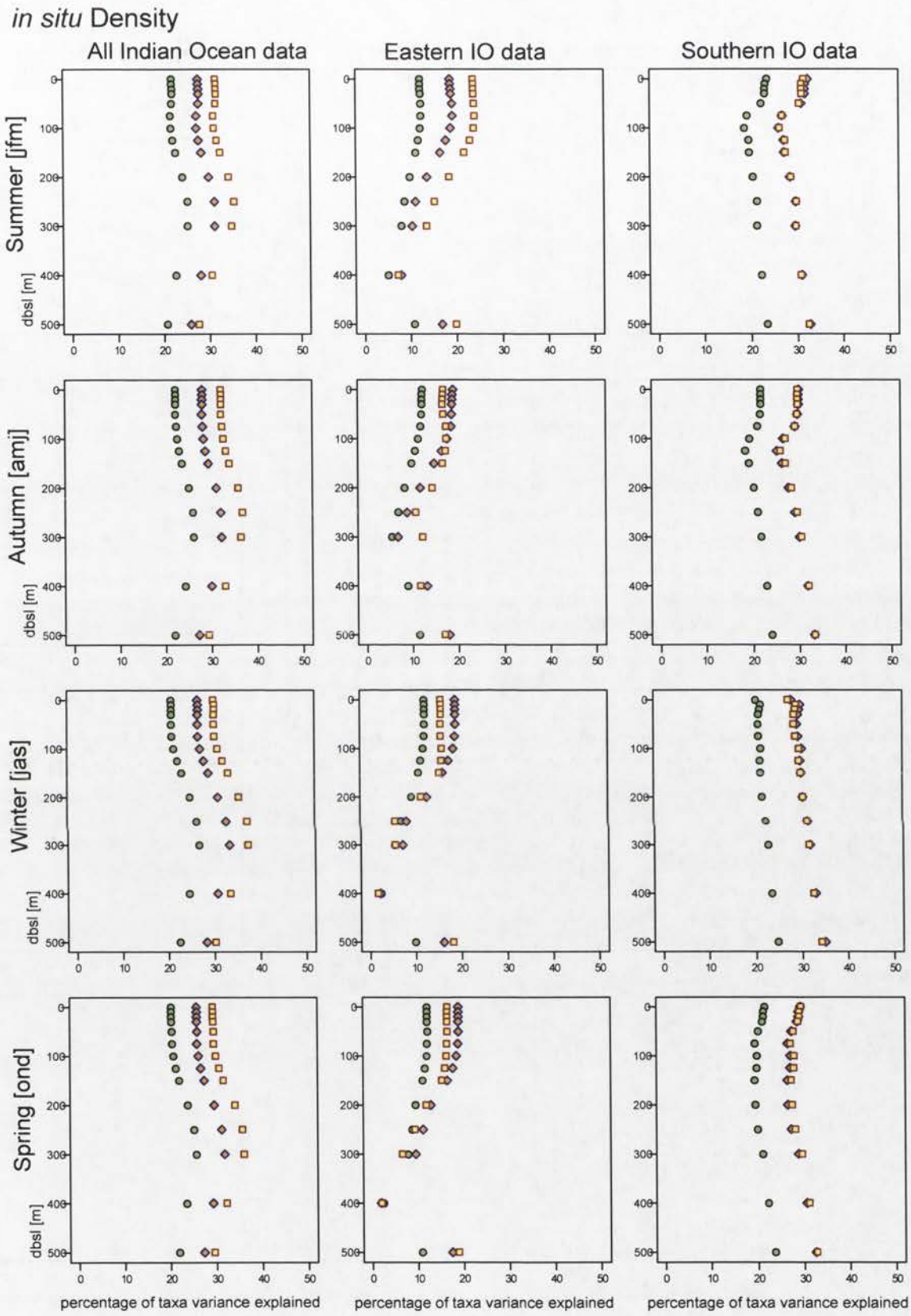

Figure 7.12b: The percentage of taxa variance explained by *in situ* density for the four (austral) seasons. Plots are provided for all the radiolarian census data and for the eastern and southern sectors of the Indian Ocean. Circles indicate all the taxa were included, diamonds the Dufrêne and Legendre significant taxa alone, and squares the chi-squared significant taxa alone.

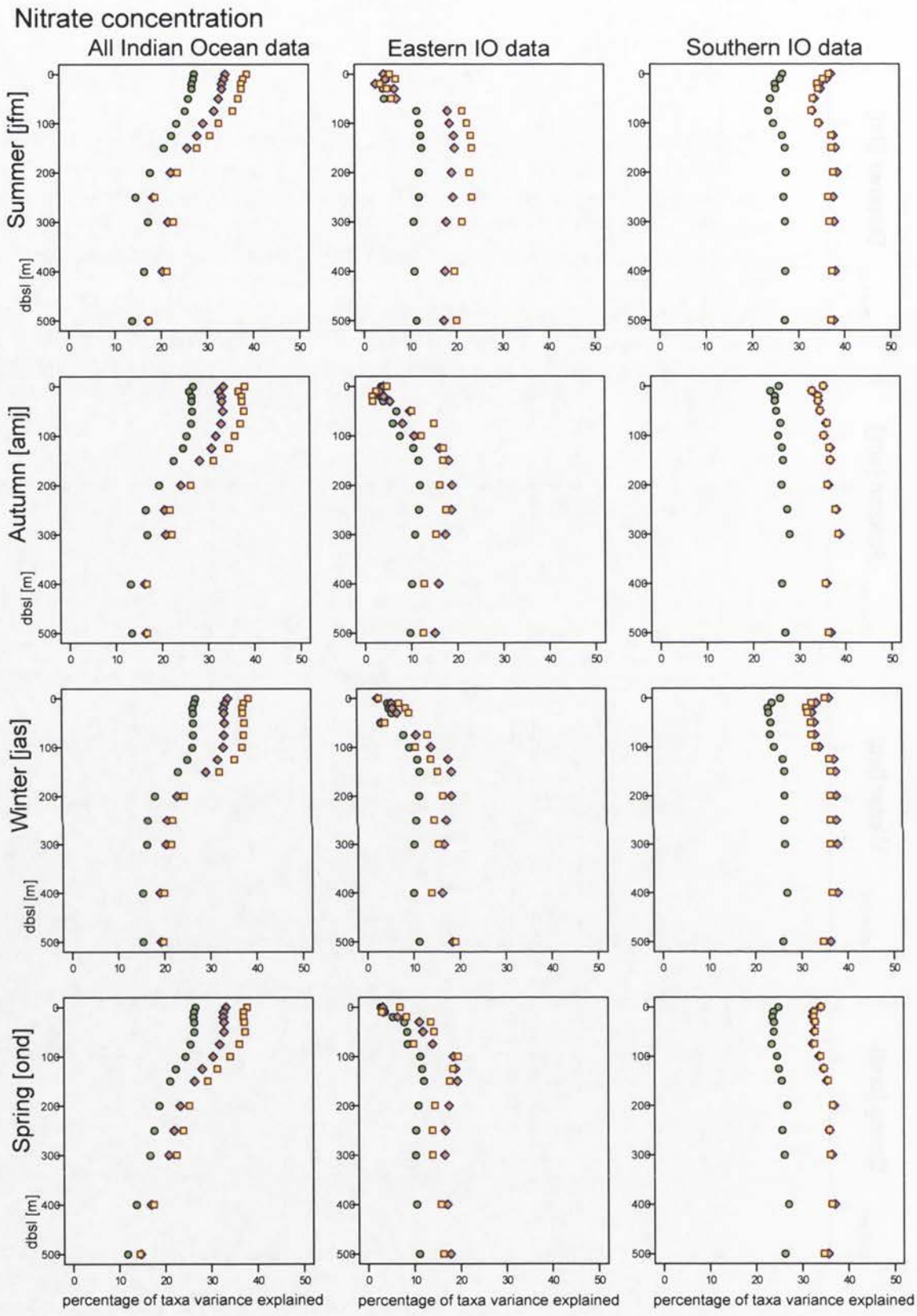

Figure 7.12c: The percentage of taxa variance explained by nitrate concentration for the four (austral) seasons. Plots are provided for all the radiolarian census data and for the eastern and southern sectors of the Indian Ocean. Circles indicate all the taxa were included, diamonds the Dufrêne and Legendre significant taxa alone, and squares the chi-squared significant taxa alone.

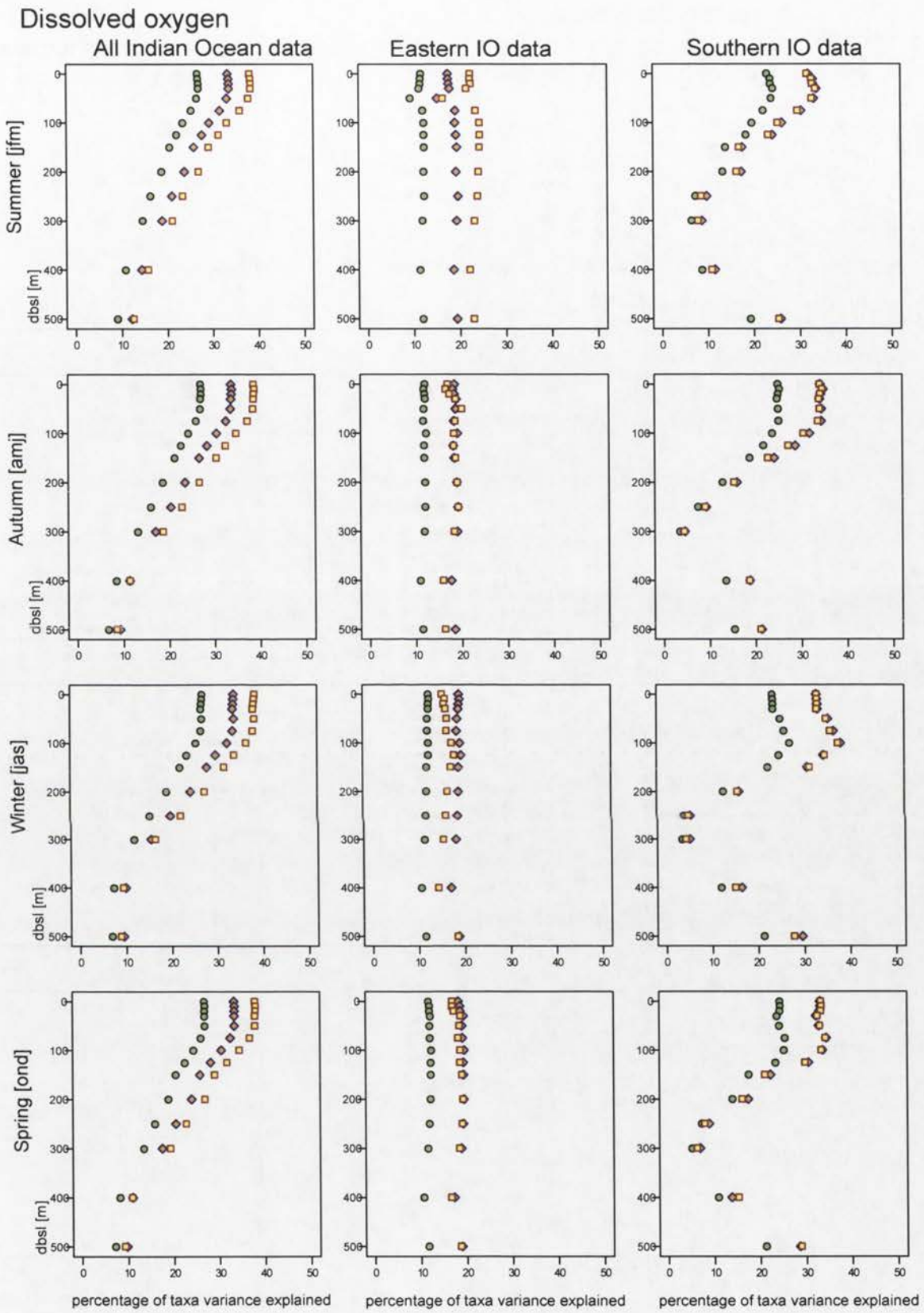

Figure 7.12d: The percentage of taxa variance explained by dissolved oxygen for the four (austral) seasons. Plots are provided for all the radiolarian census data and for the eastern and southern sectors of the Indian Ocean. Circles indicate all the taxa were included, diamonds the Dufrêne and Legendre significant taxa alone, and squares the chi-squared significant taxa alone.

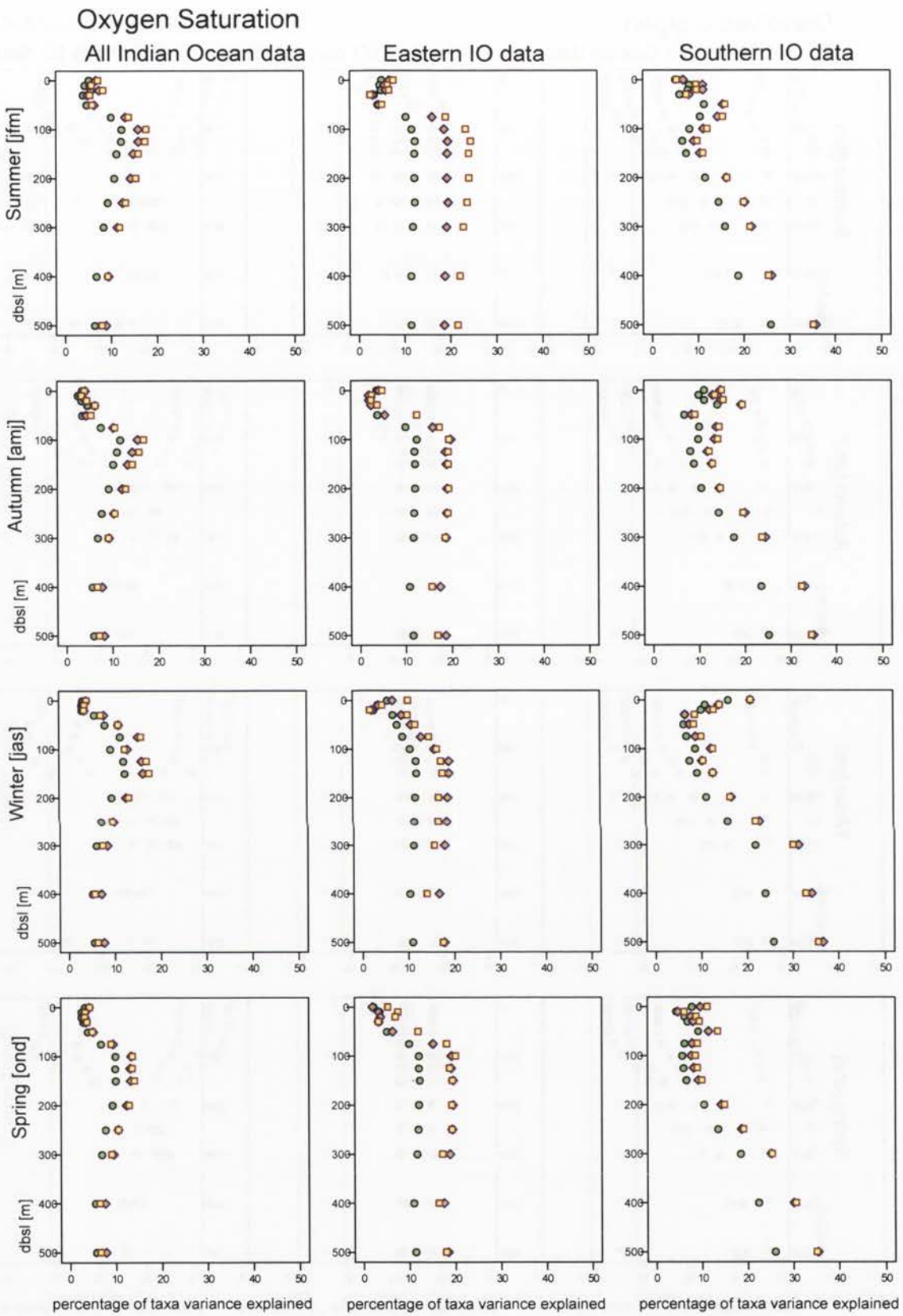

Figure 7.12e: The percentage of taxa variance explained by oxygen saturation for the four (austral) seasons. Plots are provided for all the radiolarian census data and for the eastern and southern sectors of the Indian Ocean. Circles indicate all the taxa were included, diamonds the Dufrêne and Legendre significant taxa alone, and squares the chi-squared significant taxa alone.

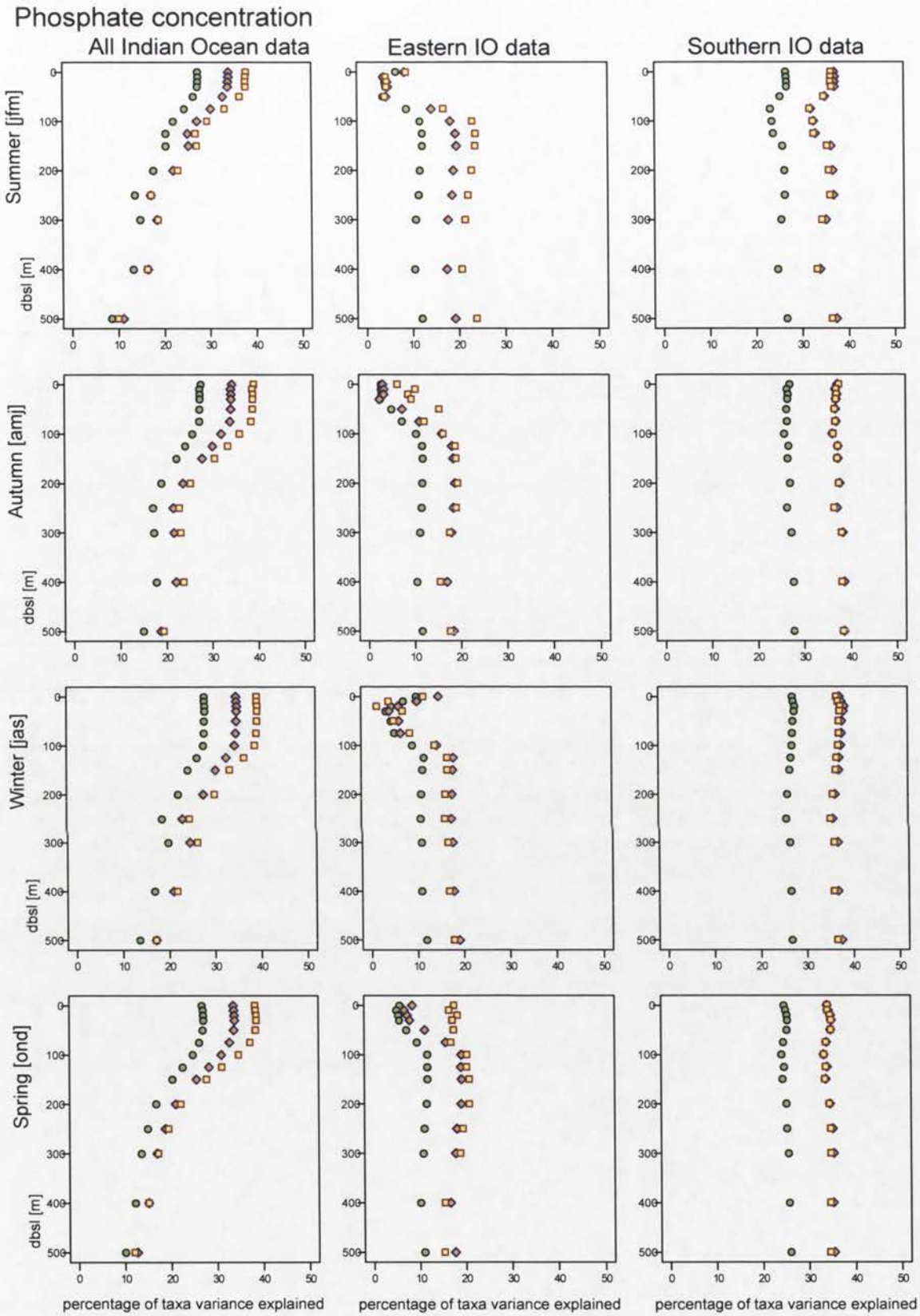

Figure 7.12f: The percentage of taxa variance explained by phosphate concentration for the four (austral) seasons. Plots are provided for all the radiolarian census data and for the eastern and southern sectors of the Indian Ocean. Circles indicate all the taxa were included, diamonds the Dufrêne and Legendre significant taxa alone, and squares the chi-squared significant taxa alone.

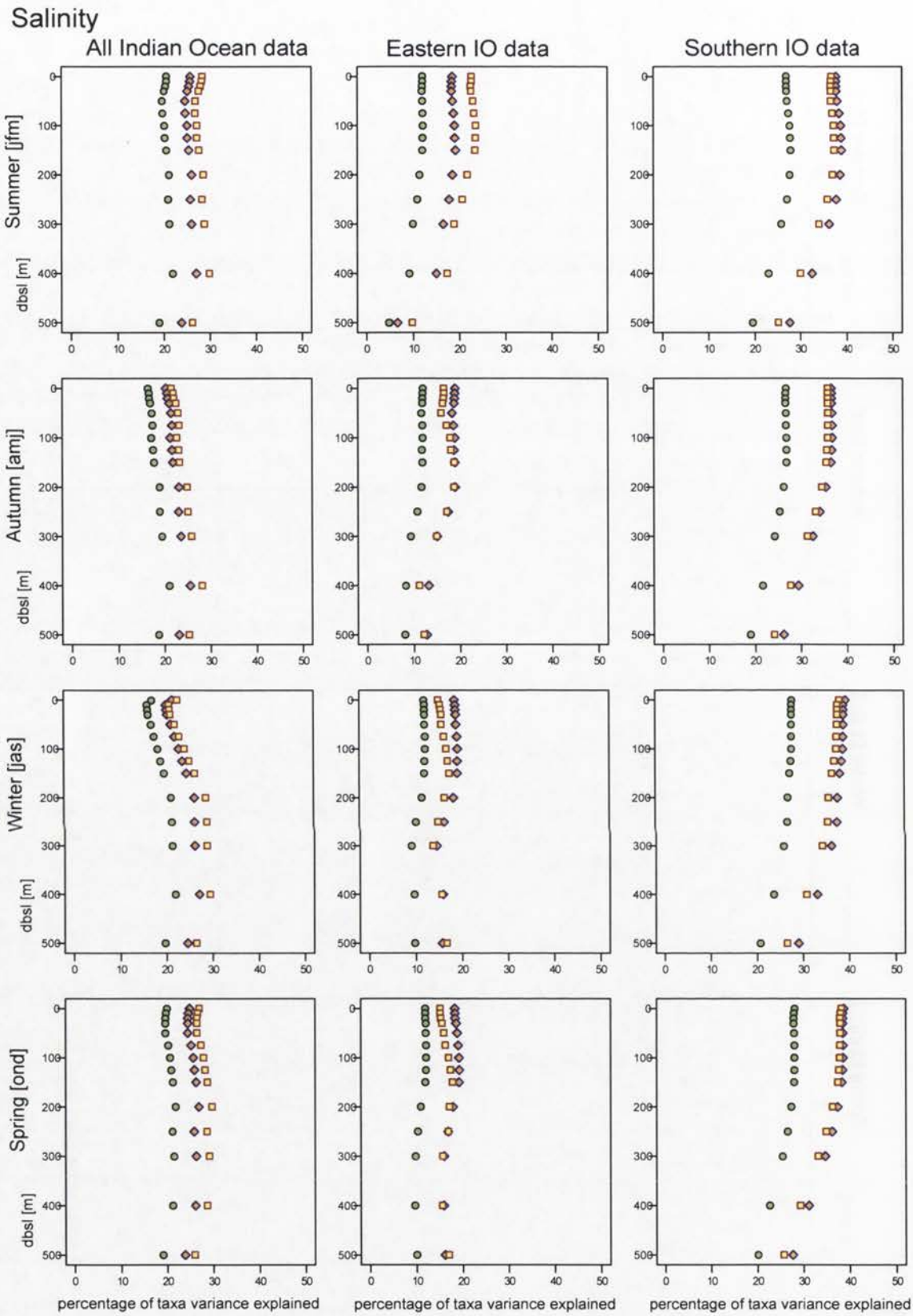

Figure 7.12g: The percentage of taxa variance explained by salinity for the four (austral) seasons. Plots are provided for all the radiolarian census data and for the eastern and southern sectors of the Indian Ocean. Circles indicate all the taxa were included, diamonds the Dufrêne and Legendre significant taxa alone, and squares the chi-squared significant taxa alone.

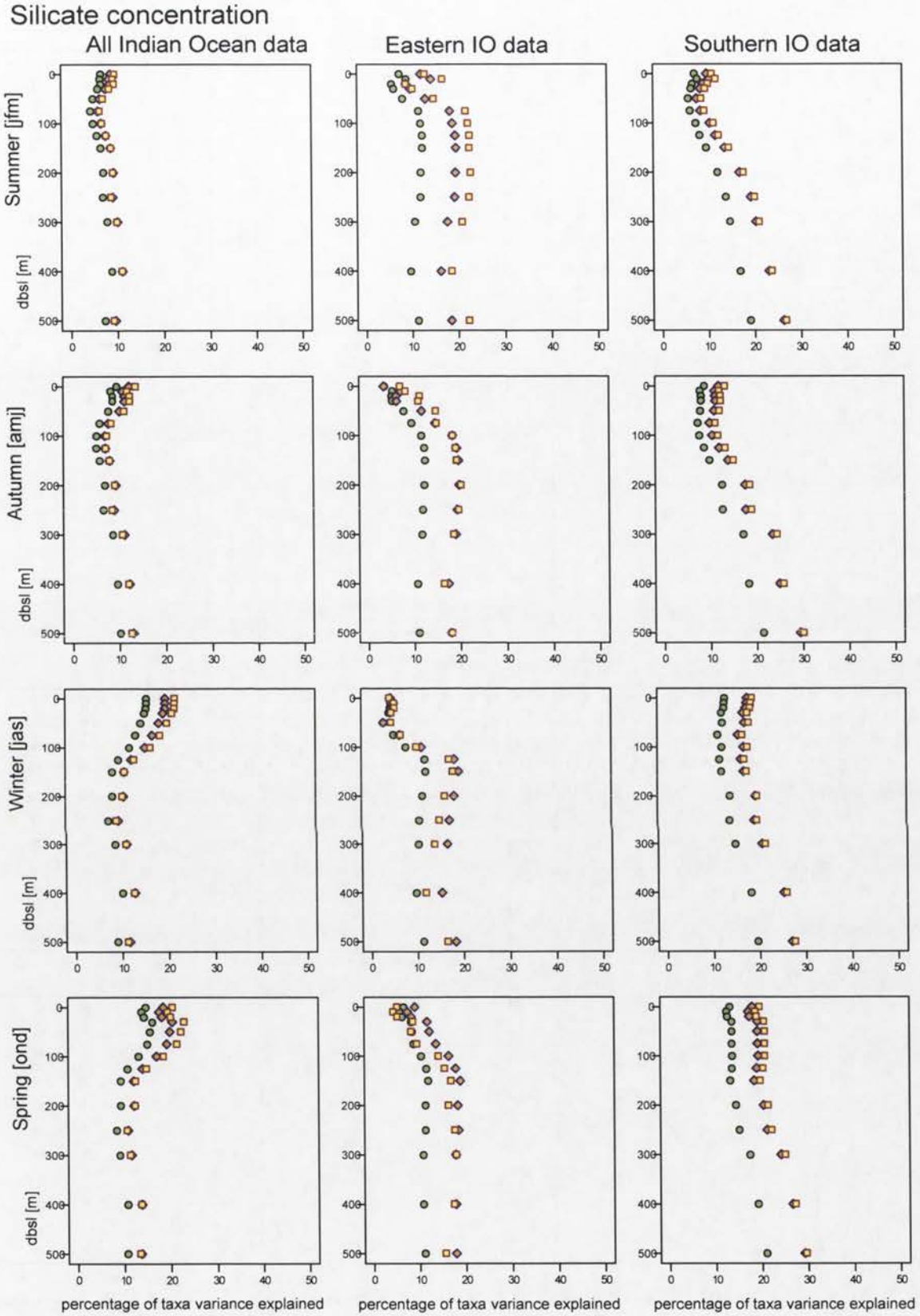

Figure 7.12h: The percentage of taxa variance explained by silicate concentration for the four (austral) seasons. Plots are provided for all the radiolarian census data and for the eastern and southern sectors of the Indian Ocean. Circles indicate all the taxa were included, diamonds the Dufrêne and Legendre significant taxa alone, and squares the chi-squared significant taxa alone.

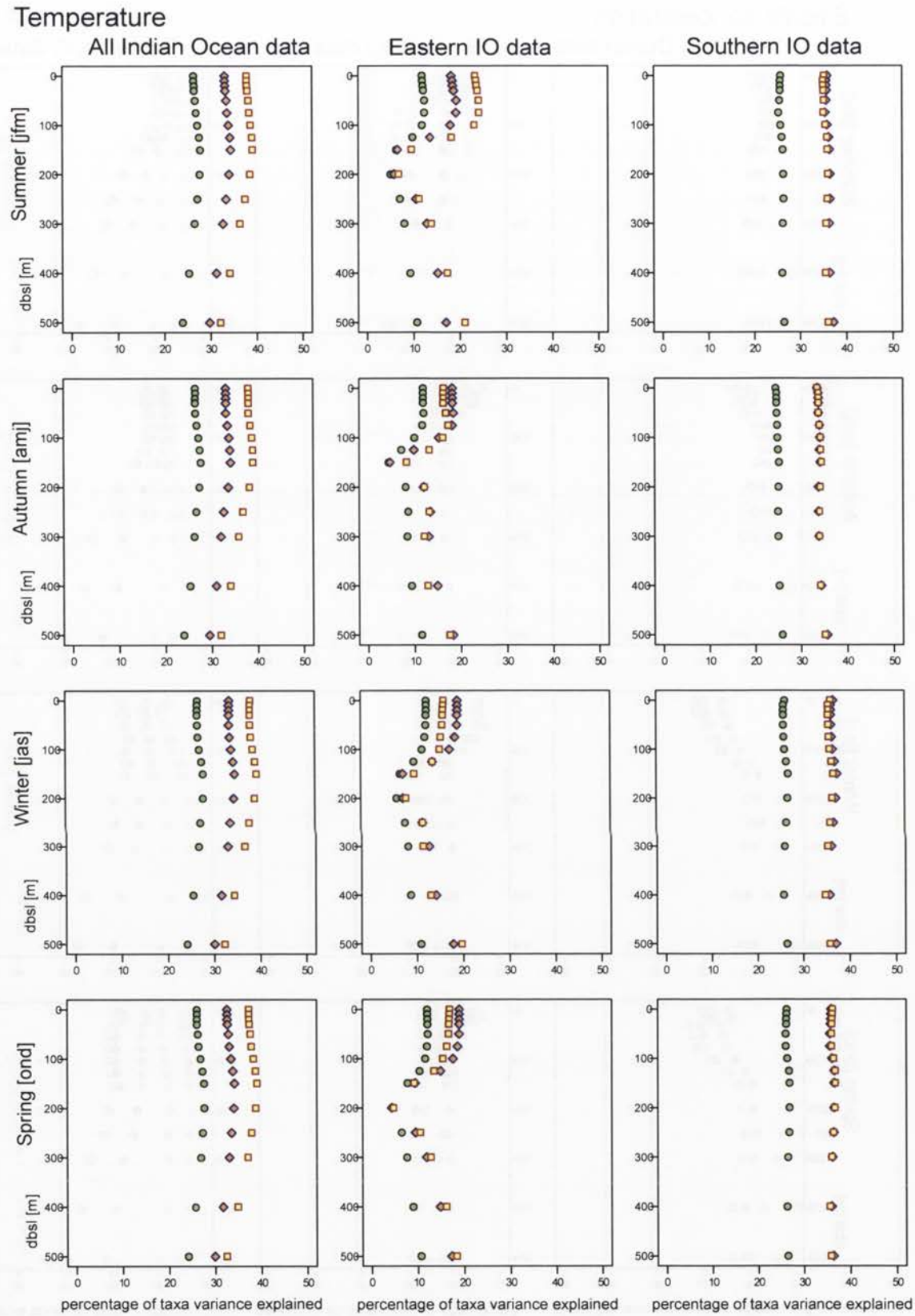

Figure 7.12i: The percentage of taxa variance explained by sea temperature for the four (austral) seasons. Plots are provided for all the radiolarian census data and for the eastern and southern sectors of the Indian Ocean. Circles indicate all the taxa were included, diamonds the Dufrêne and Legendre significant taxa alone, and squares the chi-squared significant taxa alone.

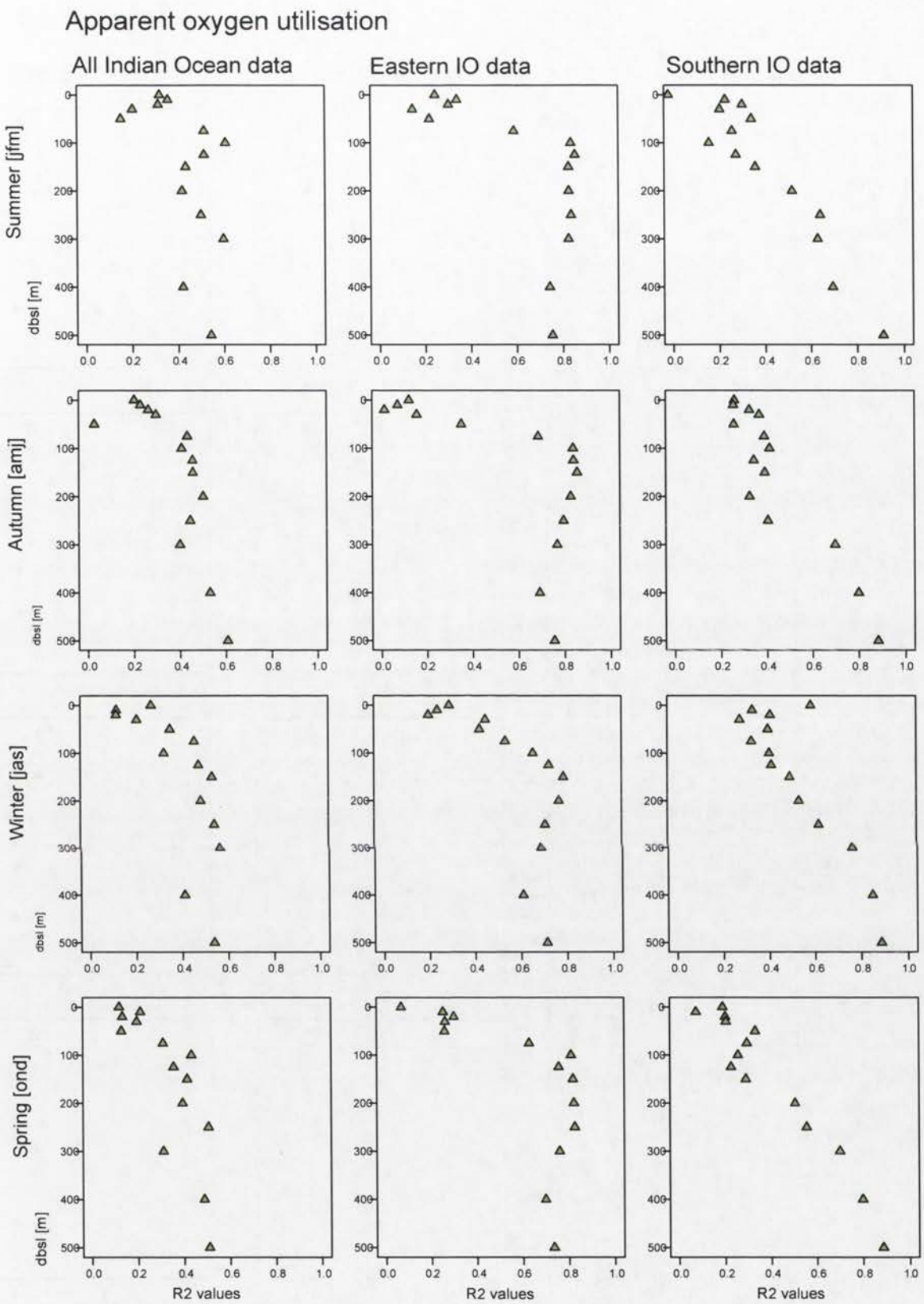

Figure 7.13a: R2 values for the prediction of apparent oxygen utilisation for the four (austral) seasons from WA-PLS applied to all the radiolarian census data, and to the eastern and southern sectors of the Indian Ocean separately. Only the more significant species based on chi-squared tests were included in the census data

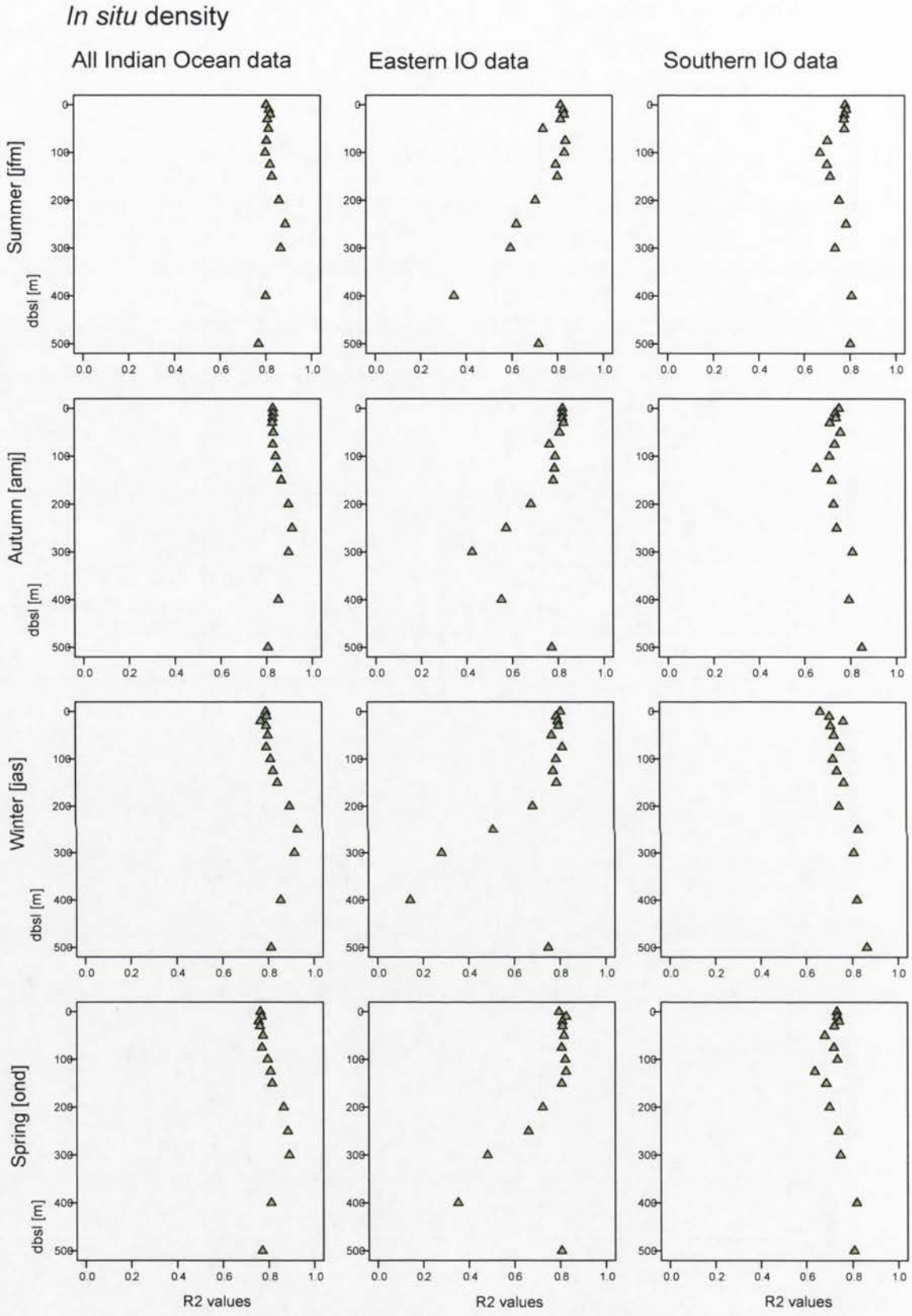

Figure 7.13b: R2 values for the prediction of *in situ* density for the four (austral) seasons from WA-PLS applied to all the radiolarian census data, and to the eastern and southern sectors of the Indian Ocean separately. Only the more significant species as determined by chi-squared tests were included in the census data.

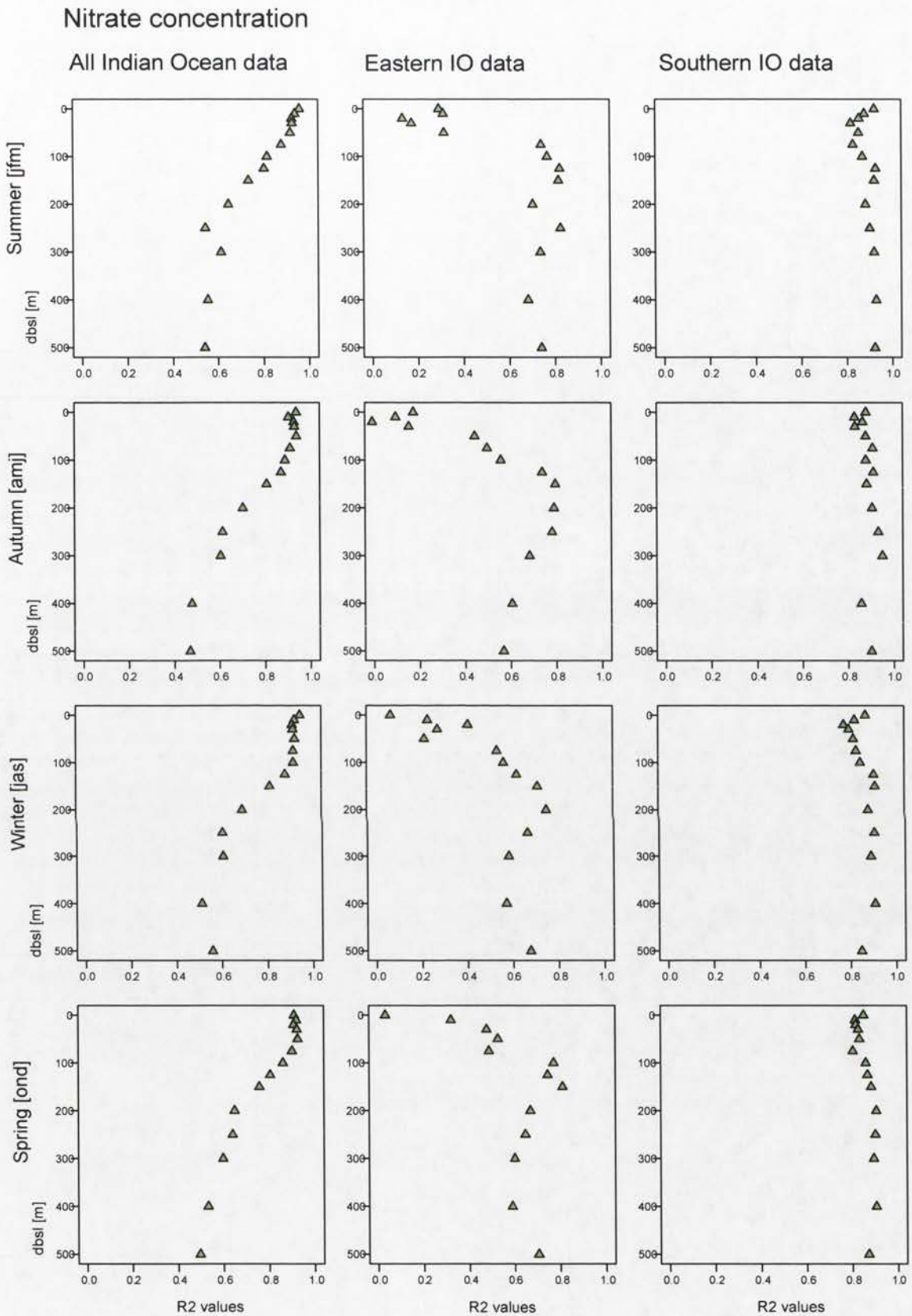

Figure 7.13c: R2 values for the prediction of nitrate concentration for the four (austral) seasons from WA-PLS applied to all the radiolarian census data, and to the eastern and southern sectors of the Indian Ocean separately. Only the more significant species as determined by chi-squared tests were included in the census data.

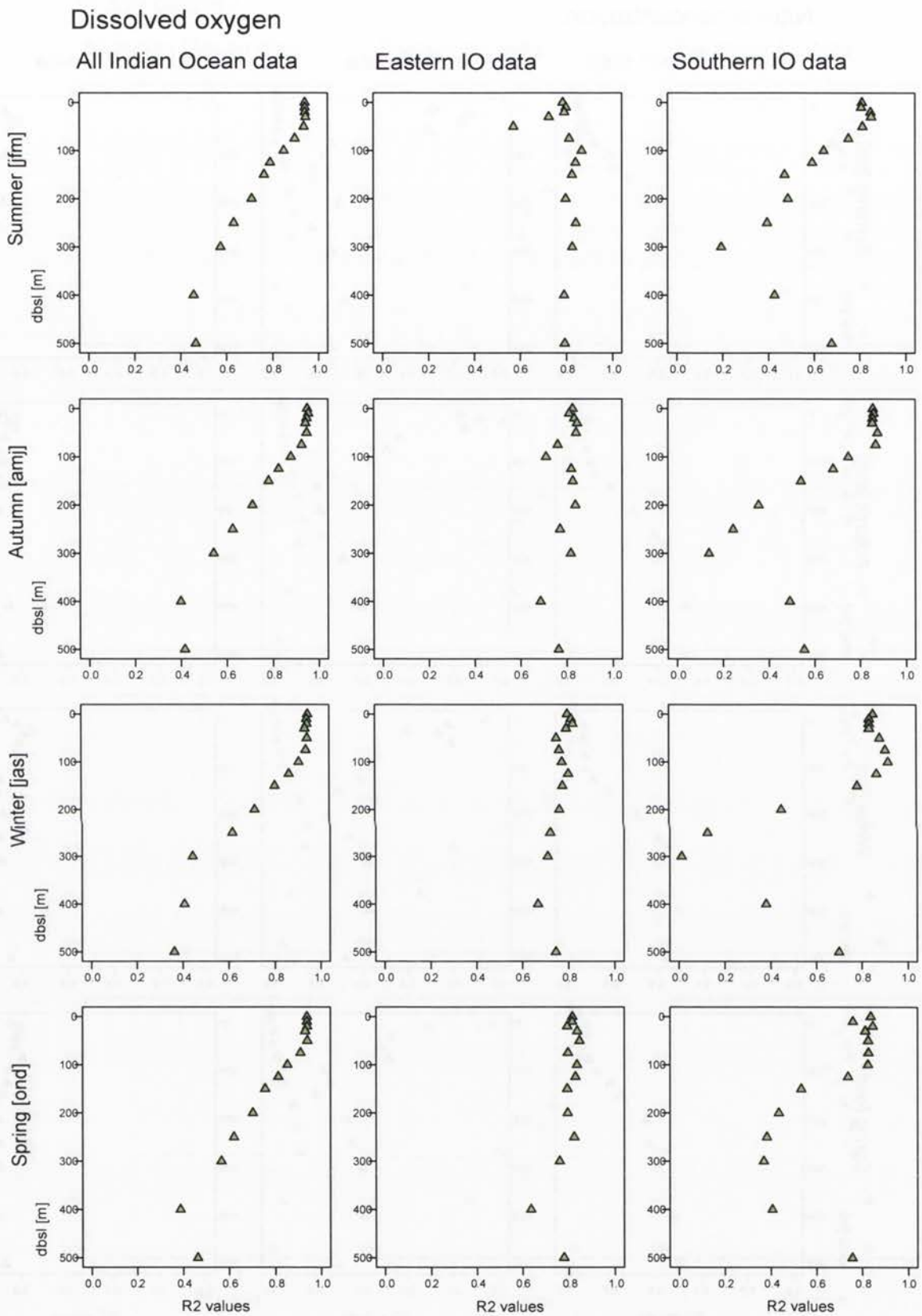

Figure 7.13d: R2 values for the prediction of dissolved oxygen for the four (austral) seasons from WA-PLS applied to all the radiolarian census data, and to the eastern and southern sectors of the Indian Ocean separately. Only the more significant species as determined by chi-squared tests were included in the census data.

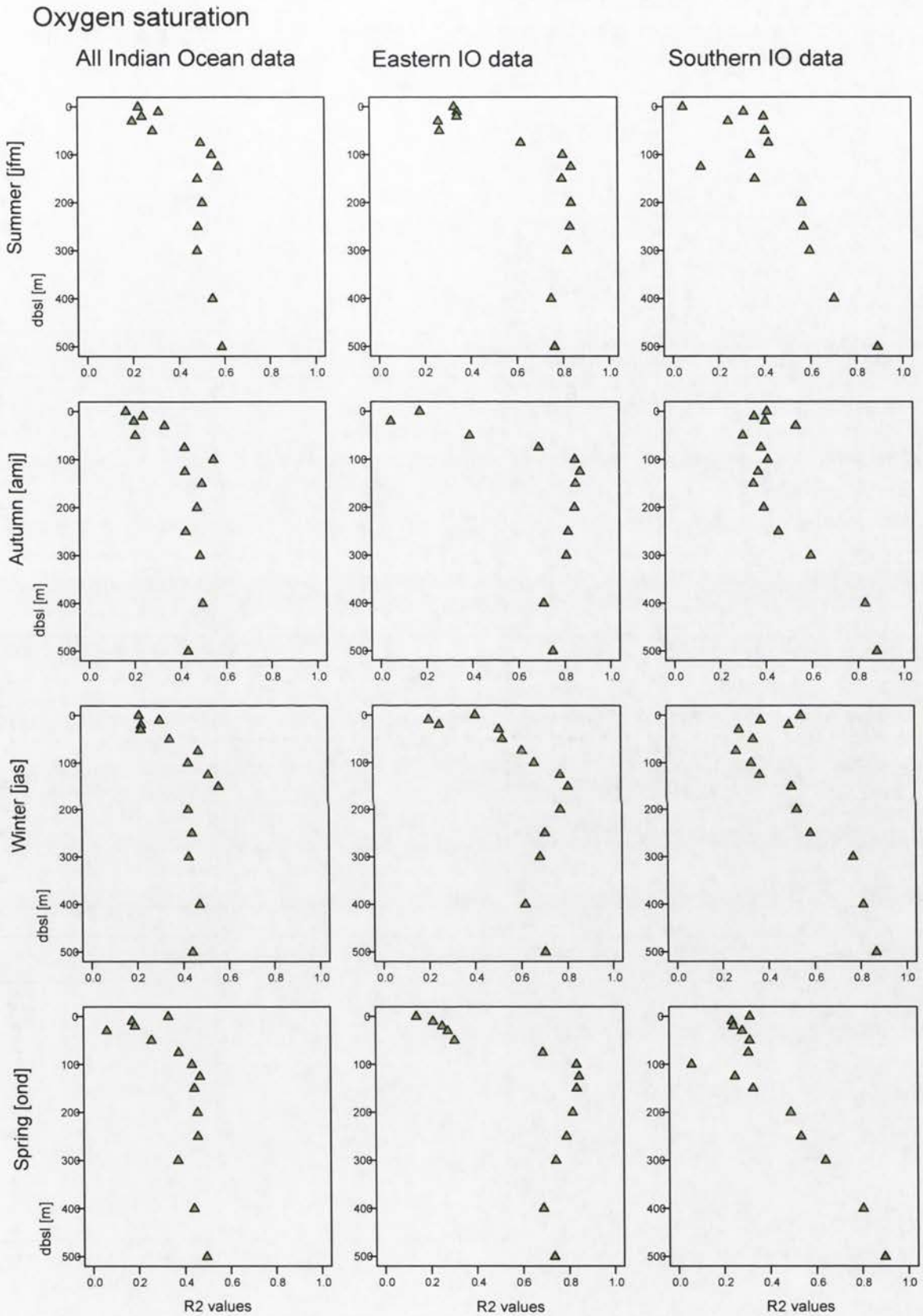

Figure 7.13e: R2 values for the prediction of oxygen saturation for the four (austral) seasons from WA-PLS applied to all the radiolarian census data, and to the eastern and southern sectors of the Indian Ocean separately. Only the more significant species as determined by chi-squared tests were included in the census data.

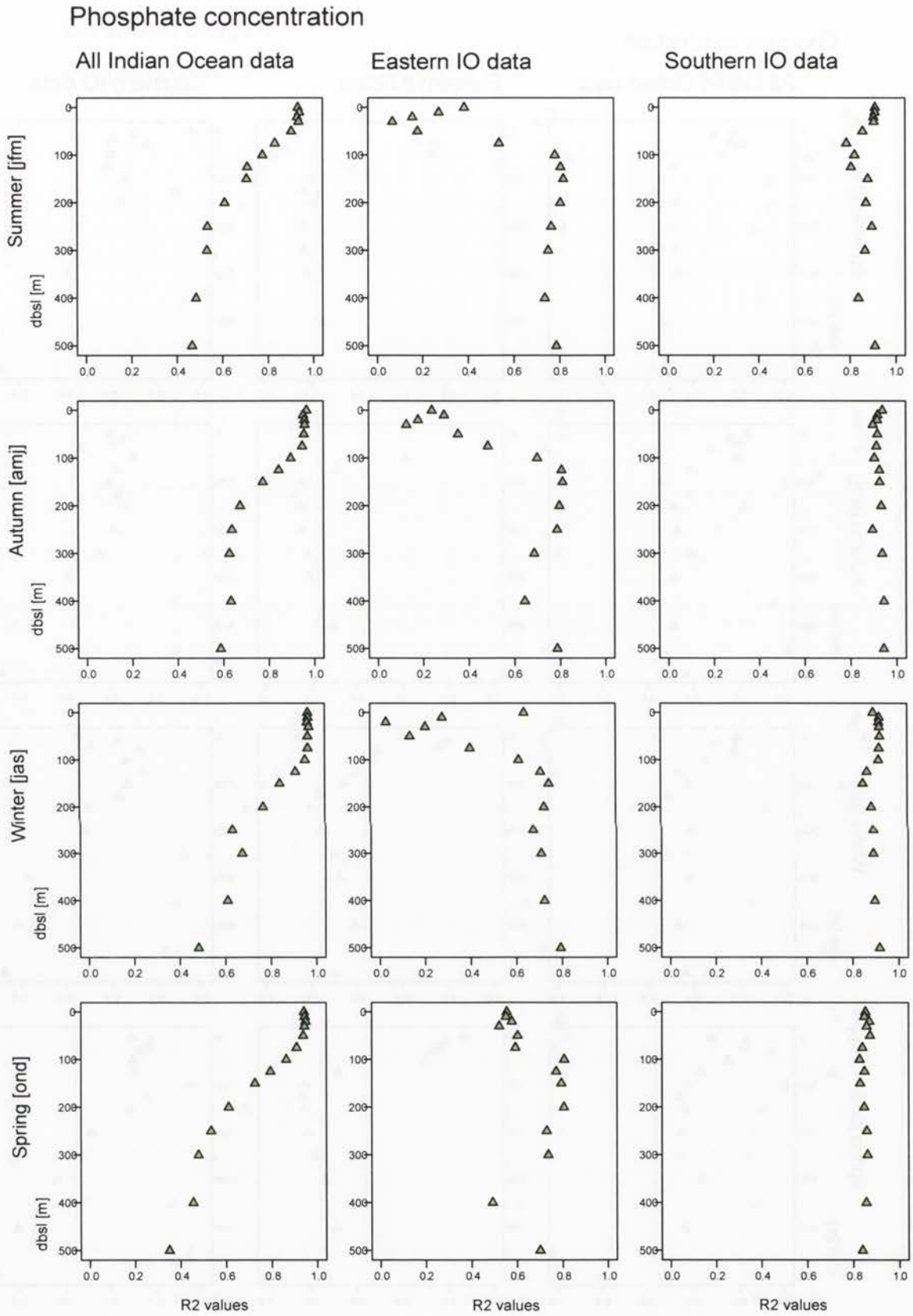

Figure 7.13f: R2 values for the prediction of phosphate concentration for the four (austral) seasons from WA-PLS applied to all the radiolarian census data, and to the eastern and southern sectors of the Indian Ocean separately. Only the more significant species as determined by chi-squared tests were included in the census data.

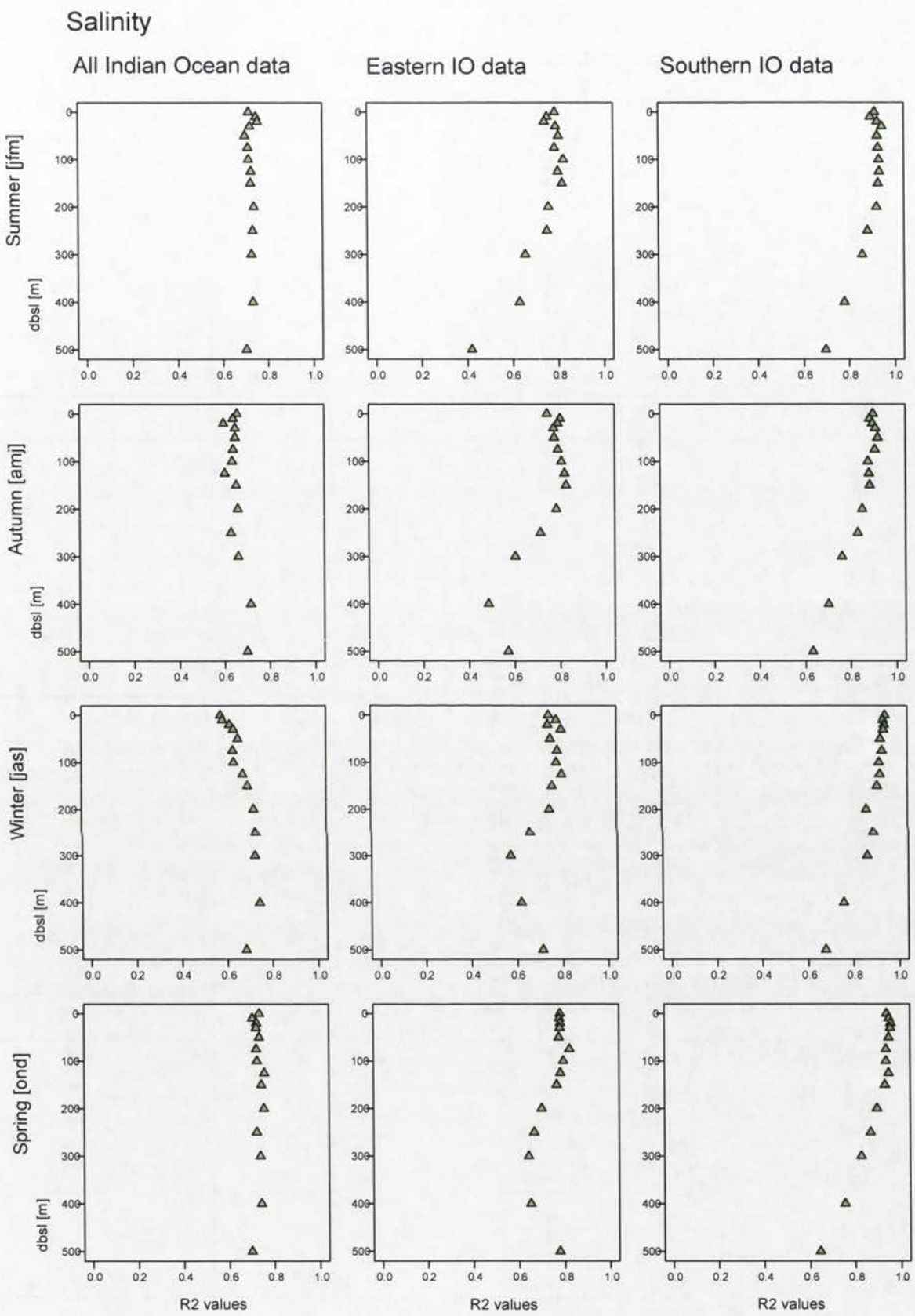

Figure 7.13g: R2 values for the prediction of salinity for the four (austral) seasons from WA-PLS applied to all the radiolarian census data, and to the eastern and southern sectors of the Indian Ocean separately. Only the more significant species as determined by chi-squared tests were included in the census data.

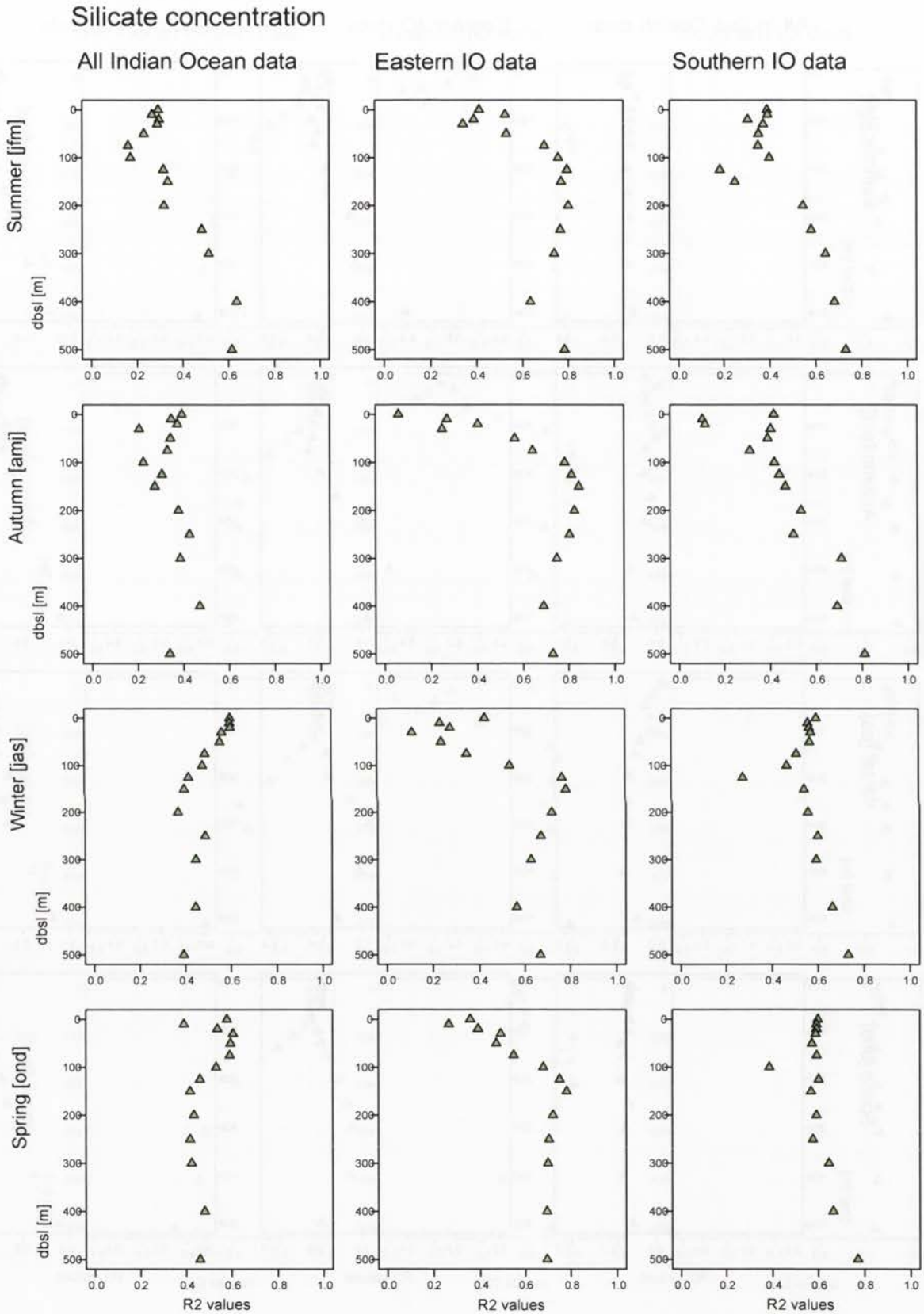

Figure 7.13h: R2 values for the prediction of silicate concentration for the four (austral) seasons from WA-PLS applied to all the radiolarian census data, and to the eastern and southern sectors of the Indian Ocean separately. Only the more significant species as determined by chi-squared tests were included in the census data.

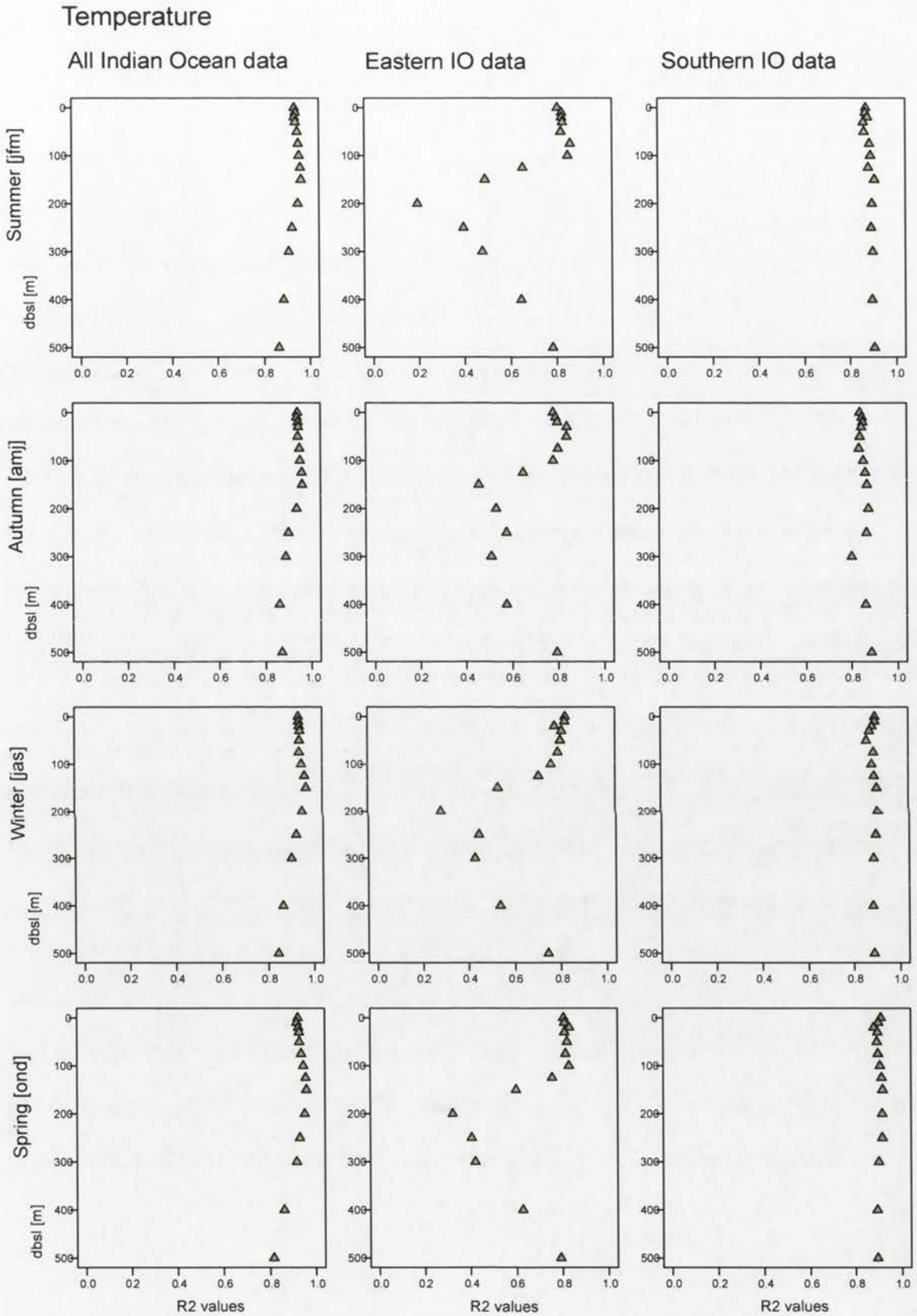

Figure 7.13i; R2 values for the prediction of sea temperature for the four (austral) seasons from WA-PLS applied to all the radiolarian census data, and to the eastern and southern sectors of the Indian Ocean separately. Only the more significant species sa determined by chi-squared tests were included in the census data.

7.2. The association between the radiolarian data and environmental variables
7.2.1. Approach 1: CCA eigenvalues and Approach 2: WA-PLS

Approaches 1 (CCA variance explained) and 2 (WA-PLS R^2 values) can be treated together because their results are very similar in both form and substance. The two techniques were applied to the radiolarian census data combined with each of the nine oceanic environmental variables available from NOAA (see §4.3 above), and salinity-normalised total alkalinity (NTA) and *in situ* density in turn. The percentages of environmental variance explained under Approach 1 are given in Tables 7.4a-c and those for WA-PLS in Table 7.5. All the results, except those for NTA and chlorophyll, were plotted – CCA eigenvalues in Figures 7.12a-i and those for WA-PLS in Figures 7.13a-i. NTA is not plotted because it is derived using Millero *et al's.* (1998) algorithm which only offers ocean surface values. Chlorophyll is omitted because NOAA does not publish data to a sufficient depth below the ocean's surface.

Both CCA eigenvalues and WA-PLS R^2 were evaluated using all taxa, the ISA taxa, and the χ^2 taxa. The WA-PLS plots tend to emphasise the important features of the two sets of plots. [Note: the R^2 values were calculated using *R:R2* which returns the unadjusted R^2, typically an over-optimistic estimator. The method of calculation can result in small negative values – presumably resulting from rounding errors when the sum of squared errors is very close to the total sum of squares.] The CCA eigenvalues and WA-PLS R^2 show a very noticeable difference in the shape of the plotted curves between the EIO and the SIO. The results from the combined IO data tend to be an average of the EIO and SIO results and, as such, provide relatively little information.

The EIO CCA eigenvalue and WA-PLS R^2 responses can be divided into three sets: temperature (~20% of the variance explained from the surface to 125 metres, then declines sharply), dissolved oxygen and salinity (15-20% surface to 500 metres), and, thirdly, AOU

and the nutrients (nitrate, phosphate, and silicate) (close to zero from the surface to ~75 metres in summer and 125 metres for the other seasons, with a sharp increase to 15-20% below that). The SIO responses fall into five sets: temperature (~35% from the surface to 500 metres), salinity (~35% from the surface to 200 metres, declining slowly thereafter), nitrate and phosphate concentrations (again ~35% at all depths but with ~4% fall between from 30-75 metres), dissolved oxygen (close to 30% but drops off sharply below 75 metres, 100 metres in winter), and silicate concentration and oxygen saturation (generally below 15% at all levels). Note that oxygen saturation and *in situ* density are not considered here because of their close relationships with AOU and temperature-salinity respectively.

7.2.2. CCA with CANOCO (Supplement to Approach 1)

Before CCA can be used successfully to establish relationships between census data and several environmental variables simultaneously, the number of environmental variables to consider must be reduced to close to the minimum. Too many constraint variables lessen the proportion each contributes to the species variance and, thus, makes identification of the major contributors more difficult. Because this study uses the full set of WOA-05 oceanic variables, there is also strong correlation between many of the potential explanatory variables. For example, as might be expected, temperature at a particular site will normally only change gradually with increasing depth below sea level, implying a high correlation between temperature values over a range of depths. Thus, it is necessary to start by limiting the number of depths below sea-level considered for any one environmental variable.

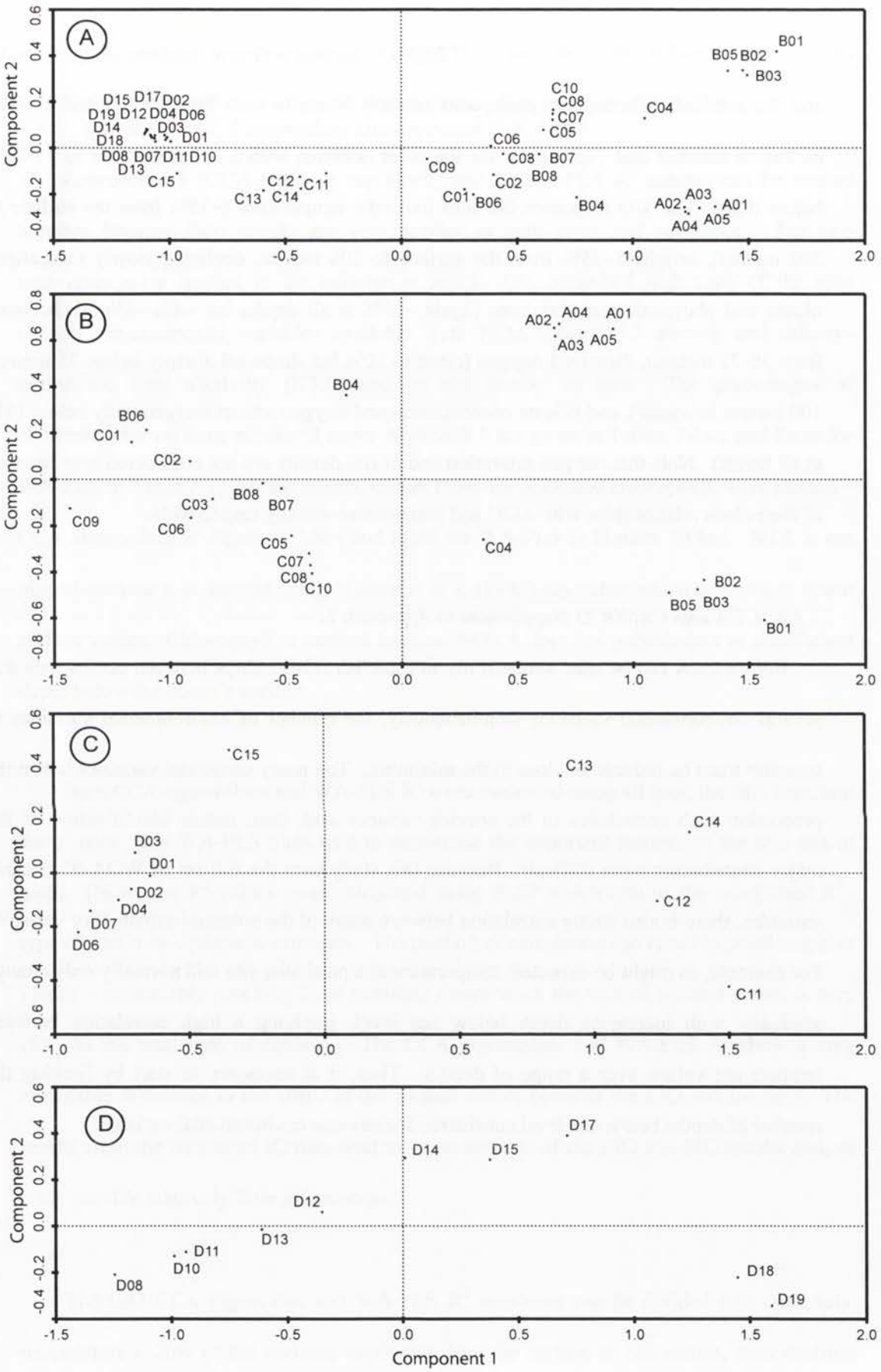

Figure 7.14: PCA for the EIO.
Plot A: the whole EIO. Note the tight clustering of Assemblage D
Plot B: 12-19°S Plot C: 19-27.5°S Plot D: 27.5- 31.5°S.
The labels have been moved slightly whenever necessary for clarity.

Principal components analysis (PCA - ter Braak and Šmilauer, 2004), when applied to the environmental data for the EIO (Table 7.6 and Figure 7.14), yields an eigenvalue of 0.948 for axis 1, suggesting that there is one major factor controlling the clustering of the sample sites. The subsequent eigenvalues indicate there may also be one or two more minor factors. Any of these factors may be a combination of collinear variables. For instance, temperature and salinity in the mixed layer are strongly negatively correlated, so either or both could be explanatory.

Examination of the PCA plot (Figure 7.14) revealed that all the sites D08-19 (which lie between 27.5°S and 31.5°S) were tightly clustered. For the clustering to occur, the value of the all-EIO major factor must be almost constant for these sites but traverse a reasonable gradient between 27.5°S and 12°S – salinity is a good candidate.

Recalculation of the PCA for sites D08-19 alone indicates there is a dominant factor which is different from that for the EIO as a whole. From consideration of the WOA-05 data, temperature seems the strongest candidate – which might imply that, over the whole EIO, the PCA results reflect the effect of a combination of temperature and salinity, with salinity carrying the greater weight. The sites between 12.0°S and 19.0°S seem to be affected by two factors. However, this finding disappears if Assemblage A is omitted. Because Assemblage A is associated with the Java Upwelling, the PCA results probably reflect enhanced nutrients but the results offer no direct evidence for this suggestion.

Latitudes \ Axes		1	2	3	4	Minimum no. of factors
12.0 – 31.5°S (i.e. all EIO)	Eigenvalues	0.948	0.012	0.006	0.012	1
	Cumulative % variance	94.8	98.8	99.4	98.8	
12.0 – 19.0°S	Eigenvalues	0.798	0.017	0.006	0.017	2
	Cumulative % variance	79.8	98.5	99.1	98.5	
19.0 – 27.5°S	Eigenvalues	0.916	0.016	0.006	0.016	1
	Cumulative % variance	91.6	99.1	99.8	99.1	
27.5 – 31.5°S	Eigenvalues	0.919	0.015	0.008	0.015	1
	Cumulative % variance	91.9	99.1	99.9	99.1	

Table 7.6: The principal components of the EIO environmental data (input limited to AOU, dissolved oxygen, nitrate, phosphate, and silicate concentrations, chlorophyll, salinity, and temperature). The table contains values for the whole EIO and for three latitude ranges.

Latitudes \ Axes		1	2	3	4	Minimum no. of factors
All SIO	Eigenvalues	0.844	0.114	0.008	0.025	2
	Cumulative % variance	84.4	95.9	99.1	98.3	
SIO excluding Assemblage L	Eigenvalues	0.858	0.103	0.008	0.015	2
	Cumulative % variance	85.8	96.1	98.4	97.6	
Assemblage G	Eigenvalues	0.873	0.113	0.000	0.014	2
	Cumulative % variance	87.3	98.6	100.0	100.0	
G01-3 and Assemblage H	Eigenvalues	0.951	0.028	0.002	0.017	1
	Cumulative % variance	95.1	97.9	99.8	99.5	
Assemblages J and K	Eigenvalues	0.853	0.74	0.017	0.31	2
	Cumulative % variance	85.3	92.6	97.4	95.8	

Table 7.7: The principal components of the SIO environmental data (input limited to AOU, dissolved oxygen, nitrate, phosphate, and silicate concentrations, chlorophyll, salinity, and temperature). The table contains values for the whole SIO and for four sets of sites chosen following examination of the All SIO results.

The PCA results for the entire SIO (Table 7.7 and Figure 7.15) indicate at least two factors over the region. The sites south of the Polar Front (broadly Assemblage L) appear to be strongly affected by silicate concentrations which increase sharply from north to south. Silicate concentration is probably a minor factor taken over the whole region, while the best contenders for the major factor are temperature and salinity. However, temperature and salinity are so strongly correlated, choosing one rather than the other is impossible.

With the information from the PCA results on the environmental variables, attempts were made to associate these variables with the census data using canonical correspondence analysis (CCA). *CANOCO* (ter Braak and Šmilauer, 2004) was employed both with and without manual selection of environmental variables (automatic forward selection was not used). Within the practicalities of trying various combinations of the WOA-05 variables, an attempt was made to maximise the proportion of taxa variance explained, both for the whole EIO and the whole SIO, and for subdivisions of both identified whilst investigating the environmental data. The results appear in Table 7.8 and Figure 7.16 for the EIO, and Table 7.9 and Figure 7.17 for the SIO.

Latitudes \ Axes		1	2	3	4	No. of factors
12.0 – 31.5°S (i.e. all EIO)	Eigenvalues	0.081	0.027	0.018	0.054	3
	Cumulative % variance	12.6	16.9	19.6	28.0	
12.0 – 19.0°S	Eigenvalues	0.059	0.033	0.63	0.49	2
	Cumulative % variance	11.0	17.1	28.8	37.9	
19.0 – 27.5°S	Eigenvalues	0.077	0.029	0.089	0.069	2
	Cumulative % variance	17.5	24.1	44.3	59.9	
27.5 – 31.5°S	Eigenvalues	0.128	0.051	0.088	0.071	2
	Cumulative % variance	23.9	33.3	49.7	63.0	

Table 7.8: Canonical correspondence results for the EIO as a whole and by latitudinal zone.

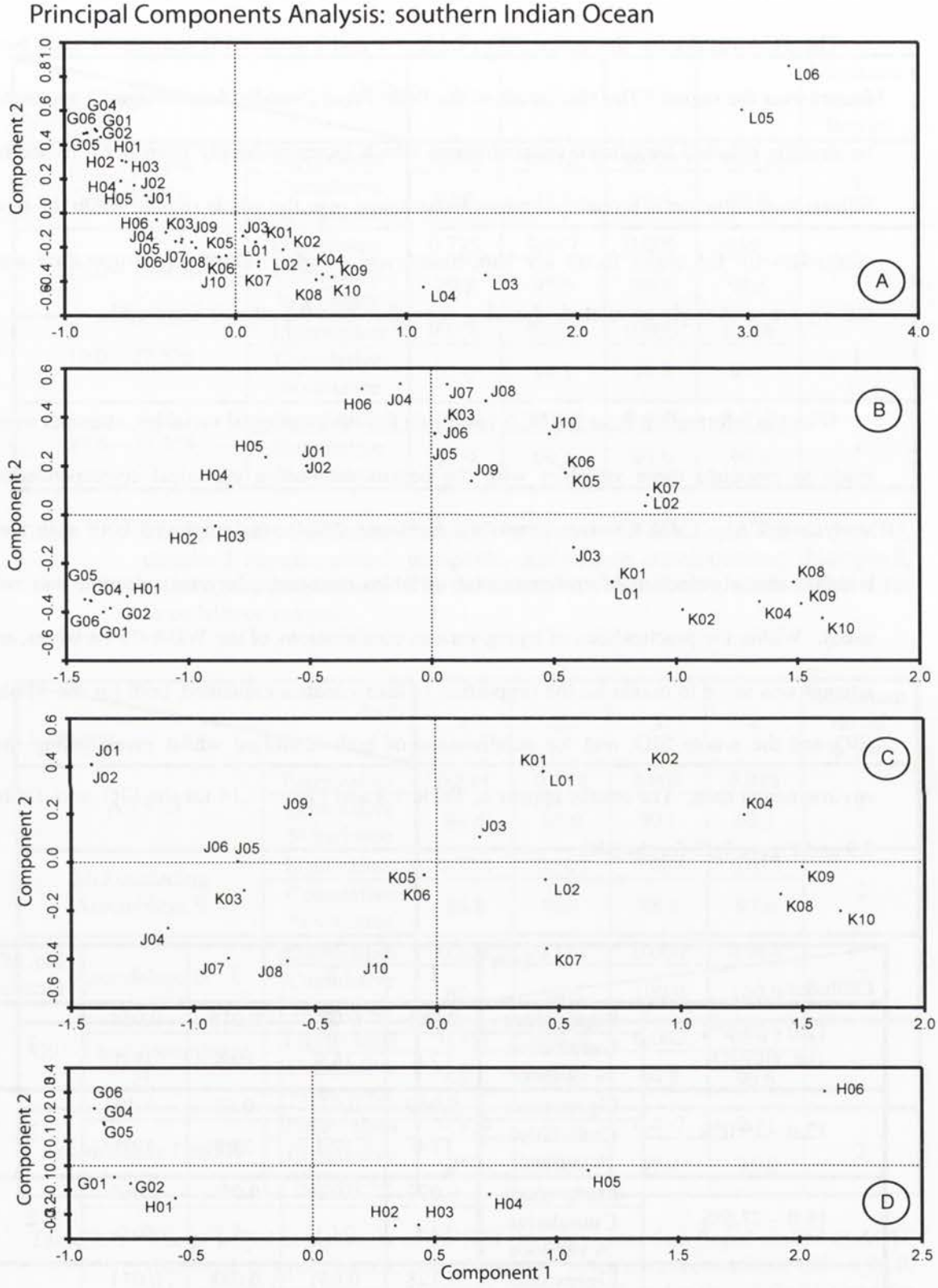

Figure 7.15: PCA plots for SIO.
Plot A: whole SIO
Plot B: SIO without the Antarctic Zone (Assemblage L).
Plot C: assemblages J (Subantarctic Zone) and K (Polar Zone)
Plot D: assemblage G (north of STF) and assemblage H (between NSTF and SSTF).

Latitudes \ Axes		1	2	3	4	No. of factors
All SIO	Eigenvalues	0.371	0.062	0.151	0.092	2
	Cumulative % variance	27.5	32.1	43.3	50.1	
SIO excluding Assemblage L	Eigenvalues	0.353	0.52	0.039	0.139	3
	Cumulative % variance	29.4	33.8	37.1	48.7	
Assemblages J and K	Eigenvalues	0.169	0.037	0.084	0.077	2
	Cumulative % variance	22.2	27.0	38.0	48.1	
Assemblages G and H	Eigenvalues	0.191	0.053	0.099	0.76	2
	Cumulative % variance	27.9	35.6	50.0	61.1	

Table 7.9: Canonical correspondence results for the SIO as a whole and by assemblage groupings.

The CCA eigenvalues for the EIO (Table 7.10) are small, indicating the census data's low information content. The ratios between the values for successive axes indicate that two or more environmental variables are factors in the site scores and assemblage composition.

In *CANOCO* CCA plots the measure of the relationship between site samples and the environmental variables is the projection of the site sample onto the line representing the environmental variable. Thus, if the plot shows a group of sites aligned parallel to an environmental variable line, that group is influenced by the environmental variable in question. If the group is aligned at right angles to an environmental line, the environmental variable has no influence on the group.

As can be seen from Figure 7.16a, the alignments of site samples with temperature, salinity, silicate, or phosphate (or a combination of these variables) break these samples into a number of groups. The plot in Figure 7.16b suggests that temperature is the main influence on sites B06-08 and C01-10 and on sites C11-15 and D03, and that these two groupings are distinguished by each having a fixed but different salinity or phosphate level. Assemblage D

appears to be entirely dominated by the effect of salinity and/or phosphate. Sites B01-3 and B05 are separated from the other assemblages by being at the extremes of temperature and salinity/phosphate. The sites of Assemblage A are separated one from the other by temperature and salinity/phosphate. They have a fixed silicate level which is different from the other assemblages.

As a by-product of CCA on the EIO, the identification of sites B01-3 and B05 as a separate assemblage to Assemblage C appears confirmed because they are completely isolated from Assemblage C in Figure 7.16b: the remaining Assemblage B sites are not clearly distinguished from Assemblage C in the plot. Sites C11-C15 and D03 apparently constitute an assemblage separate from the other Assemblage C sites for the same reason.

Region	Figure		Axis 1	Axis 2	Axis 3	Axis 4	Total
EIO	7.16 a -b	Eigenvalues	0.083	0.033	0.018	0.007	0.644
		Cumulative % variance of species data	12.9	18.0	20.8	21.9	
SIO	7.17a	Eigenvalues	0.384	0.081	0.031	0.024	1.347
		Cumulative % variance of species data	28.5	34.5	36.9	38.6	
SIO without Assemblage L	7.17b	Eigenvalues	0.361	0.050	0.036	0.031	1.249
		Cumulative % variance of species data	28.9	32.9	35.8	38.3	

Table 7.10: The CCA eigenvalues and cumulative percentage variance explained for the EIO and SIO with temperature, salinity, phosphate, and silicate as canonical variables (albeit from different depths below the sea's surface).

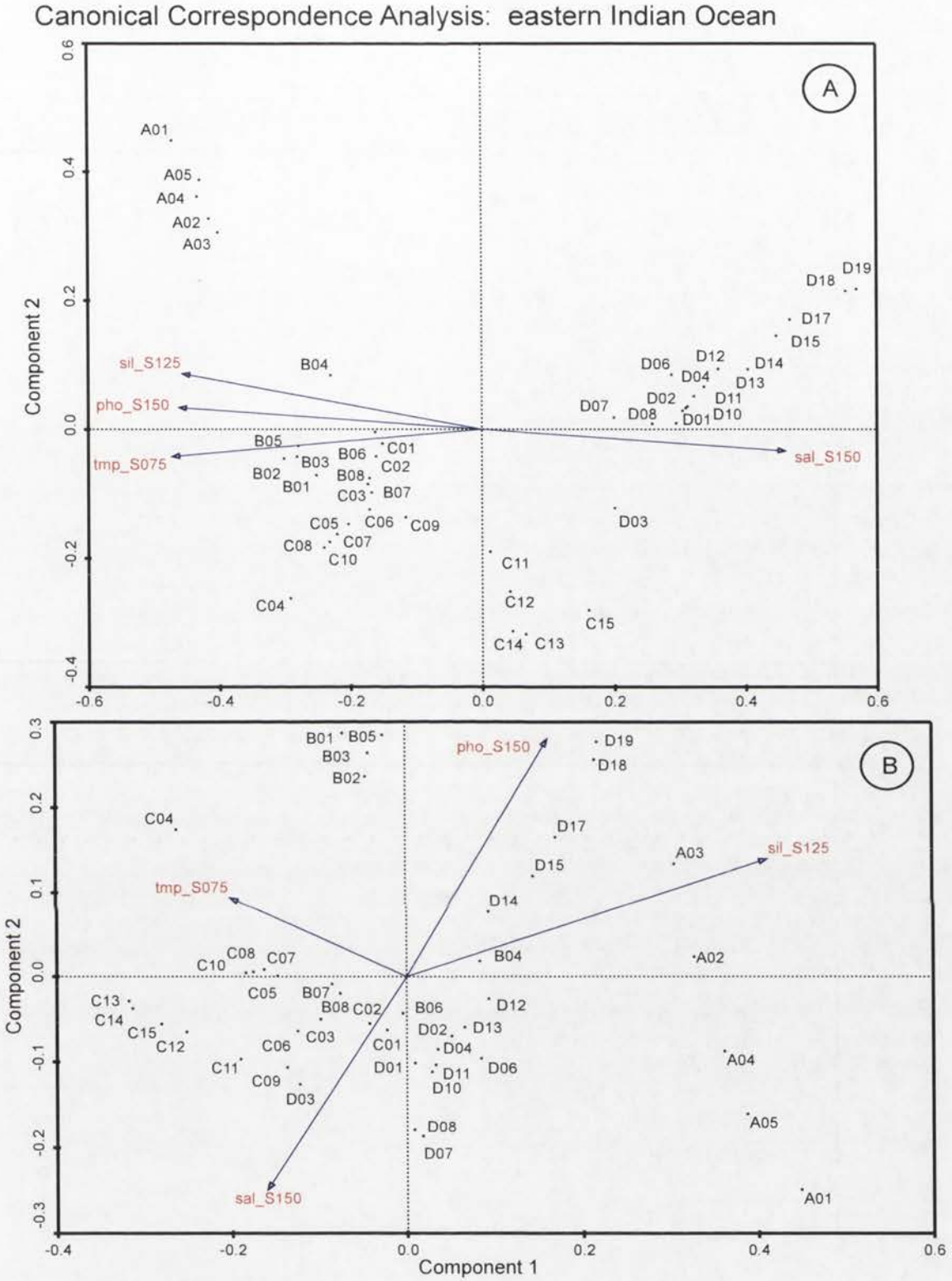

Figure 7.16: CCA applied to the whole EIO.

Plot A shows component 1 against component 2 and Plot B 2 against 3. "tmp_S075m" means summer temperature at 50 metres bsl. Similarly, "pho_S150m" and "sal_S150m" refer to summer phosphate and salinity at 150 m bsl., and "sil_S125" to silicate at 125 metres bsl. The measure of the relationships between sites and environmental variables is the projection of the site onto the variable line. Plot A suggests that the site clusters (= radiolarian assemblages) are separated by all the variables. Sites B01-08 and C01-10 may be one assemblage. Also, sites C11-15 and D03 could be a separate assemblage.
Plot B indicates assemblage A is influenced by temperature and salinity and/or phosphate. B01-03 and B05 are at the extremes of temperature and phosphate. C01-10 and C11-15 are mainly influenced by temperature but at two different salinity levels. Assemblage D is mainly influenced by phosphate/salinity. Silicate concentration appears to separate Assemblage A from the other sites but to have little influence otherwise.

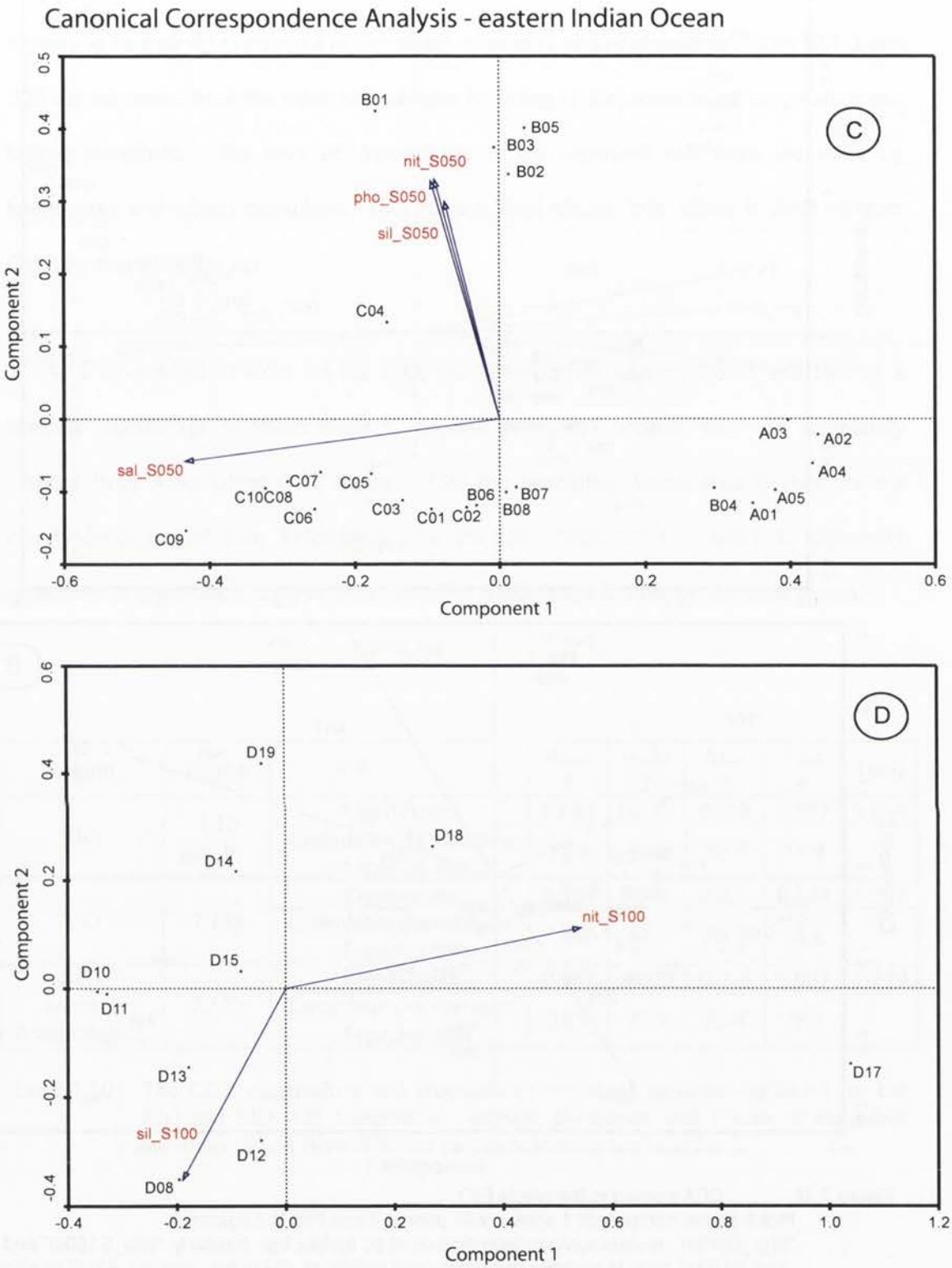

Figure 7.16: CCA applied to the EIO. Plot C covers 12-19°S and plot D 27.5-31.5°S. Plot C illustrates the collinearity of some potential explanatory variables - phosphate, nitrate, and silicate concentrations are virtually indistinguishable. In the same way, although salinity is not shown here, salinity and nitrate are almost collinear in the region covered by plot D.

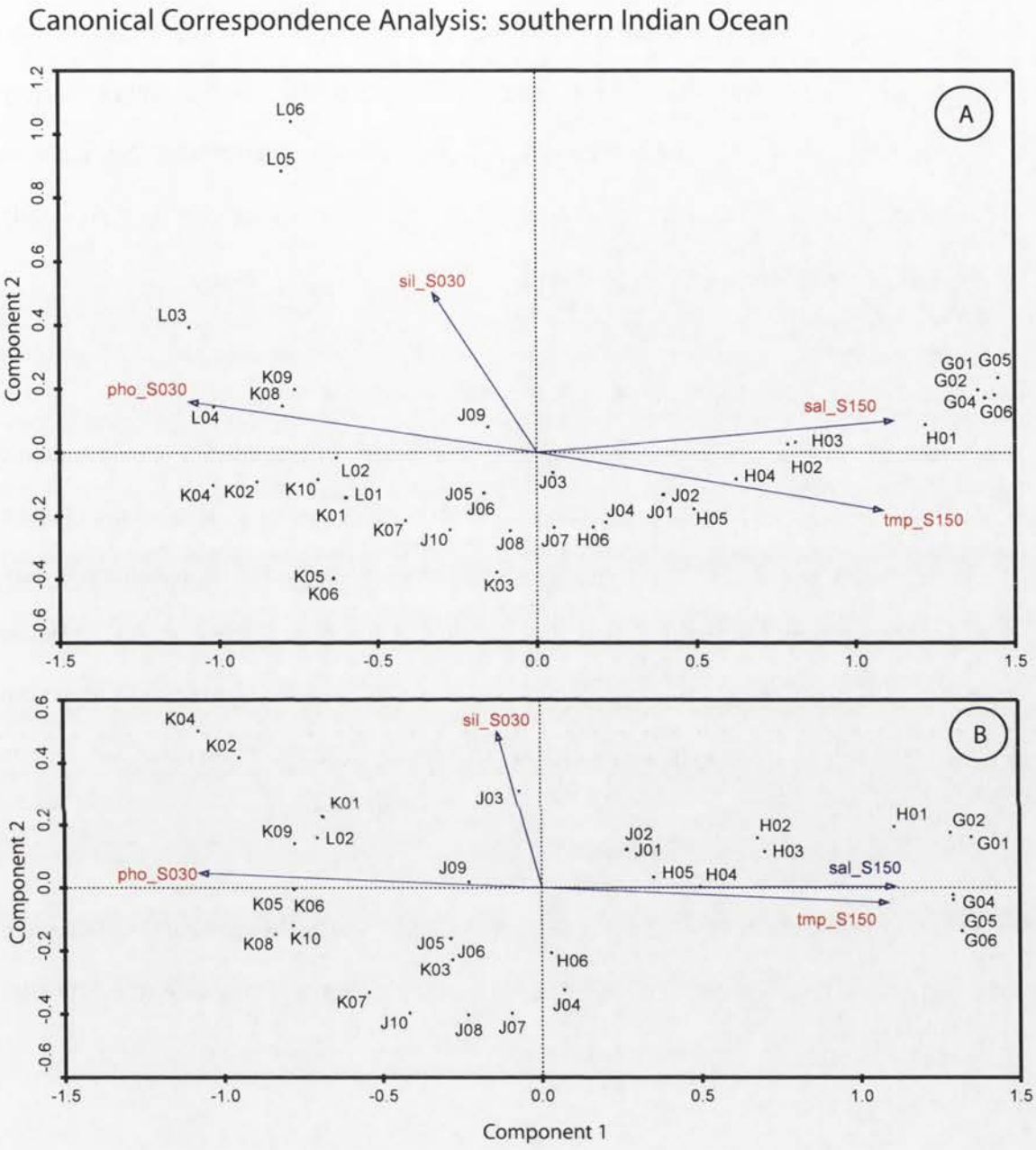

Figure 7.17: CCA plots for the SIO generated by *CANOCO*. Plot A covers the whole of the SIO and Plot B the same but without assemblage L (which lies in the Antarctic Zone). "sal_S150" means summer salinity and "tmp_S150" temperature at 150 metres bsl., and "pho_S030" phosphate and "sil_S030" silicate at 30 m bsl.
Both plots suggest that either salinity, temperature, or phosphate, or a combination of these environmental variables is the primary explanation for the distribution of the sites, and that silicate concentration is a secondary factor. The positions of sites L05 and L06 (Plot A) reflect strongly the large increase in silicate concentration south of the Polar Front

The SIO CCA eigenvalue ratios (Table 7.10) suggest that one environmental variable (or combination of correlated variables) dominates. Examination of the plots (Figures 7.17a-b) shows temperature, salinity, phosphate, or a combination of these, to be the main explanatory variable(s): the variables near-collinearity prevents separation of their effects. Silicate is an important secondary factor, particularly for Assemblages G. K, and L. The previously defined assemblages seem to be confirmed.

7.2.3. Approach 3: CA correlation with environmental variables

When CA scores are correlated with the environmental variables (results in the Electronic Supplement as Table 7.11), the EIO falls into the same three categories as were found under Approaches 1 and 2 (Electronic Supplement Tables 7.4 and 7.5). Temperature is very strongly negatively correlated between the surface and 100 metres below sea level. Below that, it switches to being positively correlated (Figure 7.18a). Salinity and dissolved oxygen are both strongly positively correlated at all depths. Nitrate, phosphate, and silicate concentrations are strongly negatively correlated below 100 metres bsl.

These correlations offer a starting point for deciding which environmental variables are explanatory. Examination of the way each variable changes longitudinally (the EIO sites cover a relatively narrow span, mostly between 110° and 115°E) shows that:

- nitrate, phosphate, and silicate are at very low concentrations in the mixed layer; their concentrations are higher and increase from south to north at 200 metres bsl (Figures 4.5e,f,g);
- dissolved oxygen and oxygen saturation decrease from south to north, both in the mixed layer and at 200 metres bsl Figures 4.5c and d);

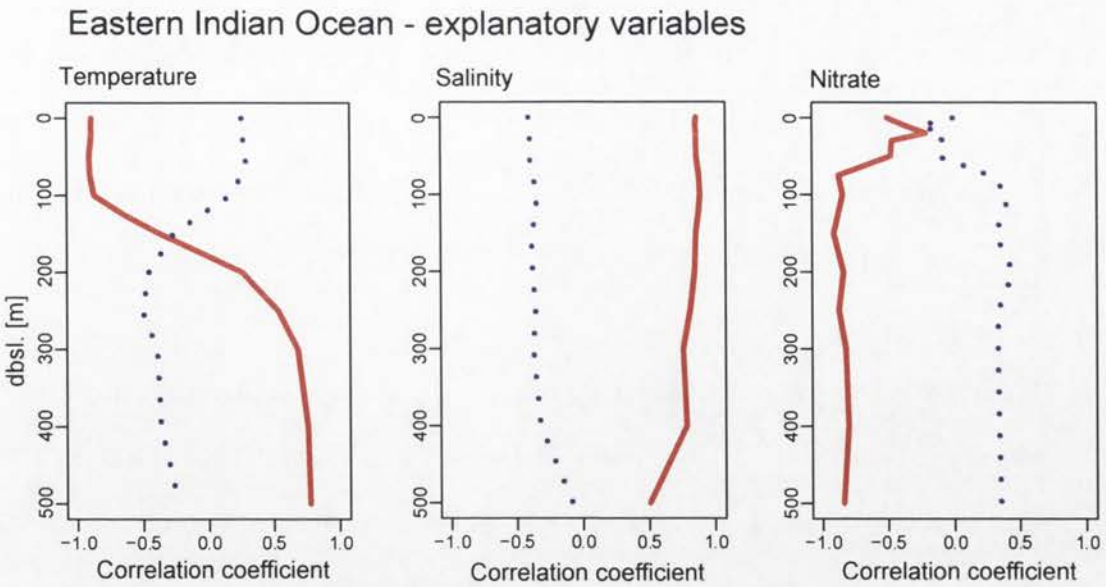

Figure 7.18a: The correlation between EIO CA site scores and three environmental variables. The red (solid) line is the correlation with the first CA axis, and the blue (dotted) line that with the second. There are 45 degrees of freedom, making absolute values greater than 0.46 significant at the 0.05% level.
Of the variables not shown, phosphate, silicate, and aou are similar to nitrate but with phosphate and aou positively correlated at the 0.1% level close to the water's surface; the correlation coefficient for dissolved oxygen is greater than 0.85 at all dbsl.
Note particularly the switch from positive to negative correlation at about 175 metres bsl in the temperature plot - apparently caused by a change of water mass at that level.

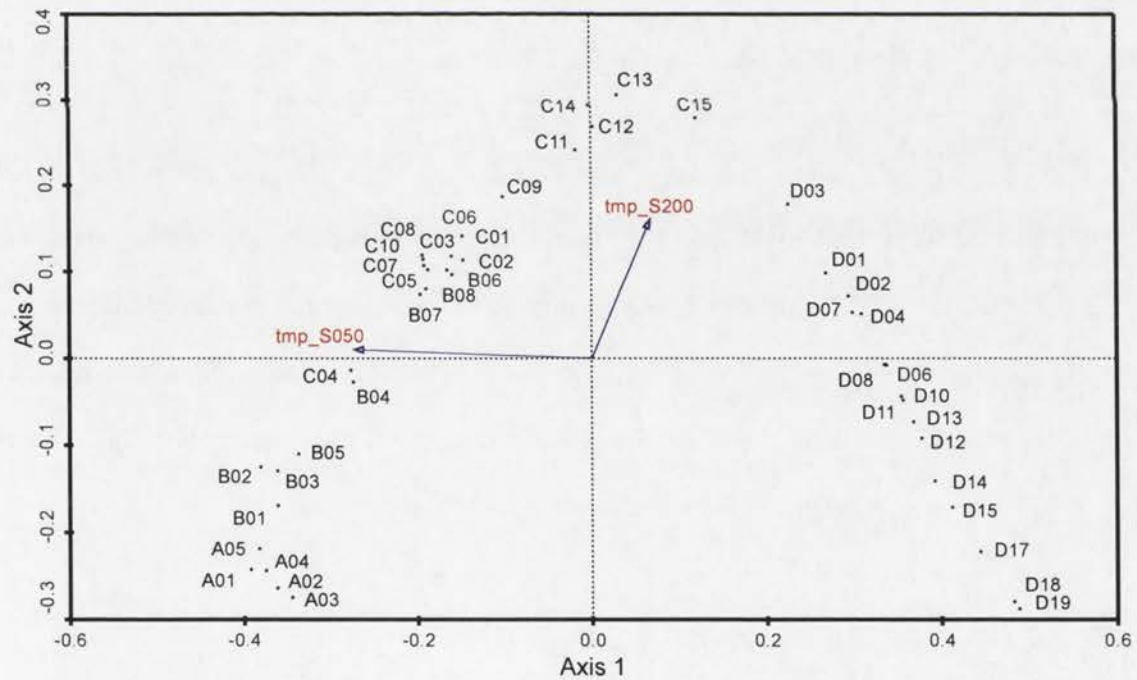

Figure 7.18b: The *CANOCO* CCA plot for the EIO sites with temperature at 50 metres bsl (tmp_S050) and 200 metres bsl (tmp_S200), austral Summer (JFM) values for both variables. The sites are labelled according to assemblage and latitude; A01 and B01 are the most northerly, D19 the most southerly. The plot implies that the radiolarians are primarily responding to the increase in sea temperature from south to north at 50 metres bsl and, secondarily, to the increase, followed by a decrease at 200 metres bsl, with a maximum at approximately 21°S.

- at the surface, salinity has a maximum value at approximately 31°S, and, at 200 metres bsl, a maximum at about 25°S (Figure 4.5b);
- at the surface, temperature in the mixed layer increases from south to north; at 200 metres bsl, it has a maximum at about 21°S (Figures 4.5a).

Thus, only one variable, temperature, changes linearly in the mixed layer and non-linearly at 200 metres bsl. The 1st CA axis varies linearly and inversely with latitude and the 2nd axis quadratically with latitude, the minimum falling at about 21°S (not illustrated). A *CANOCO* CCA plot (Figure 7.18b) with temperature at 50 and 200 metres bsl confirms these two variables as potentially explanatory. However, this finding does not exclude salinity or any of the other strongly correlated variables as explanatory: their very strong correlations with the CA scores mean they must constitute part of the explanation.

The categorisation found in the SIO correlations is also very similar to that found using Approaches 1 and 2 (Electronic Supplement Tables 7.4 and 7.5). Temperature and salinity are strongly negatively correlated with the CA scores at all depths. Nitrate and phosphate concentrations are strongly positively correlated at all depths except in that they show a slight diminution at 50-75 metres bsl; silicate follows the same pattern but its correlations are weak above 200 metres in summer (JFM). Dissolved oxygen is reasonably strongly correlated with a peak at 75 metres bsl – the correlations are stronger in spring (OND). The AOU correlations are relatively weak and increase with depth.

7.2.4. Approach 4: Multivariate Regression Trees

The multivariate regression tree software, *R:mvpart* (Oksanen, 2005), attempts to partition the set of sites by the relationship between the census data and the environmental variables. It performs this task iteratively, eventually providing a list of possible explanatory

variables and an associated set of clusters of the sites. A Monte Carlo approach with a randomised start can be used and this yields a probability estimate of the optimum number of site partitions.

Running *R:mvpart* on the EIO census data invariably yielded a high probability of there only being two possible clusters – essentially everything north of approximately 19°S as one cluster and everything south of that as the other. Typical clusters are illustrated in the CCA diagrams in Figure 7.19a. The output from *R:mvpart* on the SIO data usually provides six clusters, one more than most other indicators. The first two or three partitions occur at geographically significant points; further partitions seem random (implying the information from the data is insufficient for this subdivision and, perhaps, accounting for the extra cluster). An SIO tree appears as Figure 7.20 and the corresponding CCA diagrams as Figure 7.21.

7.2.5. Summary of radiolarian-environmental relationship results

Approach 1 (CCA eigenvalues) and Approach 2 (WA-PLS) give essentially the same results. The percentage of variance explained is typically greater and the R^2 value larger in the SIO than the EIO. In addition, the radiolarian-environmental relationships differ between the two regions: they are summarised in Tables 7.12 (EIO) and 7.13 (SIO).

The environmental variables identified under Approaches 1, 2, and 3 facilitated the selection of variables for the *CANOCO* CCA investigations, revealing significantly more about the relationships between the radiolarian census data and the environment. *R:mvpart* (Approach 4) provided some confirmatory information only.

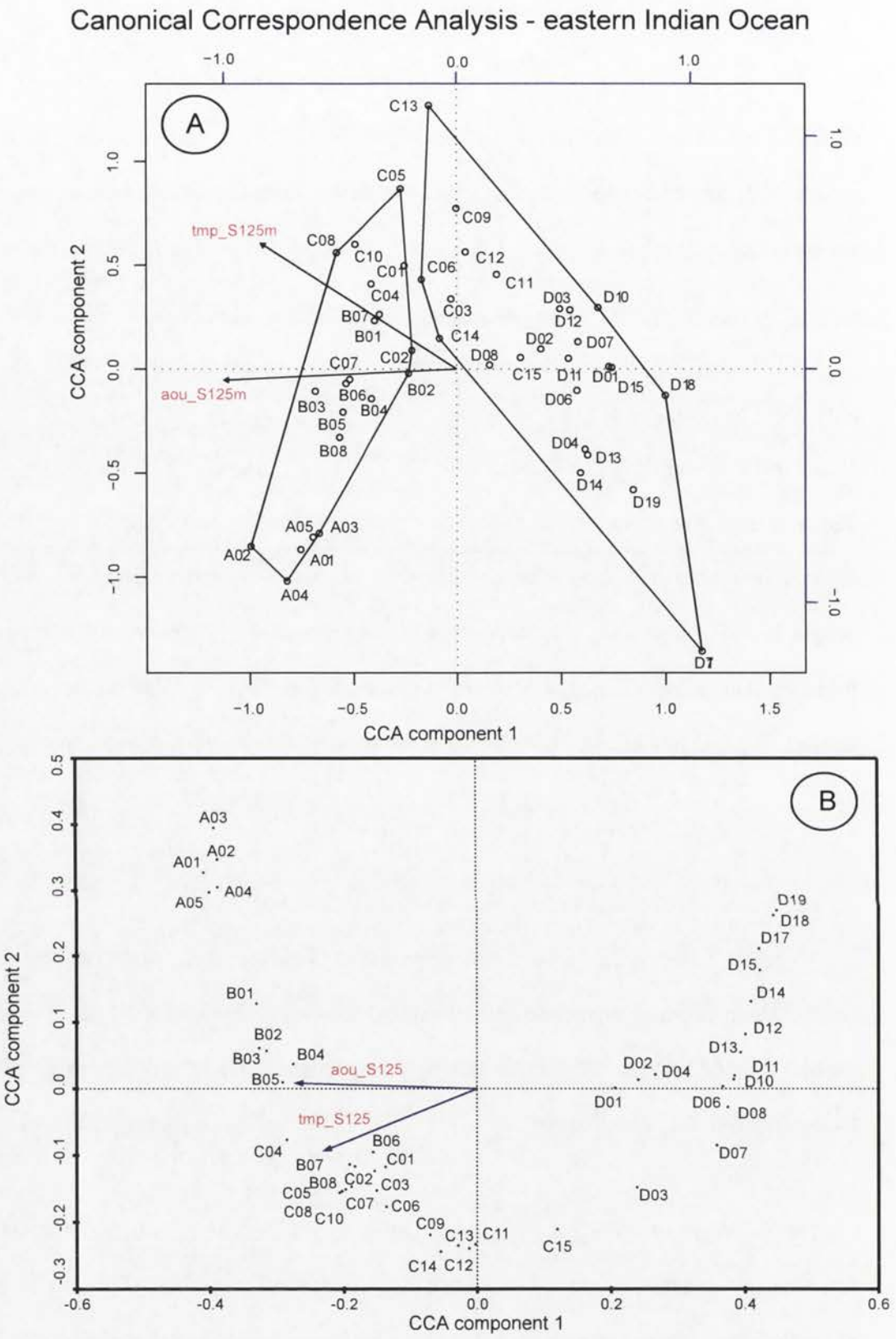

Figure 7.19: Eastern Indian Ocean canonical correspondence analysis (CCA) plots. Plot A was generated using *R:cca* with groupings from *R:mvpart* software for recursive partitioning and regression trees. Plot B is the output of *CANOCO*. The difference between the plots is mainly a matter of scaling. Both plots separate assemblages A; plot B distinguishes B-C from D, whereas this is not evident in plot A. Both plots suggest a slight distinction between assemblages B and C.
The sites are labelled according to their assemblage assignments. "tmp_S125m" means summer temperature at 125m bsl; "aou_S125m" the same for apparent oxygen utilisation. In plot A, the scales for temperature and AOU are on the upper and right-hand edges.

Variable	Depth range	Variance explained	R^2	Comment
AOU nitrate phosphate silicate [oxygen saturation]	> 125 m bsl	~20%	~0.8	Strong correlation
temperature [*in situ* density]	< 125 m bsl	~20-25%	~ 0.8	Strong correlation
dissolved oxygen salinity	0-500 m bsl	~20%	~0.8	Strong correlation

Table 7.12: The relationships between the EIO radiolarian census data and the corresponding austral summer environmental variables. It is noteworthy that the CA correlations are essentially solely due to contributions from data from north of 21°S, there being no correlation from data south of that which is significant at the 0.05% level generally used in this study. The southern data does, however correlate at the 1% level with dissolved oxygen, phosphate, and silicate.

Variable	Depth range	Variance explained	R^2	Comment
AOU silicate [oxygen saturation]	0-200 m bsl	~10%	~0.2 - 0.3	Weak correlation
	200-500 m bsl	increasing to 35%	increasing to 0.9	
nitrate phosphate [*in situ* density]	150-500 m bsl "kink" at 75 m bsl	~37%	>0.9	Very strong correlation
dissolved oxygen	0-75 m bsl sharp decline lower	~30%	>0.8	Strong correlation: winter at 100 m bsl very strong
salinity	0-200 m bsl declining slightly below 200 m.	~37%	>0.9	Very strong correlation
temperature	0-500 m bsl	~30%	~ 0.8	Very strong correlation

Table 7.13: The relationships between the SIO radiolarian census data and the corresponding environmental variables. The results are very similar for all four seasons with only the austral winter correlation with dissolved oxygen being significantly different from the values at other times of year.

7.3. Other statistical results

The Upwelling Radiolarian Index (URI) (Nigrini and Caulet, 1992) and the Water Depth Ecology index (WADE) (Lazarus *et al.*, 2006) results for each site (Table 5.1) were plotted on a map of the study area. It was observed that the WADE values were generally higher in the EIO than in the SIO but the values were so variable that no further information could be derived. The URI values showed no geographical associations.

Canonical Correspondence Analysis using *CANOCO* failed to reveal any significant relationships between either the WADE or URI values and the oceanic variables.

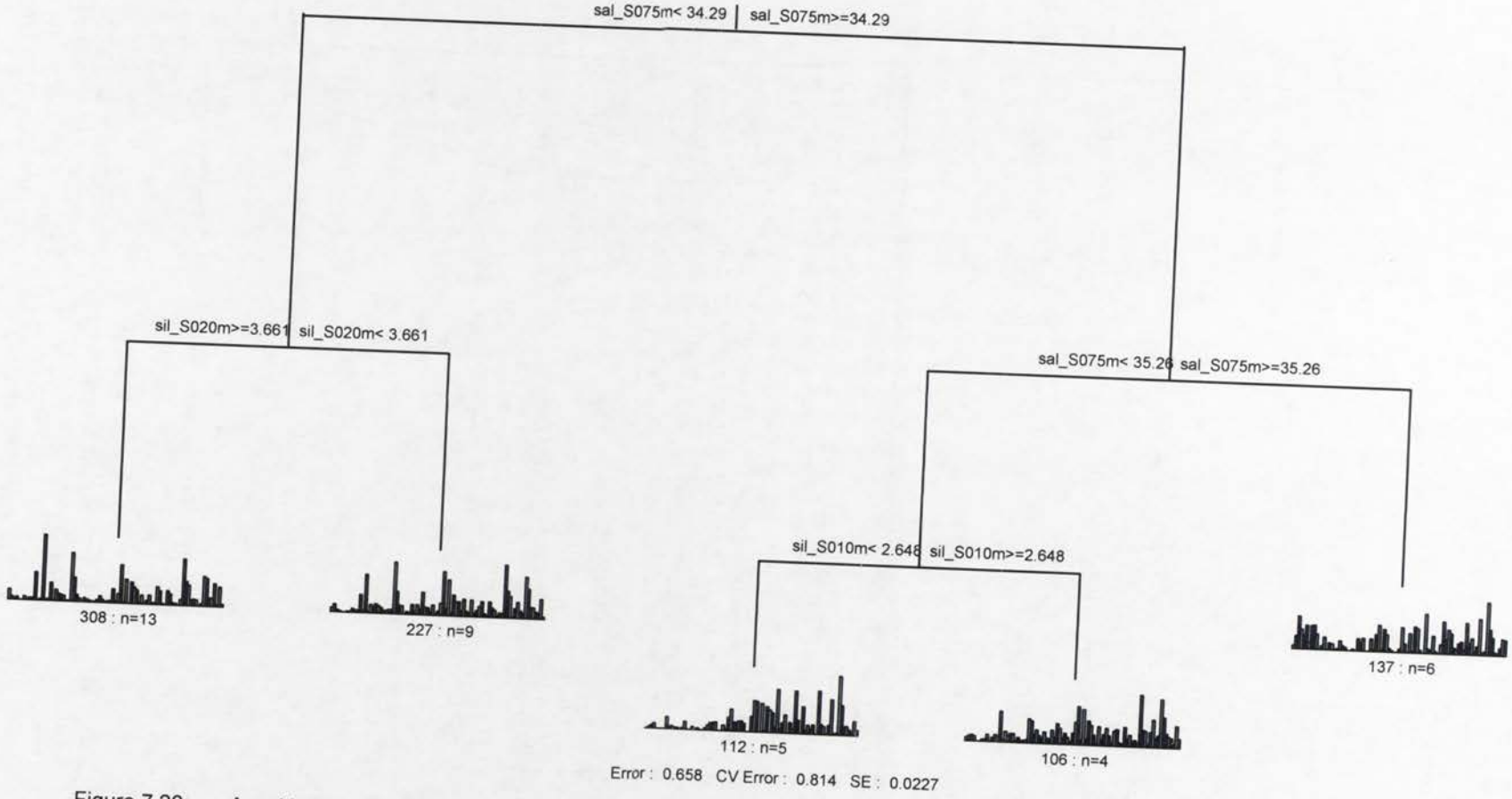

Figure 7.20: A multivariate regression tree for the SIO. "sal_S075m" = Summer salinity at 75 metres bsl., "sil_S020m" = Summer silicate at 20 metres bsl., etc. The divisions at sal_S075m = 34.29 and sil_S020m = 3.661 correspond geographically to the Subantarctic Zone and sal_S075m = 35.26 to the NSTF; the division at sil_S10m = 2.648 is not significant geographically.

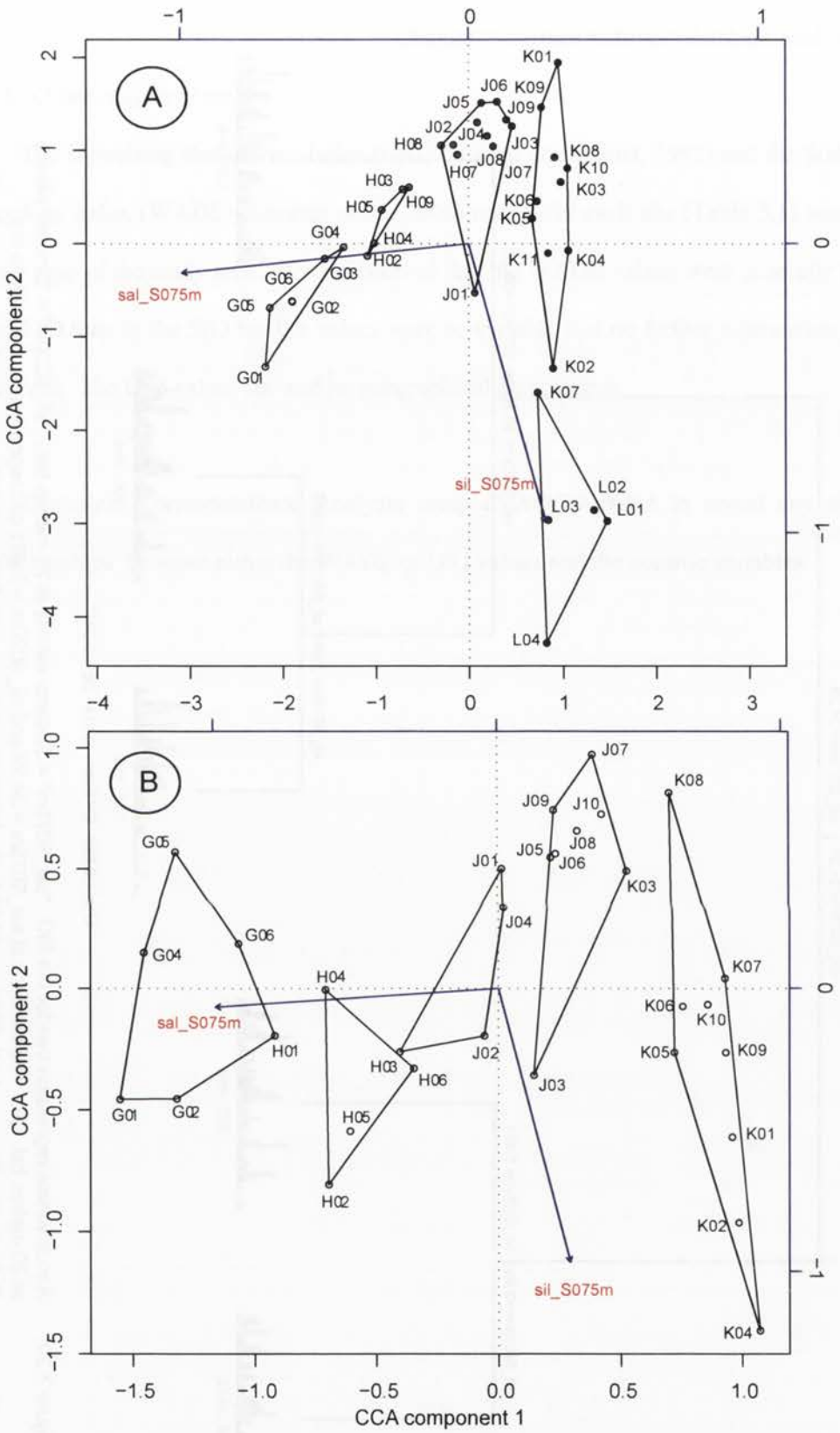

Figure 7.21: Southern Indian Ocean canonical correspondence analysis (CCA) plots. Plot A includes all the SIO census data; plot B omits the sites associated with the Antarctic Zone (assemblage L). The difference between the plots is due to the importance of silicate concentrations south of the Polar Front. The sites are labelled according to their assemblage assignments. "sal_S075m" means summer salinity at 75m bsl; "sil_S075m" the same for silicate. The scales for both are on the upper and right-hand edges of the plots. The groupings indicated by polygons are generated by *R:mvpart* software for recursive partitioning and regression trees.

Chapter 8: Analytic results from other radiolarian databases

8.1. Introduction

Most of the candidates for explanatory environmental variables in the eastern Indian Ocean (EIO) and southern Indian Ocean (SIO) proved to vary together, making it impossible to decide whether their correlations with the distribution of radiolarian taxa result from a causal connection or indirectly via their association with a genuinely explanatory variable. It is important to establish which are the genuinely explanatory variables, if possible, because their relationships with radiolarian assemblages are likely to have persisted across time, making the assemblages reliable proxies for palaeo-reconstructions. By contrast, apparent associations between environmental variables and radiolarian assemblages might not have held over geological time and, if employed in reconstructions, could lead to erroneous conclusions. A solution to this problem could be realised if radiolarian census counts from different regions of the world could be found where, optimally, some of the environmental variables of interest are constant while others vary or, at least, where the variables are not correlated in the same ways as in the Indian Ocean. Investigation of such census counts could also help confirm some of the hypotheses derived from Indian Ocean census counts.

The few comparable counts available were published by the CLIMAP Project Members (1997; 2006) for the Southern Ocean [latitude 34-60°S; longitude 123°-130°E], Kamikuri *et al.* (2008) for longitude 175°E from latitude 48°N to 15°S in the Pacific Ocean, Nimmergut and Abelmann (2001) for the Sea of Okhotsk, and Welling (2003) for the equatorial Pacific Ocean [12°N- 12°S, 135°W-141.5°W][1]. The counts were analysed both for clustering and for environmental relationships in the same way as the EIO and SIO census counts prepared for this study but using only the more efficacious techniques as described in Chapters 4 and 7.

[1] Note: after this study was complete, some further census counts were discovered in a repository not previously known to the author.

Site	Latitude	Longitude	Water depth [m]	Clustering technique					Conclusion	
				hclust	*agnes*	*pam*	*fanny*	*diana*	Assemb -lage	Code
RC12-299	-34.08	-1	4296	3	5	4	4	11	P	P01
V24-202	-34.35	59.217	5512	3	5	4	4	4	P	P02
V27-201	-34.77	-3.417	4186	3	5	4	4	4	P	P03
V18-166	-34.98	-27.12	4527	3	5	4	4	4	P	P04
RC13-243	-35.9	1.33	4790	3	5	4	4	4	P	P05
V27-192	-36.57	-16.87	3087	3	5	4	4	4	P	P06
RC12-293	-36.88	-13.15	3393	3	5	4	4	4	P	P07
RC12-269	-36.98	-32.2	4360	3	5	4	4	4	P	P08
RC12-294	-37.27	-10.1	3308	3	5	4	4	4	P	P09
RC13-242	-37.54	-3.587	4266	3	5	4	4	4	P	P10
ELT48.028-PC	-38.543	79.918	3251	3	5	4	4	4	P	P11
RC12-267	-38.68	-25.78	4144	3	5	4	4	4	P	P12
RC12-292	-39.68	-15.48	3541	3	5	4	4	4	P	P13
RC12-266	-39.82	-24.8	3939	3	5	4	4	4	P	P14
V12-53	-40.9	-20.38	3797	3	5	3	4	4	P	P15
V18-35	-36.4	-41.12	4942	1	4	3	1	1	Q	Q01
RC13-244	-36.5	3.545	5222	1	4	3	1	1	Q	Q02
V24-203	-36.98	59.983	4997	4	1	1	3	7	Q	Q03
RC14-11	-38	51.183	3268	1	4	3	1	1	Q	Q04
RC14-9	-39.02	47.883	2692	1	4	3	1	1	Q	Q05
RC11-119	-40.3	74.567	3709	1	4	3	1	1	Q	Q06
RC12-265	-40.9	-26.85	4395	1	4	3	1	1	Q	Q07
RC08-37	-41.32	33.217	4775	1	4	3	1	1	Q	Q08
V029-083	-41.5333	30.95	5059	1	4	3	1	1	Q	Q09
RC08-38	-41.88	37.817	3784	1	4	3	1	1	Q	Q10
ELT49.021-PC	-42.185	94.885	3319	1	4	3	1	1	Q	Q11
RC15-96	-42.88	-23.92	4426	1	4	3	1	1	Q	Q12
RC15-98	-42.94	-29.78	4416	1	4	3	1	1	Q	Q13
RC15-97	-42.96	-25.94	4583	1	4	1	1	1	Q	Q14
RC15-94	-42.98	-20.86	3762	1	4	3	1	1	Q	Q15
V22-108	-43.18	-3.25	4171	1	4	3	1	1	Q	Q16
ELT49.019-PC	-43.887	90.1	3057	1	4	3	1	1	Q	Q17
ELT45.029-PC	-44.877	106.518	3867	1	4	3	1	1	Q	Q18
ELT39.013-PC	-45.012	125.982	4610	1	4	3	1	1	Q	Q19
ELT45.079-PC	-45.057	114.367	4154	1	4	3	1	1	Q	Q20
V22-86	-41.6	-46.45	5110	1	4	1	1	1	R	R01
RC08-39	-42.88	42.35	4330	1	1	1	3	1	R	R02
V29-90	-43.7	25.733	5148	1	1	1	1	1	R	R03
V29-84	-43.85	27.6	5451	6	1	1	3	13	R	R04
ELT49.018-PC	-46.05	90.155	3282	1	1	1	1	1	R	R05
RC08-61	-46.53	125.57	4254	1	1	1	3	1	R	R06
ELT49.023-PC	-47.128	95.08	3285	1	1	1	3	1	R	R07
E045-074	-47.55	114.1333	5124	1	1	1	1	1	R	R08
RC09-139	-47.77	123.1	4158	1	1	1	3	1	R	R09
ELT49.024-PC	-47.988	95.037	3240	1	1	1	3	6	R	R10
ELT45.071-PC	-48.025	114.487	3700	1	1	1	3	1	R	R11
ELT45.069-PC	-48.848	114.617	3444	1	1	1	3	1	R	R12
RC08-63	-51.08	129.97	3442	1	1	1	3	6	R	R13
RC17-60	-44.5	31.182	5227	4	6	5	3	6	S	S01
V16-65	-45	45.767	1618	4	6	5	3	7	S	S02

V29-89	-45.73	25.65	5945	4	6	5	5	7	S	S03
RC15-93	-46.1	-13.23	2714	4	6	5	5	8	S	S04
RC11-80	-46.75	-0.05	3656	4	6	5	5	7	S	S05
RC11-65	-47.03	-43.68	5435	4	6	1	3	5	S	S06
V29-88	-47.85	26.783	5737	4	6	5	5	7	S	S07
RC12-289	-47.9	-23.7	4484	4	6	5	5	8	S	S08
V29-105	-48.08	17.683	4350	4	6	5	5	6	S	S09
ELT49.017-PC	-48.28	90.247	3546	4	6	5	5	5	S	S10
RC15-92	-48.49	-10.33	3378	4	6	5	5	8	S	S11
RC13-254	-48.57	5.127	3636	4	6	5	3	6	S	S12
RC08-43	-48.68	57.367	4319	4	6	5	3	7	S	S13
RC11-69	-48.9	-41	5492	4	6	5	5	8	S	S14
RC15-91	-49.92	-15.57	3775	4	6	5	5	8	S	S15
RC12-225	-53.67	-123.1	2964	4	6	5	5	5	S	S16
V29-87	-49.1	27.383	5314	2	3	2	5	8	T	T01
RC11-96	-50.47	59.583	4839	2	2	2	2	2	T	T02
RC13-255	-50.54	2.895	3332	2	3	2	2	3	T	T03
RC13-275	-50.7167	13.4333	1984	2	3	2	2	3	T	T04
RC11-78	-50.87	-9.867	3115	2	3	2	6	9	T	T05
RC13-271	-51.99	4.522	3634	2	2	2	2	2	T	T06
RC17-61	-52.2	54.462	3947	2	2	2	2	2	T	T07
ELT45.064-PC	-52.483	114.09	3871	2	2	2	2	2	T	T08
RC13-269	-52.63	-0.125	2591	2	2	2	2	2	T	T09
ELT49.007-PC	-53.037	110.047	3631	2	2	2	2	2	T	T10
RC11-77	-53.05	-16.45	4098	2	2	2	2	2	T	T11
ELT07.001-PC	-53.1	-40.833	2129	2	2	2	2	2	T	T12
ELT45.063-PC	-53.437	114.257	3969	2	2	2	2	2	T	T13
RC13-259	-53.88	-4.93	1754	2	2	2	2	2	T	T14
RC11-94	-54.48	53.05	4303	2	2	2	2	2	T	T15
RC13-257	-55	-3.002	2836	2	3	2	5	8	T	T16
RC13-273	-55.0667	11.5667	4967	2	2	2	2	2	T	T17
ELT08.008-PC	-55.2	-24.333	4003	2	2	2	2	3	T	T18
RC11-91	-56.57	34.183	5373	2	3	2	5	9	T	T19
V15-133	-56.62	-53.9	5031	2	2	2	2	2	T	T20
ELT08.012-PC	-57.108	-23	4786	2	3	2	2	3	T	T21
V14-57	-57.57	-17.1	4978	2	3	2	2	3	T	T22
ELT15.012-PC	-58.683	-108.8	4649	2	2	2	2	2	T	T23
ELT09.013-PC	-59.167	-37.258	2835	2	2	2	2	2	T	T24
RC17-63	-45.66	48.287	2947	2	6	5	5	10	U	U01
RC11-97	-50.32	61.2	4638	2	6	5	5	10	U	U02
RC13-256	-53.18	-0.355	2525	5	3	6	6	12	V	V01
RC13-263	-53.81	-8.217	3389	5	3	6	6	12	V	V02
RC13-261	-56.12	-8.687	4221	5	3	6	6	12	V	V03

Table 8.1: The results of "Single-Run" clustering applied to the CLIMAP (1997) radiolarian census data. Five clustering techniques were applied to the census data and the number of clusters determined by inspection. In the column for each technique the clusters are labelled with numbers, the numbering order being arbitrarily determined by the technique. To decide the assemblages, the sites are allocated to groups based on the majority of the techniques placing them in a single cluster.

8.2. The CLIMAP Southern Ocean census counts

The CLIMAP database (1997) consists of census counts of 26 radiolarian taxa (not all identified) from 94 sites in an area of the Southern Ocean extending from the eastern Pacific eastwards to Western Australia (locations indicated in Figure 8.1). The counts are stated to be percentages. However, the total number of specimens for each site is also provided and dividing the "percentages" (multiplied by 100) by these figures does not yield integer values, so the counts have been adjusted in some way. This fact does not seem to imply that the ratios of taxa within or between sites are invalid, thus allowing analysis to proceed.

8.2.1. Southern Ocean clustering

Single-Run clustering (Table 8.1) was applied and suggests the presence of seven radiolarian assemblages, termed Assemblages P-V. These results were refined using WA-PLS (Figure 8.2). Assemblage U appears to belong to Assemblage T and, because the two assemblages are geographically intermixed, U is subsumed into T. At the same time, although all the members of Assemblage V are geographically within Assemblage T, they are close together and the statistical indications make them very distinct from Assemblage T. They are, therefore, left as a separate assemblage.

8.2.2. Southern Ocean radiolarian-environmental associations

The CCA eigenvalues (Figure 8.3), WA-PLS R^2 values (Figure 8.4), and the CA correlations with the environmental variables (Table 8.2) were evaluated and show a consistent pattern. Temperature, salinity, nitrate, and phosphate levels all strongly influence radiolarian taxa distributions from the surface to approximately 200 metres bsl. Dissolved oxygen is influential down to about 125 metres, and silicate, aou, and oxygen saturation below 200 metres.

The CLIMAP Project sites in the Southern Ocean

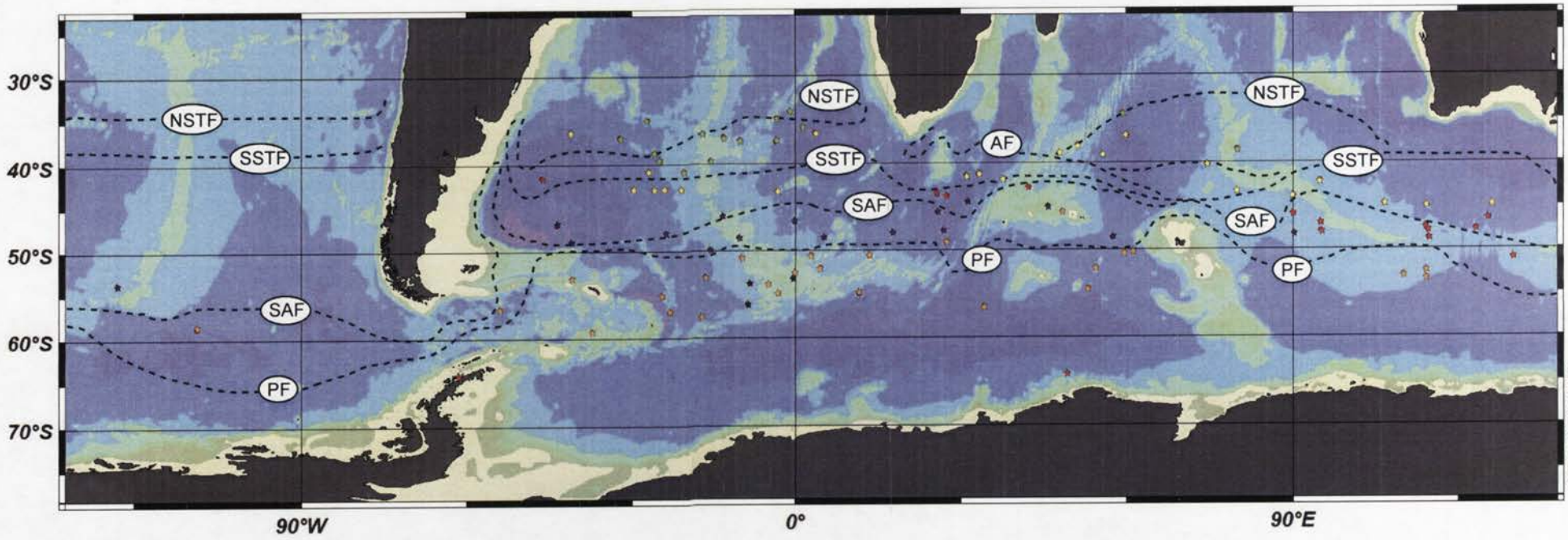

Figure 8.1: The 94 sites in the Southern Ocean investigated by the CLIMAP Project Members (1976, 1981, 1984, 1997, 2006).
The ocean fronts are plotted using data from Belkin and Gordon (1996) and are labelled:
NSTF - Northern Subtropical Front SSTF - Southern Subtropical Front AF - Agulhas Front
SAF - Subantarctic Front PF - Polar Front.
The radiolarian assemblages found in this study are marked with stars:
P - green; Q - yellow; R - red; S - blue; T - brown; V - black.
The assemblages can be seen to be contained broadly within the inter-frontal zones.

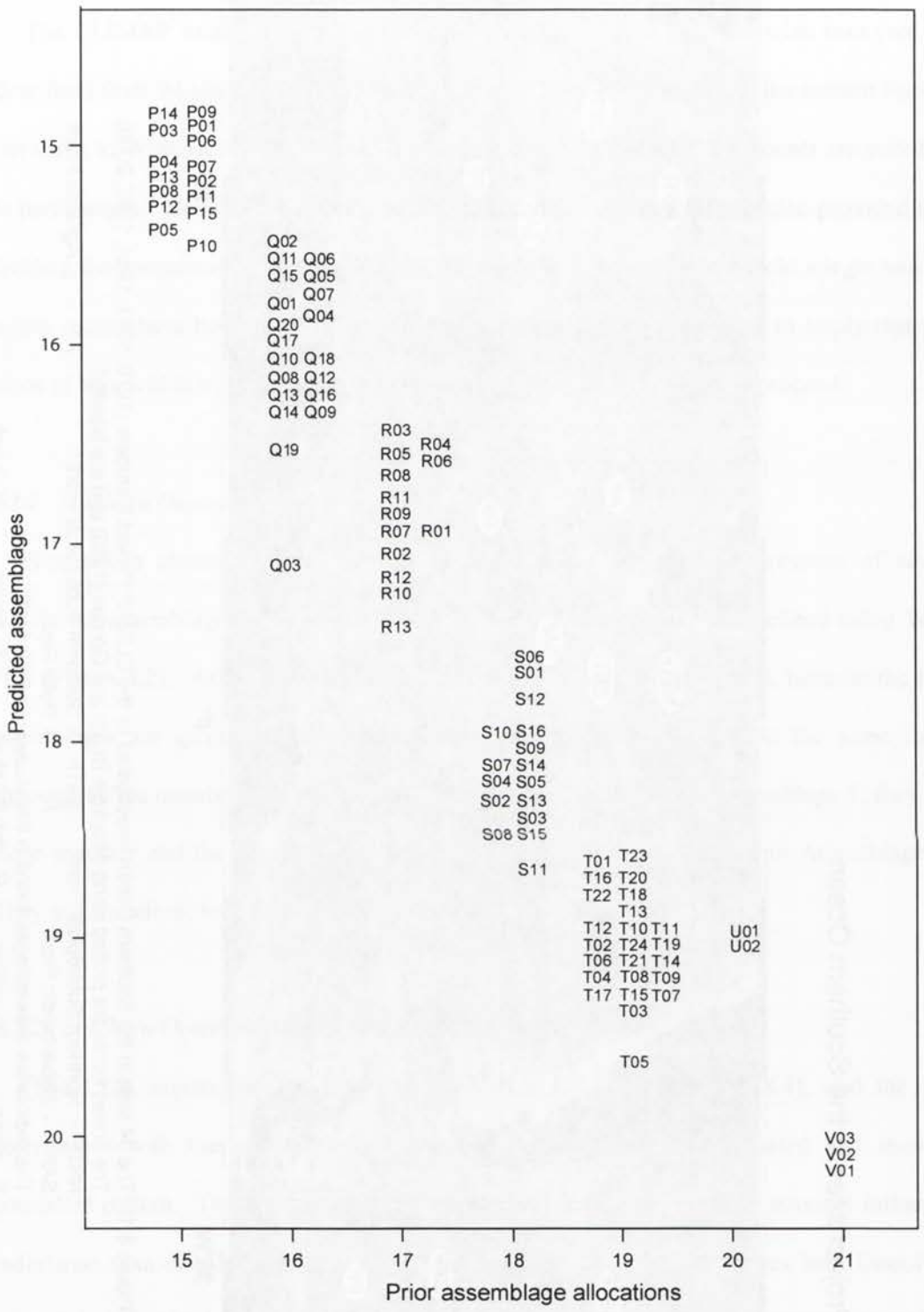

Figure 8.2: WA-PLS predictions of assemblages plotted against the Single-Run clustering assemblages which were used as input. Site labels have been moved into two columns where necessary to improve legibility.
The WA-PLS scores indicate that the assemblages tend to overlap to some extent. Q03 and Q19 appear to belong to Assemblage R, and S11, U01, and U02 to Assemblage T. Although geographically close to members of Assemblage T, Assemblage V is clearly compositionally distinct.

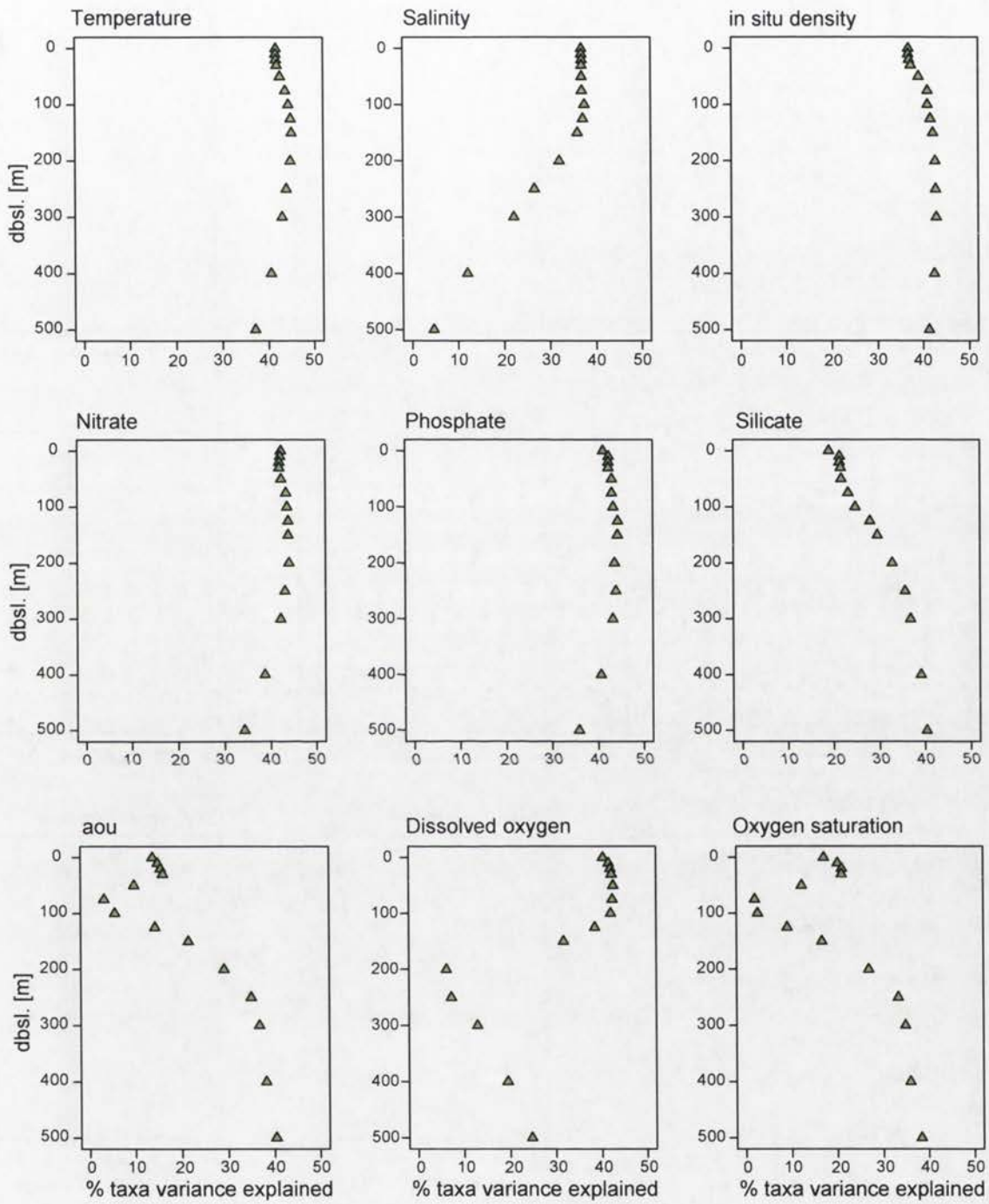

Figure 8.3: The percentage of taxa variance in CLIMAP (1997) radiolarian census counts [latitude 34-60°S; longitude 123°-130°E] in the Southern Ocean for the austral summer (jfm) explained by nine environmental variables at depths from the surface to 500 metres below sea-level (dbsl).

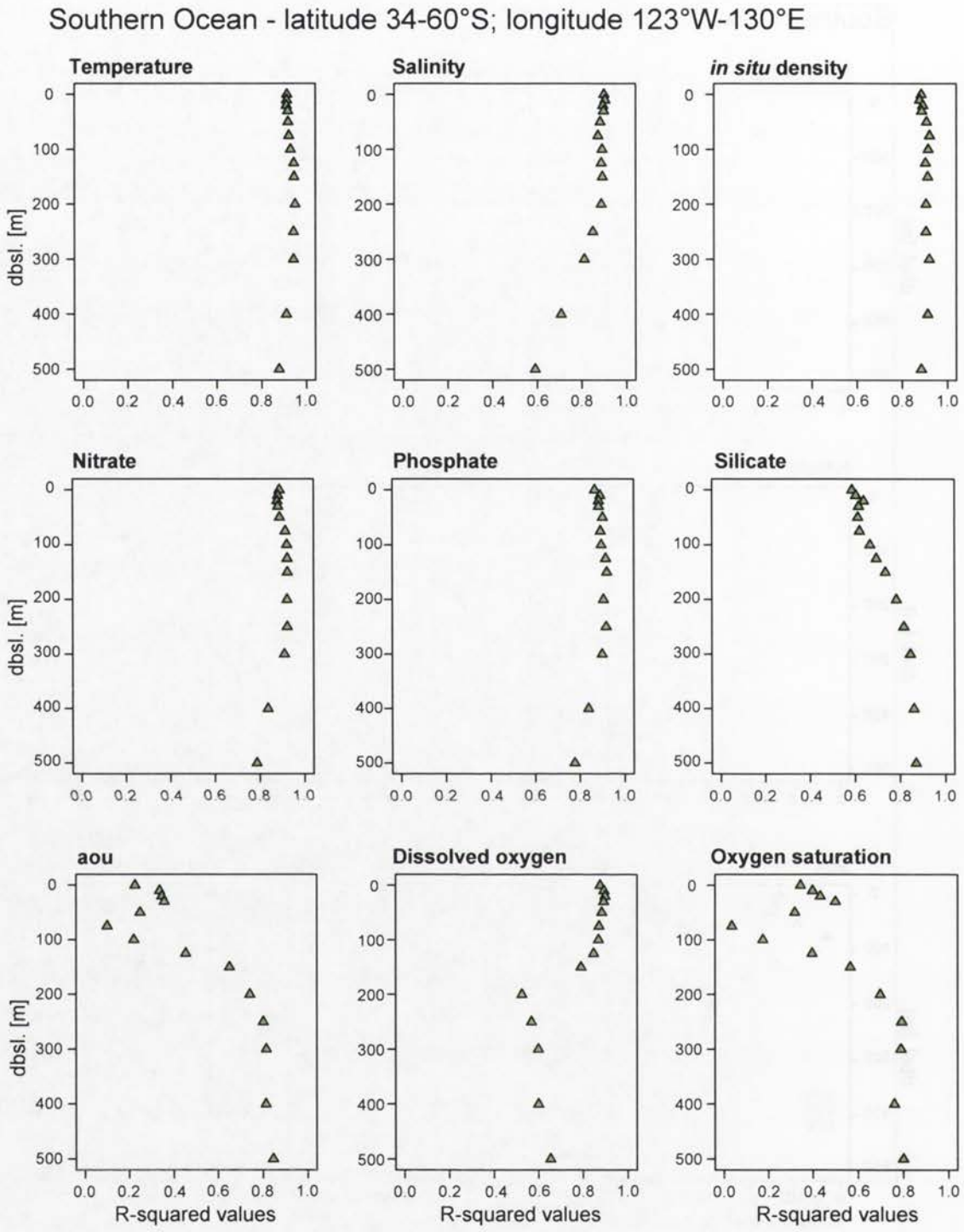

Figure 8.4: R-squared values obtained by applying WA-PLS to the CLIMAP (1997) Southern Ocean radiolarian census counts [latitude 34-60°S; longitude 123°-130°E] to each of nine environmental variables at depths from the surface down to 500 metres below sea-level (dbsl.) . Environmental values are for the austral summer (JFM).

Season	CA axis		Negative correlation					Positive correlation				
			1	2	3	4	5	1	2	3	4	5
Summer [JFM]	1	Variable	tmp 200m	tmp 150m	tmp 125m	tmp 100m	tmp 250m	sil 250m	pho 150m	isD 200m	isD 250m	sil 300m
		Correlation	-0.948	-0.945	-0.943	-0.941	-0.941	0.937	0.937	0.936	0.936	0.935
	2	Variable	sal 400m	sal 500m	sal 300m	sal 250m	sal 200m	Ods 250m	Ods 200m	Ods 300m	Ods 400m	Ods 500m
		Correlation	-0.651	-0.616	-0.586	-0.521	-0.401	0.722	0.677	0.67	0.53	0.357
	3	Variable	Ods 500m	Ods 400m	sal 150m	sal 200m	sal 125m	pho 500m	Ods 150m	Ods 125m	pho 400m	Ods 200m
		Correlation	-0.312	-0.212	-0.156	-0.156	-0.153	0.202	0.201	0.19	0.16	0.131
	4	Variable	pho 500m	pho 400m	Ods 200m	sal 020m	sal 050m	sil 000m	sil 010m	sil 020m	sil 125m	sil 050m
		Correlation	-0.115	-0.082	-0.074	-0.071	-0.069	0.146	0.127	0.098	0.085	0.078

Table 8.2: The top ten correlations between the CLIMAP radiolarian census CA scores (four axes) with austral Summer values for the environmental variables. Temperature (abbreviated "tmp"), silicate (sil), phosphate (pho), salinity (sal), dissolved oxygen (Ods), and *in situ* density (isD) all appear potentially explanatory. tmp 200m indicates temperature at 200 metres bsl.

The CCA eigenvalues (Table 8.3) show that one explanatory variable (or combination of collinear variables) explains over 46% of the variance in the radiolarian data and Figures 8.5a-b indicate that temperature, salinity, and phosphate, or a combination thereof, are major factors. In the Polar Frontal and Antarctic Zones, salinity is particularly significant and silicate may be a secondary factor, (Figure 8.5b).

Region	Figure		Axis 1	Axis 2	Axis 3	Axis 4	Total
CLIMAP	8.5	Eigenvalues	0.493	0.063	0.019	0.004	1.065
		Cumulative % variance of species data	46.3	52.2	54.0	54.4	

Table 8.3: The CCA eigenvalues and cumulative percentage variance explained for the CLIMAP Southern Ocean data with temperature, salinity, phosphate, and silicate as canonical variables (albeit from different depths below sea-level).

Southern Ocean - latitude 34°-60°S; longitude 123°W-130°E

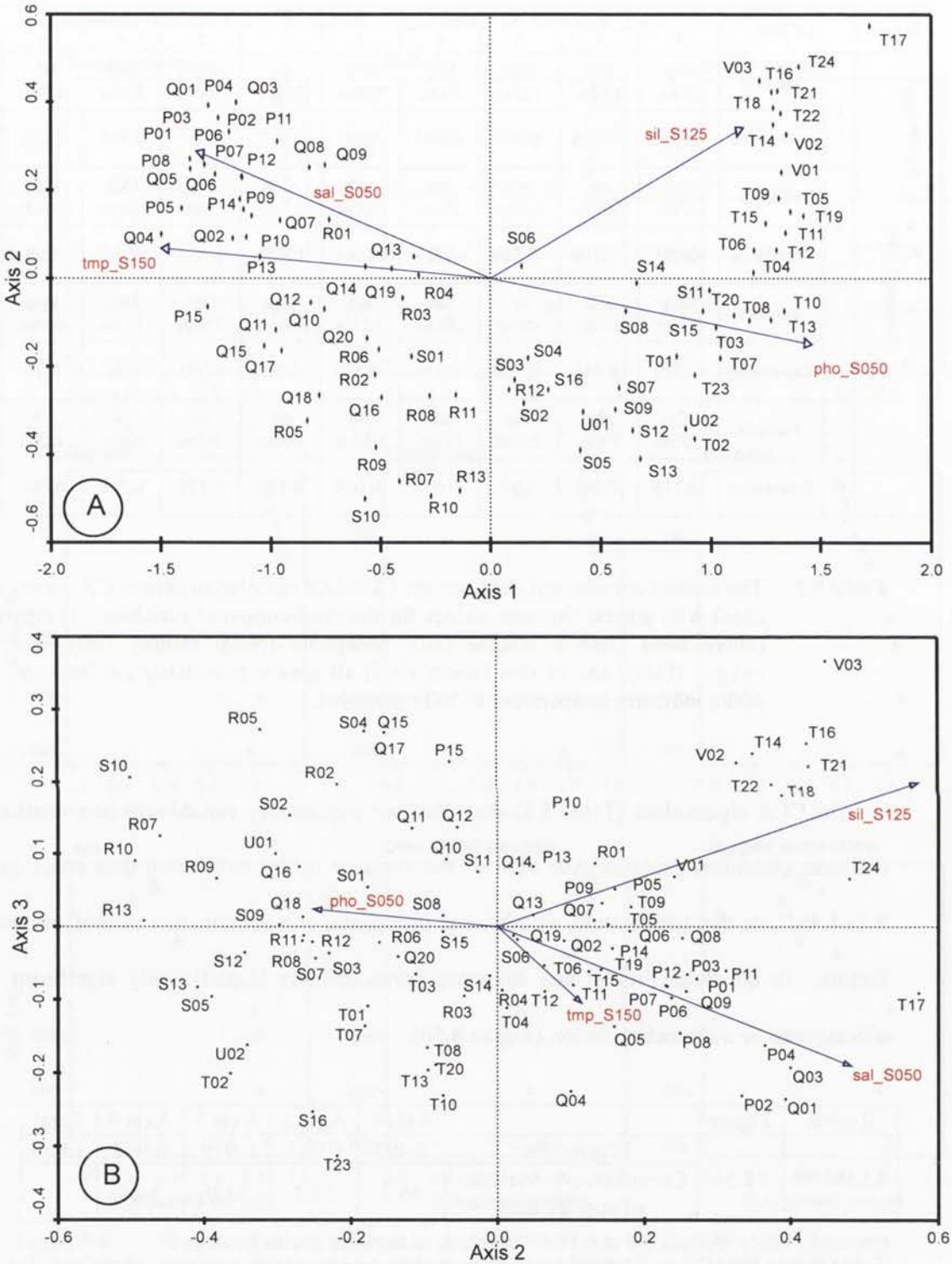

Figure 8.5: *CANOCO* CCA plots for the CLIMAP (1997) Southern Ocean radiolarian census counts [latitude 34°-60°S; longitude 123°-130°E] for the austral Summer (JFM): axis 1 against axis 2 in Plot A and axis 2 against axis 3 in Plot B.
Temperature, salinity, and phosphate are the major factors. silicate is secondary. The relative influences of temperature, salinity, and phosphate are difficult to separate: silicate's importance in the Antarctic Zone is clear.

8.3. Longitude 175°E in the Pacific Ocean (Kamikuri et al., 2008)

Kamikuri *et al.* (2008) studied twenty-four surface sediment samples between latitudes 48° and 14°S along longitude 175°E in the Pacific Ocean (Figure 8.6), counting approximately 1000 radiolarian specimens at each site. They identified five assemblages which they were able to equate to climatic zones (from south to north: the Tropical, Subtropical, Transitional, and Subarctic). Single-Run cluster analysis confirms these clusters whilst suggesting Assemblage I might be split at the Equator, something Kamikuri *et al.* also observed. Interestingly, the expectation-maximisation algorithm (Fraley and Raftery, 1998, 2006) indicates that the samples were so dissimilar, one from the other, that each might be considered a separate cluster. Examination of the raw data tends to support this conclusion.

8.3.1. Pacific Ocean radiolarian-environmental associations

The WA-PLS R^2 values and percentages of the CCA eigenvalues explained indicate that temperature, salinity, nitrate, and phosphate at depths below sea-level around 100 metres and silicate and dissolved oxygen in the upper 50 metres are important explanatory variables (Figures 8.7 and 8.8). The correlations between the CA scores and the environmental variables tend to contradict this to a degree, with temperature, nitrate, and salinity being the best candidates. The ratios of the CCA eigenvalues from *CANOCO* (Table 8.4) suggest three explanatory variables, and the plot of axes 1 against 2 and axes 2 against 3 (Figures 8.9a and b respectively) place temperature as the primary factor, salinity and nitrate also contributing.

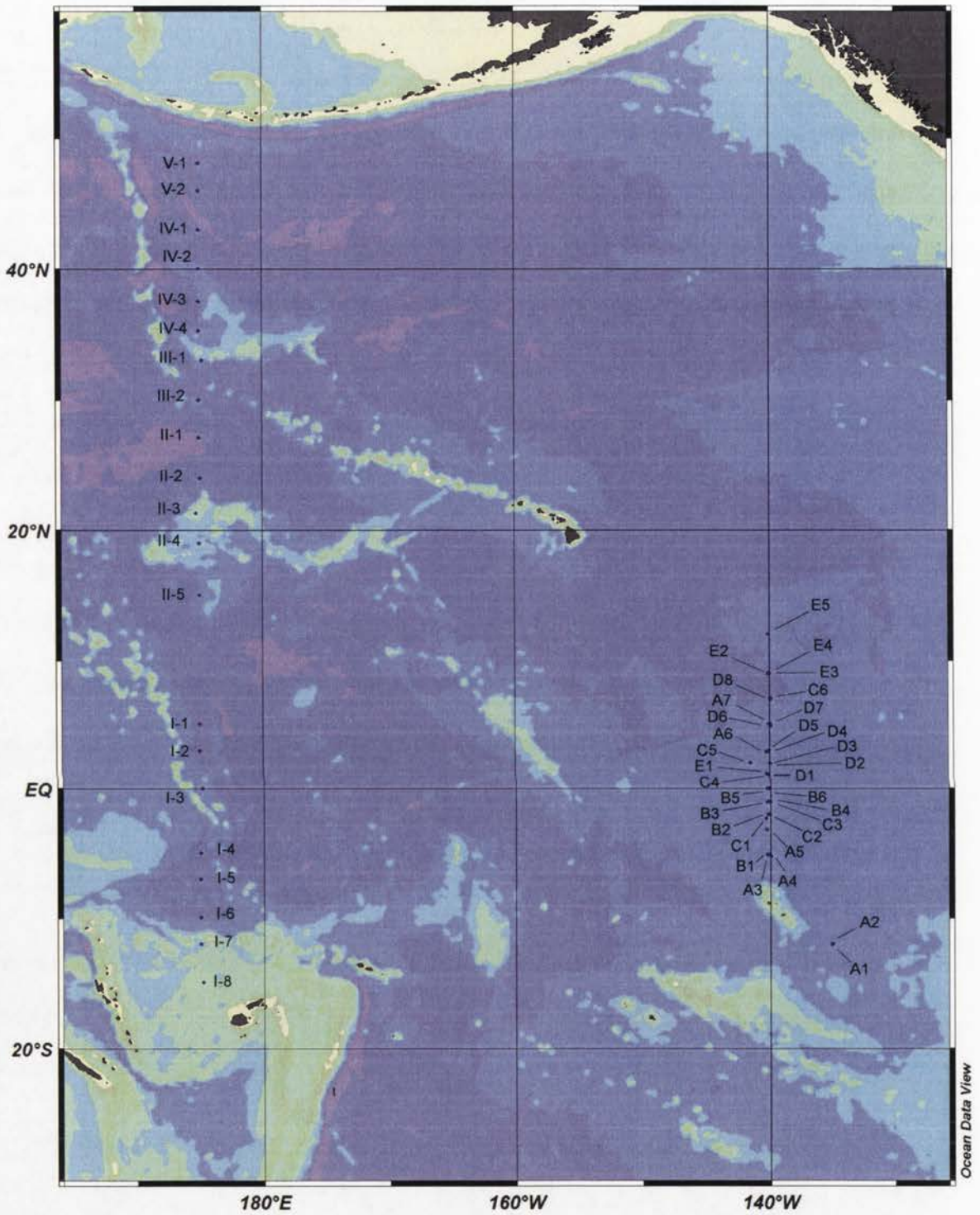

Figure 8.6: The Pacific Ocean showing the sites and assemblage designations of Kamikuri *et al's.* (2008) surface sediment samples (longitude 175°E - Assemblages I-V) and Welling's (2003) tow samples (longitude 140°W - Assemblages A-E). Kamikuri *et al's.* (2008) assemblages map climatic zones (see authors' publication). Welling's (2003) sites fall within the Tropical Zone. The Welling assemblages are only broadly related to latitude.

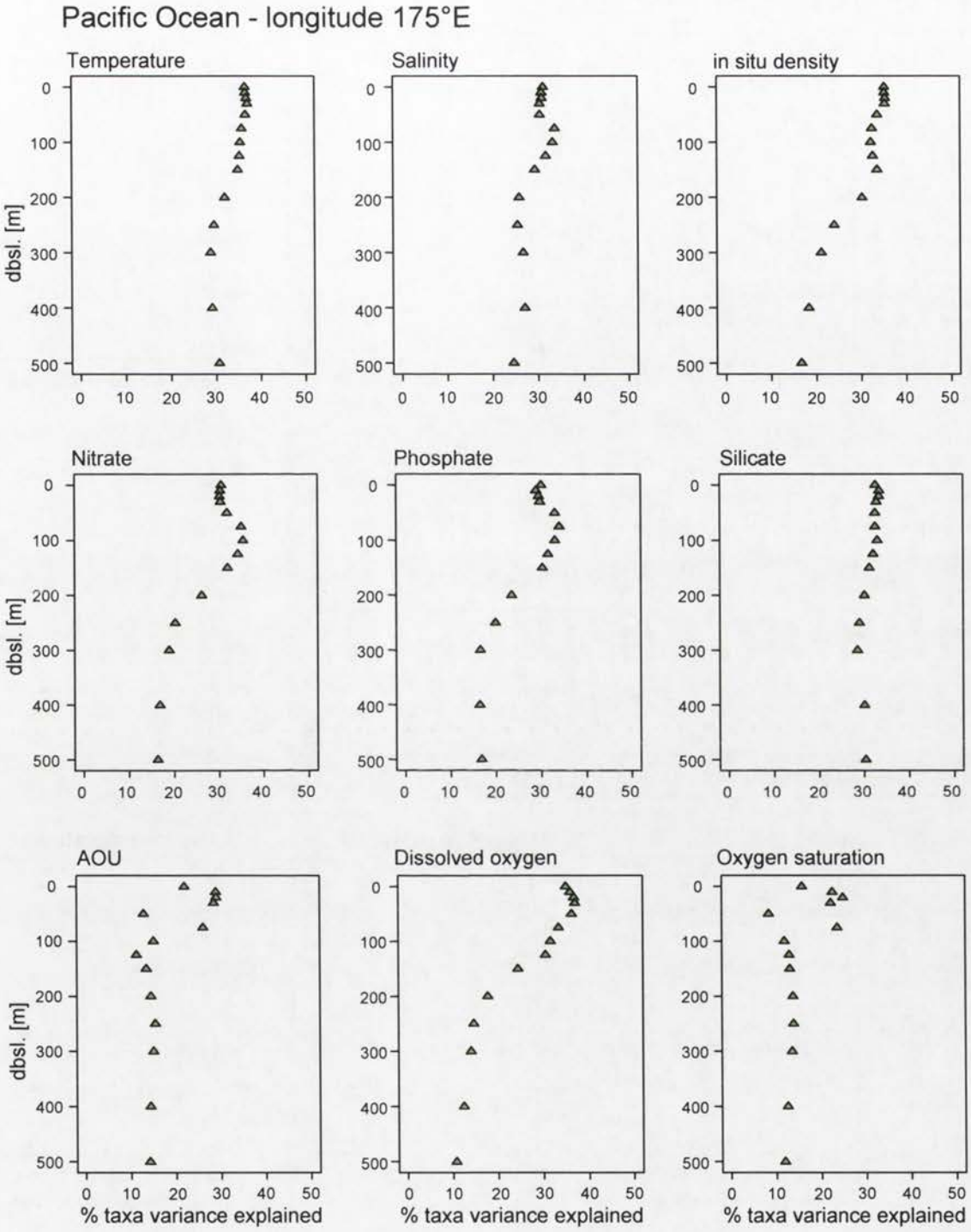

Figure 8.7: The percentage of taxa variance in the Kamikuri *et al.* (2008) Pacific Ocean [longitude 175°E from latitude 48°N to 15°S] radiolarian census counts for the boreal summer (JAS) explained by nine environmental variables from the surface to depths below sea--level (dbsl) down to 500 metres.
The relationship between the radiolarian data and temperature, salinity, *in situ* density, and silicate are strong from the surface to about 150 metres bsl. The relationship with nitrate, phosphate,and dissolved oxygen is strong in the mixed layer; that with aou and oxygen saturation occurs in the mixed layer.

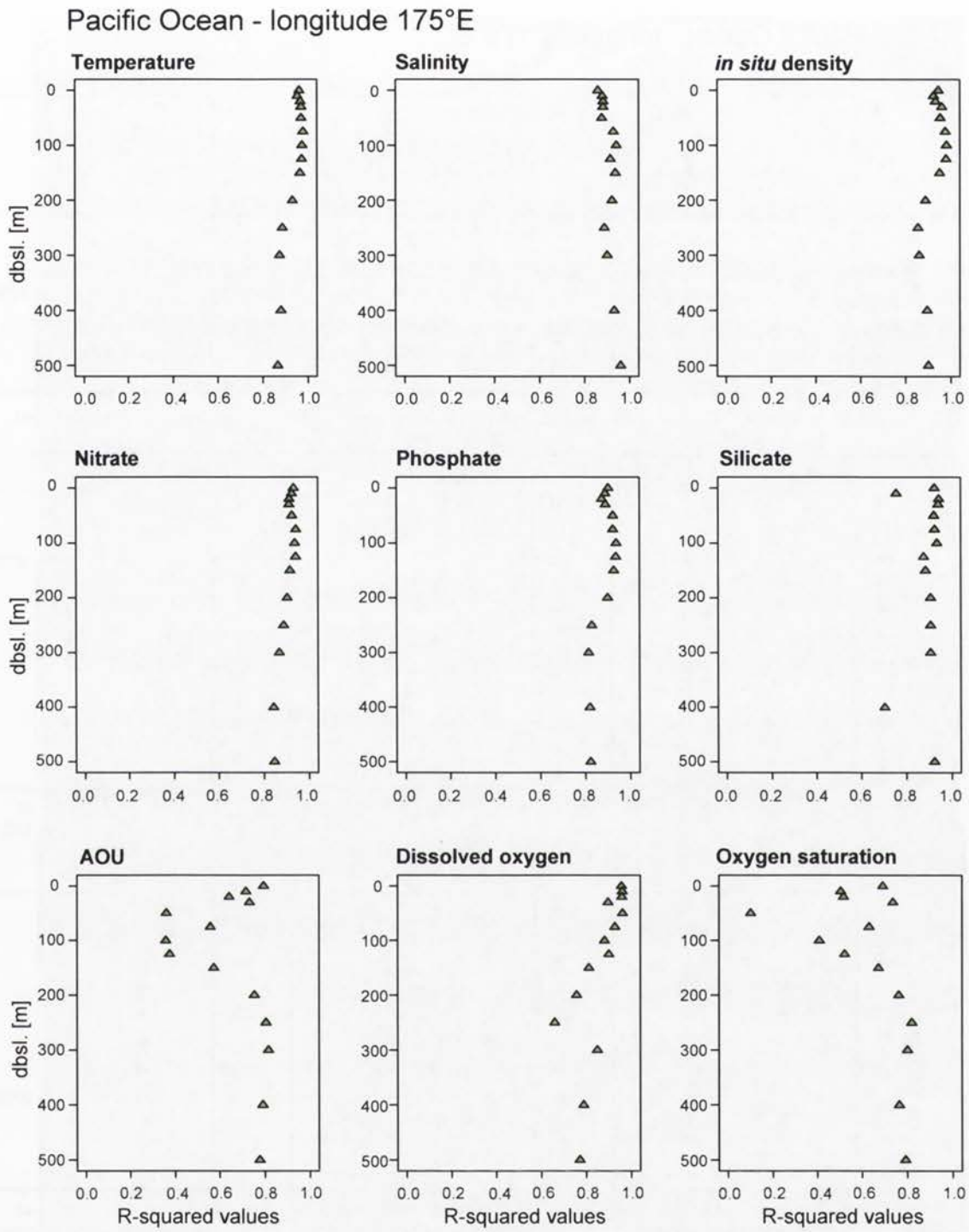

Figure 8.8: R-squared values obtained by applying WA-PLS to the Kamikuri *et al.* (2008) radiolarian census counts for longitude 175°E from latitude 48°N to 15°S in the Pacific Ocean to each of nine environmental variables at depths below sea-level (dbsl) from the surface down to 500 metres. Environmental values are for the boreal summer (JAS).
The relationship between the radiolarian data and temperature, salinity, *in situ* density, nitrate, phosphate, and silicate are very strong from the surface down to about 150 metres bsl. The relationship with dissolved oxygen is strong in the mixed layer; that with AOU and oxygen saturation is less strong and occurs below 200 metres.

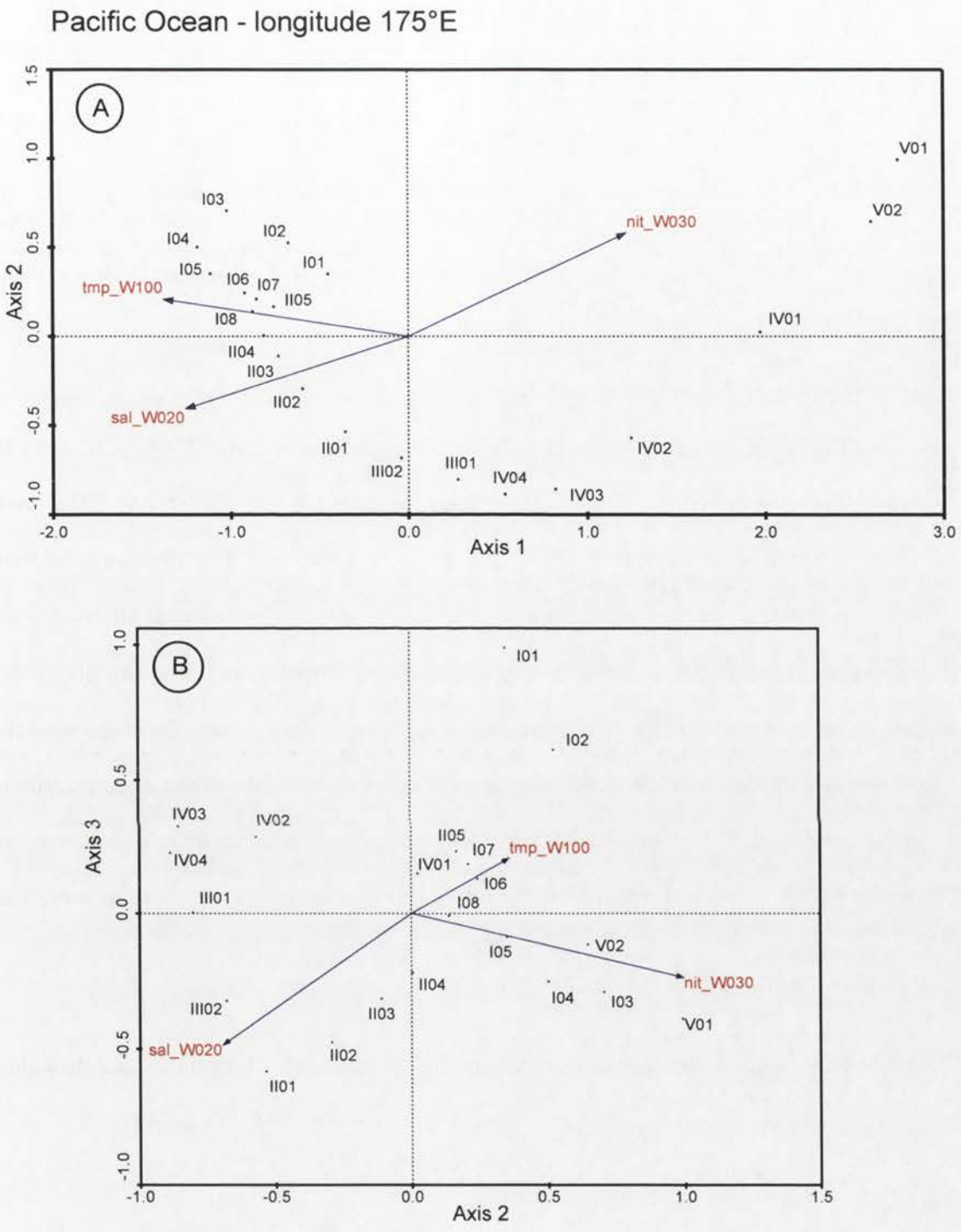

Figure 8.9: *CANOCO* CCA diagrams for the Kamikuri *et al.* (2008) Pacific Ocean radiolarian census counts for longitude 175°E from latitude 48°N to 15°S. Plot A shows axis 1 against axis 2, and Plot B axis 2 against axis 3. The assemblages I-V were identified by Kamikuri *et al.*
Plot A shows temperature and salinity to be major explanatory factor with nitrate being important for assemblages IV and V (close to the Subarctic Front).
Plot B also shows that salinity is particularly influential at latitudes 10°-30°N (i.e. approaching the Northern Subtropical Front) and 5°-15°S.

Region	Figure		Axis 1	Axis 2	Axis 3	Axis 4	Total
All Kamikuri	8.9	Eigenvalues	0.587	0.228	0.119	0.191	1.654
		Cumulative % variance of species data	35.5	49.3	56.5	68.0	

Table 8.4: The CCA eigenvalues and cumulative percentage variance explained by Kamikuri *et al's* (2008) data for the longitude 175°E in the Pacific Ocean with temperature, salinity, and nitrate as canonical variables (albeit from different depths below sea-level). The ratios of the eigenvalues suggest there are three explanatory variables.

8.3. Longitude 140°W in the Pacific Ocean (Welling, 2003)

Welling (2003) has published counts of radiolarians found in 64μm MOCNESS tows at 32 sites between latitudes 12°N and 12°S along longitude 140°W (Figure 8.6). The tows covered a range of depths at each site, mainly from the surface down to 200 metres bsl, but with some deeper. For this study, the counts for each site were summed over all tow depths to simulate the radiolarian distribution which might be found in surface sediments in the unlikely event all the tests survived descent through the water column. From the analytic viewpoint, this fiction is allowable because the objective is to determine the association between radiolarian distributions and oceanographic environmental variables and there is no reason to believe that any such association would be corrupted by a differential conservation of taxa as a result of losses in the water column.

Welling's (2003) sample sites straddle the north and south Doldrum Fronts [latitudes 11°N and 6°S respectively (Roden, 1975)] but do not extend to the Subtropical Fronts.

8.3.1. Longitude 140°W clustering

Application of the Single-Run approach gave five clusters (labelled Assemblages A-E); use of WA-PLS provided a check with no adjustment being required. Assemblages B, D, and E might be geographically associated but Assemblages A and C are definitely not (Figure

8.6). In contradiction to the clustering results, CCA plots (Figure 8.12) definitely group the sites geographically.

8.3.2. Longitude 140°W radiolarian-environmental relationships

The relationships between the radiolarian data and the WOA-05 environmental variables are rather weak. Virtually none of the environmental variables explain more than 10% of the CCA taxa variance (Figure 8.10) and few of the WA-PLS R^2 exceed 0.8 (Figure 8.11) – much less than the values in excess of 0.9 typical of the other census datasets. The eigenvalues derived from *CANOCO* CCA are very small (Table 8.5) and the ratios suggest there are between one and three explanatory variables. The percentage of variance explained is low, indicating excessive noise in the system or the absence of some important variables. Examination of the *CANOCO* plots (Figure (8.12) shows that temperature and salinity are explanatory variables with nitrate and, to a lesser extent, salinity, marking a major partition close to the Equator.

Region	Figure		Axis 1	Axis 2	Axis 3	Axis 4	Total
All Welling	8.12	Eigenvalues	0.096	0.030	0.021	0.088	0.594
		Cumulative % variance of species data	16.1	21.1	24.7	39.5	

Table 8.5: The CCA eigenvalues and cumulative percentage variance explained by Welling's (2003) data for the longitude 140°W in the Pacific Ocean with temperature, salinity, and nitrate as canonical variables (albeit from different depths below sea-level).

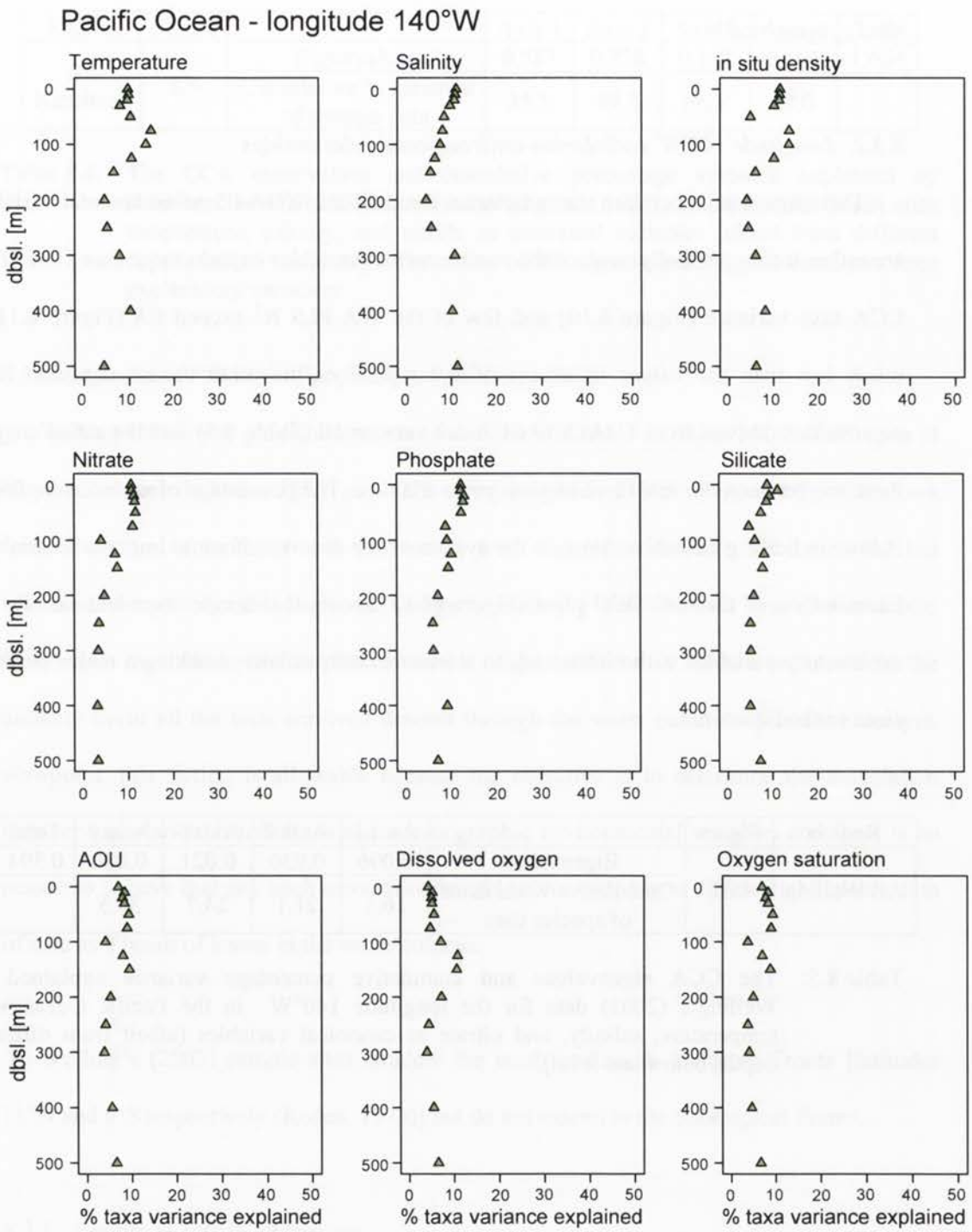

Figure 8.10: The percentage of taxa variance in the Welling (2003) Pacific Ocean [longitude 140°W from latitude 12°N to 12°S] radiolarian census counts for the boreal summer (JAS) explained by nine environmental variables at depths below sea-level (dbsl) from the surface down to 500 metres.
The relationship between the radiolarian data and each of the environmental variables tested is weak suggesting that either the important variables were not included or that the taxa variance is explained by a combination of relatively orthogonal variables.

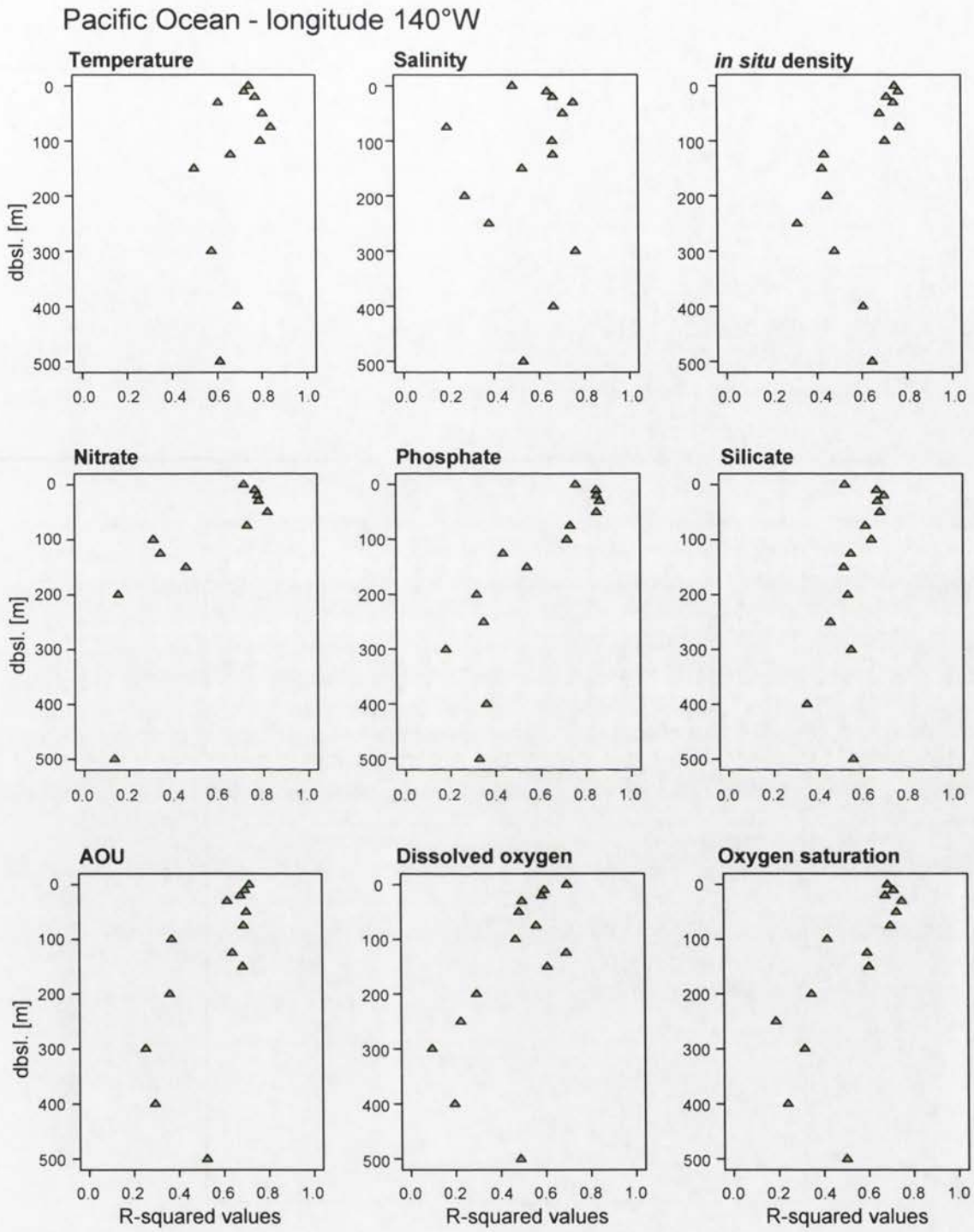

Figure 8.11: R-squared values obtained by applying WA-PLS to the Welling (2003) Pacific Ocean [longitude 140°W from latitude 12°N to 12°S] radiolarian census counts and each of nine environmental variables at depths below sea-level (dbsl.) down to 500 metres. Environmental values are for the boreal summer (JAS). The relationship between the radiolarian data and the environmental variables are generally weak. There is some evidence of the influence of temperature at about 75 metres bsl. and nitrate and phosphate around 20-50 metres bsl.

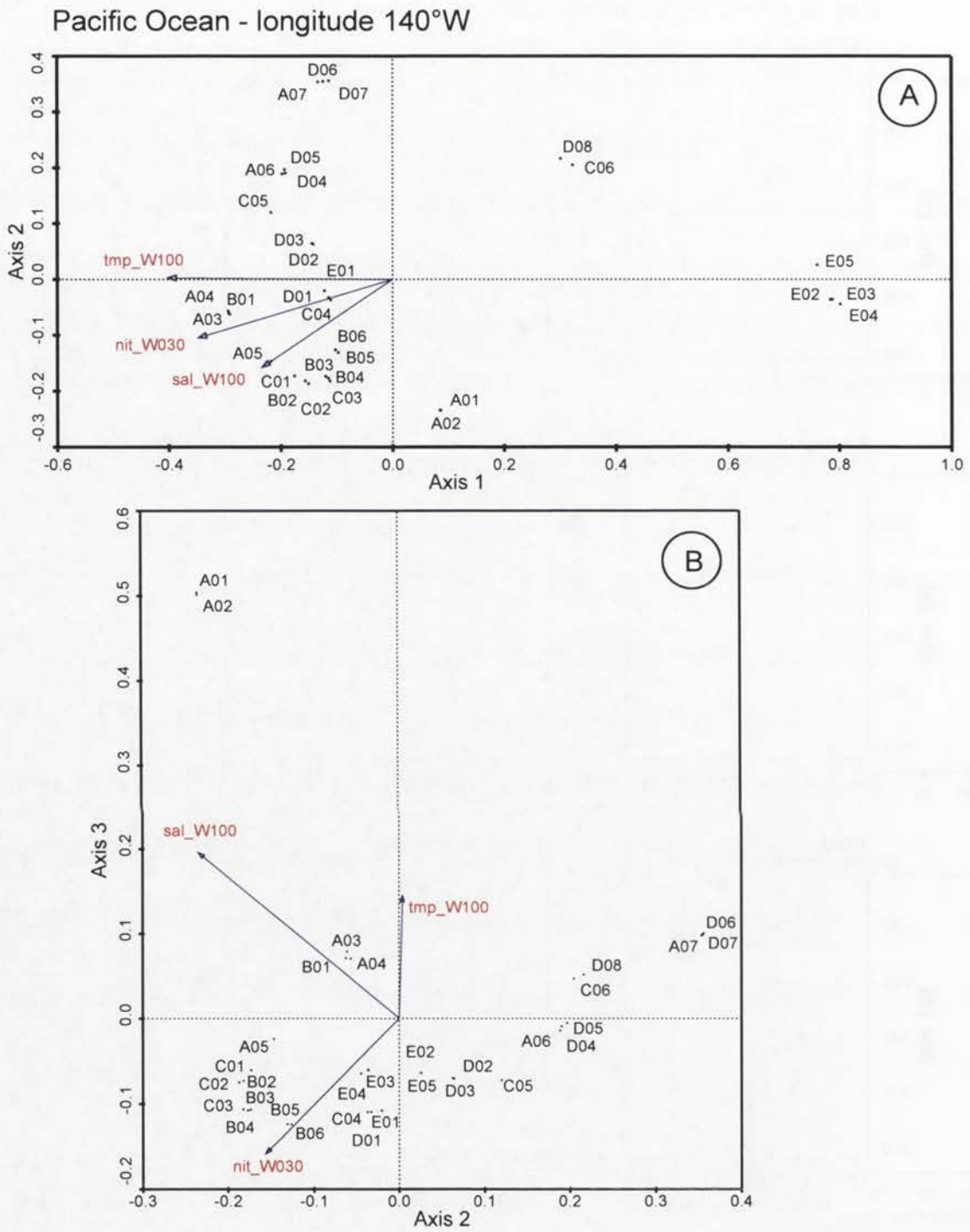

Figure 8.12: *CANOCO* CCA plots for the Welling (2003) Pacific Ocean [longitude 140°W from latitude 12°N to 12°S] radiolarian census counts. Plot A shows axis 1 against axis 2 and Plot B 2 against 3. The environmental values (temperature at 100m, nitrate at 30m, and salinity at 100m) are for the boreal summer (JAS).
Plot A shows that temperature separates a small number of sites from the majority.
Plot B indicates that nitrate is an important explanatory variable.

8.4. The Sea of Okhotsk (Nimmergut and Abelmann, 2001)

Nimmergut and Abelmann (2001) have published radiolarian census counts for surface sediments taken from thirty-three sites in the Sea of Okhotsk (Figure 8.13). Cluster analysis suggests four radiolarian assemblages (termed Assemblages A-D) which do not appear to be geographically associated. CCA against each of the nine WOA-05 environmental variables in turn reveals that little taxa variance is explained – typically no more than 10%. Similarly, the WA-PLS R^2s are less than 0.8 for almost every variable at every depth (Figure 8.14). The eigenvalues from *CANOCO* CCA results indicate two to three explanatory variables, the first two explaining 37.6% of the taxa variance (Table 8.6).

Region	Figure		Axis 1	Axis 2	Axis 3	Axis 4	Total
Sea of Okhotsk	8.15	Eigenvalues	0.281	0.142	0.048	0.020	1.125
		Cumulative % variance of species data	25.0	37.6	41.9	43.7	

Table 8.6: The CCA eigenvalues and cumulative percentage variance for the Nimmergut and Abelmann's (2001) Sea of Okhotsk data with water depth, temperature, phosphate, and nitrate as canonical variables.

Water depth for the counts ranges from 128 to 3360 metres and prove, with nitrate, phosphate, or a combination of the two, to be strong candidates for major explanatory variables: temperature at 200 metres bsl is a third (Figure 8.15).

Sea of Okhotsk

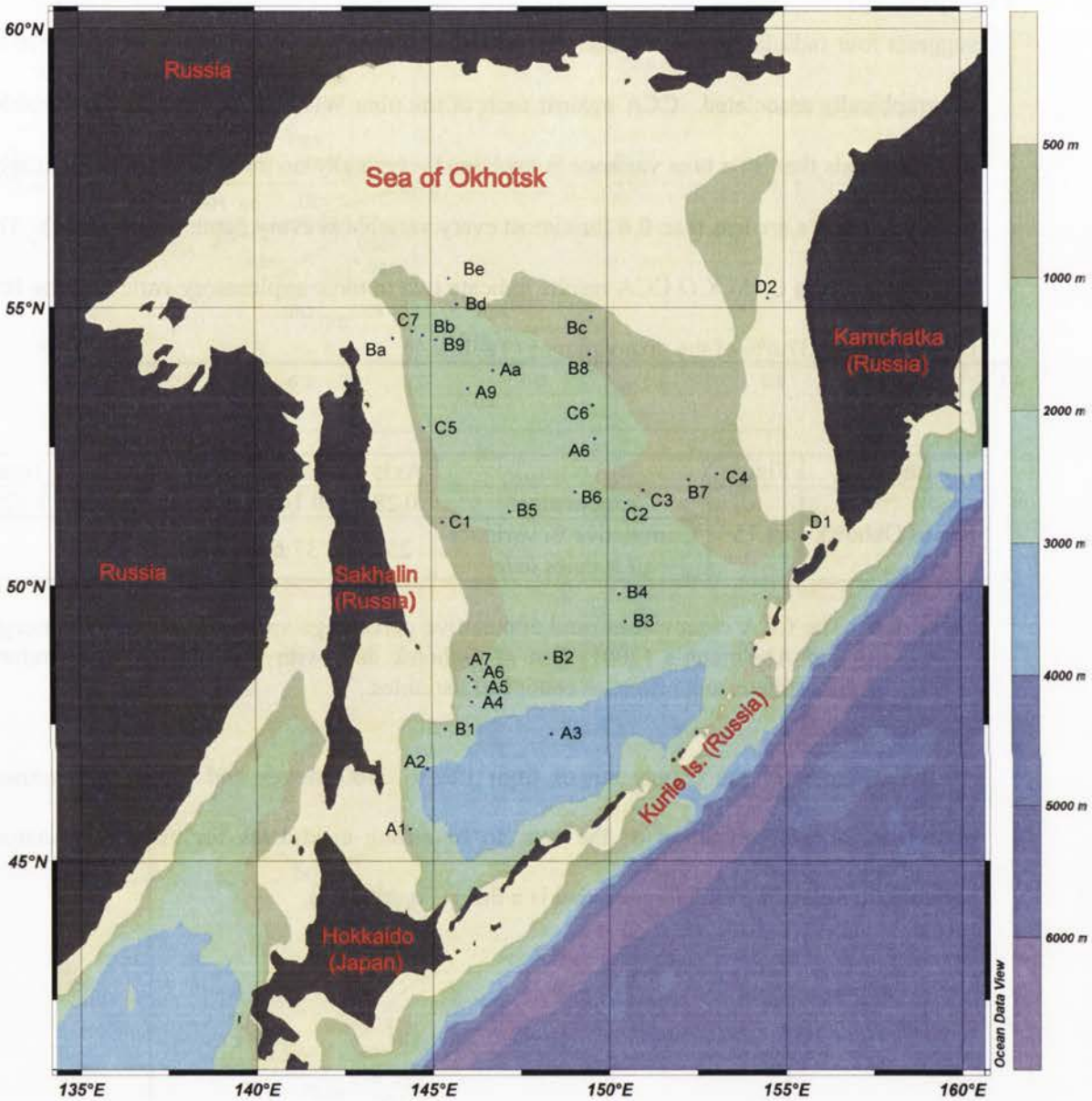

Figure 8.13: Nimmergut and Abelmann's (2005) surface sediment sites in the Sea of Okhotsk. Sites are labelled according to the results of cluster analysis - the initial letter designates the assemblage - see §8.4 of the text for further details.

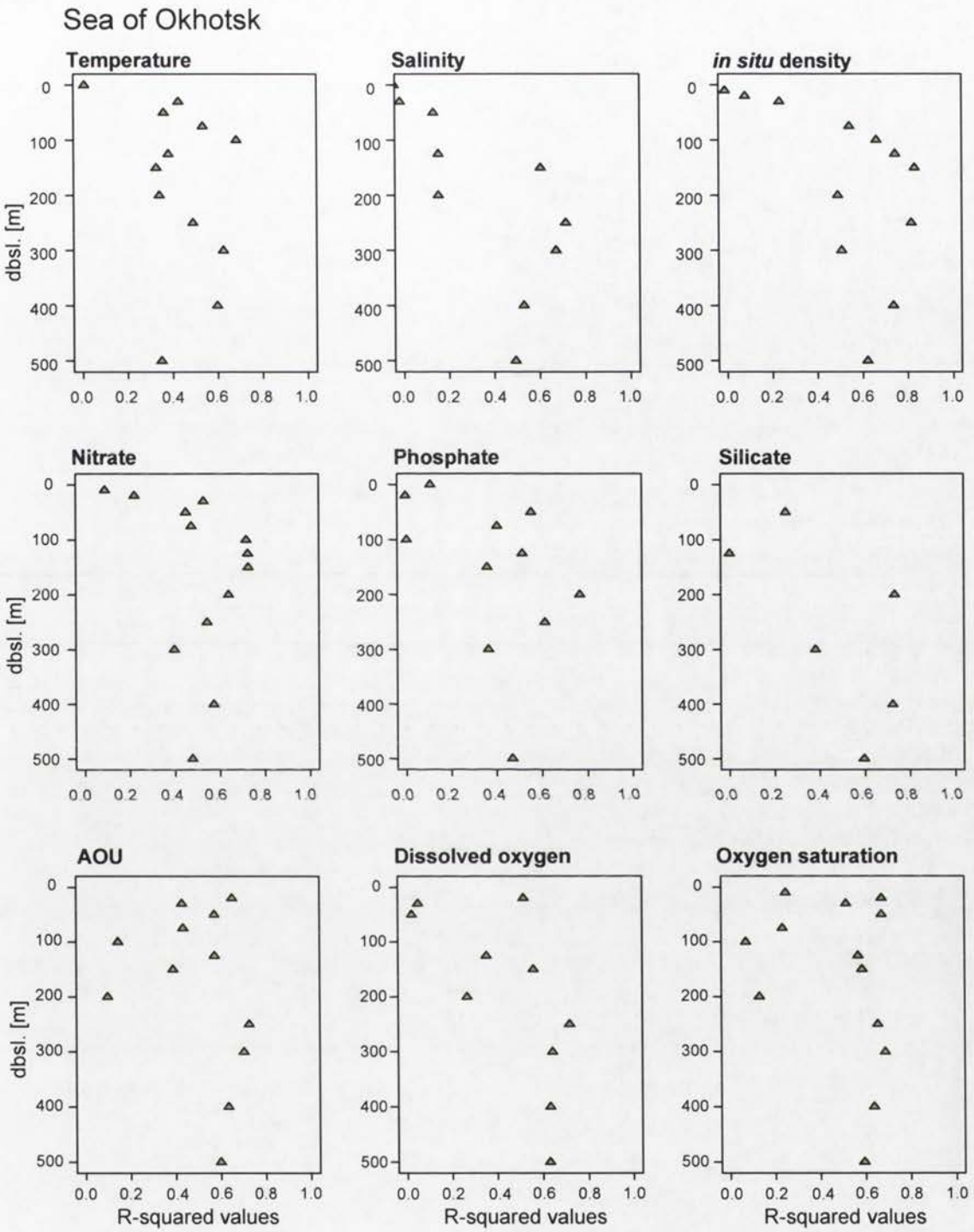

Figure 8.14: R-squared values from applying WA-PLS to the Nimmergut and Abelmann's (2003) radiolarian census counts for the Sea of Okhotsk and each of nine environmental variables at depths below sea-level (dbsl) down to 500 metres. The environmental values are for the boreal summer (JAS). There is no clear relationship between the radiolarian data and any of the environmental variables.

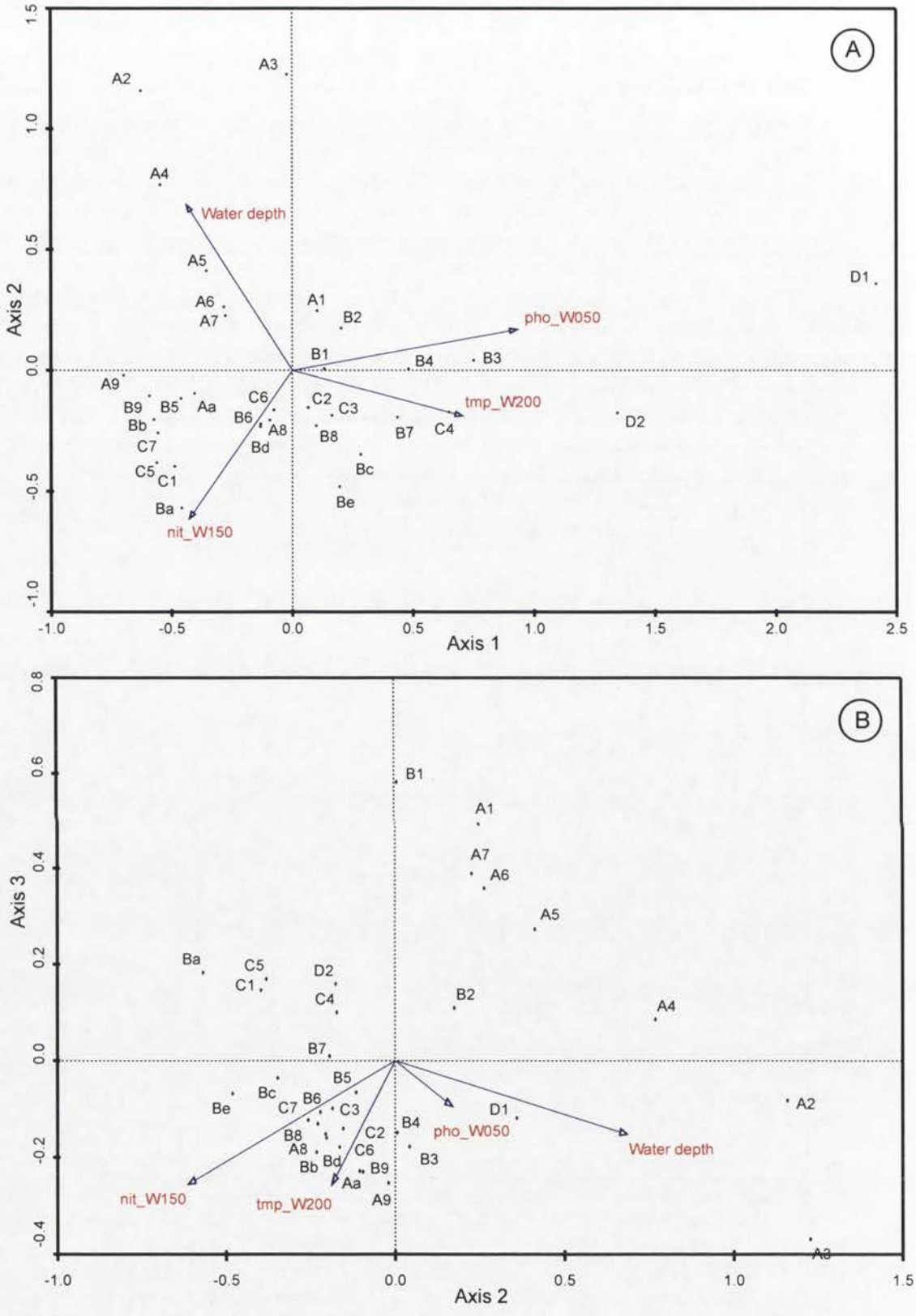

Figure 8.15: *CANOCO* CCA results for the Nimmergut and Abelmann's (2001) Sea of Okhotsk census counts. Plot A is for axis 1 against axis 2, and Plot B 2 against 3. Assemblages are indicated by the inital letter of labels.
In Plot A, two sets of sites, A2-A7 and (A9, B9, C7, C1, and Ba), amongst others, can be seen to be aligned with decreasing water depth. Nitrate, phosphate, and temperature also seem to have influenced the radiolarians.

Chapter 9: Discussion of the results of the surface sediment analysis

9.1. Radiolarian assemblages and their relationship to water masses

9.1.1. Introduction

Rogers and De Deckker (2007) spoke of there being eleven distinct radiolarian assemblages in the area of the Indian Ocean studied, six in the EIO and five in the SIO. After that paper was published, a number of the study's core tops were radiocarbon dated and five from the EIO and three from the SIO were found to be more than 5000 years old. Exclusion of the five from the EIO census counts had a significant effect on that dataset's statistical properties, although there was no discernable difference following the exclusion of the three "old" sites from the SIO counts. Only CCA, which is influenced by the explanatory environmental variables included in the analysis, revealed the six assemblages previously identified. Most of the cluster analyses suggest three assemblages only in the EIO.

A further complication with identifying assemblages arises from consideration of samples from sites on the border between two obviously distinct taxa groupings. Different forms of analysis will either distribute the samples between the major groupings in ways which depend on the particular analytic technique, or point to a separate grouping. The evidence for six assemblages in the EIO must, therefore, be regarded as weak. In the SIO, a case could be made for merging Assemblages J and K, or for redistributing them to form three principal groups.

The identification of Indian Ocean assemblages confirms and refines the work of previous researchers, particularly Johnson and Nigrini's (1982), so far as their different analytic methods allow comparison. Comparison is difficult because Johnson and Nigrini restricted themselves to the presence or absence of 74 taxa: this study analysed the abundance counts of all taxa present. Thus, for example, Johnson and Nigrini (1982) did not include

Tetrapyle octacantha in their assemblages because it is ubiquitous but it is a strong factor in this study with over 22% occurrence in the EIO assemblages against less than 6% in those from the SIO. Comparison is also difficult because Johnson and Nigrini employed larger samples to decide on the presence or absence of taxa ["two or more strewn slides" (Johnson and Nigrini, 1982) against this study's single slide]. As a result, they were able to identify a recurrent group consisting of three species, *Pterocanium praetextum eucolpum, Theocorythium trachelium dianae,* and *Trigonastrum* sp., for temperate latitudes whereas only two specimens of *P. praetextum eucolpum* were observed during the present study and none of the other two species. With regard to *Theocorythium trachelium dianae,* it is possible that some specimens were present but were misidentified as the very similar *T. trachelium trachelium.* Fortunately, even if this did occur, this study's statistical approach was such that there would have been little information loss because *T. trachelium* levels averaged 1.5% north of 32°S and only 0.5% south of that.

9.1.2. The eastern Indian Ocean (EIO)

In the EIO, six assemblages are distinguishable and map environmental provinces (labelled I-VI in Figure 9.1; see also Figure 7.16). The physico-chemical differences in the ocean's composition which the assemblages reflect appear to be influenced by the area's surface currents, although the Western Australian Current (or Leeuwin Undercurrent) may also be an important factor in the south (cf. Figure 4.4). The physico-chemical environment of the region is further affected by the cooling of currents as they flow south and evaporation which increases the salinity of the relatively fresh ITF waters to a peak about 32°S.

The EIO radiolarian assemblages

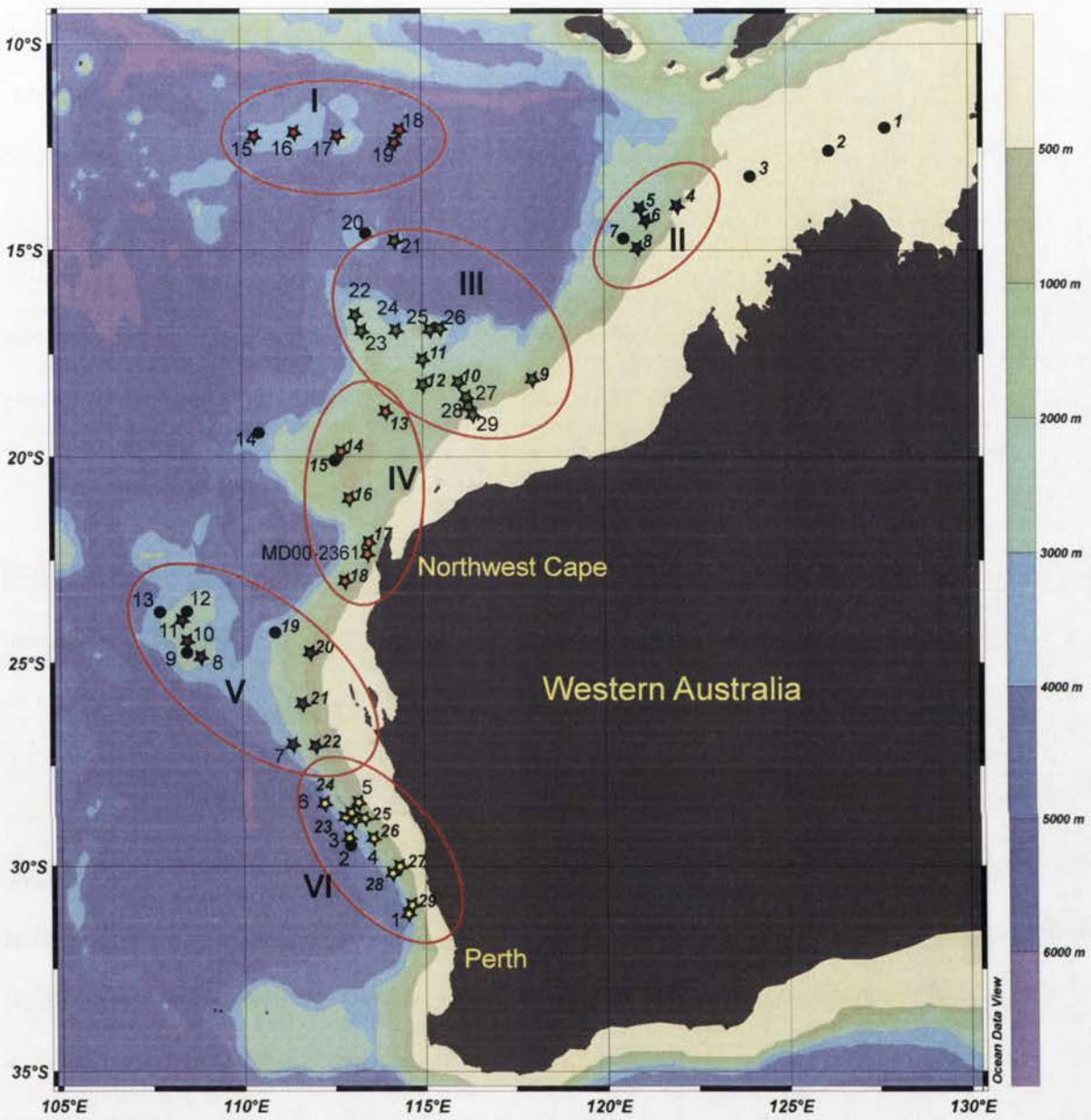

Figure 9.1: The EIO radiolarian assemblages based on cluster analysis and refined using *CANOCO* CCA results. Six assemblages are identified (I-VI). The sites are marked with stars: *RV. Franklin* 10-95 sites are labelled in italics and 02-96 in regular font. Sites marked with circles are those for which the radiolarian density was too low to provide an adequate count or sites dated as older than 5000 years.
The radiolarian assemblages shown here tend to follow the ocean currents shown in Figure 4.4.

Province I is associated with the Java Upwelling; province II with the Indonesian Throughflow (ITF), and III with the ITF, the northern leg of the Equatorial Gyral Current (EGC), and, probably the South Java Current. Province IV, whose associated radiolarian assemblage is not very different to that of province III, is located where the southern leg of the EGC meets the continuation of the ITF (termed the Leeuwin Current) and is likely to be influenced by the upwelling of the Cape and other coastal currents (Figure 4.4). Finally, provinces V and VI appear where the Leeuwin Current overlies the WAC and flows counter to the Cape Coastal Current: the difference between the two provinces arises from salinity levels in the ocean.

This disposition of assemblages and provinces in the EIO is very similar to that described by Johnson and Nigrini (1982). Unfortunately, only a limited number of Johnson and Nigrini's (1982) 74 sample sites are close to the Western Australian coast: two sites in this study's environmental Province I, two in III with two more close, three close to Province VI, and none in Provinces II, IV, or V. Despite this and the disadvantages of presence-absence against abundance data, it is possible to confirm some of their findings and develop others. Johnson and Nigrini (1982) identified three provinces in the eastern sector. Their Tropical Province covers this study's Provinces I-III, and, so far as comparison is possible, is compositionally similar. Johnson and Nigrini could not have found a distinction between Provinces I and II as they had no sample site in Province II. Their South Equatorial Province geographically includes most of Province IV and their Central Province corresponds with Provinces V and VI. In fact, using their recurrent group criteria, the South Equatorial Province is seen to extend as far south as 27°S, encompassing the whole of Province V and, perhaps, part of VI. This is consistent with the South Equatorial Province (SEP) being associated with the Equatorial Gyral Current which flows eastwards through the latitude of the SEP, then splits, part turning south along the coast of Western Australia.

Further confirmation of the validity of this study's radiolarian provinces comes from Martínez *et al.* (1998) who investigated the same EIO core-tops as used here. These authors report five planktonic foraminiferal provinces which correspond exactly with the location of this study's radiolarian assemblages except in that their Western Pacific Warm Pool province II covers three radiolarian-based provinces, II, III, and IV.

9.1.3. The southern Indian Ocean (SIO)

The evidence for five radiolarian assemblages in the SIO is very strong. It is supported not only by this study's SIO census data, but also by this study's cluster analysis of the CLIMAP Project Members (1997; 2006) data – the "re-analysed CLIMAP data" – which establishes six assemblages, five in the SIO and these five and another in the South Atlantic, as compared with the original study's three (Lozano and Hays, 1976). Johnson and Nigrini (1980; 1982) also found five assemblages spanning the same general area of the SIO but it is difficult to relate them exactly with those of this study or the CLIMAP Project Members. In all three cases, the assemblages can be associated with the frontal systems in the Southern Ocean. This study's most northerly SIO assemblage (labelled G – see Figure 9.2) is north of the NSTF and is definitely different from EIO Assemblage D, presumably because of the salinity peak at approximately 32.5°S which separates them physically (Figure 4.5b). Assemblage G is most closely associated with the South Indian Ocean Current (Figure 4.2) or, as will be discussed later, the AABW sourced from the Ross Sea and the Adélie Coast (Figure 4.3). The CLIMAP Project Members' study has no site in the region covered by

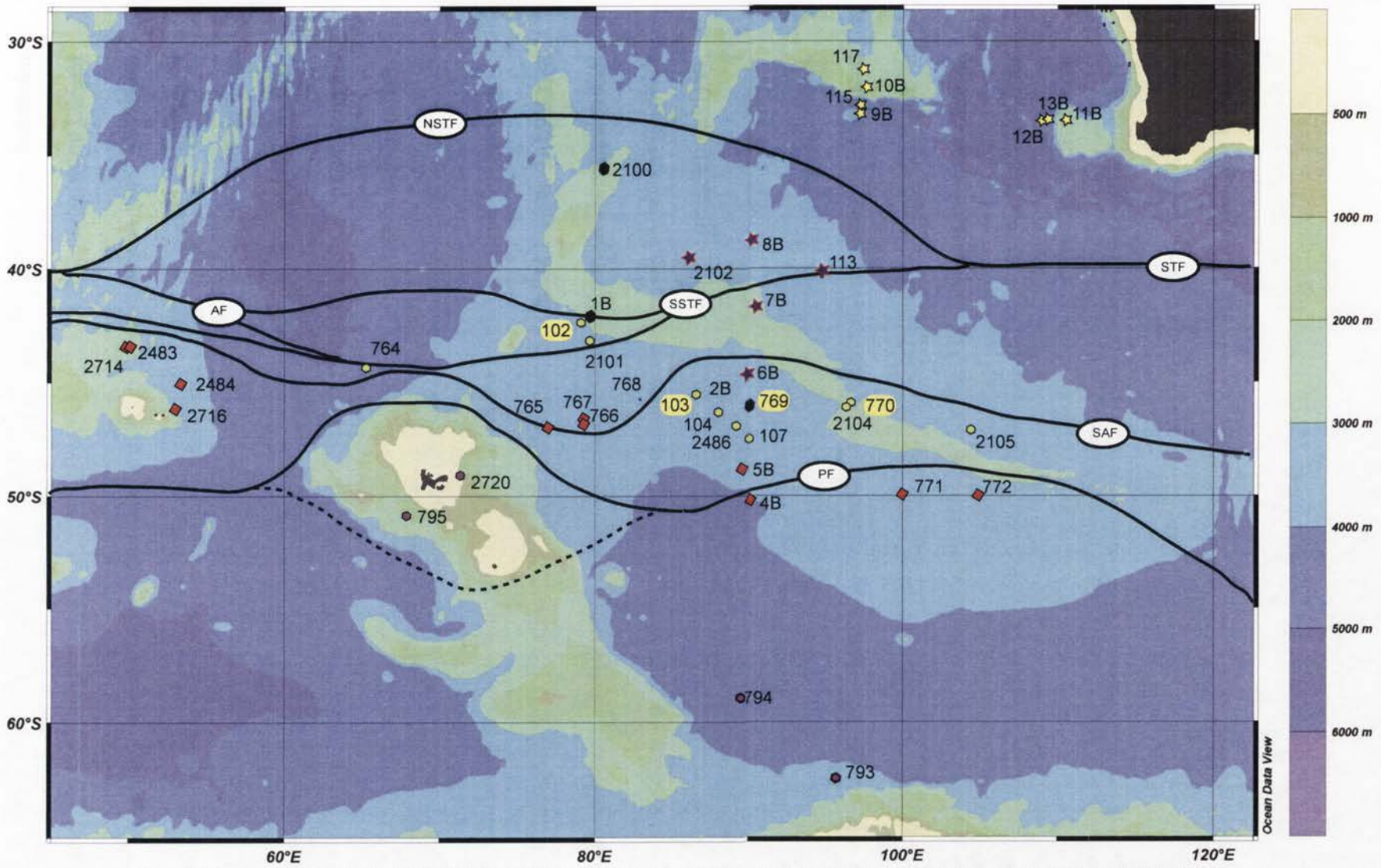

Figure 9.2: The southern Indian Ocean sites showing the radiolarian assemblages in relation to the fronts plotted from Belkin and Gordon (1996). The names of the SIO cores studied are highlighted with yellow ovals. Assemblages: G - ☆; H - ★; J - ○; K - ◆; L - ●; samples dated as older than 5000 years ⬢. Broadly, the assemblages can be seen to fall within the inter-frontal zones.

Assemblage G. The area is part of Johnson and Nigrini's (1982) Central Assemblage which they extend to the Western Australian coast but, as has been pointed out, this study finds a difference between Assemblage G and D, both of which fall into the geographical confines of the Central Assemblage.

Assemblage H may be associated with the area bounded by the NSTF and the SSTF (33°-45°S, 60°-90°E – Figure 9.2) which is the source of the Subtropical Mode Water (McCartney, 1982; Belkin and Gordon, 1996). Although the CLIMAP Members' data contains few sites in this area of the Indian Ocean, it has more than a dozen in the corresponding region of the South Atlantic Ocean and the majority fall into a single assemblage (labelled P – Figure 8.1). Assemblage J probably falls into the Subantarctic Zone and K, more definitely, into the Polar Frontal Zone. Of the CLIMAP Members' assemblages, Q belongs to the Subantarctic Zone in both Atlantic and Indian Oceans; assemblage R lies in the Polar Frontal Zone east of Kerguelen but S occupies this position west of that and, more obviously, in the South Atlantic. This study's assemblage L and CLIMAP members' T (and V) lie in the Antarctic Zone.

9.2. The census data's association with oceanic parameters

A major problem in developing transfer functions for palaeoenvironmental estimation is the plenitude of potentially explanatory parameters for marine samples. However, in the SIO, if the WOA-05 values from below 500 metres are neglected (because they do not seem to correlate well), the potentially explanatory variables fall into, at most, three groups (1: temperature and salinity, 2: nitrate, phosphate, and silicate, and 3: dissolved oxygen) and there does not seem to be a possibility of separating genuinely explanatory variables from coincidentally correlated variables within a group, even if it is not actually a combination of several or all the members or the group which constitute the explanation. Statistical argument says that for the results not to indicate a causal relationship between the five environmental parameters and the radiolarian assemblages is so improbable as to be

incredible. However, this relationship cannot be taken for granted, especially if the conclusion drawn is that radiolaria respond to all five factors when it is equally possible that response is to one or two environmental factors and, in this sector, the other three or four coincidentally vary in parallel with the explanatory parameters.

Radiolarian response to temperature is well established and confirmed by comparison with results from other proxies (Vénec-Peyré *et al.*, 1995; Pisias *et al.*, 1997; Abelmann *et al.*, 1999; Dolven *et al.*, 2002). A connection with salinity is less certain but Gupta (2003) reports the existence of salinity-sensitive radiolaria in the central Indian Ocean and Granlund (1986) found an association between salinity and the morphology of *Antarctissa* in the southern Indian Ocean. The relationship between radiolarian assemblages and nutrients such as nitrate and phosphate may be an indirect effect with the assemblages reflecting productivity which, in its turn, reflects nutrient levels (Caulet *et al.*, 1992; Kling and Boltovskoy, 1995; Jacot Des Combes *et al.*, 1999; De Wever *et al.*, 2001). However, there is no evidence in this study to confirm any indirectness. The literature does not appear to shed light on the influence of oxygen, the amount dissolved, the saturation, or the apparent oxygen utilisation (AOU).

Radiolarian census counts published by other researchers (CLIMAP Project Members, 1976; Morley and Hays, 1983; Nimmergut and Abelmann, 2001; Welling, 2003; Hays and Morley, 2004; Okazaki *et al.*, 2004; Abelmann and Nimmergut, 2005; CLIMAP Project Members, 2006; Itaki *et al.*, 2008; Kamikuri *et al.*, 2008) were analysed in the hope of identifying explanatory variables using the fact that environmental gradients would differ between widely separated research areas. Unsurprisingly, the CLIMAP Project Members (1997; 2006) data for the Southern Ocean from the eastern Pacific to Australia yielded very similar answers to those from the present study. The main difference is the fact that Lozano

and Hays (1976) identified three assemblages using Q-Mode Factor Analysis (QMFA) (Imbrie and Kipp, 1971) against the six found in this study: the difference is probably entirely the result of the use of different criteria. The census data from other researchers confirm the importance of temperature, salinity, and the nitrate and phosphate concentrations, and of the significance of the silicate concentration when it changes sharply at the Polar Front.

Results from the Welling (2003) and Kamikuri *et al.* (2008) studies reinforced the importance of temperature and salinity, both tending to suggest that salinity might be the more influential of the two. Again, the nutrient, nitrate, was an important factor. The Okhotsk Sea, whence came the Nimmergut and Abelmann (2001) data, is a basin, separated from the open ocean by a shallow sill. Climatic conditions cause well-defined layering of the waters, and, thus, water depth is the major CCA factor. Temperature and salinity have limited influence, probably because of the small range of both. After water depth, the most important factors are the nitrate and phosphate concentrations.

The detailed examination of radiolarians from the Sea of Okhotsk (including Morley and Hays, 1983; Hays and Morley, 2004; Okazaki *et al.*, 2004; Abelmann and Nimmergut, 2005; Itaki *et al.*, 2008) argues that assemblages are not determined by just a few environmental factors. This is further demonstrated by closer examination of the EIO where it can be seen that even water temperature at two different depths can have significant influence (Figure 7.18). The conclusion must, therefore, be that, whilst temperature and salinity are almost invariably dominating factors, for any particular geographic region it is their values at particular depths which are important. In addition, a number of other environmental variables are critical and, if their values change rapidly over a study area, their effects will, perhaps, even overwhelm changes in temperature or salinity. This leads to the corollary that,

in palaeo-reconstruction, radiolarian assemblages could be used to map the movement of ocean fronts because fronts are areas of rapid oceanic variable change.

In the southern Indian Ocean, and probably the Southern Ocean as a whole, temperature, salinity, nitrate and phosphate tend to be strongly correlated and, therefore, inseparable as explanatory variables. Silicate concentrations become increasing important as they increase sharply across and south of the Polar Front. In the EIO the situation is more complex and, thus, the amount of information offered rather limited. It is possible that more could be achieved if subsets were made of the surface sediment counts on the basis of the water level at which the various taxa lived. The present study's samples are probably too small for this to be practical.

9.3. Discussion of statistical techniques

9.3.1. Assemblage identification

Single-Run clustering combined with correspondence analysis and NMDS were the most efficacious techniques for the partitioning of the census data into radiolarian assemblages, whilst multivariate regression trees are useful in confirming the number of assemblages. LDA and WA-PLS provided strong additional evidence once the initial partitions were established and help with the refinement of site assignment. The Monte Carlo approach yielded too little to be worth employing in future (which is, perhaps, why it does not appear in the literature). Similarly, model-based clustering (Fraley and Raftery, 1998, 2006), which should converge to give the number of clusters, rarely did so, and provided little useful.

The selection of the potentially predictively-powerful taxa definitely strengthened results. The χ^2 test as a method of identifying the appropriate taxa was at least as successful as

Dufrêne and Legendre's (Dufrêne and Legendre, 1997) Indicator Species Analysis and has the benefit of not requiring prior assignment of sites to clusters.

9.3.2. Association of census data with oceanic variables

Canonical Correspondence Analysis (CCA) eigenvalues, WA-PLS R^2 values, and the correlations between CA scores and the environmental variables all provide information as to which environmental variables explain the observed distribution of radiolarian taxa, and are mutually confirmatory. CCA plots are the most useful in deciding which combination of environmental variables affects taxa distributions. Multivariate regression trees provide little information because they optimise at each branch, rather than over the whole tree. As a result, important environmental variables are often missed.

Chapter 10: Palaeoenvironmental reconstructions

10.1. Introduction

The strong correlations exhibited between the radiolarian census data and a number of the WOA-05 environmental variables lead to the belief that it should be possible to reconstruct oceanic palaeoenvironmental conditions from taxa counts of radiolarians obtained from samples taken at a succession of depths in a sediment core. Two sets of core samples were studied: six samples dated to the LGM taken from the eastern Indian Ocean (EIO – see §5.1.2 above) and four cores from the southern Indian Ocean (SIO – see §5.1.3 above).

Reconstructions derived from the six EIO core samples were used specifically for comparison with the LGM SSTs obtained by Barrows and Juggins (2005) to decide which of several statistical techniques was likely to give the most accurate reconstructions. The SIO reconstructions were designed to identify changes in the SIO since about 40 ka.

10.2. The LGM reconstructions

Juggins' *C2* software (2007b) offers eight calibration and regression techniques for the reconstruction of palaeoenvironmental variables. They are Weighted Average Partial Least Squares (WA-PLS) (ter Braak and Juggins, 1993), Weighted Averaging regression and calibration (WA) (Birks *et al.*, 1990), Modern Analog Technique (MAT) (Hutson, 1977), Maximum Likelihood Method (MLM) (ter Braak *et al.*, 1993), Partial Least Squares (PLS) (Wold *et al.*, 1984), Q-Mode Factor Analysis (QMFA) (Imbrie and Kipp, 1971), Correspondence Analysis regression (CAR) (ter Braak and Verdonschot, 1995), and Locally-Weighted Weighted Averaging (LWWA). All eight were employed to generate transfer functions from, firstly, the whole IO census counts and, then, the EIO and the SIO counts separately, with their corresponding present-day SSTs: the performance details are contained

in Table 10.1a and b. SIMMAX (Pflaumann *et al.*, 1996 – not available in C2) was also tried but the initial results were too poor relative to other methods to be pursued.

Radiolarian data \ Method		WA-PLS		WA classical		MAT		MLM	
		RMSEP	r^2	RMSEP	r^2	RMSEP	r^2	RMSEP	r^2
Combined EIO and SIO sectors	Annual	1.71	0.98	2.64	0.93	1.99	0.97	2.60	0.92
	Summer	1.83	0.98	2.70	0.92	1.78	0.97	1.65	0.98
	Winter	1.51	0.99	2.46	0.93	1.63	0.97	1.47	0.98
EIO sector	Annual	1.12	0.97	1.17	0.89	1.32	0.85	1.60	0.95
	Summer	1.08	0.98	1.23	0.88	1.44	0.85	1.67	0.90
	Winter	1.07	0.95	1.09	0.89	1.26	0.85	1.37	0.94
SIO sector	Annual	1.92	0.98	2.06	1.83	2.19	0.85	1.94	0.92
	Summer	2.14	0.97	2.22	0.87	2.32	0.85	2.10	0.91
	Winter	1.64	0.98	1.79	0.89	2.03	0.86	1.71	0.94

Table 10.1a: Performance statistics for the four calibration and regression techniques used to reconstruct SSTs for the EIO LGM samples. [RMSEP = root mean square error of prediction – see text for the other abbreviations]

Radiolarian data \ Method		PLS		QMFA		CAR		LWWA	
		RMSEP	r^2	RMSEP	r^2	RMSEP	r^2	RMSEP	r^2
Combined EIO and SIO sectors	Annual	1.99	0.97	2.60	0.92	2.41	0.94	1.64	0.98
	Summer	2.40	0.97	2.68	0.92	2.59	0.92	1.76	0.98
	Winter	1.98	0.97	2.50	0.92	2.21	0.94	1.47	0.98
EIO sector	Annual	1.04	0.95	1.32	0.85	1.27	0.83	1.32	0.89
	Summer	1.02	0.95	1.37	0.84	1.37	0.80	1.34	0.88
	Winter	1.04	0.94	1.23	0.85	1.21	0.83	1.27	0.89
SIO sector	Annual	2.20	0.90	2.60	0.79	2.16	0.85	1.93	0.90
	Summer	2.50	0.89	2.70	0.83	2.29	0.85	2.12	0.89
	Winter	2.05	0.91	2.25	0.84	1.79	0.90	1.69	0.91

Table 10.1b: Performance statistics for the four calibration and regression techniques not used to reconstruct SSTs for the EIO LGM samples. [RMSEP = root mean square error of prediction – see text for the other abbreviations]

The SSTs for the six EIO fossil samples were reconstructed using annual, austral summer, and austral winter WOA-05 data as the environmental training sets and the eastern sector and the combined eastern and southern sectors radiolarian data as species training sets. The reconstructions using WA-PLS, WA, MLM, and MAT and the differences between the reconstructed SSTs and Barrows and Juggins' (2005) appear as Table 10.2.

Sector(s)	Regression and calibration method	Core	Depth [cm]	SST estimates ± 1 standard error [°C]			Differences from Barrows & Juggins (2005) [°C]		
				Annual	Summer	Winter	T_{mean}	T_{max}	T_{min}
Combined eastern and southern sectors	WA-PLS	Fr10/95-GC11	27	**24.7±0.7**	**26.1±0.5**	**23.0±0.4**	**0.4**	**-0.6**	**0.8**
		Fr10/95-GC14	45	**24.0±0.5**	**25.5±0.5**	**22.2±0.4**	**2.3**	**1.6**	**2.6**
		Fr10/95-GC17	127	**25.1±0.5**	**27.0±0.7**	**23.1±0.5**	**3.8**	**3.3**	**3.5**
		Fr10/95-GC20	54	**22.2±0.7**	**24.0±0.8**	**20.5±0.6**	**0.5**	**0.1**	**0.7**
		Fr02/96-GC10	20	**21.8±0.7**	**23.3±0.5**	**20.2±0.3**	**-0.1**	**-0.7**	**0.3**
		Fr02/96-GC10	22	**22.7±0.6**	**24.0±0.5**	**21.2±0.4**	**0.8**	**0.0**	**1.3**
	WA classical deshrinking	Fr10/95-GC11	27	24.7±0.4	26.0±0.4	23.0±0.4	0.4	-0.6	0.8
		Fr10/95-GC14	45	26.0±0.3	27.4±0.4	24.3±0.3	4.3	3.5	4.6
		Fr10/95-GC17	127	24.8±0.4	26.2±0.4	23.0±0.3	3.3	2.5	3.4
		Fr10/95-GC20	54	26.5±0.4	28.0±0.4	24.7±0.4	4.8	4.1	4.9
		Fr02/96-GC10	20	23.1±0.4	24.5±0.4	21.5±0.3	1.2	0.5	1.5
		Fr02/96-GC10	22	24.4±0.4	25.7±0.4	22.7±0.3	2.5	1.7	2.8
	MAT	Fr10/95-GC11	27	26.4±0.5	27.9±0.6	24.4±0.4	2.1	1.2	2.2
		Fr10/95-GC14	45	24.3±0.7	25.6±0.8	22.6±0.7	2.6	1.7	3.0
		Fr10/95-GC17	127	26.3±0.5	27.9±0.6	24.4±0.5	4.9	4.2	4.8
		Fr10/95-GC20	54	23.5±0.6	24.9±0.7	22.0±0.6	1.8	1.0	2.1
		Fr02/96-GC10	20	22.6±1.0	24.1±0.8	21.1±0.8	0.7	0.1	1.2
		Fr02/96-GC10	22	23.8±0.7	25.2±0.8	22.2±0.7	1.9	1.2	2.3
	Maximum Likelihood	Fr10/95-GC11	27	26.3±0.5	27.9±0.4	24.4±0.4	2.0	1.2	2.2
		Fr10/95-GC14	45	24.2±0.4	25.6±0.5	22.5±0.4	2.5	1.8	2.9
		Fr10/95-GC17	127	25.6±0.6	27.3±0.5	23.7±0.6	4.2	3.6	4.1
		Fr10/95-GC20	54	22.9±0.5	24.3±0.4	21.2±0.5	1.2	0.5	1.4
		Fr02/96-GC10	20	22.1±1.3	23.6±1.2	20.8±1.1	0.2	-0.4	0.9
		Fr02/96-GC10	22	24.1±0.7	25.8±0.9	22.4±0.7	2.3	1.8	2.5
Eastern sector	WA-PLS	Fr10/95-GC11	27	27.1±0.5	28.9±0.4	24.6±0.4	2.8	2.2	2.4
		Fr10/95-GC14	45	24.9±0.5	26.4±0.5	22.4±0.5	3.2	2.5	2.8
		Fr10/95-GC17	127	26.7±0.8	28.3±0.7	23.7±0.7	5.3	4.6	4.1
		Fr10/95-GC20	54	22.4±0.6	23.5±0.7	19.6±0.6	0.3	-0.4	-0.2
		Fr02/96-GC10	20	25.5±0.6	27.3±0.5	23.2±0.4	3.6	3.3	3.3
		Fr02/96-GC10	22	25.0±0.6	26.3±0.4	22.9±0.5	3.1	2.3	3.0
	WA classical deshrinking	Fr10/95-GC11	27	26.1±0.4	28.3±0.4	24.7±0.4	2.4	1.6	2.5
		Fr10/95-GC14	45	23.1±0.5	24.5±0.5	21.5±0.5	1.4	0.6	1.9
		Fr10/95-GC17	127	26.1±0.7	27.7±0.8	24.1±0.7	4.7	4.0	4.5
		Fr10/95-GC20	54	20.4±0.6	21.8±0.8	18.9±0.6	-1.3	-2.1	-0.9
		Fr02/96-GC10	20	25.1±0.5	26.7±0.5	23.4±0.4	3.3	2.7	3.5
		Fr02/96-GC10	22	24.8±0.5	26.2±0.5	23.1±0.4	2.9	2.3	3.2
	MAT	Fr10/95-GC11	27	26.4±0.5	27.9±0.6	24.4±0.4	2.1	1.2	2.2
		Fr10/95-GC14	45	24.2±0.7	25.6±0.8	22.6±0.6	2.6	1.7	3.0
		Fr10/95-GC17	127	26.3±0.5	27.9±0.5	24.4±0.4	4.9	4.2	4.8
		Fr10/95-GC20	54	23.5±0.6	24.9±0.8	22.0±0.5	1.8	1.0	2.1
		Fr02/96-GC10	20	24.3±0.7	25.7±0.7	22.6±0.5	2.4	1.7	2.7
		Fr02/96-GC10	22	23.8±0.8	25.2±0.7	22.2±0.6	1.9	1.2	2.3
	Maximum Likelihood	Fr10/95-GC11	27	26.4±0.2	28.0±0.2	24.5±0.3	2.1	1.3	2.3
		Fr10/95-GC14	45	23.7±1.1	25.5±1.2	22.0±0.5	2.0	1.6	2.4
		Fr10/95-GC17	127	25.9±0.7	27.4±0.6	24.0±0.7	4.5	3.7	4.4
		Fr10/95-GC20	54	23.2±0.8	24.4±0.9	21.6±0.5	1.5	0.5	1.8
		Fr02/96-GC10	20	25.6±0.4	27.1±0.4	23.8±0.5	3.8	3.1	3.9
		Fr02/96-GC10	22	25.0±1.2	27.2±0.7	22.8±0.9	3.2	3.2	2.9

Table 10.2: EIO LGM reconstructions with their differences from Barrows and Juggins' (2005). The WA-PLS results, considered the most reliable overall, are in bold. The core depth corresponding to the LGM (21,000±2000 cal yr BP.) follows Martínez *et al.* (1999)

Similarity Indices (Hammer *et al.*, 2001; Hammer and Harper, 2006) indicated that there was little similarity between the fossil samples and any of the southern sector sites. As a result, no attempt was made to reconstruct LGM conditions using the southern sector data alone.

In the methods which offer a succession of increasingly close fits between the training (i.e. WOA-05) and the reconstructed environmental values, care was taken to avoid "over-fitting" because this typically results in poor predictive value (note that choosing components in this way introduces a subjective element which may result in fluctuations in the reconstructions which are not reflections of the real palaeoenvironment) . Reconstructions (using WA-PLS only) of the SIO LGM samples included in Barrows and Juggins' study (MD88-769, MD88-770, and MD94-102) are listed in Table 10.3, again, with their differences from the Barrows and Juggins' values. The SIO LGM reconstructions were made using the SIO and the combined EIO and SIO radiolarian data, the EIO-alone option being omitted for the same reasons as the SIO-alone was omitted when reconstructing the EIO LGM samples. For both the EIO and the SIO comparisons, Barrows and Juggins' T_{mean}, T_{max}, and T_{min} were taken to correspond to the annual, austral summer, and austral winter reconstructions respectively.

Sector(s)	Core	Depth [cm]	Age [ka]	SST estimates ± 1 standard error [°C]			Differences from Barrows and Juggins (2005) [°C]		
				Annual	Summer	Winter	T_{mean}	T_{max}	T_{min}
SIO	MD88-769	105	20.7	6.7±2.4	7.5±2.2	5.0±1.8	3.6	2.7	3.5
	MD88-770	150	20.9	6.9±2.4	7.2±2.4	5.2±1.7	4.0	2.8	4.1
	MD94-102	80	19.6	7.4±1.3	7.8±1.3	6.4±1.0	-0.2	-1.9	0.4
All IO	MD88-769	105	20.7	6.8±1.9	7.8±2.1	5.3±1.9	3.7	3.0	3.8
	MD88-770	150	20.9	6.5±2.4	7.3±2.7	5.0±2.3	3.6	2.9	3.9
	MD94-102	80	19.6	6.4±1.2	7.1±1.4	5.4±1.2	-1.2	-2.6	-0.6

Table 10.3: SIO LGM reconstructions using WA-PLS for cores included in Barrows and Juggins' (2005) study.

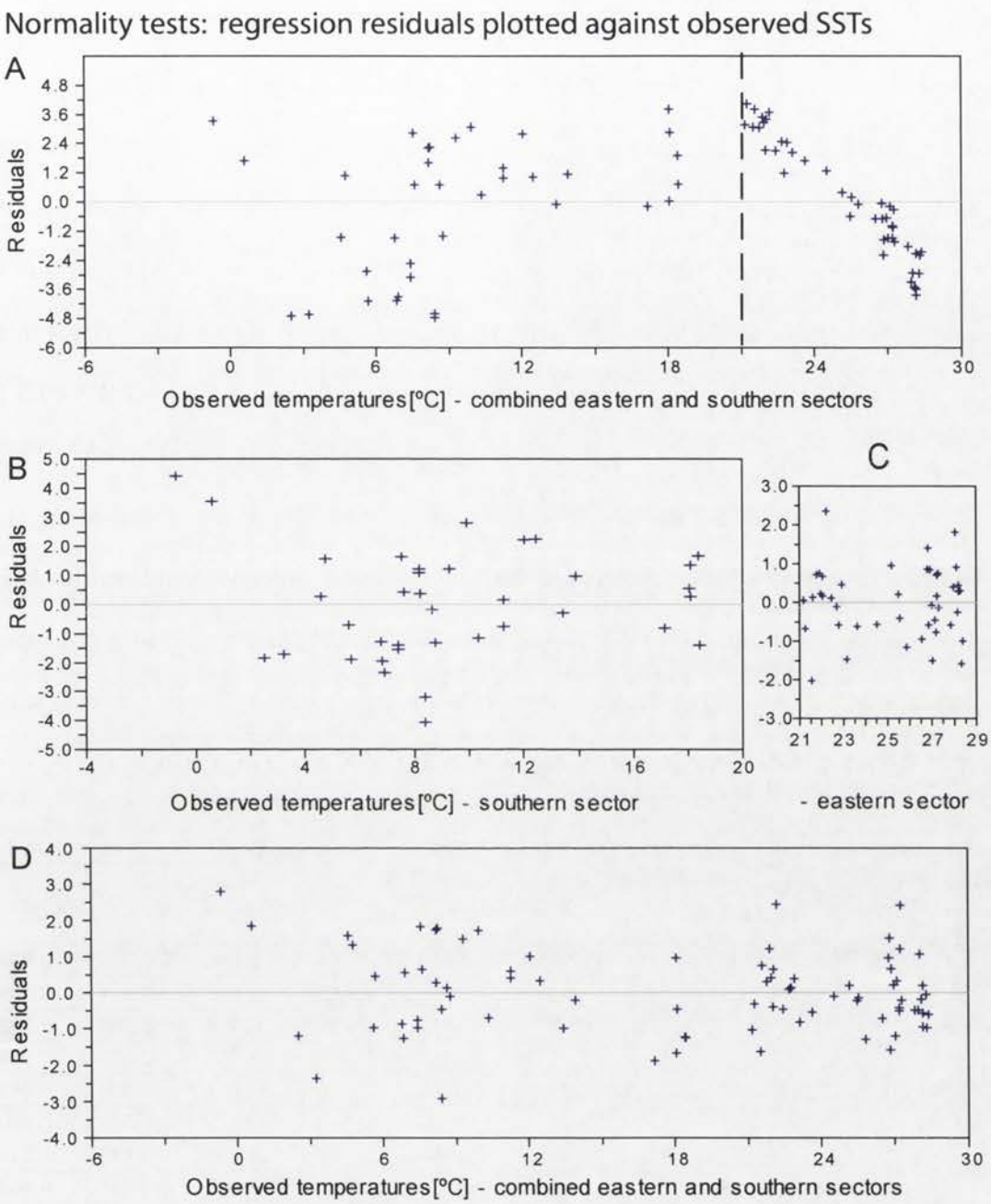

Figure 10.1: The regression residuals plotted against the observed (WOA-05) SSTs.
Plot A: WA regression using the combined EIO and SIO radiolarian data.
Plot B: WA regression using the SIO data alone.
Plot C: WA regression using the EIO data alone.
Plot D: WA-PLS regression using the combined EIO and SIO radiolarian data.
Note the linear relationship between the temperature and the residuals above 20°C (which occurs at the salinity maximum at 33°S). This relationship does not appear in plots C or D and the range of residuals is smaller in D than either A or B.

The distributions of the residual differences between the observed (i.e. WOA-05) SSTs and their reconstructions were tested for normality because, in regression analysis, prediction errors are assumed to be independent, normally-distributed, variables (Wold *et al.*, 1984; Maindonald and Braun, 2003). If the condition of normality is not met, it is an indication that one or more explanatory factors have not been included in the regression. The results of the tests for normality on the residuals from the application of all eight *C2* techniques to the combined SIO and EIO data appear in Table 10.4. The results for WA and WA-PLS are illustrated in Figure 10.1. Also included in Table 10.4 and Figure 10.1 are test results for the application of WA to the SIO and EIO data separately. It will be noted that, of the eight techniques, only WA-PLS has normally distributed residuals when the combined IO data is used. When WA is applied to the EIO or to the SIO data alone, the residual distribution is normal: this is typical of the results obtained by applying any of the *C2* techniques to the EIO or the SIO data individually.

Calibration and Regression Technique	Indian Ocean Sector	Sample size	Shapiro-Wilk		Jarque-Birk		chi-squared	
			W	p(normal)	JB	p(normal)	χ^2	p(normal)
WA-PLS	Combined	81	0.995	**0.985**	0.257	**0.880**	0.037	**0.985**
WA classical	Combined	81	0.957	0.009	4.382	0.112	2.111	0.009
	EIO	44	0.987	**0.882**	0.066	**0.968**	0.364	**0.882**
	SIO	37	0.988	**0.955**	0.283	**0.868**	2.027	**0.956**
MAT	Combined	81	0.969	0.043	13.600	0.001	3.000	0.043
MLM	Combined	81	0.933	0.000	62.580	2.582E-14	0.135	0.000
PLS	Combined	81	0.977	0.156	4.503	0.105	0.333	0.156
QMFA	Combined	81	0.971	0.064	3.286	0.193	2.210	0.064
CAR	Combined	81	0.956	0.007	4.413	0.110	6.259	0.007
LWWA	Combined	81	0.969	0.045	11.550	0.003	0.629	0.045

Table 10.4: Normality testing (using PAST software - Hammer *et al.*, 2001) of the distribution of the residuals (i.e. the differences between the observed and the estimated values) for modern IO SSTs. Probabilities of normality [p(normal)] greater than 0.8 are in bold.

Of the eight techniques, WA-PLS clearly performed the best and, so, was used for all further reconstructions. The WA-PLS Root Mean Squared Errors of Prediction (RMSEPs)

are less than 2°C in all but one case and lower than those for other methods. The WA-PLS r^2 values (the squared correlations between inferred and observed values) are higher than for the other methods (Table 10.1a-b).

Two-thirds of the EIO LGM estimates from WA-PLS applied to the combined data are within 1°C, and all are within two standard errors, of estimates based on planktonic foraminifera (Barrows and Juggins, 2005). The sample for which the radiolarian-based estimates differ most from Barrows and Juggins, Fr10/95-GC17, is from a site relatively near the coast which may account for the discrepancy.

Of the three SIO LGM samples, two, MD88-769 and MD88-770, deviate markedly from the Barrows and Juggins' estimates. The deviation is about the same as for Fr10/95-GC17 but, this time, without a geographical explanation. The deviation may be the result of an apparent tendency for radiolarian-based reconstructions of SSTs to be overestimates (cf. Molfino *et al.*, 1982). However, three other factors may contribute: firstly, it is not entirely clear that the samples used in this study came from exactly the same depth in the core as those used by Barrows and Juggins – their paper does not specify core depths, only the LGM date range, which leaves some latitude. Secondly, Barrows and Juggins' results for core E49-18, which is virtually collocated with MD88-769, are 1.5 to 2.0°C higher than their MD88-769 estimates. Thirdly, the Barrows and Juggins' MD88-769 and MD88-770 estimates were obtained from Salvignac (1998) and, as is discussed in Chapter 11, may be too low – a view supported by Dr. X. Crosta (pers. com., 2008). Finally, the standard errors for the SIO reconstructions are two to four times larger than those for the EIO and, thus, this study's SST estimates lie within two standard errors of Barrows and Juggins' results.

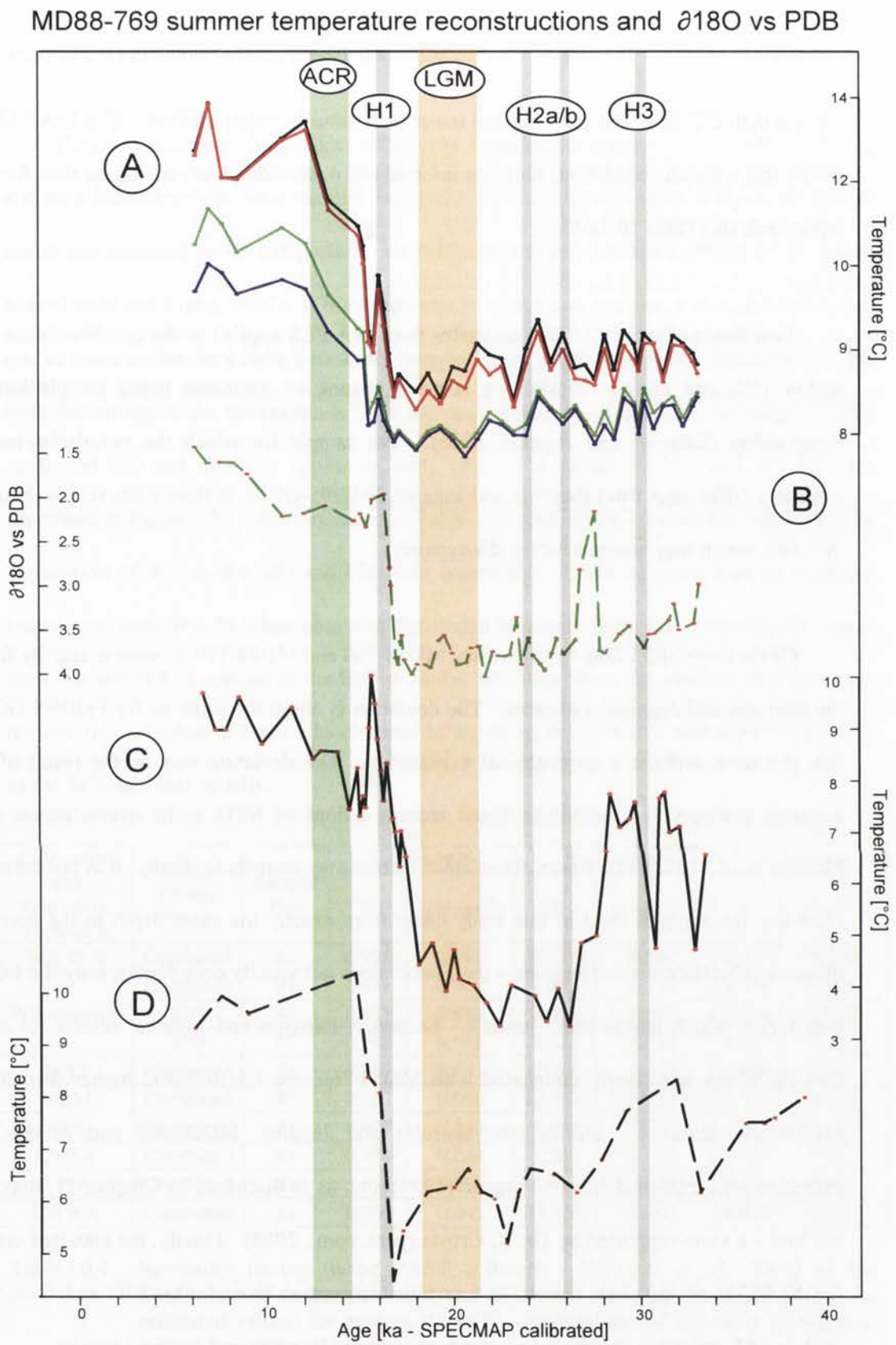

Figure 10.2a: A: Radiolarian austral summer temperature reconstructions at surface (black), 50m (red), 125m (green), and 250m (blue) bsl. Note scale differs from scales of C and D.
B: ∂18O vs PDB *N. pachyderma* left (200-250µ) (courtesy Dr E. Michel)
C. SSST reconstruction from foraminifera (Dr. M-E. Salvignac, unpublished thesis, 1998)
D. SSST reconstruction from diatomacea (Dr. X. Crosta, pers. com., 2008).
Grey vertical bars: Heinrich events (Bond *et al.* 1992, 1993) - see text for details.
Green bar: the Antarctic Cold Reversal; orange bar: the LGM.

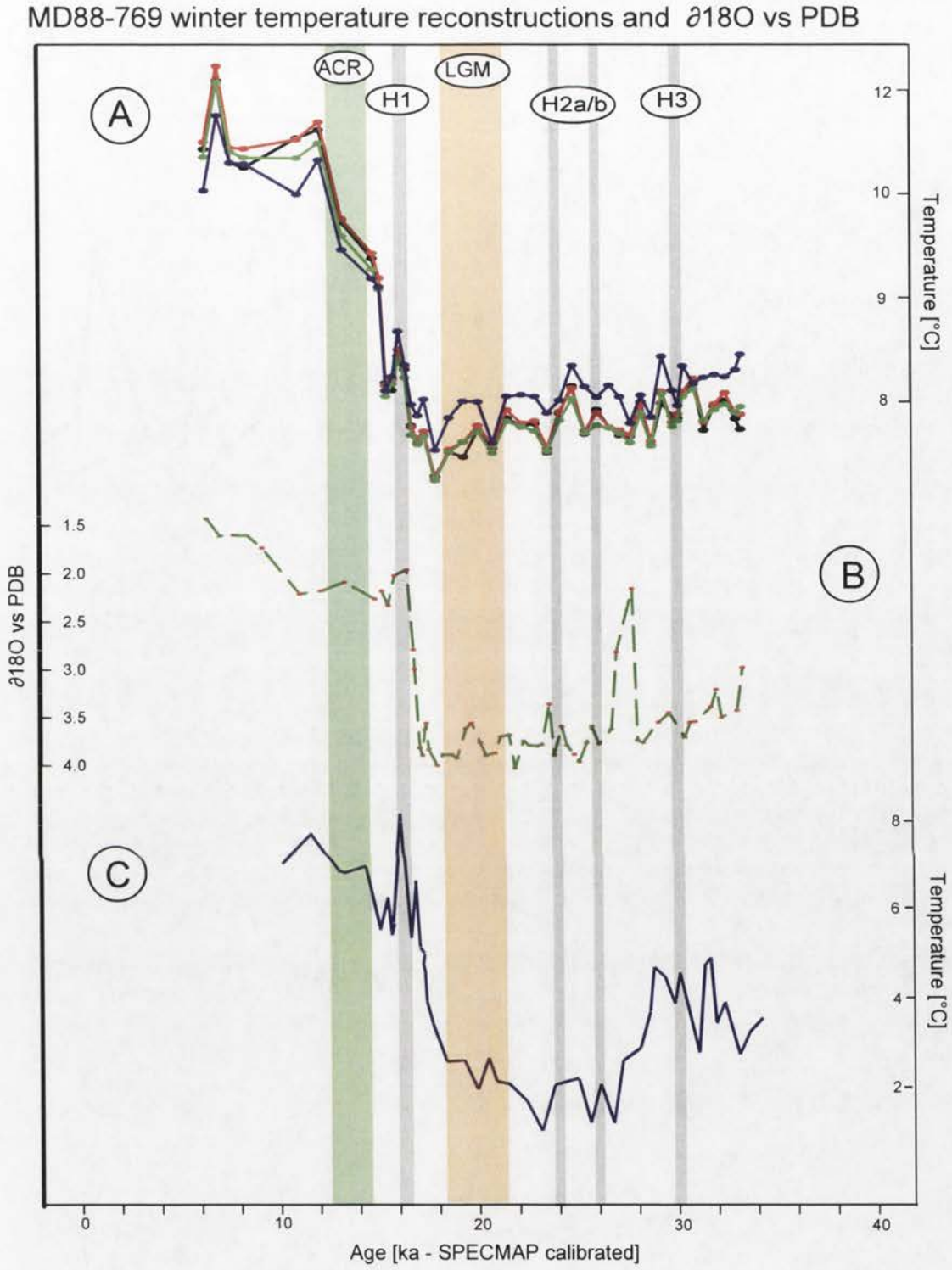

Figure 10.2b: A: Radiolarian austral winter temperature reconstructions at surface (black), 50m (red), 125m (green), and 250m (blue) bsl.
B: ∂18O vs PDB *N. pachyderma* left (200-250μ) (courtesy Dr E. Michel)
C. WSST reconstruction from foraminifera from a diagram in Dr. M-E. Salvignac's doctoral thesis (1998) - some detail has been lost.
Grey vertical bars: Heinrich events (Bond *et al.*, 1992, 1993) - see text for details.
Green bar: the Antarctic Cold Reversal; orange bar: the LGM.

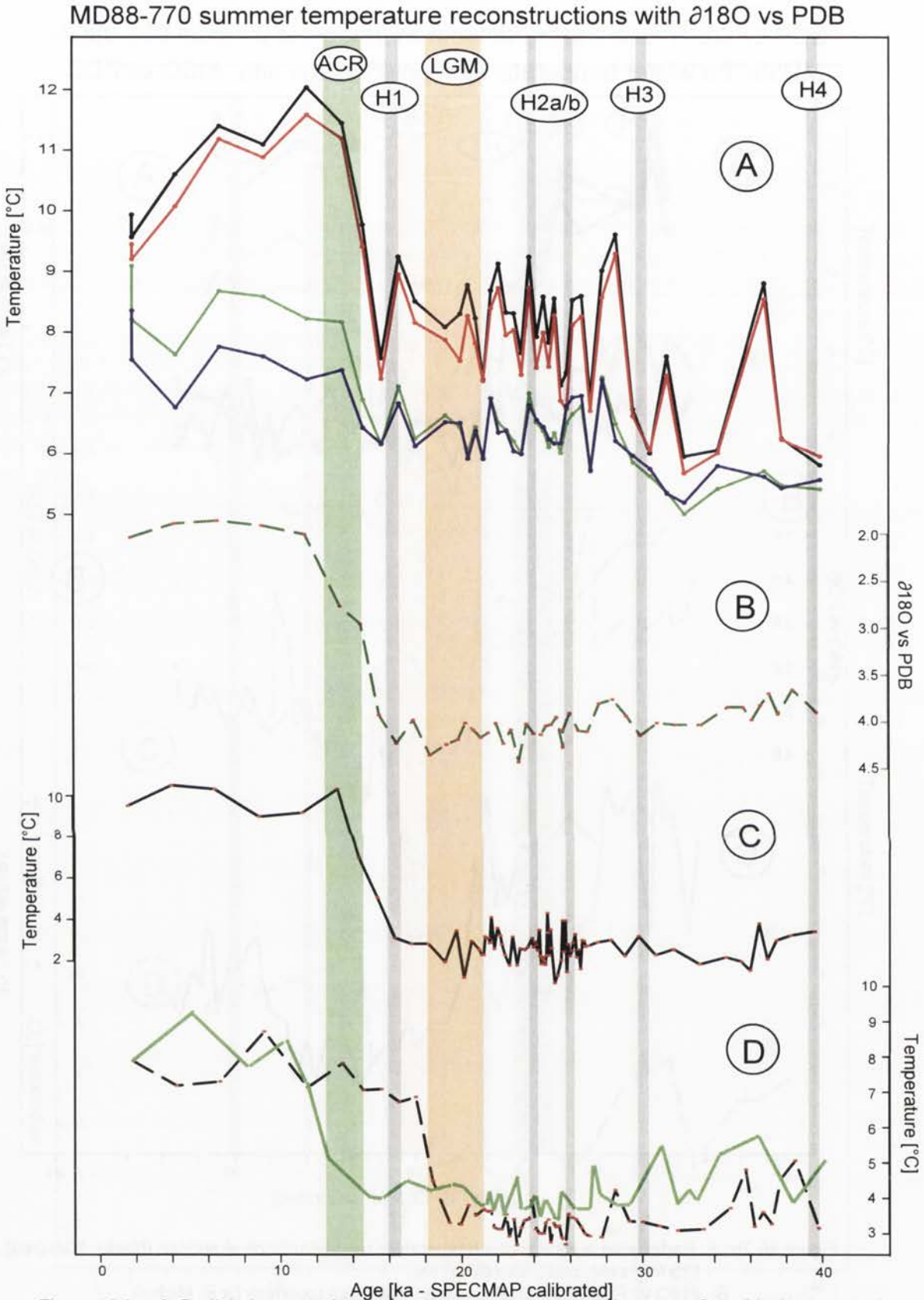

Figure 10.3a: A: Radiolarian austral summer temperature reconstructions at surface (black), 50m (red), 125m (green), and 250m (blue) bsl. Temperature scale differs from plots C and D.
B: ∂18O vs PDB *N. pachyderma* left (200-250μ) (courtesy Dr E. Michel)
C. SSST reconstruction from diatomacea (Dr. X. Crosta, pers com., 2008)
D. SSST reconstruction from foraminifera - dashed line: Rickaby and Elderfield (1999) solid line - Salvignac (unpublished thesis, 1998) - traced and some detail lost.
Grey vertical bars: Heinrich events H1-4 (Bond *et al.*, 1992, 1993) - see text for details.
Green bar: the Antarctic Cold Reversal; orange bar: the LGM.

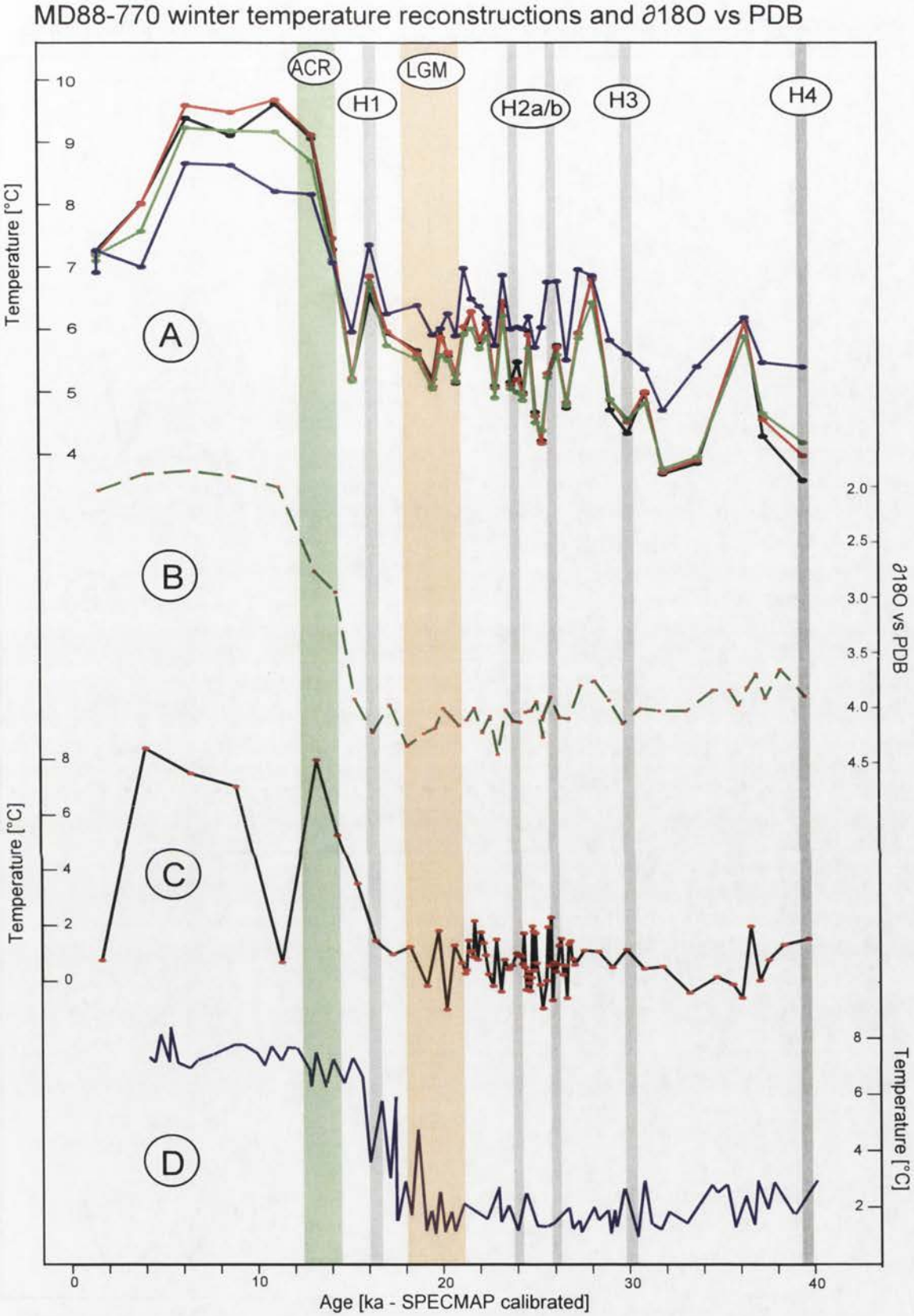

Figure 10.3b: A: Radiolarian austral winter temperature reconstructions at surface (black), 50m (red), 125m (green), and 250m (blue) bsl. Temperature scale differs from plots C and D.
B: ∂18O vs PDB *N. pachyderma* left (200-250µ) (courtesy Dr E. Michel)
C. WSST reconstruction from diatomacea (courtesy Dr. X. Crosta)
D. WSST reconstruction from foraminifera taken from a diagram in M-E Slavignac's unpublished doctoral thesis (1998) - some detail has been lost.
Grey vertical bars: Heinrich events H1-4 (Bond *et al.*, 1992, 1993) - see text for details.
Green bar: the Antarctic Cold Reversal; orange bar: the LGM.

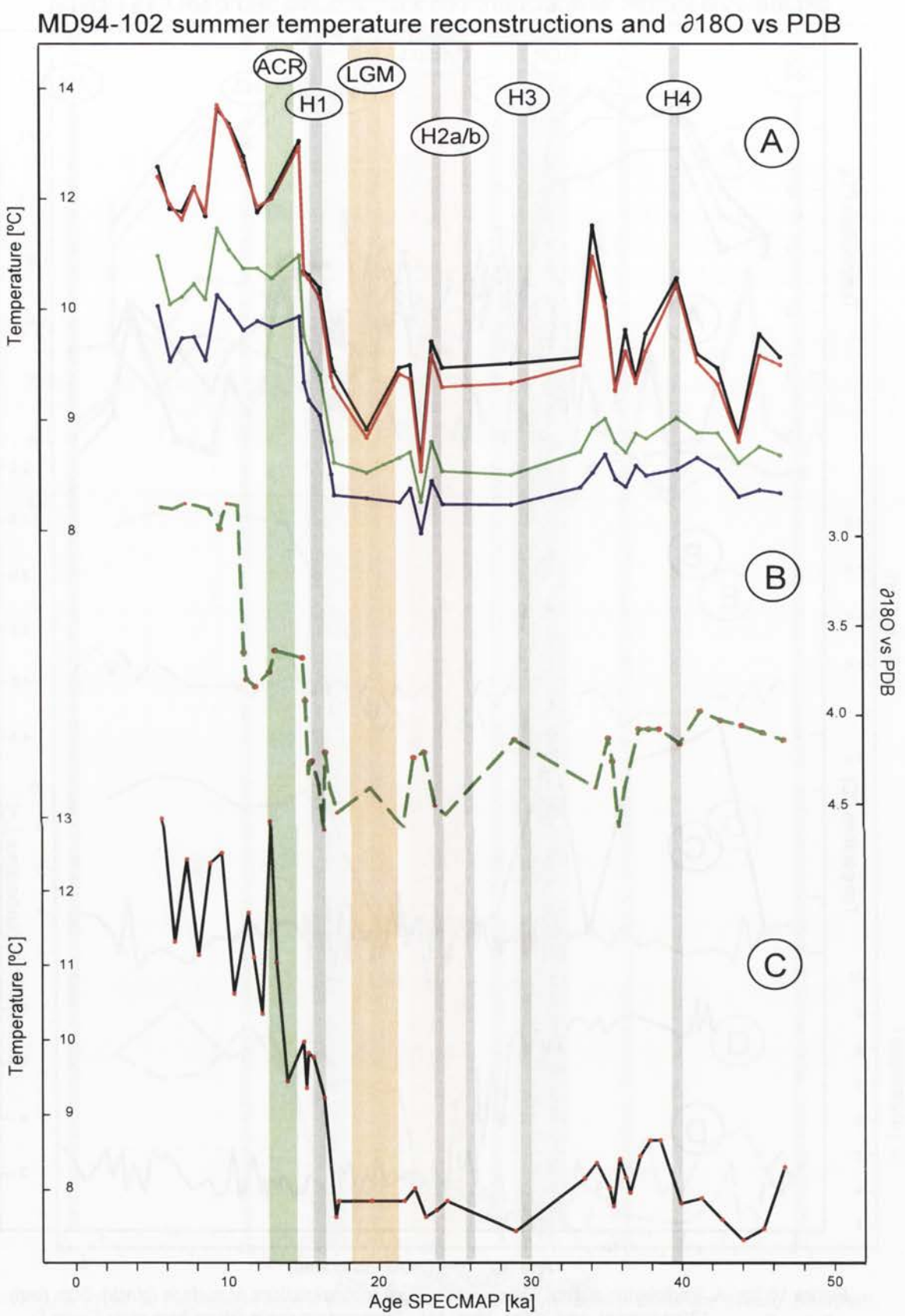

Figure 10.4a: A: Radiolarian austral summer temperature reconstructions at surface (black), 50m (red), 125m (green), and 250m (blue) bsl. Temperature scale differs from plots C and D.
B: ∂18O vs PDB *N. pachyderma* left (200-250µ) (courtesy Dr E. Michel)
C. SSST reconstruction from foraminifera (courtesy Dr. C. Waelbroeck).
Grey vertical bars: Heinrich events H1-4 (Bond *et al.*, 1992, 1993) - see text for details.
Green bar: the Antarctic Cold Reversal: orange bar: the LGM.

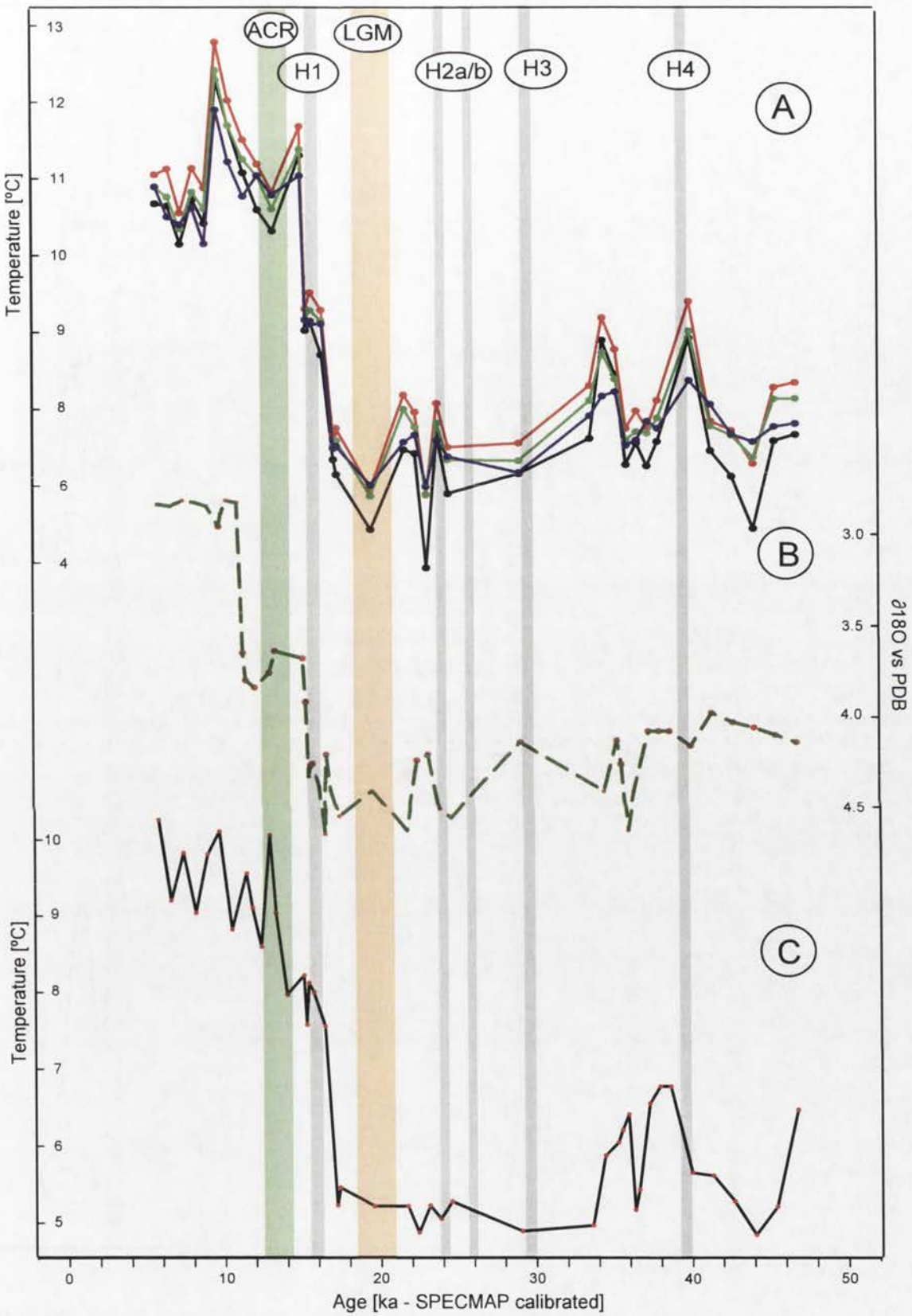

Figure 10.4b: A: Radiolarian austral winter temperature reconstructions at surface (black), 50m (red), 125m (green), and 250m (blue) bsl.
B: ∂18O vs PDB *N. pachyderma* left (200-250μ) (courtesy Dr E. Michel)
C. WSST reconstruction from foraminifera (courtesy Dr. C. Waelbroeck).
Grey vertical bars: Heinrich events H1-4 (Bond *et al.,* 1992, 1993) - see text for details.
Green bar: the Antarctic Cold Reversal; orange bar: the LGM.

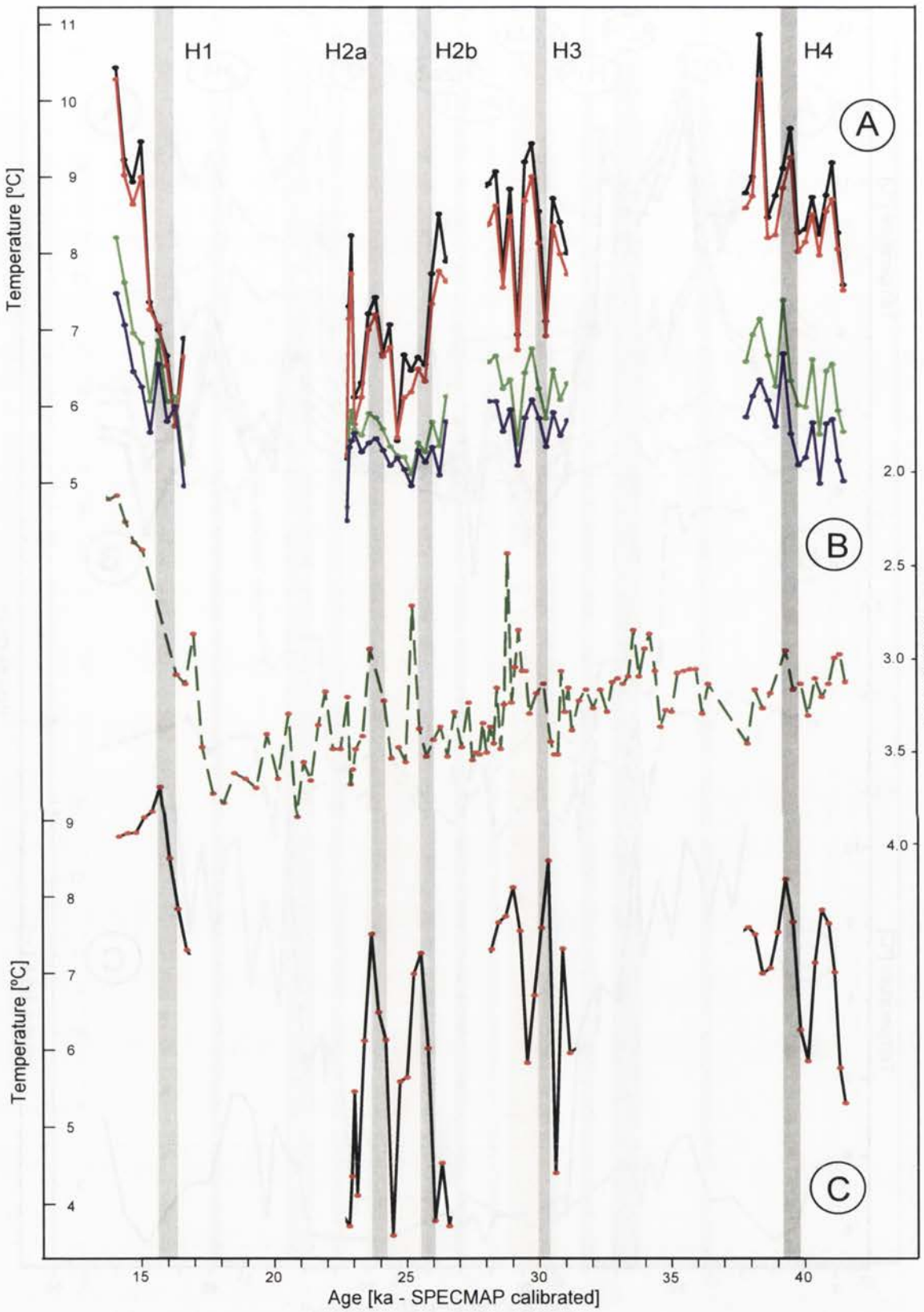

Figure 10.5a: A: Radiolarian austral summer temperature reconstructions at surface (black), 50m (red), 125m (green), and 250m (blue) bsl.
B: ∂18O vs PDB *N. pachyderma* left (200-250µ)
C. SST reconstruction from foraminifera from Sicre *et al.* (2005 - supplementary data).
Grey vertical bars: Heinrich events after Sicre *et al.* (2005) - see text for details.

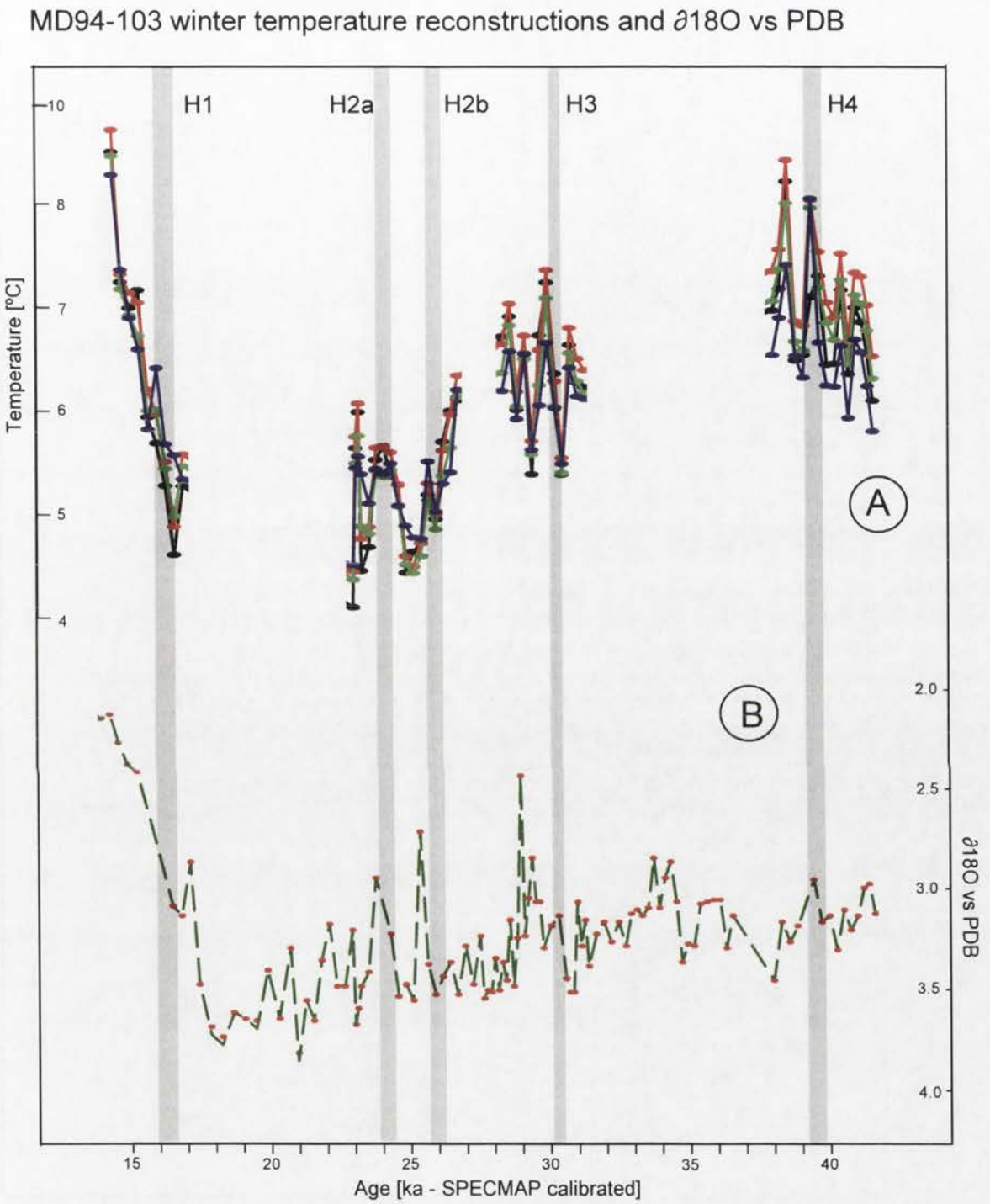

Figure 10.5b: A: Radiolarian austral winter temperature reconstructions at surface (black), 50m (red), 125m (green), and 250m (blue) bsl.
B: ∂18O vs PDB *N. pachyderma* left (200-250µ)
No independent reconstructions of WSSTs were available.
Grey vertical bars: Heinrich events H1-4 after Sicre *et al.* (2005) - see text for details.

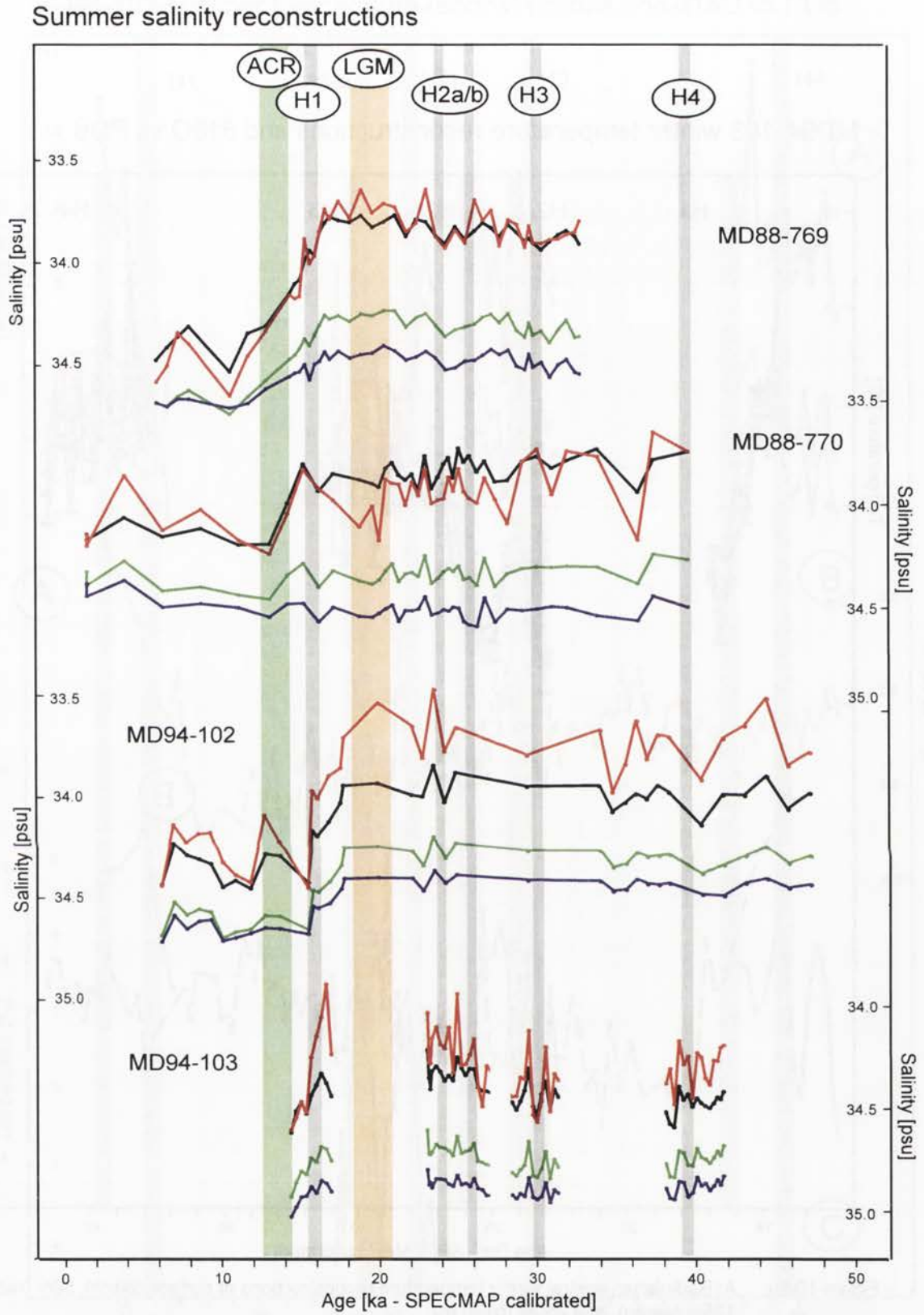

Figure 10.6a: Reconstructions of austral summer salinity [psu] for MD88-769, MD88-770, MD94-102, and MD94-103 at the surface (black), and at 50m (red), 125m (green) and 250m (blue) bsl. Note that, in MD88-769, MD88-770, and MD94-102, there is a greater difference between salinity levels at the surface and 50m and those at 125 and 250m bsl before 15ka than after - see text for details. Note the inverted vertical scales.
Grey vertical bars: Heinrich Events H1-4 (Bond *et al.*, 1992, 1993); green bar: the Antarctic Cold Reversal; orange bar: the LGM.

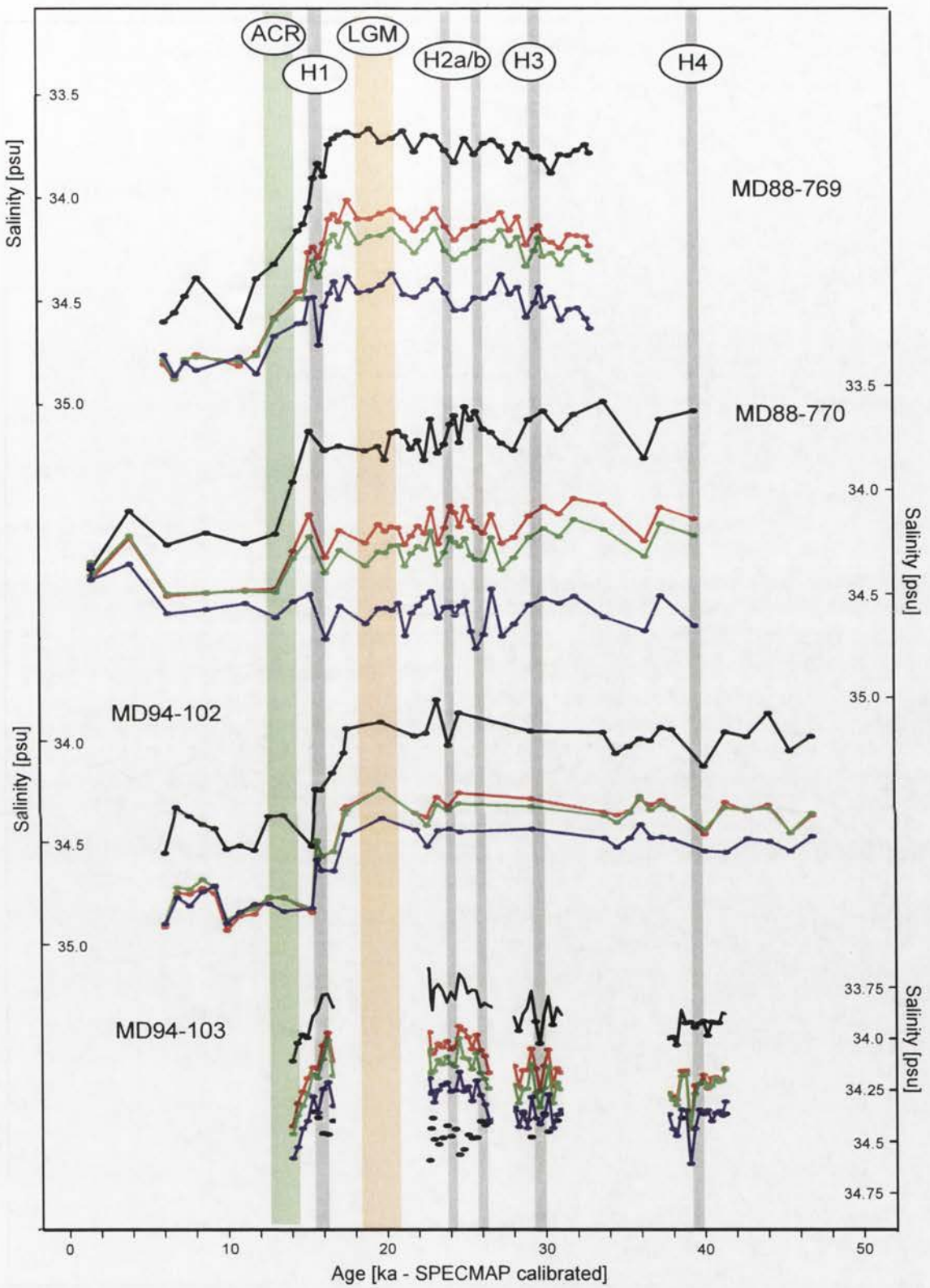

Figure 10.6b: Reconstructions of austral winter salinity [psu] for MD88-769, -770, MD94-102, and -103 at the surface (black), and at 50m (red), 125m (green) and 250m (blue) bsl. Note that, in MD88-769, MD88-770, and MD94-102, there is a greater difference between salinity levels nearer the surface and that at 250m bsl before 15ka than after - see text for details.
Grey vertical bars: Heinrich Events H1-4 (Bond *et al.*, 1992, 1993); green bar: the Antarctic Cold Reversal; orange bar: the LGM.
Note that the vertical scales are inverted.

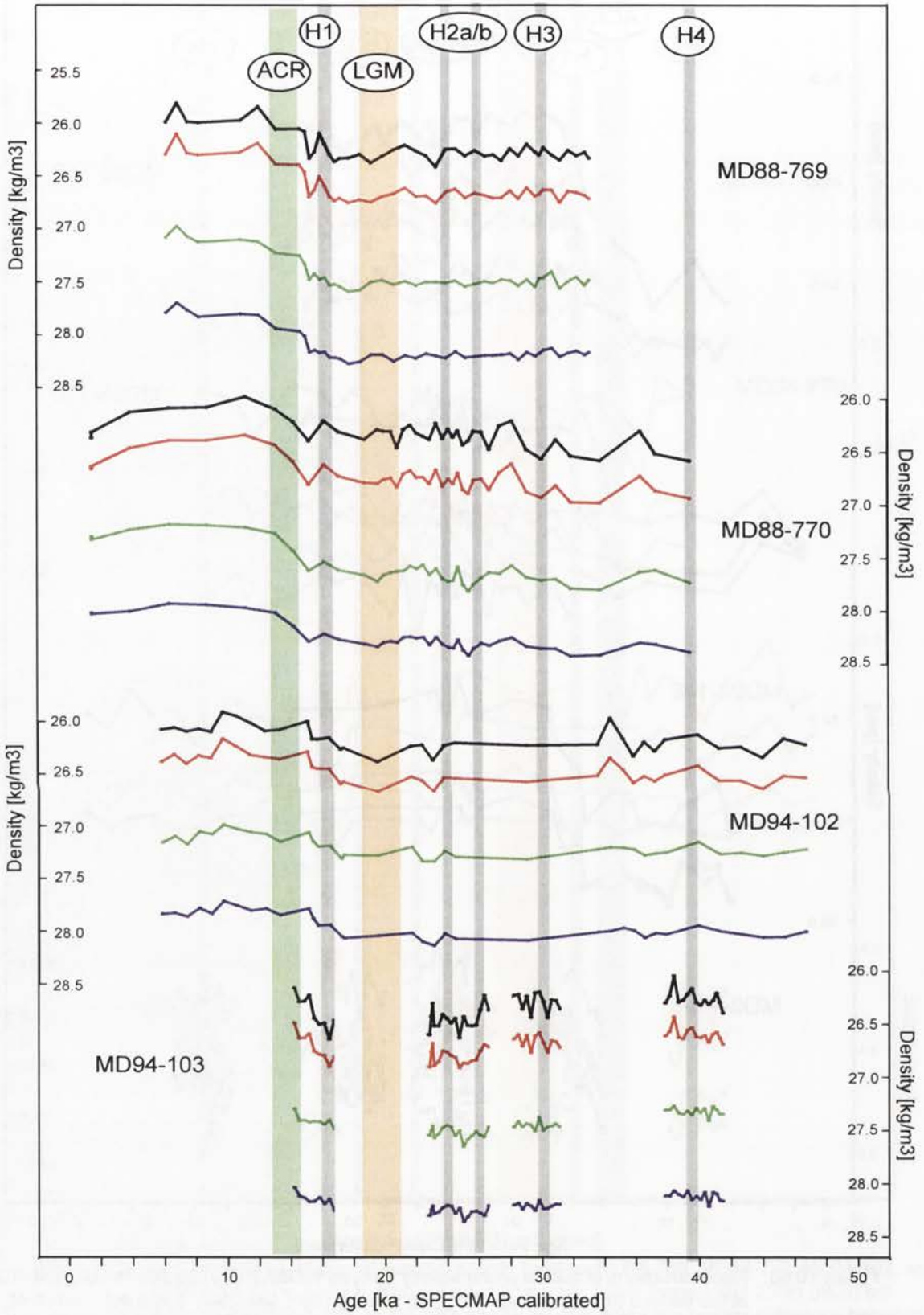

Figure 10.7a: Reconstructions of summer *in situ* density [[kg/m^{-3}] for MD88-769, MD88-770, MD94-102, and -103 at the surface (black), and at 50m (red), 125m (green) and 250m (blue) bsl. Vertical bars as previous plots. The vertical scales are inverted.
Note that in all the cores density decreases at about 15ka and that the plots for the four depths are approximately parallel - see text for details.

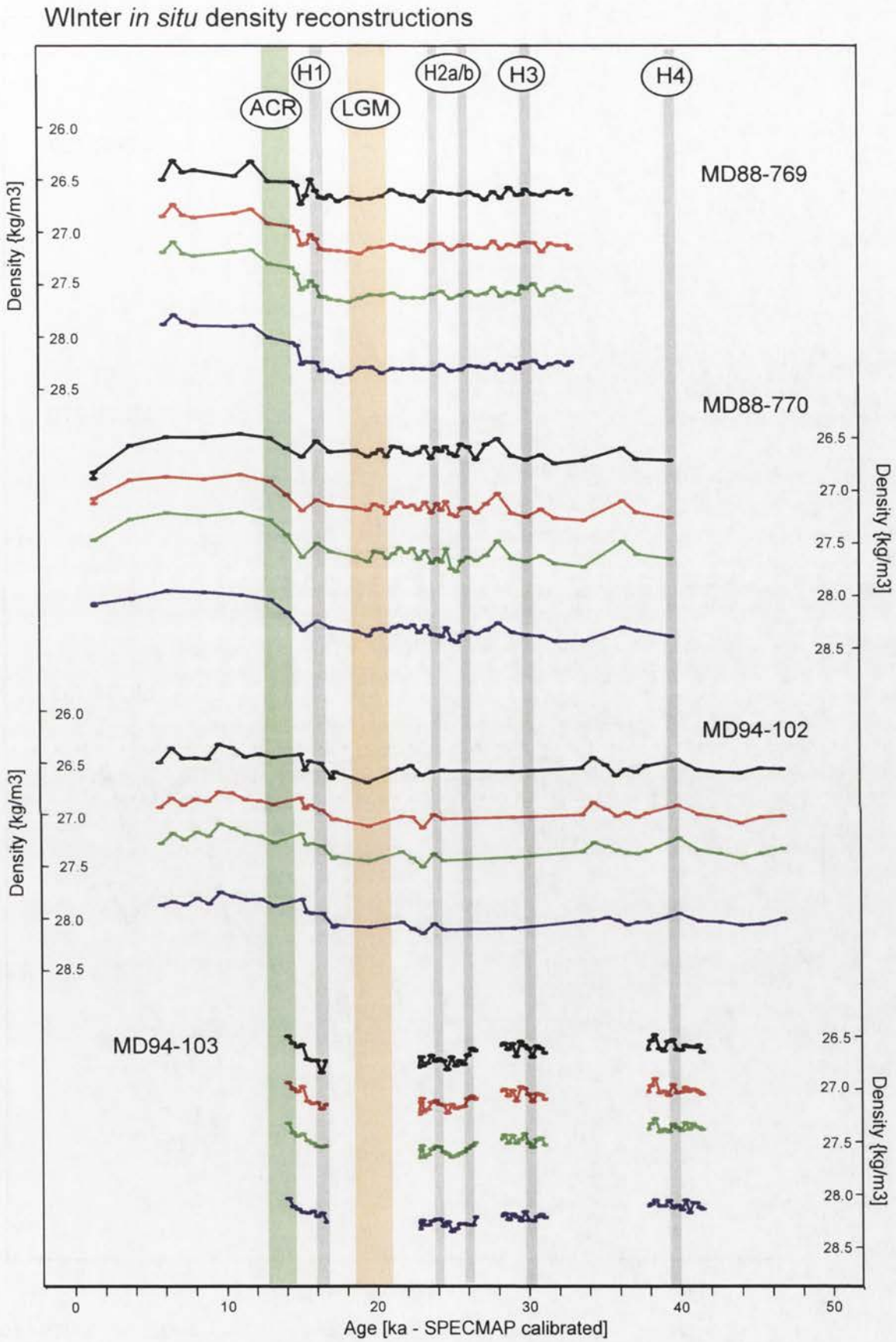

Figure 10.7b: Reconstructions of austral winter *in situ* density [[kg/m^3] for MD88-769, MD88-770, MD94-102, and -103 at the surface (black), and at 50m (red), 125m (green) and 250m (blue) bsl. Vertical bars as previous plots.
Note that in all the cores density decreases at about 15ka and that the plots for the four depths are approximately parallel - see text for details.

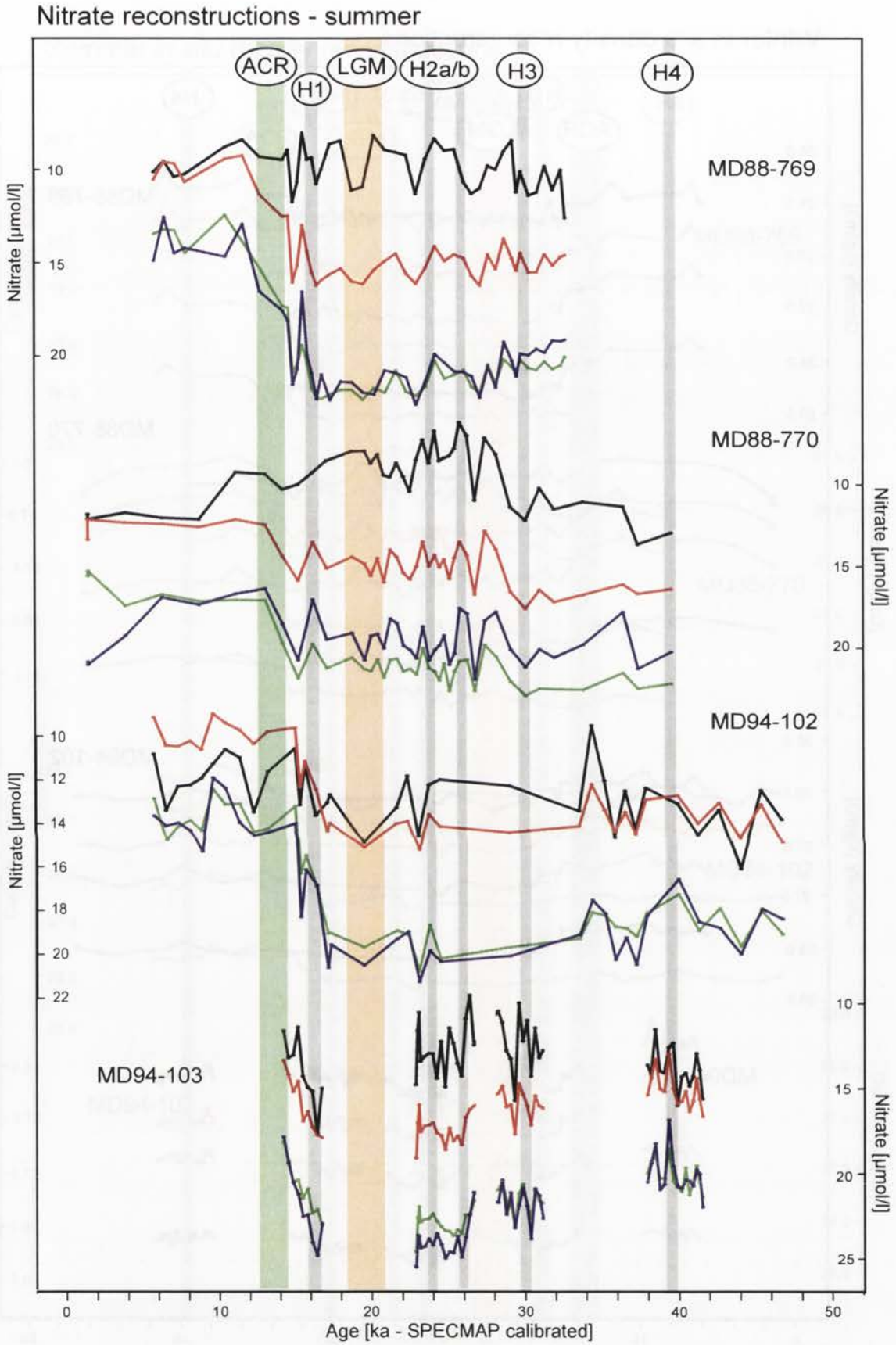

Figure 10.8a: Reconstructions of austral summer nitrate [µmol/l] for MD88-769, MD88-770, MD94-102, and MD94-103 at the surface (black), and at 50m (red), 125m (green) and 250m (blue) bsl - not all on the same vertical scale. Vertical bars as previous plots. Vertical scales are inverted. Note that there is a greater difference between nitrate at the surface and 50m and at 125 and 250m bsl between 15ka and 35ka than before or after - details in text.

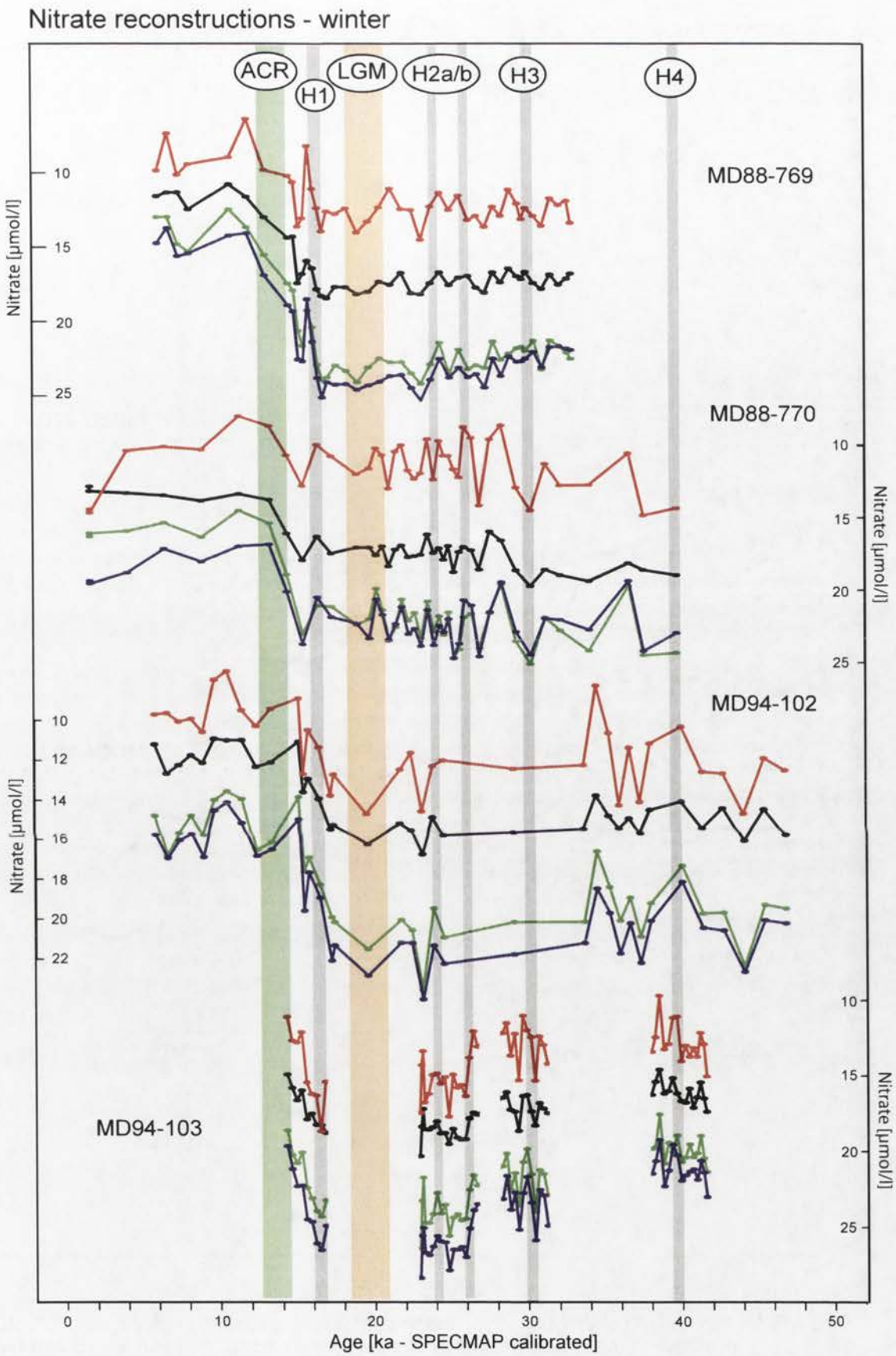

Figure 10.8b: Reconstructions of austral winter nitrate [µmol/l] for MD88-769, -770, MD94-102, and -103 at the surface (black), and at 50m (red), 125m (green) and 250m (blue) bsl - not all on the same vertical scale. Vertical bars as previous plots. Vertical scales inverted. There is a greater difference between nitrate levels at the surface and 50m and those at 125 and 250m bsl between 15ka and 35ka than before or after - see text for details.

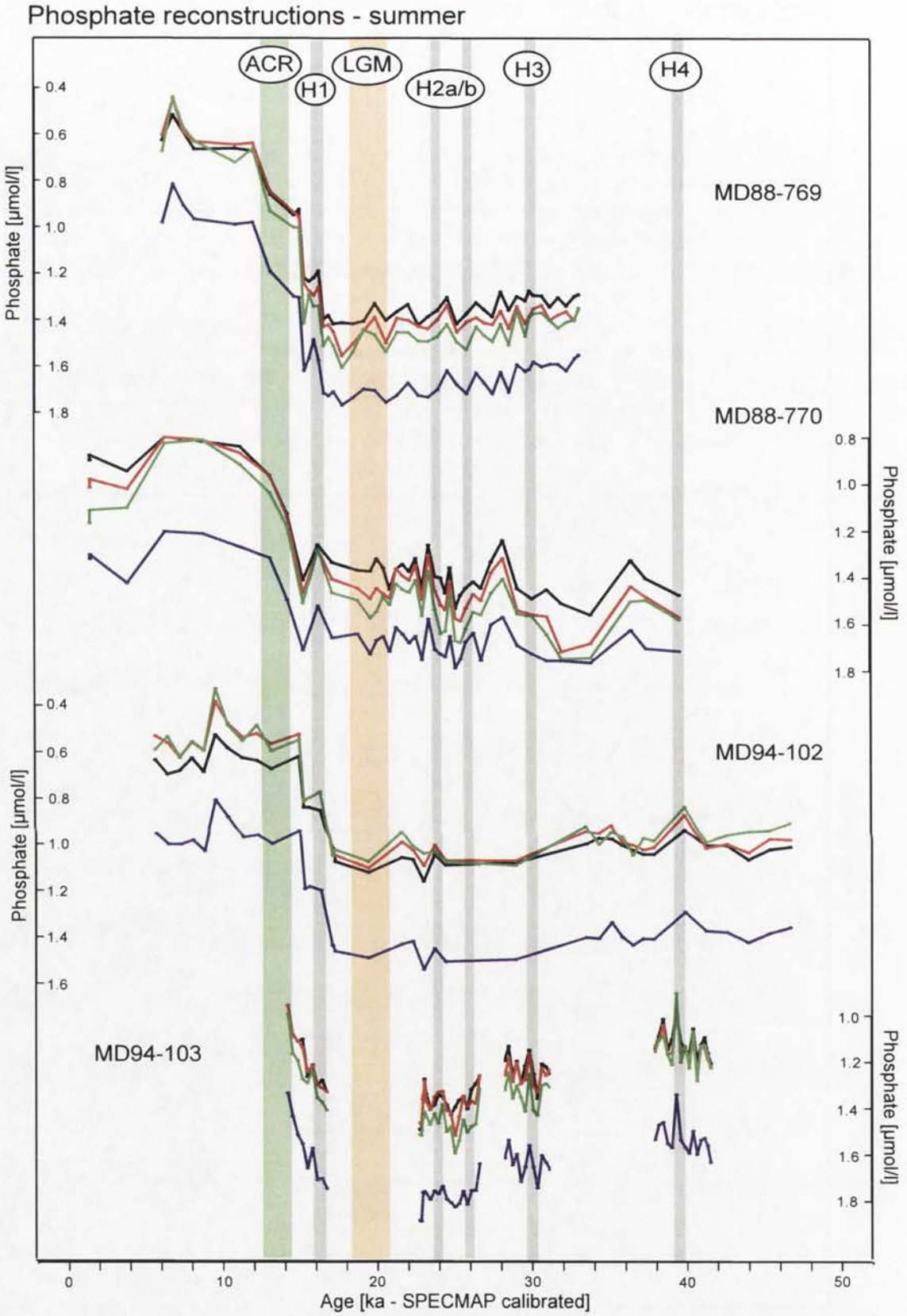

Figure 10.9a: Reconstructions of summer phosphate concentrations [µmol/l] for MD88-769, -770, MD94 -102, and -103 at the surface (black), and at 50m (red), 125m (green) and 250m (blue) bsl - all plots on the same scale. Vertical bars as in previous plots. Vertical scales inverted. Note that in MD88-770 there is a greater difference between phosphate levels at the surface, 50m, and 125m and those at 125 and 250m bsl between 15ka and the present than before. This phenomenon is not evident in the other cores except, possibly, MD94 -102. See text for details.

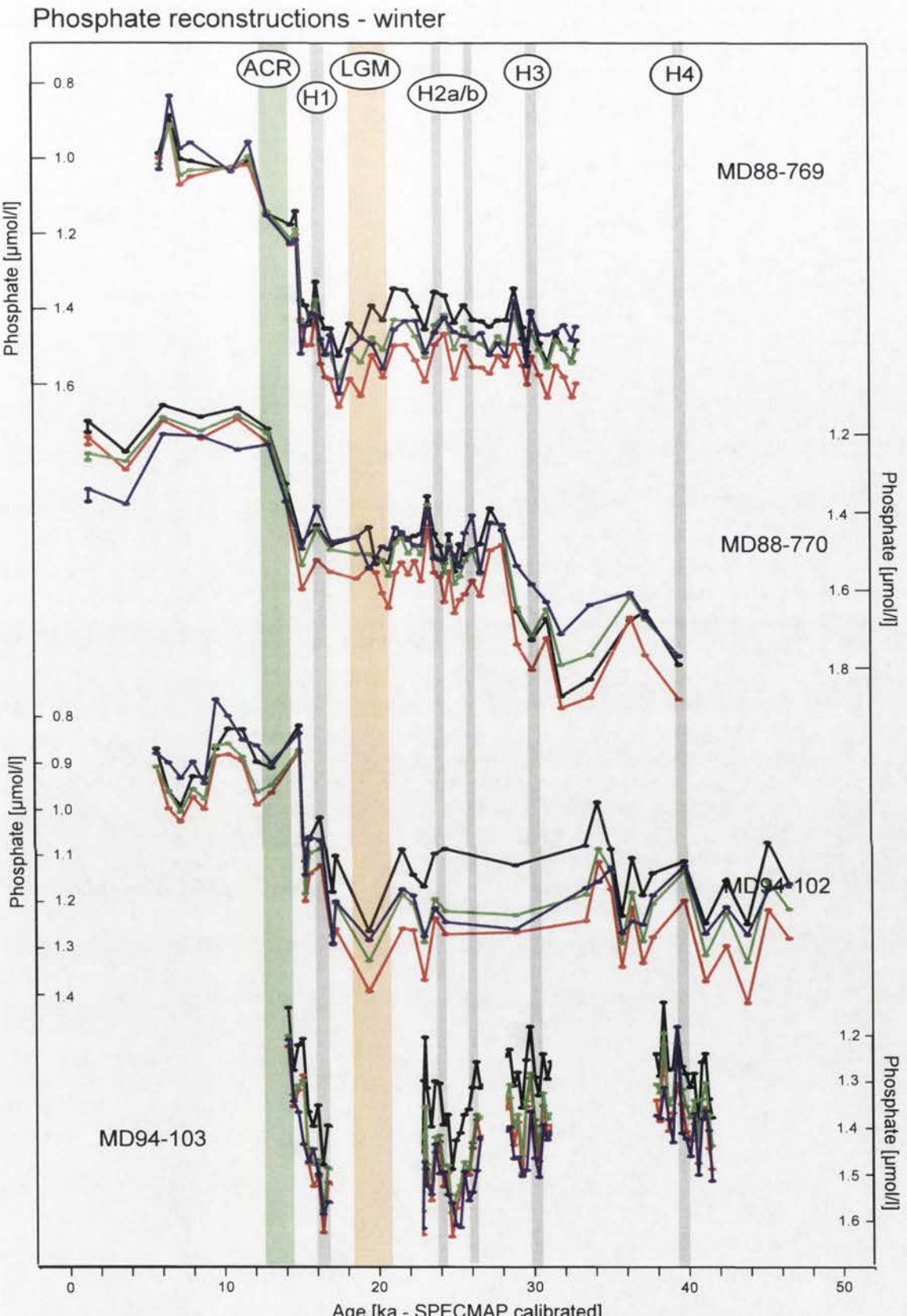

Figure 10.9b: Reconstructions of austral winter phosphate [µmol/l] for MD88-769, -770, MD94-102, and -103 at the surface (black), and at 50m (red), 125m (green) and 250m (blue) bsl. Note: vertical scales are inverted and not all the same. Vertical bars as in previous plots. In MD88-769 and MD95-102 there is a greater difference between phosphate levels at the surface and those at greater depth between 15ka and 35ka than before or after. The phenomenon is not evident in MD88-770 or MD94-103 (which does not cover a sufficient time interval to display it). See text for details.

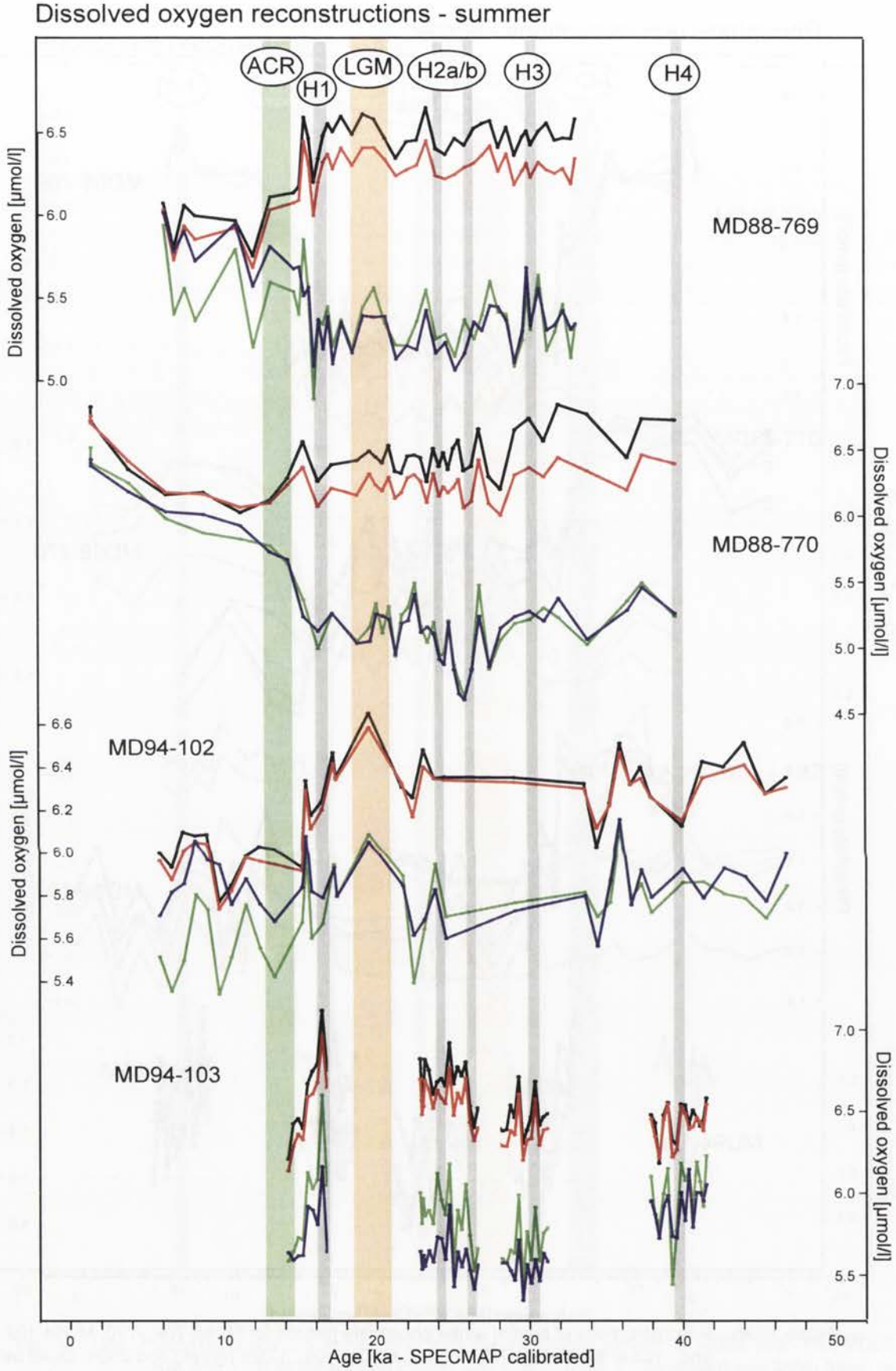

Figure 10.10a: Reconstructions of austral summer dissolved oxygen [µmol/l] for MD88-769, -770, MD94-102, and -103 at the surface (black), and at 50m (red), 125m (green) and 250m (blue) bsl - not all on the same vertical scale. Vertical bars as in previous plots. Note that there is a greater difference between dissolved oxygen levels at the surface and 50m and those at 125 and 250m bsl between 15ka and 35ka than before or after - see text for details.

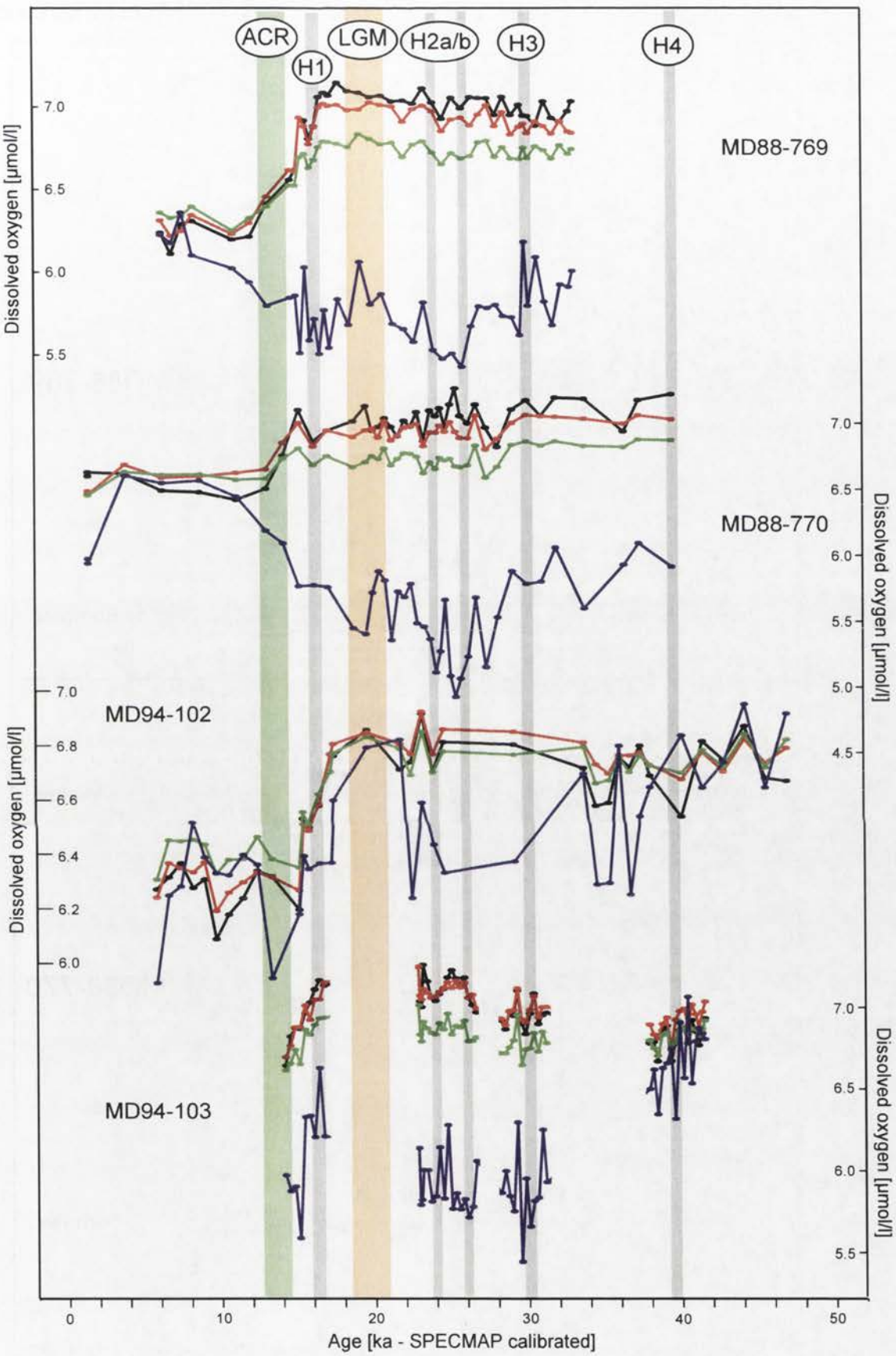

Figure 10.10b: Reconstructions of austral winter dissolved oxygen [µmol/l] for MD88-769, -770, MD94-102, and -103 at the surface (black), and at 50m (red), 125m (green) and 250m (blue) bsl - not all on the same vertical scale. Vertical bars as in previous plots.
Note that there is a greater difference between dissolved oxygen levels at the surface, 50m, and 125 and those at 250m bsl between 15ka and 35ka than before or after - details in text.

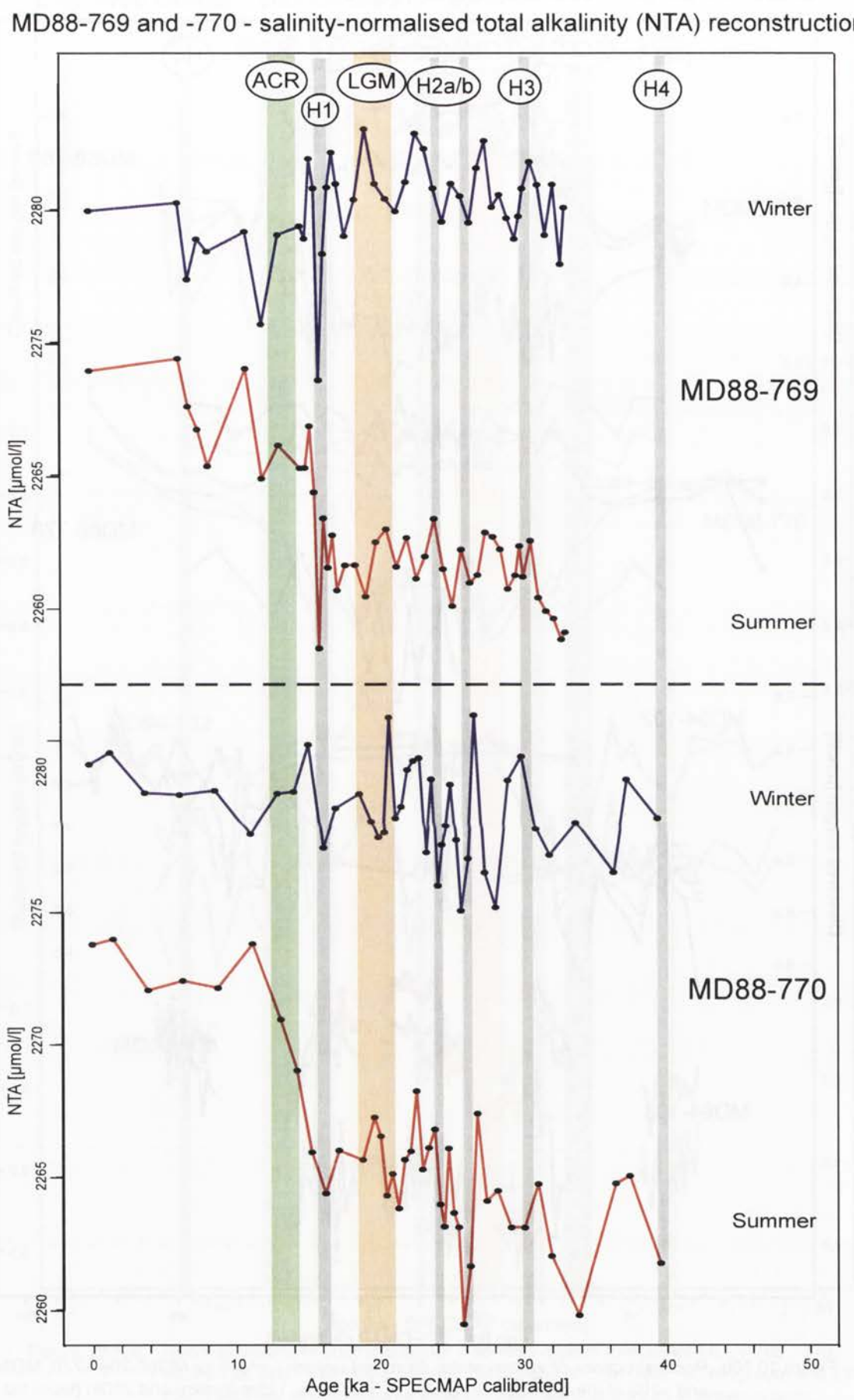

Figure 10.11a: summer and winter NTA for MD88-769 and MD88-770 derived from SST reconstructions using Millero *et al's* (1998) formulae. Vertical bars as in previous plots.

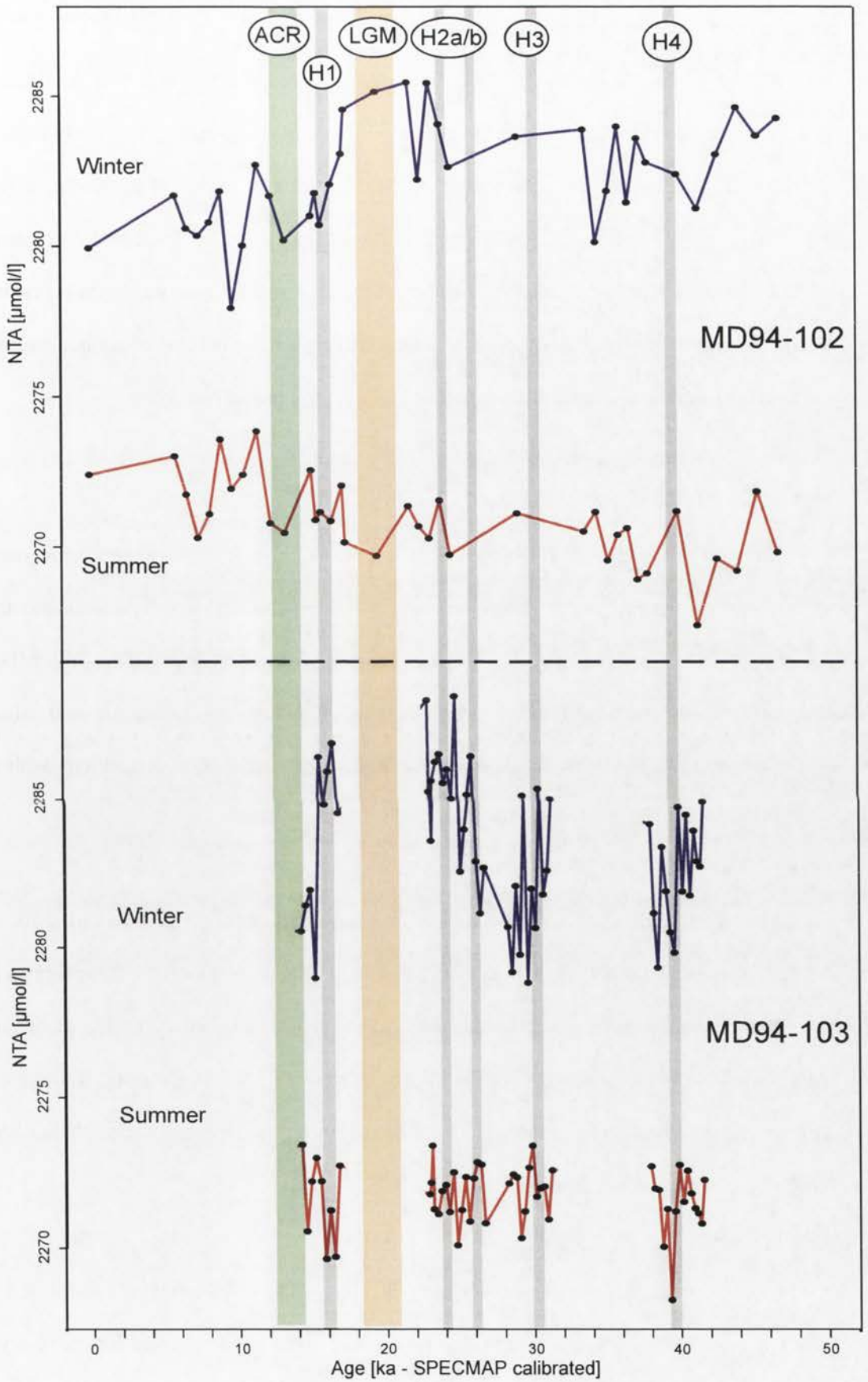

Figure 10.11b: summer and winter NTA for MD94-102 and MD94-103 from SST reconstructions using Millero *et al's* (1998) formulae. Vertical bars as in previous plots.

WA-PLS's nearest rival on the basis of performance is LWWA (Table 10.1b). However, when used to reconstruct SSTs from the EIO and SIO LGM samples, the differences from the Barrows and Juggins' (2005) values are considerably greater than any of the reconstructions listed in Table 10.2 and, so, the LWWA results are not reported here. The LWWA constructs a local training set of a user-specified number of the closest sub-fossil analogues (as defined by the minimum squared χ^2 distance) and is most effective if the number of surface sediment samples is large. This study's thirty-eight SIO samples are probably too few.

10.3. The SIO environmental variable reconstructions

The austral summer and winter values of the environmental variables temperature, salinity, *in situ* density, nitrate, phosphate, dissolved oxygen, and salinity-normalised total alkalinity (NTA) were reconstructed for each sample of the four cores MD88-769, MD88-770, MD94-102, and MD94-103. The variables AOU, oxygen saturation, and silicate concentration were not reconstructed because of their relatively poor correlations with the surface sediment radiolarian data (see Chapter 7).

Plots of the summer and winter temperature reconstructions at the surface and at 50, 125 and 250 metres bsl against age appear as Figures 10.2-10.5. Also plotted in these figures are the $\partial^{18}O$ versus PDB *N. pachyderma* left (200-250μ) values provided by Dr E. Michel and, where available, foraminifera-based SST reconstructions (the sources varying from core to core and are assumed to be annual SSTs unless otherwise marked) and diatom-based SSTs (Dr X. Crosta, pers. com., 2008).

The age model for the four cores used in this study is that originally employed by Labeyrie *et al.* (1996). Radiocarbon dates for the four cores were corrected for the reservoir effect following Bard *et al.* (1993) and Stuiver and Reimer (1993) and further modified using

the Pisias *et al.* (1984) "short stack" and Martinson *et al's.* (1982) inverse correlation "SPECMAP" (Labeyrie *et al.*, 1996; Salvignac, 1998). Sicre *et al.* (2005) confirmed their age model for MD94-103 by reference to the Laschamp excursion and, thus, there can be high confidence in the alignments they report between Heinrich events and features in their alkenone- and foraminiferal-based SST reconstructions. For cores other than MD94-103, the significance of similar alignments between Heinrich events and features in the radiolarian-based SST reconstructions presupposes, of course, that the cores' age models are sufficiently similar to that for MD94-103 for this to be justified. Comparison of the estimated timing of the one major feature common to all the plots, the acute increase in temperature at the end of the last Glacial indicates the age models are essentially the same.

Recently, a new age model has been proposed for four cores from the Australasian sector of the Southern Ocean (Barrows *et al.*, 2007). The cores used are SO136-GC3, DSDP site 594, MD92-2120, and, common to this study, MD88-770. For MD88-770, the difference between the two models over the last 40 ka is 5% or less from 40-35 ka, an average of 9%, peaking at 12.2% (3.27 ka) from 35-20 ka, and less than 5% since 20 ka. The Barrows *et al.* (2007) chronology has not been adopted for this thesis, partly because the majority of papers relating to the cores studied here follow Labeyrie *et al.* (1996), and partly because not all the radiocarbon dating information which would be required to make the change is available to the author.

The timing of Heinrich Events, following Bond *et al's.* (1992; 1993) chronology, is indicated in Figures 10.2-10.11 and 10.16-10.23. The dates used for the Heinrich events is the same as used those used by Sicre *et al.* (2005), ensuring that comparisons with their findings for MD94-103 are on the same age scale. The LGM is also indicated in Figures 10.2-10.11 and 10.16-10.23 as between 18.2 ka and 21.4 ka, the equivalent on the Labeyrie *et*

al. (1996) age model of the Barrows *et al.* (2007) estimate of 21±2 ka for the timing of the LGM on their age model. In addition, the timing of the Antarctic Cold Reversal (ACR) (Jouzel *et al.*, 1995) is shown using dates from Calvo *et al.* (2007) slightly adjusted. It should be noted that the resolution of the age scales in Figures 10.2-10.11 and 10.16-10.23 is insufficient to draw firm conclusions on relationships between the Heinrich Events and the ACR on one hand and features in the reconstructions on the other: such conclusions could only be drawn from the numeric data.

Figures 10.6 to 10.10 are plots of salinity, *in situ* density, nitrate and phosphate concentrations, and dissolved oxygen, again at the surface and at 50, 125 and 250 metres bsl, against age – both austral summer (JFM) and austral winter (JAS) plots are presented. Figures 10.11a and b present salinity-normalised total alkalinity reconstructions (NTA) at the ocean's surface based on Millero *et al's* (1998) formulae for summer and winter respectively: NTA below the sea-surface cannot be estimated by this method. The salinity, nitrate, and dissolved oxygen plots show a greater difference between the near surface and the deeper water reconstructions between approximately 35 ka and 15 ka (i.e. the MIS-2 glacial) than before or after that period. This phenomenon is not consistently evident in all the cores and is reversed in the case of temperature. The observation has implications for changes in ocean stratification and the speed of downwelling and, so, has been illustrated as "time slices" of dbsl against age for the reconstructed variables, one set of slices for each core for summer and winter (Figures 10.12-15). These time slices have been restricted to cover the surface to 250 bsl because going to greater depth only increases the information content marginally and does so at the expense of decreasing the scale of the plots.

In an attempt to test the validity of the reconstructions, it was assumed that the values of the oceanic variables had not changed a great deal over the last 10 ka and would be similar to

the present-day values. [Note that this assumption is not strictly justified because temperatures in early MIS-1 were higher than at present, peaking at about 7 ka, and other oceanic variables show similar variations.] Using cores MD88-769, MD88-770, and MD94-102 (there are no MD94-103 data available to the author for the relevant period), the average of the reconstructed values over approximately the last 10 ka was calculated for each environmental variable at each dbsl and, from this was subtracted the present-day, WOA-05, value. The average of the absolute value of these differences for each variable appears in Table 10.5 with this value as a percentage of the WOA-05 values.

	Unit	MD88-769		MD88-770		MD94-102	
Age range of reconstructions	ka	6.9-10.9		1.5-8.8		5.8-10.5	
Season		JFM	JAS	JFM	JAS	JFM	JAS
Temperature	°C	-2.05	-2.41	-0.37	-1.04	-0.07	-0.67
Salinity	psu	-0.22	-0.36	-0.01	-0.05	0.10	0.04
	%	0.63	1.04	0.09	0.21	0.30	0.10
In situ density	kg/m^3	0.21	0.14	0.09	0.15	0.11	0.11
	%	0.79	0.50	0.33	0.54	0.40	0.41
Nitrate	µmol/l	4.93	5.52	0.54	2.05	-0.30	0.77
	%	29.22	32.91	5.91	13.29	7.66	7.39
Phosphate	µmol/l	0.27	0.20	0.09	0.04	0.09	0.03
	%	26.56	16.08	7.59	2.99	11.04	4.58
Dissolved oxygen	µmol/l	0.57	0.26	0.26	-0.08	-0.01	-0.11
	%	8.84	4.10	3.96	1.95	2.01	2.43

Table 10.5: The average difference between WOA-05 data and the average of the reconstructions for cores MD88-769, MD88-770, and MD94-102 over approximately the last 10 ka over depths from the surface to 500 metres and that value as a percentage of the average WOA-05 value (except for temperature where percentage would be meaningless).

In Table 10.5, the very low averages and percentages for salinity and *in situ* density indicate that their reconstructions are reliable for all three cores. The temperature reconstructions for MD88-770 and MD94-102 also differ very little from present-day values, and the nitrate, phosphate, and dissolved oxygen reconstructions are reasonably close. However, all but the salinity and *in situ* density reconstructions for MD88-769 differ

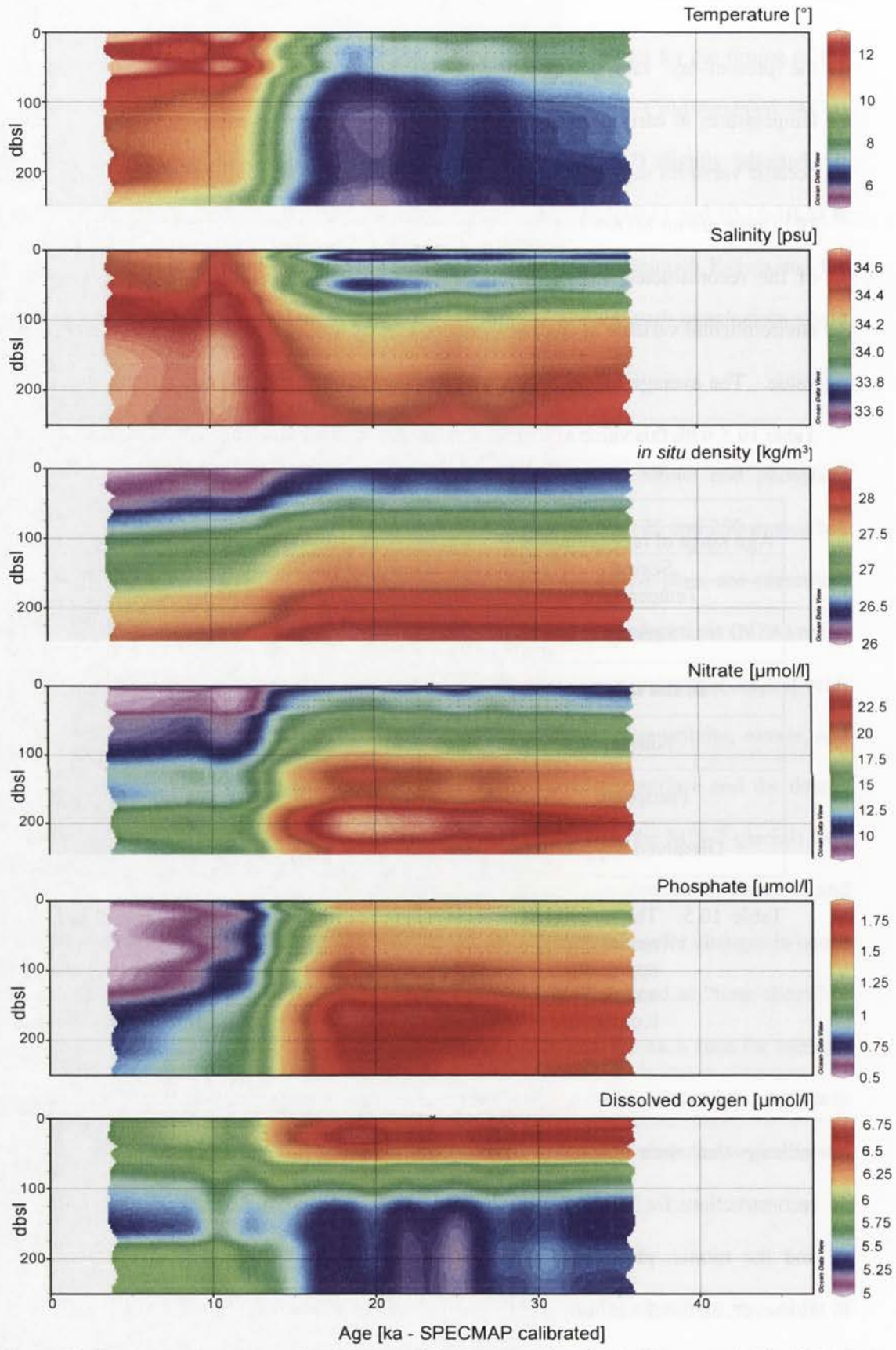

Figure 10.12a: austral summer palaeoceanographic reconstructions for 0-250 metres bsl for MD88-769 plotted against age.

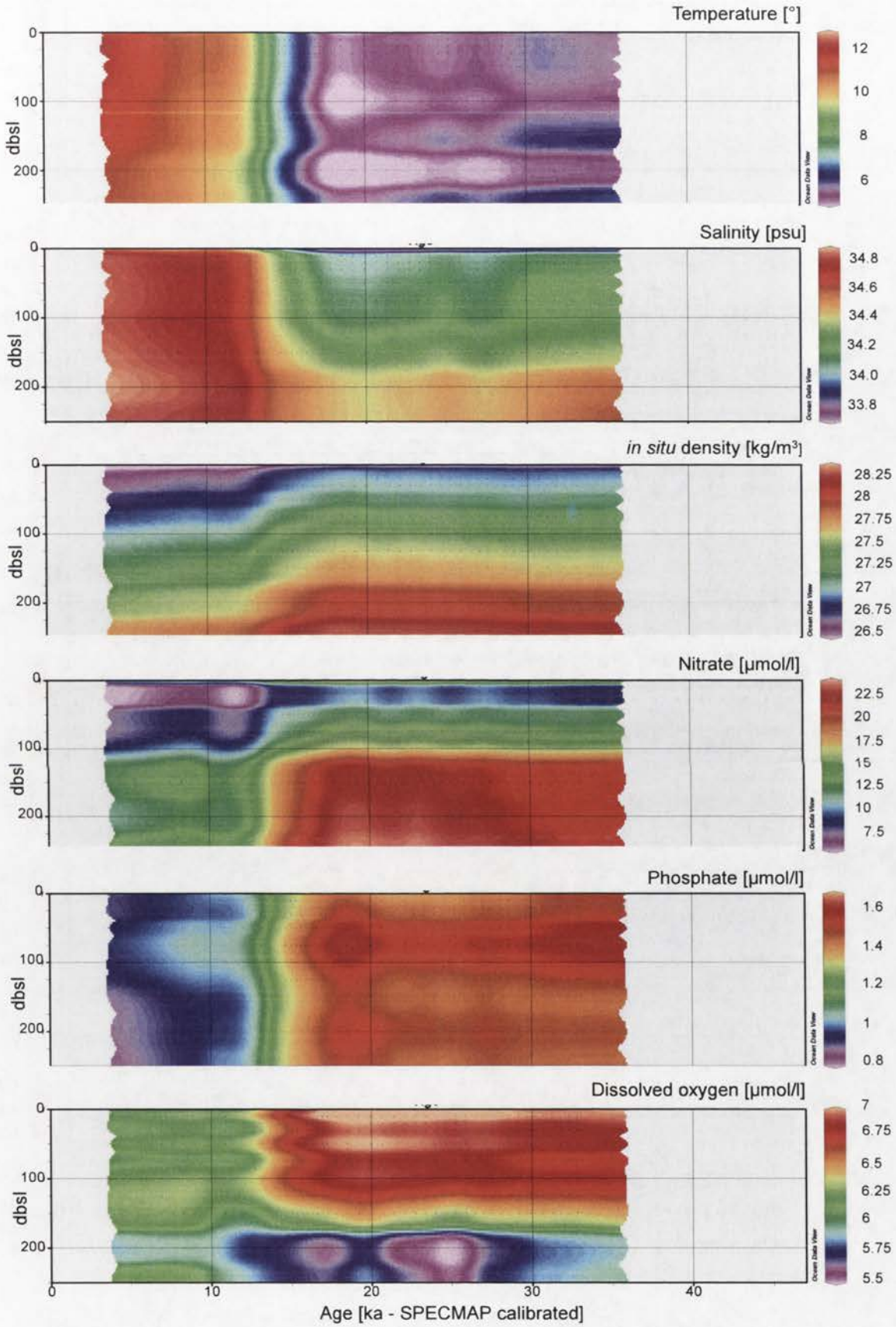

Figure 10.12b austral winter palaeoceanographic reconstructions for 0-250 metres bsl for MD88-769 plotted against age.

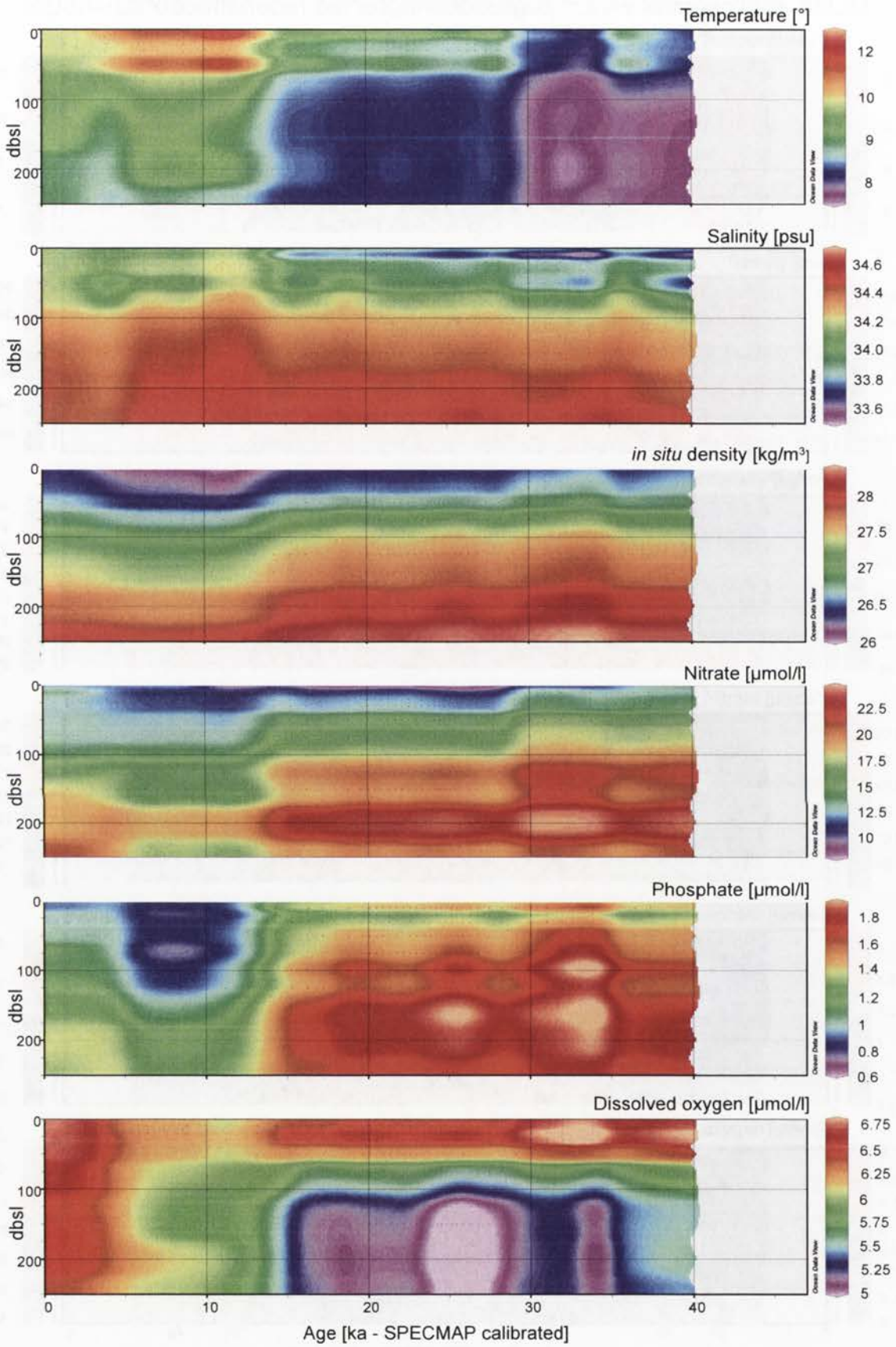

Figure 10.13a: austral summer palaeoceanographic reconstructions for 0-250 metres bsl for MD88-770 plotted against age.

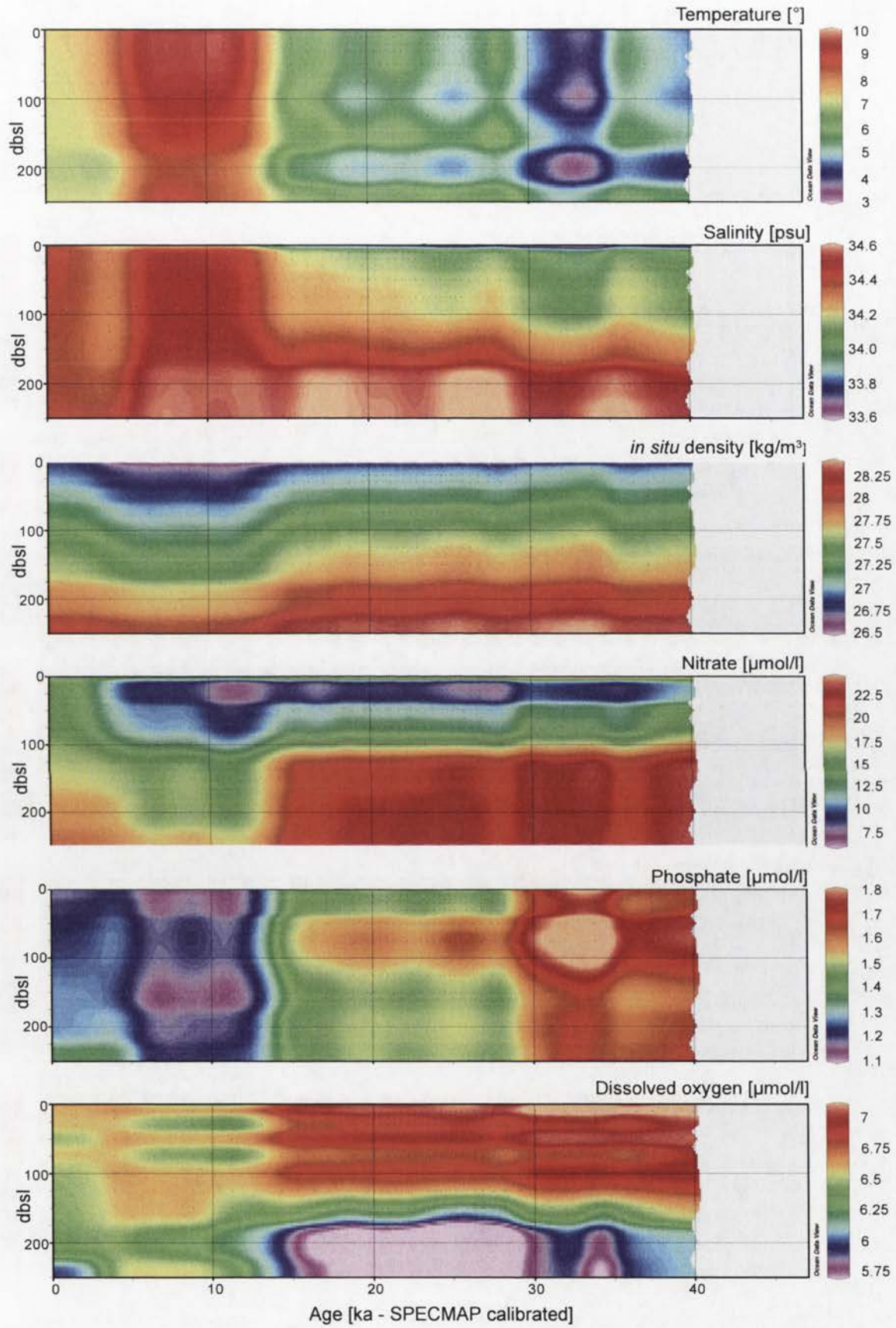

Figure 10.13b austral winter palaeoceanographic reconstructions for 0-250 metres bsl for MD88-770 plotted against age.

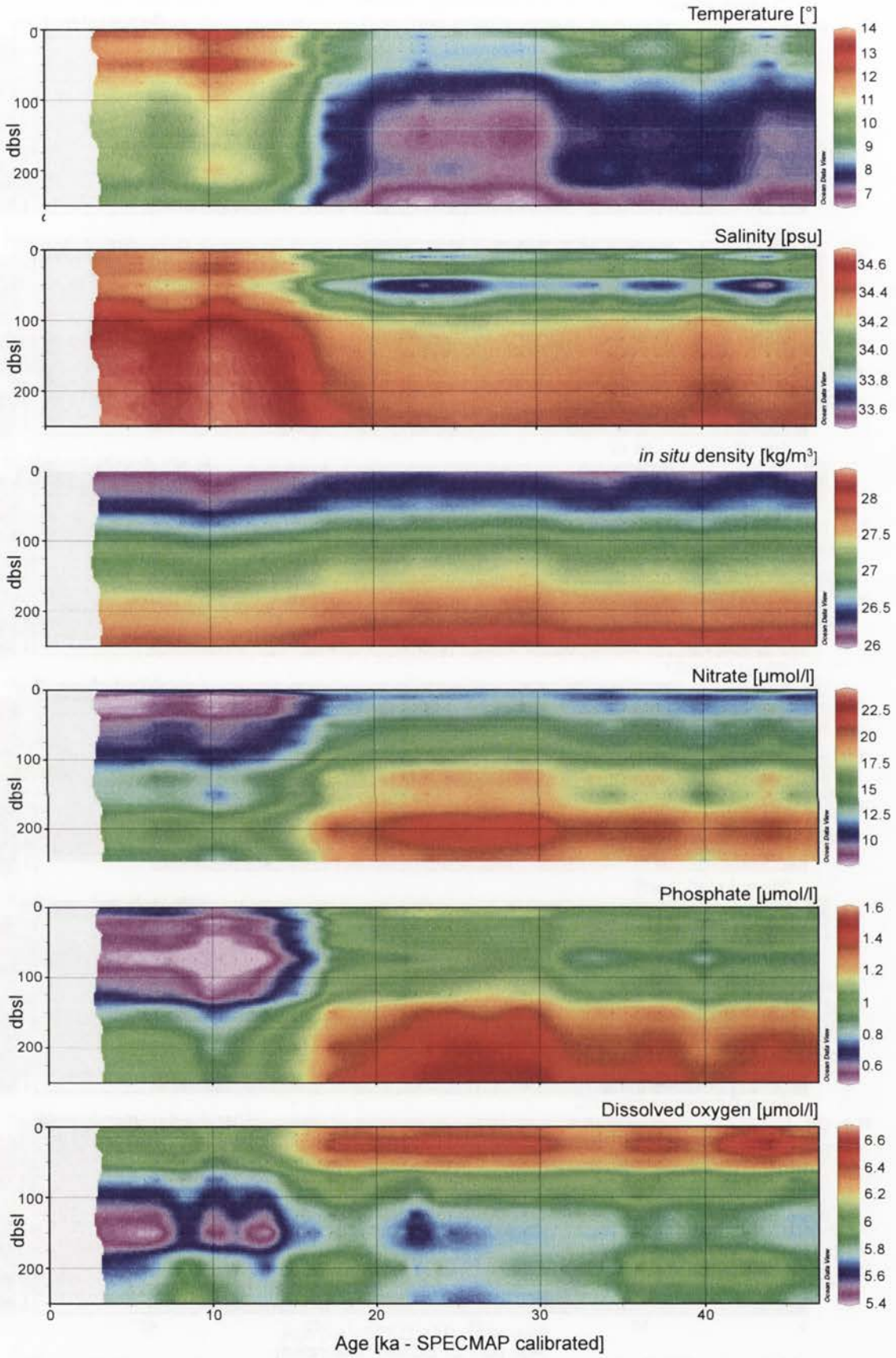

Figure 10.14a: austral summer palaeoceanographic reconstructions for 0-250 metres bsl for MD94-102 plotted against age.

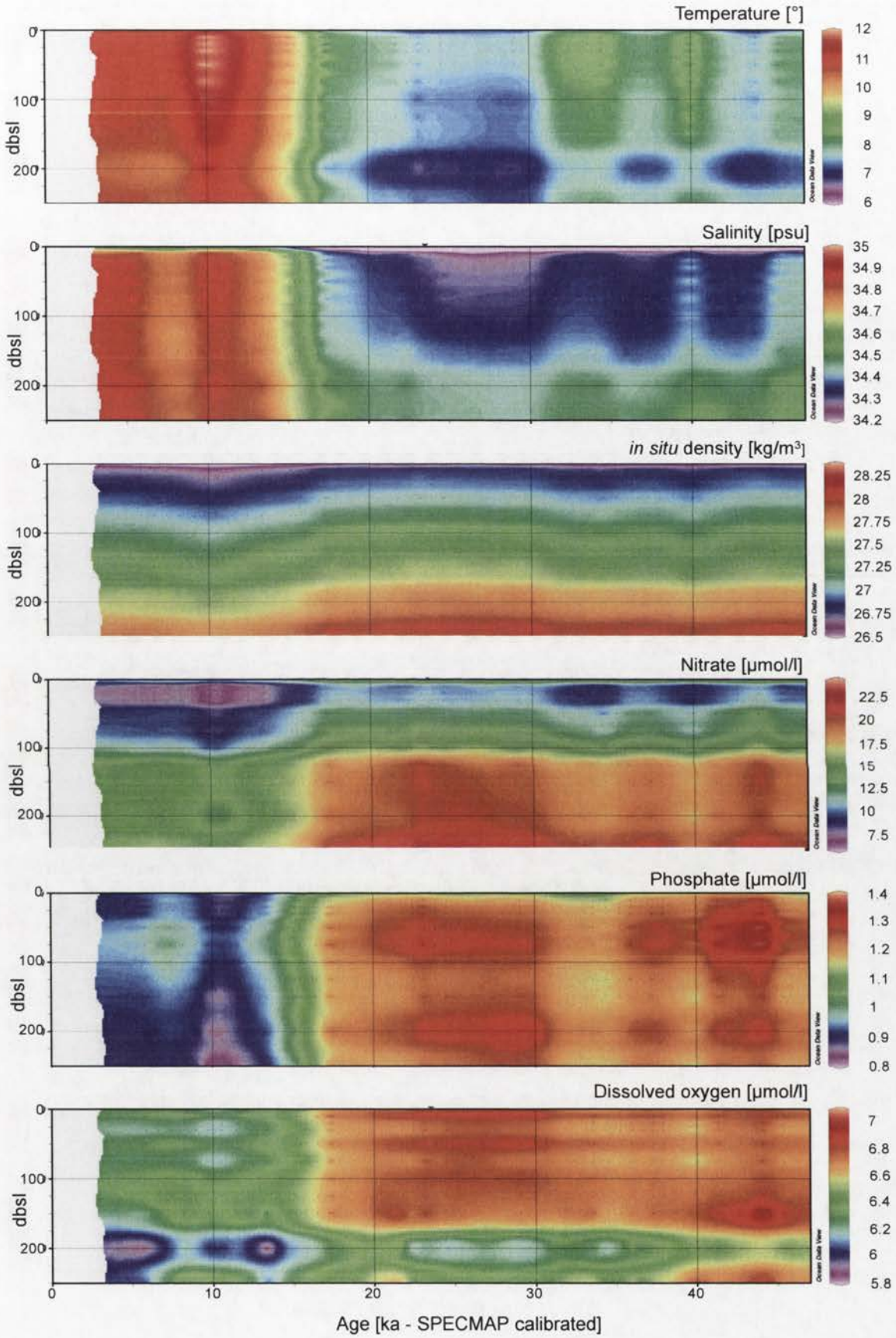

Figure 10.14b: austral winter palaeoceanographic reconstructions for 0-250 metres bsl for MD94-102 plotted against age.

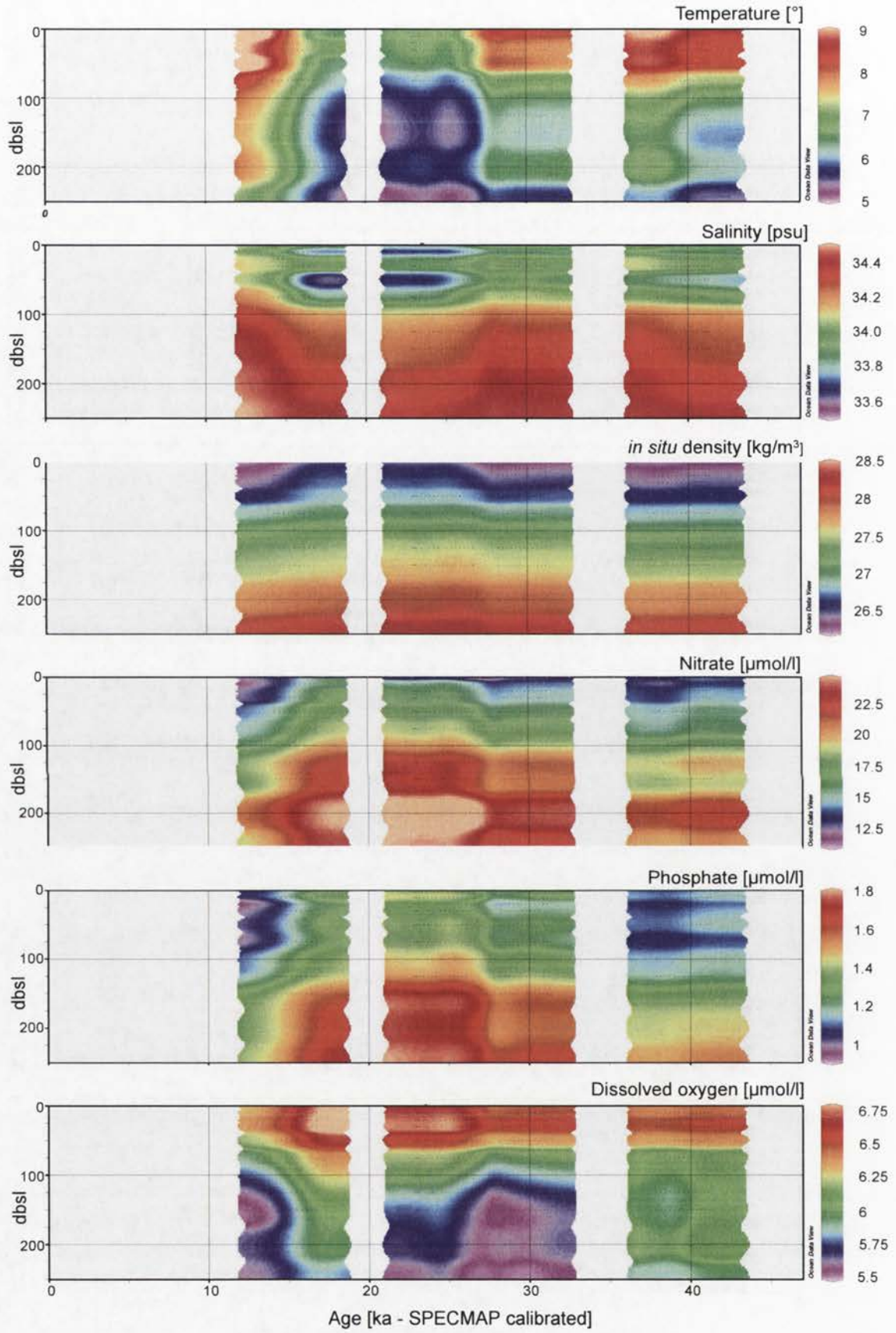

Figure 10.15a: austral summer palaeoceanographic reconstructions for 0-250 metres bsl for MD94-103 plotted against age.

MD94-103 - austral winter palaeoceanographic reconstructions

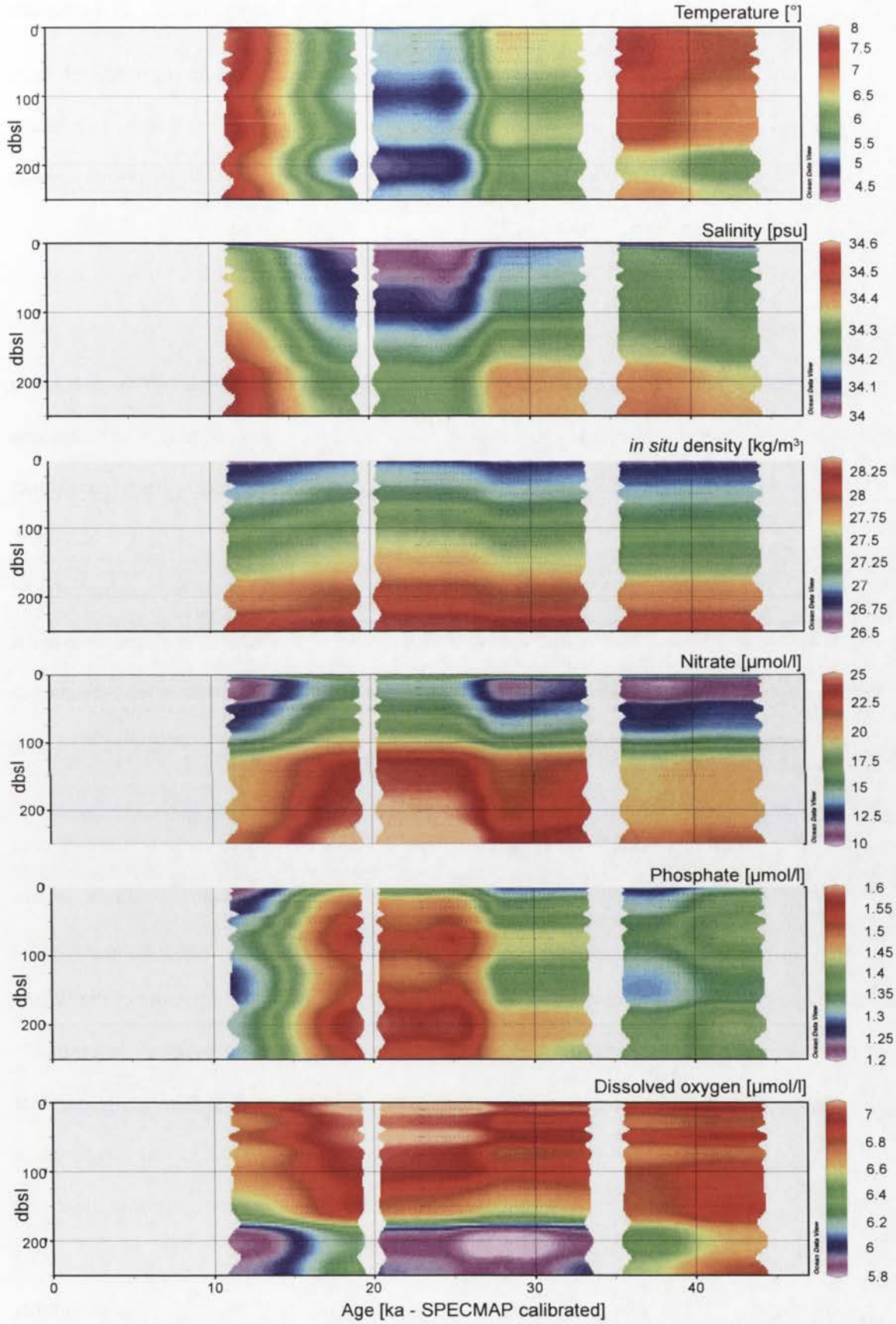

Figure 10.15b: austral winter palaeoceanographic reconstructions for 0-250 metres bsl for MD94-103 plotted against age.

markedly from present-day values. Some of these differences may be the result of there being no MD88-769 data younger than 6 ka, but, if this be the case, the MD94-102 results should show similar discrepancies. Detailed examination of the MD88-769 results showed the greatest discrepancies occurred in the values close to the ocean surface.

10.4. Reconstruction of frontal movements over time

Ocean fronts move north and south seasonally and over longer periods in association with such phenomena as ENSO (Tomczak and Godfrey, 2003). In this study, an attempt was made to reconstruct movements over the last 30-40 ka. The first approach was to reconstruct (using C2 - Juggins, 2007b) the radiolarian assemblages to which each core sample belonged, with the expectation of seeing fluctuations between more northerly and more southerly-based assemblages. This method produced credible results but was eventually replaced by what is considered a more robust approach which has the added refinement of allowing estimates to be made for different ranges of water depth.

The second method consists of forming both summer and winter vectors for every core sample, each vector consisting of the reconstructed values of temperature, salinity, *in situ* density, dissolved oxygen, nitrate, and phosphate for a selected water-depth range: a maximum of 84 reconstructed values for each core sample. Datasets of vectors of the WOA-05 data for the same environmental variables at the same depths for every point on the 1° latitude by 1° longitude grid covering the study area was constructed for both austral summer and winter, over 4500 vectors in all. Every vector of reconstructed values was compared, in turn, with every vector in the WOA-05 dataset and the best five matches, based on least sum of squared differences, published. This approach is very similar to the modern analog method (Hutson, 1977) of reconstructing palaeoenvironmental SSTs using a large number (best if greater than 500 - Juggins, 2007a) of modern surface samples.

Because the plots of the environmental variable reconstructions seem to suggest that the changes over time differ between near-surface and deeper waters, two sets of comparisons of the reconstructed and the WOA-05 vectors have been made. The first consists of comparing the vectors formed from values from above 100 metres bsl (36 values per vector), and the second from those from 100 to 500 metres bsl (48 values per vector). For any given vector of reconstructed values, the maximum sum of squared differences is typically at least a factor of 100 greater than the minimum. The best matches are tightly clustered with respect to latitude, the difference between the highest and lowest rarely being more than one degree. Longitude matches varied more, sometimes by as much as 40° one from another: this seems to be a function of the rough symmetry of ocean conditions between latitudes 40 and 50°S about longitude 90°E. Because of the symmetry, the best match has roughly the same chance of being found to the east of 90°E as to the west of that longitude.

In order to reconstruct the movements of the fronts, the difference in latitude between the position of each sample's best match and the location of the Subantarctic and Polar Fronts (interpolated from Belkin and Gordon, 1996) at the longitude of that match was calculated and to this was added the latitude of the core site. The inferred positions of the Subantarctic Front thus derived appear in Figures 10.16-19; the Polar Front positions in Figures 10.20-23.

The latitudinal shifts of the SAF and the PF between the glacial and interglacial periods MIS-2 and MIS-1 and between MIS-3 and MIS -2 are summarised in Table 10.6. In almost every case, the frontal movement for waters above 100 m bsl is greater than that below that depth. The major exception is the apparent movement of the PF between MIS-2 and MIS-1 in winter. Also notable is the indication that, in summer in MIS-2, the SAF and the PF in the area of MD94-102 and MD94-103 were displaced further north relative to their present locations than they were in the region of MD88-769 and MD88-770. Near MD94-102 and MD94-103, both the

SAF and the PF were displaced about 5° north, whereas, near MD88-769 and MD88-770, the SAF was displaced only 2° north and the PF 4° north.

It should be noted that Belkin and Gordon's (1996) data do not distinguish summer from winter frontal paths. The data include winter as well as summer measurements and, thus, the published positions of the fronts may be regarded as an annual average, probably trending towards summer values because of the greater availability of records for that season. Comparison of the summer and winter profiles of the Southern Ocean in Figures 4.4-4.10 indicates that the mixed layer of the SAF and the PF probably move about 2° over the course of the year; below the mixed layer the movement is little or nothing. The winter values for water depth less than 100 metres bsl in Figures 10.16-23 may be underestimates of about 2°.

MIS periods	Season (austral)	Fronts	Water depth [m]	MD88-769 [° latitude]	MD88-770 [° latitude]	MD94-102 [° latitude]	MD94-103 [° latitude]
2-1	Summer [JFM]	SAF	<100	2.5	1.8	5.3	(4.0)
			≥100	1.4	-1.2	1.5	(1.4)
		PF	<100	3.8	4.2	5.1	(4.9)
			≥100	2.3	1.6	2.3	(2.3)
	Winter [JAS]	SAF	<100	3.2	2.2	3.2	(3.2)
			≥100	1.9	-0.2	2.4	(1.9)
		PF	<100	0.9	-0.1	3.7	(2.9)
			≥100	2.9	3.2	2.6	(3.0)
3-2	Summer [JFM]	SAF	<100	no data	no data	-2.2	-1.3
			≥100			0.7	-1.1
		PF	<100			-2.3	-1.7
			≥100			-0.2	-1.1
	Winter [JAS]	SAF	<100			-0.5	-0.9
			≥100			-0.7	-0.4
		PF	<100			-1.3	-1.4
			≥100			-0.8	-0.3

Table 10.6: The average southward movement (negative value signifies northward movement) of the Subantarctic Front (SAF) and the Polar Front (PF) reconstructed from cores MD88-769, MD88-770, MD94-102, and MD94-103 between MIS-2 and 1 and between MIS-3 and MIS-2 for austral summer and winter at water depths less than 100m and for depths greater than 100m. Parentheses indicate values based on limited data.

10.5. Spectral analysis

Spectral analysis (Hammer *et al.*, 2001; Hammer and Harper, 2006) was applied to the reconstructed sequences to identify any environmental cycles over time. The time period covered by this study is insufficient to reveal Milankovitch cycles and no shorter cycles are evident, probably because the study was not conducted at high enough resolution.

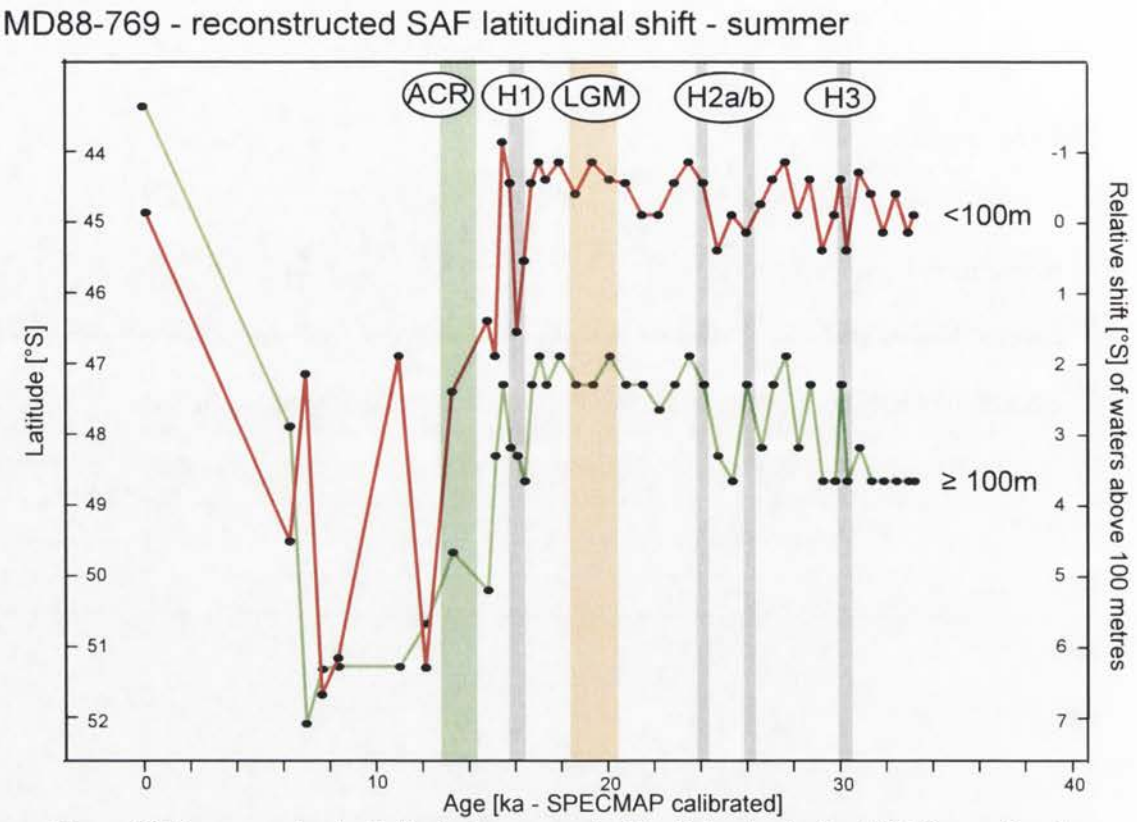

Figure 10.16a: reconstructed latitudinal movement of the Subantarctic Front (SAF) over time from MD88-769 summer data (see text for details). The shift of waters above 100 metres bsl is plotted in red and those from 100 to 500 metres in green.

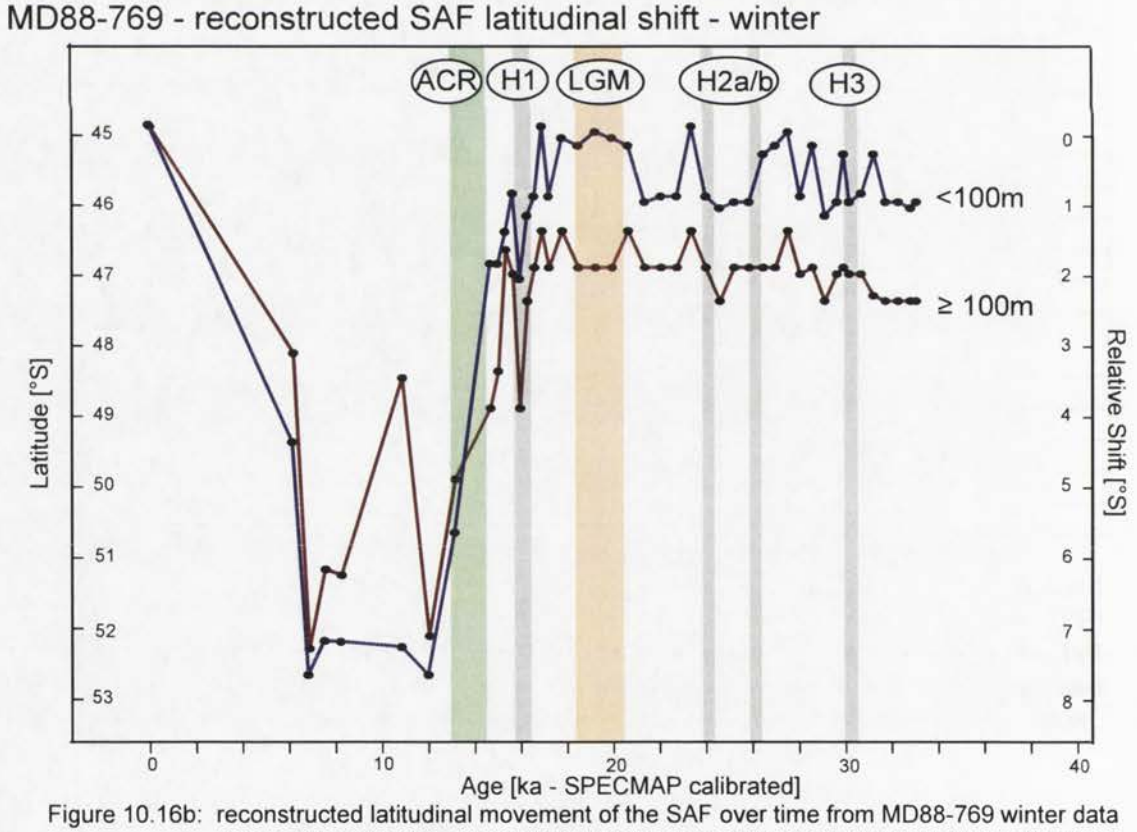

Figure 10.16b: reconstructed latitudinal movement of the SAF over time from MD88-769 winter data (see text for details). The shift of waters above 100 metres bsl is plotted in blue and those from 100 to 500 metres in brown.

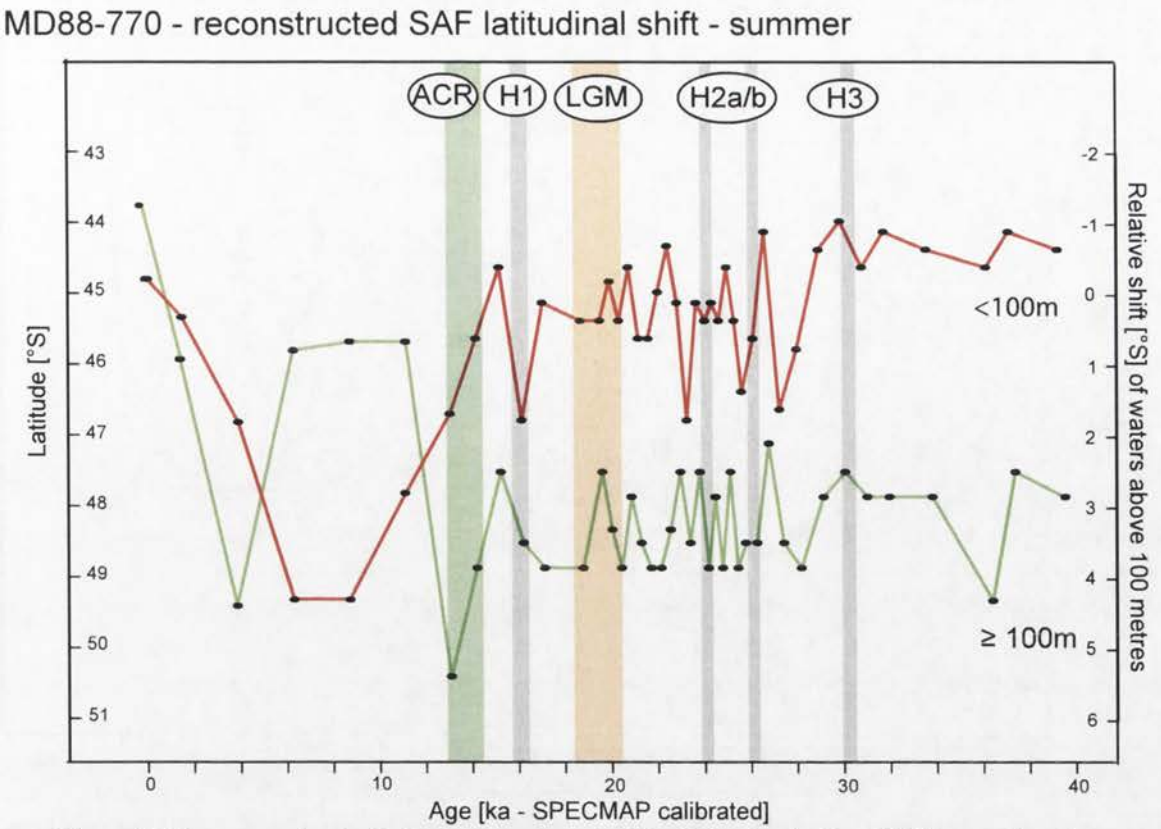

Figure 10.17a: reconstructed latitudinal movement of the Subantarctic Front (SAF) over time from MD88-770 summer data (see text for details). The shift of waters above 100 metres bsl is plotted in red and those from 100 to 500 metres in green.

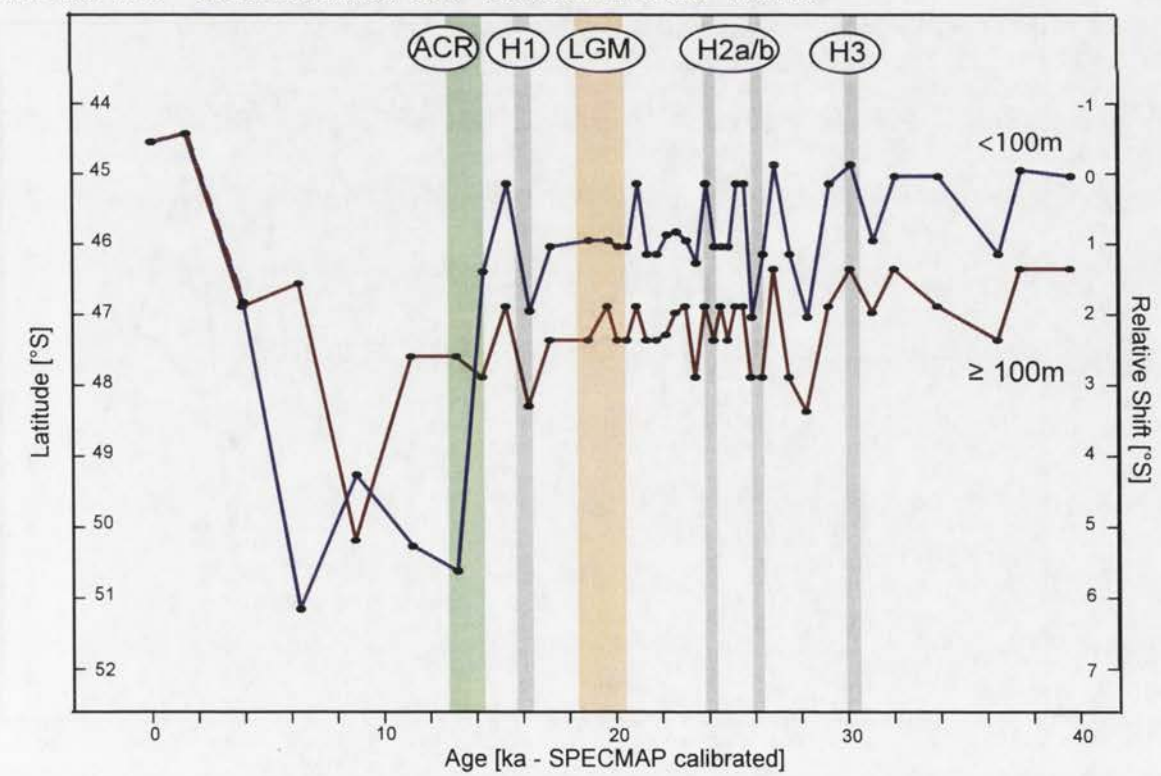

Figure 10.17b: reconstructed latitudinal movement of the SAF over time from MD88-770 winter data (see text for details). The shift of waters above 100 metres bsl is plotted in blue and those from 100 to 500 metres in brown.

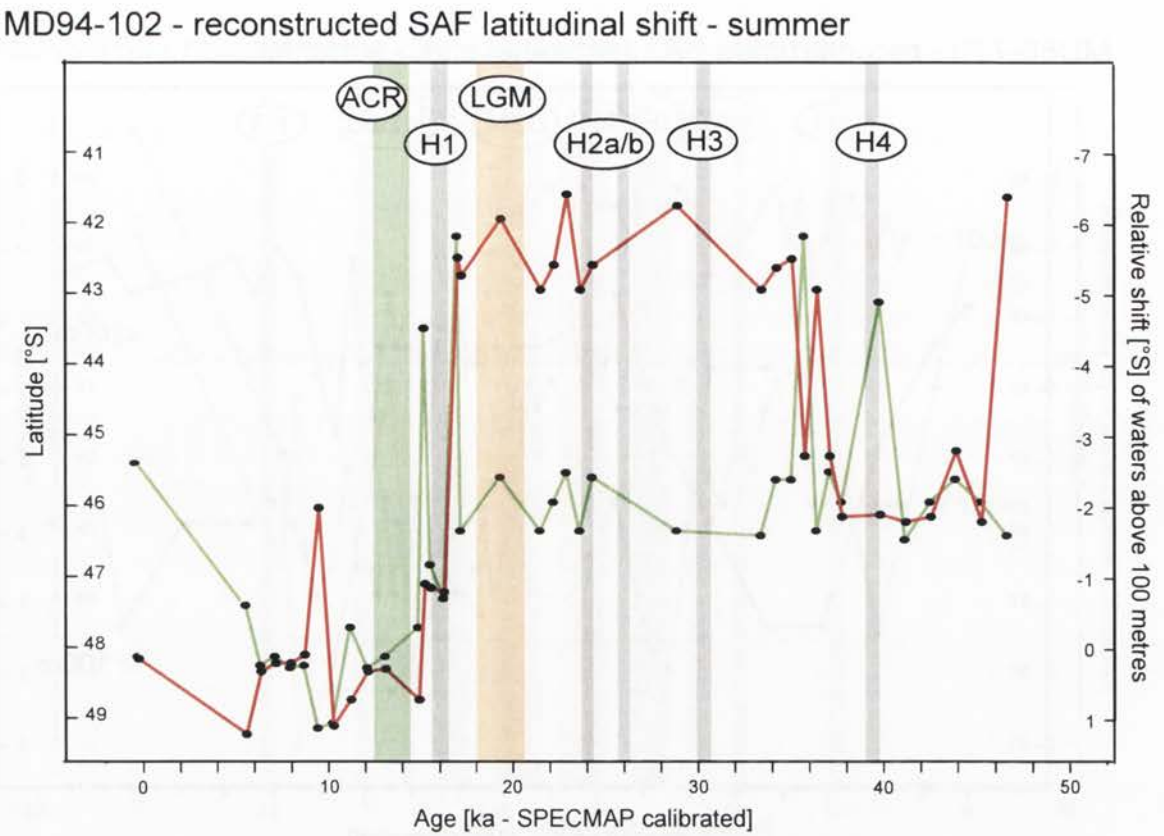

Figure 10.18a: reconstructed latitudinal movement of the Subantarctic Front (SAF) over time from MD94-102 summer data (see text for details). The shift of waters above 100 metres bsl is plotted in red and those from 100 to 500 metres in green.

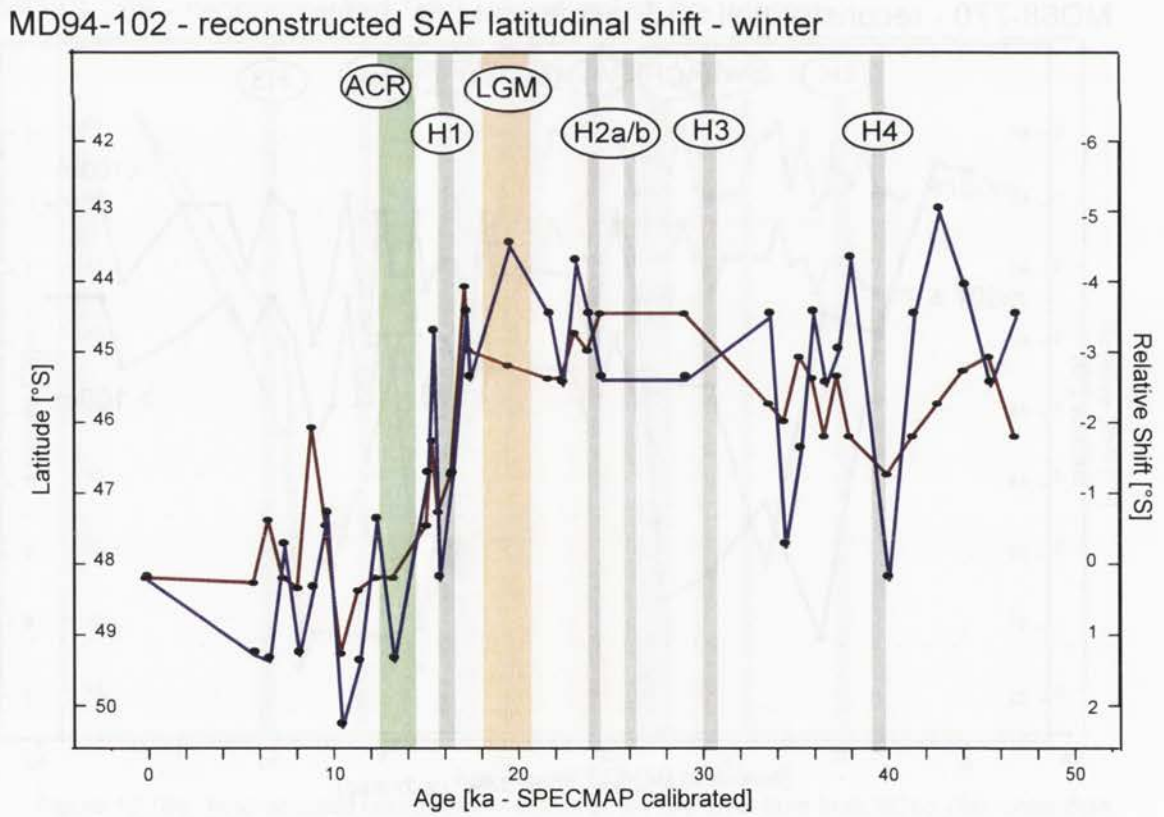

Figure 10.18b: reconstructed latitudinal movement of the SAF over time from MD94-102 winter data (see text for details). The shift of waters above 100 metres bsl is plotted in blue and those from 100 to 500 metres in brown.

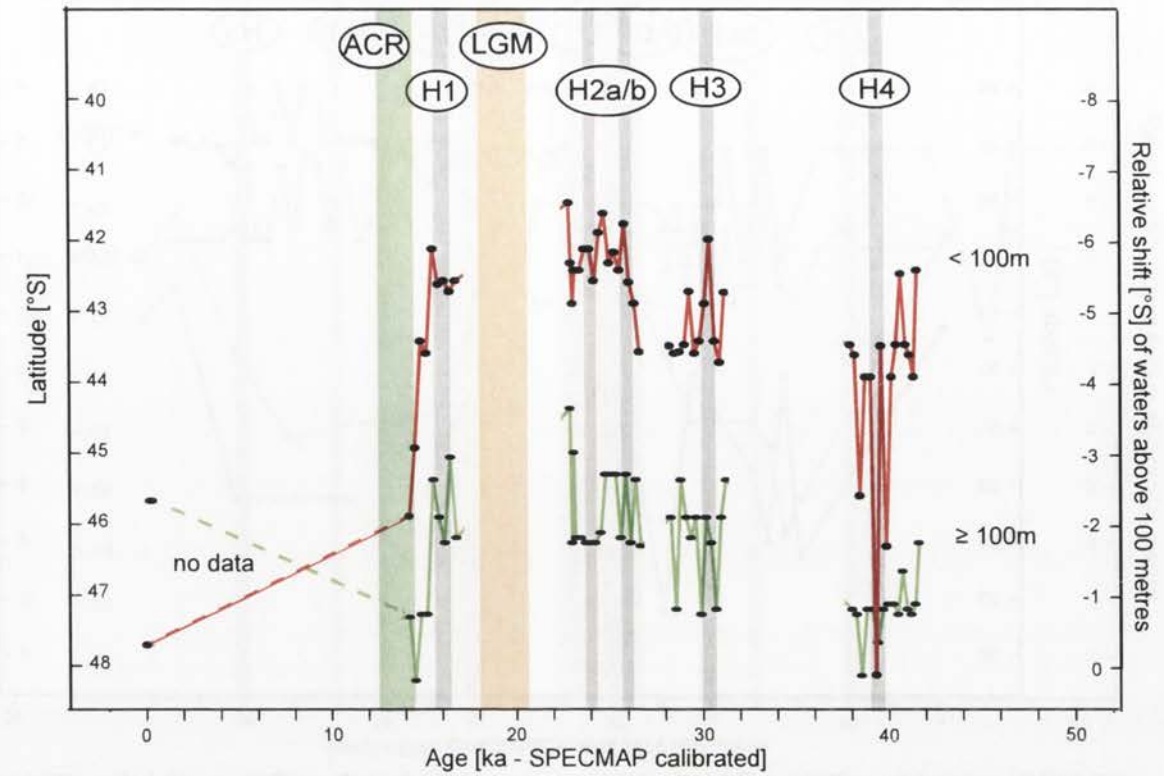

Figure 10.19a: reconstructed latitudinal movement of the Subantarctic Front (SAF) over time from MD94-103 summer data (see text for details). The shift of waters above 100 metres bsl is plotted in red and those from 100 to 500 metres in green.

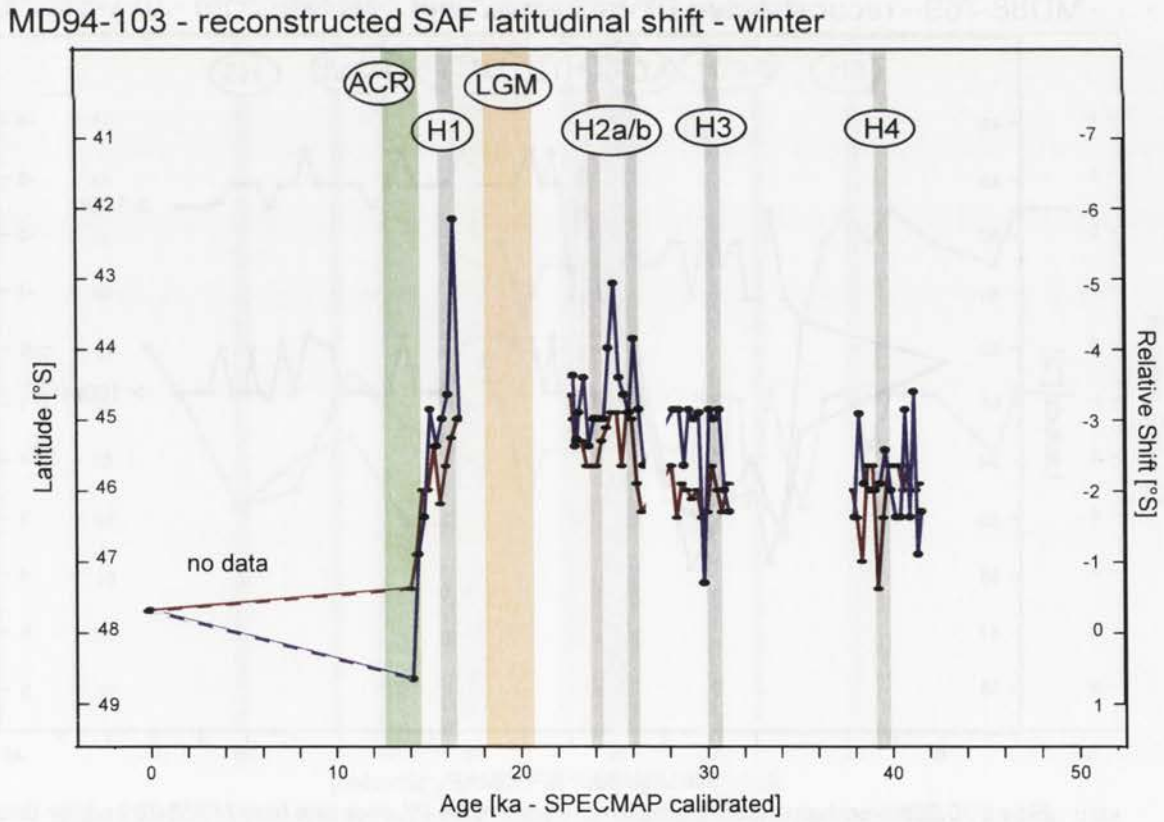

Figure 10.19b: reconstructed latitudinal movement of the SAF over time from MD94-103 winter data (see text for details). The shift of waters above 100 metres bsl is plotted in blue and those from 100 to 500 metres in brown.

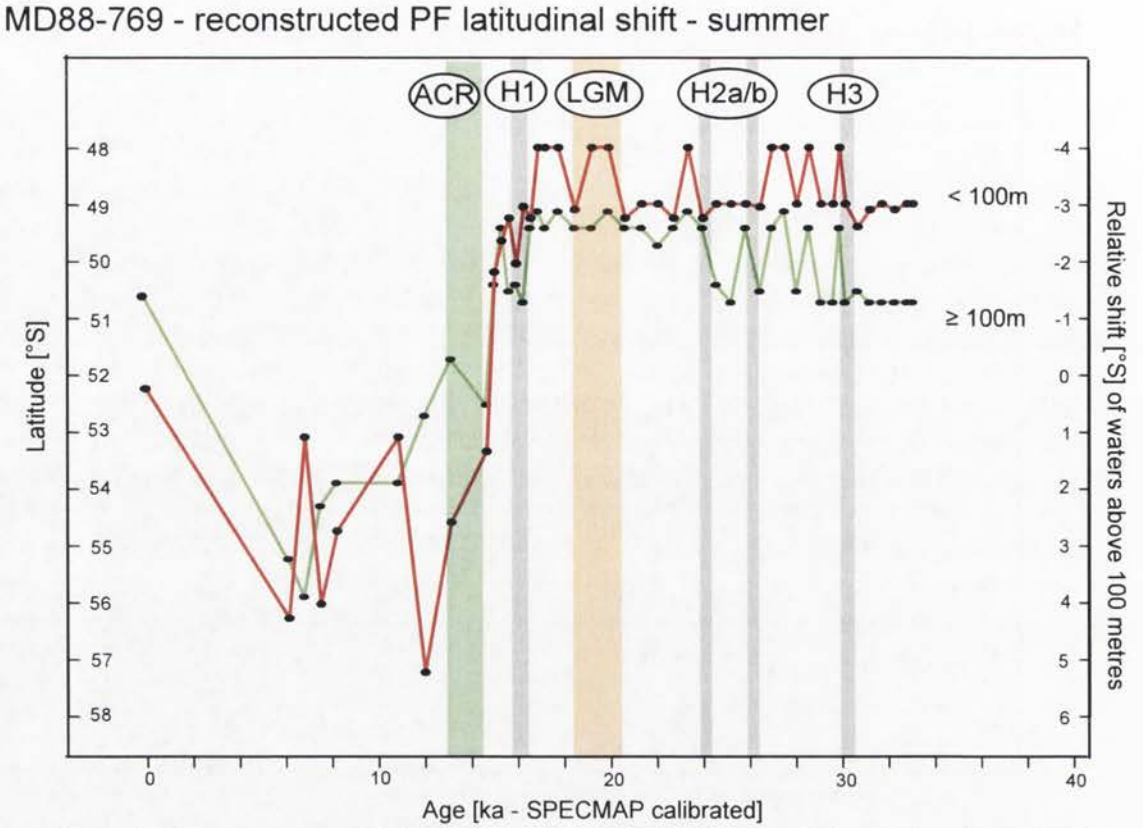

Figure 10.20a: reconstructed latitudinal movement of the Polar Front (PF) over time from MD88-769 summer data (see text for details). The shift of waters above 100 metres bsl is plotted in red and those from 100 to 500 metres in green.

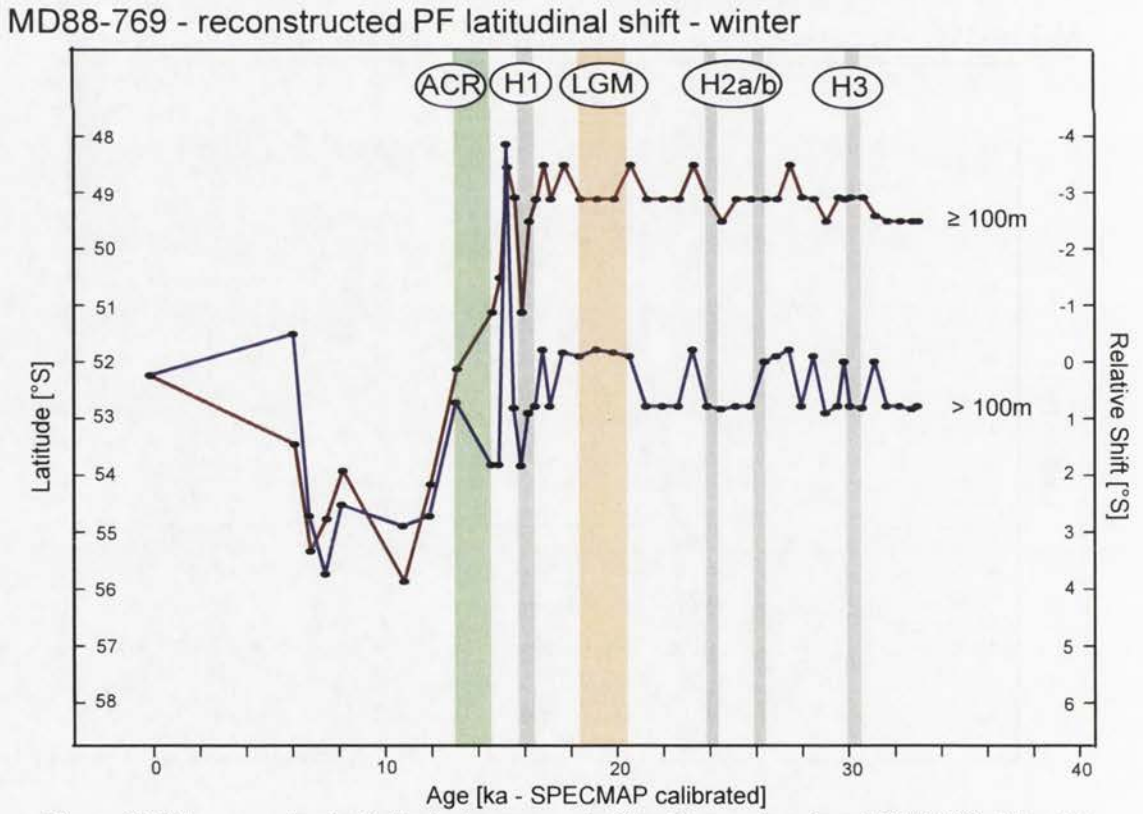

Figure 10.20b: reconstructed latitudinal movement of the PF over time from MD88-769 winter data (see text for details). The shift of waters above 100 metres bsl is plotted in blue and those from 100 to 500 metres in brown.

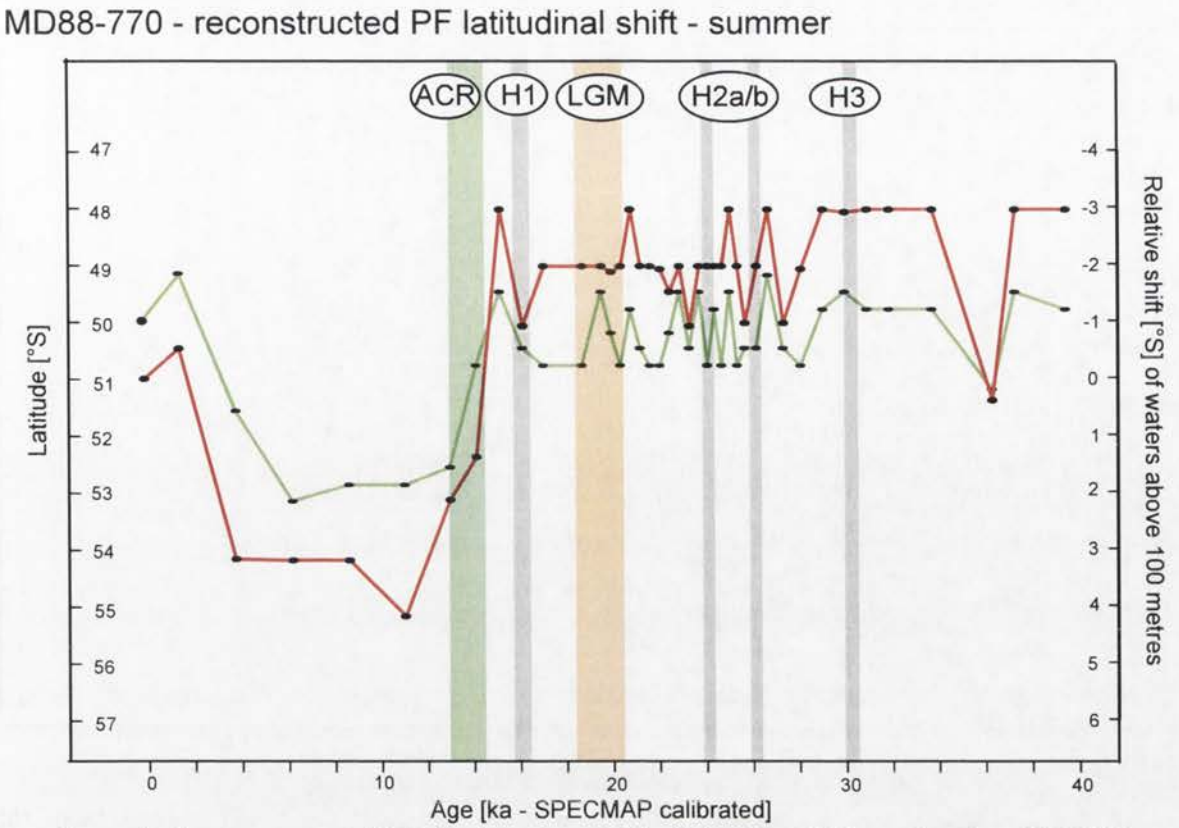

Figure 10.21a: reconstructed latitudinal movement of the Polar Front (PF) over time from MD88-770 summer data (see text for details). The shift of waters above 100 metres bsl is plotted in red and those from 100 to 500 metres in green.

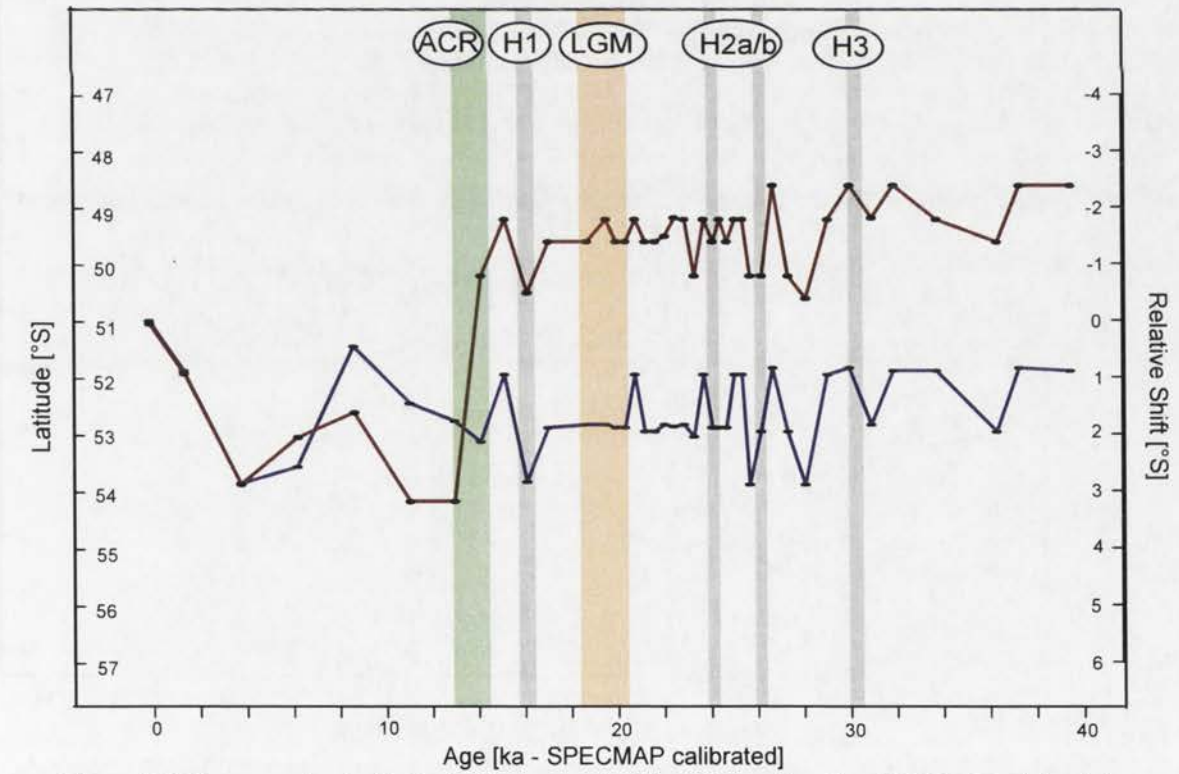

Figure 10.21b: reconstructed latitudinal movement of the PF over time from MD88-770 winter data (see text for details). The shift of waters above 100 metres bsl is plotted in blue and those from 100 to 500 metres in brown.

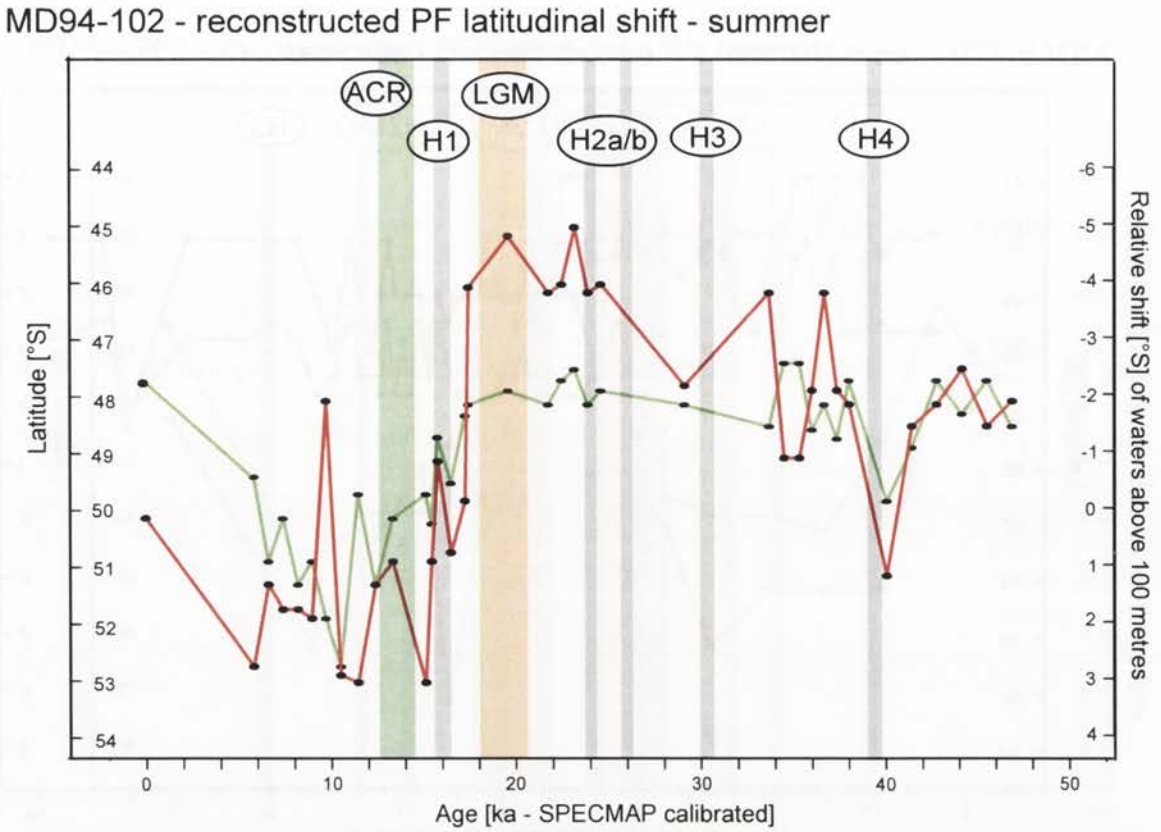

Figure 10.22a: reconstructed latitudinal movement of the Polar front (PF) over time from MD94-102 summer data (see text for details). The shift of waters above 100 metres bsl is plotted in red and those from 100 to 500 metres in green.

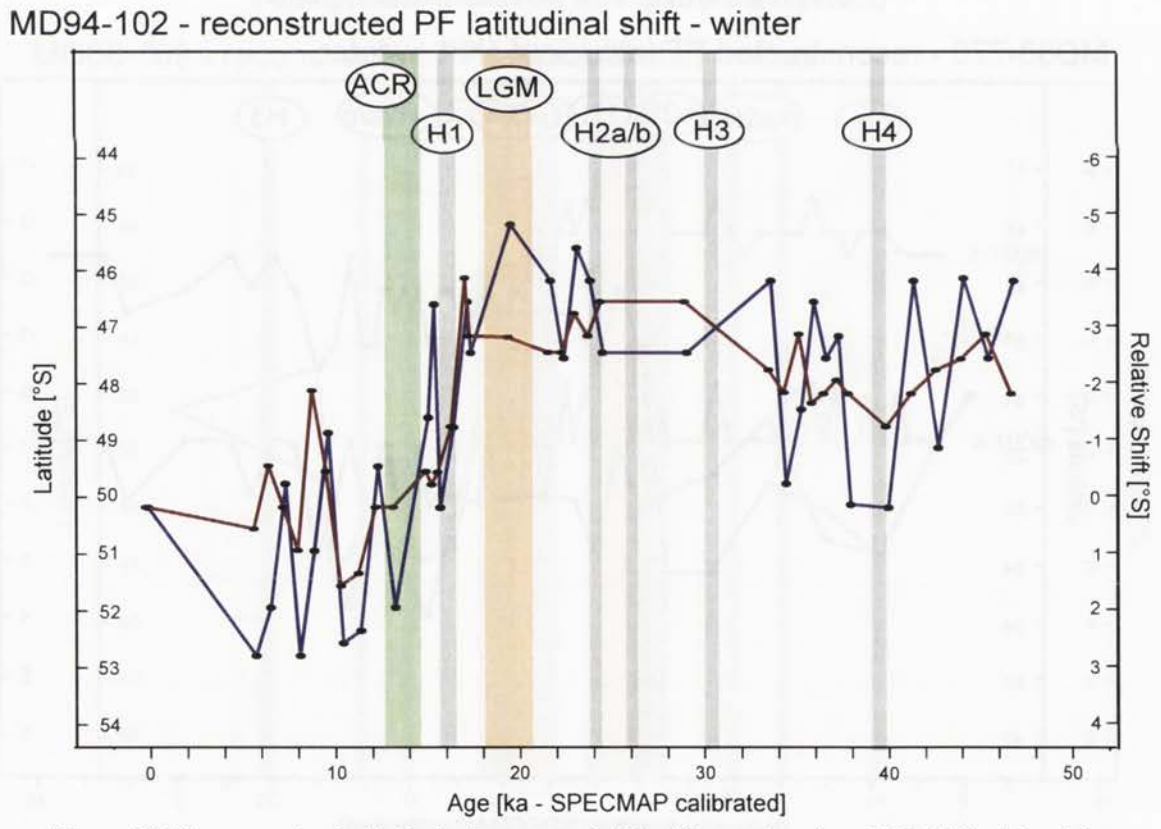

Figure 10.22b: reconstructed latitudinal movement of the PF over time from MD94-102 winter data (see text for details). The shift of waters above 100 metres bsl is plotted in blue and those from 100 to 500 metres in brown.

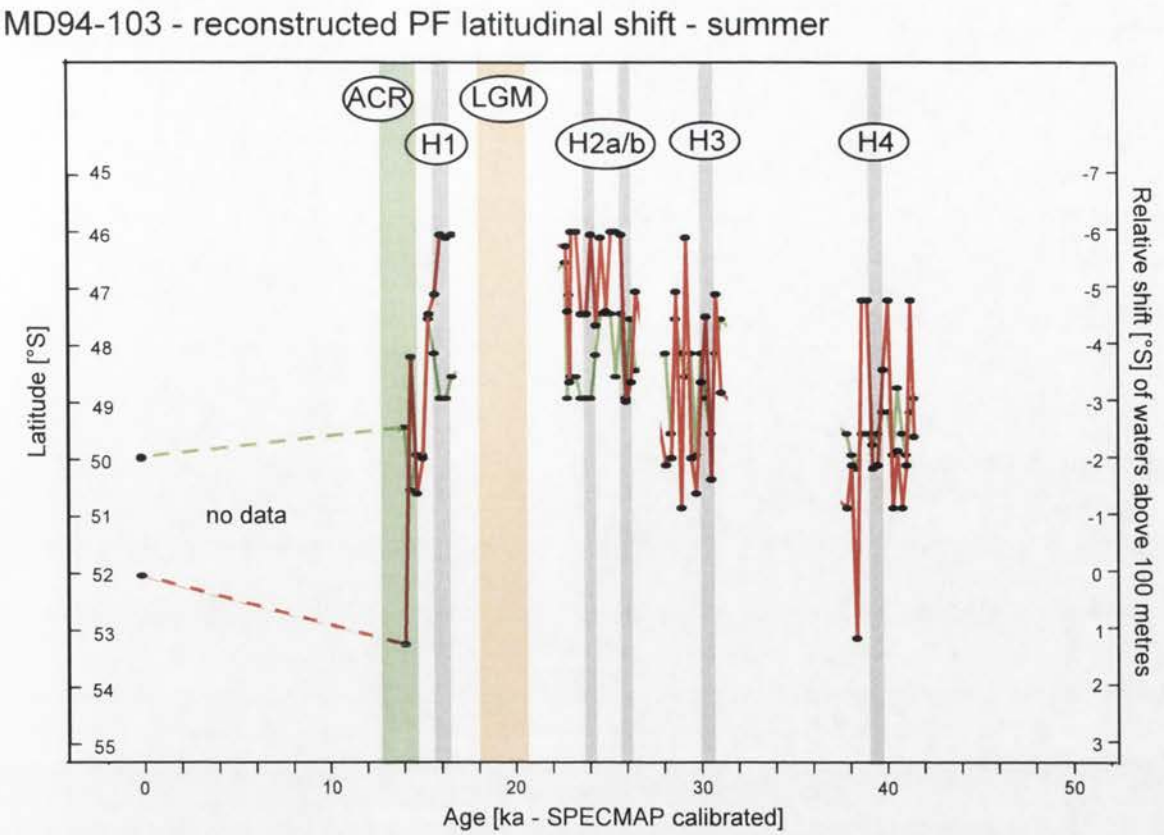

Figure 10.23a: reconstructed latitudinal movement of the Polar (PF) over time from MD94-103 summer data (see text for details). The shift of waters above 100 metres bsl is plotted in red and those from 100 to 500 metres in green.

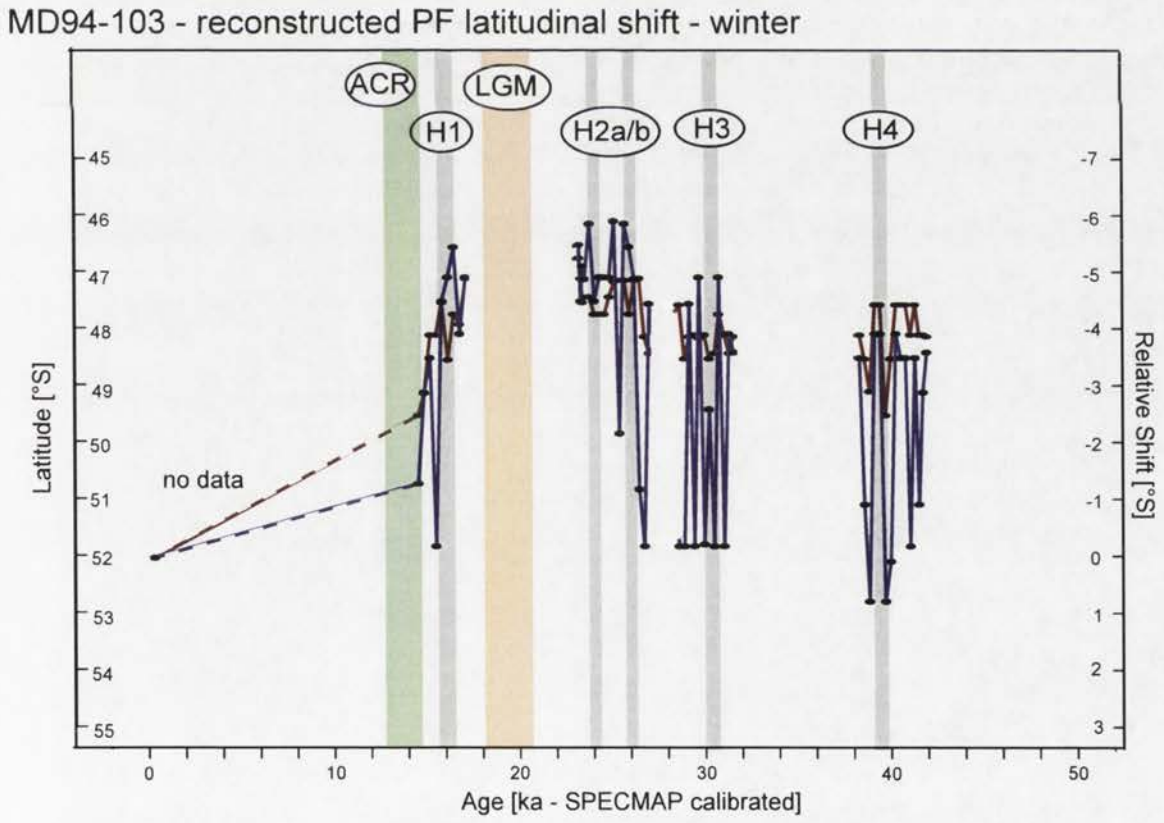

Figure 10.23b: reconstructed latitudinal movement of the PF over time from MD94-103 winter data (see text for details). The shift of waters above 100 metres bsl is plotted in blue and those from 100 to 500 metres in brown.

Chapter 11: Discussion of palaeoenvironmental reconstructions

11.1. The SST reconstructions

When compared with plots of SSTs reconstructed from foraminiferal and diatomaceal data, the plots of this study's SST reconstructions (Figures 10.2-10.5) are very similar in shape and the difference between the maximum and minimum temperatures very similar. However, the radiolarian-based SSTs are consistently higher than those from the other plankton. The difference for MD94-102 and MD94-103 is between 0°C and 2.5°C, so within one standard error for either this study's or the other plankton's reconstructions. The difference for these two cores cannot, therefore, be considered statistically significant, although the fact that the radiolarian reconstructions are consistently higher than the others must still be justified. By comparison, for MD88-769 and MD88-770, the difference is approximately 4°C. This cannot be random error because it is too large and is consistent in magnitude and sign. The LGM SST reconstructions from the EIO (Table10.2) also show a tendency for radiolarian estimates to exceed others, although the difference is small. Only two reconstructions based on diatoms are available for this study: they lie between the radiolarian-based and the foraminiferal-based reconstructions (Figures 10.2a and 10.3a).

Some of the discrepancy in the temperature reconstructions could derive from the use in this study of WOA-05 (Locarnini *et al.*, 2006) oceanic values. The foraminiferal and diatomaceal studies used for comparisons all use the 1994 version of the World Ocean Atlas (Levitus, 1994). As Figure 11.1 shows, WOA-05 values range between 1°C below Levitus (1994) and 1.5°C above those values, and the differences are neither evenly distributed across the study area nor down the water column. The maximum excess of the WOA-05 temperatures over Levitus (1994) for this study's surface sample sites is 1.3°C and values of this order occur at 30-70 metres bsl. The greatest excess for any one depth below

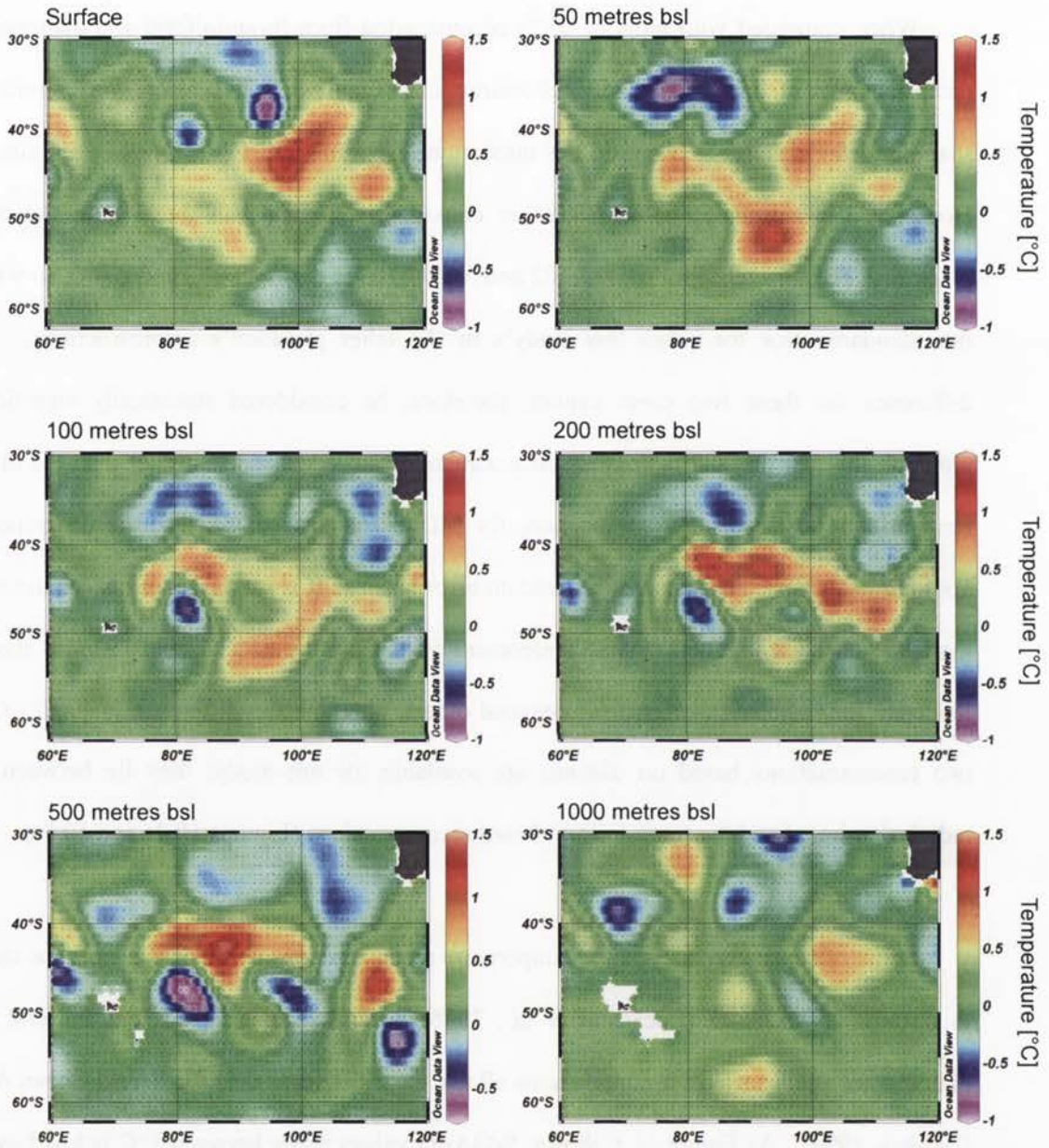

Figure 11.1: austral summer temperature differences between the World Ocean Atlas 2005 (Locarnini *et al.*, 2006) and the World Ocean Atlas 1994 (Levitus, 1994) at depths from the surface down to 1000 metres bsl for a section of the southern Indian Ocean. Positive values mean that the 2005 version of the Atlas indicates higher values than the 1994 version; negative values imply the reverse.

sea-level, averaged over the SIO sites, is 0.27°C, and values of this size are found in the top 50 metres of the water column. Thus, whilst it seems likely that the use of the WOA-05 Atlas causes higher temperatures to be reconstructed from plankton proxies than those obtained using earlier versions of the Atlas, the maximum difference will probably not be more than 0.5°C, a figure well within reconstruction error bounds. These higher temperatures are sufficient to account for the differences in the EIO reconstructions (Table 10.2) and for those in MD94-102 and MD94-103, but not for those in MD88-769 and MD88-770.

Of course, the difference between the 1994 and 2005 versions of the World Ocean Atlas places marine micropalaeontologists on the horns of a dilemma. WOA-05 is based on much more comprehensive data than the 1994 version, and, with the advent of the Argo floats, future versions (eg. Chang, Y-S. *et al.*, 2009) will be derived from far greater databases. At the same time, at least some parts of the Southern Ocean are heating rapidly (for instance, see Böning *et al.*, 2008; Whitehouse *et al.*, 2008). Thus, researchers who continue to use Levitus (1994) will have ocean temperatures close to those when surface sediments were deposited but, being based on limited data with relatively large error bounds. The researchers who use new versions of the World Ocean Atlas will have much more accurate data for the modern ocean but, perhaps, significantly different from the conditions under which their surface samples were deposited.

It has been previously suggested (for instance Howard and Prell, 1984), differences between reconstructed SSTs based on a range of plankton could result from the variety of depths in the water column in which the different plankton live. This might account for the differences between the foraminiferal-derived and the radiolarian-derived SSTs for MD94-102 and MD94-103. It does not, however, account for the fact that, for MD88-769 and

MD88-770, the differences are around 4°C and, for MD94-102 and MD94-103, they are closer to 1°C. It could only be concluded that habitat was the cause if (a) a large proportion of the radiolarian population lived in one or more sections of the water column relatively devoid of foraminifera, and (b) the water-column temperature profiles for the two sets of sites diverged greatly over those sections. In fact, the water-column profiles are essentially parallel. The hypothesis that radiolarian and foraminiferal habitat explains the discrepancy between the SST reconstructions must be rejected, in this instance, at least.

The possibility of "no-analog" problems (Hutson, 1977) can be dismissed because such problems would affect both core sets equally. Similarly, neither MD88-770, nor MD94-102, nor MD94-103 figure as outliers during calibration of the transfer function (the surface sample of MD88-769 is dated to 6.2 ka, so is not included in the training dataset). Howard and Prell (1984) show radiolarian- and foraminiferal-based SSTs for RC11-120, a core collocated with MD94-103, as falling into exactly the same range. [Note: Howard and Prell (1984) also observed a time lag of about 3.2 ka between the radiolarian indications of warming at the MIS-6 to MIS-5e transition and the indications from foraminifera: no such lag is discernable at the MIS-2 to MIS-1 transition as recorded by the present study.]

A possible explanation of the discrepancy is that foraminiferal proxies tend to yield underestimates of SSTs, whereas radiolarian proxies yield overestimates, due to one or more oceanic variables other than temperature. Comparison of WOA-05 data for the four core sites reveals substantial elevated nitrate and phosphate concentrations and depressed silicate concentrations and apparent oxygen utilisation for MD88-769 and MD770 (which are both very close to and just south of the SAF) relative to MD94-102 and MD94-103 (both north of the SAF). Table 11.1 gives the differences between the average of the reconstructed values and the present day SSTs. With the exception of MD88-769, winter values (for which no

explanation is offered at present), the radiolarian and foraminiferal values are roughly equidistant above and below present day SSTs. This finding suggests that diatoms may be better proxies for SSTs than either foraminifera or radiolaria, an unsurprising conclusion given that diatoms dwell closer to the sea-surface than the other planktons. At the same time, both radiolarian and foraminiferal proxies provide good estimates of SSTs: why one gives an overestimate and the other an underestimate cannot be determined with certainty from the data currently available. However, against the suggestion that diatoms provide the best SST estimates and radiolaria overestimates, and foraminifera underestimates, respectively, is the fact that SSTs early in MIS-1 exceeded present-day values, so all the values in Table 11.1 should be positive. Only the radiolarian-based temperature differences are positive, perhaps suggesting that radiolaria provide better estimates of SSTs than the other two proxies.

	Proxy	MD88-769		MD88-770		MD94-102	
Age range of reconstructions [ka]		6.9-10.9		1.5-8.8		5.8-10.5	
Season		JFM	JAS	JFM	JAS	JFM	JAS
Temperature difference [°C]	Radiolaria	1.0	2.6	1.2	1.0	0.5	0.9
	Foraminifera	-1.2	-0.8	-1.8	0.2	0	-0.4
	Diatomacea	0.1	n/d	0.1	n/d	n/d	n/d

Table 11.1: The differences between reconstructed SSTs averaged over approximately 10 ka and present day SSTs for MD88-769, MD88-770, and MD94-102 (n/d indicates that no data are available). MD94-103 is not included because no radiolarian reconstructions have been made for the relevant period.

11.2. The SIO reconstructions

11.2.1. Temperature

The sea temperature reconstructions for cores MD88-769, MD88-770, MD94-102, and MD94-103, plotted at four depths (the surface and 50, 125, and 250 metres below sea-level) in Figures 10.2-10.5 and as time-slices in Figures 10.12-10.15, are notable for two features. Firstly, in summer (JFM), the temperature gradient with increasing depth is much smaller between approximately 15 and 35ka (i.e. during MIS-2) than before or after. This feature is more pronounced in MD88-769 and MD88-770 than in the more northerly core, MD94-102;

MD94-103 provides relatively little evidence due to the limited time periods it covers. Secondly, in winter (JAS), the temperature gradient is very much smaller than in summer for the whole of the period covered by this study and the waters closer to the surface are typically warmer than those at greater depth after 15ka, whereas the reverse is the case before that.

The fact that the summer temperature gradient is less during MIS-2 than during MIS-1 or MIS-3 could, *a priori,* be due either to higher surface wind speeds causing mixing of the ocean waters to a much greater depth than is now the case, or to much cooler atmospheric conditions (and, perhaps, reduced insolation) limiting the warming of surface waters so that they are closer in temperature to the underlying waters. A third possibility, that increased convection caused deeper mixing, is probably belied by the fact that the *in situ* density gradients does not change between MIS-2 and MIS-1 (Figure10.7a).

Millero (2006) states that, at high latitudes (typically greater than 50°), there is no permanent thermocline. Instead, a seasonal thermocline may form and lead to the creation of a dicothermal layer at 50-100 m bsl. Such a dicothermal layer consists of cool water [Millero says at -1.6°C but others (for instance Pickard and Emery, 1982) indicate that the layer is 1.6°C below the temperature of the surface waters] sandwiched between warmer surface and deeper waters. The layer results from intense cooling of the upper waters in winter, followed by summer warming, with stability being maintained by an increase in salinity with depth. A dicothermal layer during MIS-2 is clearly apparent in the MD88-769 (Figure 10.12a), MD88-770 (Figure 10.13a), and MD94-103 (Figure 10.15a) reconstructions but only just discernable in the more northerly MD94-102 (Figure 10.14a). The existence of a dicothermal layer argues against deep mixing because the mixing would destroy the comparatively shallow layer, suggesting that the reduced temperature gradient may be due to lower atmospheric

temperatures (and/or decreased insolation) in summer and little warming of the surface waters, rather than higher wind speeds.

In winter, the MIS-2 reconstructions indicate that near-surface waters are cooler than those around 250 m bsl (see Figures 10.2b, 3b, 4b, and 5b). The reconstructions also show stratification of surface water down to 200-250 metres bsl with a dicothermal layer at about 200 metres bsl (see Figures 10.12b, 13b, 14b, and 15b). Interestingly, winter dicothermal layers is not evident in present-day data (at least, not north of 64°C, the southerly limit of this study – see Figures 4.1a-n). Deep stratification suggests increased convection of the very cold surface waters and ice-free seas, higher wind speeds being excluded because wind-induced mixing does not extend below 50-100 metres bsl (Dr A. Hogg, pers com., 2009). A deep dicothermal layer would result naturally from winter loss of heat from the ocean's surface coupled with mixing to about 200 metres bsl (the dicothermal layer marks the limit of mixing). However, the phenomenon does not seem to have been reported previously.

The reconstruction time-slices also show significantly higher ocean temperatures than those found at present in the period from about 13 ka to 5 ka with a peak at about 10 ka. The phenomenon lasted longer at the latitude of MD88-769 and MD88-770 (about 46°S) than at that of MD94-102 (43°30'S) and is evident for both summer and winter. This warmer period (the Holocene Optimum or Hypsithermal) immediately follows the steep increase in temperatures at the end of the MIS-2 glacial.

11.2.2. Salinity

The salinity reconstructions for the cores MD88-769, MD88-770, MD94-102, and MD94-103 are plotted against time in Figure 10.6a (summer) and 10.6b (winter). They also appear in the time-slice plots (Figures 10.12-10.15). In contrast to the temperature gradients,

the difference in summer between the sea surface and depths greater than 100 m are greater during MIS-2 than MIS-1 or MIS-3. This is interpreted as resulting from the limit of the winter ice being further north during MIS-2, with the result that a pool of low salinity water was created at the surface when the ice melted in summer. The pool of low salinity water can be seen at the surface in the MD88-769 and MD88-770 time-slices; in MD94-102 the pool is seen to be centred on 75 metres bsl. This is compatible with the Polar Front lying between 46° and 42°S: subduction at the Antarctic Convergence would cause the low-salinity pool to sink provided low water temperatures also resulted in sufficiently low water densities, which density reconstructions indicate was the case.

Labeyrie *et al.* (1996) also observe reduced salinity at the MD88-770 site during periods of global cooling with an increase at the start of the next sea-surface warming. They interpret this as the shifting of the polar fronts which separate warm and saline subtropical waters from cool, fresher, polar waters across the site, essentially the same explanation as above. The salinity data published in Labeyrie *et al.* (1996) only overlaps with that of this study for the period 14-20 ka and this overlap is too short to say more than that the reconstructed salinity levels are broadly the same. The fact that Labeyrie *et al.* (1996) derived their salinity values from benthic foraminiferal $\delta^{18}O$ values provides some mutual support for their approach and the radiolarian-based reconstructions of this study.

Coinciding with the higher-than-modern temperatures of the period 13-5 ka (§11.2.1 above), salinity increases from the MIS-2 levels but not to the same degree as temperature, a fact revealed by the dip in *in situ* density levels. This can be explained by a lag in the retreat of the Antarctic Convergence southwards to its present location, the speed of retreat being mediated by the gradual melting of the Antarctic icecap and, perhaps, permanent ice on the Kerguelen Plateau. In fact, the rate of increase in salinity associated with the southward

movement of subtropical waters would have been slowed if there were ice melting from the Kerguelen Plateau. MD88-770 reconstruction indicates that the attainment of present-day *in situ* density at about 5 ka was comparatively sudden. No reason is advanced for this observation: it suggests the ice-melt was rapidly replaced by subtropical waters. A sudden increase in Southern Ocean circulation could result from the melting of ice blocking the Drake Passage. However, no real evidence can be adduced from this study as to the existence of an ice barrier or its subsequent melting.

11.2.3. Dissolved oxygen

The dissolved oxygen reconstructions for the cores MD88-769, MD88-770, MD94-102, and MD94-103 exhibit two important features: firstly, in summer, there is a greater difference between the values for the near-surface waters than those more than 100 m bsl for MIS-2 than for MIS-1. Secondly, in winter, that situation changes to place the gap between waters above 200 m bsl and those below that depth (Figures 10.10a-b). Although the MD88-770 reconstruction does not conform exactly, it is also the case that the near-surface waters were more highly oxygenated during MIS-2 than MIS-1. These phenomena can be explained by hypothesising that stronger winds led to greater air-sea mixing during MIS-2 than since. In addition, stratification due to the shallow pool of low-salinity water at the ocean's surface and the dicothermal layer (and, probably, lower wind speeds) prevented deep mixing in summer and, in winter, these constraints were no longer present, allowing mixing to about 200 metres bsl.

11.2.4. Nitrate concentrations

MD88-769, MD88-770, MD94-102, and MD94-103 nitrate reconstructions (Figures 10.8a-b) evidence the same changes in the degree of mixing of surface waters between MIS-2 and MIS-1, as do other oceanic variable reconstructions. The one observed peculiarity is the

fact that in winter the lowest nitrate concentration above 300 m bsl is at about 50 m bsl. In summer, this might be explained by high levels of biological activity denuding waters of nitrates: in winter, this seems less likely. It may be that the feature is actually to be viewed as an unexpectedly high concentration very close to the surface – perhaps sourced from airborne dust but not immediately removed due to the lack of biological activity at that time of year.

11.2.5. Phosphate concentrations

The reconstructions for the cores MD88-769, MD88-770, MD94-102 (Figures 10.9a-b) show a sharp decline in phosphate concentrations between MIS-2 and MIS-1. This is to be expected under the hypothesis that the Antarctic Convergence was located at about 44°S during MIS-2. The reconstructions also show mixing to around 200 metres bsl in winter. Anomalously, the MD88-770 reconstruction shows a greater difference between concentrations at 250 m bsl than above that level during MIS-1: no explanations is advanced for this observation. Also anomalous is the fact that the reconstructions show the winter phosphate concentrations above 250 m bsl peak at 75 m bsl (Figures 10.12b, 10.13b, 10.14b, and 10.15b). The explanation for this peak could be the same as that for high nitrate concentrations close to the surface in winter, i.e. that phosphate concentrations were being enhanced by dust but were not being consumed by biota. However, the question remains as to why the peak for phosphate is at 75 m bsl and that for nitrate is at 10 m bsl.

11.2.5. Salinity-normalised total alkalinity (NTA)

MD88-769 and MD88-770 reconstructions of summer NTA show a sharp increase between MIS-2 and MIS-1 which is not seen in the MD94-102 reconstruction. This is a further indication that the Antarctic Convergence lay between 42°S and 46°S during MIS-2, i.e. between cores MD88-769 and MD88-770 on the one hand and MD94-102 (and MD94-103) on the other. Winter NTA for all three cores shows little change between MIS-1 and MIS-2.

NTA levels are determined solely by oceanic biology (Sarmiento and Gruber, 2006 page 328) and the increase in NTA between MIS-2 and MIS-1 can be related to an increase in the formation of organic matter (*ibid.* page 331). Estimations of palaeo-values of NTA are potentially valuable because, combined with estimates of dissolved inorganic carbon (DIC), reasonable approximations of carbonate and bicarbonate concentrations are possible (*ibid.* page 326). Alternatively, DIC may be estimated from NTA and either carbonate or bicarbonate concentrations.

11.2.6. Heinrich Events

Following investigations of MD94-103, Sicre *et al.* (2005) conclude, *inter alia,* that, superimposed on the long term trends for SST during the last glacial period, alkenone-based SSTs show cooling during Heinrich events (Dansgaard *et al.*, 1993) and foraminiferal-based SSTs show warming. The samples from MD94-103 examined in this study were specifically selected to provide a high-resolution record over the period of the Heinrich events covered by the Sicre *et al.* (2005) study with the intention of deciding whether radiolarian fossils also reflect these events. For this reason, the occurrence of Heinrich events (Bond *et al.*, 1992; Bond *et al.*, 1993), as well as the Antarctic Cold Reversal (ACR) and the LGM, is recorded on the reconstruction plot figures (Figures 10.2-10.11) as vertical bars. However, the limited resolution of these plots mean that the width of these bars do not reflect the duration of the events accurately.

Despite the plot limitations, the radiolarian-based temperature reconstructions for all four cores strongly suggest warming in the SIO coincident with Heinrich event H1 and H2a. There is no consistent evidence of warming at H2b or H3 but there is warming during H4 for cores MD94-102 and MD94-103. MD92-102 shows cooling at about the ACR but neither MD88-769 nor MD88-770 reflect that event – possibly due to inadequate resolution. With

respect to MD94-103, the radiolarian data does not cover the ACR and neither the alkenone-based nor the foraminiferal-based SSTs appear to reflect that event. The nitrate, phosphate, and NTA reconstructions show a decline in these variables during the ACR, H1, and H2a, those for NTA being particularly large. The results for H2b, H3, and H4 are less clear. Similarly the reconstructions of salinity, dissolved oxygen, and *in situ* density show no definite features in association with these events.

Unfortunately, this study's data are probably insufficient to draw firm conclusions about the relationship between the ACR and the Heinrich events and conditions in the SIO. A statistically sound basis is needed and this could be achieved by:

- increasing the resolution of the reconstructions during and immediately before and after each event to about a quarter of the duration of the event (this is necessary to ensure the actual location of the maxima or minima);
- ensuring the resolution of the remainder of the period under consideration is sufficient to identify every peak and trough (optimally this would be the same resolution as over the duration of the events); and
- calculating the number of the peaks (or troughs) which coincide with the ACR and the Heinrich events as a percentage of the total number of peaks (or troughs).

The higher the percentage, the more likely the relationship.

11.3. The reconstruction of frontal movements

Reconstructions of the movement of the SAF and the PF (Figures 10.6-10.23 and Table 10.6) shows, as might be expected, that the fronts moved north at the end of MIS-3 and south again at the MIS-2 to MIS-1 transition, the latter movement being considerably more than the former. Three features of these reconstructions need explanation:

- why the frontal movement is less below 100 metres bsl than above that depth;

- why the movement of both the SAF and the PF in summer is greater at MD94-102 and MD94-103 than at MD88-769 or MD88-770; and
- why the PF reconstruction using variables from above 100 metres bsl shows so little movement in winter with respect to MD88-769 and MD88-770.

The difference between the frontal movements derived from variables above and below 100 metres bsl indicates a steepening of the subduction gradient during MIS-2 as the PF moves north and the Polar Frontal Zone (PFZ) narrows (Figure 4.1a-n). Contraction of the PFZ is also indicated by the fact that summer advances of the PF during MIS-2 are greater than those of the SAF (Table 10.6). Reduction of the PFZ (and the Subantarctic Zone) is the natural result of the PF and the SAF being forced north by increased Antarctic glaciation but movement of the more northerly fronts being constrained by bottom topography (Belkin and Gordon, 1996; Craneguy and Park, 1999).

There are two possible explanations for MD94-102 and MD94-103 summer reconstructions indicating a greater movement of the SAF and PF than is shown by MD88-769 and MD88-770. The first possibility is that the MD88-769 and MD88-770 temperature reconstructions are substantial overestimates. If this were the case, the comparison of the environmental variable vectors with WOA-05 data (10.4 above) would give best matches at lower than the correct latitudes. However, it appears the overestimate hypothesis can be dismissed – see §11.1 above. The alternative hypothesis is that permanent glaciation on the Kerguelen Plateau forced the whole of the PF north of the Kerguelen Plateau during MIS-2. Although Belkin and Gordon (1996) suggest the PF lies north of Kerguelen at present, other researchers (Park *et al.*, 1993; Olbers *et al.*, 2004) consider the front is south of Kerguelen (see Figure 4.2). This study's MIS-1 reconstructions for MD88-769, MD88-770, and MD94-103 place the PF at the longitudes of those sites in approximately the locations determined by

Belkin and Gordon (1996), whereas the MD94-102 reconstruction places the PF at 52°S, i.e. south of Kerguelen and close to the location proposed by Olbers *et al.* (2004) and Park *et al.* (1993). If, during MIS-2, the PF lay north of the Kerguelen Plateau, its latitude at 70°E would have been around 46.5°S. Further east than, perhaps, 80-85°E the front's northerly movement would be constrained by the Southeast Indian Ridge. The reconstructed frontal movements shown in Table 10.6 are compatible with this hypothesis in that the MD94-102 [43°30'S 79°50'E] reconstructions indicate that the PF moved from about 46.5°S to about 52°S between MIS-2 and MIS-1, and that the other three cores indicate a reducing movement to the east.

A modification to the second hypothesis, which would fit better with Belkin and Gordon (1996), would take into account the period around 10 ka which may have been warmer than at present (see Figures 10.2-10.4). Under this scenario, it is possible the PF was forced north of the Kerguelen Plateau during MIS-2, then, during the warm start to MIS-1, lay south of Kerguelen, and now is usually to the north of Kerguelen again.

The location of the fronts south of present day positions between 13ka and 5ka is assumed to reflect the Holocene Optimum.

11.4. The analysis of the radiolarian census data

11.4.1. Validity and accuracy of results

Proxies are used to reconstruct palaeoenvironmental conditions because no direct estimates are possible. The fact that reconstructions are indirect opens questions as to the validity of associating the proxy with the palaeo-condition it is desired to estimate. Further, even if the associations are at least partially valid, errors in the estimates will accumulate due to the limitations entailed in data-gathering and the statistical analysis of that data.

Guiot and de Vernal (2007) state that three assumptions form the basis for the use of transfer function models and methods (and, although not explicitly mentioned, all other, including analogue, methods) to reconstruct palaeoenvironmental conditions. To quote, they are:

1. "Climate is the ultimate cause of change in the palaeobiological data.
2. The ecological properties of the species considered has not changed between the period analysed and the present time, and the relationship between the species and the climate is thus uniform over time.
3. The modern observations contain all the necessary information to interpret the fossil data."

The word "climate" here is shorthand for "climatic and/or oceanic conditions". Prior discussion in Guiot and de Vernal's (2007) article indicates this is the case and, of course, the biota under consideration will, undoubtedly, be affected, not only by conditions normally thought of as part of the climate, but other aspects of the environment such as the supply of nutrients.

All three of Guiot and de Vernal's (2007) assumptions may be questioned in relation to any particular proxy of biological origin. Firstly, random mutation in one (or more) species of the proxy may make the mutated species better adapted to the extant environmental conditions. The result would be a significant change in the distribution of species in the proxy group despite the environment remaining unchanged. The truth of the second assumption is clearly limited as it is known that most organisms have some flexibility of habitat. However, this flexibility may be limited in the case of very simple organisms.

An unfortunate corollary of the third assumption is that the researcher may, unknowingly, have little or no information on the primary factor or factors determining the distribution of the species being studied. For instance, although there is comprehensive data on the temperature and salinity of the Indian Ocean, data on iron and trace elements, factors potentially decisive in plankton species distribution, are very sparse so determination of the correlation, if any, between proxy species and these possible factors is impossible. If one of the factors is a major explanatory variable for the species distribution, interpretation of the fossil record may be flawed.

In addition to Guiot and de Vernal's (2007) three assumptions, for palaeo-reconstruction to be successful, it is also essential that applicable statistical techniques be identified. Many commonly-used techniques demand that species distributions be linear or normal with respect to the explanatory environmental factors. This is particularly important because it means these techniques cannot be used if even one of the explanatory variables (possibly one unknown to the researcher – see previous paragraph) is not monotonically increasing or decreasing over the environmental gradient being considered. This is a strong argument in favour of using weighted-averaging partial least squares (WA-PLS), artificial neural networks, or analogue techniques, none of which demand linearity or normality in species distribution.

In this study, the problem of linear and/or normal distribution has been avoided by the use of WA-PLS. Analogue techniques (such as the Modern Analog Technique – MAT) were not an option because they require a much larger surface-sediment database than was available. Researchers using foraminiferal proxies in the southern Indian Ocean had 245 surface samples on which to base their MAT reconstructions (Salvignac, 1998) and Juggins (2007a)

recommends 500. WA-PLS also has the advantage of minimising the "no-analog" problem (Hutson, 1977).

Statistical techniques usually provide rigorous estimates of error. The quantification of the effects of species classification is, however, far more problematic. Misidentification has, in itself, no adverse effect on statistical analysis: inconsistency in classification could be a serious source of error but the name applied to a species is irrelevant. Although consistency is very difficult to maintain when a large number of samples are counted over a long period, there are ways to improve data quality, albeit expensively. For example, (some of) the samples could be counted by more than one person. Independent checking of census counts was not possible in the present study. However, all data was visually examined for apparent discrepancies and, whenever found, a second, confirmatory, count was conducted or the data was rejected.

The main difficulties with classification arise in the degree of "lumping" or "splitting" applied. Excessive lumping, i.e. ascribing too wide a range of specimens to a single species category, may result in a serious loss of information. The appropriate degree of splitting is a more difficult decision. For instance, it was observed during the present study that the juvenile forms of *Tetrapyle octacantha* Müller 1858 far outnumbered the more mature forms in the surface samples of a group of geographically-proximate sites and in other areas the reverse was the case. It does not seem clear that both forms should be treated as a single category because it is possible that some factor, such as silicate lack, prevented the juveniles maturing. Equally, how could they be successfully split into two categories, given that maturation consists of the gradual accretion of skeletal elements?

11.4.2. Precision of results

The error bars in reconstruction of the four cores' temperatures at the ocean's surface and at 50, 125, and 250 metres bsl are shown in Figures 11.2 a-d. The standard error (SE) can be seen to diminish with increased depth below sea level in all four cores. If this phenomenon were a statistical artefact, the magnitude of the SE would be correlated with the temperature range and this is not the case. When the SEs are considered as proportions of the temperature range, all four cores yield local minima at the surface, and at 50, and 200, 300 metres bsl, with corresponding local maxima at 30, 75, 250, and 400 metres bsl. Closer investigation would be required to determine whether these observations are due to radiolarian habitat or changes in oceanic conditions down the water column.

The error envelope is smaller during MIS-1 than prior to that. This reflects the fact that oceanic conditions since the MIS2-1 transition are closer to those of the present than the conditions before the transition were.

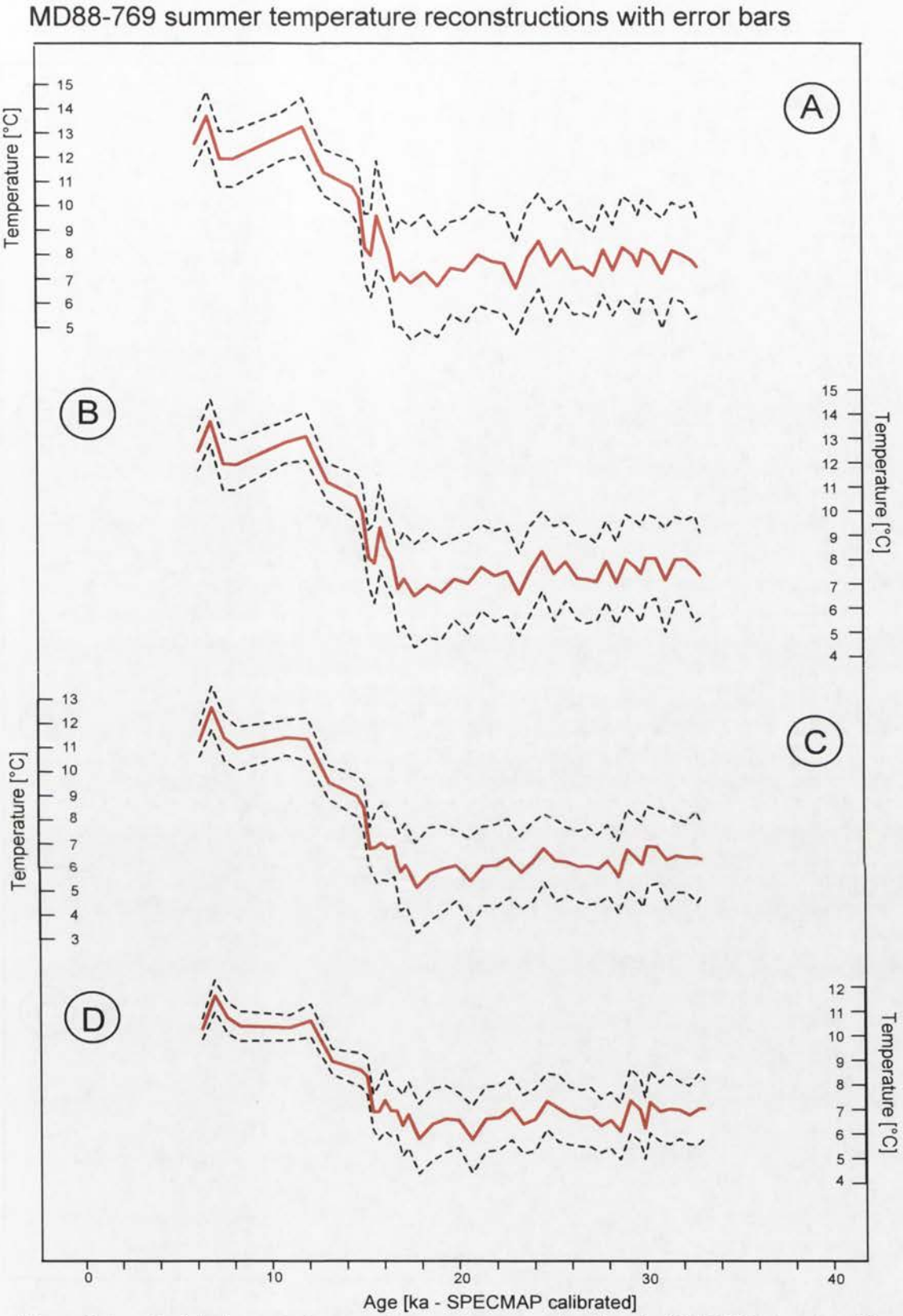

Figure 11.2a: Radiolarian austral summer temperature reconstructions for MD88-769 at surface (A), 50m (B), 125m (C), and 250m (D) bsl with the error bars for each depth. The error bars are those generated by WA-PLS, the calibration and regression technique used for the reconstructions. The bars do not include the errors in the WOA-05 environmental data. All the reconstructions are on same scale - note how the error declines with increasing depth below sea level.

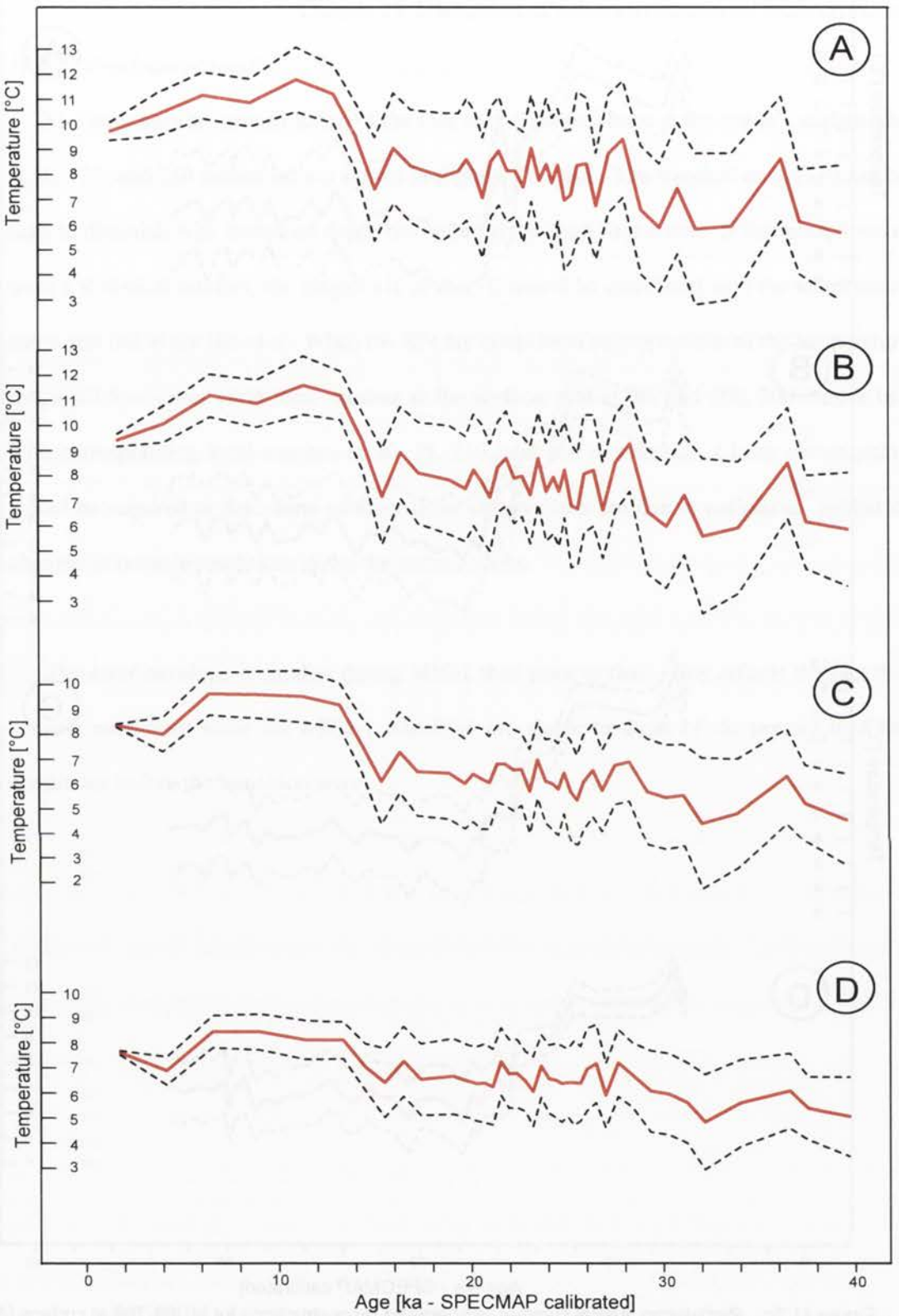

Figure 11.2b: Radiolarian austral summer temperature reconstructions for MD88-770 at surface (A), 50m (B), 125m (C), and 250m (D) bsl with the error bars for each depth. The error bars are those generated by WA-PLS, the calibration and regression technique used for the reconstructions. The bars do not include the errors in the WOA-05 environmental data. All the reconstructions are on same scale - note how the error declines with increasing depth below sea level.

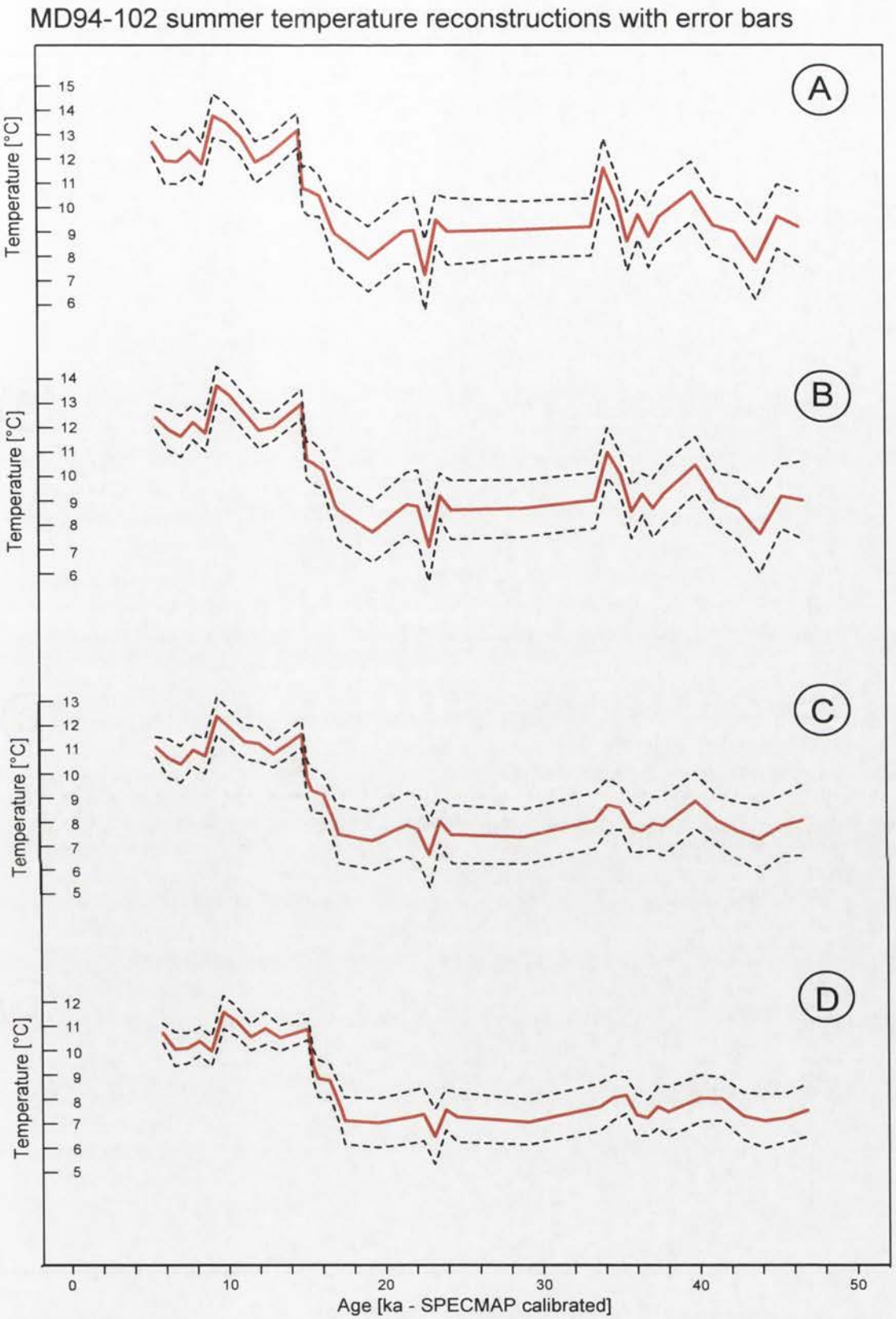

Figure 11.2c: Radiolarian austral summer temperature reconstructions for MD94-102 at surface (A), 50m (B), 125m (C), and 250m (D) bsl with the error bars for each depth. The error bars are those generated by WA-PLS, the calibration and regression technique used for the reconstructions. The bars do not include the errors in the WOA-05 environmental data. All the reconstructions are on same scale - note how the error declines with increasing depth below sea level.

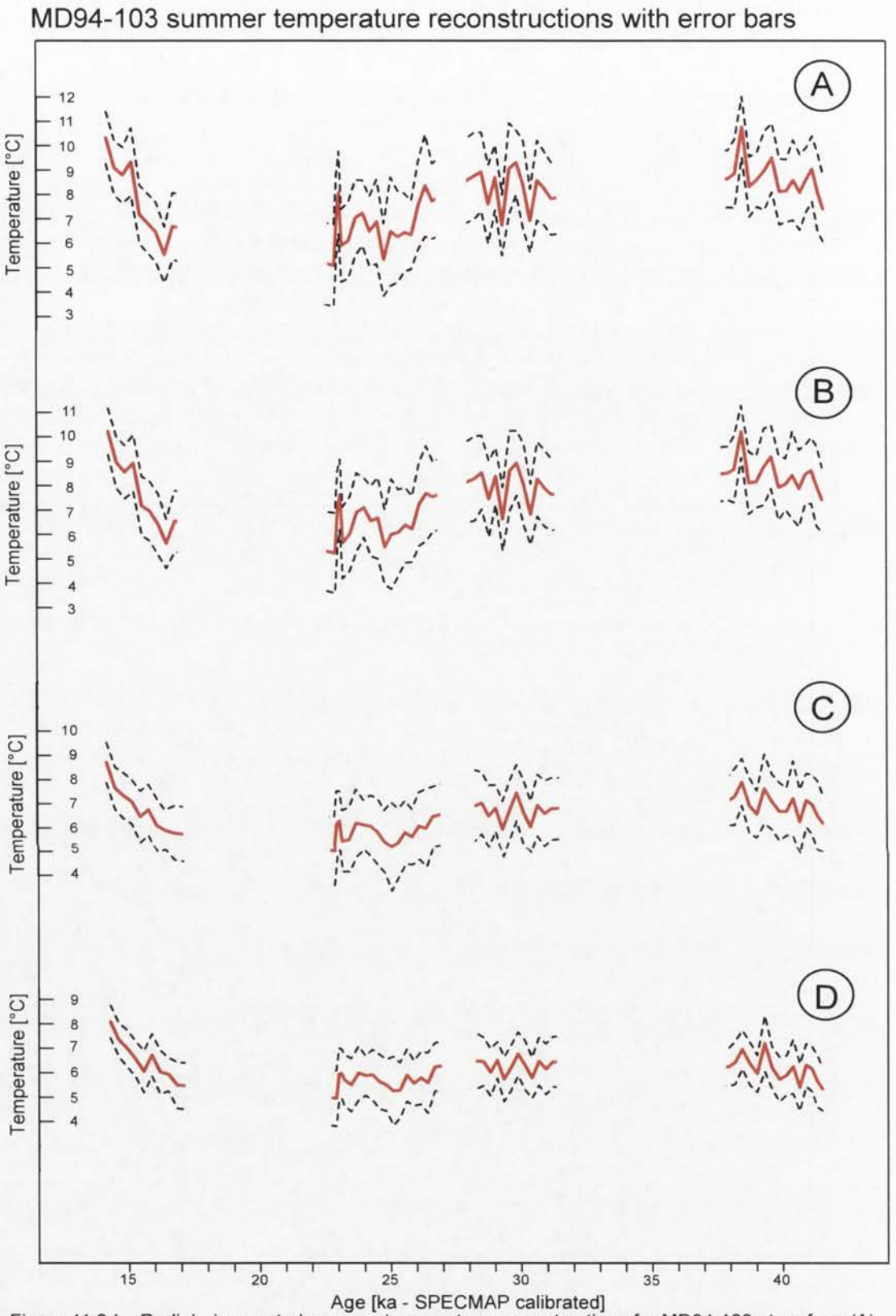

Figure 11.2d: Radiolarian austral summer temperature reconstructions for MD94-103 at surface (A), 50m (B), 125m (C), and 250m (D) bsl with the error bars for each depth. The error bars are those generated by WA-PLS, the calibration and regression technique used for the reconstructions. The bars do not include the errors in the WOA-05 environmental data. All the reconstructions are on same scale - note how the error declines with increasing depth below sea level.

Chapter 12: Conclusions and Future Work

12.1. Introduction

The object of this study was to examine the utility and limitations of radiolarian census counts as proxies for palaeoenvironmental conditions in the Indian Ocean, to investigate, mainly statistically, techniques for the analysis of the data, and, whenever possible, to advance the knowledge of environmental conditions in the southern Indian Ocean over the last forty thousand years.

The bulk of previous investigations using radiolarian census data for palaeoenvironmental reconstruction has concentrated on estimating SSTs (*inter alia* Lozano and Hays, 1976; Johnson and Nigrini, 1980, 1982; Morley, 1989; Abelmann *et al.*, 1999) and, for the statistical analysis, has employed Q-mode factor analysis (QMFA - Imbrie and Kipp, 1971) or the modern analog technique (MAT - Hutson, 1980). This study has been an attempt to extend reconstructions beyond SSTs, both by considering a range of oceanic conditions – not just temperature alone – and by applying the relationships between the census data and oceanic conditions over the water column from the surface to 500 metres bsl. The study has also sought and found statistical techniques that would be more powerful or more appropriate to the available data than QMFA or MAT.

Whilst it would be difficult to claim that this study significantly advances knowledge of the palaeo-Southern Ocean, it does provide additional support to previous reconstructions of radiolarian assemblages and SSTs (*inter alia* Johnson and Nigrini, 1980, 1982; CLIMAP Project Members, 1984; Morley, 1989; Labeyrie *et al.*, 1996; Salvignac, 1998; Rickaby and Elderfield, 1999; Sicre *et al.*, 2005). The study also supports and refines previous research on the movement of Southern Ocean fronts between MIS-2 and MIS-1 and, to a limited extent, between MIS-3 and MIS-2 (Hays *et al.*, 1976; Prell *et al.*, 1979; Prell *et al.*, 1980): in

particular, it distinguishes the amount of movement of the Polar Front (PF) in the vicinity of the Kerguelen Plateau from the situation further east.

Two topics covered in this study are essentially new. Apart from temperature and, to a limited extent, salinity (Labeyrie *et al.*, 1996), planktonic proxies have not commonly been used to reconstruct palaeoceanic conditions: this study provides reconstructions of *in situ* density, dissolved oxygen, alkalinity, and nitrate and phosphate concentrations. The second new area is reconstruction below the sea surface: the study contains reconstructions to 500 metres bsl. Reconstructions of the top 500 metres of the water column provide a view of the changes in water masses over the last 40 ka. Being new, the findings from these two areas of study are subject to confirmation by the use of different estimation methods.

12.2. The results from surface sediments

The surface sediment samples from the eastern and southern Indian Ocean were investigated for two reasons: firstly, to establish an association between the radiolarian census data and Indian Ocean water masses, and, secondly, to associate the census data with oceanic variables (temperature, salinity, etc).

In the eastern Indian Ocean (EIO), an association between the census data and currents, including sub-surface currents, has been demonstrated. This extends the work of Johnson and Nigrini (1982), both by showing where the radiolarian assemblages they discovered are located close to the Western Australian coast, adding an assemblage, and by establishing that the assemblages are sometimes determined by sub-surface conditions. Similarly, this study identifies two more assemblages in the SIO than did Lozano and Hays (1976): both studies equate their assemblages with ocean fronts and in an almost identical way.

The association between radiolarian census data and oceanic variables presents a complex picture. Firstly, the relationship with any one environmental variable differs between the EIO and the SIO and even between subdivisions of those regions. For instance, the relationship with temperature reflects the thermocline. As a result, the SIO census data is strongly positively correlated with temperature throughout the water column from the surface to (at least) 500 metres bsl. In the EIO, there is strong correlation from the surface down to 100 metres bsl; below that depth, correlation declines to a minimum at 200 metres bsl before slowly increasing again down to at least 500 metres bsl (Figures 7.12i and 7.13i). As an example of relationships differing within regions, in the SIO, Assemblages G, K, and L are much more strongly influenced by silicate concentrations than Assemblages H and J (Figure 7.17).

The second complexity lies in the differing importance of one environmental variable relative to another. Again, this phenomenon exists between the EIO and the SIO and within each of these regions. For instance, dissolved oxygen is a major factor throughout the year in the EIO and is only important in the top layer of the water column (the thickness of the layer varying with the season) in the SIO (Figures 7.12d and 7.13d). The situation is almost exactly reversed with respect to temperature (Figures 7.12i and 7.13i). This phenomenon probably reflects important differences in radiolarian habitat and trophic type between the EIO and SIO. Within the EIO, Figure 7.16 shows that Assemblage D is strongly influenced by salinity and/or phosphate concentrations at 150 metres bsl but not by temperature at 75 metres bsl, whereas the reverse is true for Assemblage C (although salinity splits Assemblage C into two sub-assemblages). Assemblage D is mainly determined by the Leeuwin Undercurrent and Assemblage C by the Indonesian Throughflow and the Equatorial Gyral Current (Figures 4.4 and 9.1).

The differing relative importance of environmental variables on radiolarian taxa distributions is also evident in the results obtained from analysing the census counts of other researchers – the CLIMAP Project (1984) in the Southern Ocean, Kamikuri *et al.* (2008) and Welling (2003) in the Pacific Ocean, and Nimmergut and Abelmann (2001) in the Sea of Okhotsk. Although all these census counts indicate temperature is almost invariably an important determinant in species distribution, they also indicate the SST is never the major factor, and other oceanic variables are often more important in their effects than temperature at any depth.

It must be concluded that radiolaria are adapted to a wide range of ecological niches, and that each niche is defined by its own combination of oceanic variables (almost certainly including some which are not included in the WOA-05 datasets). The factors which control radiolarian distributions differ between ecological niches. Thus, the limiting factor in one niche might be nutrient concentrations, in another it might be dissolved oxygen. Furthermore, if the availabilities of two or more major explanatory variables are close to their limiting values, a slight increase in the availability of the most important factor could result in it being displaced by the second most important. It is probably a change in the relative availabilities of important (to radiolaria, that is) oceanic variables which explains why silicate concentrations are of more importance south of the Polar Front than north of it. In the SIO and north of the PF, silicate concentrations are very low, and the small changes in concentration over an extended longitudinal range (and large changes in temperature, salinity, etc) fail to be reflected in the radiolarian census data. South of the PF, silicate concentrations are very much higher and increase rapidly with increasing latitude. These large changes dominate radiolarian species' distribution, and can even be observed directly in the increasingly robust tests of some species.

The corollary of the conclusion that the variables which explain radiolarian species' distribution change from one area of the ocean to another validates this study's assumptions that assemblages delineate currents and fronts. Further, that frontal movements can be traced by matching vectors consisting of reconstructions of several variables with present-day conditions. An additional corollary is that, to reconstruct a particular variable using calibration and regression, the technique employed must, like WA-PLS, be designed to minimise the influences of the other variables on the reconstruction (ter Braak and Juggins, 1993; ter Braak *et al.*, 1993; Guiot and de Vernal, 2007).

The second conclusion which can be reached from the analysis of the surface sediments is that it is possible to exploit correlations between the census data and oceanic conditions at a range of depths in the water column to reconstruct the movement of water masses over time.

12.3. Palaeoenvironmental reconstructions

The palaeoenvironmental reconstructions conducted during this study cover two main areas: the changes in oceanic variables, and the movements of fronts and water masses (both at the surface and deeper).

The examination of variable reconstruction was conducted in several phases. Initially, it was demonstrated that radiolarian-based LGM SST reconstructions broadly conformed with the widely-accepted values obtained by previous researchers (principally Barrows and Juggins, 2005). Next, SSTs were estimated for the last 40 ka from the four SIO cores, MD88-769, MD88-770, MD94-102, and MD94-103. The radiolarian-derived results and those from foraminifera (Labeyrie *et al.*, 1996; Salvignac, 1998; Sicre *et al.*, 2005) and diatomacea (Labeyrie *et al.*, 1996; Crosta *et al.*, 2004) were compared and the discrepancies resolved. Reconstructions were also produced for salinity, dissolved oxygen, *in situ* density, and nitrate and phosphate concentrations, all variables not normally the subjects of

reconstruction. Finally, the estimates of the palaeo-oceanic variables were used to provide a "time-slice" for each of the four cores, showing the changes over the last 40 ka. The time slices give an indication of the vertical structure of the SIO over the last 40 ka.

It can be concluded that, in the southern Indian Ocean, diatoms may be better proxies for SSTs than either radiolaria or foraminifera. However, the error bounds of all three proxies overlap, and radiolarian census counts (and, probably, foraminiferal counts as well) can be used as proxies for ocean temperature from the surface to at least 500 metres bsl. The radiolarian-based reconstructions of other oceanic variables appear credible and are, for the most part, the first estimates of these variables made. It is hoped that they will form the basis of multiproxy reconstructions of these variables to establish their validity, and will be used in studies to improve the overall knowledge of the SIO.

Estimates have been made of the movement of Southern Ocean fronts. Although previous estimates exist (Hays *et al.*, 1976; Prell *et al.*, 1979; Prell *et al.*, 1980), this study's reconstructions of the movements of the SAF and PF are derived from a range of oceanic variables and a range of depths in the water column and are considered to be more soundly based than those derived from SST considerations alone. In addition, instead of making movement estimates at an ocean basin level, it is now possible to obtain values which cover as little as ten degrees of longitude. This degree of resolution allows the hypothesis that the SAF and the PF moved further north during MIS-2 in the vicinity of the Kerguelen Plateau than further east and, thus, that the Plateau was under permanent glaciation at the time.

12.4. Summary

This study has demonstrated the utility of radiolarian census counts as proxies for a wide range of oceanic variables and changes in water masses, including some for which no proxies have been found previously. The error bonds for the palaeo-reconstructions are seen to be comparable with other proxies and, therefore, acceptable for continuing research into conditions in the palaeo-Indian Ocean.

12.5. Recommendations and plans for future work

12.5.1. The surface sediment database

The outcomes of this study depend critically on the quality of the census data obtained from the surface sediment samples. Three criteria need to be satisfied:

- There must be good reason to believe that the samples were deposited within the period that present day oceanic conditions have been extant so as to justify the use of databases such as WOA-05.
- There must be a sufficiently large number of samples, well distributed over the study area. Statistical techniques invariably yield better results from large samples than from small ones.
- Each sample must be counted consistently and must comprise enough specimens to meet the aims of the study. It is anticipated this will demand larger counts than have been common hitherto.

As is discussed in Chapter 9 above (§9.1.1), the criterion for accepting surface sediment samples as sufficiently "modern" for comparison with WOA-05 was set at deposition within the last 5000 years. The exclusion of five samples which had been included in an earlier study (Rogers and De Deckker, 2007) changed the EIO database significantly. Radiocarbon dates were available for some of the surface sediments included in this study (Table 5.1). The remainder were accepted on trust, although it is likely that some had been dated and

were known to be modern. In an extension of this study or any similar future study, all, or at least a large proportion of the samples should be radiocarbon-dated. The lack of a date should be enough reason for excluding a sample if, during statistical analysis, it appears to be an outlier. There is a balance to be struck here between the cost of radiocarbon dating and the labour in counting enough surface samples that undated outliers can be excluded without affecting the statistical integrity of the study.

The precision of this study's results is undoubtedly constrained by the relatively few SIO surface samples counted. In particular, the paucity of samples from south of 50°S limits (unquantifiably) the quality of the results. A first step in furthering this study would be to obtain, if possible, twenty or more surface samples from the region south of 50°S and between 40°E and 120°E and to raise the total number of surface samples in the SIO to not less than 100. For the author, this would represent three to six months work.

With a single researcher performing all the census counts, consistency should not be a great problem, although care must be taken to avoid "identification drift", the tendency, gradually and unconsciously, to change the range of specimens included in a single taxonomic group. As explained in Chapter 5 (§5.3), correct identification to a described genus or species is not necessary for the purposes of statistical analysis. What is important is consistency in categorisation and this is achievable by a single researcher who is careful to guard against identification drift. A team of several researchers will speed the overall counting process but at the cost of regular cross-checking of each other's results.

Once samples of less than 100 specimens were removed, this study averaged a count of 500 specimens per core top. Five hundred specimens per sample is adequate for the work done. However, the relationship between census data and subsurface water masses would be more easily analysed if sample counts to be divided by taxa into groups correlated with

specific depths below sea level. The optimum specimen count per sample could only be determined by experiment, but would probably exceed 1000. Raising the SIO surface sample census data to this level represents around two month's work for a single researcher. It is probably impossible to achieve for the EIO at present because the surface samples for many of the sites are now exhausted.

12.5.2 Eastern Indian Ocean Currents

The association between the radiolarian census data and EIO surface and sub-surface currents opens the possibility of reconstructing both the Leeuwin Current and the Western Australian Current (WAC – also called the South Indian Ocean Current and, for that part which flows under the Leeuwin Current, the Leeuwin Undercurrent). In particular, changes in the temperature, salinity, and other oceanic conditions in the WAC should be traceable, regardless of the presence or absence of the Leeuwin Current. Hitherto, the WAC would only have been traceable in the absence of the Leeuwin Current because transfer function were only available for SSTs. The discovery that radiolarian data reflect sub-surface waters (see §7.2.3 and Figure 7.18) means the WAC could be reconstructed even when the Leeuwin Current was flowing above it – as is the case during interglacials (during glacials, the Leeuwin Current is reduced or absent).

Reconstruction of the WAC would entail counting the radiolaria in samples from cores taken offshore Western Australia from about 22°S to about 35°S. Cores taken during the *RV. Franklin* cruises Fr94 and Fr95 would probably suffice, as would the existing surface sample database. The resolution, both in terms of how many sample sites would be appropriate and how many samples from each core, would be depend on the exact aims of the research. Similarly, it would be possible to improve knowledge of the palaeo-currents north of 22°S.

12.5.3 Southern Indian Ocean frontal movements

The quickest way of improving frontal movement reconstruction would be to examine more down-core samples from MD94-103, the core having only been sampled to-date to look for associations between the radiolarian census data and Heinrich and similar events. The next step would be to examine a series of cores mainly from between 40°S and 50°S, but also including some from south of 50°S and from north of 40°S. This second step would entail up to five years work, depending on the number of cores investigated, but would be very valuable. Further examination of MD94-103 would be quite quick (six to nine months, perhaps, depending on the resolution of the examination) and would provide further information on possible North Atlantic/Southern Ocean interconnections (see next paragraph).

12.5.4 Southern Ocean/North Atlantic interconnections

The MD94-103 core samples were specifically selected to investigate the possibility of radiolarian reconstructions of SIO conditions reflecting events in the North Atlantic in a similar way to that in which foraminiferal reconstructions appear to do (Sicre *et al.*, 2005). There is now *prima facie* evidence that the radiolarian reconstructions reflect North Atlantic events, and this should now be put on a firm basis by sampling the time periods not yet counted and by increasing the resolution of those periods already examined. This represents, perhaps, six to nine months work and may open an opportunity for a collaborative study.

12.5.5 The reconstructions of oceanic variables

The study provides estimates of a number of palaeoenvironmental variables which have rarely, if ever, been the focus of proxy studies previously. The variables are dissolved oxygen, nitrate and phosphate concentrations, alkalinity, and *in situ* density. Salinity, which has been the subject of some previous researches (e.g. Labeyrie *et al.*, 1996), is emphasised and there is sufficient information to reconstruct silicate concentrations in specific regions of the ocean. Two new areas of work are opened: firstly, the validity of these variable

reconstructions needs to be confirmed using a multiproxy approach, and, secondly, the variables need to be employed to provide useful information about the palaeo-Indian Ocean, for instance by relating alkalinity to pCO_2.

12.5.6 Future work priorities

Subject to being able to obtain appropriate samples, the author proposes to conduct the following work, in this order of priority, commencing immediately after this thesis is submitted:

- Extension of the SIO surface sediment database to approximately 100 sites.
- Improvement of the coverage and resolution of MD94-103.

Until the samples can be obtained, the author proposes to extend the sampling of MD88-769 and MD88-770 back to 50 ka and to sample MD94-101. The material for these investigations is already at hand. In addition, the author intends to investigate more fully the data already obtained on the movement of ocean fronts and water masses.

References

Abelmann, A. and Gowing, M., 1996. Horizontal and vertical distribution pattern of living radiolarians along a transect from the Southern Ocean to the South Atlantic subtropical region. *Deep-Sea Research I,* 43(3):361-382.

Abelmann, A. and Nimmergut, A., 2005. Radiolarians in the Sea of Okhotsk and their ecological implication for paleoenvironmental reconstructions. *Deep-Sea Research,* 11(52):2302-2331.

Abelmann, A., Brathauer, U., Gersonde, R., Sieger, R., and Zielinski, U., 1999. Radiolarian-based transfer function for the estimation of sea surface temperature in the Southern Ocean (Atlantic Sector). *Paleoceanography,* 14(3):410-421.

Anderson, A. and Gupta, S., 1998. Evidence of binary division in mature colonial capsules of a Collosphaerid colonial radiolarian: implications for shell ontogenetic patterns in modern and fossil species. *Palaeontologia Electronica,* 1998(1).

Anderson, O.R., 1981. Radiolarian Fine Structure and Silica Deposition, in *Silicon and Siliceous Structures in Biological Systems*, T. Simpson and B. Volcani (eds), pp. 347-380. New York: Springer-Verlag.

---, 1983. *Radiolaria.* New York: Springer-Verlag pp.

Anderson, O.R., Bennett, P., and Bryan, M., 1988. Experimental and Observational Studies of Radiolarian Physiological Ecology: 1. Growth, Abundance and Opal Productivity of the Spongiose Radiolarian *Spongaster tetras tetras*. *Marine Micropaleontology,* 14:257-265.

---, 1989. Experimental and Observational Studies of Radiolarian Physiological Ecology: 3. Effects of Temperature, Salinity and Light Intensity on the Growth and Survival of *Spongaster tetras tetras* Maintained in Laboratory Culture. *Marine Micropaleontology,* 14:275-282.

Anderson, O.R., Bryan, M., and Bennett, P., 1990. Experimental and observational studies of radiolarian physiological ecology: 4. Factors determining the distribution and survival of *Didymocyrtis tetrathalamus tetrathalamus* with implications for paleoecological interpretations. *Marine Micropaleontology,* 16:155-167.

Anderson, O.R., Bennett, P., Angel, M., and Bryan, M., 1989. Experimental and Observational Studies of Radiolarian Physiological Ecology: 2. Trophic Activity and Symbiont Primary Productivity of *Spongaster tetras tetras* with Comparative Data on Predatory Activity of Some Nassellarida. *Marine Micropaleontology,* 14:267-273.

Andrews, J., 1977. Eddy structure and the West Australian Current. *Deep-Sea Research,* 24:1133-1148.

Antonov, J., Locarnini, R., Boyer, T., Mishonov, R., and Garcia, H., 2006. *World Ocean Atlas 2005 Volume2: Salinity,* Washington, D.C.: US Government Printing Office.

Bard, E., Arnold, M., and Fairbanks, R., 1993. 230Th-234U and 14C ages obtained by mass spectrometry on corals. *Radiocarbon,* 35:191-199.

Bareille, G., Grousset, F., and Labracherie, M., 1994. Origin of detrital fluxes in the southeast Indian Ocean during the last climatic cycles. *Paleoceanography,* 9(6):799-819.

Bareille, G., Labracherie, M., Bertrand, P., Labeyrie, L., Lavaux, G., and Dignan, M., 1998. Glacial-interglacial changes in the accumulation rates of major biogenic components in Southern Indian Ocean sediments. *Journal of Marine Systems,* 17:527-539.

Barker, P. and Thomas, D., 2004. Origin, signature and palaeoclimatic influence of the Antarctic Circumpolar Current. *Earth-Science Reviews,* 66:143-162.

Barrows, T.T. and Juggins, S., 2005. Sea-surface temperatures around the Australian margin and Indian Ocean during the Last Glacial Maximum. *Quaternary Science Reviews,* 24:1017-1047.

Barrows, T.T., Juggins, S., De Deckker, P., and Calvo, E., 2007. Long-term sea surface temperatures and climate change in the Australian-New Zealand region. *Paleoceanography,* 22(PA2215):1-17.

Belkin, I. and Gordon, A., 1996. Southern Ocean fronts from the Greenwich meridian to Tasmania. *Journal of Geophysical Research,* 101(C2):3675-3696.

Berger, W., 1968. Radiolarian Skeletons: Solution at Depths. *Science,* 159(3820):1237-1239.

Berger, W. and Garner, J., 1975. On the determination of Pleistocene temperatures from planktonic foraminifera. *Journal of Foraminiferal Research,* 5(2):102-113.

Berggren, W., 1978. Marine Micropaleontology: an introduction, in *Introduction to Marine Micropaleontology*, B. Haq and A. Boersma (eds), pp. 1-376. New York: Elsevier North-Holland Inc.

Birks, H., Line, J., Juggins, S., Stevenson, A., and Ter Braak, C., 1990. Diatoms and pH Reconstruction. *Philosophical Transactions of the Royal Society of London, Series B, Biological Sciences,* 327(1240):263-278.

Blain, S., Quéguiner, B., Armand, L., Belviso, S., Bombled, B., Bopp, L., Bowie, A., Brunet, C., Brussaard, C., Carlotti, F., Christaki, U., Corbière, A., Durand, I., Ebersbach, F., Fuda, J.-L., Garcia, N., Gerringa, L., Griffiths, G., Guigue, C.G., c., Jacquet, S., Jeandel, J., Laan, P., Lefèvre, D., Lo Monaco, C., Malits, A., Mosseri, J., Obernosterer, I., Park, Y.-H., Picheral, M., Pondaven, P., Remenyi, T., Sandroni, V., Sarthou, G., Savoye, N., Scouarnac, L., Souhaut, M., Thuiller, D., Timmermans, K., Trull, T., Ulitz, J., van Beek, P., Veldhuis, M., Vincent, D., Viollier, E., Vong, L., and Wagener, T., 2007. Effect of natural iron fertilization on carbon sequestration in the Southern Ocean. *Nature,* 446:1070-1075.

Boltovskoy, D., 1998. Classification and Distribution of South Atlantic Recent Polycystine Radiolaria. *Palaeontologia Electronica,* 1(2):1-116.

Boltovskoy, D., Kogan, M., Alder, V., and Mianzan, H., 2003. First record of a brackish radiolarian (Polycystina): Lophophaena rioplatensis n. sp in the Rio de la Plata estuary. *Journal of Plankton Research,* 25(12):1551-1559.

Bond, G., Broecker, W., Johnsen, S., McManus, J., Labeyrie, L., Jouzel, J., and Bonani, G., 1993. Correlations between climate records from the North Atlantic and Greenland ice. *Nature,* 365:143-147.

Bond, G., Heinrich, H., Broecker, W., Labeyrie, L., McManus, J., Andrews, J., Huon, S., Jantschik, R., Clasen, S., Simet, C., Tedesco, K., Klas, M., Bonani, G., and Ivy, S., 1992. Evidence for massive discharges of icebergs into the North Atlantic Ocean during the last glacial period. *Nature,* 360(6401):245-249.

Böning, C., Dispert, A., Visbeck, M., Rintoul, S., and Schwarzkopf, F., 2008. The response of the Antarctic Circumpolar Current to recent climate change. *Nature Geoscience,* 1:864-869.

Brathauer, U., Abelmann, A., Gersonde, R., Niebler, H.-S., and Fütterer, D., 2001. Calibration of *Cycladophora davisiana* events versus oxygen isotope stratigraphy in the subantarctic Atlantic Ocean - a stratigraphic tool for carbonate-poor Quaternary sediments. *Marine Geology,* 175:167-181.

Breiman, L., Friedman, J., Olshen, R., and Stone, J., 1984. *Classification and Regression Trees*. Belmont, Ca.: Wadsworth pp. 358.

Calvo, E., Pelejero, C., De Deckker, P., and Logan, G., 2007. Antarctic deglacial pattern in the 30 kyr record of sea surface temperature offshore South Australia. *Geophysical Research Letters,* 34(L13707):1-6.

Campbell, A. and Moore, R., 1954. *Treatise on Invertebrate Paleontology*. Part D Protista 3 Protozoa (Chiefly Radiolaria and Tintinnina). Boulder, Colorado: University of Kansas Press and Geological Society of America, Inc. pp. 195.

Casey, R., 1967a. Distribution of polycystine radiolarians in the oceans in relation to physical and chemical conditions, in *The Micropalaeontology of Oceans*, B. Funnell and W. Riedel (eds), pp. 151-159. Cambridge: Cambridge University Press, 1971.

---, 1967b. Radiolarians as indicators of past and present water-masses, in *The Micropalaeontology of Oceans*, B. Funnell and W. Riedel (eds), pp. 331-342. Cambridge: Cambridge University Press, 1971.

---, 1993. Radiolaria, in *Fossil Prokaryotes and Protists*, J. Lipps (ed.), pp. 249-284. Boston: Blackwell Scientific Publications.

Caulet, J.-P., Vénec-Peyré, M.-T., Vergnaud Grazzaini, C., and Nigrini, C., 1992. Variation of the South Somalian upwelling during the last 160 ka; radiolarian and foraminifera records in core MD 85674, in *Upwelling Systems: Evolution since the Early Miocene*, C. Summerhayes, W. Prell and K. Emeis (eds), pp. 379-389. London: Geological Society of London.

Cavalier-Smith, T., 1993. Kingdom Protozoa and its 18 Phyla. *Microbiological Reviews,* 57(4):953-994.

Chang, F., Zhuang, L., Li, T., Yun, J., Cao, Q., and Cang, S., 2003. Radiolarian fauna in the surface sediments of the northeastern East China Sea. *Marine Micropaleontology,* 48:169-204.

Chang, Y.-S., Rosati, A., Zhang, S.-Q., and Harrison, M., 2009. Objective analysis of monthly temperature and salinity for the world ocean in the 21st century: Comparison with World Ocean Atlas and application to assimilation validation. *Journal of Geophysical Research,* 114(C02014):1-24.

Charnock, H., 1996. The Atmosphere and the Ocean, in *Oceanography: and illustrated guide*, C. Summerhayes and S. Thorpe (eds), pp. 27-40. Southampton: Manson.

CLIMAP Project Members, 1976. The Surface of the Ice-Age Earth. *Science,* 191(4232):1131-1137.

---, 1981. *Seasonal reconstructions of the Earth's surface at the Last Glacial Maximum.* Map and Chart Series. New York: Geological Society of America pp. 1-18.

---, 1984. The last interglacial ocean. *Quaternary Research,* 21:123-224.

---, 1997. Relative abundance of radiolaria in surface sediments. PANGEA. DOI:doi:10.1594/PANGAEA.51928 accessed May 2008.

---, 2006. Abundance of microfossils of sediment core RC11-83. PANGEA. DOI:10.1594/PANGAEA.401041 accessed May 2008.

Corliss, B., 1979. Recent deep-sea benthonic foraminiferal distributions in the southeast Indian Ocean: infered bottom-water routes and ecological implications. *Marine Geology,* 31:116-138.

Cortese, G. and Bjørklund, K., 1998. Morphometry and Taxonomy of Hexacontium Species from Western Norwegian Fjords. *Micropaleontology,* 44(2):161-172.

Cortese, G., Abelmann, A., and Gersonde, R., 2007. The last five glacial-interglacial transitions: A high-resolution 450,000-year record from the subantarctic Atlantic. *Paleoceanography,* 22(PA4203):1-14.

Craneguy, P. and Park, Y.-H., 1999. Contrôle topographique du courant circumpolaire antarctique dans l'océan Indien sud. *Comptes Rendus de l'Académie des Sciences - Series IIA: Sciences de la terre et des planètes* 328(9):583-589.

Cresswell, G., 1991. The Leeuwin Current - observations and recent models. *Journal of the Royal Society of Western Australia,* 74:1-14.

Cresswell, G. and Golding, T., 1980. Observations of a south-flowing current in the southeastern Indian Ocean. *Deep-Sea Research,* 27A:449-466.

Crosta, X., Sturm, A., Armand, L., and Pichon, J., 2004. Late Quaternary sea ice history in the Indian sector of the Southern Ocean as recorded by diatom assemblages. *Marine Micropaleontology,* 50:209-223.

Dansgaard, W., Johnsen, S., Clausen, H., Dahl-Jensen, D., Gundestrup, N., Hammer, C., Hvidberg, C., Steffensen, J., Svelnbjorndottir, A., Jouzel, J., and Bond, G., 1993. Evidence for general instability of past climate from a 250-kyr ice-core record. *Nature,* 364:218-220.

De'ath, G., 2002. Multivariate regression trees: a new technique for modeling species-environment relationships. *Ecology,* 83(4):1105-1117.

De Wever, P., Dumitrica, P., Caulet, J.-P., Nigrini, C., and Caridroit, M., 2001. *Radiolarians in the Sedimentary Record.* Amsterdam: Gordon and Breach Science Publishers pp.

Dezileau, L., Bareille, G., and Reyss, J., 2002. Enrichissement en uranium authigène dans les sédiments glaciaires de l'océan Austral. *Comptes rendus de l'Academie des Sciences - Géoscience,* 334:1039-1046.

Dezileau, L., Bareille, G., Reyss, J., and Lemoine, F., 2000. Evidence for strong sediment redistribution by bottom currents along the southeast Indian ridge. *Deep-Sea Research I,* 47:1899-1936.

Dolven, J., 2004. 'Radiolaria.org', http://www.radiolaria.org, accessed frequently.

Dolven, J., Cortese, G., and Bjørklund, K., 2002. A high-resolution radiolarian-derived paleotemperature record for the late Pleistocene-Holocene in the Norwegian Sea. *Paleoceanography,* 17(4):24.21-24.13.

Dow, R., 1978. Radiolarian distribution and the Late Pleistocene history of the southeastern Indian Ocean. *Marine Micropaleontology,* 3:203-227.

Dufrêne, M. and Legendre, P., 1997. Species assemblages and indicator species: the need for a flexible asymmetrical approach. *Ecological Monographs,* 67(3):345-366.

Durgadoo, J., Lutjeharms, J., Biastoch, A., and Ansorge, I., 2008. The Conrad Rise as an obstruction to the Antarctic Circumpolar Current. *Geophysical Research Letters,* 35(L20606):1-6.

Dworetzky, B. and Morley, J., 1987. Vertical distribution of Radiolaria in the eastern Equatorial Atlantic: analysis of a multiple series of closely-spaced plankton tows. *Marine Micropaleontology,* 12:1-19.

Emiliani, C., 1955. Pleistocene Temperatures. *Journal of Geology,* 63:538-578.

Erickson III, D., Hernandez, J., Ginoux, P., Gregg, W., McClain, C., and Christian, J., 2003. Atmospheric iron delivery and surface ocean biological activity in the Southern Ocean and Patagonian Region. *Geophysical Research Letters,* 30(12):11-11 - 11-14.

Fagel, N., Dehairs, F., André, L., Bareille, G., and Monnin, C., 2002. Ba distribution in the surface Southern Ocean sediments and export production estimates. *Paleoceanography,* 17(2-1011):1.1-20.

Faith, D., Minchin, P., and Belbin, L., 1987. Compositional dissimilarity as a robust measure of ecological distance. *Vegetatio,* 69:57 68.

Faria, J., Grosjean, P., and Jelihovschi, E., 2008. 'Tinn-R - GUI/Editor for R language and environment statistical computing', https://sourceforge.net/projects/tinn-r, accessed 18 December 2008.

Fatela, F. and Taborda, R., 2002. Confidence limits of species proportions in microfossil assemblages. *Marine Micropaleontology,* 45:169-174.

Feng, M., Meyers, G., Pearce, A., and Wijffels, S., 2003. Annual and interannual variations of the Leeuwin Current at 32°S. *Journal of Geophysical Research,* 108(C11):19/11-19/21.

Fieux, M., Andrié, C., Delecluse, P., Ilahude, A., Kartavtseff, A., Mantisi, F., Molcard, R., and Swallow, J., 1994. Measurements within the Pacific-Indian Oceans throughflow region. *Deep-Sea Research I,* 41(7):1091-1130.

Fine, R., 1993. Circulation of Antarctic Intermediate Water in the South Indian Ocean. *Deep-Sea Research I,* 40(10):2021-2043.

Foreman, H. and Riedel, W., 1972. *Catalogue of polycystine Radiolaria, US National Technical Information Service PB281000/LC.* New York: The American Museum of Natural History.

Fraley, C. and Raftery, A., 1998. How many clusters? Which clustering method? Answers via model-based cluster analysis. *The Computer Journal,* 41(8):578-588.

---, 2006. *MCLUST Version 3 for R: Normal Mixture Modeling and Model-Based Clustering, Technical Report no. 504.* Department of Statistics, University of Washington.

Gille, S., 1994. Mean sea surface height of the Antarctic Circumpolar Current from Geosat data: Method and application. *Journal of Geophysical Research,* 99(C9):18,255-218,273.

Gingele, F., De Deckker, P., and Hillenbrand, C.-D., 2001. Clay mineral distribution in surface sediments between Indonesia and NW Australia - source and transport by ocean currents. *Marine Geology,* 179:135-146.

Granlund, A., 1986. Size and shape patterns in the Recent Radiolarian genus *Antarctissa* from a South Indian Ocean transect. *Marine Micropaleontology,* 11:243-250.

Greenland Project (GRIP) Members, 1993. Climate instability during the last Interglacial period recorded in the GRIP ice core. *Nature,* 364:203-207.

Guiot, J. and de Vernal, A., 2007. Transfer functions: methods for quantitative paleoceanography based on microfossils, in *Proxies in Late Cenozoic Paleoceanography*, C. Hillaire-Marcel and A. de Vernal (eds), pp. 521-563. Elsevier.

Gupta, S., 2002. Pyloniid Stratigraphy - a new tool to date tropical radiolarian ooze from the central tropical Indian Ocean. *Marine Geology,* 184:85-93.

---, 2003. Orbital frequencies in radiolarian assemblages of the central Indian Ocean: implications on the Indian summer monsoon. *Palaeogeography, Palaeoclimatology, Palaeoecology,* 197:97-112.

Haeckel, E., 1887. 'Report on the Radiolaria collected by H.M.S. Challenger. Vol. XVIII - Zoology', *Her Majesty's Stationery Office,* http://caliban.mpiz-koeln.mpg.de/~stueber/haeckel/challenger/index.htm, accessed 2005-present.

Hammer, Ø. and Harper, D., 2006. *Paleontological Data Analysis.* Oxford: Blackwell Publishing pp. 351.

Hammer, Ø., Harper, D.A.T., and P.D., R., 2001. PAST: Paleontological Statistics Software Package for Education and Data Analysis. *Palaeontologia Electronica,* 4(1).

Hanawa, K. and Talley, L., 2001. 5.4 Mode Waters, in *Ocean circulation and climate, 77,* G. Siedler, J. Church and J. Gould (eds), pp. 373-386. San Diego: Academic Press.

Haslett, S., 1995. Mapping Holocene upwelling in the eastern equatorial Pacific using Radiolaria. *The Holocene,* 5(4):470-478.

Hays, J. and Morley, J., 2004. The Sea of Okhotsk: A Window on the Ice Age Ocean. *Deep-Sea Research I,* 51:593-618.

Hays, J., Lozano, J., Shackleton, N., and Irving, G., 1976. Reconstruction of the Atlantic and Western Indian Ocean Sectors of the 18.,00 B.P. Antarctic Ocean, in *Investigation of Late Quaternary Paleoceangraphy and Paleoclimatology, Memoir 145,* R. Cline and J. Hays (eds), pp. 338-372. Boulder, Co: Geological Society of America.

Howard, W. and Prell, W., 1984. A comparison of radiolarian and foraminiferal paleoecology in the southern Indian Ocean: new evidence for the interhemispheric timing of climate change. *Quaternary Research,* 21:244-263.

Hutson, W., 1977. Transfer functions under No-analog Conditions: experiments with Indian Ocean Planktonic Foraminifera. *Quaternary Research,* 8:355-367.

---, 1980. The Agulhas Current during the Late Pleistocene: Analysis of modern faunal analogs. *Science,* 207(4426):64-66.

Imbrie, J. and Kipp, N., 1971. A new micropaleontological method for Quantitative Paleoclimatology: Application to a late Pleistocene Caribbean Core, in *The Late Cenozoic Glacial Ages,* K. Turekian (ed.), pp. 71-181. New Haven: Yale University Press.

Itaki, T., 2003. Depth-related radiolarian assemblage in the water-column and surface sediments of the Japan Sea. *Marine Micropaleontology,* 47:253-270.

Itaki, T., Khim, B.-K., and Ikehara, K., 2008. Last glacial-Holocene water structure in the southwestern Okhotsk Sea inferred from radiolarian assemblages. *Marine Micropaleontology,* 67:191-215.

Itaki, T., Ito, M., Narita, H., Ahagon, N., and Sakai, H., 2003. Depth distribution of radiolarians from the Chukchi and Beaufort Seas, western Arctic. *Deep-Sea Research,* 50:1507-1522.

Jacot Des Combes, H., Caulet, J.-P., and Tribovillard, N., 1999. Pelagic productivity changes in the equatorial area of the northwest Indian Ocean during the last 400,000 years. *Marine Geology,* 158:27-55.

Johnson, D. and Nigrini, C., 1980. Radiolarian biogeography in surface sediments of the western Indian Ocean. *Marine Micropaleontology,* 5:111-152.

---, 1982. Radiolarian biogeography in surface sediments of the eastern Indian Ocean. *Marine Micropaleontology,* 7:237-281.

Jongman, R., ter Braak, C., and van Tongeren, O., 1987. *Data analysis in community and landscape ecology.* Den Haag: PUDOC Wageningen pp. 299.

Jouzel, J., Vaikmae, R., Petit, J., Martin, m., Duclos, Y., Stievenard, M., Lorius, C., Toots, M., Méliières, M.-A., Burckle, L., Barkov, N., and Kotlyakov, V., 1995. The two-step shape and timing of the last deglaciation in Antarctica. *Climate Dynamics,* 11:151-161.

Juggins, S., 2007a. Analysis of Environmental Data. Unpublished course text.

---, 2007b. 'C^2: Software for ecological and palaeoecological data analysis and visualisation'. Version 1.5.1 (build 1) http://www.campus.ncl.ac.uk/staff/Stephen.Juggins/software/c2home.htm.

Kamikuri, S., Motoyama, H., and Nishimura, A., 2008. Radiolarian assemblages in surface sediments along longitude 175°E in the Pacific Ocean. *Marine Micropaleontology,* 69:151-172.

Kaufman, L. and Rousseeuw, P., 1990. *Finding Groups in Data: An Introduction to Cluster Analysis.* New York: Wiley pp.

Kling, S., 1975. Relation of radiolarian distributions to subsurface hydrography in the North Pacific. *Deep-Sea Research,* 23:1943-1058.

---, 1978. Radiolaria, in *Introduction to Marine Micropaleontology*, B. Haq and A. Boersma (eds), pp. 203-244. New York: Elsevier.

---, 1979. Vertical distribution of polycystine radiolarians in the Central North Pacific. *Marine Micropaleontology,* 4:295-318.

Kling, S. and Boltovskoy, D., 1995. Radiolarian vertical distribution patterns across the southern California Current. *Deep-Sea Research I,* 42(2):191-231.

Kolla, V., Sullivan, L., Streeter, S., and Langseth, M., 1976. Spreading of Antarctic bottom water and its effects on the floor of the Indian Ocean inferred from bottom-water potential temperature, turbidity, and sea-floor photography. *Marine Geology,* 21:171-189.

Kunitomo, Y., Sarashina, I., Iijima, M., Endo, K., and Sashida, K., 2006. Molecular phylogeny of acantharian and polycystine radiolarians based on ribosomal DNA sequences, and some comparisons with data from the fossil record. *European Journal of Protistology,* 42(2):143-153.

Labeyrie, L., Labracherie, M., Gorfti, N., Pichon, J., Vautravers, M., Arnold, M., Duplessy, J.-C., Paterne, M., Michel, E., Duprat, J., Caralp, M., and Turon, J.-L., 1996. Hydrographic changes over the Southern Ocean (southeast Indian sector) over the last 230 kyr. *Paleoceanography,* 11(1):57-76.

Lazarus, D., Bittniok, B., Diester-Haass, L., Meyers, P., and Billups, E., 2006. Comparison of radiolarian and sedimentologic paleoproductivity proxies in the latest Miocene-Recent Benguela Upwelling System. *Marine Micropaleontology,* 60:269-294.

Legendre, P. and Legendre, L., 1998. *Numerical Ecology*. 2nd English. Amsterdam: Elsevier pp.

Levitus, S., 1994. 'World Ocean Atlas. Vol. 1: Temperature', http://iridl.ldeo.columbia.edu/SOURCES/.NOAA/.NODC/.WOA98, accessed January, 2009.

Linacre, E. and Geerts, B., 1997. *Climates and Weather Explained.* London: Routledge pp.

Locarnini, R., Mishonov, R., Antonov, J., Boyer, T., and Garcia, H., 2006. *World Ocean Atlas 2005 Volume 1: Temperature,* Washington, D.C.: US Government Printing Office.

Lozano, J. and Hays, J., 1976. Relationship of Radiolarian Assemblages to Sediment Types and Physical Oceanography in the Atlantic and Western Indian Ocean Sectors of the Antarctic Ocean. *Geological Society of America Memoir,* 145:303-336.

Lüer, V., Cortese, G., Neil, H., Hollis, C., and Willems, H., 2009. Radiolarian-based sea surface temperatures and paleoceanographic changes during the Late Pleistocene–Holocene in the subantarctic southwest Pacific. *Marine Micropaleontology,* 70:151-165.

Maindonald, J. and Braun, J., 2003. *Data Analysis and Graphics: Using R - an example-based approach.* Cambridge: Cambridge University Press pp. 362.

Martin, J., Coale, K., Johnson, K., Fitzwater, S., Gordon, R., Tanner, S., Hunter, C., Elrod, V., Nowicki, J., Coley, T., Barber, R., Lindley, S., Watson, A., Van Scoy, K., Law, C., Liddicoat, M., Ling, R., Stanton, T., Stockel, J., Collins, C., Anderson, A., Bidigare, R., Ondrusek, O., Latase, M., Millero, F., Lee, K., Yao, W., Zhang, J., Friederich, G., Sakamoto, C., Chavez, F., Bucj, K., Kolber, Z., Greene, R., Falkowski, P., Chisholm, S., Hoge, F., Swift, R., Yungel, J., Turner, S., Nightingale, P., Hatton, A., Liss, P., and Tindale, N., 1994. Testing the iron hypothesis in ecosystems of the equatorial Pacific Ocean. *Nature,* 371:123-129.

Martínez, J., De Deckker, P., and Barrows, T.T., 1999. Palaeoceanography of the last glacial maximum in the eastern Indian Ocean: planktonic foraminiferal evidence. *Palaeogeography, Palaeoclimatology, Palaeoecology,* 147:73-99.

Martínez, J., Taylor, L., De Deckker, P., and Barrows, T.T., 1998. Planktonic foraminifera from the eastern Indian Ocean: distribution and ecology in relation to the Western Pacific Ocean Warm Pool (WPWP). *Marine Micropaleontology,* 34:121-151.

Martinson, D., Menke, W., and Stoffa, P., 1982. An inverse approach to signal correlation. *Journal of Geophysical Research,* 87:4807-4818.

McCarthy, M. and Talley, L., 1999. Three-dimensional isoneutral potential vorticity structure in the Indian Ocean. *Journal of Geophysical Research,* 104(C6):13251-13267.

McCartney, M., 1977. Subantarctic Mode Water, in *A Voyage of Discovery*, M. Angel (ed.), pp. 103-119. Oxford: Pergamon Press.

---, 1982. The subtropical recirculation of Mode Waters. *Journal of Marine Research,* 40 supplement:427-464.

Meissener, K., 2007. Reconstructing and Modeling Past Oceans, in *Proxies in Late Cenozoic Paleoceanography*, C. Hillaire-Marcel and A. de Vernal (eds), pp. 799-811. Elsevier.

Meyers, G., Bailey, R., and Worby, A., 1995. Geostrophic transport of Indonesian throughflow. *Deep-Sea Research I,* 42(7):1163-1174.

Millero, F., 2006. *Chemical oceanography*. Boca Raton: CRC/Taylor and Francis pp. 496.

Millero, F., Lee, K., and Roche, M., 1998. Distribution of alkalinity in the surface waters of the major oceans. *Marine Chemistry,* 60:111-130.

Minchin, P., 1987. An evaluation of relative robustness of techniques for ecological ordinations. *Vegetatio,* 71:145-156.

Molfino, B., Kipp, N., and Morley, J., 1982. Comparison of Foraminiferal, Coccolithophorid, and Radiolarian Paleotemperature Equations: Assemblage Coherency and Estimate Concordancy. *Quaternary Research* 17:279-313.

Moore, C., Hickman, A., Poulton, A., Seeyave, S., and Lucas, M., 2007. Iron–light interactions during the CROZet natural iron bloom and EXport experiment (CROZEX): II—Taxonomic responses and elemental stoichiometry. *Deep-Sea Research II,* 54(18-20):2066-2084.

Moore, C., Seeyave, S., Hickman, A., Allen, J., Lucas, M., Planquette, H., Pollard, R., and Poulton, A., 2007. Iron–light interactions during the CROZet natural iron bloom and EXport experiment (CROZEX) I: Phytoplankton growth and photophysiology. *Deep-Sea Research II,* 54(18-20):2045-2065.

Moore, J.K., Abbott, M., and Richman, J., 1999. Locations and dynamics of the Antarctic Polar Front from satellite sea surface temperature data. *Journal of Geophysical Research,* 104(C2):3059-3073.

Morley, J., 1989. Radiolarian-based Transfer Functions for Estimating Paleoceanographic Conditions in the Southern Ocean. *Marine Micropaleontology,* 13:293-307.

Morley, J. and Hays, J., 1983. Oceanographic conditions associated with high abundances of the radiolarian *Cycladophora davisiana*. *Earth and Planetary Science Letters,* 66:63-72.

Murgese, S. and De Deckker, P., 2005. The distribution of deep-sea benthic foraminifera in core tops from the eastern Indian Ocean. *Marine Micropaleontology,* 56:25-49.

Nigrini, C., 1967. *Radiolaria in pelagic sediments from the Indian and Atlantic Oceans.* Bulletin of the Scripps Institution of Oceanography. La Jolla, Ca.: University of California Press pp. 1-125.

Nigrini, C. and Moore, T.C., 1979a. *A Guide to Modern Radiolaria.* Special Publication No. 16. Cushman Foundation for Foraminiferal Research Inc. pp.

---, 1979b. 'A Guide to Modern Radiolaria (online)', *Cushman Foundation for Foraminiferal Research Inc.,* http://gdcmp1.ucsd.edu/geol_coll/radlit/nm79titl.html, accessed January 2004.

Nigrini, C. and Caulet, J.-P., 1992. Late Neogene radiolarian assemblages characteristic of Indo-Pacific areas of upwelling. *Micropaleontology,* 38(2):139-164.

Nigrini, C., Caulet, J.-P., and Sanfilippo, A., 2004. 'RadWorld', http://www.mnhn.fr/mnhn/geo/radworld/radworldsite/radsearch.html, accessed 15 March 2004.

Nimmergut, A. and Abelmann, A., 2001. Abundance of radiolaria in surface sediment, Sea of Okhotsk. PANGEA. DOI:10.1594/PANGAEA.60186 accessed May 2008.

Okazaki, Y., Takahashi, K., Itaki, T., and Kawasaki, Y., 2004. Comparison of radiolarian vertical distributions in the Okhotsk Sea near the Kuril Islands and in the northwestern North Pacific off Hokkaido Island. *Marine Micropaleontology,* 51:257-284.

Oke, T., 1987. *Boundary Layer Climates.* 2nd edition. Padstow, Cornwall: Routledge pp. 1-435.

Oksanen, J., 2005. Multivariate analysis of ecological communities in R: vegan tutorial.

Olbers, D., Borowski, D., Völker, C., and Wölff, J.-O., 2004. The dynamical balance, transport, and circulation of the Antarctic Circumpolar Current. *Antarctic Science,* 16(4):439-470.

Orsi, A., Whitworth, T., and Nowlin, W., 1995. On the meridional extent and fronts of the Antarctic Circumpolar Current. *Deep-Sea Research I,* 42(5):641-673.

Overpeck, J., Webb, T., and Prentice, I., 1985. Quantitative Interpretation of Fossil Pollen Spectra: Dissimilarity Coefficients and the Method of Modern Analogs. *Quaternary Research,* 23:87-108.

Park, Y.-H., Gamberoni, L., and Charriaud, E., 1993. Frontal structure, water masses, and circulation in the Crozet Basin. *Journal of Geophysical Research,* 98(C7):12361-12385.

Pearce, A., 1991. Eastern boundary currents of the southern hemisphere. *Journal of the Royal Society of Western Australia,* 74:35-45.

Pearce, A. and Cresswell, G., 1985. Ocean Circulation off Western Australia and the Leeuwin Current. *CSIRO Information Service,* 16(3).

Pearce, A. and Phillips, B., 1988. ENSO events, the Leeuwin Current, and larval recruitment of the western rock lobster. *Journal of the International Council for the Exploration of the Sea,* 45:13-21.

Pearce, A. and Pattiaratchi, C., 1999. The Capes Current: a summer countercurrent flowing pass Cape Leeuwin and Cape Naturaliste, Western Australia. *Continental Shelf Research,* 19:401-420.

Petit, J., Jouzel, J., Raynaud, D., Barkov, N., Barnola, J., Basile, I., Bender, M., Chappellaz, J., Davis, M., Delaygue, G., Delmotte, M., Kotlyakov, V., Legrand, M., Lipenkov, V., Lorius, C., Pépin, L., Ritz, C., Saltzman, E., and Stievenard, M., 1999. Climate and atmospheric history of the past 420,000 years from the Vostok ice core, Antarctica. *Nature,* 399:429-436.

Petrushevskaya, M., 1967. Radiolaria in the plankton and Recent sediments from the Indian Ocean and Antarctic, in *The Micropalaeontology of the Oceans*, B. Funnell and W. Riedel (eds), pp. 319-330. Cambridge: Cambridge University Press 1971.

Pflaumann, U., Duprat, J., Pujol, C., and Labeyrie, L., 1996. SIMMAX: A modern analog technique to deduce Atlantic sea surface temperatures from planktonic foraminifera in deep-sea sediments. *Paleoceanography,* 11(1):15-35.

Pichon, J., Bareille, G., Labracherie, M., Labeyrie, L., Baudrimont, A., and Turon, J.-L., 1992. Quantification of biogenic silica distribution in Southern Ocean sediments. *Quaternary Research,* 37(3):361-378.

Pickard, G. and Emery, W., 1982. *Descriptive Physical Oceanography: an introduction.* 4th. Oxford: Pergamon Press pp. 247.

Pisias, N., Roelofs, A., and Weber, M., 1997. Radiolarian-based transfer functions for estimating mean surface ocean temperatures and seasonal range. *Paleoceanography,* 12(3):365-379.

Pisias, N., Martinson, D., Moore, C., Shackleton, N., Prell, W., Hays, G., and Boden, G., 1984. High resolution stratigraphic correlation of benthic oxygen isotope records spanning the last 300,000 years. *Marine Geology,* 56:119-136.

Pollard, R. and Read, J., 2001. Circulation pathways and transports of the Southern Ocean in the vicinity of the Southwest Indian Ridge. *Journal of Geophysical Research,* 106(C2):2881-2898.

Prell, W., Hutson, W., and Williams, D., 1979. The Subtropical Convergence and Late Quaternary Circulation in the Southern Indian Ocean. *Marine Micropaleontology,* 4:225-234.

Prell, W., Hutson, W., Williams, D., Bé, A., Geitzenauer, K., and Molfino, B., 1980. Surface circulation of the Indian Ocean during the Last Glacial Maximum, approximately 18,000 yr B.P. *Quaternary Research,* 14:309-336.

Quadfasel, D. and Cresswell, G., 1992. A note on the seasonal variability of the South Java Current. *Journal of Geophysical Research,* 97(C3):3685-3688.

Quadfasel, D., Frische, A., and Cresswell, G., 1996. The circulation in the source area of the South Equatorial Current in the eastern Indian Ocean. *Journal of Geophysical Research,* 101(C5):12483-12488.

R Development Core Team, 2008. 'R: A language and environment for statistical computing', *R Foundation for Statistical Computing, Vienna, Austria,* http://cran.ms.unimelb.edu.au/, accessed 18 December 2008.

Ragueneau, O., Tréguer, P., Leynaert, A., Anderson, R., Brzezinski, M., DeMaster, D., Dugdale, R., Dymond, J., Fischer, G., François, R., Heinze, C., Maier-Reimer, E., Martin-Jézéquel, V., Nelson, D., and Quéguiner, B., 2000. A review of the Si cycle in the modern ocean: recent progress and missing gaps in the application of biogenic opal as a paleoproductivity proxy. *Global and Planetary Change,* 26:317-365.

Renz, G., 1976. *The Distribution and Ecology of Radiolaria in the central Pacific: Plankton and Surface Sediments*. Bulletin of the Scripps Institution of Oceanography of the University of California. Berkley: University of California pp.

Ribbe, J., 2004. The southern supplier. *Nature,* 427:23-24.

Rickaby, R. and Elderfield, H., 1999. Planktonic foraminiferal Cd/Ca: Paleonutrients or Paleotemperature? *Paleoceanography,* 14(3):293-303.

Ridgway, K. and Condie, S., 2004. The 5500-km-long boundary flow off western and southern Australia. *Journal of Geophysical Research,* 109(C04017):1-18.

Ridgway, K. and Dunn, J., 2007. Observational evidence for a Southern Hemisphere oceanic supergyre. *Geophysical Research Letters,* 34(L13612):1-5.

Rintoul, S., Hughes, C., and Olbers, D., 2001. 4.6 The Antarctic Circumpolar Current System, in *Ocean circulation and climate, 77,* G. Siedler, J. Church and J. Gould (eds), pp. 271-302. San Diego: Academic Press.

Roden, G., 1975. On North Pacific Temperature, Salinity, Sound Velocity and Density Fronts and their Relation to the Wind and Energy Flux Fields. *Journal of Physical Oceanography,* 5(4):557-571.

Roemmich, D., 2007. Super spin in the southern seas. *Nature,* 449:34-35.

Rogers, J. and De Deckker, P., 2007. Radiolaria as a reflection of environmental conditions in the eastern and southern sectors of the Indian Ocean: A new statistical approach. *Marine Micropaleontology,* 65:137-162.

Salvignac, M.-E., 1998. *Variabilité hydrologique et climatique dans l'Océan Austral (secteur indien) au cours du Quaternaire terminal. Essai de corrélations inter-hémisphériques.*, Thèse de doctorat, Océanographie-Paléo-Océanographie, Université de Bordeaux I, Bordeaux.

Sanfilippo, A., Westberg-Smith, M., and Riedel, W., 1985. Cenozoic radiolaria, in *Plankton stratigraphy, 2: Radiolaria, diatoms, silicoflagellates, dinoflagellates, and ichthyoliths*, Paperback, H. Bolli, J. Saunders and K. Perch-Nielsen (eds), pp. 631-712. Cambridge: Cambridge University Press 1989.

Sarmiento, J. and Gruber, N., 2006. *Ocean Biochemical Dynamics*. Princeton: Princeton University Press pp. 503.

Sarmiento, J., Gruber, N., Brzezinski, M., and Dunne, J., 2004. High-latitude controls of thermocline nutrients and low-latitude biological productivity. *Nature,* 427(6969):56-60.

Schlitzer, R., 2005. 'Ocean Data View', http://www.awi.de, accessed 18 December 2008.

Sedwick, P., Bowie, A., and Trull, T., 2008. Dissolved iron in the Australian sector of the Southern Ocean (CLIVARSR3 section): Meridional and seasonal trends. *Deep-Sea Research I,* 55:911-925.

Sicre, M.-A., Labeyrie, L., Ezat, U., Duprat, J., Turon, J.-L., Schmidt, S., Michel, E., and Mazaud, A., 2005. Mid-latitude Southern Indian Ocean response to Northern Hemisphere Heinrich events. *Earth and Planetary Science Letters,* 240:724-731.

Smith, R., Huyer, A., Godfrey, J., and Church, J., 1991. The Leeuwin Current off Western Australia, 1986-1987. *Journal of Physical Oceanography,* 21:323-345.

Stramma, L., 1991. The South Indian Ocean Current. *Journal of Physical Oceanography,* 22:421-430.

Stuiver, M. and Reimer, P., 1993. Radiocarbon age calibration. *Radiocarbon,* 35:215-230.

Sugiyama, K. and Anderson, O.R., 1997. Experimental and observational studies of radiolarian physiological ecology, 6. Effects of silicate-supplemented seawater on the longevity and weight gain of spongiose radiolarians *Spongaster tetras* and *Dictyocoryne truncatum*. *Marine Micropaleontology,* 29:159-172.

Swanberg, N., 1983. The trophic role of colonial Radiolaria on oligotrophic oceanic enviroments. *Limnology and Oceanography,* 28(4):655-666.

Swanberg, N. and Anderson, O.R., 1985. The nutrition of radiolarians: Trophic activity of some solitary Spumellaria. *Limnology and Oceanography,* 30(3):646-652.

Swanberg, N. and Bjørklund, K., 1986. The radiolarian fauna of Western Norwegian fjords: patterns of abundance in the plankton. *Marine Micropaleontology,* 11:231-241.

---, 1992. The radiolarian fauna of western Norwegian fjords: a multivariate comparison of the sediment and plankton assemblages. *Micropaleontology,* 38(1):57-74.

Takahashi, K., 1991. *Radiolaria: flux, ecology, and taxonomy in the Pacific and Atlantic.* Ocean Biocoenosis Series No 3. Woods Hole, Ma: Woods Hole Oceanographic Institution pp.

Takahashi, K. and Okada, H., 2000. The paleoceanography for the last 30,000 years in the southeastern Indian Ocean by means of calcareous nannofossils. *Marine Micropaleontology,* 40:83-103.

Takahashi, K. and Yamashita, H., 2004. Temporal and vertical flux changes of radiolarians in the western and central equatorial Pacific during the 1999 La Niña conditions. *Journal of the Geological Society of Japan,* 110(8):463-479.

Takahashi, O., Yuasa, T., Honda, H., and Mayama, S., 2004. Molecular phylogeny of solitary shell-bearing Polycystinea (Radiolaria) *Revue de micropaléontologie,* 47(3):111-118.

Taylor, J. and Pearce, A., 1999. Ningaloo Reef Currents: implication for coral spawn dispersal, zooplankton, and whale shark abundance. *Journal of the Royal Society of Western Australia,* 82:57-65.

Tchernia, P., 1980. *Descriptive Regional Oceanography.* Oxford: Pergamon Press pp.

ter Braak, C. and Juggins, S., 1993. Weighted averaging partial least squares regression (WA-PLS): an improved method for reconstructing environmental variables from species assemblages. *Hydrobiologia,* 269/270:485-502.

ter Braak, C. and Verdonschot, P., 1995. Canonical correspondence analysis and related multivariate methods in aquatic ecology. *Aquatic Sciences,* 57(3):255-289.

ter Braak, C. and Šmilauer, P., 2004. 'Canoco for Windows 4.53'. Biometris - Plant Research International

ter Braak, C., Juggins, S., Birks, H., and van der Voet, H., 1993. Weighted averaging partial least squares regression (WA-PLS): definition and comparison with other methods for species-environment calibration, in *Multivariate Environmental Statistics, 6,* G. Patil and C. Rao (eds), pp. 525-560. Amsterdam: Elsevier Science Publishers.

Thompson, R., 1983. Observations of the Leeuwin Current off Western Australia. *Journal of Physical Oceanography,* 14:623-648.

Tomczak, M. and Godfrey, J., 2003. *Regional Oceanography: an introduction.* 2nd Edition. Delhi: Daya Publishing House pp. 390.

Toole, J. and Warren, B., 1993. A hydrographic section across the subtropical South Indian Ocean. *Deep-Sea Research I,* 40(10):1973-2019.

van de Paverd, P., 1995. *Recent Polycystine Radiolaria from the Snellius-II Expedition*, Published PhD thesis, Center for Marine Earth Science, Faculty of Earth Science, Free University, Amsterdam.

van der Kaars, S. and De Deckker, P., 2003. Pollen distribution in marine surface sediments offshore Western Australia. *Review of Palaeobotany and Palynology,* 124:113-129.

Venables, W. and Ripley, B., 2002. *Modern Applied Statistics with S.* New York: Springer-Verlag pp.

Vénec-Peyré, M.-T., Caulet, J.-P., and Grazzaini, C., 1995. Paleohydrographic changes in the Somali Basin (5°N upwelling and equatorial areas) during the last 160 kyr, based on correspondence analysis of foraminiferal and radiolarian assemblages. *Paleoceanography,* 10(3):473-491.

Vranes, K. and Gordon, A., 2005. Comparison of Indonesian Throughflow transport observations, Makassar Strait to eastern Indian Ocean. *Geophysical Research Letters,* 32:L10606/10601-10605.

Waelbroeck, C., Jouzel, J., Labeyrie, L., Lorius, C., Labracherie, M., Stiévenard, M., and Barov, N., 1995. A comparison of the Vostok ice deuterium record and series from Southern Ocean core MD-88-770 over the last two glacial-interglacial cycles. *Climate Dynamics,* 12:113-123.

Walker, G. and King, D., 2008. *The Hot Topic: how to tackle global warming and still keep the lights on.* London: Bloomsbury pp. 1-309.

Wang, R., Clemens, S., Huang, B., and Chen, M., 2003. Quaternary palaeoceanographic changes in the northern South China Sea (ODP 1146): radiolarian evidence. *Journal of Quaternary Science,* 18(8):745-756.

Welling, L., 2003. Polycystine radiolarian counts from 64 mym MOCNESS tows. Woods Hole Oceanographic Institution, USA. DOI:10.1594/PANGAEA.123365 accessed May 2008.

Whitehouse, M., Meredith, M., Rothery, P., Atkinson, A., Ward, P., and Korb, R., 2008. Rapid warming of the ocean around South Georgia, Southern Ocean, during the 20th century: Forcings, characteristics and implications for lower trophic levels. *Deep-Sea Research I,* 55:1218-1228.

Wijffels, S., Bray, N., Meyers, G., and Werner, M., 1996. The WOCE Indonesian Throughflow Repeat Hydrography Sections: I10 and IR6. *International WOCE Newsletter,* 24:25-28.

WOA05, 2005. 'World Ocean Atlas 2005', *National Oceanographic Data Center, National Oceanic and Atmospheric Administration,* http://www.nodc.noaa.gov/OC5/WOA05/, accessed September, 2008.

Wold, S., Ruhe, H., Wold, H., and Dunn, W., 1984. The collinearity problem in linear regression: the partial least squares (PLS) approach to generalized inverses. *SIAM Journal on Scientific and Statistical Computation,* 5:735-743.

Yamashita, H., Takahashi, K., and Fujitani, N., 2002. Zonal and vertical distribution of radiolarians in the western and central Equatorial Pacific in January 1999. *Deep-Sea Research II,* 49:2823-2826.

Young, M., 2006. *The distribution of organic- and calcareous-walled dinoflagellate cysts from the eastern Indian Ocean; a proxy for late Quaternary palaeo-oceanographic reconstructions*, Unpublished PhD thesis, Earth and Marine Sciences, The Australian National University, Canberra.

Yuasa, T., Takahashi, O., Honda, H., and Mayama, S., 2005. Phylogenetic analyses of the polycystine Radiolaria based on the 18s rDNA sequences of the Spumellarida and the Nassellarida. *European Journal of Protistology,* 41(4):287-298.

Zettler, L., Sogin, M., and Caron, D., 1997. Phylogenetic relationships between the *Acantharea* and the *Polycystinea*: A molecular perspective on Haeckel's *Radiolaria. Proceedings of the National Academy of Sciences, USA.,* 94:11411-11416.

Zettler, L., Anderson, O.R., and Caron, D., 1999. Towards a molecular phylogeny of colonial spumellarian radiolaria. *Marine Micropaleontology,* 36:67-69.

Appendix 1: Frequently observed species

The following 244 identified species were observed often enough to be included in the statistical analyses. The "Source" column indicates the source of the identification: if "*", the source is 'radiolaria.org' (Dolven, 2004). Images of the taxa appear in the Electronic Supplement.

Species	Source	Plate
Acanthodesmia vinculata Müller 1858	*	1.1
Acanthosphaera angulata Haeckel 1862	(Haeckel, 1887)	1.2
Acrobotrys cribosa Popofsky 1913	*	1.3
Acrosphaera australis Lazarus 1990	*	1.4
Acrosphaera murrayana Haeckel 1887	*	1.5
Acrosphaera spinosa Haeckel 1861	*	1.6
Actinomma antarcticum Haeckel 1887	*	1.7-9
Actinomma arcadophorum Haeckel 1887	(Takahashi, K., 1991)	1.10
Actinomma boreale Cleve (1899)	*	1.11
Actinomma circumtexta (Haeckel) van de Paverd 1995	(van de Paverd, 1995)	1.12
Actinomma delicatulum (Dogiel and Reschetnjak) 1952	*	1.13
Actinomma hastatum Haeckel 1887	(van de Paverd, 1995)	1.14
Actinomma leptoderma longispina Cortese and Bjørklund 1998	*	1.15
Actinomma medianum Nigrini 1967	*	1.16
Actinomma sol Cleve 1901	*	1.17
Actinomma sp aff. *trinacria* (Haeckel) 1860	*	1.19
Actinomma sp. det. Benson 2003	*	1.18
Actinosphaera acanthophora Popofsky 1912	*	1.20
Amphiplecta acrostoma Haeckel 1887	*	2.1
Amphirhopalum ypsilon Haeckel 1887	*	2.2
Amphispyris reticulata (Ehrenberg) Nigrini 1967	(Nigrini and Moore, 1979a)	2.3
Amphitholus acanthometra Haeckel 1887	*	2.4
Amphitholus spp. indet.		
Antarctissa spp. = *A. cylindrica* Petrushevskaya 1975 + *A. denticulata* (Ehrenberg) 1844	*	2.5 2.6-7
Antarctissa strelkovi Petrushevskaya 1975	*	2.8
Anthocyrtidium ophirense Ehrenberg 1872	*	2.9
Anthocyrtidium zanguebaricum Ehrenberg 1872	*	2.10
Anthocyrtium sp aff. *A. anthemis* Haeckel 1887	*	2.11
Arachnocorys umbellifera Haeckel 1862	*	2.12
Artostrobus annulatus (Bailey) 1856	*	2.13
Artostrobus joergenseni Petrushevskaya 1967	*	2.14
Artostrobus sp aff. *A. quadriporus* Bjørklund 1976	*	2.15
Axoprunum (?) monostylum Caulet 1986	*	2.16
Botryocampe sp cf *B. inflata* Bailey 1856	(Petrushevskaya, 1971)	2.17-18
Botryocyrtis scutum Harting 1863	*	2.19
Botryopyle dictyocephalus Haeckel 1887	(Petrushevskaya, 1971)	2.20
Botryostrobus aquilonaris Bailey 1856	*	3.1
Callimitra emmae Haeckel 1887	(Takahashi, K., 1991)	3.2
Calocyclas monumentum Haeckel 1887	*	3.3-4
Carpocanarium papillosum Ehrenberg 1872	*	3.5

Species	Source	Plate
Carpocanistrum sp. aff sp A Nigrini 1970	*	3.6
Carpocanium obliquum Haeckel 1862	(van de Paverd, 1995)	3.7-8
Carpocanium spp. indet		
Carposphaera melitomma Haeckel 1887	(van de Paverd, 1995)	3.9
Cenosphaera sp cf C. reticulata Haeckel 1860	*	3.11
Cenosphaera sp indet Benson 2003	*	3.10
Centrocubus sp. cf. C. octostylus Haeckel 1887	(Takahashi, K., 1991)	3.12
Ceratocyrtis galeus Cleve 1899	*	3.13
Ceratocyrtis histricosus (Jørgensen) 1905	*	3.14-5
Ceratocyrtis sp cf. *C. robustus* Bjørklund 1976	*	3.16
Ceratocyrtis sp cf. *C. mashae* Bjørklund 1976	*	3.17
Ceratospyris hyperborea Jørgensen 1905	*	3.18
Ceratospyris sp cf *C. borealis* Benson 1983	*	3.19
Circodiscus sp. (Stöhr) 1880	*	3.20
Cladococcus abietinus Haeckel 1887	*	4.1-2
Cladoscenium sp cf. C. ancoratum Haeckel 1887	*	4.3
Cladoscenium sp cf. C. *limbatum* Jørgensen 1905	*	4.4
Cladoscenium sp cf. *C. tricolpium* (Haeckel) 1887	*	4.5-8
Clathrocanium coarctatum Ehrenberg 1860	*	4.9
Clathrocanium spp.		
Clathrocircus ?stapedius Haeckel 1887	*	4.10
Clathrocorys murrayi Haeckel 1887	*	4.11
Clathromitra sp cf. *C. pterophormis* Haeckel 1887	*	4.12
Clinorhabdus sp.cf. *C. longithorax* (Petrushevskaya) 1975	*	4.13
Collosphaera huxleyi Müller 1855	(Takahashi, K., 1991)	4.14
Collosphaera invaginata (Haeckel) 1887	*	4.15
Collosphaera macropora Haeckel 1887	*	4.16
Collosphaera tuberosa Haeckel 1887 Nigrini 1971	*	4.17
Cornutella profunda Ehrenberg 1854	*	4.18
Coracalyptra cervus (Ehrenberg) 1872	*	4.19
Corocalyptra (=Clathrocyclas) sp.		
Corocalyptra craspedota (Jørgensen) 1900	*	4.20
Cubotholus octoceras Haeckel 1887	*	5.1
Cubotholus spp.		
Cycladophora bicornis (Popofsky) Lombari-Lazarus (1988)	*	5.2
Cycladophora davisiana Ehrenberg 1862	*	5.4-5
Cycladophora sp cf. *conica* Lombari and Lazarus 1988	*	5.3
Cypassis irregularis Nigrini 1968	*	5.6
Cyrtopera laguncula Haeckel 1887	*	5.7
Dictyocircus sp cf. *D. clathratus* (Jørgensen) 1905	* (archive plate)	5.8
Dictyocoryne profunda Ehrenberg 1886	*	5.9
Dictyocoryne truncatum (Ehrenberg 1861)	*	5.10
Dictyophimus bicornis (Ehrenberg)	(Petrushevskaya, 1971)	5.11-13
Dictyophimus crisiae Ehrenberg 1854	*	5.14-16
Dictyophimus hirundo (Haeckel) 1887	*	5.19
Dictyophimus histricosus Jørgensen 1905	*	5.17
Dictyophimus sp. cf. *D. tripus* Benson 1966	*	5.18
Didymocyrtis tetrathalamus (Haeckel) 1887	*	5.20
Diplosphaera sp cf. *D. hexagonalis* Haeckel 1887	(van de Paverd, 1995)	6.1
Dipylissa bensoni Dumitrica 1988	*	6.2-3

Species	Source	Plate
Druppatractus hastatus Blueford 1982	*	6.5
Druppatractus spp. with *Dorydruppa* spp.	*	6.4
Euchitonia elegans/furcata group Boltovskoy 1998	*	6.6
Euchitonia triangulum Ehrenberg 1872	*	6.7
Eucyrtidium acuminatum (Ehrenberg) 1844	*	6.8
Eucyrtidium annulatum (Popofsky) 1913	*	6.9
Eucyrtidium anomalum Haeckel 1861	*	6.10
Eucyrtidium cienkowskii Haeckel 1887	*	6.11
Eucyrtidium inflatum Kling 1973	(Kling, 1973)	6.14
Eucyrtidium sp. aff. *E. hexagonatum* Haeckel 1887	*	6.13
Eucyrtidium sp. cf. *E. erythromystax* Nigrini and Caulet 1992	*	6.12+6.16
Eucyrtidium sp. aff. *E. dictyopodum* Haeckel 1887	(van de Paverd, 1995)	6.15
Eucyrtidium teuscheri teuscheri Caulet 1986	*	6.17
Euscenium corynephorum Jørgensen 1900	*	6.18
Gondwanaria campanulaeformis (Campbell and Clark) 1944	*	6.19
Gondwanaria sp. indet.	*	6.20
Haliomma hexacanthum Müller 1858	(van de Paverd, 1995)	7.1
Haliomma hexagonum Ehrenberg 1854	(van de Paverd, 1995)	7.2
Heliodiscus asteriscus Haeckel 1887	*	7.3
Heliodiscus echiniscus Haeckel 1887	*	7.4
Helotholus sp. cf. *H. haysi* Lazarus 1992	*	7.5
Helotholus sp. cf. *H. vema* Hays 1965	*	7.6
Helotholus sp. indet.		
Hexacontium melpomene Haeckel 1887	*	7.7
Hexapyle dodecantha group Haeckel 1887	*	7.8
Hexastylus dimensivus Haeckel 1887	*	7.9
Lamprocyclas maritalis Haeckel 1887 *maritalis* Nigrini 1967	(Nigrini and Moore, 1979a)	7.10
Lamprocyclas maritalis Haeckel 1887 *polypora* Nigrini 1967	(Nigrini and Moore, 1979a)	7.11
Lamprocyrtis hannai (Campbell and Clark) Kling 1973	(Nigrini and Moore, 1979a)	7.12
Lamprocyrtis nigriniae Caulet 1971	*	7.13
Lampromitra quadricuspis Haeckel 1887	*	7.14-15
Lampromitra sp. aff. *L. latonae* Takahashi 1991	*	7.16
Larcopyle hayesi (Chen) 1975	*	7.17
Larcospira sp.	new species?	7.18
Larcopyle polyacantha titan Lazarus *et al* 2005	*	7.20
Larcospira quadangulata Haeckel 1887	*	7.19
Larcospira sp. Bjørklund *et al.* 1998	*	8.1
Lipmanella bombus (Haeckel) 1887	*	8.2
Lipmanella dictyoceras (Haeckel) 1861	*	8.3
Litharachnium sp cf. *L. tentorium* Haeckel 1862	*	8.4
Lithelius minor Jorgensen 1889	(Nigrini and Moore, 1979a)	8.5-8
Lithelius nautiloides Popofsky 1908	(Nigrini and Moore, 1979a)	8.9
Lithocampe platycephala (Ehrenberg) 1873	*	8.10-11
Lithomelissa araneosa Haeckel 1887	(van de Paverd, 1995)	8.12
Lithomelissa hystrix Jørgensen (1900)	*	8.13
Lithomelissa setosa Jørgensen 1900	*	8.15
Lithomelissa sp. cf. *L .laticeps* Jørgensen 1905	*	8.14
Lithomelissa sp. cf. *L. thoracites* Haeckel 1862	*	8.16
Lithopera bacca Ehrenberg 1872	*	8.17
Lithostrobus cuspidatus (Bailey) 1856	*	8.18

Species	Source	Plate
Lithostrobus hexagonalis Haeckel 1887	*	8.19
Lophophaena bütschlii (Haeckel) Petrushevskaya 1971	*	8.20
Lophophaena sp. cf. *L. capito* Ehrenberg 1874	(Takahashi, K., 1991)	9.4-5
Lophophaena hispida Ehrenberg 1872	*	9.1-2
Lophophaena nadezdae Petrushevskaya 1971	*	9.3
Lophophaena variabilis Petrushevskaya 1971	*	9.6
Lophophaena witjazii Petrushevskaya 1971	*	9.7-8
Lophospyris pentagona pentagona (Ehrenberg) Goll 1976	*	9.9
Lophospyris pentagona quadriforis (Haeckel), emend. Goll 1976	*	9.10
Mitrocalpis araneafera Popofsky 1908	*	9.11
Neosemantis distephanus distephanus Goll 1979	*	9.12
Nephrospyris renilla Haeckel 1887	*	9.13
Otosphaera polymorpha Haeckel 1887	(Takahashi, K., 1991)	9.14
Pentapylonium implicatum Dumitrica 1991	*	9.15
Peridium longispinum Jørgensen 1900	*	9.16
Peridium sp. cf. *P. longispinum* Benson 1966	*	9.17
Peripyramis circumtexta Haeckel 1887	*	9.18
Peromelissa sp. cf. *P. thoracites scaphopodium* (Haeckel) 1862	(van de Paverd, 1995)	9.19
Phormacantha sp. aff. *P. hystrix* (Jørgensen) 1905	*	9.20/10.1
Phormospyris sp. cf. *P. ophirensis* Ehrenberg *1872*	*	10.2
Phormospyris stabilis scaphipes (Haeckel) 1887	*	10.3
Phormospyris stabilis stabilis Goll 1976	*	10.4
Phormostichoartus corbula Harting 1863	*	10.5
Phormostichoartus sp.aff. *P. caryoforma* (Caulet) 1992		10.6
Phorticium circumtextum group Haeckel 1887	(van de Paverd, 1995)	10.7
Phorticium octopyle (Haeckel 1887)	(van de Paverd, 1995)	10.8
Phorticium pylonium Haeckel 1887	*	10.9-10
Plectacantha oikiskos (Jørgensen) 1905	*	10.11-12
Plectacantha sp. Benson 1966 (5-29)	*	10.13
Plectacantha trichoides (Jørgensen 1905)	*	10.14
Plectopyramis dodecomma Haeckel 1887	*	10.15
Plegmosphaera exodictyon Haeckel 1887	(Haeckel, 1887)	10.16
Plegmosphaera pachyplegma Haeckel 1887	(Haeckel, 1887)	10.17
Polysolenia lappacea Nigrini 1967	(Nigrini and Moore, 1979a)	10.18
Prunopyle sp B Abelmann 1990	(Abelmann, 1990)	10.19
Prunopyle tetrapila Hays 1965	*	10.20
Pseudocubus obeliscus Haeckel 1887	*	11.1
Pseudodictyophimus gracilipes (Bailey) 1856	*	11.2
Pseudodictyophimus platycephalus (Haeckel) 1887	*	11.3
Pterocanium praetextum eucolpum Haeckel 1887	*	11.4
Pterocanium praetextum praetextum (Ehrenberg) 1872	*	11.5
Pterocanium sp. cf. *P. auritum* Nigrini and Caulet 1992	*	11.6
Pterocanium sp. cf. *P. elegans* Haeckel 1887	*	11.7
Pterocanium trilobum (Haeckel) 1861	*	11.8
Pterocorys zancleus (Müller) 1855	*	11.9
Saccospyris antarctica Haecker 1907	*	11.10-12
Saturnalis circularis Haeckel 1887	*	11.13
Sethoconus tabulatus (Ehrenberg) 1873	*	11.14
Sethophormis pentalactis Haeckel 1887	*	11.15
Sethophormis rotula Haeckel 1887	*	11.16-17

Species	Source	Plate
Sethophormis spp. indet		
Siphocampe arachnea (Ehrenberg) 1838	(Takahashi, K., 1991)	11.18
Siphonosphaera magnisphaera Takahashi 1990	*	11.19
Siphonosphaera martensi Brandt 1905	(Takahashi, K., 1991)	11.20
Siphonosphaera polysiphonia (Haeckel 1887) Nigrini 1967	(Nigrini and Moore, 1979a)	12.1
Sphaeropyle langii Dreyer 1889	*	12.2
Sphaerozoum punctatum Müller 1858	*	12.3
Spirocyrtis scalaris Haeckel 1887	*	12.4
Spongaster pentas Riedel and Sanfilippo 1991	(Takahashi, K., 1991)	12.5
Spongaster tetras Ehrenberg 1860	*	12.6
Spongocore puella Haeckel 1887	*	12.7
Spongodiscus anomalus (Popofsky 1912)		12.8
Spongodiscus biconcavus Haeckel 1887	*	12.9
Spongodiscus sp.		12.10
Spongoplegma rugosa Hollande and Enjumet 1960	(Boltovskoy, 2005)	12.11-12
Spongopyle osculosa Dreyer 1889	*	12.13
Spongosphaera polyacantha Müller 1857	*	12.14-17
Spongotrochus glacialis Popofsky 1908	*	12.18
Spongurus pylomaticus Riedel 1958	(Nigrini and Moore, 1979a)	12.19-20
Stichocorys sp. aff. *S. peregrina* (Riedel) 1953	*	13.1
Stichocorys sp. aff. *S. seriata* Jørgensen 1905	*	13.2
Stichopilium bicorne Haeckel 1887	*	13.3
Stylatractus neptunus Haeckel 1887	*	13.4
Stylatractus pluto Haeckel 1887	*	13.5
Stylatractus sp. aff. *S. hispida*	*	13.6
Stylatractus sp. cf. *S. universus* Hays	(Lazarus, 1990)	13.7
Stylatractus spp.		
Stylochlamydium venustum (Bailey) 1856	*	13.8
Stylodictya aculeata Jørgensen 1905	*	13.9-11
Stylodictya validispina Jørgensen 1905	*	13.12-13
Stylosphaera coronata laevis Ehrenberg 1873	*	13.14
Stylosphaera sp. aff. *S. radiosa* Ehrenberg 1854	*	13.15
Styptosphaera sp. aff. *S. spumacea* Haeckel 1887	*	13.16
Tetrapyle larnacilla (Haeckel 1887)	(van de Paverd, 1995)	13.17
Tetrapyle octacantha Müller 1858	*	13.18-19
Theocorythium trachelium Ehrenberg 1872	*	13.20
Theopilium tricostatum Haeckel 1887	*	14.1
Tholospironium cervicorne Haeckel 1887	(van de Paverd, 1995)	14.2-3
Tholospyris baconiana baconiana Goll 1972	*	14.4
Tholospyris devexa Goll 1969	*	14.5
Tholospyris ramosa Haeckel 1887	(Takahashi, K., 1991)	14.6
Tholospyris sp. cf. *T. gephyristes* Hülsemann 1963	*	14.7
Tholospyris sp.	*	14.8
Tholospyris tripodiscus Haeckel 1887	(Boltovskoy, 2005)	14.9
Triceraspyris antarctica (Haecker) 1907	*	14.10
Tripospyris angulata Popofsky 1913	(Petrushevskaya, 1971)	14.11
Trisolenia megalactis megalactis Bjørklund & Goll 1979	*	14.12-13
Trisolenia zanguebarica Ehrenberg 1872	(van de Paverd, 1995)	14.14
Trisulcus triacanthus Popofsky 1913	(van de Paverd, 1995)	14.15
Zygocircus productus Goll 1979	*	14.16

Sources:

Abelmann, A., 1990. Oligocene to Middle Miocene Radiolarian stratigraphy of Southern High Latitudes from Leg 113, Sites 689 and 690, Maud Rise, in *Proceedings of the Ocean Drilling Program, 113*, P. Barker (ed.), pp. 675-708.

Boltovskoy, D., 2005. Zooplankton of the South Atlantic Ocean. ETI Bioinformatics. CD.

Dolven, J., 2004. 'Radiolaria.org', http://www.radiolaria.org, accessed frequently.

Haeckel, E., 1887. 'Report on the Radiolaria collected by H.M.S. Challenger. Vol. XVIII - Zoology', *Her Majesty's Stationery Office,* http://caliban.mpiz-koeln.mpg.de/~stueber/haeckel/challenger/index.htm, accessed 2005-present.

Kling, S., 1973. Radiolaria from the Eastern North Pacific, Deep Sea Drilling Project, Leg 18., in *Initial Reports of the DSDP, 18* L. D. Kulm (ed.), pp. 617-671. U.S. Government Printing Office.

Lazarus, D., 1990. Middle Miocene to recent radiolarians from the Weddell Sea, Antarctica, ODP Leg 113, in *Proceedings of the Ocean Drilling Program, 113*, P. F. Barker (ed.), pp. 709-727.

Nigrini, C. and Moore, T.C., 1979. 'A Guide to Modern Radiolaria (online)', *Cushman Foundation for Foraminiferal Research Inc.,* http://gdcmp1.ucsd.edu/geol_coll/radlit/nm79titl.html, accessed January 2004.

Petrushevskaya, M., 1971. *Nassellarian Radiolarians in the Plankton of the World Ocean.* Explorations of the fauna of the seas, IX (XVII). Leningrad: Academy of Sciences of the USSR, Institute of Zoology pp. 1-294 + Appendix pp. 374-397.

Takahashi, K., 1991. *Radiolaria: flux, ecology, and taxonomy in the Pacific and Atlantic.* Ocean Biocoenosis Series No 3. Woods Hole, Ma: Woods Hole Oceanographic Institution pp.

van de Paverd, P., 1995. *Recent Polycystine Radiolaria from the Snellius-II Expedition,* Published PhD thesis, Center for Marine Earth Science, Faculty of Earth Science, Free University, Amsterdam.

Appendix 2: Rarely observed species

The following 88 species were identified but were too rarely observed to be included in the statistical analyses. Where available, images appear in the Electronic Supplement of both these and those taxa which could not be identified. In general, none of the taxa listed here were observed more than once or twice in the approximately 150,000 specimens counted during this study. An asterisk in the column marked "Source" indicates the identification was obtained through 'radiolaria.org' (Dolven, 2004): otherwise the source is referenced.

Species	Source
Acanthosphaera dodecastyla Mast	* (archive)
Acanthosphaera macropora Haeckel 1887	*
Acanthosphaera sp aff. *A. pinchuda*	(Boltovskoy, 2005)
Acrobotrys sp cf. *A. teralans* Renz 1976	*
Actinomma ?magnifenestra Lazarus 1992	*
Actinomma leptoderma (Jørgensen) 1900	*
Actinomma medusa? (Ehrenberg) 1844	*
Actinomma sp cf *A. holtedahli* Bjørklund 1976	*
Amphimelissa sp cf. *A. setosa* (Cleve) 1899	*
Amphisphaera sp cf. *A. cristata* Carnevale 1908	*
Amphistylus sp.cf. *A. angelinus* (Campbell and Clark) 1944	*
Amphymenium sp aff. *A.challengerae* Weaver 1983	*
Androcyclas gamphonycha (Jørgensen) 1900	*
Androspyris sp aff. *A. reticulidisca* Takahashi 1991	(Takahashi, 1991)
Anomalacantha sp cf. A. *dentata* (Mast) 1910	*
Antarctissa cylindrica Petrushevskaya 1975	*
Antarctissa longa? (Popofsky)	(Boltovskoy, 2005)
Antarctissa whitei Bjørklund 1976	*
Arachnocalpis sp. Haeckel 1881	(Takahashi, 1991)
Arachnocorys sp cf. *A. dubius* Dogiel	(Petrushevskaya, 1971)
Artopilium undulatum Popofsky 1913	*
Botryocampe conythorax (Petrushevskaya)	(Petrushevskaya, 1971)
Botryocampe inflata (Bailey) 1856	*
Botryocyrtis quinaria(?) Ehrenberg 1872	*
Campylacantha sp cf *C. cladophora* Jørgensen 1905	*
Cannosphaera sp aff. *C. geometrica* Bogert 1901	*
Carposphaera sp cf. *C. subbotinae* (Borisenko) 1958	*
Centrobotrys thermophila Petrushevskaya	(Takahashi, 1991)
Cladococcus cervicornis Haeckel 1862	*
Collosphaera huxleyi with pylom	new species?
Corocalyptra kruegeri Popofsky 1913	
Corocalyptra murrayi Popofsky 1908	
Corythomelissa sp aff *C. horrida* Petrushevskaya 1975	*
Cycladophora sp cf. *C. humerus* (Petrushevskaya) 1975	*
Cyrtocapsella sp. aff. *C. cornuta* Haeckel 1887	*
Dictyophimus platycephalus Haeckel 1887	*
Dictyophimus sp cf. *D. killmari* (Renz) 1974	*
Dictyophimus sp aff. *D. mawsoni* Riedel 1958	*
Druppatractus multihasta	
Druppatractus sp aff D. irregularis	*
Druppatractus variabilis	*
Eucyrtidium sp cf. *E. hexastichum* (Haeckel) 1887	(Takahashi, 1991)
Hexacontium gigantheum Cortese and Bjørklund 1998	*
Hexalonche pythagorea Haeckel 1887	
Hexacontium sp cf *H.pachydermum* Jørgensen 1900	*

Species	Source
Hexastylus sp cf. *H. triaxonius* Haeckel 1887	*
Lamprocyrtis sp cf *L. heteroporos*	*
Lampromitra spinosiretis Takahashi 1991	(Takahashi, 1991)
Larcopyle bütschlii Dreyer 1889	*
Larcopyle titan (Campbell and Clark) 1944	*
Lipmanella sp cf *L. xiphephorum*	*
Lithomelissa pentacantha (Popofsky) 1913	*
Lophophaena sp cf. *L. araneosa* (Haeckel 1887)	(van de Paverd, 1995)
Lophospyris dictyopus (Haeckel 1881)	(van de Paverd, 1995)
Lophospyris sp cf *L. damaecornis* (Haeckel 1887)	(van de Paverd, 1995)
Octodendron cubocentron Haeckel 1887	2
Peromelissa sp. cf. P. phalacra (Haeckel 1887)	*
Phormospyris stabilis Goll 1976 forma novum	new species?
Phormostichoartus pitomorphus Caulet 1986	*
Phorticium group Haeckel 1887	
Plegmosphaera entodictyon Haeckel 1887	(Takahashi, 1991)
Prunopyle sp cf. *P. frakesi* Chen 1975	*
Prunopyle sp cf. *P. hayesi* Chen 1975	*
Prunopyle sp cf. *P. titan* Chen 1975	*
Pseudocubus sp cf. *P. warreni* Goll 1980	*
Pseudodictyophimus sp.aff. *P. cienkowskii* (Haeckel) 1887	(van de Paverd, 1995)
Pterocanium sp cf *P. grandiporus* Nigrini, 1968	(Takahashi, 1991)
Pterocanium sp cf *P. prismaticum* Riedel 1957	*
Pterocorys sp cf *P. clausus* (Popofsky) 1913	*
Pterocorys sp aff. *P. hirundo* Haeckel 1887	*
Pterocorys sp cf *P. longicollis* Caulet 1986	*
Pterocorys sp cf. *P. minythorax* (Nigrini) 1968	*
Rhizoplegma boreale (Cleve) 1899	*
Sethoconus anthocyrtis Haeckel 1887	(van de Paverd, 1995)
Sethophormis aurelia Haeckel 1887	(van de Paverd, 1995)
Siphocampe lineata (Ehrenberg) 1838	*
Solenosphaera zanguebarica (Ehrenberg)	(Boltovskoy, 2005)
Sphaeropyle sp aff. *S. robusta* Kling 1973	*
Spongodiscus sp cf. *S. resurgens* Ehrenberg 1854	*
Spongodrymus sp.	(van de Paverd, 1995)
Spongurus sp. cf. *S. elliptica* Ehrenberg 1872	*
Stylacontarium sp cf. *S. bispiculum* Popofsky 1912	*
Stylatractus cronos (Haeckel) 1887	*
Stylatractus sp cf. *S. santaeannae* (Campbell and Clark) 1944	*
Theocorys sp cf *T. veneris* Haeckel 1887	*
Tripospyris tricostata (Haeckel 1887)	(van de Paverd, 1995)
Udan sp aff. *U. undulata* Renz 1976	
Verticillata hexacantha Popofsky 1913	*

Sources

Boltovskoy, D., 2005. Zooplankton of the South Atlantic Ocean. ETI Bioinformatics. CD.

Dolven, J., 2004. 'Radiolaria.org', http://www.radiolaria.org, accessed frequently.

Petrushevskaya, M., 1971. *Nassellarian Radiolarians in the Plankton of the World Ocean.* Explorations of the fauna of the seas, IX (XVII). Leningrad: Academy of Sciences of the USSR, Institute of Zoology pp. 1-294 + Appendix pp. 374-397.

Takahashi, K., 1991. *Radiolaria: flux, ecology, and taxonomy in the Pacific and Atlantic.* Ocean Biocoenosis Series No 3. Woods Hole, Ma: Woods Hole Oceanographic Institution pp.

van de Paverd, P., 1995. *Recent Polycystine Radiolaria from the Snellius-II Expedition*, Published PhD thesis, Center for Marine Earth Science, Faculty of Earth Science, Free University, Amsterdam.

Plain black scale bars are 100 microns; chequered bars are 50 microns.

Plate 1

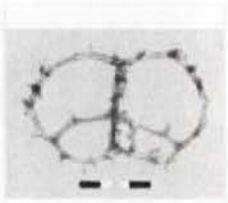

1. *Acanthodesmia vinculata*

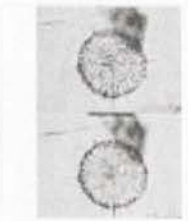

2. *Acanthosphaera angulata*

3. *Acrobotrys cribosa*

4. *Acrosphaera australis*

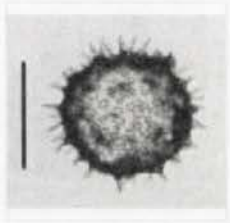

5. *Acrosphaera murrayana*

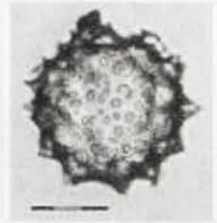

6. *Acrosphaera spinosa*

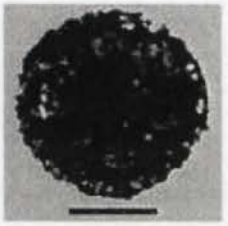

7. *Actinomma antarcticum*

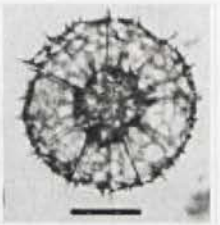

8. *Actinomma antarcticum*

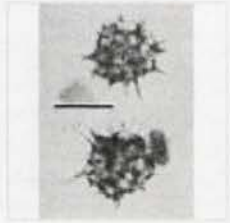

9. *Actinomma antarcticum*
- medullar shells

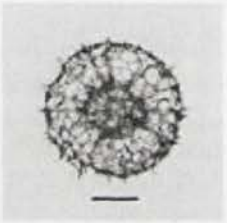

10. *Actinomma arcadophorum*

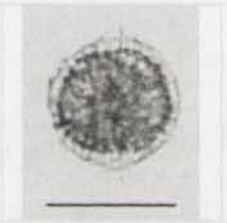

11. *Actinomma boreale*

12. *Actinomma circumtexta*

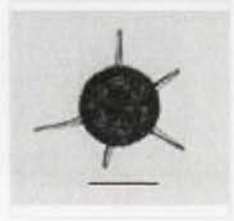

13. *Actinomma delicatulum*

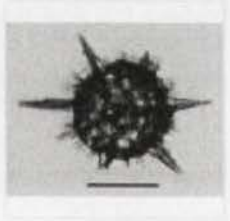

14. *Actinomma hastatum*

15. *Actinomma leptoderma longispina*

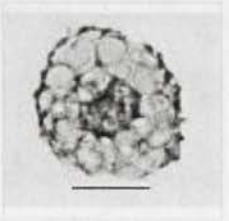

16. *Actinomma medianum*

17. *Actinomma sol*

18. *Actinomma* sp. B (Abelmann 1990)

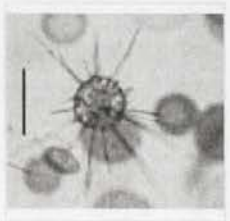

19. *Actinomma* sp aff. *A. trinacria*

20. *Actinosphaera acanthophora*

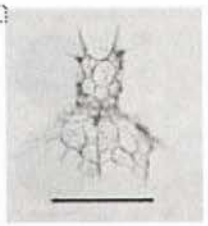

1. *Amphiplecta acrostoma*

2. *Amphirhopalum ypsilon*

3. *Amphispyris reticulata*

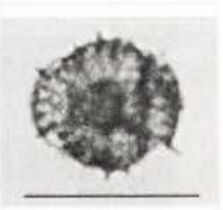

4. *Amphitholus acanthometra*

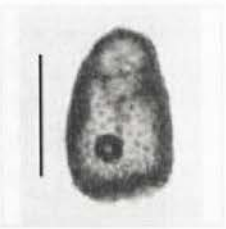

5. *Antarctissa cylindrica*

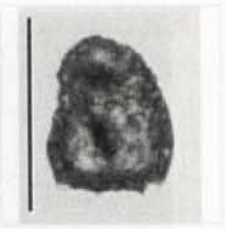

6. *Antarctissa denticulata*

7. *Antarctissa denticulata*

8. *Antarctissa strelkovi*

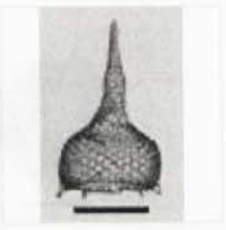

9. *Anthocyrtidium ophirense*

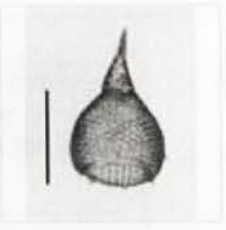

10. *Anthocyrtidium zanguebaricum*

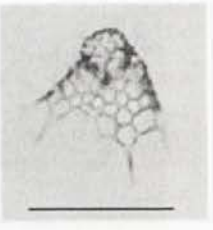

11. *Anthocyrtium* sp aff. *A. anthemis*

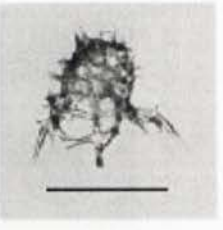

12. *Arachnocorys umbellifera*

13. *Artostrobus annulatus*

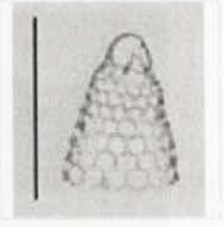

14. *Artostrobus joergenseni*

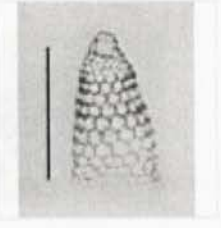

15. *Artostrobus* sp aff. *A. quadriporus*

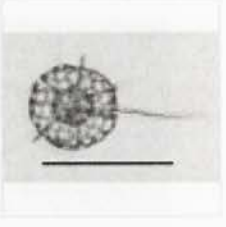

16. *Axoprunum (?) monostylum*

17. *Botryocampe* sp cf *B. inflata*

18. *Botryocampe* sp cf *B. inflata*

19. *Botryocyrtis scutum*

20. *Botryopyle dictyocephalus*

1. *Botryostrobus aquilonaris*

2. *Callimitra emmae*

3. *Calocyclas monumentum*

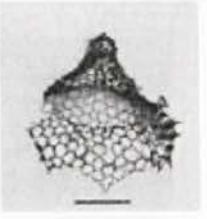

4. *Calocyclas monumentum*

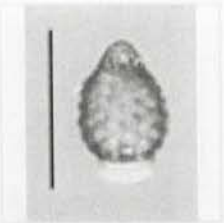

5. *Carpocanarium papillosum*

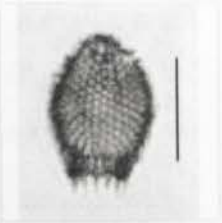

6. *Carpocanistrum* sp. aff sp A Nigrini

7. *Carpocanium obliquum*

8. *Carpocanium obliquum*

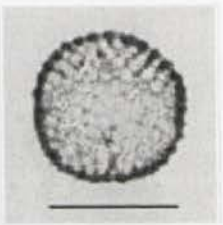

9. *Carposphaera melitomma*

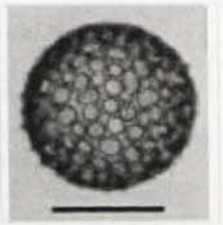

10. *Cenosphaera* sp indet Benson 2003

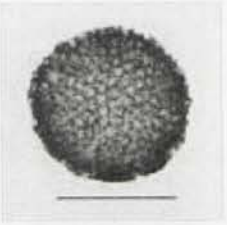

11. *Cenosphaera* sp cf *C. reticulata*

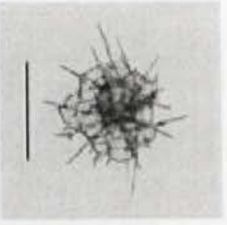

12. *Centrocubus* sp. cf. *C. octostylus*

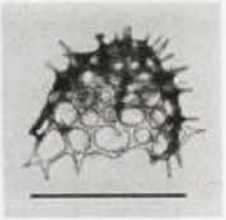

13. *Ceratocyrtis galeus*

14. *Ceratocyrtis histricosus*

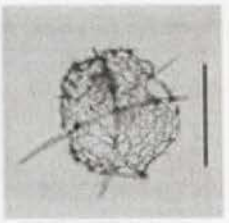

15. *Ceratocyrtis histricosus*

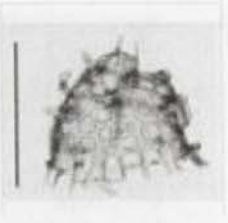

16. *Ceratocyrtis* sp cf. *C. robustus*

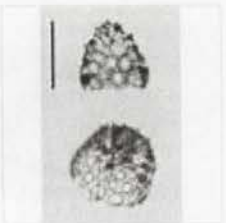

17. *Ceratocyrtis* sp cf. *C. mashae*

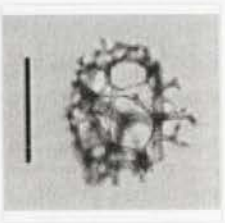

18. *Ceratospyris hyperborea*

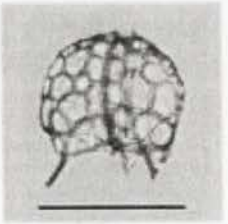

19. *Ceratospyris* sp cf *C. borealis*

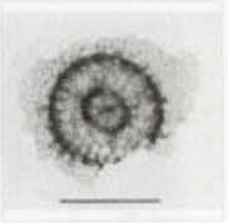

20. *Circodiscus* sp.

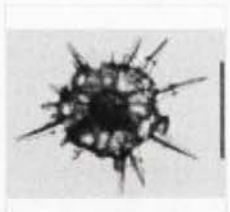

1. *Cladococcus abietinus*

2. *Cladococcus abietinus*

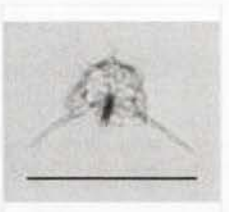

3. *Cladoscenium* sp cf. *C. ancoratum*

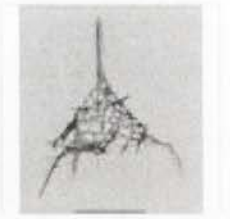

4. *Cladoscenium* sp cf. *C. limbatum*

5. *Cladoscenium* sp cf. *C. tricolpium*

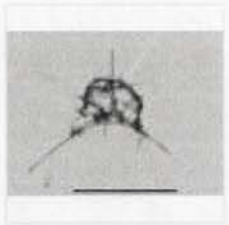

6. *Cladoscenium* sp cf. *C. tricolpium*

7. *Cladoscenium* sp cf. *C. tricolpium*

8. *Cladoscenium* sp cf. *C. tricolpium*

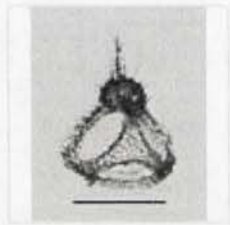

9. Clathrocanium *coarctatum*

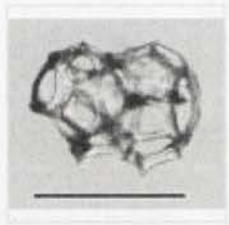

10. Clathrocircus *?stapedius*

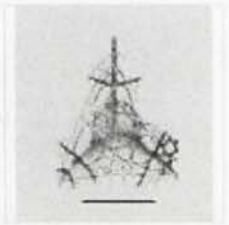

11. Clathrocorys *murrayi*

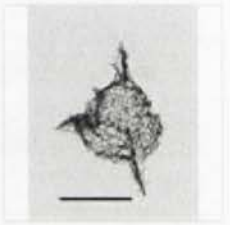

12. Clathromitra sp cf. *C. pterophormis*

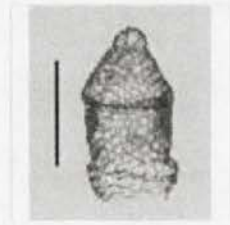

13. *Clinorhabdus* sp. cf. *C. longithorax*

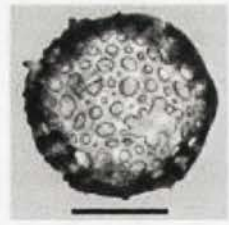

14. *Collosphaera huxleyi*

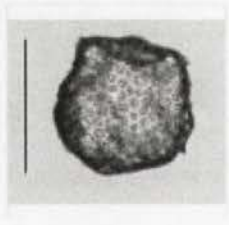

15. *Collosphaera invaginata*

16. *Collosphaera macropora*

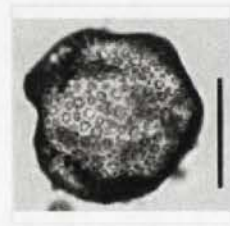

17. *Collosphaera tuberosa*

18. *Cornutella profunda*

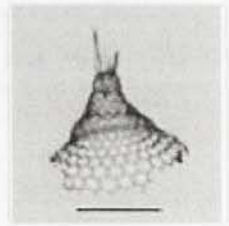

19. *Coracalyptra cervus*

20. *Corocalyptra craspedota*

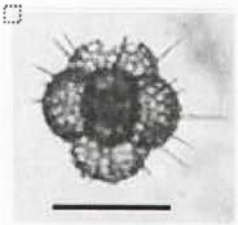

1. *Cubotholus octoceras*

2. *Cycladophora bicornis*

3. *Cycladophora* sp cf. *conica*

4. *Cycladophora davisiana*

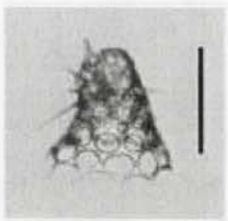

5. *Cycladophora davisiana*

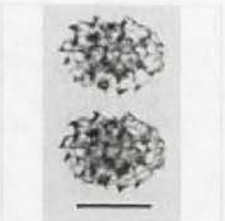

6. *Cypassis irregularis*

7. *Cyrtopera laguncula*

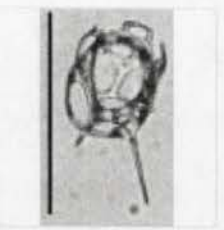

8. *Dictyocircus* sp cf. *D. clathratus*

9. *Dictyocoryne profunda*

10. *Dictyocoryne truncatum*

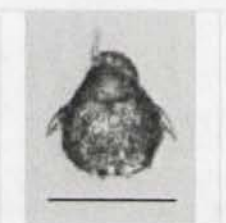

11. *Dictyophimus bicornis*

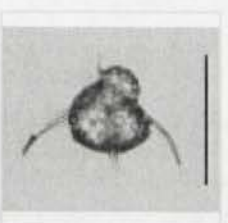

12. *Dictyophimus bicornis*

13. *Dictyophimus bicornis*

14. *Dictyophimus crisiae*

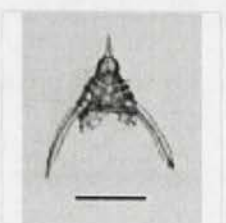

15. *Dictyophimus crisiae*

16. *Dictyophimus crisiae*

17. *Dictyophimus histricosus*

18. *Dictyophimus* sp. cf. *D. tripus*

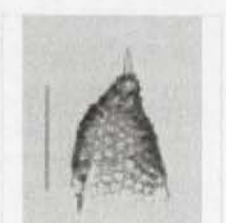

19. *Dictyophimus hirundo*

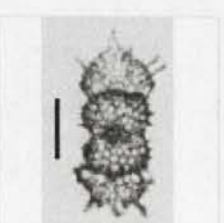

20. *Didymocyrtis tetrathalamus*

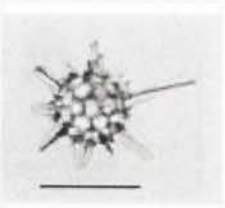

1. *Diplosphaera* sp cf. *D. hexagonalis*

2. *Dipylissa bensoni*

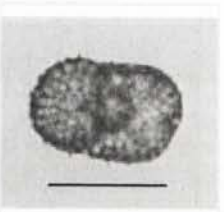

3. *Dipylissa bensoni*

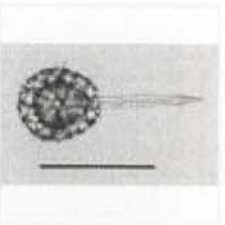

4. *Dorydruppa bensoni*

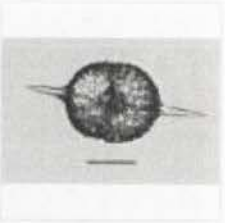

5. *Druppatractus hastatus*

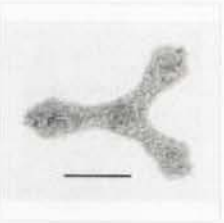

6. *Euchitonia elegans -furcata* group

7. *Euchitonia triangulum*

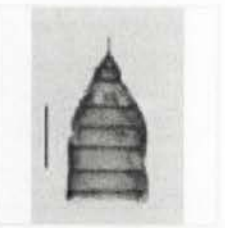

8. *Eucyrtidium acuminatum*

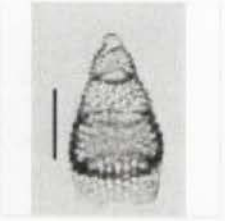

9. *Eucyrtidium annulatum*

10. *Eucyrtidium anomalum*

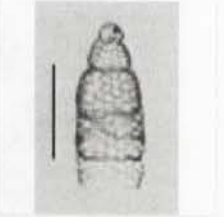

11. *Eucyrtidium cienkowskii*

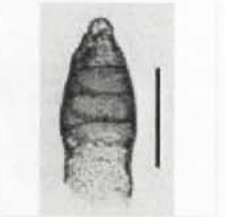

12. *Eucyrtidium* sp. cf. *E. erythromystax*

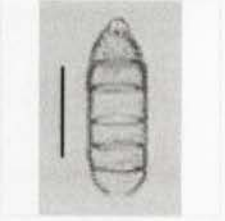

13. *Eucyrtidium* sp. aff. *E. hexagonatum*

14. *Eucyrtidium inflatum*

15. *Eucyrtidium* sp. aff. *E. dictyopodum*

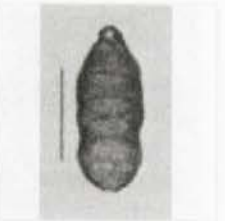

16. *Eucyrtidium* sp. aff. *E. erythromystax*

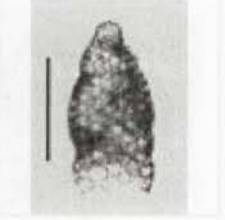

17. *Eucyrtidium teuscheri teuscheri*

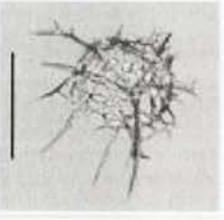

18. *Euscenium corynephorum*

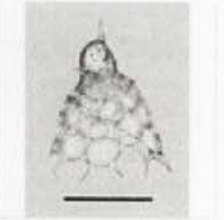

19. *Gondwanaria campanulaeformis*

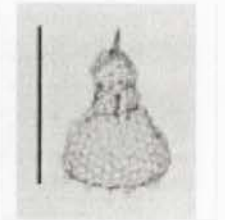

20. *Gondwanaria* sp. indet.

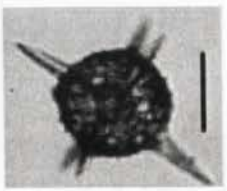

1. *Haliomma hexacanthum*

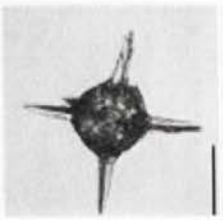

2. *Haliomma hexagonum*

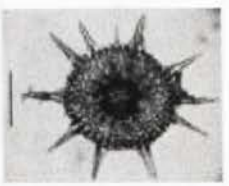

3. *Heliodiscus asteriscus*

4. *Heliodiscus echiniscus*

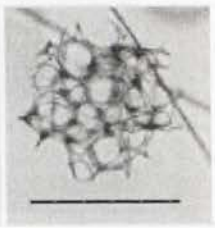

5. *Helotholus* sp. cf. *H. haysi*

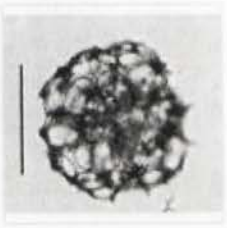

6. *Helotholus* sp. cf. *H. vema*

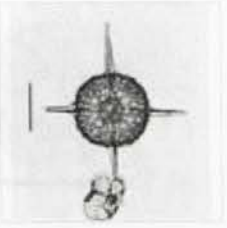

7. *Hexacontium melpomene*

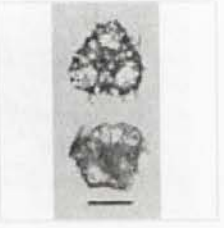

8. *Hexapyle dodecantha* group

9. *Hexastylus dimensivus*

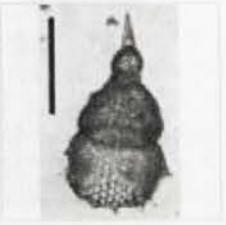

10. *Lamprocyclas maritalis maritalis*

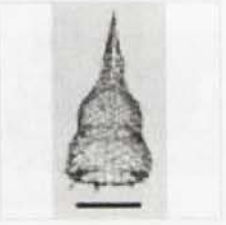

11. *Lamprocyclas maritalis polypora*

12. *Lamprocyrtis hannai*

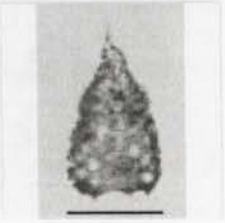

13. *Lamprocyrtis nigriniae*

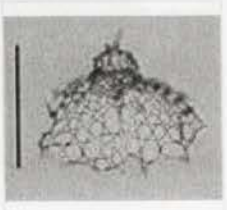

14. *Lampromitra quadricuspis*

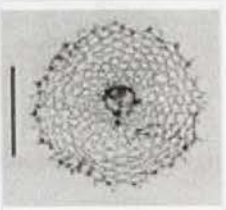

15. *Lampromitra quadricuspis*

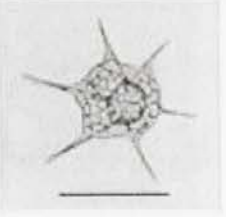

16. *Lampromitra* sp. aff. *L. latonae*

17. *Larcopyle hayesi*

18. *Larcospira* sp. (new species?)

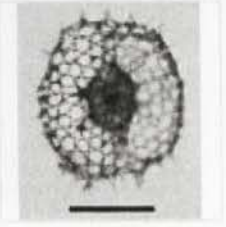

19. *Larcospira quadangula*

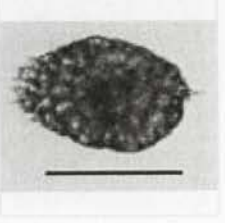

20. *Larcopyle polyacantha titan*

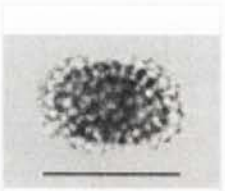

1. *Larcospira sp.* Bjørklund *et al.* 1998

2. *Lipmanella bombus*

3. *Lipmanella dictyoceras*

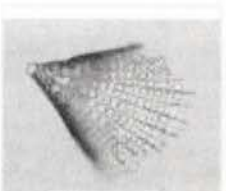

4. *Litharachnium* sp. cf. *L. tentorium*

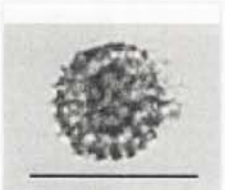

5. *Lithelius minor*

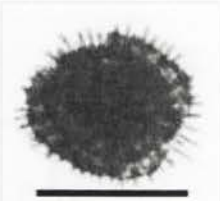

6. *Lithelius minor*

7. *Lithelius minor*

8. *Lithelius minor*

9. *Lithelius nautiloides*

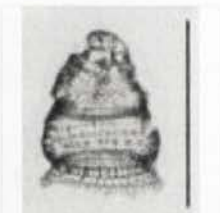

10. *Lithocampe platycephala*

11. *Lithocampe platycephala*

12. *Lithomelissa araneosa*

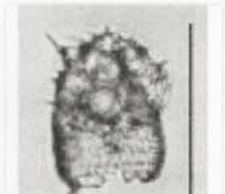

13. *Lithomelissa hystrix*

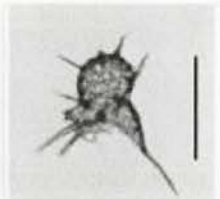

14. *Lithomelissa* sp. cf. *L .laticeps*

15. *Lithomelissa setosa*

16. *Lithomelissa* sp. cf. *L. thoracites*

17. *Lithopera bacca*

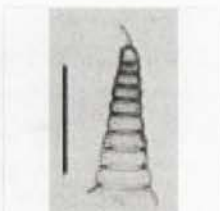

18. *Lithostrobus cuspidatus*

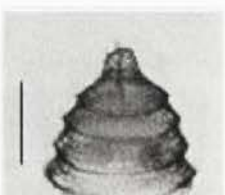

19. *Lithostrobus hexagonalis*

20. *Lophophaena bütschlii*

1. *Lophophaena hispida*

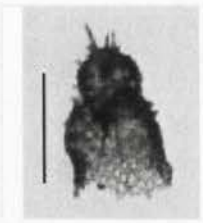

2. *Lophophaena hispida*

3. *Lophophaena nadezdae*

4. *Lophophaena* sp. cf. *L. capito*

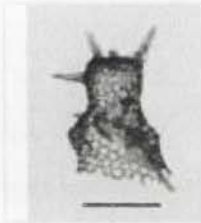

5. *Lophophaena* sp. cf. *L. capito*

6. *Lophophaena variabilis*

7. *Lophophaena witjazii*

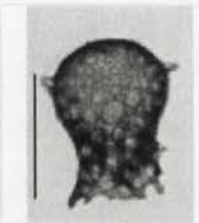

8. *Lophophaena witjazii*

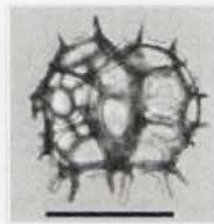

9. *Lophospyris pentagona pentagona*

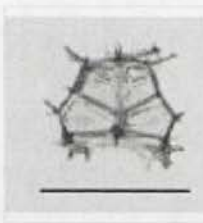

10. *Lophospyris pentagona quadriforis*

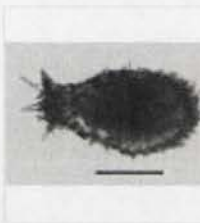

11. *Mitrocalpis araneafera*

12. *Neosemantis distephanus distephanus*

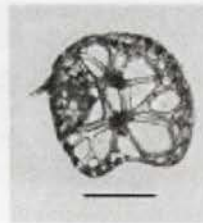

13. *Nephrospyris renilla*

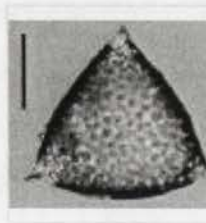

14. *Otosphaera polymorpha*

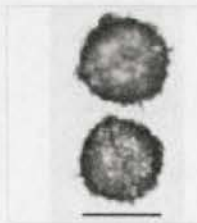

15. *Pentapylonium implicatum*

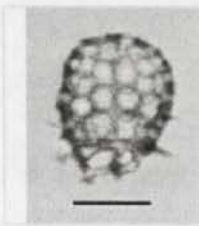

16. *Peridium longispinum*

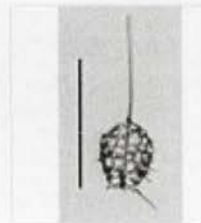

17. *Peridium* sp. cf. *P. longispinum*

18. *Peripyramis circumtexta*

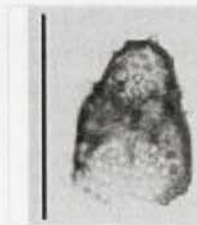

19. *Peromelissa* sp. cf. *P. thoracites scaphopodium*

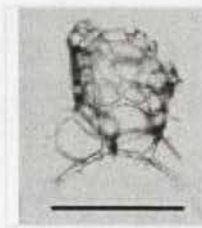

20. *Phormacantha* sp. aff. *P. hystrix*

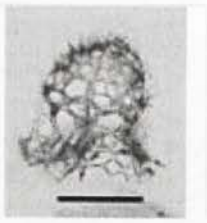

1. *Phormacantha* sp. aff. *P. hystrix*

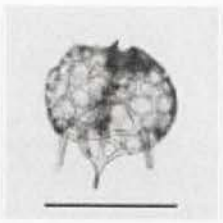

2. *Phormospyris* sp. cf. *P. ophirensis*

3. *Phormospyris stabilis scaphipes*

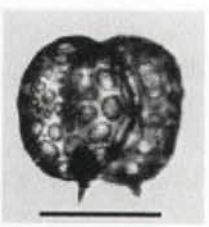

4. *Phormospyris stabilis stabilis*

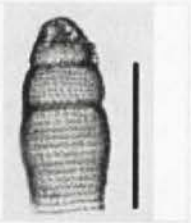

5. *Phormostichoartus corbula*

6. *Phormostichoartus* sp.aff. *P. caryoforma*

7. *Phorticium circumtextum* group

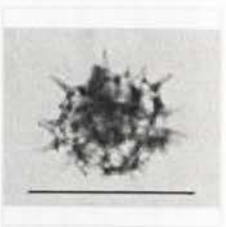

8. *Phorticium octopyle*

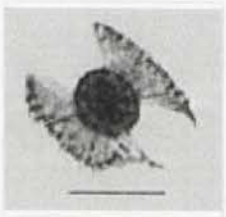

9. *Phorticium pylonium*

10. *Phorticium pylonium*

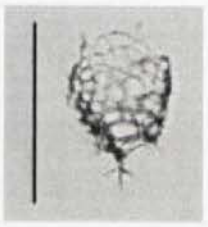

11. *Plectacantha oikiskos*

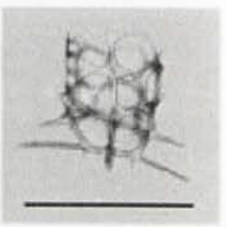

12. *Plectacantha oikiskos*

13. *Plectacantha* sp. Benson 1966

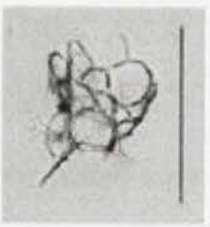

14. *Plectacantha trichoides*

15. *Plectopyramis dodecomma*

16. *Plegmosphaera exodictyon*

17. *Plegmosphaera pachyplegma*

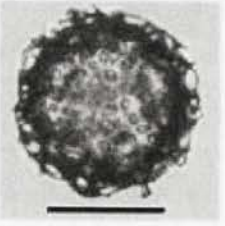

18. *Polysolenia lappacea*

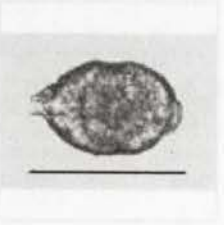

19. *Prunopyle* sp. B Abelmann 1990

20. *Prunopyle tetrapila*

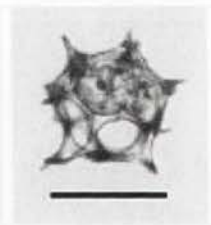

1. *Pseudocubus obeliscus*

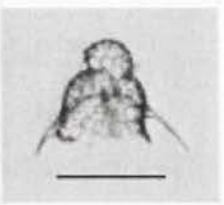

2. *Pseudodictyophimus gracilipes*

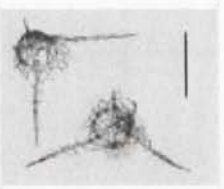

3. *Pseudodictyophimus platycephalus*

4. *Pterocanium praetextum eucolpum*

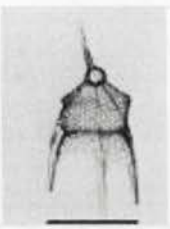

5. *Pterocanium praetextum praetextum*

6. *Pterocanium* sp. cf. *P. auritum*

7. *Pterocanium* sp. cf. *P. elegans*

8. *Pterocanium trilobum*

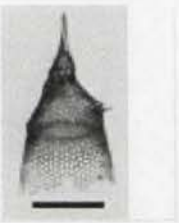

9. *Pterocorys zancleus*

10. *Saccospyris antarctica*

11. *Saccospyris antarctica*

12. *Saccospyris antarctica*

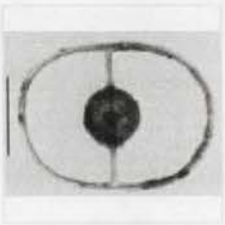

13. *Saturnalis circularis*

14. *Sethoconus tabulatus*

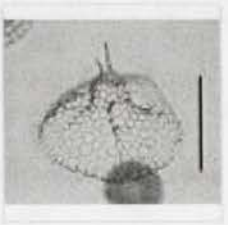

15. *Sethophormis pentalactis*

16. *Sethophormis rotula*

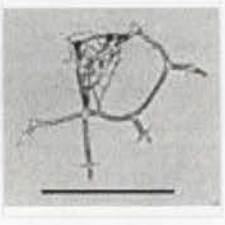

17. *Sethophormis rotula*

18. *Siphocampe arachnea*

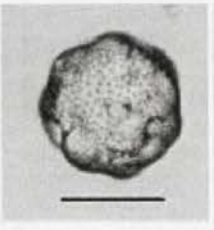

19. *Siphonosphaera magnisphaera*

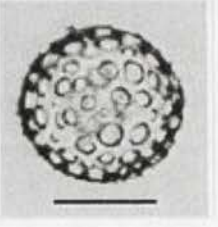

20. *Siphonosphaera martensi*

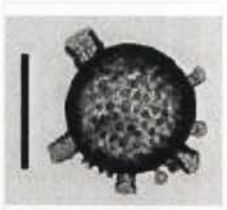

1. *Siphonosphaera polysiphonia*

2. *Sphaeropyle langii*

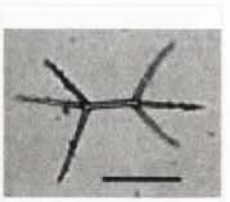

3. *Sphaerozoum punctatum*

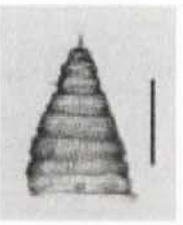

4. *Spirocyrtis scalaris*

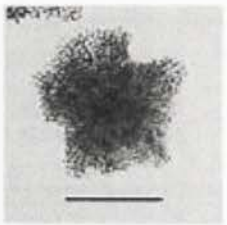

5. *Spongaster pentas*

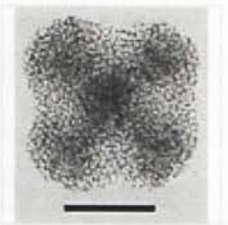

6. *Spongaster tetras*

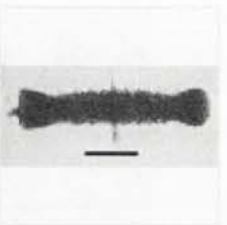

7. *Spongocore puella*

8. *Spongodiscus anomalus*

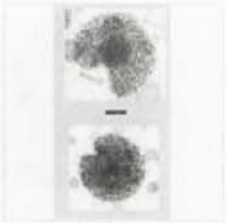

9. *Spongodiscus biconcavus*

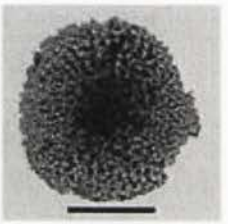

10. *Spongodiscus* sp.

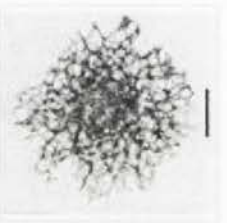

11. *Spongoplegma rugosa*

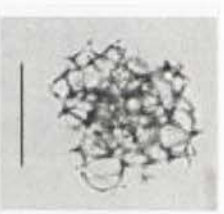

12. *Spongoplegma rugosa*

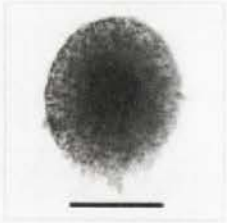

13. *Spongosphaera osculosa*

14. *Spongosphaera polyacantha*

15. *Spongosphaera polyacantha*

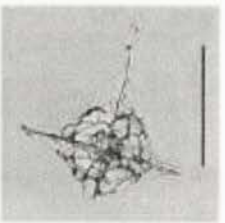

16. *Spongosphaera polyacantha*

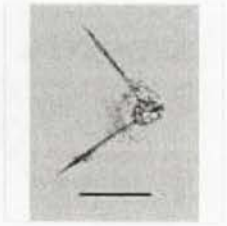

17. *Spongosphaera polyacantha*

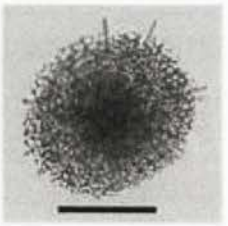

18. *Spongotrochus glacialis*

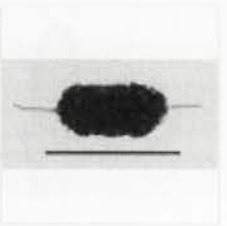

19. *Spongurus pylomaticus*

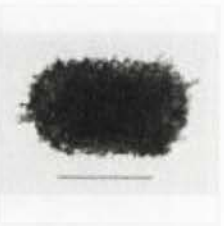

20. *Spongurus pylomaticus*

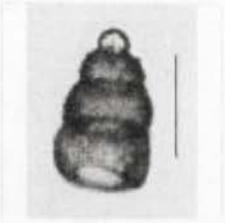

1. *Stichocorys* sp. aff. *S. peregrina*

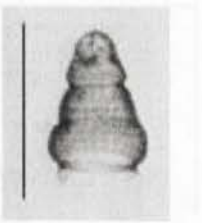

2. *Stichocorys* sp. aff. *S. seriata*

3. *Stichopilium bicorne*

4. *Stylatractus neptunus*

5. *Stylatractus pluto*

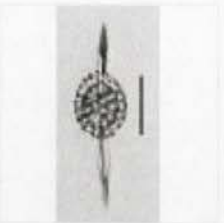

6. *Stylatractus* sp. aff. *S. hispida*

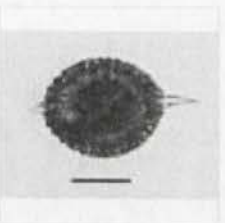

7. *Stylatractus* sp. cf. *S. universus*

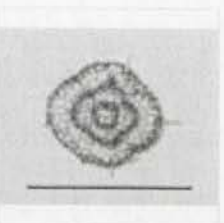

8. *Stylochlamydium venustum*

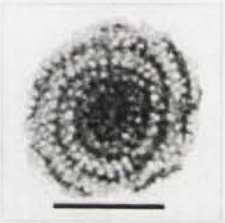

9. Stylodictya *aculeata*

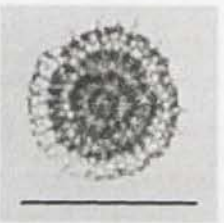

10. Stylodictya *aculeata*

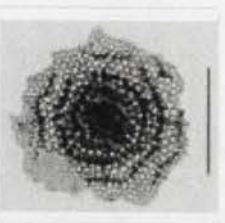

11. Stylodictya *aculeata*

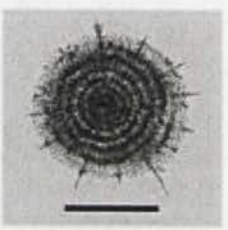

12. Stylodictya *validispina*

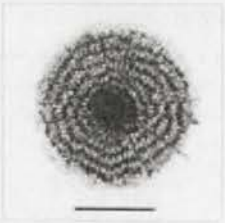

13. *Stylodictya validispina*

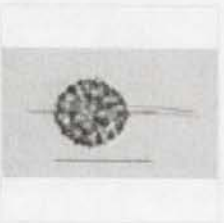

14. *Stylosphaera coronata laevis*

15. *Stylosphaera* sp. aff. *S. radiosa*

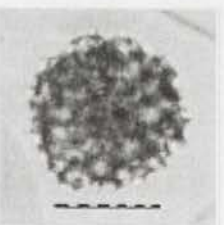

16. *Styptosphaera* sp. aff. *S. spumacea*

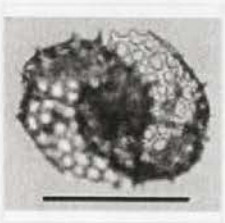

17. *Tetrapyle larnacilla*

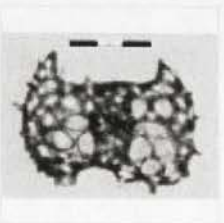

18. *Tetrapyle octacantha*

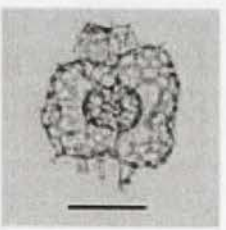

19. *Tetrapyle octacantha*

20. *Theocorythium trachelium*

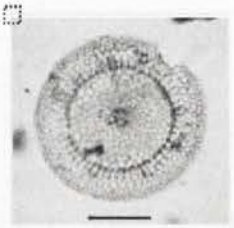

1. *Theopilium tricostatum*

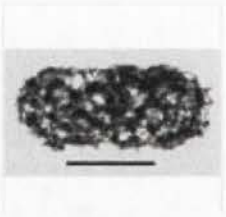

2. *Tholospironium cervicorne*

3. *Tholospironium cervicorne*

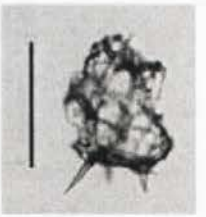

4. *Tholospyris baconiana baconiana*

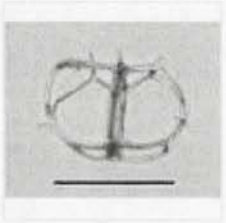

5. *Tholospyris devexa*

6. *Tholospyris ramosa*

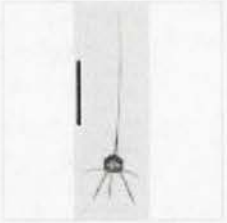

7. *Tholospyris* sp. cf. *T. gephyristes*

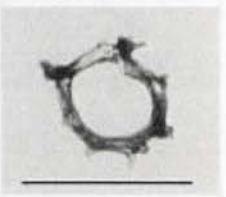

8. *Tholospyris* sp.

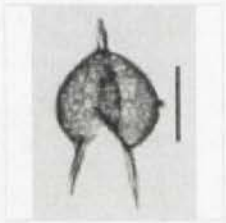

9. *Tholospyris tripodiscus*

10. *Triceraspyris antarctica*

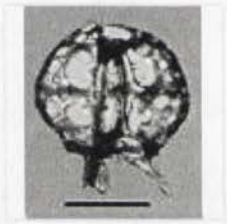

11. *Tripospyris angulata*

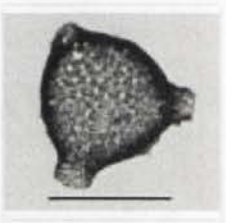

12. *Trisolenia megalactis megalactis*

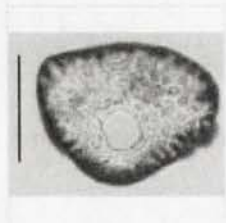

13. *Trisolenia megalactis megalactis*

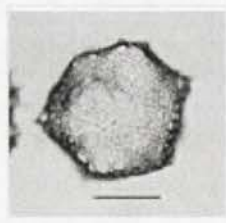

14. *Trisolenia zanguebarica*

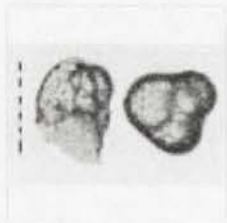

15. *Trisulcus triacanthus*

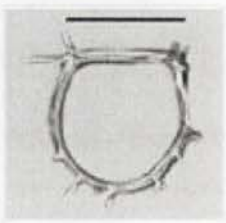

16. *Zygocircus productus*